National Defence
Research and
Development Branch

Défense nationale
Bureau de recherche
et développement

ABSTRACTS and SUMMARIES
of the
2nd CANADIAN FORCES / CRAD MEETING
on

NAVAL APPLICATIONS of MATERIALS TECHNOLOGY

2 - 3 - 4 MAY 1995

Defence
Research
Establishment
Atlantic

Centre de
Recherches pour la
Défense
Atlantique

Canada

Compiled by J. R. Matthews

2nd CF/CRAD MEETING

on

NAVAL APPLICATIONS OF MATERIALS TECHNOLOGY

Baronet Room
8th floor
Chateau Halifax

2nd, 3rd and 4th May 1995

Tuesday May 2nd

Welcome: Capt(N) G.D. Humby, Commanding Officer, Fleet Engineering Maintenance Unit (FEMU)

Opening Remarks: Dr. Roger Hollingshead, DREA

SESSION I:

Chairman: Dr. R.S. Hollingshead

page

1. Development of CAN/MIL HYW700QT Steel, Part II: Welding Procedures and Conclusions, Stéphane Garneau and J.F. Boucher, NDHQ/DGMEM/DSE 5, R. René and F. Racicot, MIL Davie Inc., and C. Billard, MétaSoudage 1

COFFEE

2. Monitoring Pulsed GMAW Parameters in HY Weldments, R. Robicheau, J.and R. Consultants Inc, and J.R. Matthews, DREA 2
3. Microstructural Characterization of NiAl Bronze Weldments, Jim Gianetto, M. Sahoo, M.W. Letts and C.Bibby, CANMET 24
4. Evaluation of Fracture Toughness of High Strength Steels from Stretch Zones, M.N. Bassim and Jason V. Smith, University of Manitoba and J.R. Matthews, DREA 56

LUNCH

SESSION II:

Chairman: Dr. Richard Morchat, CRAD, NDHQ

1. Application of the APHIUS System in DND Submarine Inspection Applications, D. Robert Hay and André Pelletier Tektrend International Inc., James R. Matthews, DREA, Stéphane Garneau, NDHQ/DGMEM/DSE, and Richard Morchat, NDHQ/CRAD 80

2. Introduction of the Signature Classification Development System, Larry Brown, Naval Surface Warfare Center, Carderock Division, Annapolis Detachment, Annapolis, Maryland and Jeff Lin, John Hopkins Applied Physics Laboratory, Laurel, Md 118

3. NDE for Thick Section Composite Laminates, Carol Lebowitz, Naval Surface Warfare Center, Carderock Division, Annapolis Detachment, Annapolis, Maryland 125

COFFEE

4. NDE for Thick Section, Layered Composite Structures, Johnnie DeLoach Naval Surface Warfare Center, Carderock Division, Annapolis Detachment 154

5. Microbiological Contamination of Shipboard Fuel Systems, Causes-Consequences-Control, R.D. Haggett, DREA 177

6. The Ultrasonic Destruction of Microbiological Contamination in Shipboard Fuel Systems, Dr. K.M. Valter McConville, Aastra Aerospace Inc., Downsview, Ont 188

7. High Temperature Firesafe Electrical Cables, D.E. Veinot, DREA, S.Johar, Z. Wang and S. DasGupta, The Electrofuel Manufacturing Company, Ltd., Toronto, and Dr. M.K.Murthy, MKM Consultants International, Toronto,Ont. 196

TUESDAY EVENING, 2nd MAY

RECEPTION and BANQUET

Chateau Halifax

Bluenose Room 8th Floor

7:00 pm
(for 8:00 dinner)

Wednesday, 3rd May

SESSION III:

Chairman: Stéphane Garneau, DSE, NDHQ

1. Laser Processing of Components for Naval Applications, Terri A. Marsico, P.E. Denney, D.F. Farson, Materials and Manufacturing Division, Applied Research Laboratory, The Pennsylvania State University 209

2. Laser Weld Cladding of Nickel Aluminum Bronzes, C.V. Hyatt, DREA K.H. Magee and J. Hewitt, The Laser Institute and T. Betancourt, NSRF 226

COFFEE

3. Laser Cladding for Surface Protection, J. Hewitt and V.E. Merchant, The Laser Institute, Edmonton Alta 253

4. Current US Navy Welding Consumables Research, by P.W. Holsberg J.J. DeLoach, Jr., J.M. Blackburn, G.L. Franke, R.J. Wong and R.DeNale Naval Surface Warfare Center, Carderock Division, Annapolis Detachment, Annapolis, Maryland, USA 21402 266

LUNCH

SESSION IV:

chairman: Mr. Dwight Veinot

1. Computational Evaluation of Shipboard Cathodic Protection Systems, V.G. DeGiorgi, E.D. Thomas III and K.E. Lucas, Mechanics of Materials Branch and Environmental Effects Branch, Naval Research Laboratory, Washington, and A. Kee, Geo-Centers, Maryland 296

2. CPBEM Program Suite For The Design Of Cathodic Protection Systems For Ships, D. Brennan, J. Wallace, M.W. Chernuka, and M. Palmeter, Martec Ltd., and K. KarisAllen, Facts Engineering 325

3. Fracture Control for Surface Ships, Ken KarisAllen, Facts Engineering and Jim Matthews, DREA 326

COFFEE

4. Crack Arrest Toughness of a Heat Affected Zone Containing LBZ, L. Malik and L.N. Pussegoda, Fleet Technology Ltd., B.A. Graville, Graville Assoc., and W.R. Tyson, MTL, CANMET 342

5. Effect of Undermatching Weld Metal on the Measured Fracture Toughness of HSLA 100 Joints, R. Yee and L. Malik, Fleet Technology, Ltd., and J. Morrison, Esquimalt Defence Research Detachment 361

6. Preservation and Painting - Meeting the Environmental Challenge, David Allison, Director of Naval Architecture, Ministry of Defence (Procurement Executive), Foxhill, Bath 390

106-04129/

Thursday, 4th May

SESSION V:

Chairman: Dr. John Hiltz, GL/Materials Chemistry, DREA

1. Evaluation of Noise Reduction Coatings, C.A. Hamm, Guigné International Ltd., Newfoundland and J.P. Szabo, DREA 409

2. Inorganic Intumescent Fire Protective Coatings for Marine Use, D.E. Veinot, DREA and D. Nguyen, J.O. Bernt and Associates, Ltd., Mississauga 432

COFFEE

3. DDH 205 Class Structural Integrity History 1951-1994, D.J. Hussey and C.D. Roushorn, Donelad Hydronautics Ltd, D.G. Smith, Paint and Preservation Officer (retired) and LCdr K.B. Holt and Lt(N) K. Kirkov, Surface Ship Structures, Naval Architectural Services, NDHQ 444

4. An Overview of Fatigue Assessment and Control in Naval Welded Details, Dr. A.M. Abdel-latif, Materials Engineering and Applied Physics, Quality Engineering Test Establishment, Ottawa 510

LUNCH

SESSION VI:

Chairman: Mr. John Porter

1. X-ray Diffraction Determination of Residential Strain for Marine Platforms John F. Porter, DREA, and Michael E. Brauss and James A. Pineault, Proto Manufacturing Ltd. 534

2. Diffraction Measurements on CPF Steel Fatigue Samples, Perry Clarke, and Tom Holden, Atomic Energy of Canada Ltd., J.F. Porter, DREA and Richard Yee, Fleet Technology Ltd. 535

3. Implementation of Accuracy Control on the Canadian Patrol Frigate Program, Brian McGrath, Saint John Shipbuilding Ltd. 551

COFFEE

4. Fatigue Crack Initiation Prediction for Naval Platform Weldments, J.F. Porter, DREA, and R. Yee, Fleet Technology Ltd. 577

5. Acoustic Emission Inspection of Compressed Gas Cylinders D.R. Hay, Tektrend International Inc. 608

6. Prediction of Hydrogen Cracking in Multipass Welds in Low Carbon Steels, B.A. Graville, Graville Assoc., and L.N. Pussegoda and L. Malik, Fleet 632

7. Acoustic Properties of Sonar Dome Materials, J.Y. Guigné and Quanshun Liu Guigné International Ltd., Newfoundland, and J.P. Szabo, DREA 646

#510344 C

Development of CAN/MIL HYW700QT Steel. Part II: Welding Procedures and Conclusions

by

S. Garneau, J-F Boucher - DND/DGMEM/DSE 5
National Defence Headquarters, Ottawa, Canada, K1A 0K2

R. René, F. Racicot - MIL Davie Inc, R&D Center
22 George D. Davie Lévis, QC, G6V 6N7

C. Billard, MétaSoudage, 115 De la Rive
Ste-Anne de Sorel QC, J3P 1K1

ABSTRACT

This project consisted of the acquisition of a Canadian know-how for the production and the welding of an HY100 type steel, dubbed CAN/MIL HYW700QT. The project was started in June 1988 and ended in July 1994. the main contractor, MIL Davie Inc. had the CAN/MIL HYW700QT made, rolled, and heat treated in three separate Canadian steelmaker's facilities.

The experimental steel was characterized with regard to it's hardenability and cold cracking susceptibility. The extensive mechanical testing performed showed that the steel had the high level of toughness required for pressure hull applications. The other mechanical properties met or exceeded the American military requirements for HY100 grade steel plates.

The filler materials hygroscopic behaviour, in relation to the diffusible hydrogen content of the resulting welds, was assessed. Valuable information about moisture pickup, the moisture retention effect, shelf life of opened containers, and the ability to reclaim by baking, several filler materials was collected.

Finally, welding procedures using GMAW, MCAW, SAW and FCAW processes were developed and qualified. The SMAW procedures, developed with one particular MIL E11018M electrode, did not pass the final qualification test, the DREA/DL developed Underwater Monoblast Explosion Bulge Test.

#510345 ②

Pulsed GMAW Parameters in HY Weldments

by

R.M. Robicheau
J & R Consultants, Dartmouth, N.S.

and

J.R. Matthews
Defence Research Establishment Atlantic

ABSTRACT

The Parameters in Synergic Pulsed GMAW welding are a direct result of the logic programmed into each specific welding machine and are dependent on the shielding gas, weld wire composition and wire size. In many systems, the pulsing parameters cannot be varied from manufacturer's pre-programmed settings.

This project evaluated the electrical output characteristics of the following three welding systems to determine the pulsing parameters of each of the power sources;

1) Fronius T.I.M.E. 450 Synergic
2) Fronius T.I.M.E. 540 coupled with a TR-19 synergic pulsing unit, and
3) Linde 650

These machines had been utilized to produce weldments for evaluation on previous DREA projects. Lincoln LA 100 welding wire and T.I.M.E. gas were used on each machine but C-5 gas was also evaluated on the T.I.M.E. 540. Pulsing parameters were determined at wire feed speeds ranging from 100 to 500 IPM, various synergic settings, and for welding procedures conducted in previous projects.

Pulsed gas metal arc welding is the superior process for all positional welding of HY steels, however, it is essential that pulsing parameters be recorded during welding procedures qualification in order to establish calibration criteria for production welds.

1.0 INTRODUCTION

Synergic Pulsed GMAW shows promise as the welding process of choice for joining HY steels. However, pulsing parameters are pre-programmed into the equipment and therefore not only varies from manufacturer to manufacturer, but are also dependent on the shielding gas, weld wire composition and wire size. In order to fully characterise a welding procedure, it is essential to understand the synergic logic programmed into each machine. Therefore, the purpose of this project was to evaluate Welding Procedures from selected previous DREA projects to determine the pulsing parameters of each welding machine.

2.0 SCOPE OF THE PROJECT

This project involved the evaluation of the following three welding machines;

a) T.I.M.E. 450 Synergic,
b) T.I.M.E. 540, and
c) LINDE 650.

The latter two machines had been used on previous DREA projects and weldments from optimised procedures were evaluated. T.I.M.E. gas was used as the shielding medium for all three machines but a 95 % Ar, 5 % CO_2 (C-5) gas mixture was also reviewed using the T.I.M.E. 540 system.

3.0 BACKGROUND

3.1 Pulse Welding with T.I.M.E.^{TM} Process

The Transferred Ionized Molten Energy (T.I.M.E.) Process is a modification of the gas metal arc welding (GMAW) technique consisting of a four component shielding gas and new types of welding equipment. The Patented T.I.M.E. gas is a mixture of argon, helium, carbon dioxide and oxygen. The gas creates a unique arc plasma that provides stability at wire feed speeds up to 2000 IPM with 0.045" diameter wire. This compares to less than 800 IPM for conventional GMAW welding processes. The result is a process capable of depositing weld metal with high quality (i.e. higher toughness, no spatter, no undercut) at a very high deposition rate and welding speed (up to 8 times faster than SMAW).

The pulsed gas metal arc welding(P-GMAW) process is a technique developed over 15 years ago to bridge the gap between short circuit and spray mass transfer of weld metal. In this process a pulsating current is superimposed over the steady DC-GMAW causing brief inputs of energy. These current pulses produce a controlled droplet transfer which corresponds to the rhythm of the pulse frequency. The background current ensures that the tip of the electrode and the welding pool are kept molten. With each rise in current, a droplet is transferred to the workpiece due to the "pinch effect". In sophisticated pulsing systems, the size of the droplet can be controlled and adjustable to provide one droplet per pulse.

The background current is adjustable to suit the weld wire material and shielding gas composition. Since the critical level of current necessary to shed the droplets is a function of pulse current, the amount of heat produced is relatively low compared with conventional methods.

There are two features of P-GMAW that are of interest in welding HY80/HY100 steels. First, the critical level of current needed to achieve spray transfer is low enough to allow deposition rates in excess of that which can be easily controlled in normal GMAW for making out-of-position welds hence providing operation economy. Second, it has also been found that pulsing can actually enhance the quality and toughness of the deposited weld metal while maintaining acceptable levels of other mechanical properties.

Pulse welding introduces a number of new variables in addition to the those normally controlled in the T.I.M.E.™ Process (i.e. WFS, tip recess, voltage, travel speed). These are shown in Figure 3.1.

Figure 3.1 Pulse Parameters

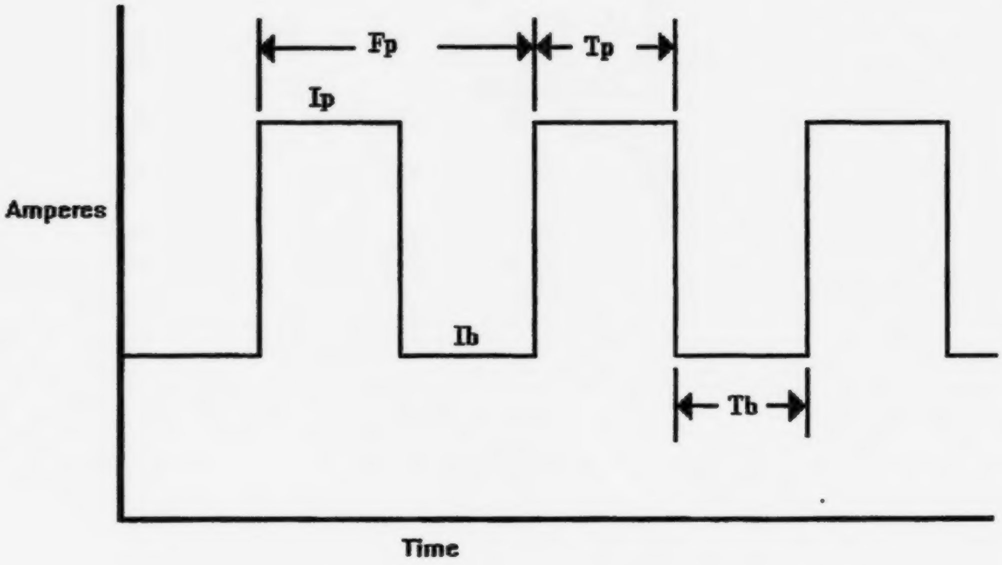

I_p - pulse current
T_p - pulse duration
I_b - background current
T_b - background current duration
F_p - pulse frequency

4.0 EXPERIMENTAL PROCEDURE

4.1 Consumable Wires and Shielding Gases for the Program

Lincoln LA 100 weld wire (classed by AWS as ER100S-1) was used for all welding. The weld wire was 1.2 mm in diameter. The chemical analysis is given in Table 4-1. T.I.M.E gas was used on all machines. However, 95 %Ar, 5 % CO_2 (C-5) mixture was evaluated on the T.I.M.E. 540 system.

4.2 Arc Voltage and Current Measurements

All arc voltages were measured between the base metal and wire feeder. Welding currents were measured using a LEM shunt Model LT-500-S modified for Fronius welding machines. A low pass 5 kHz filter was used for some readings. A data acquisition card coupled with a 386 computer was used to collect readings and were transformed into data points for statistical and graphical evaluation (See Figure 4.1)

Figure 4.1 Equipment Set-up

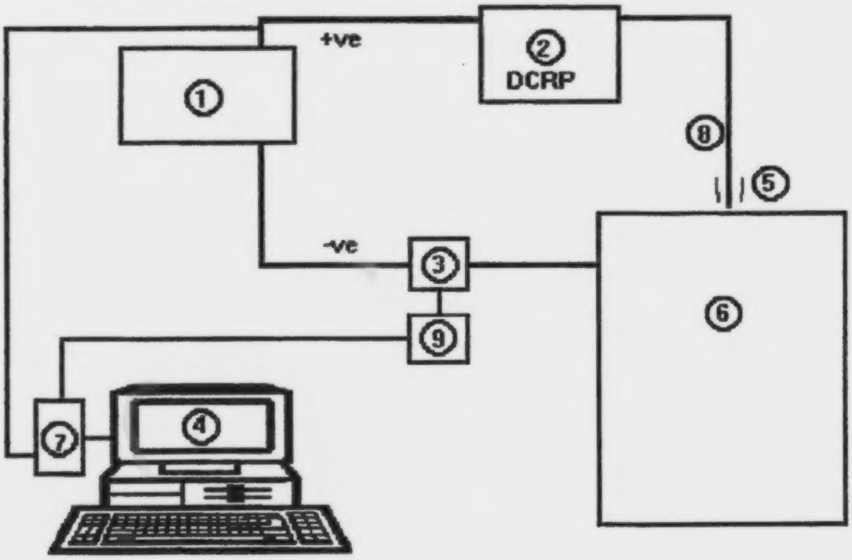

1)	**Power Source**	**6)**	**Base Metal**
2)	**Wire feeder Unit**	**7)**	**Data Acquisition card**
3)	**LEM Shunt**	**8)**	**Filler Metal**
4)	**PC**	**9)**	**5 kHz low pass filter (optional)**
5)	**Welding Torch**		

5.0 EXPERIMENTAL RESULTS

There were several tests that were carried out on three different welding machines. Table 5.1 gives the explanation for each experiment.

The first series of experiments was conducted with the T.I.M.E. 450 Synergic welding machine. Although no welding procedure qualification tests had been conducted with this machine in previous D.R.E.A. studies, a series of experiments were conducted to give a comparison of the synergic settings on this machine as compared with the T.I.M.E. 540. The T.I.M.E. 450 Synergic is the latest T.I.M.E. technology available from Fronius and the machine is based upon a much different inverter technology than its predecessor. Therefore the experiments that were conducted with this machine included a series that evaluated changes in the fine tuning controls (Weld 450A), synergic settings varied by the power control alone changing the wire feed speed from 50 to 500 IPM (Weld 450 B), and two welding schedules that were prepared and practised as part of a T.I.M.E. training program held in 1994 (Welds 450 C and 450 D.

The T.I.M.E. 540 system coupled with the TR-19 synergic controller has been used in its present and modified form in various projects sponsored by D.R.E.A. A series of experiments were developed to evaluate many of the welding procedure parameters developed in those earlier projects (Welds 540 B, 540C, 540D and 540E). Also, in order to evaluate the pulsing characteristics of the machine, a series of experiments were conducted which allowed direct comparison with the T.I.M.E. 450 series. These experiments consisted of varying the synergic settings to achieve WFS's from 50 to 500 IPM (Weld 540A), evaluating changes in the fine tuning controls (Weld 540F). Additional experiments were conducted to evaluate the effect of using a 5 kHz low pass filter in the circuit. These results are given in Weld 540G(no filter) and can be compared to Weld 540A(using a 5 kHz filter).

A final series of experiments were conducted to compare another mixed gas, C-5 (95 % Ar - 5% CO_2) with T.I.M.E. gas, which was used for all other experiments. This experiment used the Ar-CO_2 synergic program provided with the TR-19 controller (Weld 540H) and varied the power control to achieve WFS' of 50 to 500 IPM. This series can be directly compared with the results from Weld 540A

The last series of experiments employed the Linde 650 welding machine and is not designed to allow pulsed synergic output. This series consisted of adjusting the voltage to achieve a stable arc for WFS's from 50 to 500 IPM.

Table 5.1 Description of Experiments

1) T.I.M.E. 450 Synergic

I)	Series 450 A:	WFS constant, change Pv, WF
ii)	Series 450B:	Synergic Settings, WFS 50 - 500 IPM
iii)	Series 450C:	Weld Program #3 (overhead welding)
iv)	Series 450D:	Weld Program #3 (vertical welding)

2) T.I.M.E. 540 c/w TR-19 Synergic Controller

I)	Series 540A:	Synergic Settings, WFS 50 - 500 IPM
ii)	Series 540B:	Flat Procedure from CR/93/436
iii)	Series 540C:	Vertical Procedure from CR/93/436
iv)	Series 540D:	Overhead Procedure from CR/93/436
v)	Series 540E:	L.O.F. Settings from CR/94/436
vi)	Series 540F:	WFS constant, change Pv, WF
vii)	Series 540G:	Synergic Settings but without low pass filter
viii)	Series 540H:	Synergic Settings but with C-5 gas

3) LINDE 650 c/w DigiMig Wire Feeder

I)	Series 650A:	WFS 50 - 500 IPM
ii)	Series 650A:	Horizontal Welding procedure

The following results compare the pulse characteristic of all four major machine set-ups at a wire feed speed of 450 IPM.

Synergic Settings to achieve 450 IPM

	T.I.M.E. 450	**T.I.M.E. 540**	**T.I.M.E. 540 (C-5)**	**Linde 650**
	450B	*540A*	*540H*	*650A*
I_{avg}	316 amps	300.6 amps	238.5 amps	370.0 amps
V_{avg}	27.5 volts	29.1 volts	24.2 volts	29.9 volts
I_p	543.6 amps	502.5 amps	528.3 amps	421.0 amps
I_b	148.1 amps	91.2 amps	30.2 amps	334.0 amps
T_p	2.84 ms	3.32 ms	4.48 ms	2.08 ms
F_p	227.3 Hz	223 Hz	115.7 Hz	320.5 Hz

6.0 DISCUSSION

Synergic pulsed gas metal arc welding incorporates a number of pulsing features which can be characterised by the electrical characteristics of the machine output. In the synergic relationship, the correct combination of each of the variables is pre-programmed into an EPROM (erasable, programmable, read only memory) and is accessed by changes in the position of the main Power Control on the controller. Different relationships are therefore required for different welding consumable and shielding gas. Also, each manufacturer of equipment may have different views on how the synergic relationship should be constructed in order to maintain a stable arc. In fact this synergic logic was found to be different between the T.I.M.E. 450 Synergic and the T.I.M.E. 540 machines even though each machine is manufactured by Fronius of Austria.

Generally each machine follows the same basic rules when applying the synergic logic. As the wire feed speed is increased in each machine by varying the Power Control, the I_b, T_p and F_p increase accordingly to maintain a stable arc. However, the I_p appears to remain constant throughout the range of wire feed speeds examined.

In comparing the four major combinations of this project, namely Experimental Welds 450B, 540A, 540H, and 650A, in which the synergic relationship at a wire feed speed of 450 IPM was examined (see Figures 6.1 - 6.4), the changes in the pulse characteristics of each machine can be seen graphically. The T.I.M.E. 450 appears to have excellent control over the pulsing parameters and is able to maintain arc stability in a superior manner to the T.I.M.E. 540. The 450 system employs a different synergic relationship and although I_p is common to the 540 system, T_p is smaller while the I_b increases to maintain the same average current for a given wire feed speed. F_p remains the same.

In comparing the T.I.M.E 540 system equipped with T.I.M.E. gas versus C-5 gas, the synergic relationship is entirely different with respect to all pulsing parameters except I_p. It would appear that the synergic logic in both Fronius machines is to keep pulse height at the maximum output of the machine thus varying the other pulse parameters as much as possible on lower settings while approaching a constant voltage/constant current relationship as the wire feed speed continues to increase to a point where the arc current must be over 500 amps to melt the wire in a stable arc condition.

Arc stability is an important feature that dictates weldment quality and was found to be different between the 450 and 540 systems. Figures 6.5 - 6.8 show the pulse output characteristics over a range of 4000 sample points versus 1500 points used in Figures 6.1 - 6.4. It was found that the 450 system is again superior in maintaining arc stability over time, and this contrast is more prominent in Figure 6.9, the setting used in a previous project for Flat welding. The figure shows that over a time period representing 4000 sample points, the arc goes through zones of arc instability. Extrapolated over 12000 sample points this instability exhibits a cyclic nature but at a much lower frequency to the synergic pulse relationship. During actual welding operations, the welding operator noted changes in arc length (i.e. arc voltage) which is verified by Figure 6.9. The 450 system did not display this arc instability problem and during actual welding operations was noted to have a much more consistent and stable arc than the 540 system.

The Linde 650 machine also exhibits superior arc stability to the 540 system as shown in Figure 6.8. The arc characteristics detected during welding operations with this machine show a smooth, stable arc.

The synergic settings on the 540 system for C-5 gas did not produce a stable arc and made it difficult interpret the experimental results. This arc instability is readily apparent in Figures 6.3 and 6.7. Although the current pulse appears to constant, the corresponding arc voltage is not able to maintain a stable arc and therefore results in an erratic voltage trace.

Another interesting feature that was observed while using the C-5 gas involved the brightness of the arc of the C-5 compared to the T.I.M.E. gas. The stable arc region in gas metal arc welding is very dependent upon the shielding gas mixture. Generally, each shielding gas maintains a stable arc at different arc voltages but due to the presence of helium in the T.I.M.E. gas, the arc voltage and hence arc energy increases. Comparing the experimental results from Figure 6.6 and 6.7, taken from the 540 system, one can see that in order to maintain a stable arc for T.I.M.E. gas (Fig. 6.6), an arc voltage of 29.1 volts is required. However, for the C-5 gas mixture, an arc voltage of only 24.2 volts was required. The difference in arc voltage and hence arc energy results in the T.I.M.E. gas displaying a much greater amount of light emanated from the arc. This problem is easily rectified by changing to a darker lens shade in the welding helmet. No change in the protective clothing was deemed to be necessary.

FIGURE 6.1 T.I.M.E. 450, SYNERGIC SETTING AT 450 IPM, T.I.M.E. GAS

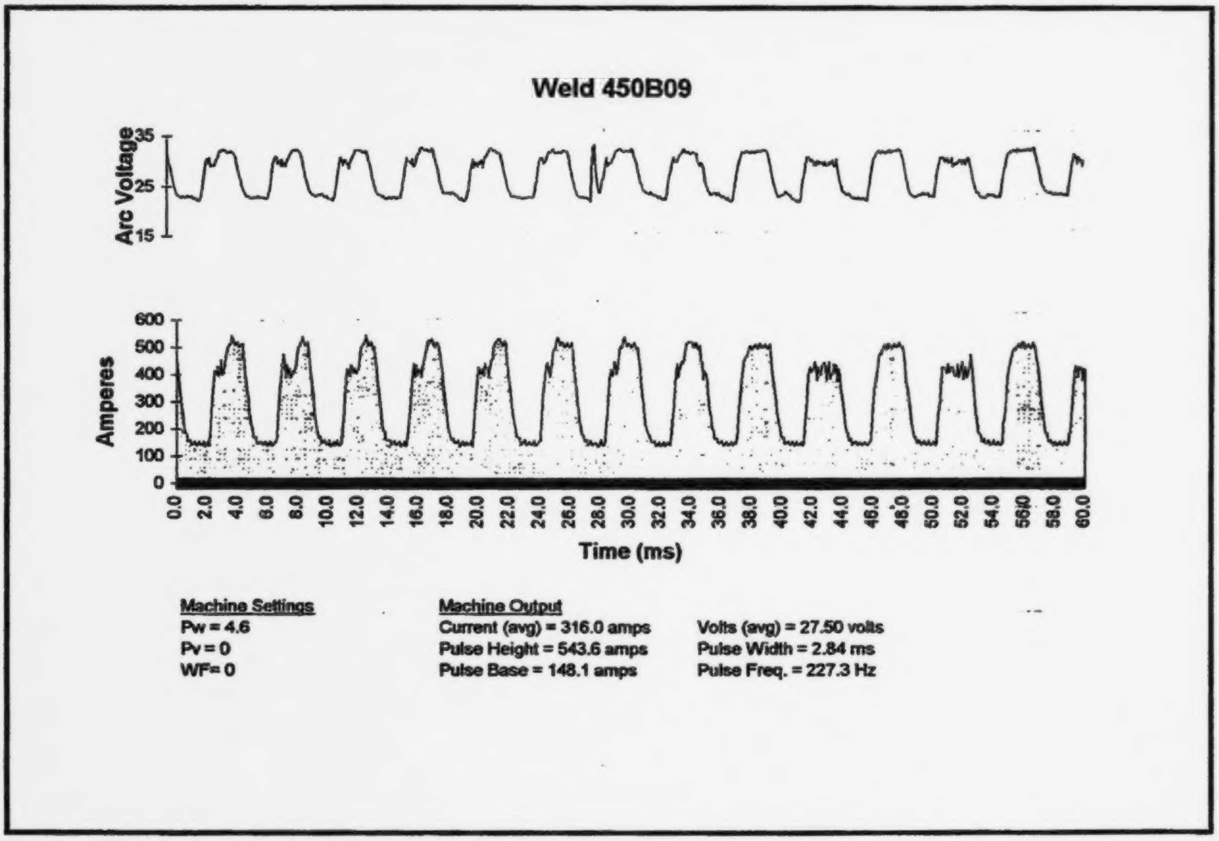

Machine Settings
Pw = 4.6
Pv = 0
WF= 0

Machine Output
Current (avg) = 316.0 amps
Pulse Height = 543.6 amps
Pulse Base = 148.1 amps
Volts (avg) = 27.50 volts
Pulse Width = 2.84 ms
Pulse Freq. = 227.3 Hz

FIGURE 6.2 T.I.M.E. 540, SYNERGIC SETTING AT 450 IPM, T.I.M.E. GAS

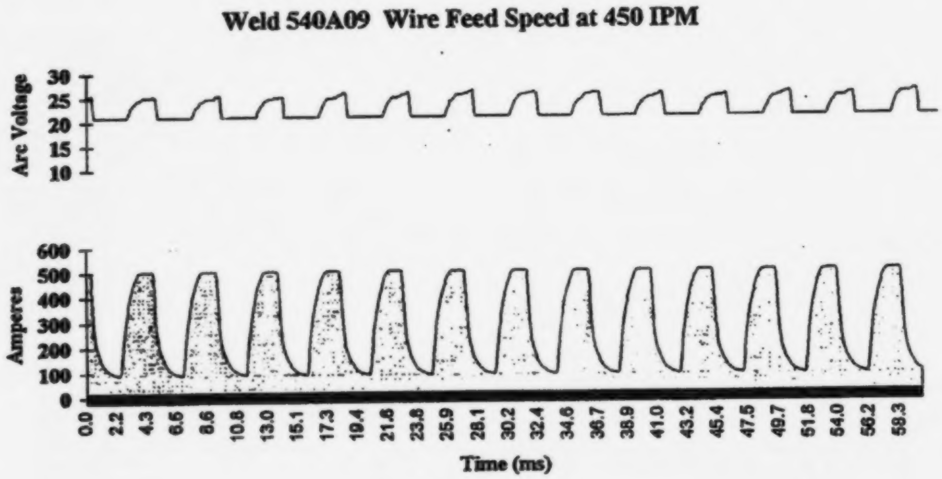

Machine Settings
Pw = 5.75
Pv = 0
WF = 0

Machine Output
Current (avg) = 300.6 amps
Pulse Height = 502.5 amps
Pulse Base = 91.2 amps

Volts (avg) = 29.1 volts
Pulse Width = 3.32 ms
Pulse Freq. = 223.0 Hz

FIGURE 6.3 T.I.M.E. 540, SYNERGIC SETTING AT 450 IPM, C-5 GAS

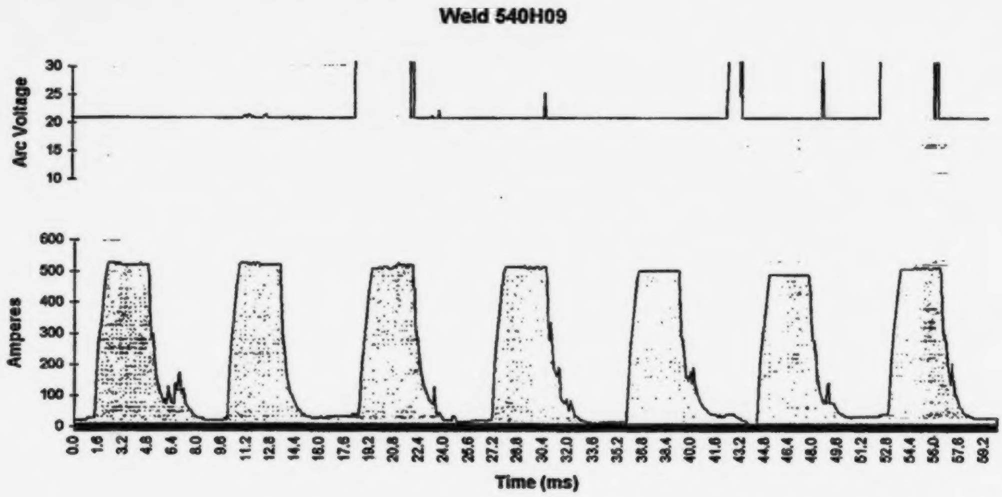

Machine Settings
Pw = +4.5
Pv = 0.0
WF= 0.0

Machine Output
Current (avg) = 238.3 amps
Pulse Height = 528.3 amps
Pulse Base = 30.2 amps

Volts (avg) = 24.2 volts
Pulse Width = 4.48 ms
Pulse Freq. = 115.7 Hz

FIGURE 6.4 LINDE 650, WIRE FEED SETTING AT 450 IPM, T.I.M.E. GAS

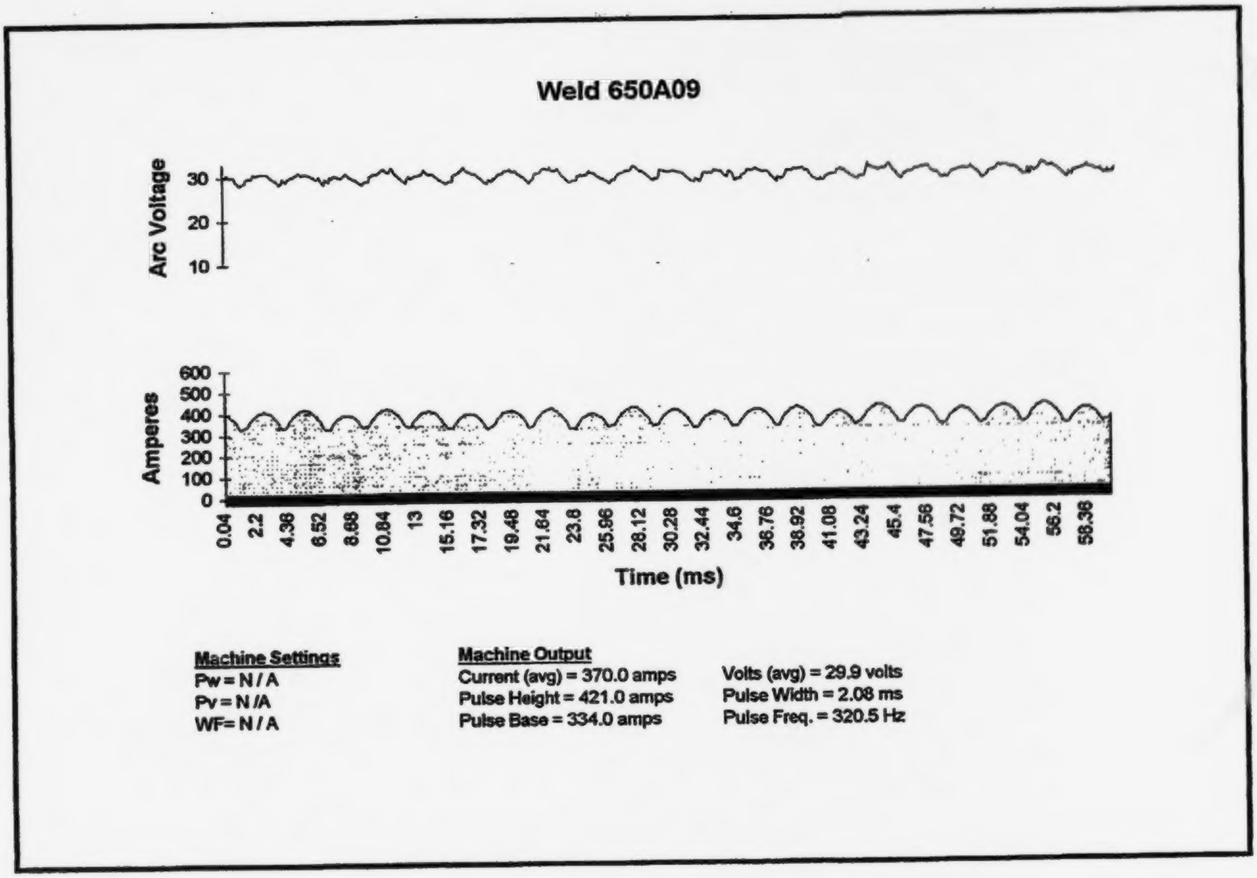

Machine Settings
Pw = N / A
Pv = N /A
WF= N / A

Machine Output
Current (avg) = 370.0 amps
Pulse Height = 421.0 amps
Pulse Base = 334.0 amps

Volts (avg) = 29.9 volts
Pulse Width = 2.08 ms
Pulse Freq. = 320.5 Hz

FIGURE 6.5 T.I.M.E. 450, SYNERGIC SETTING AT 450 IPM (4000 DATA POINTS), T.I.ME. GAS

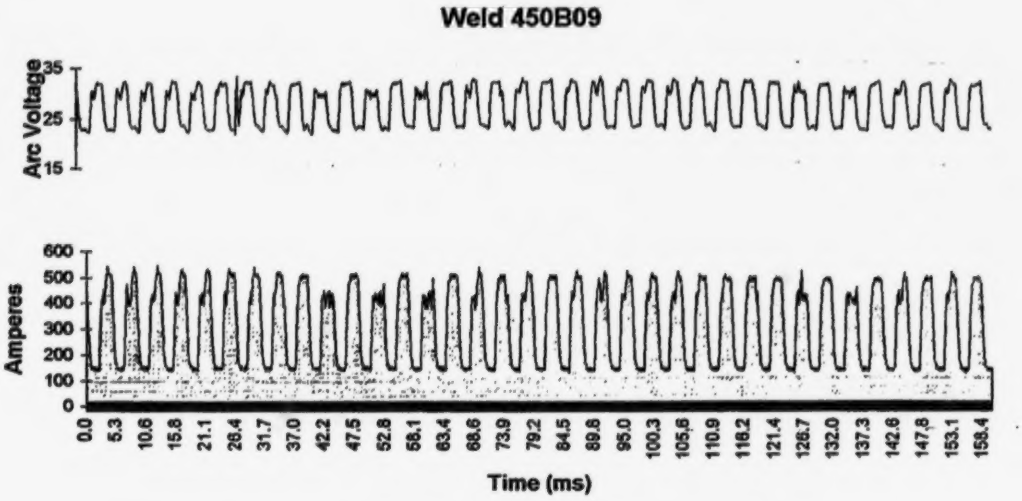

Machine Settings
Pw = 4.6
Pv = 0
WF= 0

Machine Output
Current (avg) = 316.0 amps
Pulse Height = 543.6 amps
Pulse Base = 148.1 amps

Volts (avg) = 27.50 volts
Pulse Width = 2.84 ms
Pulse Freq. = 227.3 Hz

FIGURE 6.6 T.I.ME. 540, SYNERGIC SETTING AT 450 IPM (4000 DATA POINTS), T.I.ME. GAS

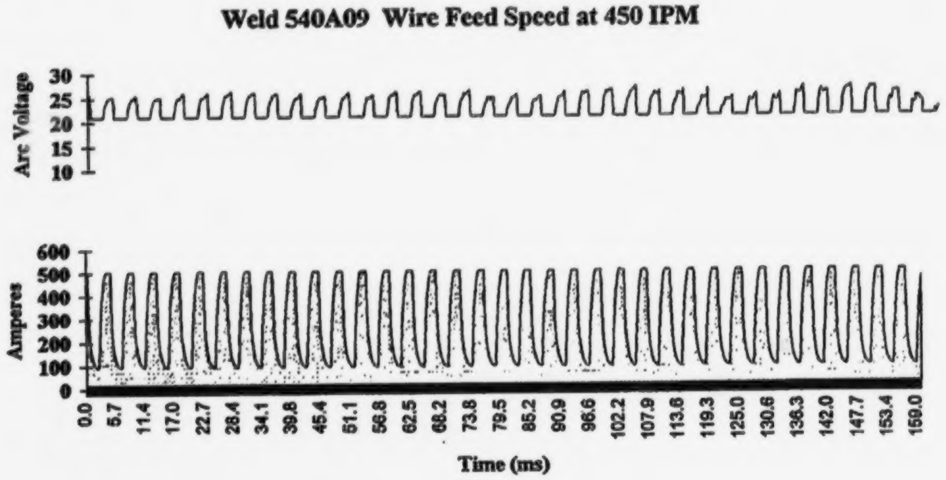

Machine Settings
Pw = 5.75
Pv = 0
WF = 0

Machine Output
Current (avg) = 300.6 amps
Pulse Height = 502.5 amps
Pulse Base = 91.2 amps

Volts (avg) = 29.1 volts
Pulse Width = 3.32 ms
Pulse Freq. = 223.0 Hz

FIGURE 6.7 T.I.ME. 540, SYNERGIC SETTING AT 450 IPM (4000 DATA POINTS), C-5 GAS

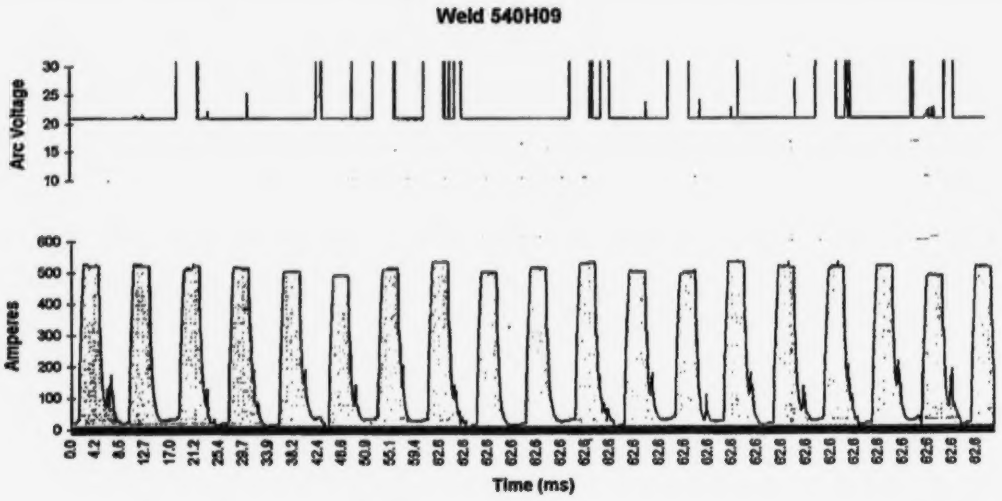

Machine Settings
Pw = +4.5
Pv = 0.0
WF= 0.0

Machine Output
Current (avg) = 238.3 amps
Pulse Height = 528.3 amps
Pulse Base = 30.2 amps

Volts (avg) = 24.2 volts
Pulse Width = 4.48 ms
Pulse Freq. = 115.7 Hz

FIGURE 6.8 LINDE 650, SYNERGIC SETTING AT 450 IPM (4000 DATA POINTS), T.I.M.E. GAS

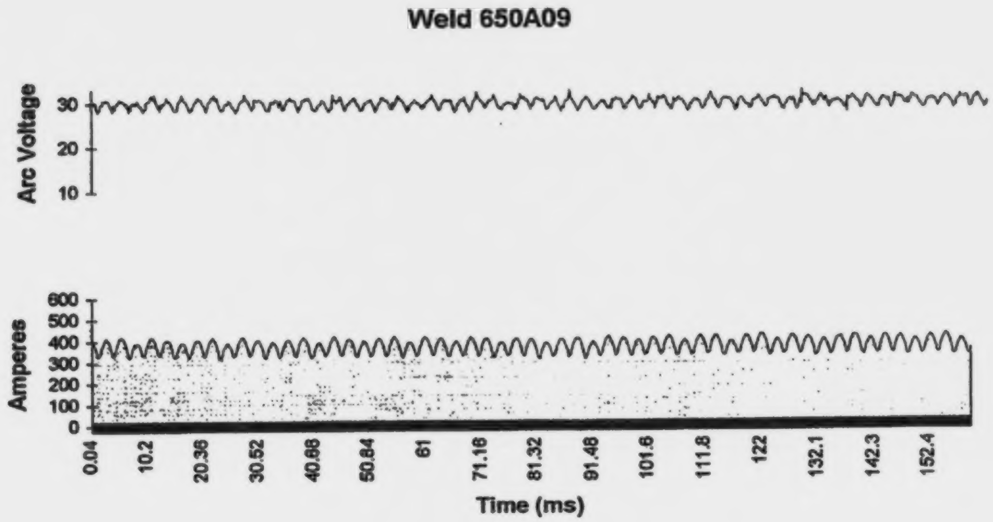

Machine Settings	Machine Output	
Pw = N / A	Current (avg) = 370.0 amps	Volts (avg) = 29.9 volts
Pv = N /A	Pulse Height = 421.0 amps	Pulse Width = 2.08 ms
WF= N / A	Pulse Base = 334.0 amps	Pulse Freq. = 320.5 Hz

FIGURE 6.9 T.I.ME. 540, WELDING PROCEDURE FOR FLAT POSITION, T.I.ME. GAS

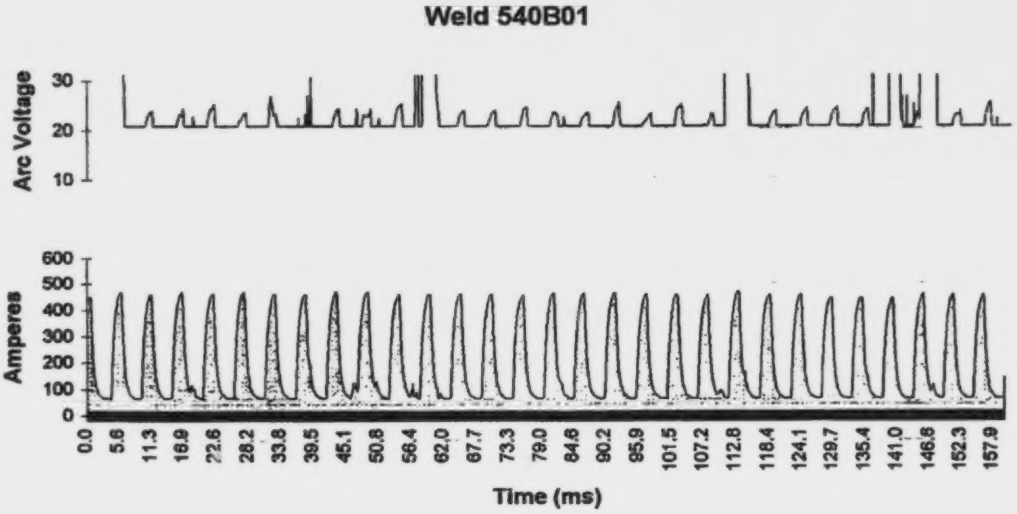

Machine Settings
Pw = 5.25
Pv = -3.5
WF= 0

Machine Output
Current (avg) = 204.3 am Volts (avg) = 25.11 volts
Pulse Height = 452.5 amp Pulse Width = 2.96 ms
Pulse Base = 70.3 amps Pulse Freq. = 186.6 Hz

7.0 CONCLUSIONS

1) P-GMAW has superior benefits for welding HY steels and is clearly the process of choice that should be followed for all positional welding.

2) Pulse waveforms must be taken during the qualification of welding procedures to fully calibrate the electrical characteristics of the welding arc and could be used to determine the conditions promoting fusion defects during production welding.

3) The T.I.M.E. 450 Synergic employs a slightly different pulse logic than the T.I.M.E. 540 with the end result being that the T.I.M.E. 450 has much better arc control than the T.I.M.E. 540. The T.I.M.E. 450 Synergic also has much better operational characteristics than the Linde 650.

4) T.I.M.E. process welding causes a much brighter arc than C-5 gas, but a change in lens shade corrects the problem.

5) The Linde 650, although not a pulsed GMAW machine, actually produces a P-GMAW output at lower wire feed speeds.

Acknowledgements

The authors would like to thank Mr. Ken KarisAllen of FACTS Engineering for his help and support in capturing and subsequent processing of the data obtained for this paper.

#510346 ③

METALS TECHNOLOGY LABORATORIES
REPORT MTL 95-3(TR-R)

MICROSTRUCTURAL CHARACTERIZATION OF NiAl BRONZE WELDMENTS

by

J.A. Gianetto, M. Sahoo, M.W. Letts and C. Bibby

EXECUTIVE SUMMARY

The objective of this study was to develop and evaluate a series of simulation techniques to provide a better understanding of the transformation behaviour of both the weld metal and heat-affected zone (HAZ) regions formed in Ni-Al bronze (NAB) weldments. The welds investigated were produced by (i) laser cladding, (ii) gas-tungsten-arc welding (both autogenous and with filler-wire), and (iii) a Gleeble 2000 weld simulator. In the latter case the aim was to develop melting and reheating experiments that would accurately simulate the HAZ and weld metal regions found in the laser clad weldments. Optical microscopy and microhardness surveys were used to characterize the structures formed in the real and Gleeble simulated weldments. In addition, radial dilatometry was performed to assist with the interpretation of the complex microstructures formed as a result of dynamic thermal cycling. In general, the microstructures formed in NAB weldments were found to be strongly dependent on the alloy composition, particularly Al content, and the thermal cycle conditions including the heating rate, peak temperature, hold time and cooling rate. In addition, there is evidence to suggest that the original starting microstructure e.g. base metal, weld metal or HAZ plays an important role in the formation of the final microstructure. The results of this study clearly demonstrate that Gleeble simulation techniques can be used effectively to understand the transformation behaviour of NAB weldments.

SUMMARY AND CONCLUSIONS

The results from this study clearly demonstrate that Gleeble simulation can be used to gain a better understanding of the transformation behaviour of both the heat-affected zone and weld metal regions formed in NAB weldments. Using optical microscopy and hardness surveys it was possible to characterize the complex microstructures formed in both weld metal and HAZ regions of NAB alloys. It is evident from these results that the microstructures formed in NAB weldments are strongly dependent on the alloy content, particularly Al, and the thermal cycle variables including the heating rate, peak temperature, hold time and cooling rate. In addition, there is evidence to suggest that the original starting microstructure, e.g. base metal, weld metal or HAZ, plays an important role in the formation of the final microstructure. The main observations and conclusions are summarized below.

(i) Significant variation in microstructure and hardness of the as-received laser clad weld metal was observed within the as-deposited as well as the reheated weld metal regions. This included a transition from columnar (mainly martensite) to equiaxed (Widmanstätten α) grains as the center of a weld bead was approached. The reheated weld metal region exhibited lower hardness as a result of transformation to a predominantly Widmanstätten α microstructure. Both regions had allotriomorphic and Widmanstätten α which decorated the prior β boundaries. Gleeble reheating of these structures to Tp = 800°C ($\Delta t_{800-500} = 0.7 - 0.8$ s) produced significant softening, which was associated with annealing of the original martensitic structure. A further reduction in hardness was observed for reheating to Tp =1000°C ($\Delta t_{800-500} = 0.5 - 0.6$ s), and corresponded to the formation of a large volume fraction of α with a eutectoid phase between the laths.

(ii) For the series of GTA bead-on plate autogenous welds and those produced with filler-wire additions the variations in microstructure and microhardness were attributed to the strong effect of Al content and the relatively low energy input (estimated to be between 0.3 to 0.5 kJ/mm). With higher Al content the microstructure and microhardness were similar to those found in the central top portion of the as-deposited region in the laser clad weld where the predominant constituent was Widmanstätten α. In both cases, the prior β grain boundaries were decorated by both allotriomorphic and Widmanstätten α.

(iii) Radial dilatometry was performed to provide HAZ transformation data for dynamic thermal cycling of the 9.2% Al alloy. On heating, the major transformation corresponding to $\alpha + \kappa \rightarrow \alpha + \beta + \kappa$ and $\alpha + \beta + \kappa \rightarrow \alpha + \kappa$ could be detected. On cooling, it was possible to detect the following transformation sequence: a suppression of the $\alpha + \beta \rightarrow \alpha + \beta + \kappa$ to ~ 855-875°C followed by $\alpha + \beta + \kappa \rightarrow \alpha + \kappa$ which occurred at lower temperatures (650-760°C) depending on the cooling rate.

(iv) In the experiments designed to produce simulated weld metal, it was possible to produce microstructures representative of those observed in the original laser clad weldment by heating to Tp = 1040 and 1060°C and varying the cooling time (e.g. martensite ($\Delta t_{800-500} = 0.4$ s) and Widmanstätten α ($\Delta t_{800-500} \geq 1.6$ s). Subsequent reheating of the almost fully martensitic structure to Tp = 800 or 1000°C produced significant reductions in hardness and corresponding changes in microstructures. Reheating to Tp = 800°C ($\Delta t_{800-500} = 0.5$ and 1.3 s) produced an annealed martensitic structure with γ_2 decorating the martensite plate boundaries. Reheating to Tp =1000°C followed by fast cooling ($\Delta t_{800-500} = 0.1$ s) produced a martensitic structure, whereas air cooling ($\Delta t_{800-500} = 1.6$ s) produced a significantly softer mainly Widmanstätten α microstructure. These results clearly show that the final reheated weld metal microstructure is greatly affected by peak temperature and cooling time.

OBJECTIVE

To develop and evaluate a series of simulation techniques to provide a better understanding of the transformation behaviour of both the weld metal and heat-affected zone (HAZ) regions formed in NAB weldments.

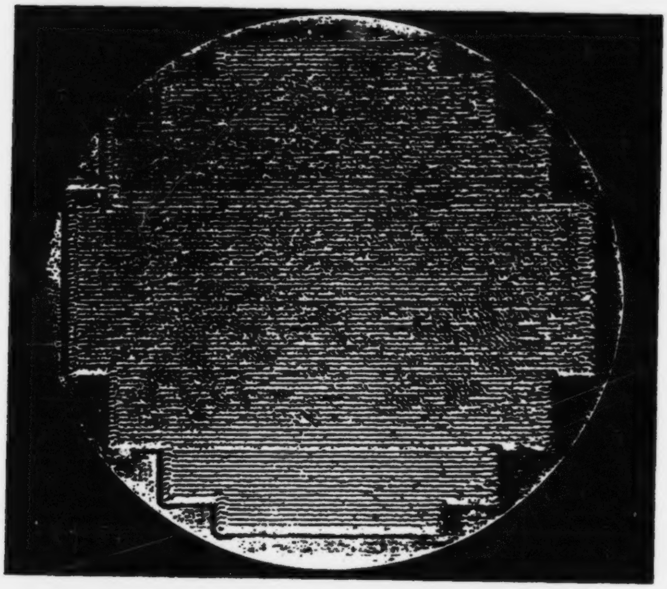

(a)

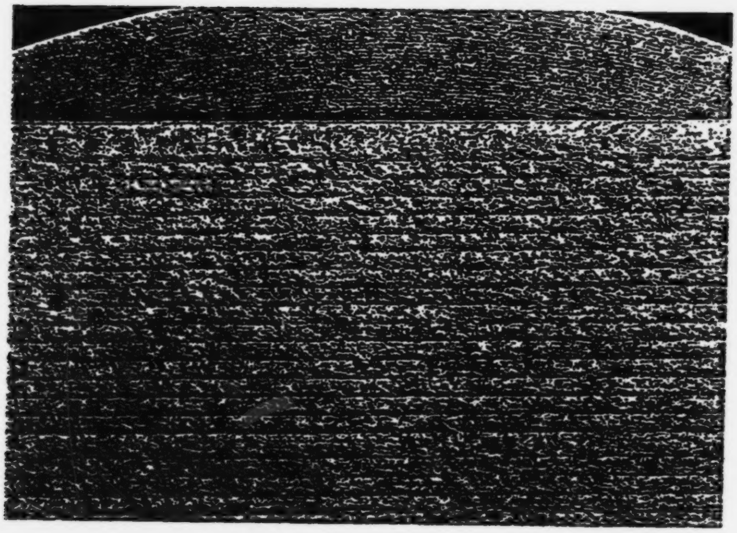

(b) 2x

Fig. 1. Photographs showing the as-received laser clad weldment prepared on the 8.5% Al NAB alloy.

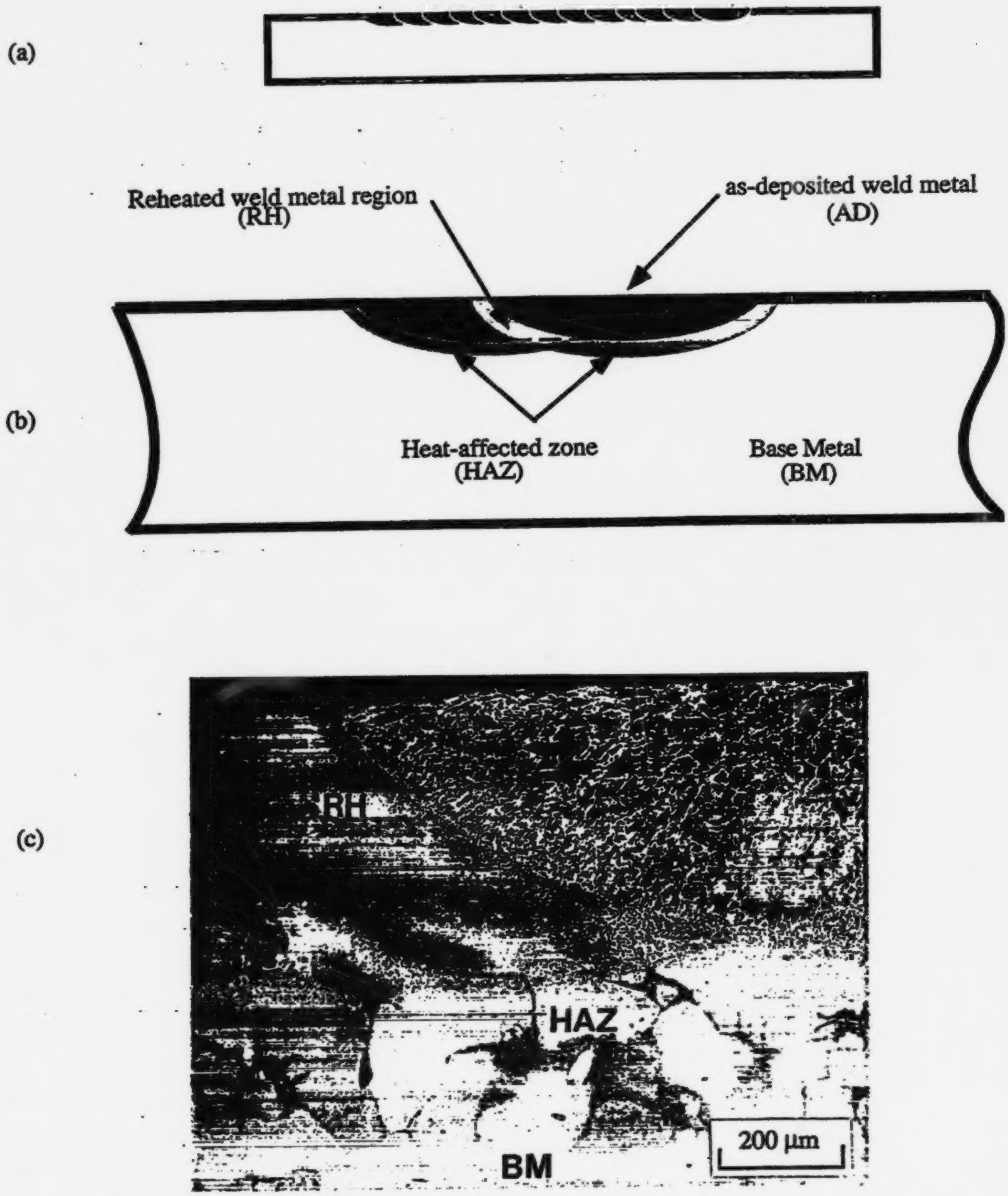
(a)
Reheated weld metal region
(RH)
as-deposited weld metal
(AD)
(b)
Heat-affected zone
(HAZ)
Base Metal
(BM)
(c)
RH
HAZ
BM
200 μm

Fig. 2. Schematic diagrams and micrograph showing regions within laser clad NAB weldment.

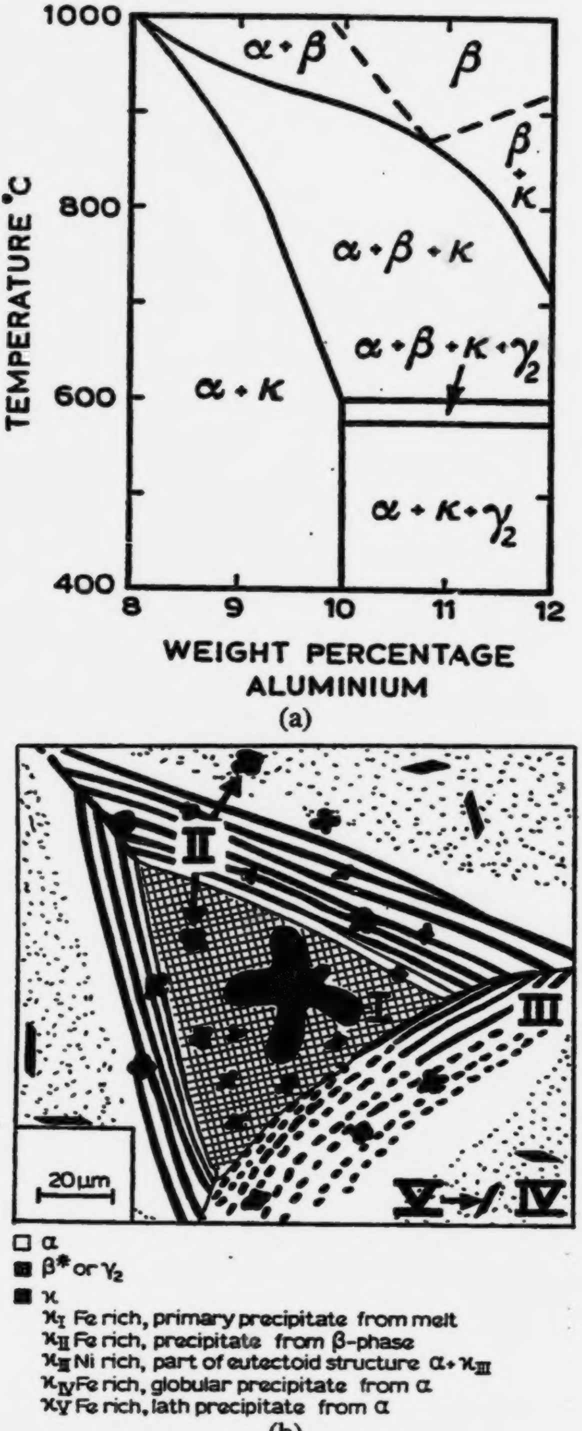
1000
800
600
400
TEMPERATURE °C
8
9
10
11
12
WEIGHT PERCENTAGE ALUMINIUM
α + β
β
β + κ
α + β + κ
α + β + κ + γ2
α + κ
α + κ + γ2
II
I
III
IV
V
20µm
□ α
▨ β* or γ2
■ κ
κI Fe rich, primary precipitate from melt
κII Fe rich, precipitate from β-phase
κIII Ni rich, part of eutectoid structure α + κIII
κIV Fe rich, globular precipitate from α
κV Fe rich, lath precipitate from α

(a)

(b)

Fig. 3. Vertical section of phase diagram for (a) Cu-Al-4Ni-4Fe alloy (1) and (b) schematic illustration of different κ morphologies in NAB alloys (6).

Casting/ Alloy	Heat No.	Element wt %				
		Al	Ni	Fe	Mn	Cu
NAB-1	1260	8.0	4.8	3.4	0.66	balance
NAB-2	1303-2	9.2	4.7	3.4	0.77	balance
Laser Clad*	Base Metal	8.5	4.7	4.1	1.6	balance
Laser Clad*	Weld Metal	8.0	4.6	4.2	1.6	balance
GTA-8.0% Al	Filler wire Weld Metal	8.1	2.4	2.2	0.34	balance
GTA-9.2% Al	Filler wire Weld Metal	9.2	2.6	2.4	0.47	balance

* Supplied by DREA

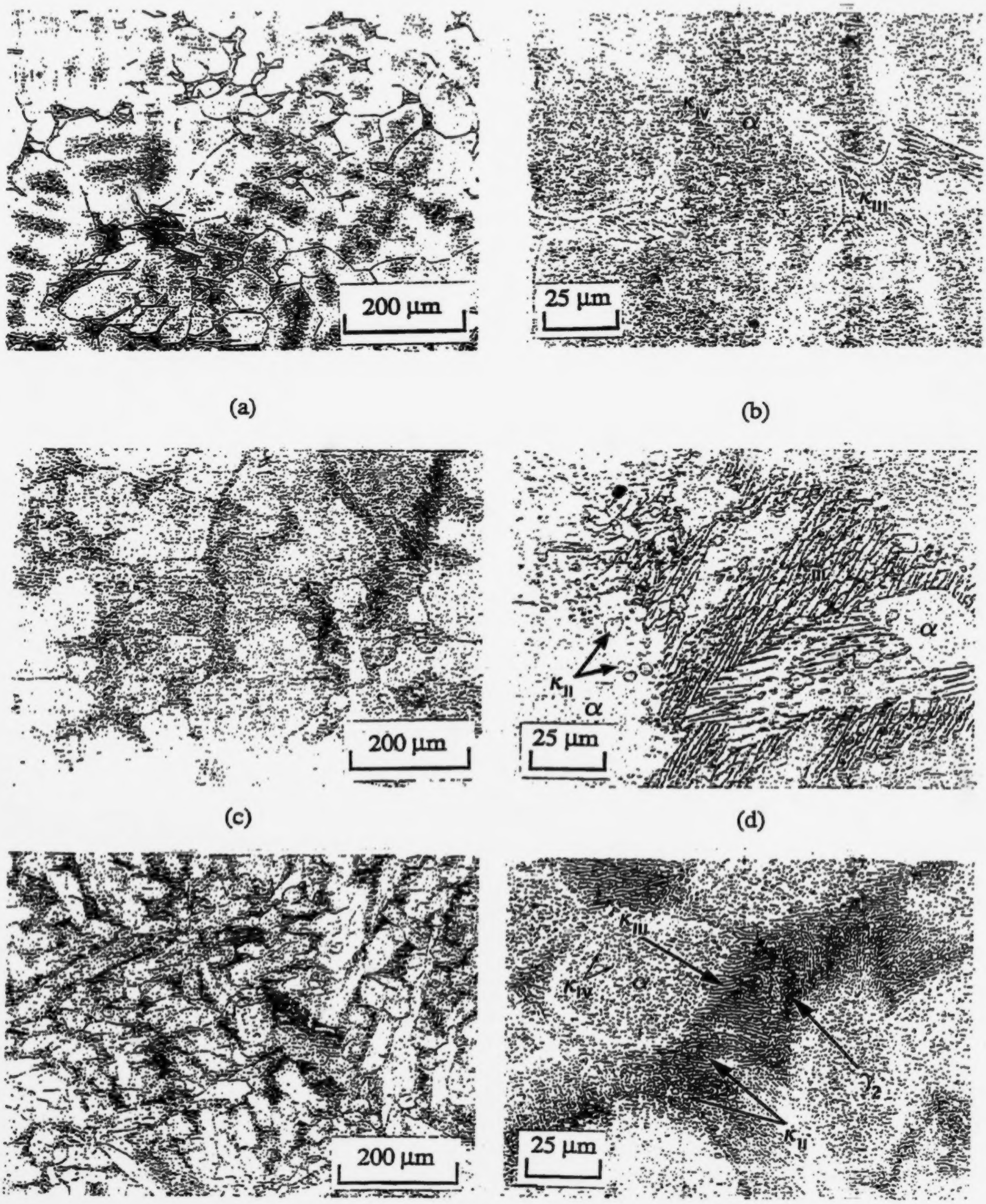
200 μm
κ_{IV}
α
κ_{III}
25 μm
200 μm
κ_{II}
α
α
25 μm
200 μm
κ_{III}
κ_{IV}
α
γ_2
κ_{II}
25 μm

(a) (b)

(c) (d)

(e) (f)

Fig. 8. Optical micrographs of base metals (a,b) 8.0% Al (NAB-1), (c, d) 8.5% Al (laser clad) and (e, f) 9.2% Al (NAB-2).

Microhardness, HV100g			
Identification	Al Content wt %	Overall Avg. (range)	Individual Phases Avg.
NAB-1	8.0	164 (129-203)	$\alpha = 150$ $\alpha + \kappa = 177$
Laser Clad	8.5	170 (141-207)	$\alpha = 142$ $\alpha + \kappa = 198$
NAB-2	9.2	179 (141-207)	$\alpha = 167$ $\alpha + \kappa = 191$

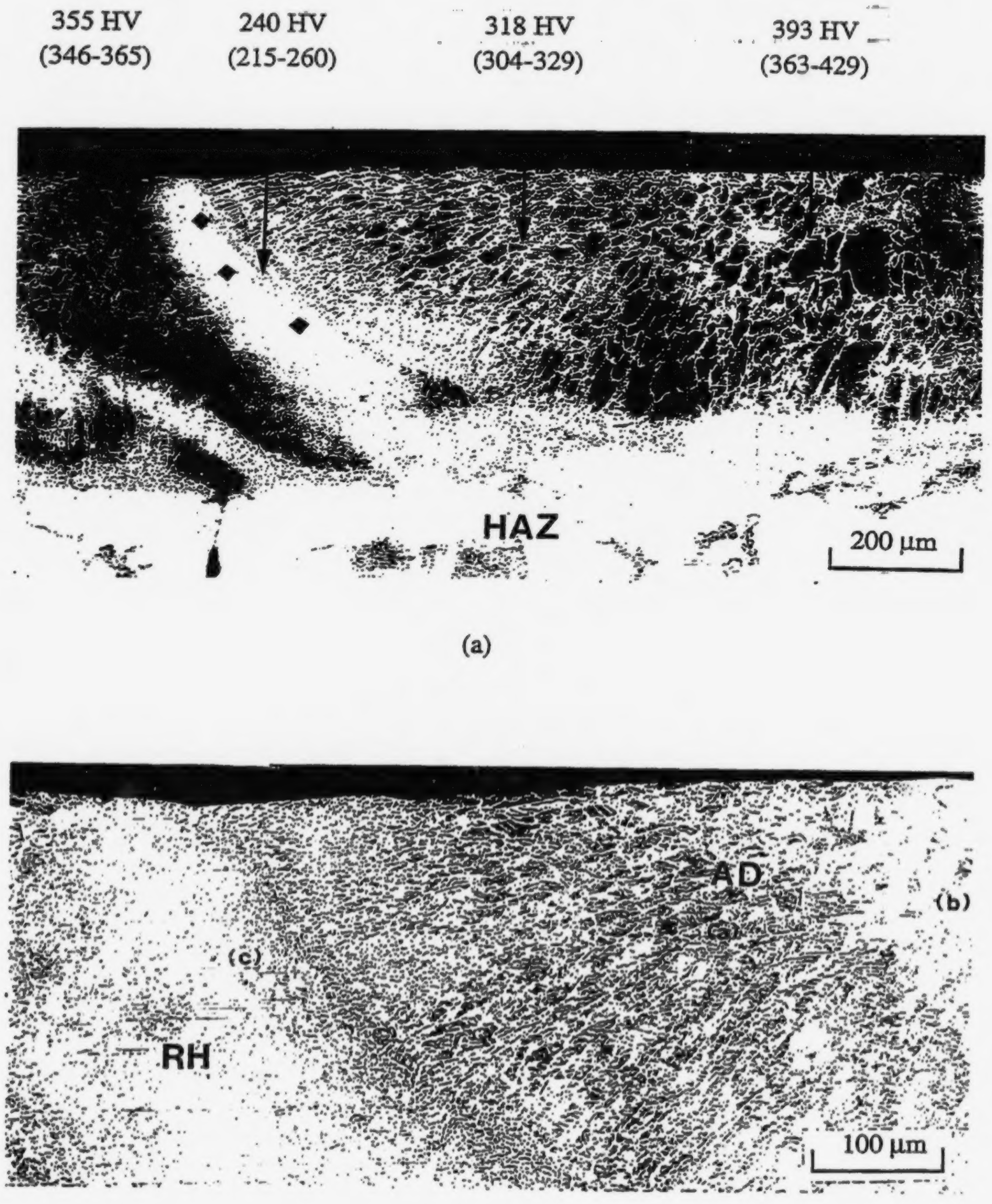
355 HV
(346-365)
240 HV
(215-260)
318 HV
(304-329)
393 HV
(363-429)
HAZ
200 µm
AD
(b)
(a)
(c)
RH
100 µm

(a)

(b)

Fig. 9. Overview of laser-clad NAB weldment. Shown are the as-deposited (AD), reheated (RH) and base metal heat-affected zone (HAZ) regions. Higher magnification micrographs of locations (a), (b) and (c) are shown in Fig. 10(a), (b) and (c), respectively.

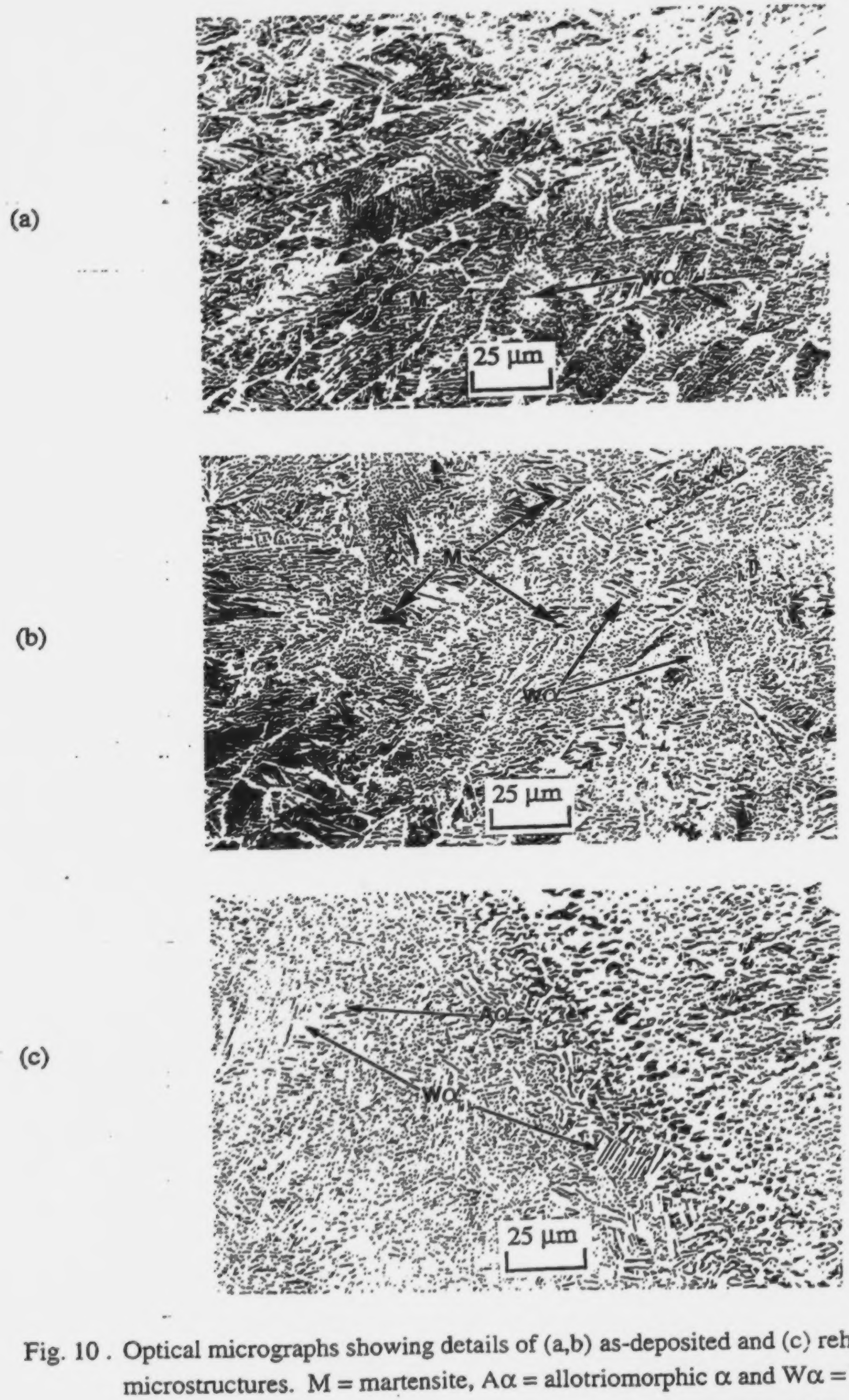
(a)
Aα
Wα
M
25 µm
(b)
M
Wα
25 µm
(c)
Aα
Wα
25 µm

Fig. 10 . Optical micrographs showing details of (a,b) as-deposited and (c) reheated weld metal microstructures. M = martensite, Aα = allotriomorphic α and Wα = Widmanstätten α.

EFFECT OF REHEATING THE LASER CLAD WELDMENT

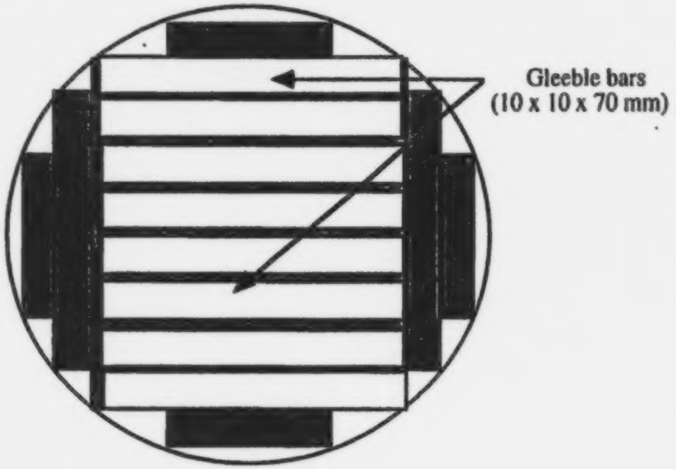
Gleeble bars
(10 x 10 x 70 mm)

(a) Location and orientation of Gleeble bars extracted from laser weld clad NAB.

(b) Gleeble bar with laser weld cladding on top surface.

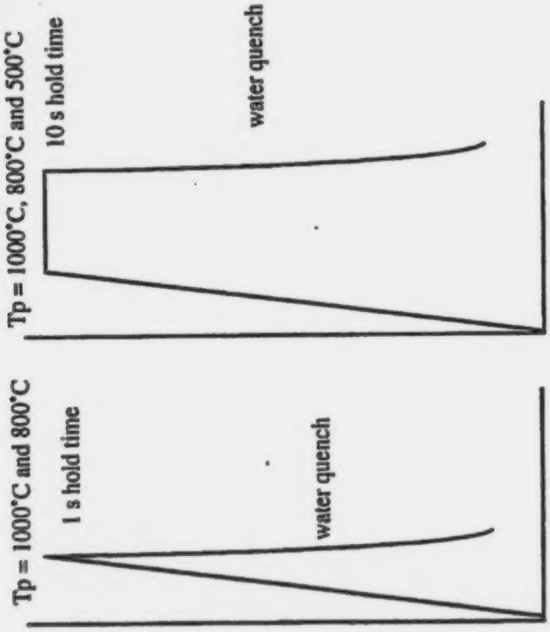
Tp = 1000°C and 800°C
1 s hold time
water quench
Tp = 1000°C, 800°C and 500°C
10 s hold time
water quench

Microhardness, HV100g		
Laser Weld Samples	As-deposited Region	Reheated Region
As-received (overall)	361 (304-429)	298 (215-365)
Dark Regions (martensite)	393 (363-429)	355 (346-365)
Light Regions (Widmanstätten α)	318 (304-329)	240 (215-260)
Tp=500 - 10s hold + WQ	333 (311-365)	281 (252-300)
Tp=800 - 1s hold + WQ	259 (252-269)	262 (240-276)
Tp=800 - 10s hold + WQ	261 (250-268)	233 (220-245)
Tp=1000 - 1s hold + WQ	214 (203-230)	210 (200-220)
Tp=1000 - 10s hold + WQ	242 (215-266)	221 (212-230)

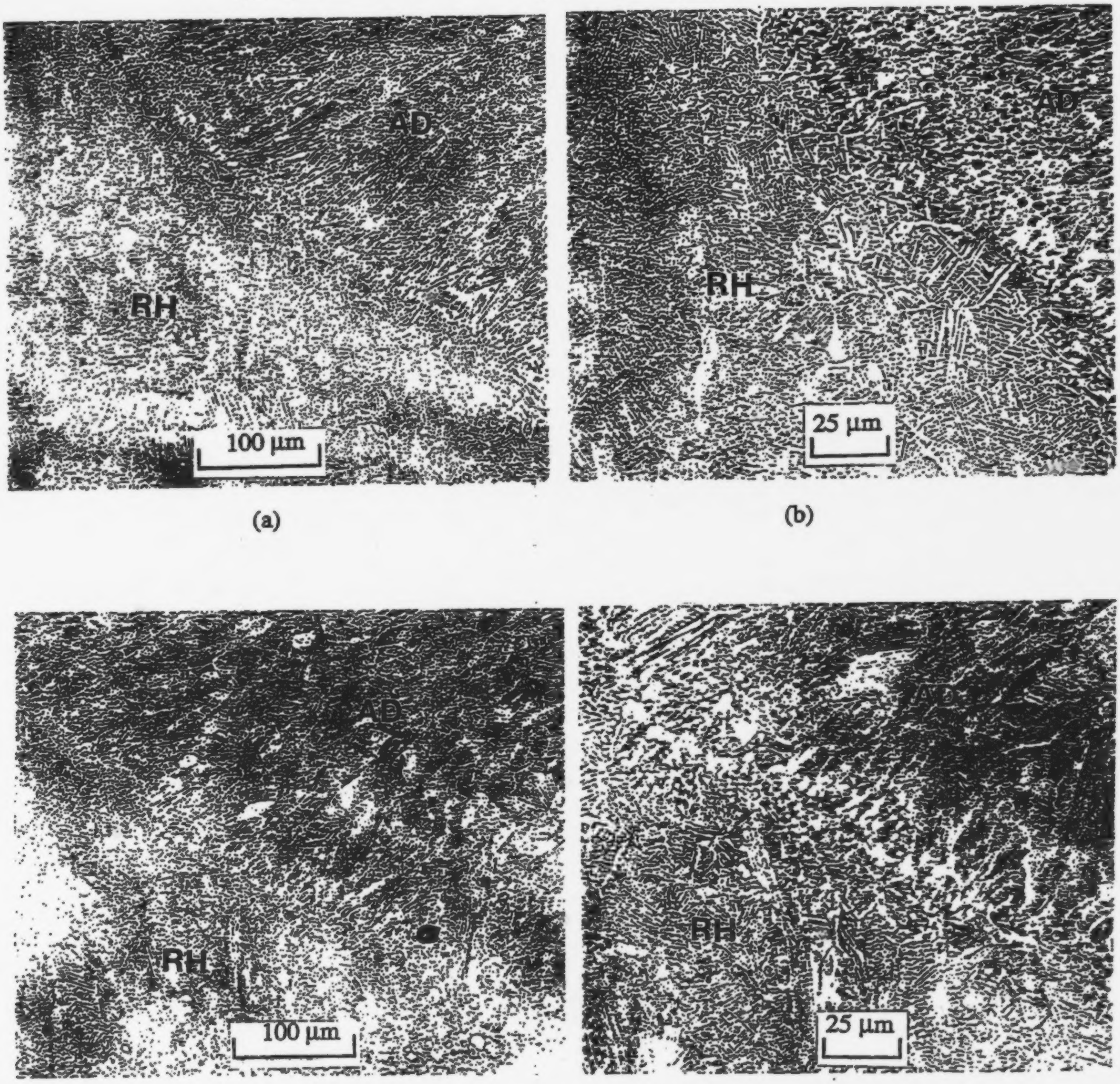
AD
RH
100 µm
AD
RH
25 µm
AD
RH
100 µm
AD
RH
25 µm

(a) (b)

(c) (d)

Fig. 11. Optical micrographs of laser clad weld metal reheated to Tp =800°C ($\Delta t_{800-500}$ = 0.7 - 0.8 s) with (a,b) hold time = 1 s and (c, d) hold time = 10 s.

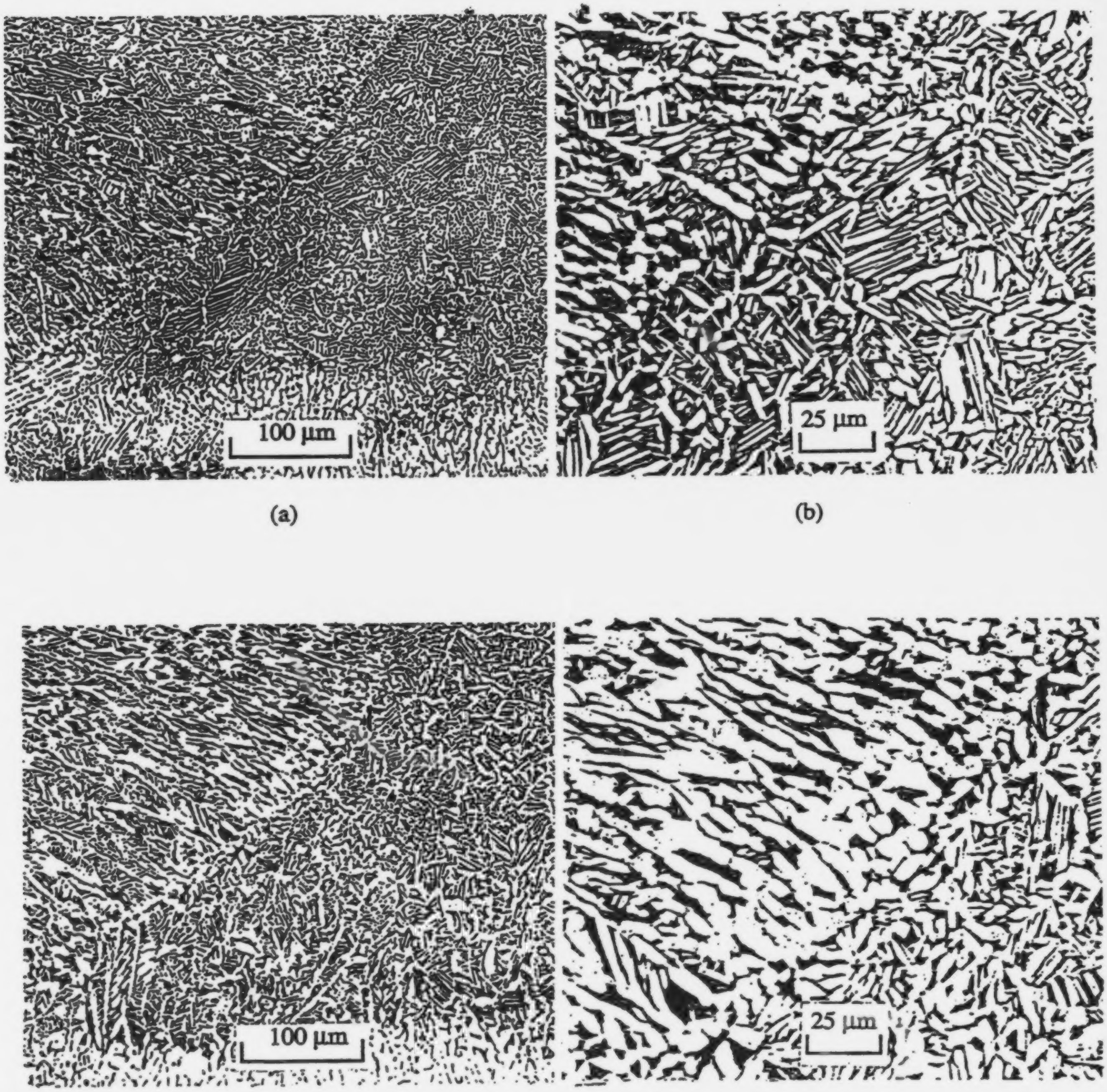
100 µm
25 µm
100 µm
25 µm

(a) (b)

(c) (d)

Fig. 12. Optical micrographs of laser clad weld metal reheated to Tp = 1000°C ($\Delta t_{800-500}$ = 0.5 - 0.6 s) with (a,b) hold time =1 s and (c, d) hold time = 10 s.

Microhardness, HV100g		
Conditions for reheating laser clad base metal.	Base Metal HAZ Region Overall	Individual Phases (avg.)
Base Metal – As-received	170 (141-207)	$\alpha = 142$ $\alpha + \kappa = 198$
Tp=500 - 10s hold + WQ	161 (145-188)	$\alpha = 155$ $\alpha + \kappa = 171$
Tp=800 - 1s hold + WQ	192 (140-300)	$\alpha = 146$ $\alpha + \kappa = 201$ M = 300 (high)
Tp=800 - 10s hold + WQ	208 (138-323)	$\alpha = 149$ $\alpha + \kappa = 222$ M = 323 (high)
Tp=1000 - 1s hold + WQ	259 (113-394)	$\alpha = 143$ M = 394 (high)
Tp=1000 - 10s hold + WQ	276 (147-415)	$\alpha = 161$ M = 415 (high)

Note: M refers to martensite

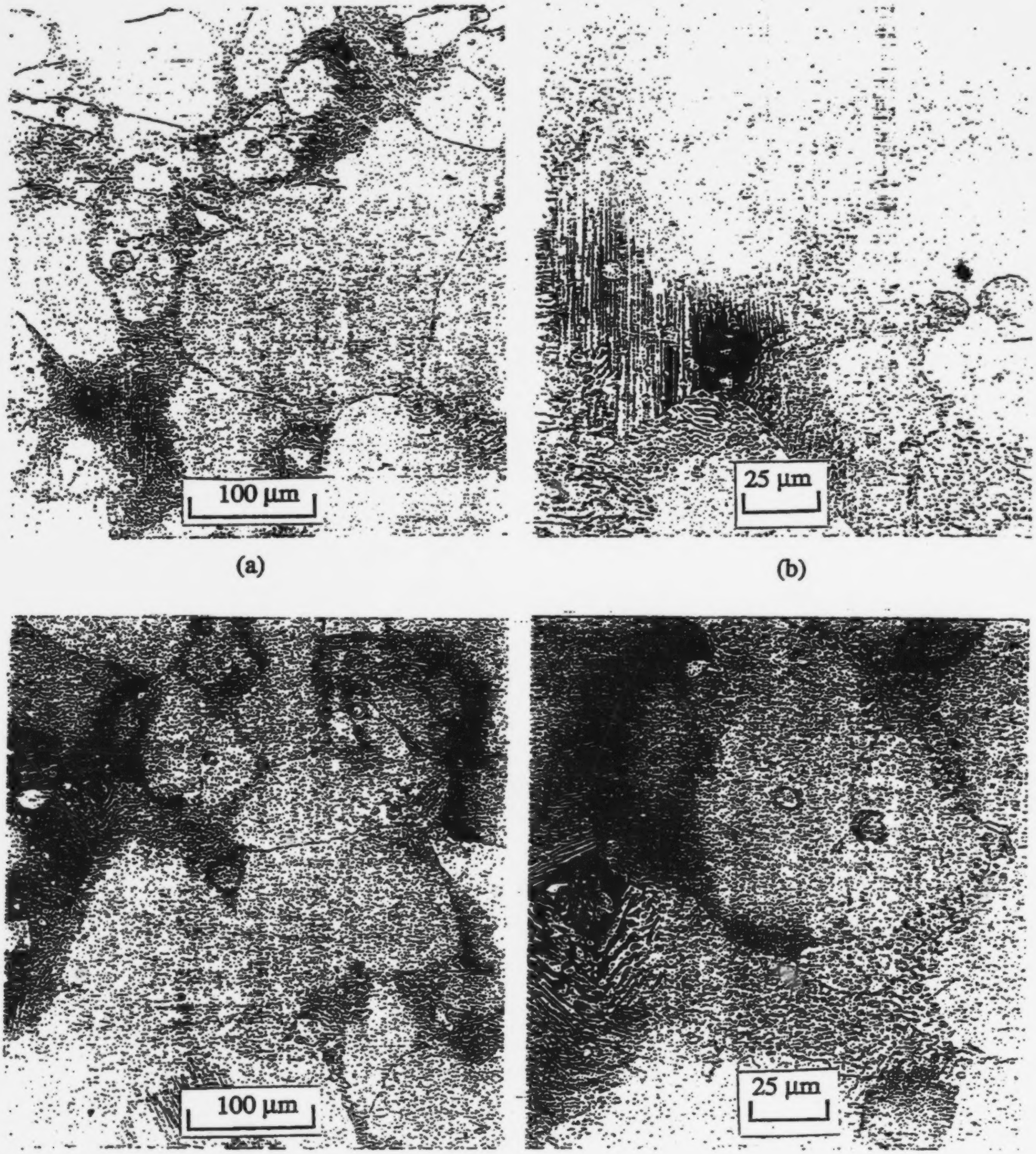
100 µm
25 µm
100 µm
25 µm

(a) (b)

(c) (d)

Fig. 13. Optical micrographs of laser clad base metal reheated to Tp =800°C ($\Delta t_{800-500}$ = 0.7 - 0.8 s) with (a,b) hold time =1 s and (c, d) hold time = 10 s.

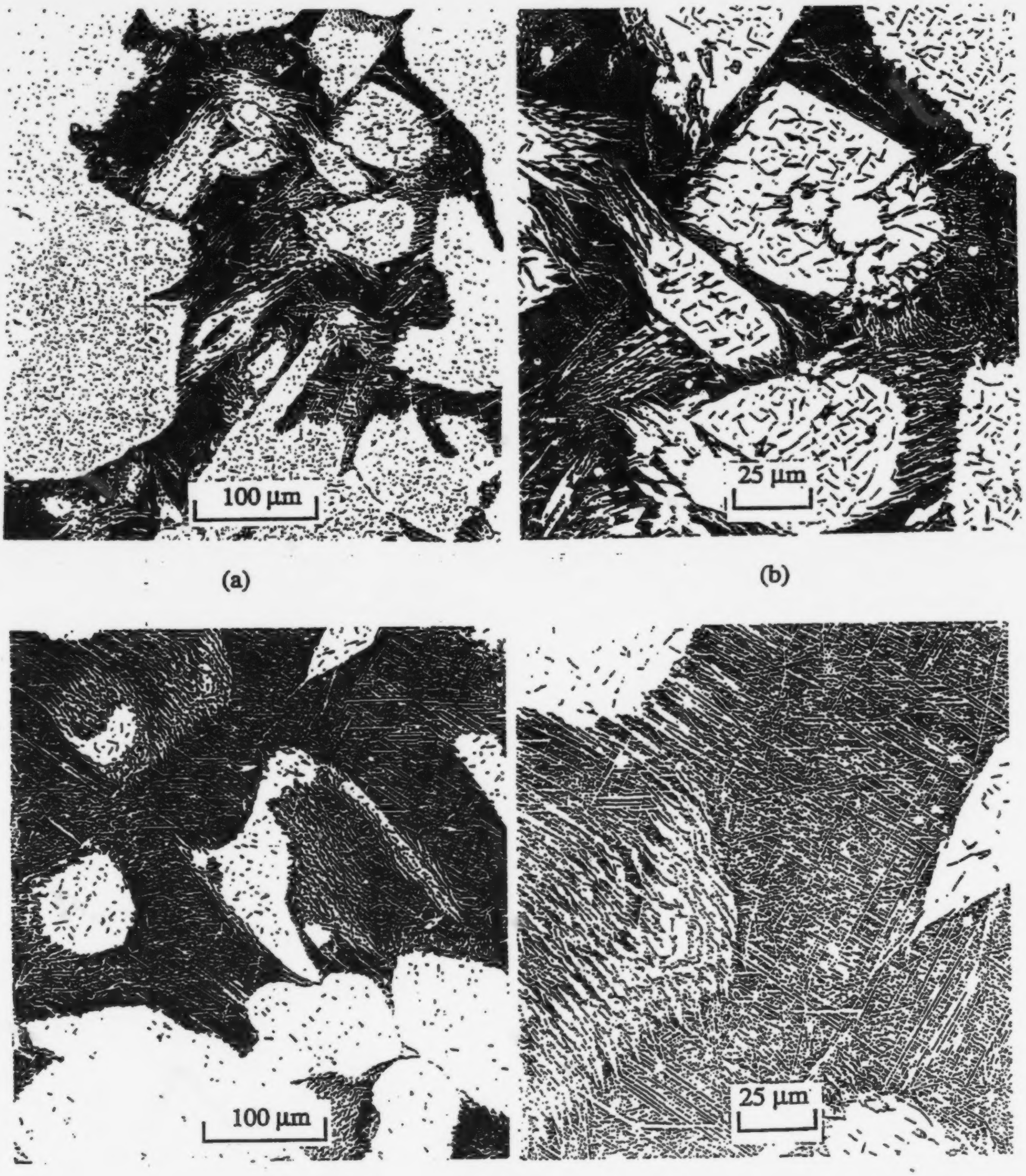
100 µm
25 µm
100 µm
25 µm

(a) (b)

(c) (d)

Fig. 14. Optical micrographs of laser clad base metal reheated to Tp = 1000°C ($\Delta t_{800-500}$ = 0.5 - 0.6 s) with (a,b) hold time = 1 s and (c, d) hold time = 10 s.

EVALUATION OF SIMULATION TECHNIQUES

GTA Bead-on Plate Welds

GLEEBLE SIMULATION TECHNIQUES

Simulated Heat-Affected Zone Regions

Simulated Weld Metal Regions

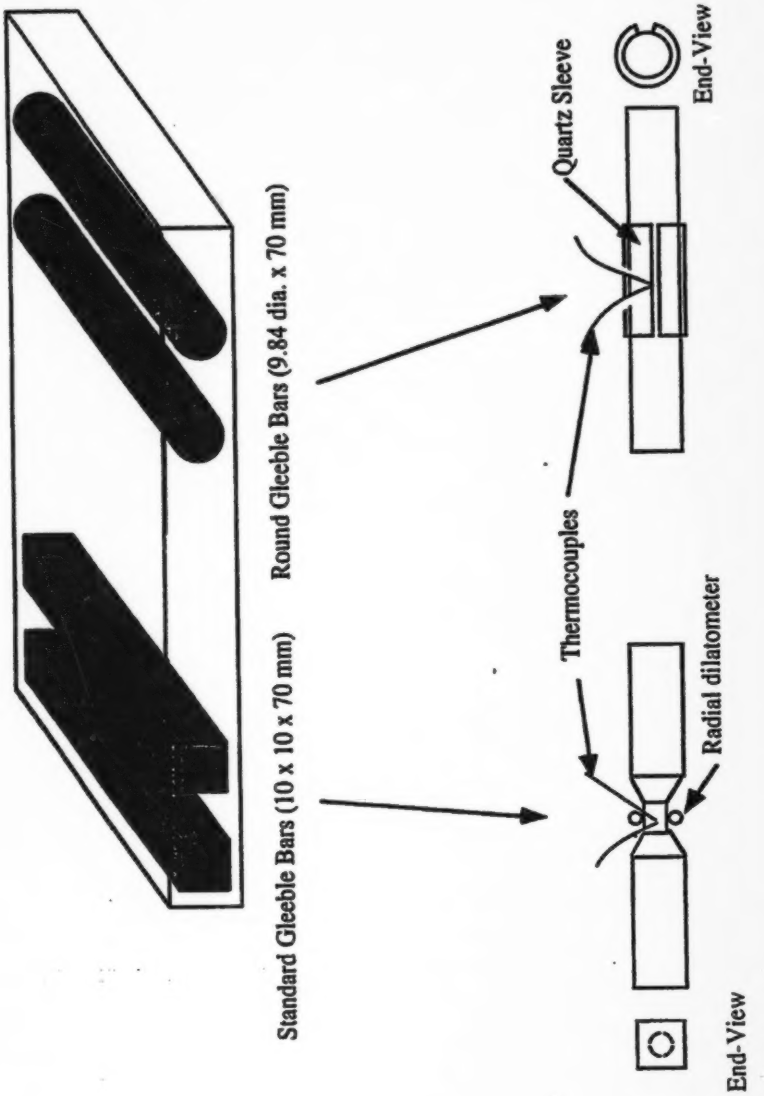
Standard Gleeble Bars (10 x 10 x 70 mm)
Round Gleeble Bars (9.84 dia. x 70 mm)
End-View
Thermocouples
Radial dilatometer
Quartz Sleeve
End-View

(a) Radial dilatometer bar.

(b) Round melt specimen.

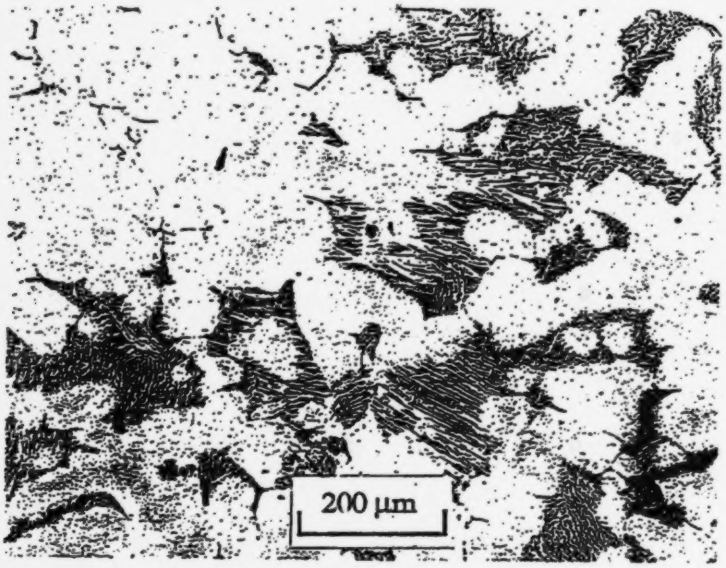

(a) Tp = 1018°C - air cooled

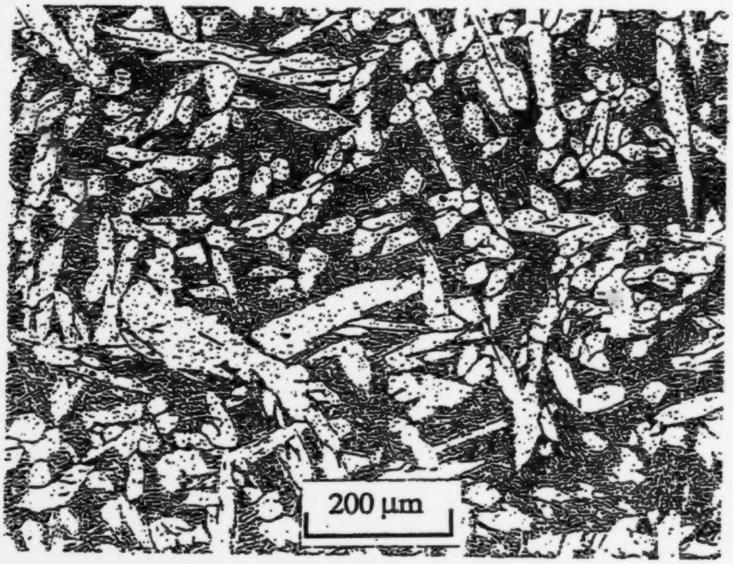

(b) Tp = 1030°C - air cooled

Fig. 17. Microstructures of Gleeble simulated HAZ region in (a) 8.0 % Al and (b) 9.2% Al NAB alloy.

Thermal Cycle Condition	Microhardness, HV100g	
	Overall Average (range)	Individual Phases Average (range)
Tp=1030°C $\Delta t_{800-500}$=1 s	253 (151-394)	α = 160 (151-178) $\alpha + \kappa$ = 345 (289-394)
Tp=1030°C $\Delta t_{800-500}$=11 s	247 (158-326)	α = 167 (158-172) $\alpha + \kappa$ = 310 (282-326)
Tp=1030°C $\Delta t_{800-500}$=31 s	207 (123-321)	α = 143 (123-155) $\alpha + \kappa$ = 271 (233-321)
Tp=1030°C Slow Heat Hold 10 s $\Delta t_{800-500}$=1 s	254 (150-337)	α = 189 (150-226) $\alpha + \kappa$ = 320 (304-337)

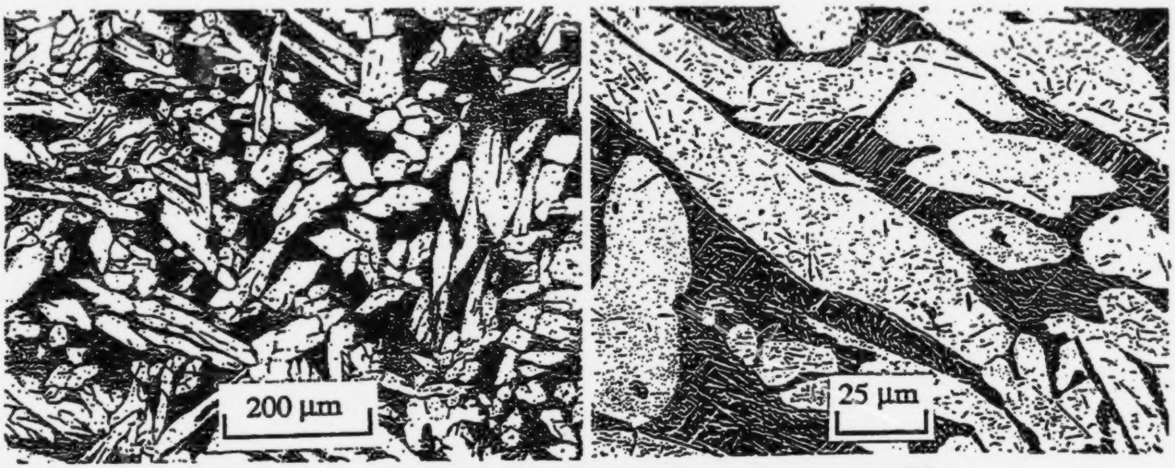

(a) Tp =1033°C- hold 1 s, $\Delta t_{800\text{-}500} = 1$ s (b)

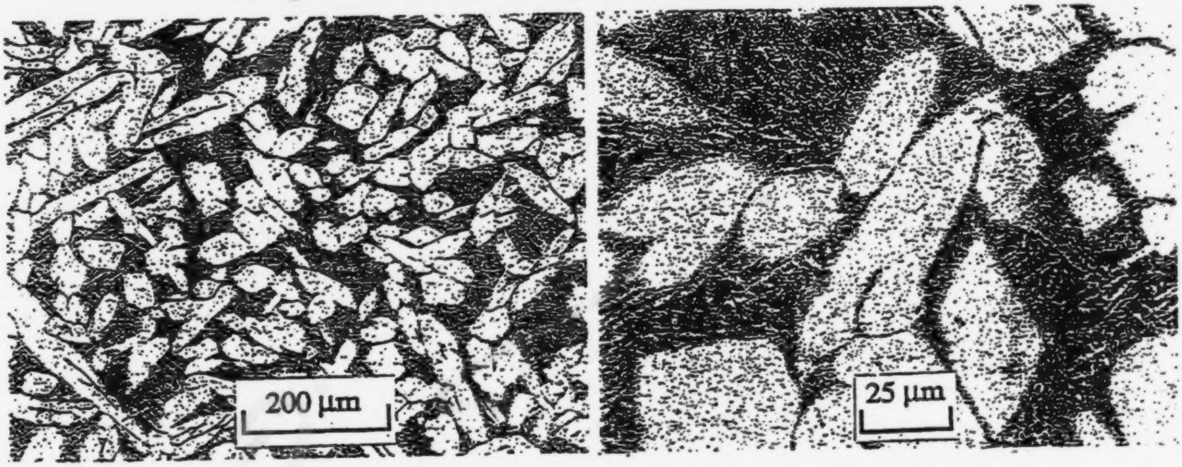

(c) Tp =1033°C- hold 1 s, $\Delta t_{800\text{-}500} = 31$ s (d)

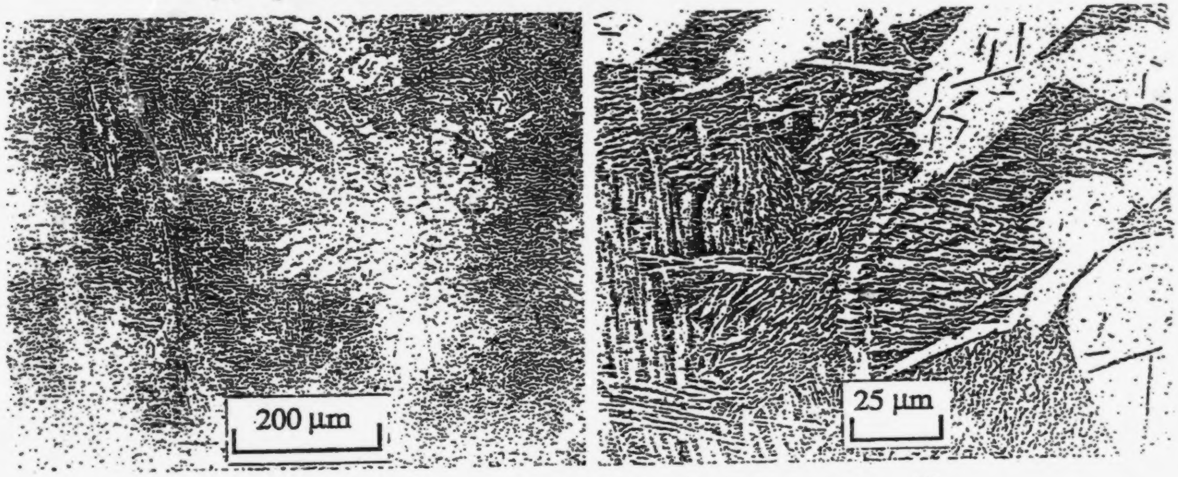

(e) Tp =1030°C- slow heat + hold 10 s, $\Delta t_{800\text{-}500} = 1$ s (f)

Fig. 18. Microstructures formed in the 9.2% Al NAB and showing the effect of (a-d) cooling time and (e,f) hold time.

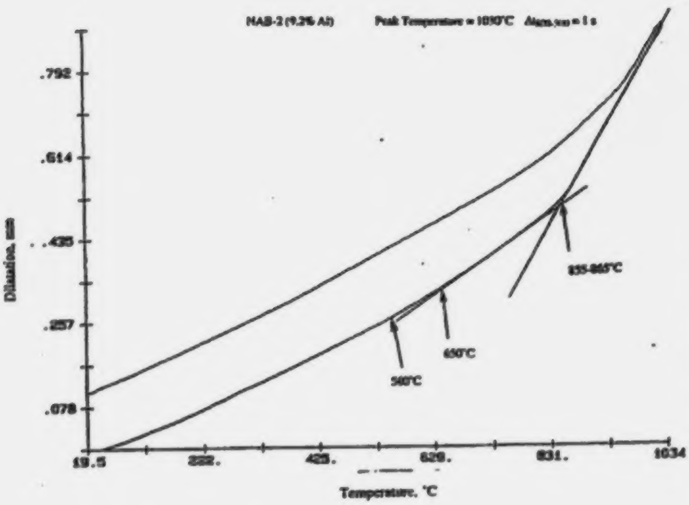

(a) Tp =1033°C- hold 1 s, $\Delta t_{800\text{-}500}$ = 1 s

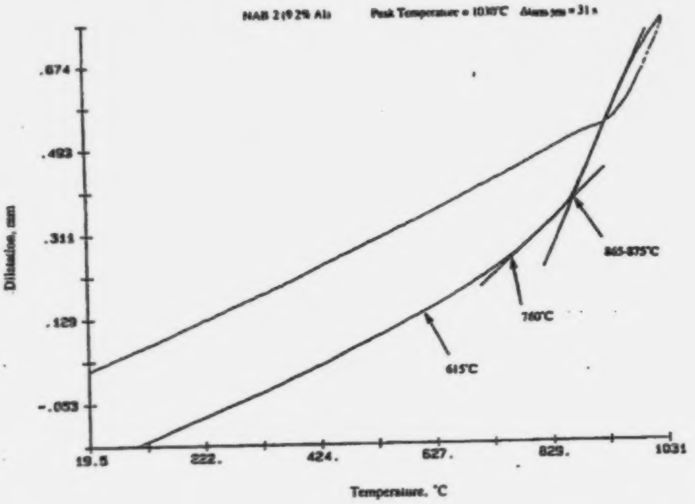

(b) Tp =1033°C- hold 1 s, $\Delta t_{800\text{-}500}$ = 31 s

Fig. 19. Dilatometric curves for simulated HAZ structures (9.2% Al) shown in Fig. 18 (a, b) and (c, d).

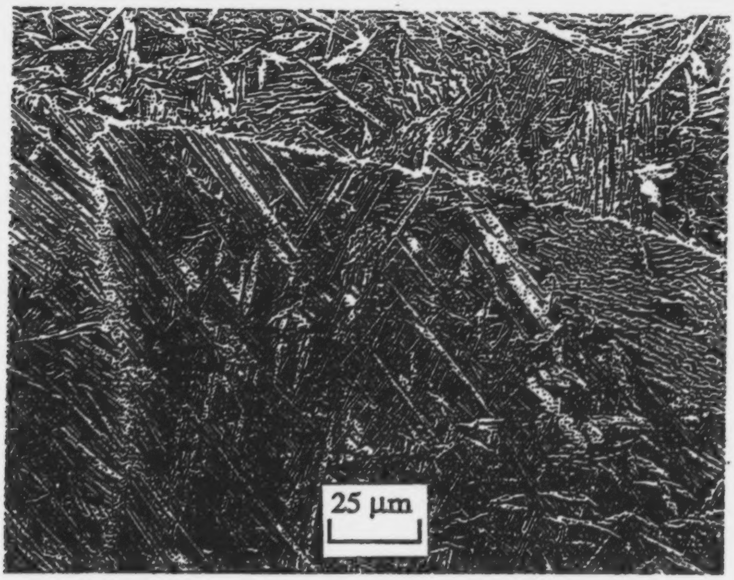

(a)

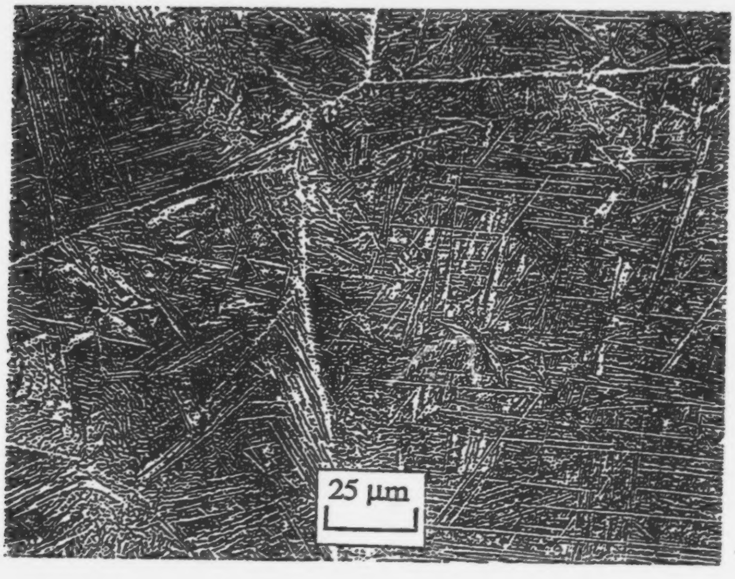

(b)

Fig. 21. Microstructures of 9.2% Al alloy cycled to (a) Tp = 1040°C and (b) Tp = 1064°C followed by water quenching ($\Delta t_{800-500}$ = 0.4 s, cooling rate = 750°C/s).

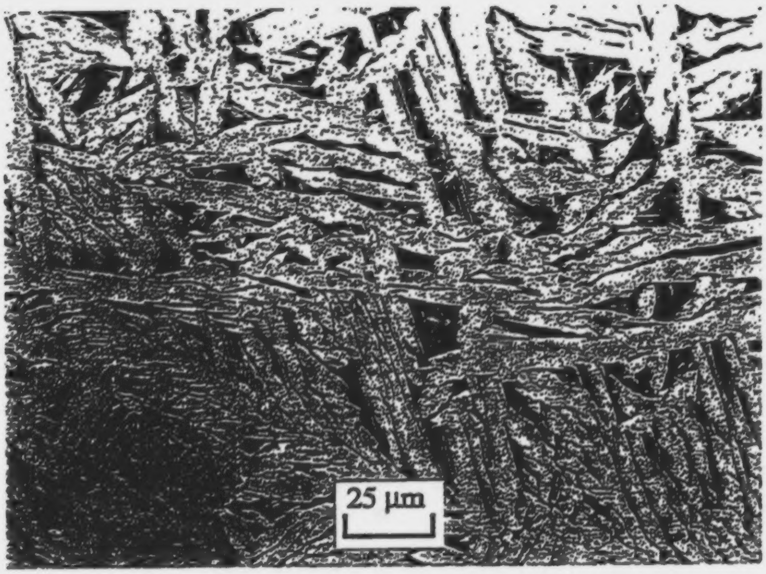

(a)

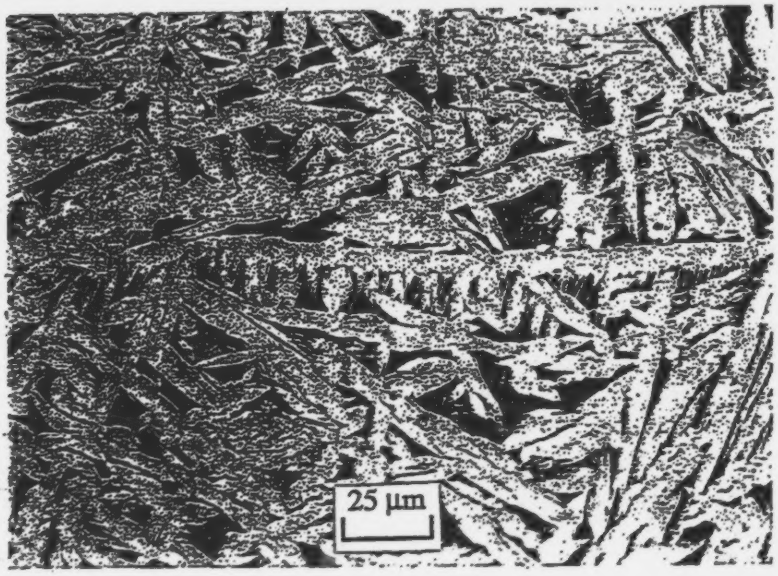

(b)

Fig. 22. Microstructures of 9.2% Al alloy cycled to (a) Tp = 1040°C followed by air quenching ($\Delta t_{800\text{-}500}$ = 1.6 s, cooling rate = 188°C/s) and (b) Tp = 1064°C followed air cooling ($\Delta t_{800\text{-}500}$ = 6.7 s, cooling rate = 45°C/s), respectively.

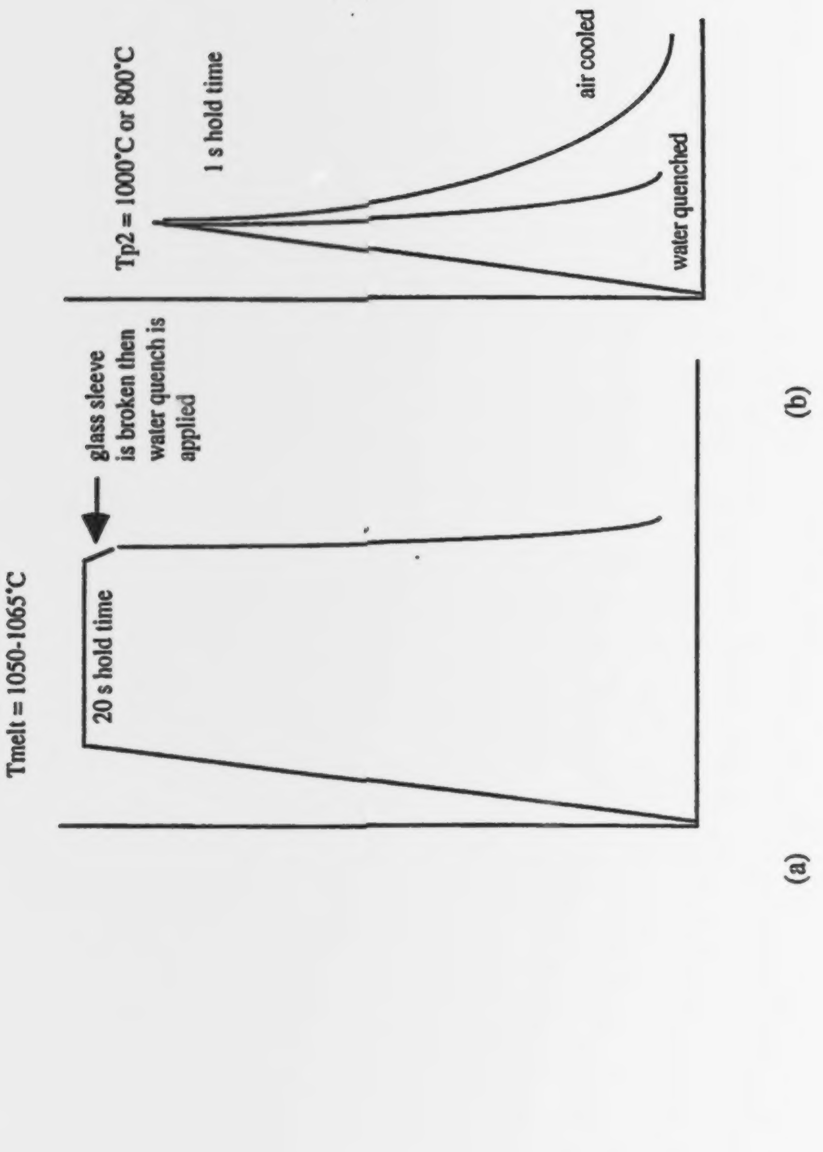
Tmelt = 1050-1065°C
20 s hold time
glass sleeve is broken then water quench is applied
(a)
Tp2 = 1000°C or 800°C
1 s hold time
air cooled
water quenched
(b)

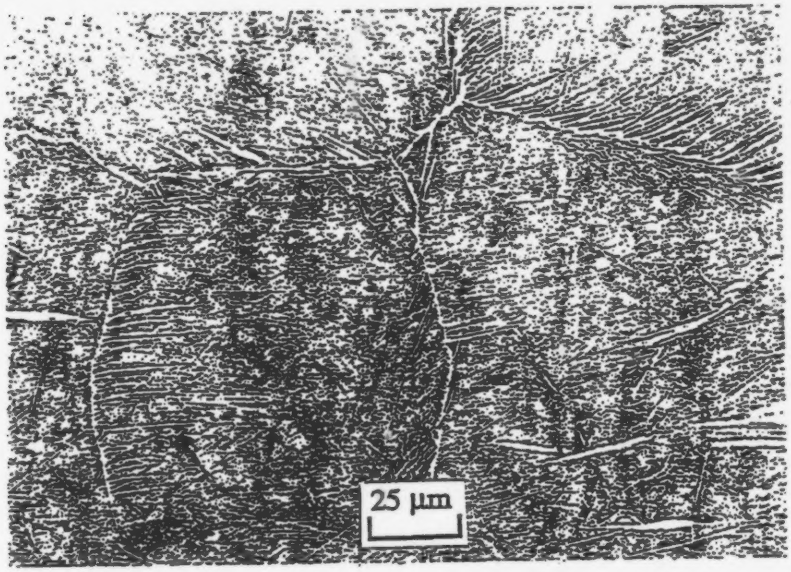

(a)

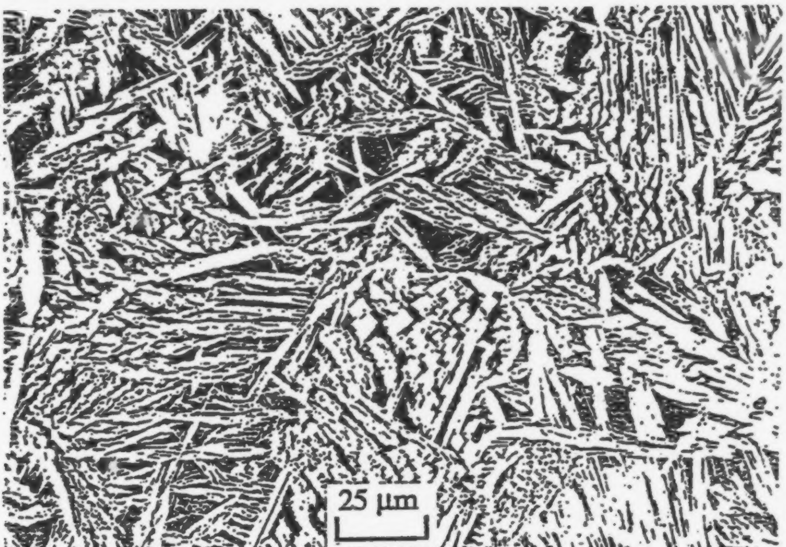

(b)

Fig. 24. Microstructures of samples cycled to $Tp_1 = \sim 1050°C$ + WQ and then reheated to $Tp_2 = 1000°C$ followed by (a) water quenching ($\Delta t_{800\text{-}500} = 0.1$ s) and (b) air cooling ($\Delta t_{800\text{-}500} = 1.6$ s).

SUMMARY AND CONCLUSIONS

The results from this study clearly demonstrate that gleeble simulation can be used to gain a better understanding of the transformation behaviour of both the heat-affected zone and weld metal regions formed in NAB weldments.

#510347 ④

Evaluation of Fracture Toughness of High Strength Steels from Stretch Zones

by M. Nabil Bassim*, Jason V. Smith* and J.R. Matthews**

*Department of Mechanical and Industrial Engineering
University of Manitoba
Winnipeg, Manitoba R3T 5V6
** Defence Research Establishment Atlantic, Dockyard Laboratory
FMO Halifax, Halifax, Nova Scotia, Canada, B3K 2X0

ABSTRACT

High strength steels exhibit elastic-plastic fracture behavior at the crack tip even at low temperature and/or high strain rates. Characterization of their fracture toughness under these conditions by means of standardized J_{IC} tests is extremely difficult. This is particularly the case at very high strain rates such as those obtained using Split Hopkinson Bar devices. Alternatively, measurements of the stretch zone ahead of the crack on the fracture surface allows evaluation of the fracture toughness. It was found, however, that the stretch zone, which is indicative of the plasticity at the crack tip is affected by several factors such as the level of loading during fatigue precracking, the extent of strain hardening which occurs at the crack tip, the length of the crack and the corresponding a/w ratio and the occurrence of transverse and compressive strains ahead of the crack.

In this study, the effect of these factors of the measured stretch zone width and the corresponding J_{IC} is evaluated systematically. Factors examined are a/w values, $\Delta K_{fatigue}$, temperature and strains ahead of the crack. The results emphasize the importance of using stretch zone measurements for fracture toughness evaluation.

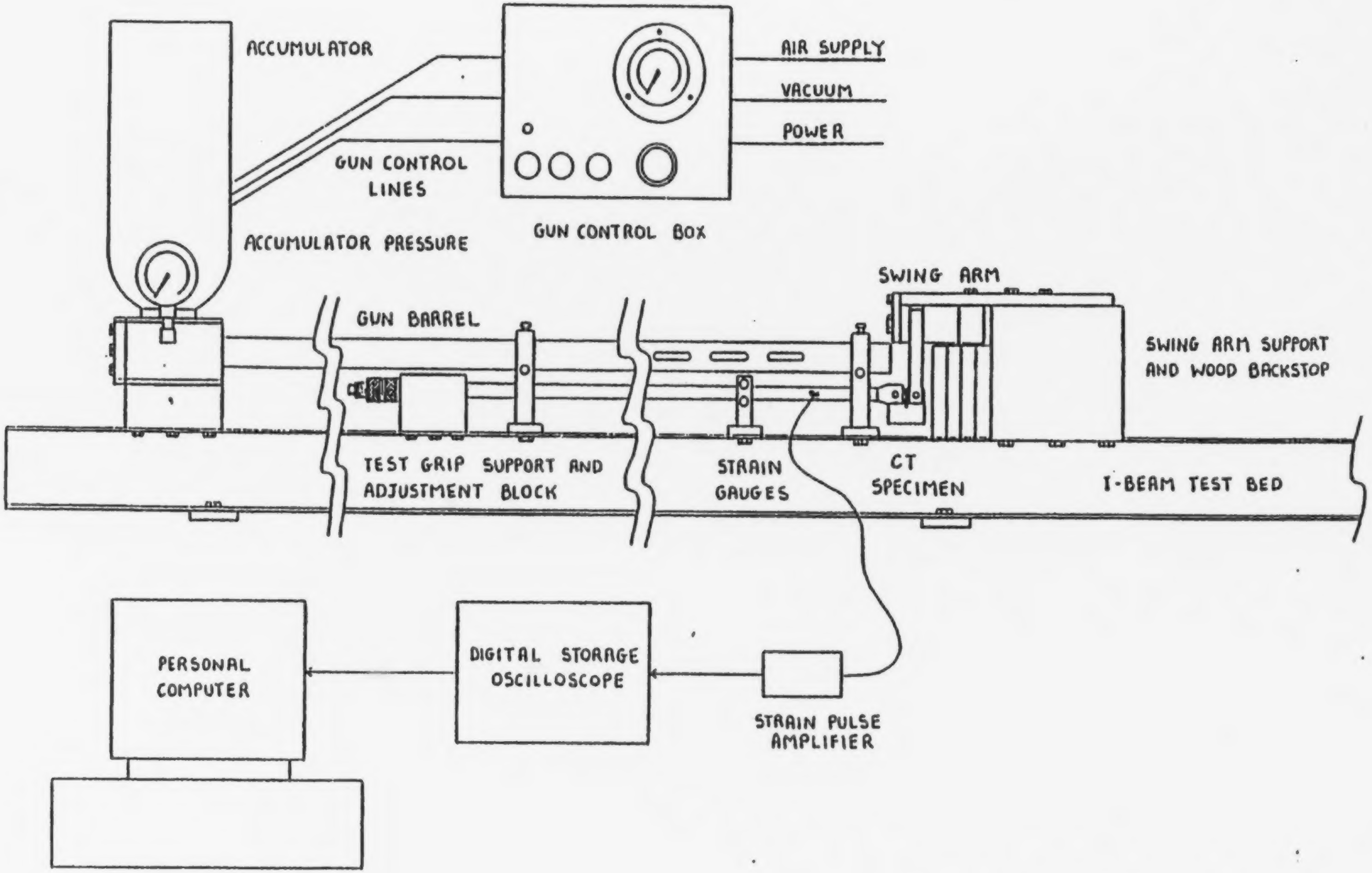
ACCUMULATOR
GUN CONTROL LINES
ACCUMULATOR PRESSURE
GUN CONTROL BOX
AIR SUPPLY
VACUUM
POWER
SWING ARM
GUN BARREL
SWING ARM SUPPORT AND WOOD BACKSTOP
TEST GRIP SUPPORT AND ADJUSTMENT BLOCK
STRAIN GAUGES
CT SPECIMEN
I-BEAM TEST BED
PERSONAL COMPUTER
DIGITAL STORAGE OSCILLOSCOPE
STRAIN PULSE AMPLIFIER

FIG. SPLIT HOPKINSON BAR ASSEMBLY FOR CT SPECIMEN TESTING

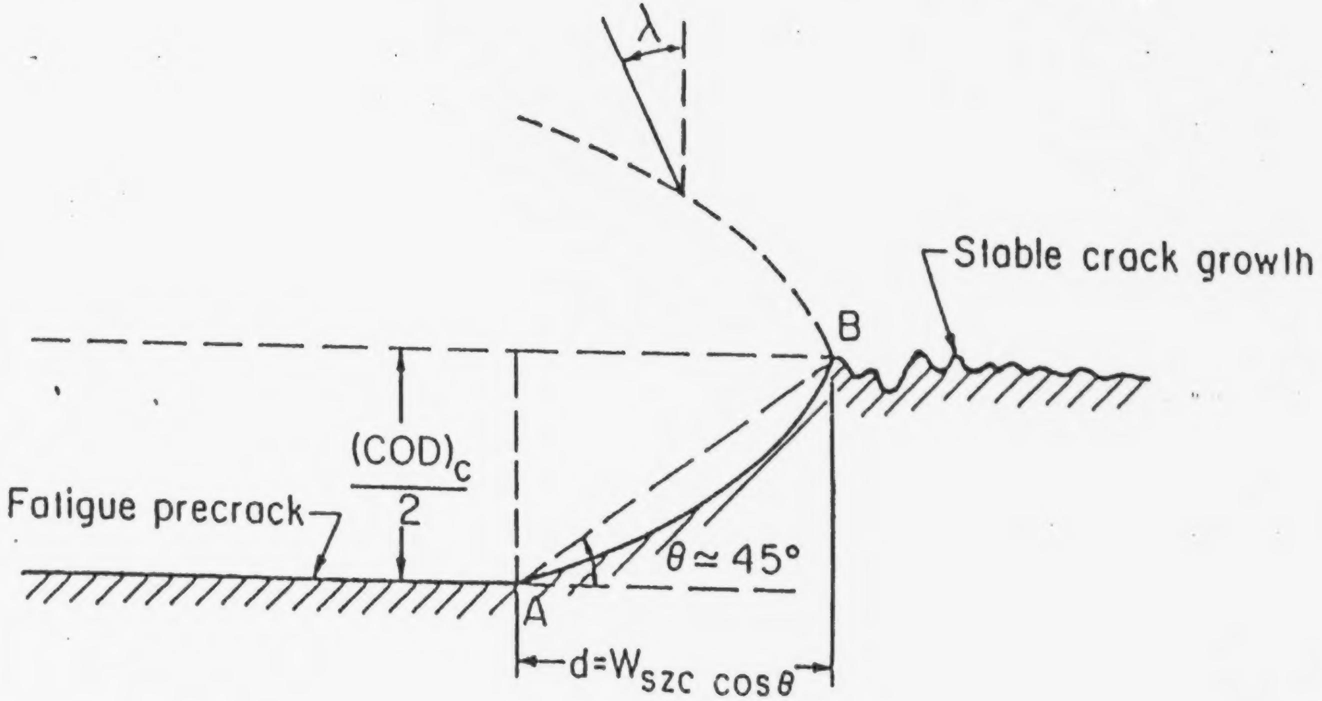
λ
Stable crack growth
B
(COD)c/2
Fatigue precrack
θ ≃ 45°
A
d=Wszc cosθ

FIG CONCEPT OF THE STRETCH ZONE ANALYSIS

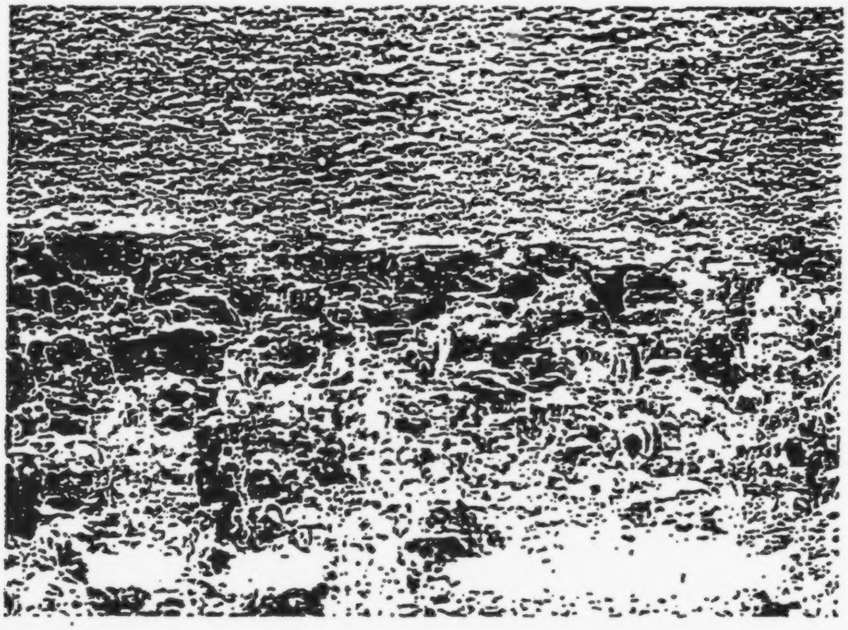

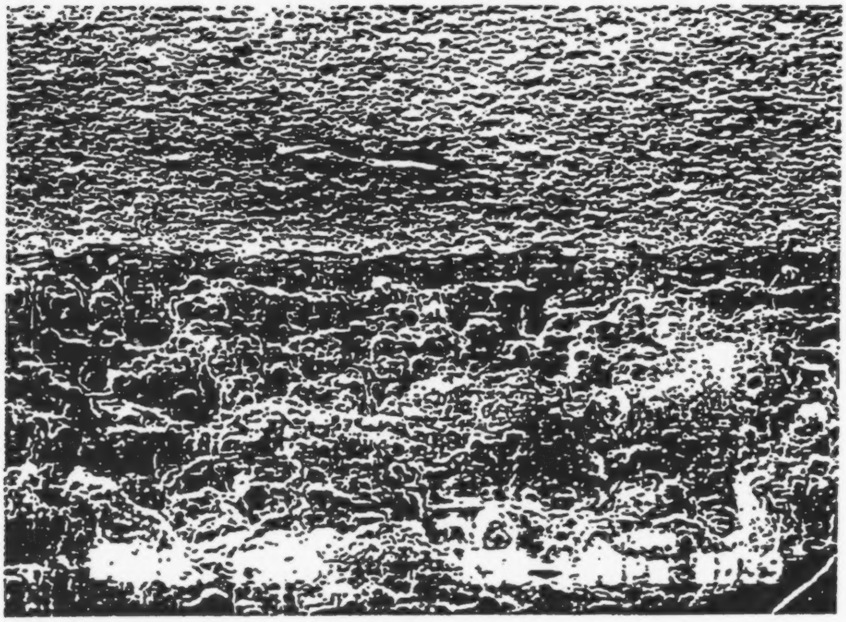

No.	Temp	Load Speed	Stretched Zone width 10^{-6} m									
	°C	m/S	1	2	3	4	5	6	7	8	9	Average
2	24	10^{-5}	100	200	142	186	88	100	140	136	100	132.4
3	24	10^{-3}	225	110	140	138	65	124	138	144	70	128.2
4	24	10^{-1}	176	180	166	174	140	110	128	110	132	145.7
7	24	19.5	190	216	180	168	150	148	190	240	144	180.7
1	24	26.7	208	580	352	200	392	134	225	260	200	258.4
6	24	32.0	185.7	190	300	325	282.5	356	162.5	154	222.2	242.3
11	-20	10^{-5}	140	89	149.3	149.3	105.5	128.9	185	81.4	155	131.5
8	-20	10^{-3}	178	178.5	128.9	138.7	83	157.1	154.7	67	70	128.2
9	-20	10^{-1}	136.5	130	96.7	178.5	105.5	149.3	224	58	118	132.9
14	-30	19.5	131.7	61	165.7	172.3	146.3	58	84	137.6	207.3	129.3
12	-30	26.7	127.8	97	95	118	134.1	154.7	162.9	129	117.9	126.3
13	-30	32.0	116	176.9	136.4	116	178.5	136.5	178.5	203.6	128.9	152.4

Table 1: Stretch zone measurements of HY100 Specimens Tested at Different Loading Rates and Temperatures.

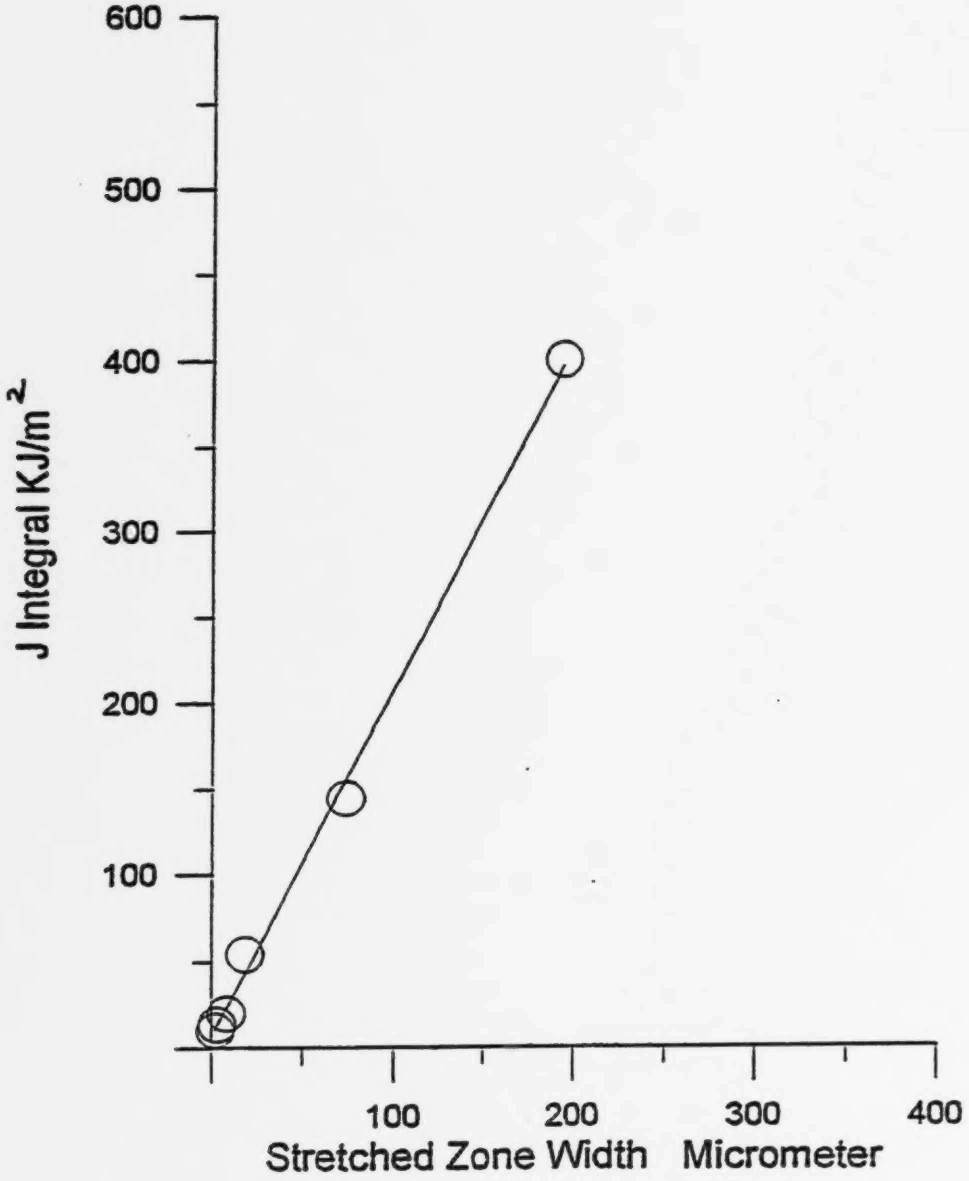

FIG. J-integral vs stretch zone for HY100 steel.

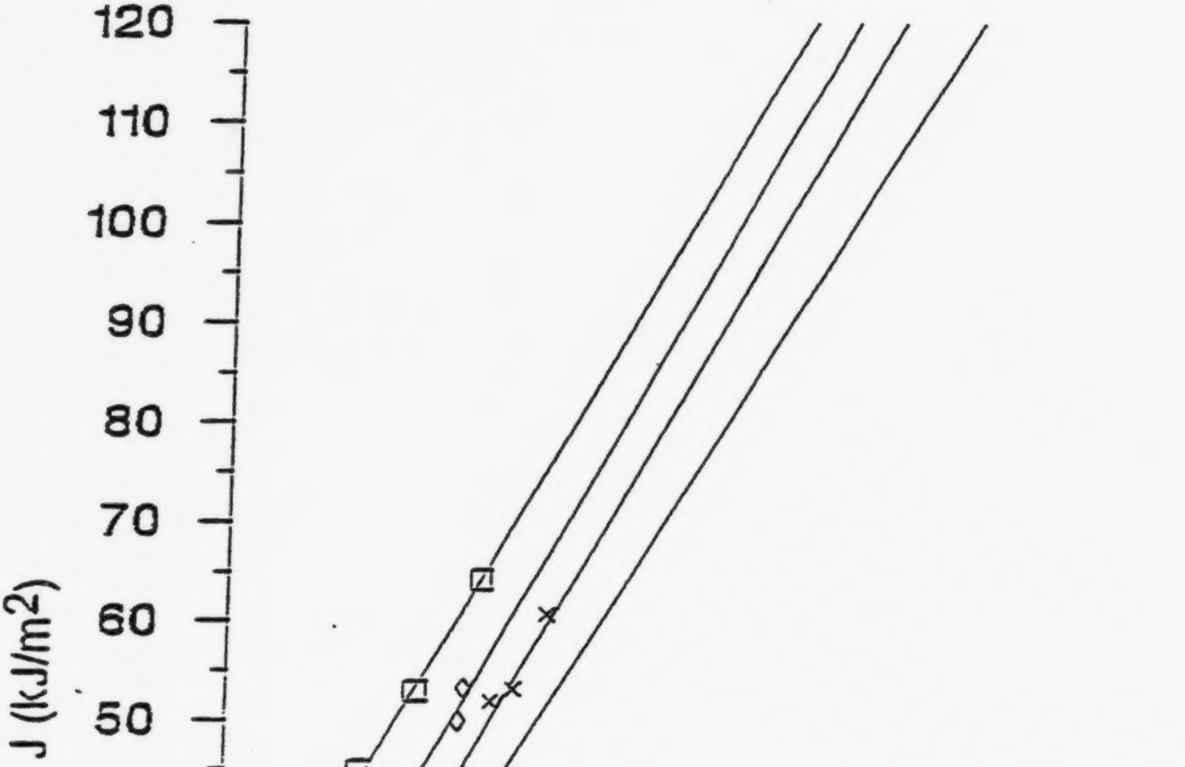

FIG. Effect of fatigue precracking on fracture toughness of 4340 steel.

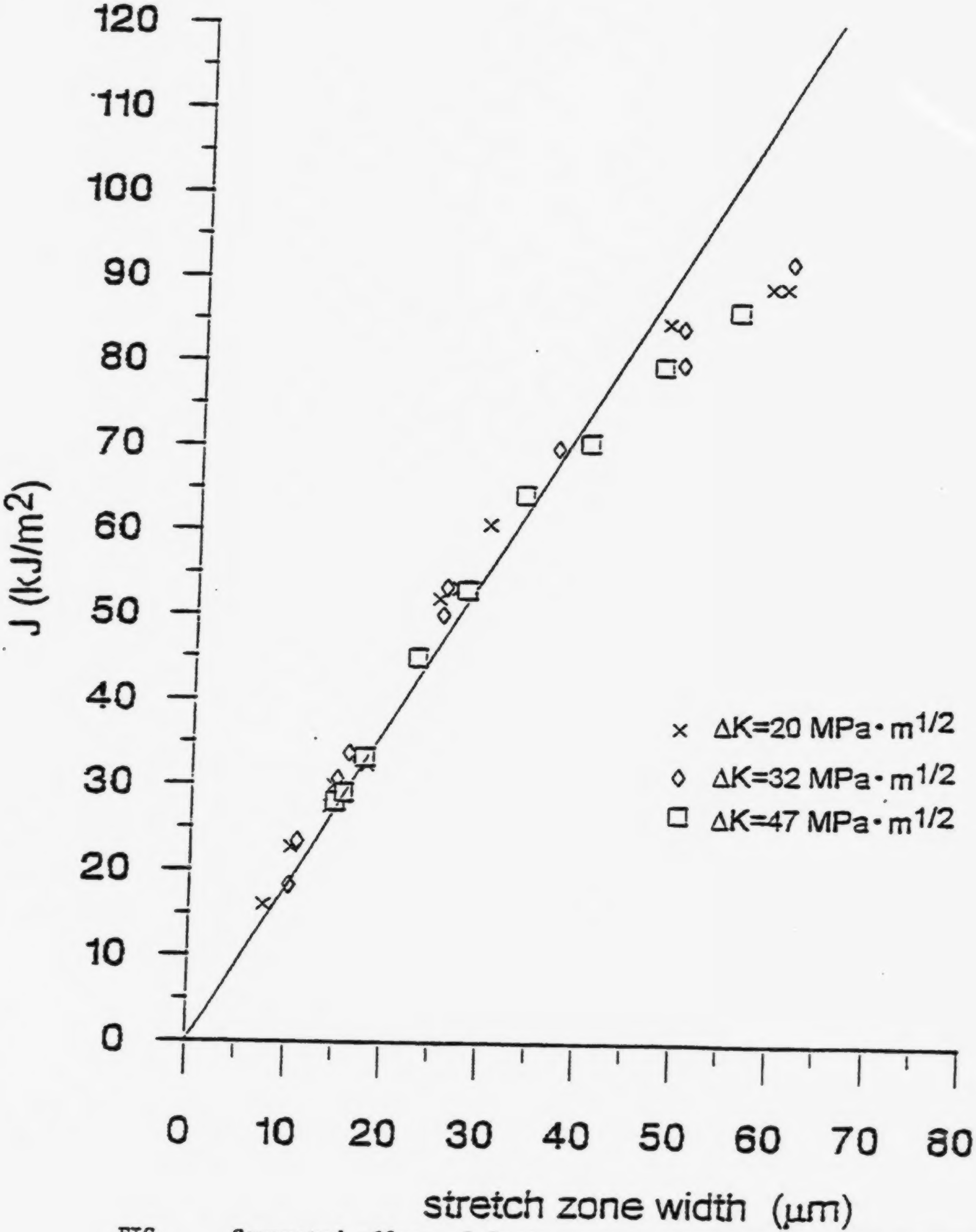

FIG. Corrected effect of fatigue precracking on fracture toughness.

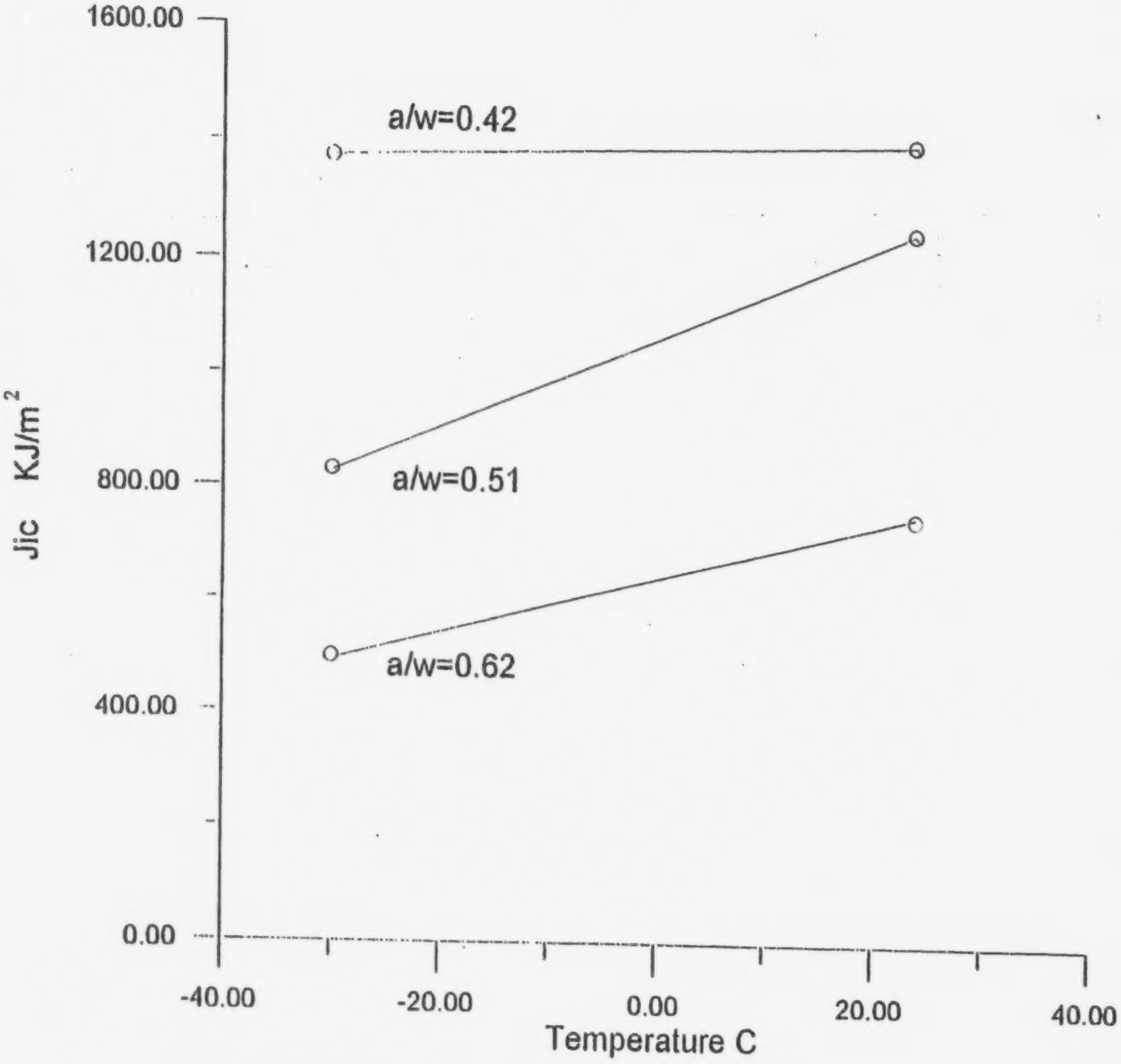

FIG. Effect of temperature and crack length on J-integral.

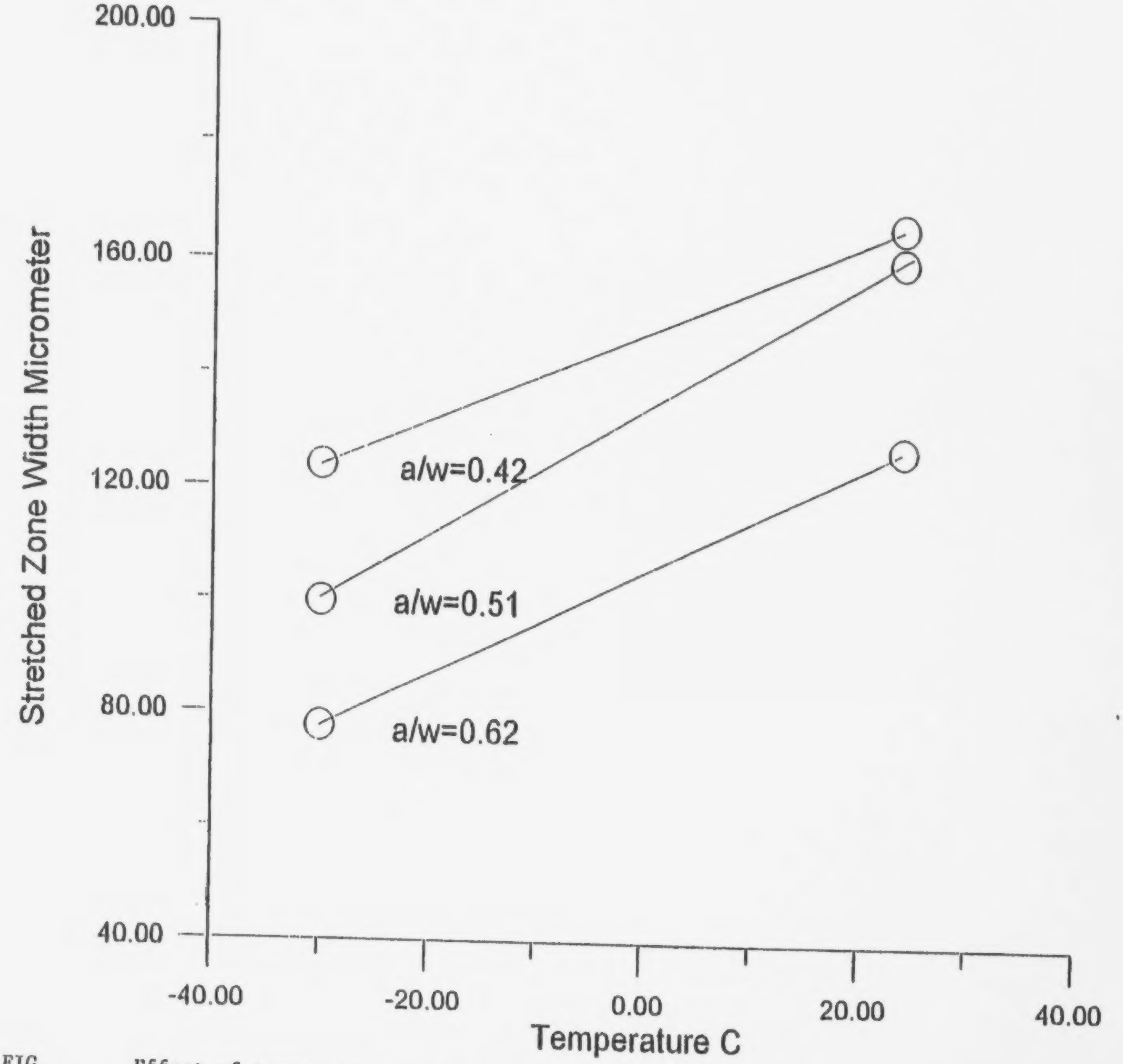

FIG. Effect of temperature and crack length

B = 12.7mm (0.5")
B_n = 10.7mm (0.4213")
a_0 = 17.70mm (0.7")
b_0 = 33.0mm (1.3")
W = 51mm (2")
$2H$ = 63.5mm (2.5")

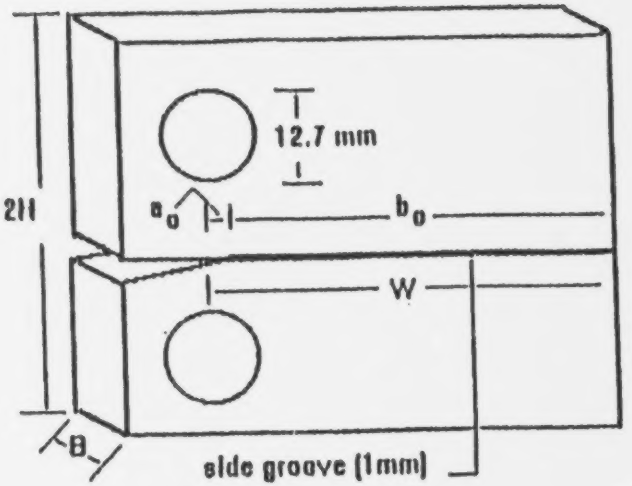
12.7 mm
2H
a0
b0
W
B
side groove (1mm)

FIG. Large CT specimen dimensions.

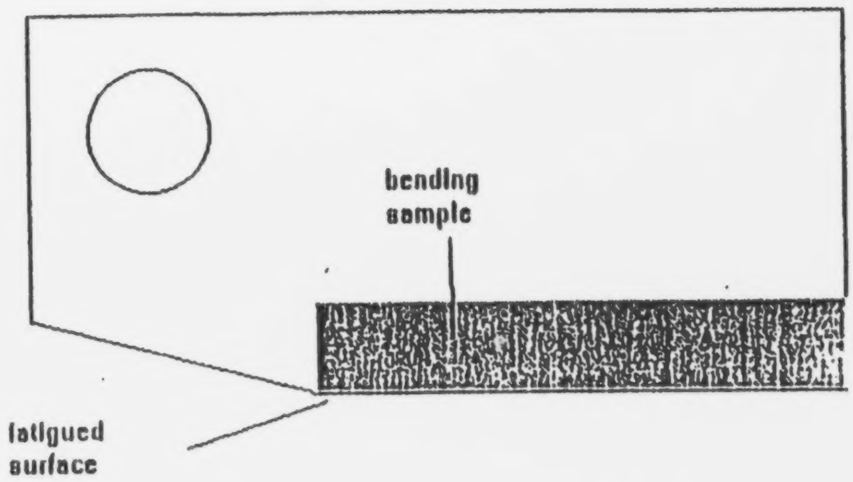
bending sample
fatigued surface

FIG. . Configuration of bending specimen from large CT specimen.

$L = 25.4\text{mm}\ (1.0")$
$H = 5.00\text{mm}\ (0.2")$
$D = 0.64\text{mm}\ (0.025")$
$B = 10.44\text{mm}\ (0.411")$
$L_0 = 36.93\text{mm}\ (1.455")$

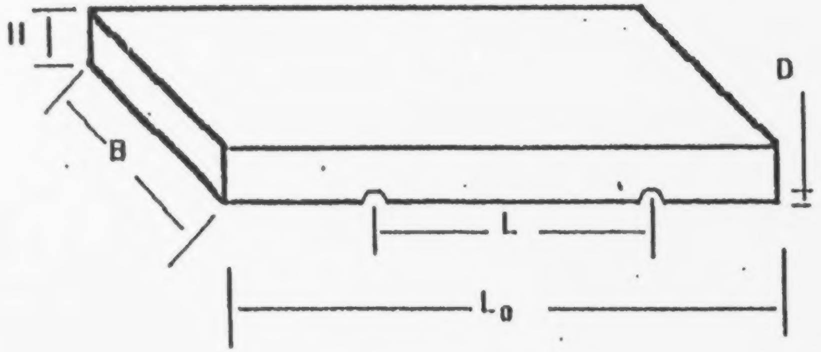

FIG. Dimensions of bending specimen used in strain measurements.

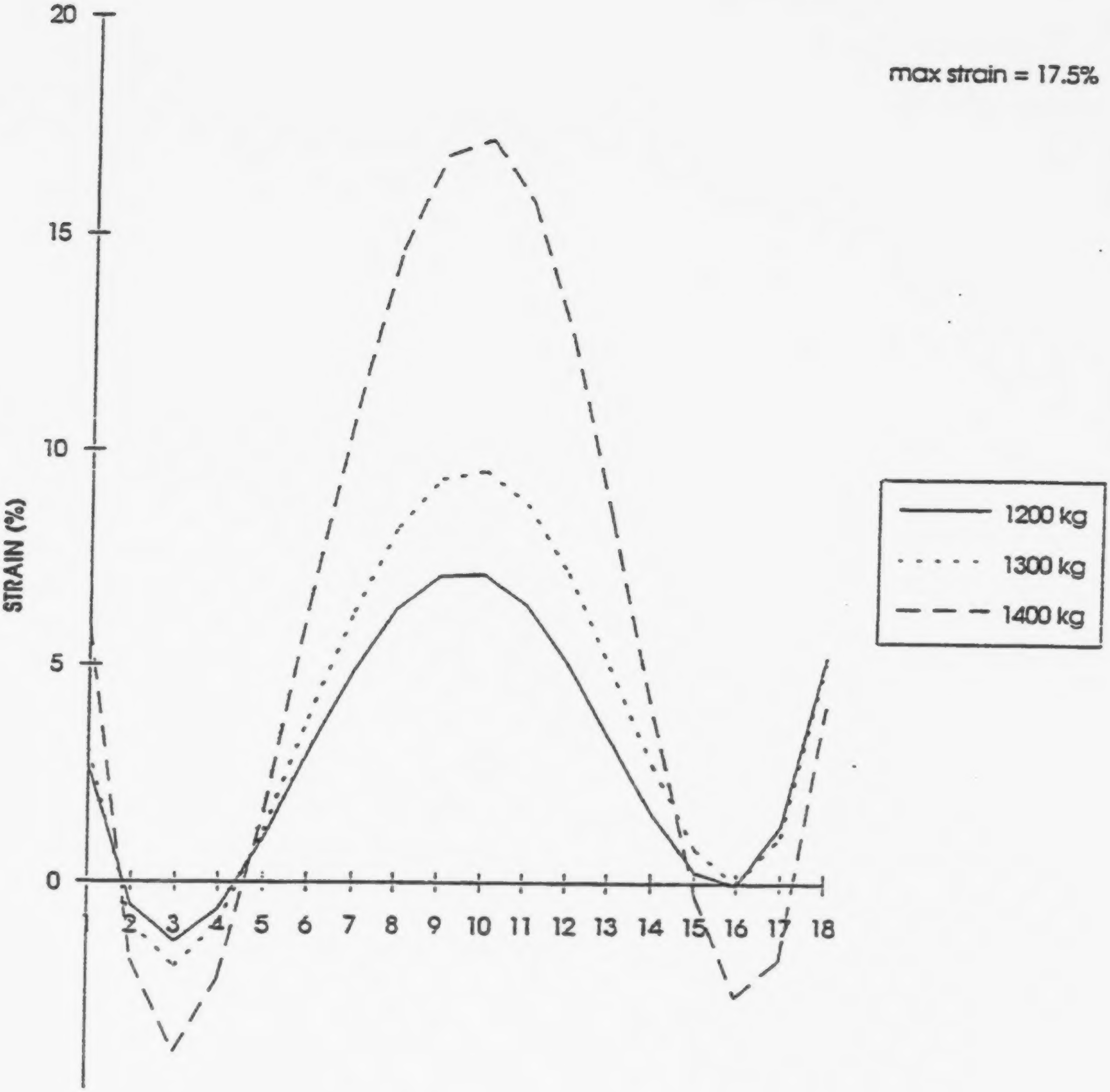

FIG. Strain distribution on polished bending specimen.

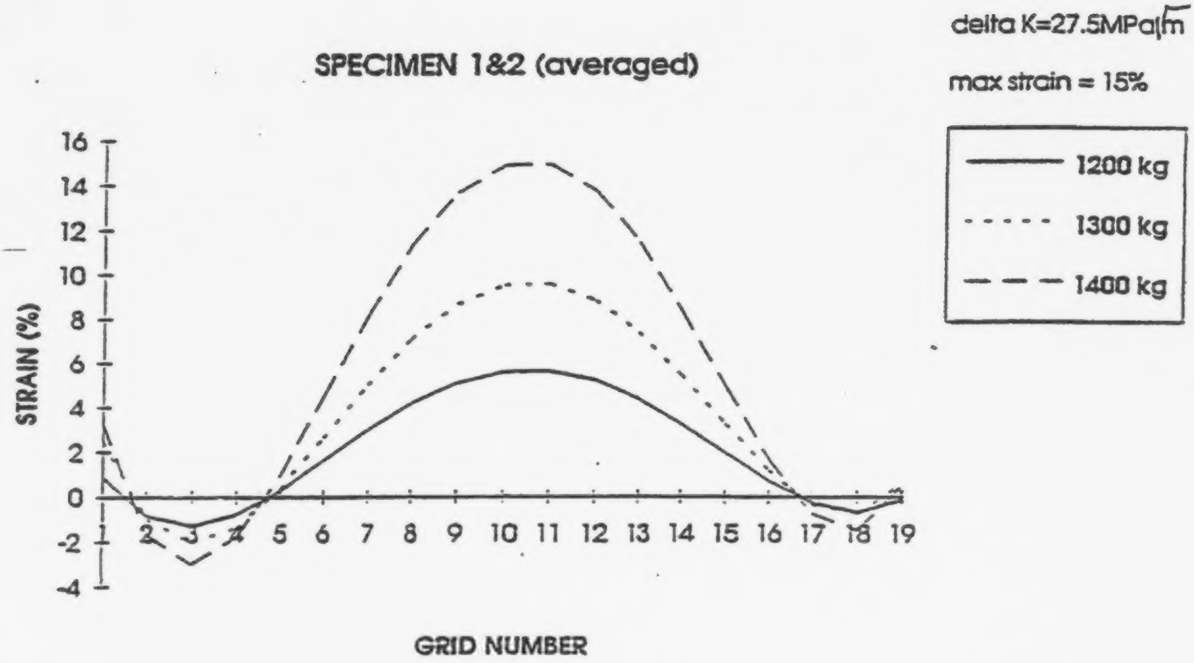

FIG. Strain distribution on fatigued bending specimen. (delta K = 27.5MPa$\sqrt{m}$)

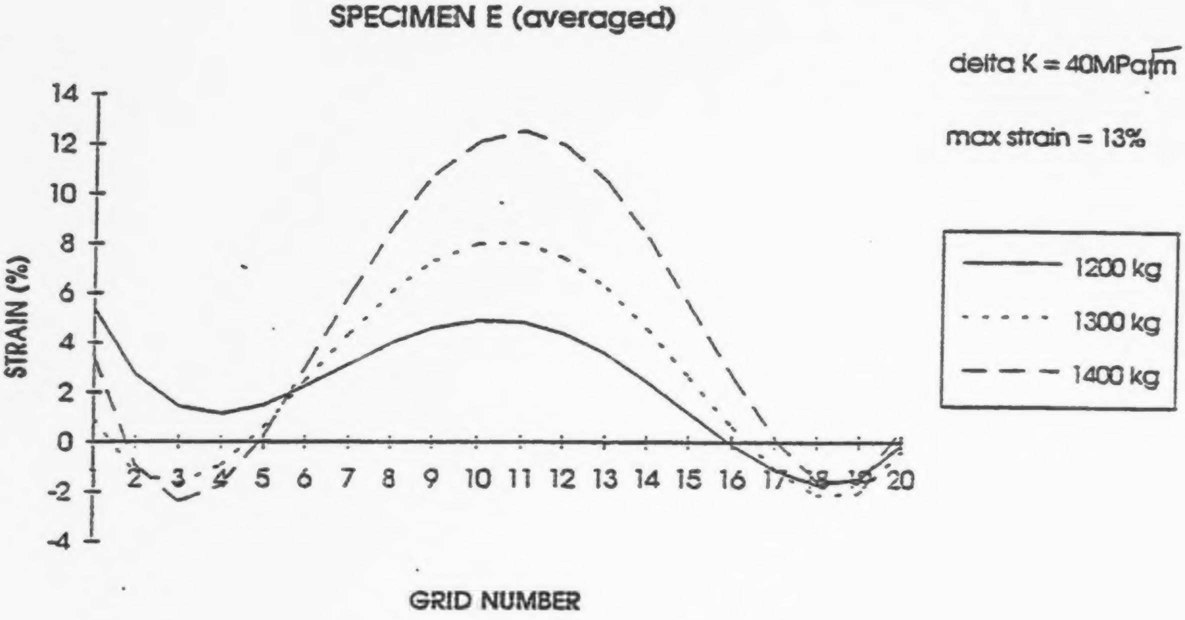

FIG. Strain distribution on fatigued bending specimen. (delta K = 40MPa$\sqrt{m}$)

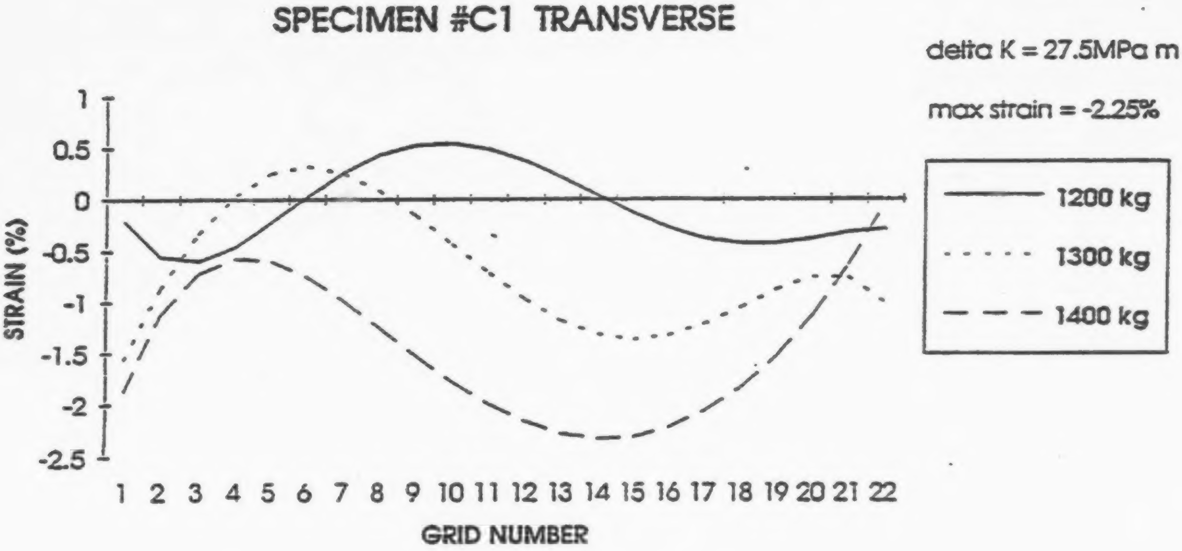

FIG. Strain distribution in transverse direction.

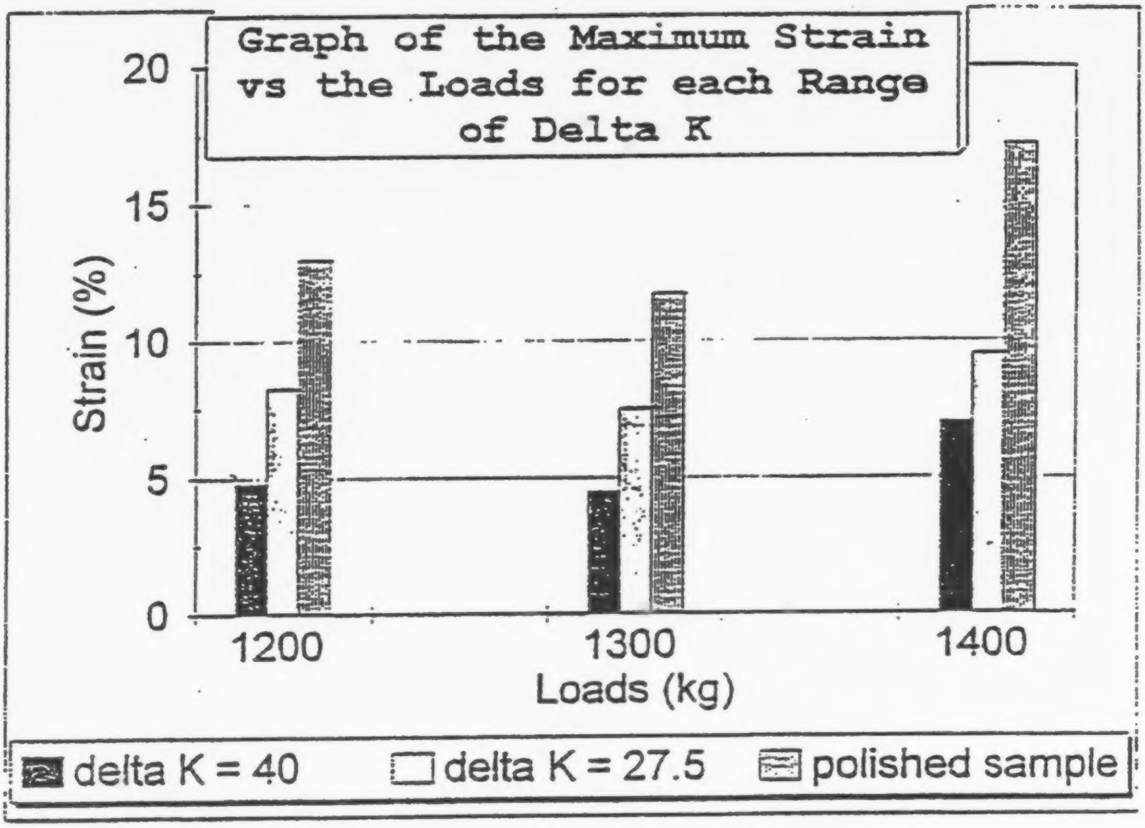

FIG. Summary of strain distribution results.

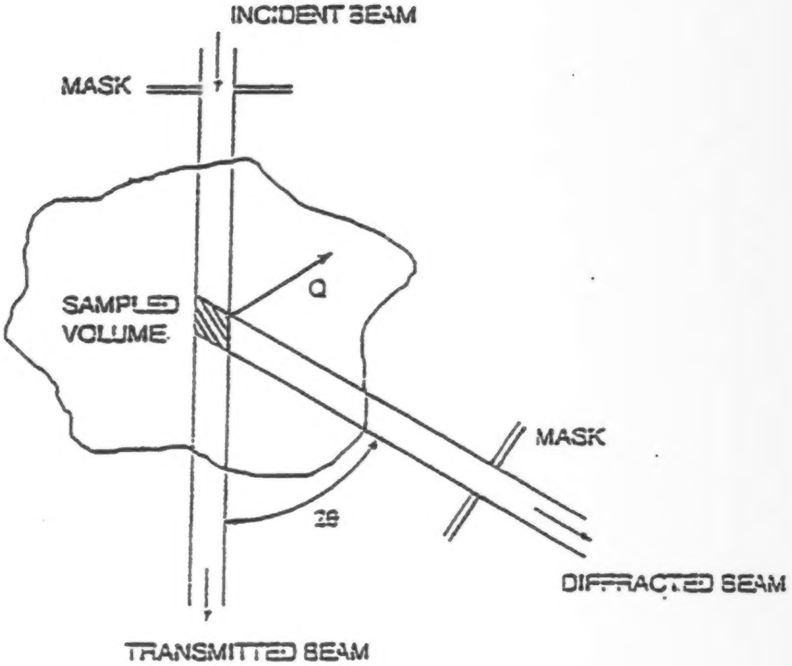
INCIDENT BEAM
MASK
SAMPLED VOLUME
Q
MASK
2θ
DIFFRACTED BEAM
TRANSMITTED BEAM

FIG. Configuration of neutron diffraction testing.

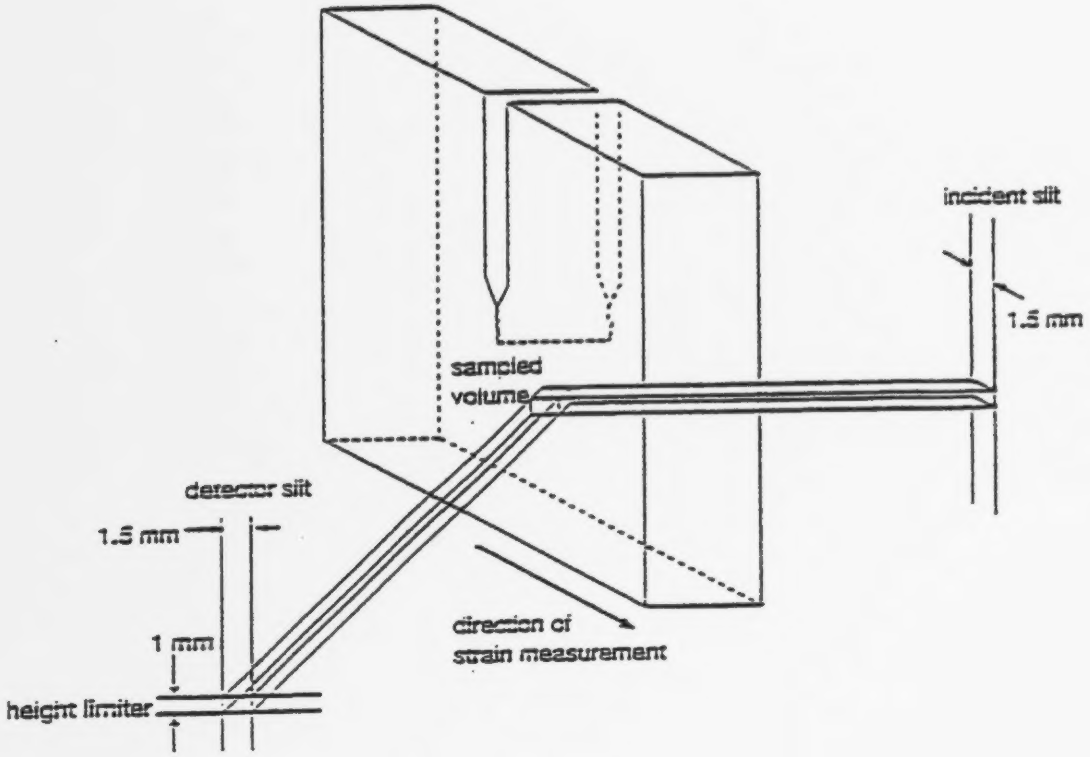
incident slit
1.5 mm
sampled volume
detector slit
1.5 mm
1 mm
height limiter
direction of strain measurement

FIG. Neutron diffraction arrangement for CT specimen.

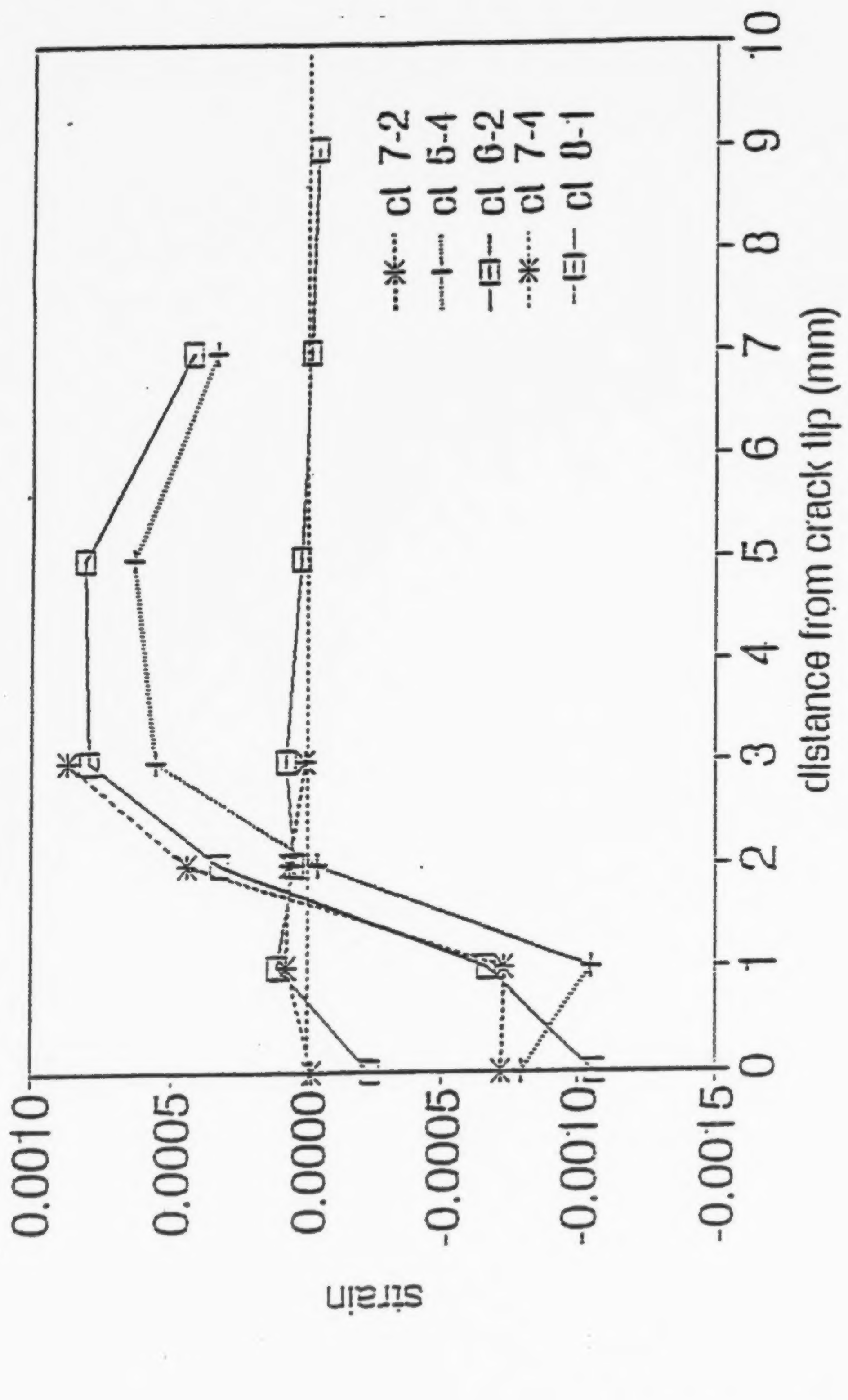

FIG. Residual elastic strains.

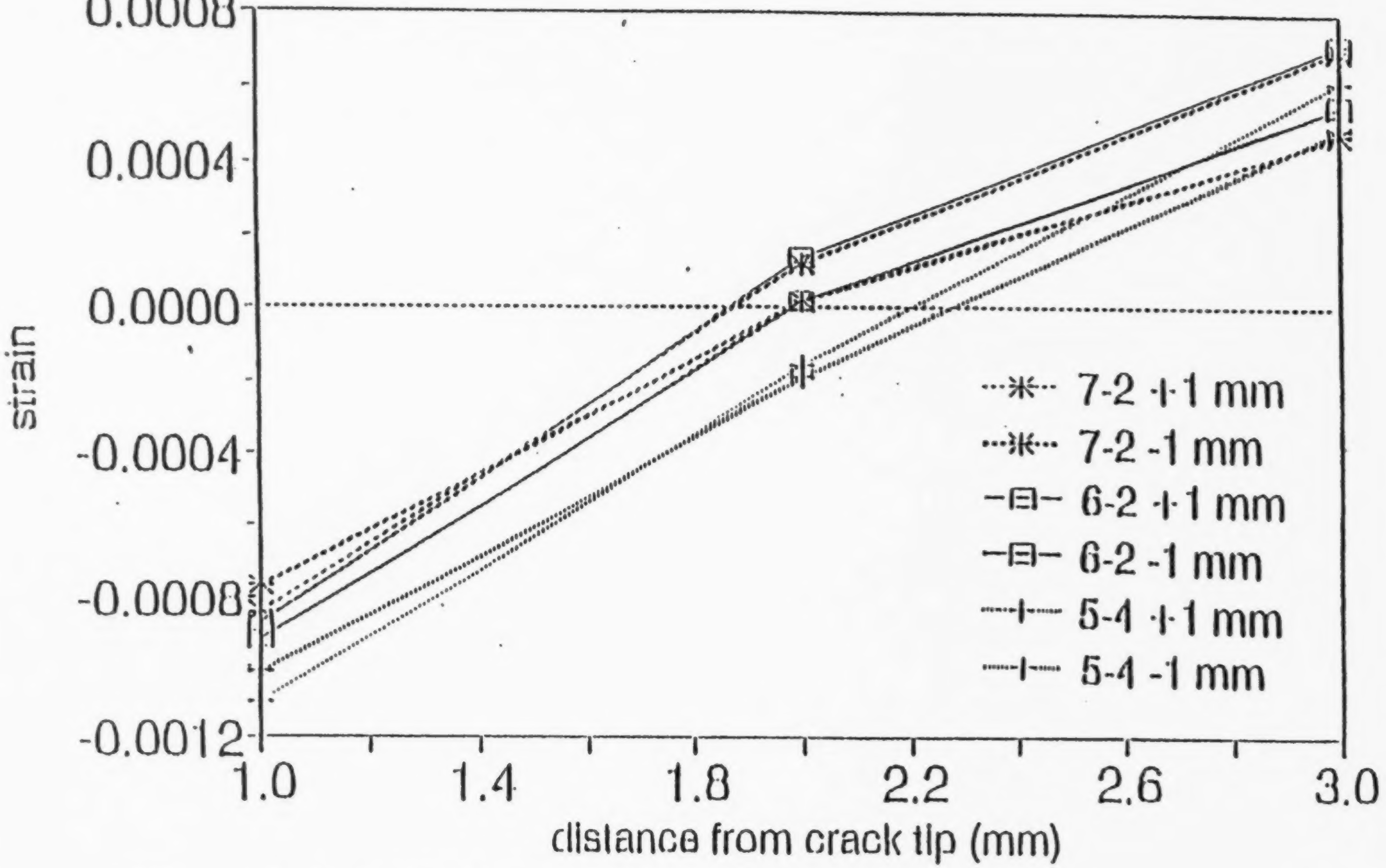

FIG. Residual elastic strains offset ± 1 mm from the crack plane.

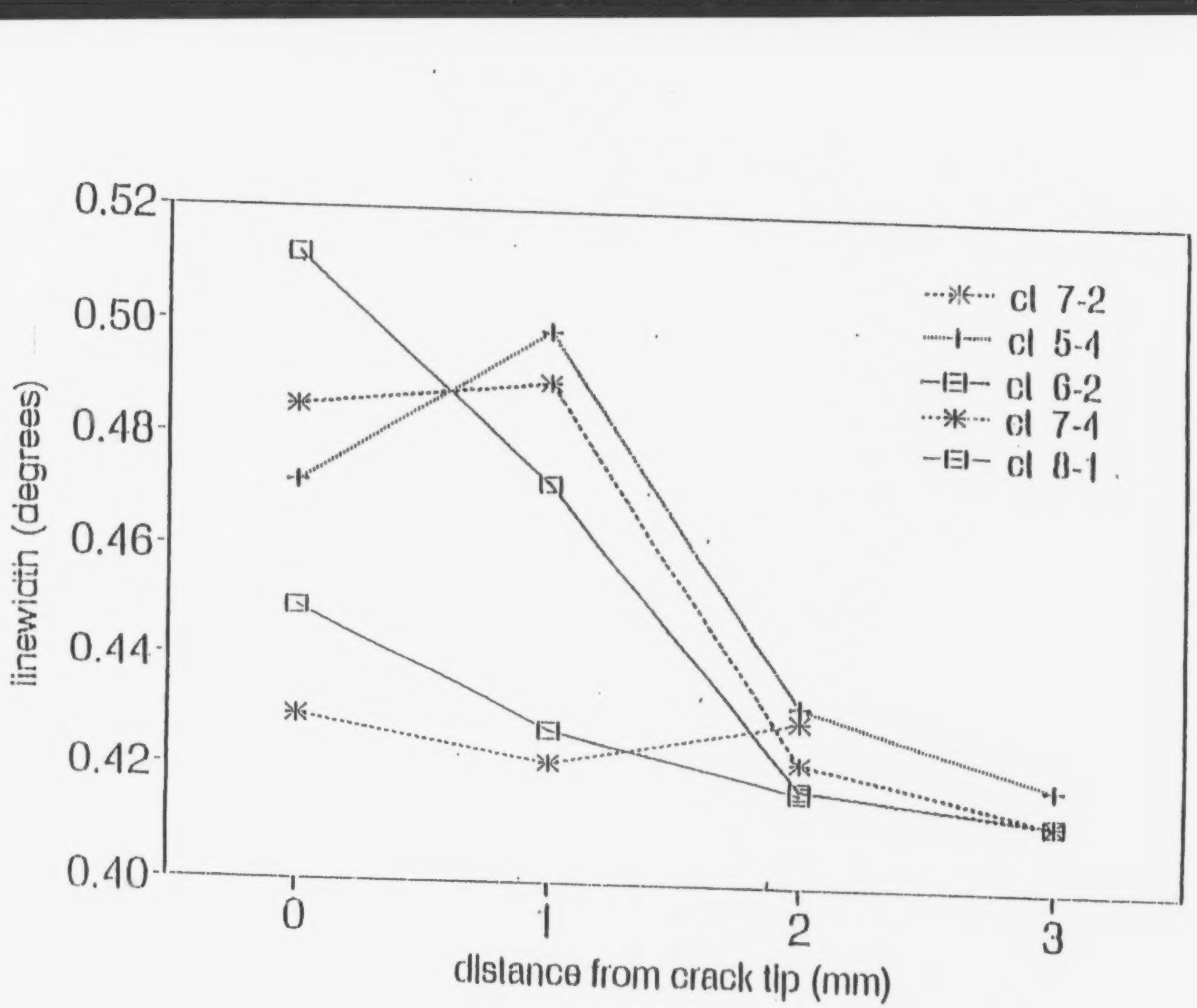

FIG. Linewidths arising from plastic deformation.

CONCLUSIONS

The research described deals with consideration of the effects which may influence the stretch zone with measurements and hence the determination of the fracture toughness of the high strength low alloy steels. Among these factors are the effect of crack size, temperature, loading rates as well as other factors related to the pre cracking process such as prestraining and strain hardening of the crack surface. The results obtained provide an in-depth understanding of these factors. Equations for compensation of these factors were also developed.

#510348 (5)

Application of the APHIUS System
in
DND Submarine Inspection Applications

by

D. Robert Hay and André Pelletier
Tektrend International Inc.

James R. Matthews
Defence Research Establishment Atlantic

Stéphane Garneau
DND/NDHQ/DGMEM/DSE

and

Richard Morchat
DND/NDHQ/CRAD

ABSTRACT

The Automated Pressure Hull Intelligent Ultrasonic System (APHIUS) was applied to submarine pressure hull inspection applications during the latter stages of its development. These included lamination inspections in critical areas and large-area mapping prior to major cuts in a submarine and weld inspection. The overall capabilities of APHIUS will be reviewed and examples of the field work that was carried out will be presented.

APHIUS

D. Robert Hay **André Pelletier**
Tektrend International Inc.

James R. Matthews
Defence Research Establishment Atlantic, Dockyard Laboratory

Stéphane Garneau
DGMEM/DSE 6-3-4, NDHQ

Richard Morchat
DND/CRAD/DRDM 8

TEKTREND

Metallic Materials

TEKTREND

APHIUS

Automated Pressure Hull Intelligent Ultrasonic System

Objectives

Submarine Pressure Hull Steel Plate and Weld Inspection using Ultrasonics

Increase Safety and Reliability

Lower Refit Costs

Metallic Materials

TEKTREND

APHIUS

Data Acquisition

Primary Target: Submarine Pressure Hulls

Primary Inspection Method: Ultrasonic

Primary Inspection Mode: Manual

Expansion Capabilities

Methods: Eddy Current, Acousto-Ultrasonics

Modes: Automated - Scanners
Crawlers
Probes

APHIUS

IMAGING

Assist in Interpretation

Provide Hard Copy

Metallic Materials

TEKTREND

APHIUS

Capabilities

- Software
  - Intelligence
  - Imaging
- Hardware
  - Data Acquisition
  - Data Storage

Metallic Materials

TEKTREND

APHIUS

INTELLIGENCE

To distinguish between tolerable defects and those calling for materials condemnation

This differentiation will enable decisions to be made that will eliminate certain repairs that are carried out automatically at present thus achieving the desired cost reductions

TEKTREND

APHIUS INSPECTION KIT

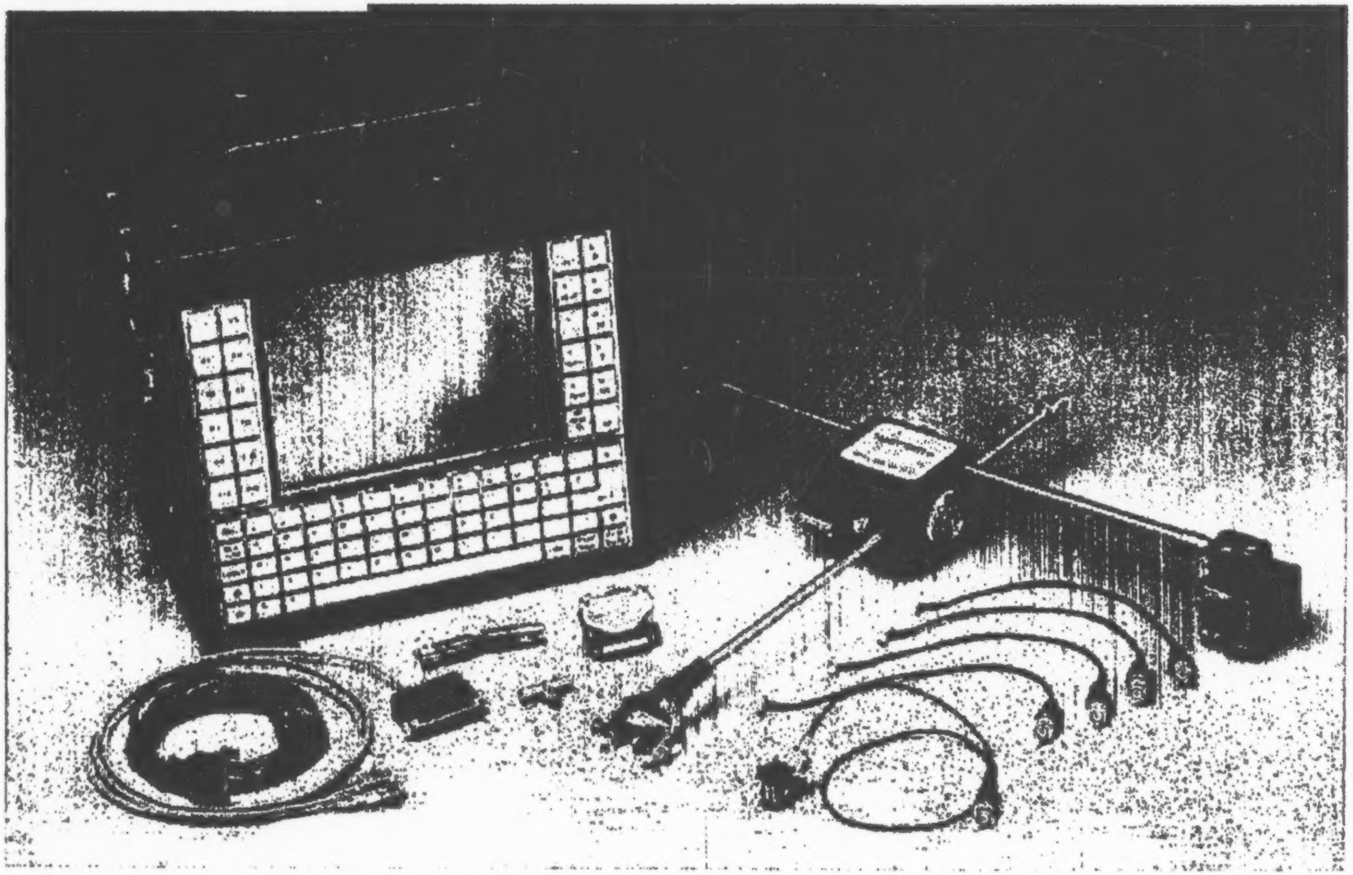

TEKTREND

APHIUS MAIN CONSOLE

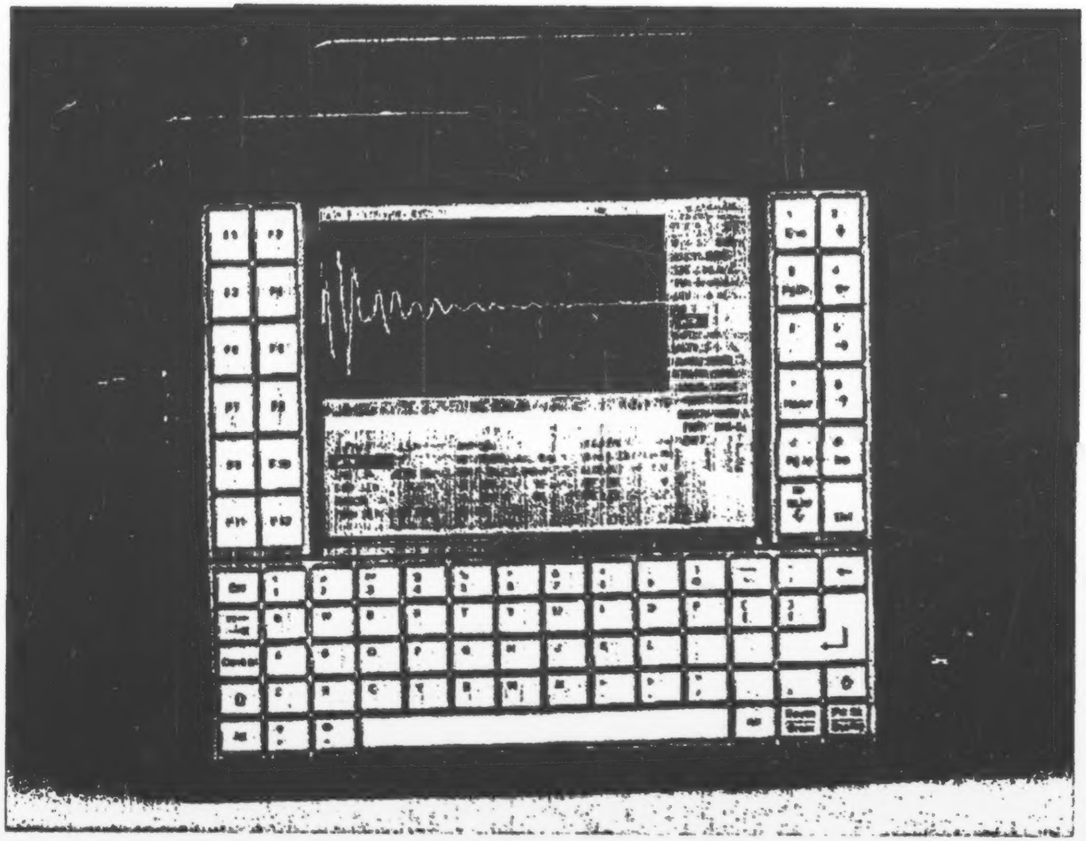

Metallic Materials

TEKTREND

APHIUS

HARDWARE

Main Console

- Small Form Factor to fit in Submarine
- High Digital Data Storage Capability
  - 525 MB Hard Disk
  - 2 GB DAT
- Flat Panel Color VGA
- Touch Screen
- Integrated Membrane Keypad

APHIUS

MAIN CONSOLE

APHIUS meets the requirements of demanding field inspections.

A high-performance ultrasonic inspection instrument, it is housed in an extremely compact, ruggedized enclosure.

The system provides high-speed, high-capacity data acquisition.

The combination of functionality and performance of APHIUS provides high inspection productivity and reliability.

The Console provides the ultrasonic pulser/receiver, full waveform digitization, large digital storage capacity, a full high-speed, powerful computer microprocessor, 9-inch color VGA monitor and integral keyboard all in a single module.

No separate monitor or detachable keyboard need be carried to the field. The single unit simplifies set up and operation in the field, significantly improving inspection productivity.

The ruggedized chassis resists moisture and dust and critical components are shock mounted. Thus, downtime due to field-induced handling is reduced and system availability with APHIUS is expected to be high.

An efficient point-and-click user interface is achieved through use of a touch screen. The advantages of a mouse-like interface are achieved without the need for a detached mouse.

All instrument settings are settable under the graphical user interface using the touch screen.

Access to a number of advanced display, analysis and interpretation capabilities of the APHIUS software is also provided through this touch-and-click interface.

APHIUS

MAIN CONSOLE

APHIUS meets the requirements of demanding field inspections.

A high-performance ultrasonic inspection instrument, it is housed in an extremely compact, ruggedized enclosure.

The system provides high-speed, high-capacity data acquisition.

The combination of functionality and performance of APHIUS provides high inspection productivity and reliability.

The Console provides the ultrasonic pulser/receiver, full waveform digitization, large digital storage capacity, a full high-speed, powerful computer microprocessor, 9-inch color VGA monitor and integral keyboard all in a single module.

No separate monitor or detachable keyboard need be carried to the field. The single unit simplifies set up and operation in the field, significantly improving inspection productivity.

The ruggedized chassis resists moisture and dust and critical components are shock mounted. Thus, downtime due to field-induced handling is reduced and system availability with APHIUS is expected to be high.

An efficient point-and-click user interface is achieved through use of a touch screen. The advantages of a mouse-like interface are achieved without the need for a detached mouse.

All instrument settings are settable under the graphical user interface using the touch screen.

Access to a number of advanced display, analysis and interpretation capabilities of the APHIUS software is also provided through this touch-and-click interface.

APHIUS

ULTRASONIC DATA ACQUISITION

APHIUS contains a high-performance ultrasonic pulser with receiver and state-of-the-art digitization for rapid data acquisition and processing.

PULSER

The ultrasonic pulser features both square wave and tone burst operation in one complete digitally controlled package. It can operate in the Pulse/Echo mode through the same transducer or Pitch/Catch with dual transducers. All pulser parameters are adjustable including voltage, damping, and pulse shape.

PULSER SPECIFICATIONS

Output Voltage:
12-375 volts, switchable in 16 steps.
Pulse Shape:
(a) Positive unipolar
(b) Negative unipolar
(c) Tone burst, 1-8 cycles
Pulse width:
25 nsec - 780 nsec, in .2 nsec steps
Rise time: <7 nsec, (square wave mode)
Fall time: dependent on damping
Damping: 16 levels (40-634)
Trigger: external or internal
Burst frequency:
640 khz - 20.00 MHz 5khz steps
Pulse repetition rate:
100-5000 per second (dependent on pulse width)

SCOPE

APHIUS is digital and modular in hardware and software and houses the following system elements:

- Data Acquisition
- Analysis and Interpretation
- Display

OPERATOR INTERFACE

Heavy-duty, industrial NEMA4 display, keypad and 1024x1024 touch-point touch screen

MICROPROCESSOR

The APHIUS II system is built around the IBM PC/INTEL 80X86 open architecture.

- 80486DX 33MHz processor
- 2 Serial Ports
- 1 Parallel Port
- Up to 32 MB DRAM
- AMI BIOS

DISPLAY

A flat panel 9", 512-color VGA, thin-film technology VGA monitor is used in the field inspection console. The display panel is combined with a full 101-key membrane keyboard and touch screen to facilitate field use. The front panel is sealed to moisture and dust to NEMA 4 specifications.

DISK STORAGE DRIVES

- 3½" floppy disk drive
- 500 MB high-speed hard disk for data acquisition
- 1.2 GB DAT drive for data archiving

KEYBOARD: Full 101-key membrane keypad

CHASSIS: 14 in. x 15 in. x 9 in. (WxLxD)

DATA ACQUISITION

All pulser, receiver and digitizer parameters operate under software control.

A/D CONVERSION

Full waveform storage at a 100 MHz transient sampling rate and, with equivalent-time sampling, up to 800 MHz. 64K on-board high speed memory buffer provides maximum data acquisition flexibility. One- or two-channel configurations.

DIGITIZER SPECIFICATIONS

TRIGGERS: Pretrigger, internal, external, threshold, software, continuous

MEMORY BUFFER:
- 64K high speed static RAM per channel
- Segmentable in 1 byte increments
- Addressable at 16K boundaries through a 16K window in user memory

ANALOG SPECS:
- DC to 110 MHz bandwidth, -3db
- 50 Ohm input impedance
- .03 to 4 volts through software selection
- 2 channels with common trigger

A/D CONVERSION:
- 100 MHz base rate (flash converter)
- 7 software selectable lower rates
- 200, 400, and 800 MHz time equivalent sampling

SPECIAL FEATURES:
- Threshold-exceeded alarm output
- External clock input
- Interrupt polling for multiple board applications
- Hardware peak detector

POWER SUPPLY:
300 w, 36 cfm, 46 dbA, UL, CSA, TUV

APHIUS

ULTRASONIC DATA ACQUISITION

RECEIVER

Combined with the pulser is a high quality receiver with a 60 dB gain operating in broadband and tuned modes. A coarse-step attenuator before the amplifier avoids saturation effects. A fine- step attenuator after the amplifier permits the user to fine tune the gain. The receiver also provides adjustable high- and low-pass filters.

RECEIVER SPECIFICATIONS

Overall Gain:-60 to 60 db, 1 db steps
H.P. Filter:
0.1, 0.5, 2.3, 2.8 MHz
L.P. Filter: 2.2, 2.4, 2.6, 3.0, 9.0, 14, 24, 50MHz
Bandwidth:
30 MHz ± 3 db
Output: RF, ± 1 volt
Input impedance:
50 ohms
Output impedance: 50 ohms

TEKTREND

APHIUS HAND SCANNER

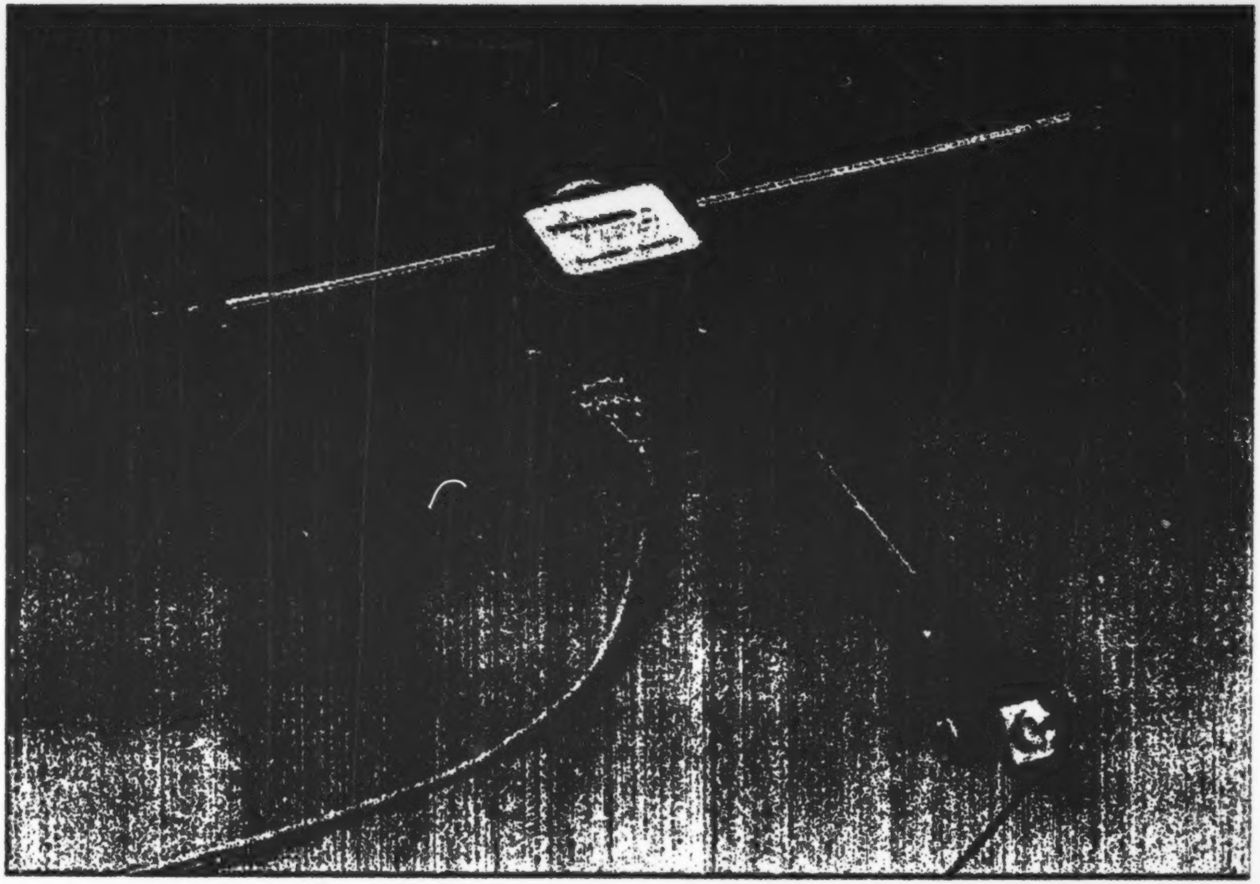

Metallic Materials

APHIUS

TEKTREND

APPLICATIONS

CORROSION MAPPING

DELAMINATION DETECTION AND MAPPING

WELD INSPECTION

TEKTREND

SETUP FOR

APHIUS

PRESSURE HULL INSPECTION

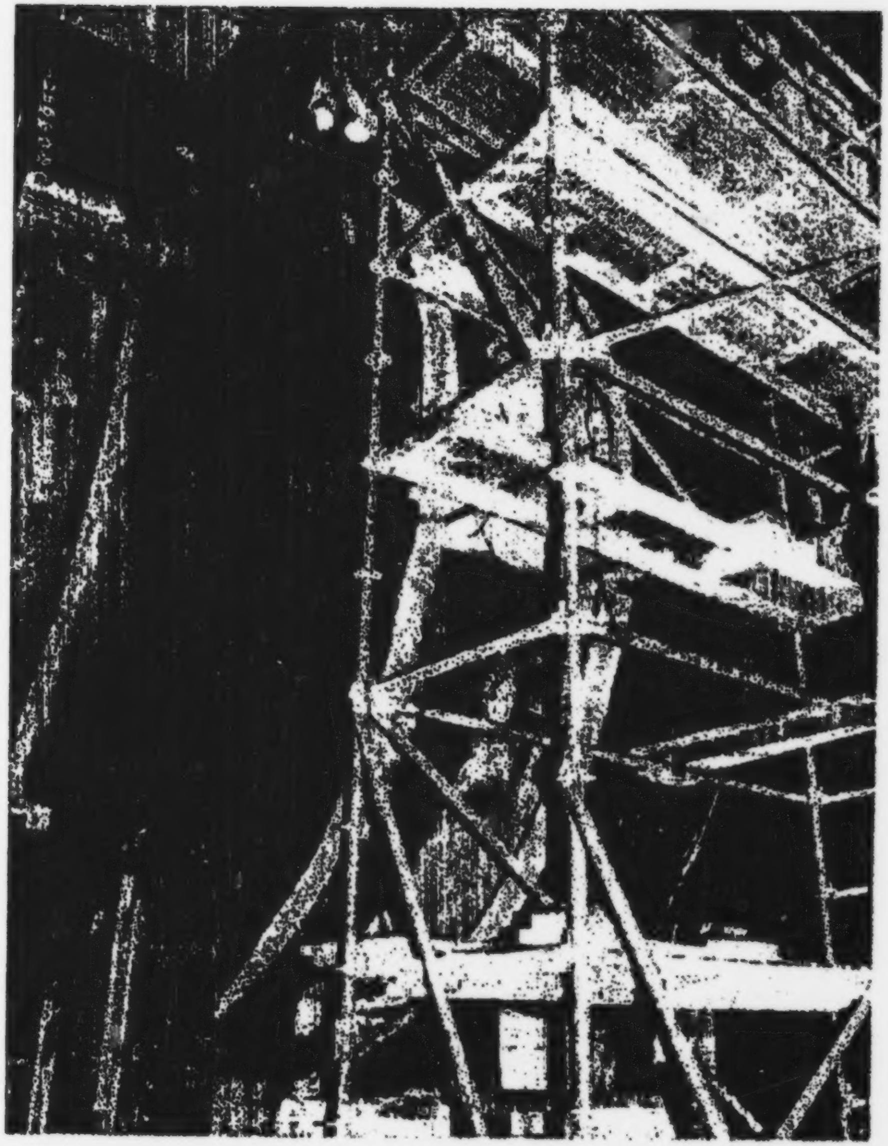

TEKTREND

APHIUS

INSTRUMENTATION

SETUP ON THE

OUTSIDE OF THE

SUBMARINE PRESSURE HULL

TEKTREND

APHIUS

CALIBRATION

ON THE

SUBMARINE PRESSURE HULL

TEKTREND

APHIUS

INSPECTION

OF THE

SUBMARINE PRESSURE HULL

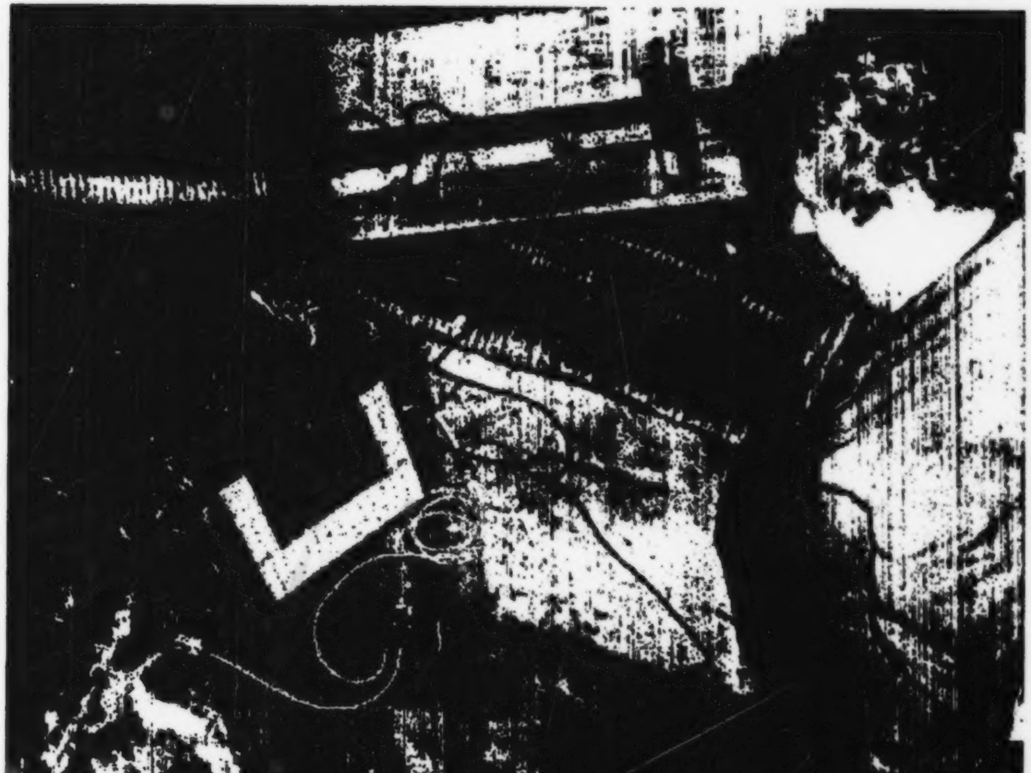

TEKTREND

APHIUS

INSPECTION

REFERENCE SYSTEM

ON THE PRESSURE HULL

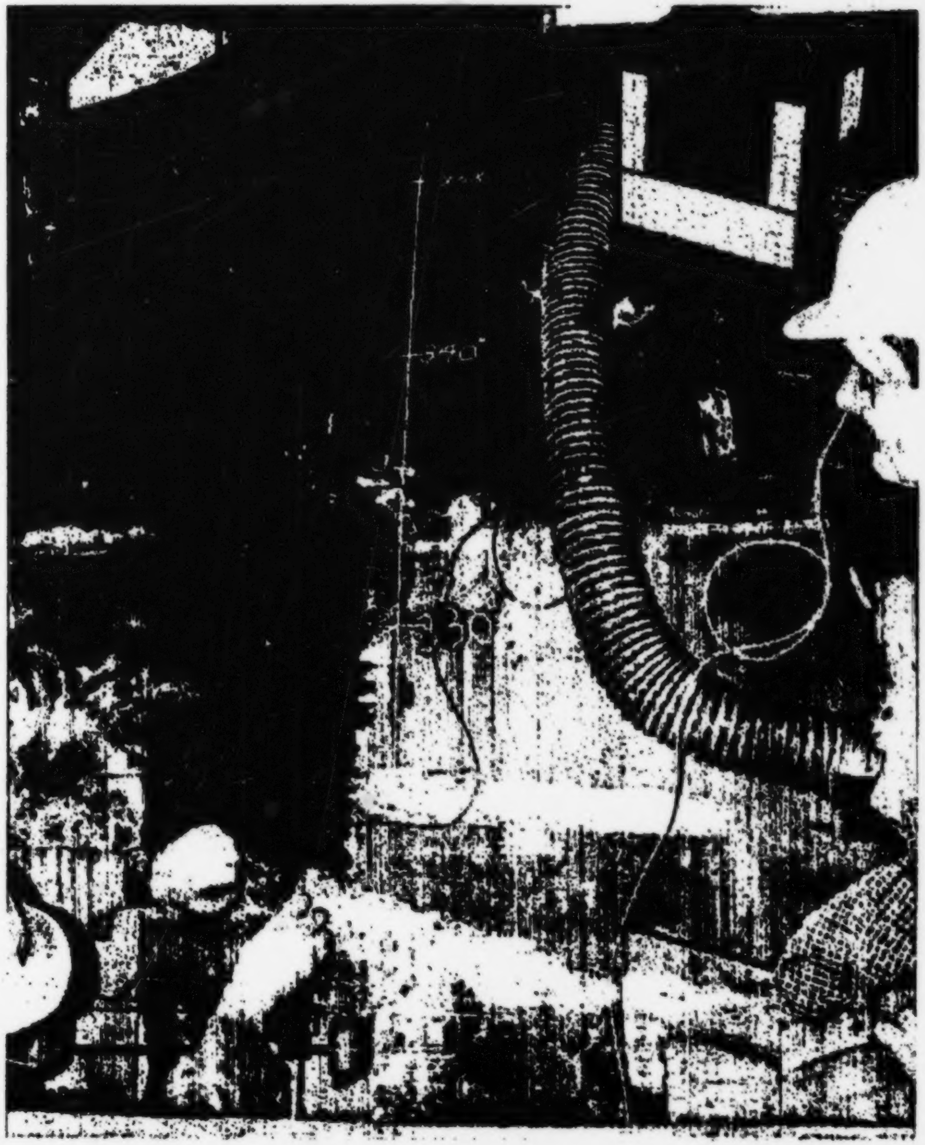

TEKTREND

APHIUS

The longitudinal B-scan shows the depth of the defects and the transverse B-scan their location in the weld profile.

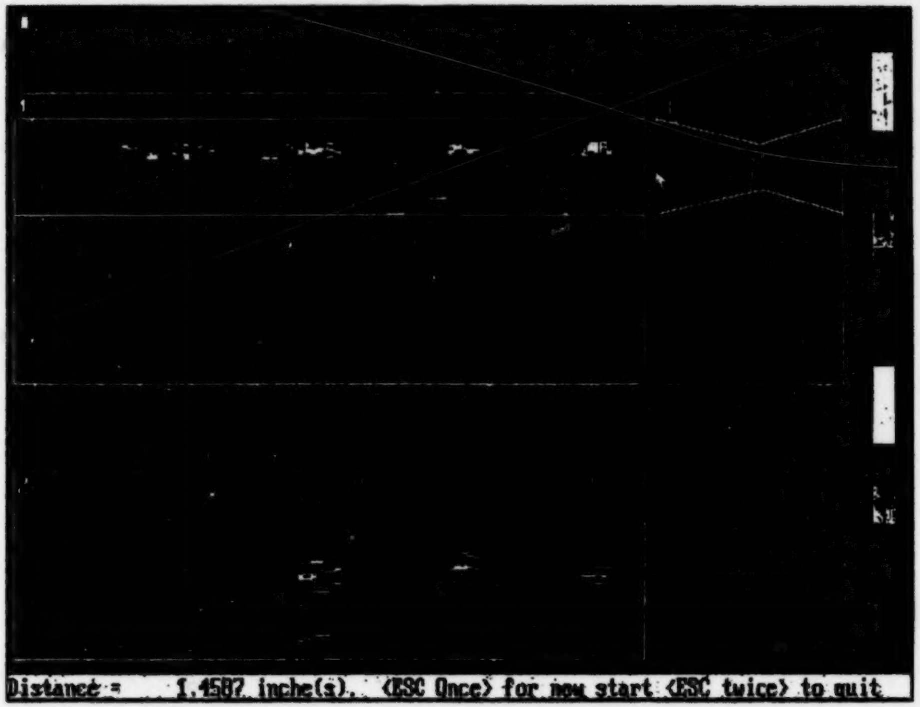

```
Distance =    1.4587 inche(s).  <ESC Once> for new start <ESC twice> to quit
```

- ☐ *C-scan (upper left)*
- ☐ *longitudinal B-scan along the weld through the line of defects (lower left)*
- ☐ *a transverse B-scan across the weld (upper right).*

APHIUS

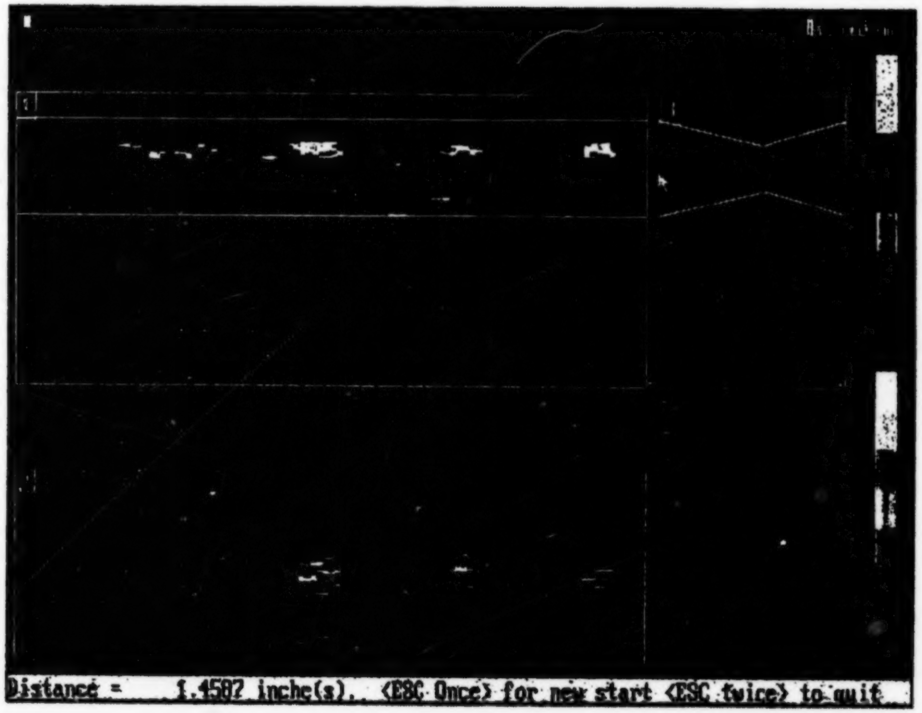

```
Distance =      1.4587 inche(s).  <ESC Once> for new start <ESC twice> to quit
```

The longitudinal B-scan shows the depth of the defects and the transverse B-scan their location in the weld profile.

- ☐ ***C-scan (upper left)***
- ☐ ***longitudinal B-scan along the weld through the line of defects (lower left)***
- ☐ ***a transverse B-scan across the weld (upper right).***

Metallic Materials

TEKTREND

APHIUS

INTELLIGENCE

Artificial Intelligence Methods used in APHIUS:

- Statistical Pattern Recognition
  - Linear Discriminant
  - **Nearest Neighbor**
  - **Empirical Bayesian**
  - **Minimum Distance**
- Neural Network

Artificial Intelligence in Ultrasonic Inspection

Artificial Intelligence (AI) is indicated when:

- *there is a lack of skilled people to do the work.*
- *the application has resisted other forms of automation*
- *functions are isolated and performed by an individual or small group.*
- *the working environment may be hazardous to human health*

Interpretation of ultrasonic signals

- *can vary from operator to operator*
- *human factors such as a training and fatigue influence judgment*
- *large bodies of knowledge are held by a few experts acquired through extensive inspection experience*

Additional advantages

- *computer programs can extract more information from data than a human in a reasonable time frame*
- *effective extraction and encoding of expert and physical knowledge into a knowledge-based system can disseminate expertise to related inspection requirements or focus it on a particular inspection procedure*
- *these AI methods can also provide new physical insight into the phenomena involved*
- *an AI system permits faster, more reliable and robust routine interpretation.*

Pattern Recognition and Artificial Intelligence

AI methods simulate certain advanced human functions and interface man and machine with techniques humans use for problem solving in a number of fields:

Pattern Recognition
Intelligent Sensing
Theorem Proving
Knowledge-Based Systems
Natural Language Understanding
Connectionist Systems
Man-Machine Communication
Expert Systems
Computer Vision
Game Theory
Robotics
Decision Theory
Neural Networks
Problem Solving

Knowledge-Based AI Methods
for
Interpretation, Diagnosis and Analysis

EXPERT SYSTEMS

RULE-BASED

PATTERN RECOGNITION

FEATURE-BASED

Pattern recognition is well-suited to interpretation of waveform data generated in ultrasonic inspection and models the methods that humans actually use.

PATTERN CLASSIFICATION APPROACH

Pattern classification methods are well established and largely application independent.

Research in classifier design lies in selection of the pattern elements or ***features*** with powerful pattern representation capabilities. Feature definition and selection is largely application dependent although generic feature sets applicable over a wide range of applications can be defined.

Once the knowledge is organized and formalized using the known identity of the feature classes, it can be used to train the computer to characterize an unknown set of input features or for modifying decision parameters.

Pulse Shape Descriptors

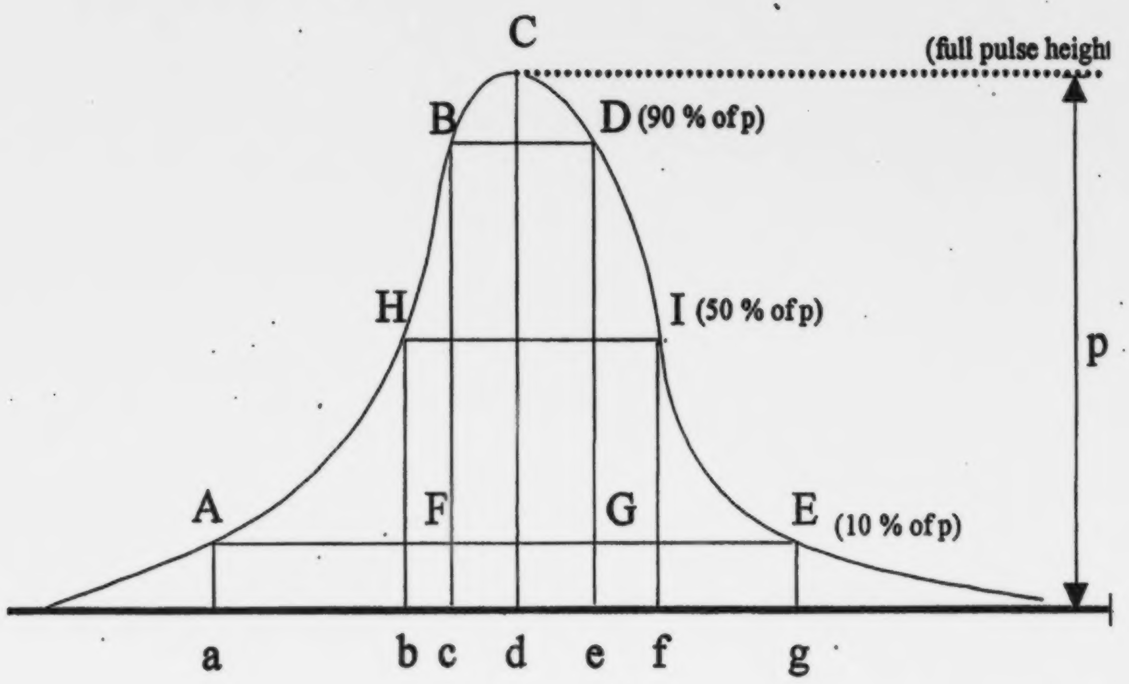
C
(full pulse height
B
D (90 % of p)
H
I (50 % of p)
p
A
F
G
E (10 % of p)
a
b c
d
e
f
g

Rise Time = AF
Rise Slope = BF / AF
Pulse Location = d
Pulse Width = AE
Peak Width = BD

Fall Time = GE
Fall Slope = DG / GE
Pulse Amplitude = p
Half Max Width = HI

ICEPAK Version 4.0

Waveform Features by Domain

					Correlation	
Feature	**Time**	**Power**	**Phase**	**Cepstral**	**Auto-**	**Cross-**
# peaks above signal base line	x	x	x	x	x	x
# peaks above 10% max. signal amplitude	x	x	x	x	x	x
# peaks above 25% max. signal amplitude	x	x	x	x	x	x
Greatest peak position	x	x	x	x	x	x
Greatest peak amplitude	x	x	x	x	x	x
2nd greatest peak position	x	x	x	x	x	x
2nd greatest peak amplitude	x	x	x	x	x	x
3rd to 5th greatest peak position	x					
3rd to 5th greatest peak amplitude	x					
% of total area under greatest peak	x	x	x	x	x	x
% of total area under 2nd greatest peak	x	x	x	x	x	x
% of total area under 3rd, 4th, 5th greatest peak	x					
Inter-peak distance from 1st to 2nd greatest	x	x	x	x	x	x
Inter-peak distance from 1st to 3rd greatest	x					
Inter-peak distance from 2nd to 3rd greatest	x					
Greatest peak rise time	x					
Greatest peak rise slope	x					
Greatest peak fall time	x					
Greatest peak fall slope	x					
Greatest peak full pulse width	x					
Greatest peak half pulse width	x					
Greatest peak peak width	x					
2nd - 5th greatest peak rise time	x					
greatest peak rise slope	x					
greatest peak fall time	x					
greatest peak fall slope	x					
greatest peak full pulse width	x					
greatest peak half pulse width	x					
greatest peak peak width	x					
% of partial power in 1st octant		x	x	x	x	x
% of partial power in 2nd octant		x	x	x	x	x
% of partial power in 3rd octant		x	x	x	x	x
% of partial power in 4th octant		x	x	x	x	x
% of partial power in 5th octant		x	x	x	x	x
% of partial power in 6th octant		x	x	x	x	x
% of partial power in 7th octant		x	x	x	x	x
% of partial power in 8th octant		x	x	x	x	x
Normalized energy of the signal (RMS)	x	x	x	x	x	x
Standard deviation of the signal	x	x	x	x	x	x
Variance of the signal	x	x	x	x	x	x

Pattern Recognition

A pattern recognition system, in general, comprises four phases

- *data acquisition*
- *data transformation*
- *feature extraction*
- *classification*

During development, a training and testing phase is also required.

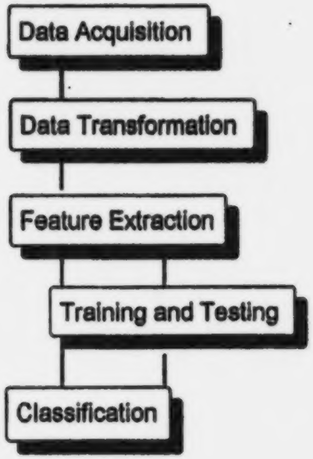
Data Acquisition
Data Transformation
Feature Extraction
Training and Testing
Classification

TEKTREND

Classifier design and indication identification processes

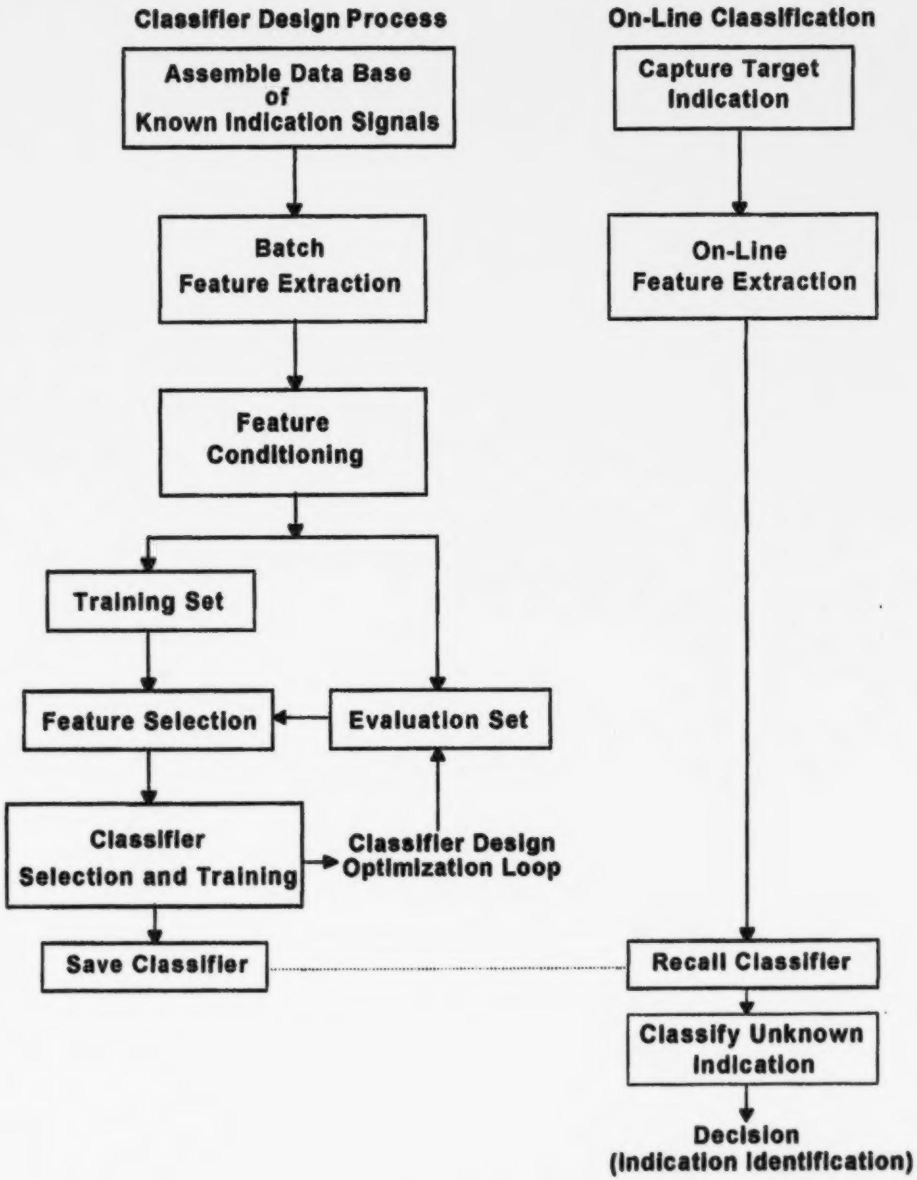

Classifier Design Process

Assemble Data Base of Known Indication Signals

Batch Feature Extraction

Feature Conditioning

Training Set

Evaluation Set

Feature Selection

Classifier Selection and Training

Classifier Design Optimization Loop

Save Classifier

On-Line Classification

Capture Target Indication

On-Line Feature Extraction

Recall Classifier

Classify Unknown Indication

Decision (Indication Identification)

Types of Pattern Classifiers

There are several types of pattern classifiers to meet a wide range of applications. The following represent linear, parametric, and nonparametric classifiers:

Linear discriminant function classifier
K-nearest neighbor classifier
Empirical bayesian classifier
Minimum distance classifier
Neural network classifier

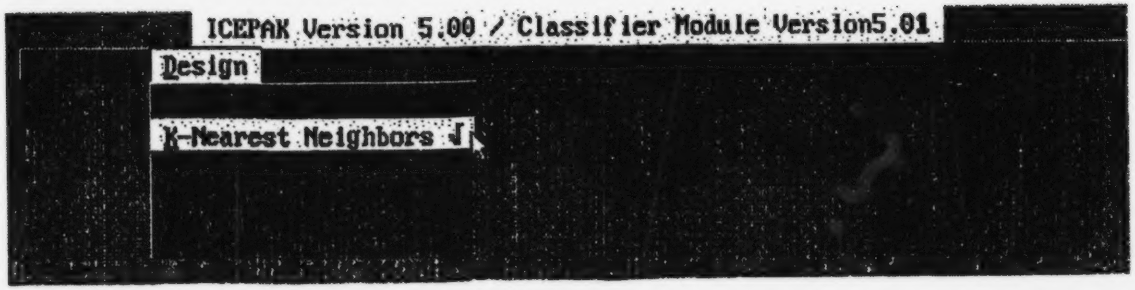
ICEPAK Version 5.00 / Classifier Module Version5.01
Design
K-Nearest Neighbors √

CLASIFICATION RESULTS TABLE

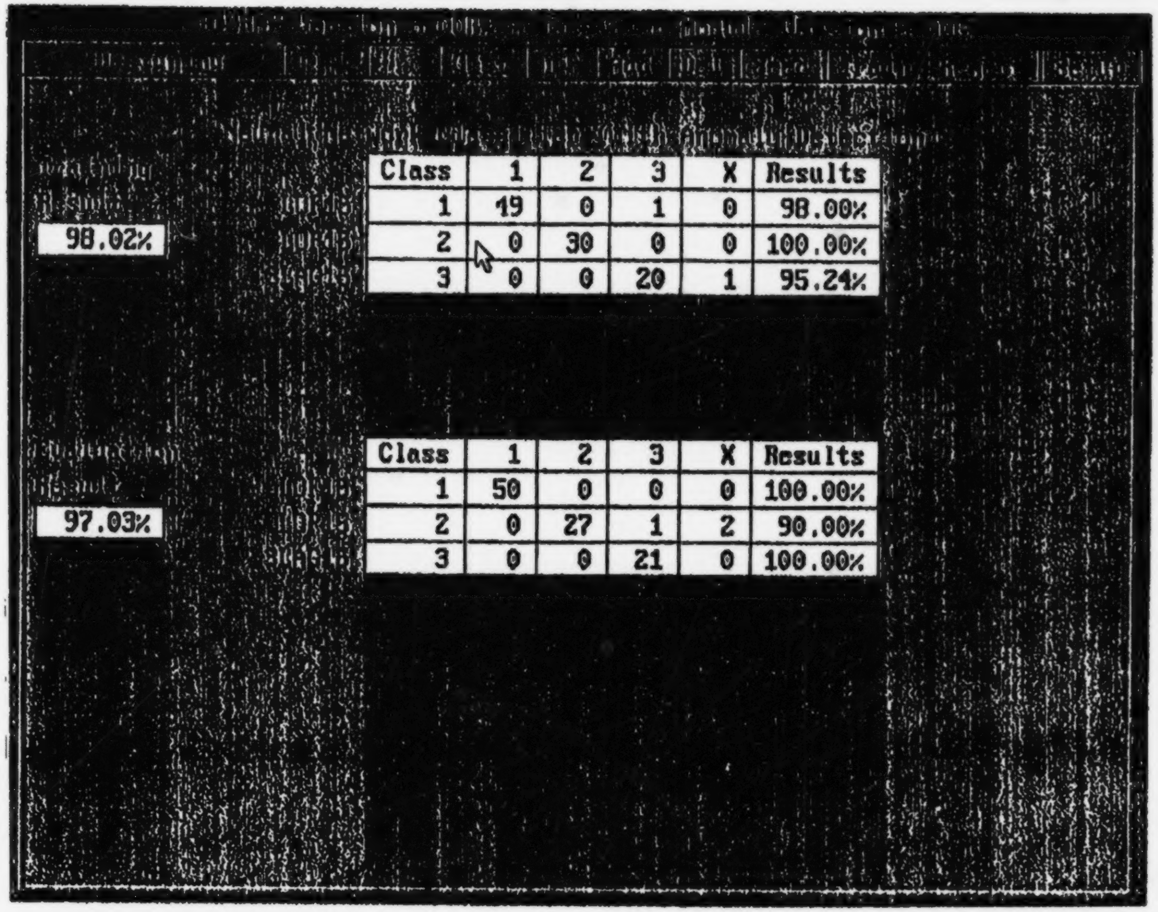

98.02%

Class	1	2	3	X	Results
1	19	0	1	0	98.00%
2	0	30	0	0	100.00%
3	0	0	20	1	95.24%

97.03%

Class	1	2	3	X	Results
1	50	0	0	0	100.00%
2	0	27	1	2	90.00%
3	0	0	21	0	100.00%

CLASSIFICATION RESULTS

15 mm Plate Classifier

Training Results: 98 %   Evaluation Results 97 %

The 15 mm Plate Classifier was successful in distinguishing between its three classes (slag inclusions, lack of penetration and lack of fusion).

12 mm Plate Classifier

Training Results: 95 %   Evaluation Results 93 %

This classifier confused lack of penetration and slag inclusion defects.

10 mm Plate Classifier

Training Results: 97 %   Evaluation Results 88 %

The confusion occurred between lack of fusion and slag inclusion defects.

8 mm Plate Classifier

Training Results: 92 %   Evaluation Results 89 %

Longitudinal cracks made this Classifier the only with four classes. The results from this Classifier were generally excellent except for the identification of longitudinal cracks. Training Results were 77.78 % and Evaluation Results were 58.82 %. This classifier had trouble distinguishing between slag inclusions and longitudinal cracks.

6 mm Plate Classifier (3 classes)

Training Results: 100 %   Evaluation Results 73 %

This classifier confused slag inclusion defects with both lack of penetration defects and lack of fusion defects. The success rate for slag inclusions, lack of penetration and lack *of fusion were 31 %, 86 %* and 87 % respectively.

6 mm Plate Classifier (2 classes)

Training Results: 100 %   Evaluation Results 96 %

When the slag inclusion class was not included in the classifier the classifier identified the lack of penetration and lack of fusion successfully.

CONCLUSIONS

The data from defects examined in this study provide

- Good separability permitting the design of
  - ☐ *high performance*
  - ☐ *user-tolerant defect classifiers for ultrasonic inspection of submarine pressure hull steels*

- Recognition rates down to 512 points remain acceptable
- This will increase the speed of classification
- Applying a filter window to the data before feature extraction can substantially improve the classifier performance

#510349 (6

INTRODUCTION OF THE SIGNATURE CLASSIFICATION DEVELOPMENT SYSTEM

Lawrence M. Brown
Carderock Division
Naval Surface Warfare Center
Annapolis, Maryland

Jeffery S. Lin
Applied Physics Laboratory
Johns Hopkins University
Laurel, Maryland

ABSTRACT

The Carderock Division of the Naval Surface Warfare Center and the Applied Physics Laboratory of the Johns Hopkins University are currently developing a Signature Classification Development System (SCDS) to transfer signature classification technology to NDE inspection equipment in the field. The SCDS is a PC-based software tool-kit designed to aid in the analysis of NDE signatures and to support the development of classification algorithms. Three modules are integral to the Signature Classification Development System: 1) the digital signal processing module (DSP), the classification module, and the code generation module. The DSP module supports user-written C routines to facilitate signal processing, definition of templates, assignment of signature gates, and generation of feature vectors. The SCDS classification module incorporates an artificial neural network and both parametric and non-parametric statistical techniques for classification of the NDE signatures. After a satisfactory classification algorithm has been developed and tested, the SCDS can generate run-time source code for integration of the processing and classification algorithm into NDE field equipment or laboratory systems.

The Signature Classification Development System is an on-going program sponsored by the Office of Naval Research. This paper briefly describes the current capabilities of the SCDS and outlines the plans for future enhancements.

INTRODUCTION

Discontinuities of various types and sizes may be introduced into a material during the manufacturing process and during the service life of the component. Discontinuities generated during the manufacturing process may include stress cracking, slag inclusions, lack of fusion, and gas or shrinkage porosity, whereas typical discontinuities generated during the service life may include fatigue cracks and corrosion (Hull and John, 1988). Before the component can be accepted for inventory or continued service, an accurate nondestructive evaluation of the component must be performed.

In addition to discontinuity detection, nondestructive evaluation (NDE) can provide signature information to characterize the discontinuity. Because each discontinuity type can result in a degradation of a specific mechanical property, characterization of the discontinuity permits the development and application of acceptance criterion that are defect specific, providing additional assurance that the material is suitable for use in the intended structural application.

Advancements in intelligent processing algorithms and high speed computers have brought forward increased capabilities to characterize material discontinuities and to determine the location and size of the discontinuities. For example, in Japan and the United States artificial neural networks have been employed to characterize discontinuities in weld metal based on information in the ultrasonic signatures (Song and Schmerr, 1991, Ogi, et al., 1991). Similarly, ultrasonic signatures of discontinuities in thick graphite epoxy composites have been characterized using artificial neural networks (Brown, et al., 1992). Parameterization of eddy current signatures using the Fourier descriptor method has lead to classification of defects in Inconel® tubing (Udpa and Udpa, 1990). Signal processing techniques and neural networks have been used to determine the depth of surface breaking cracks in steel plates (Kitahara, et al., 1991). In addition, processing of acoustic emissions data has aided Pacific Northwest Laboratory in the detection and location of leaks in curved aluminum plates designed for the U.S. Space Station (Friesel, et al., 1992).

Industrial competitiveness will continually drive technological advances in the field of nondestructive evaluation, increasing the application of intelligent processing of materials and in-service inspections (Schwartz, 1991). As advancements are made in NDE sensors, and both mathematical and physical models of materials, the scientific community will see increased research in material characterization.

The U.S. Navy has recognized the significant advancements in intelligent processing and classification of discontinuities in the field of NDE. Furthermore, the U.S. Navy recognizes the need for generic classification development systems. These intelligent systems would aid the design engineer in selecting signature processing and classification algorithms for a broad spectrum of NDE technologies and applications. A signature classification development system will speed the introduction of material characterization procedures to field inspection sites, reduce expenses and increase material safety and world competitiveness.

SYSTEM DESIGN

The Applied Physics Laboratory of the Johns Hopkins University and the Carderock Division of the Naval Surface Warfare Center have jointly developed a prototype of the Signature Classification Development System. The prototype, SCDS Version 1.02, runs on a IBM® PS/2® or AT compatible computer operating under Microsoft® Windows™ 3.1 or above. SCDS Version 1.02 contains a functional library for the analysis of ultrasonic signatures, but will support the analysis of any signature that is a function of a single variable (i.e. amplitude versus time).

In general, the Signature Classification Development System (SCDS) is a software tool-kit aimed at assisting the research engineer in developing algorithms for classification of signatures. The targeted design architecture of the SCDS is comprised of three major functional modules: data processing, signature classification, and code generation. The data processing module supports selection of signatures for analysis, digital signal processing (DSP) and calculation of parameter vectors for input to the classifiers. The classification module will include an artificial neural network and both parametric and nonparametric statistical classifiers. In addition, the classification module will provide resources for selection of optimal input features to the classifiers, and provide verification of stochastic assumptions required for the parametric classifiers. Lastly, SCDS will support source code generation, where the functional libraries are accessed to build a single source code file to perform the signature classification. The source code file will contains the required DSP routines, feature parameter functions and the classification algorithm to create a run-time version of the specified classifier. The stand-alone source code can later be integrated into NDE inspection systems in the field.

The technologies targeted for the SCDS are NDE and manufacturing process control. However, flexibility of the SCDS architecture will support analysis and classification of data originating from a large spectrum of technological areas--meteorology, geophysics, finance and marketing, biology, psychology, etc.

Not all components of the design architecture are provided in the initial prototype. Specifically, the classifiers and source code generator are not fully operational, but will be made available in future versions of the product. Currently, the SCDS supports data processing and feature generation. Further design specifications for the SCDS Version 1.02 is presented in the following sections.

USER INTERFACE AND DATA PROCESSING

Microsoft® Windows™ was selected as the interface between the user and the SCDS software tool-kit. Microsoft® Windows™ is a mouse supported operating system with a graphical user interface (GUI) to provide full text and graphics display. Microsoft® Visual Basic™ was selected to develop all displays in the SCDS GUI. Microsoft® Visual Basic™ is an object oriented high-level language which supports the Microsoft® Windows™ environment and Dynamic Link Libraries (Microsoft, 1991). Dynamic Link Libraries (DLL's) are standard Windows™ functional units that provide seamless integration between various programming languages.

The GUI interface provides the following control of the SCDS:

- selection of data files and signatures,
- allocation of signatures for training and verification sets,
- selection of DSP functions, templates, and gates,
- selection and calculation of signature feature parameters,
- graphical review of the features,
- selection of statistical tests and classification algorithms,
- source code generation,
- modification of the system libraries.

Where appropriate, process control and computations are achieved through DLL routines written in Borland® C++.

DSP AND FEATURE PARAMETERS

The success of any classification algorithm is dependent on the input parameters selected to represent each unique population. Ideally, the feature parameters chosen should exhibit the greatest orthogonality between the class populations, and address the underlying physics of the problem, therefore processing of the raw signatures may be necessary to obtain a robust set of parameters for classification of the various discontinuity types under investigation.

The SCDS data processing module supports 1-D digital signal processing, selection of templates to locate discontinuities in the signatures, assignment of (multiple) gates, and generation of feature vectors. The end objective of the data processing module is to produce input feature vectors for the classification algorithms, however, the module is mainly structured around the signature gates. In this regard, the user needs to specify which features to calculate from which user-defined gates.

A signature gate can be fixed-gate, with a specified starting and ending index, or can be a floating gate based on the templates used to locate discontinuities in the signatures. Pre- and post-processing, can be performed on the signature for locating discontinuities and transforming the data prior to calculation of the feature parameters. Specification of the data processing is recorded in a Microsoft® Access™ database, therefore, the number of possible gates is limited by availability of hard-disk space. Any or all of the features available in the library may be applied to each gate.

All the DSP and feature routines are implemented in Dynamic Link Libraries compiled under Borland® C++ for Windows, Version 4.02. The user has the capability to add new DSP routines, templates, and/or feature routines to the Libraries.

SIGNATURE CLASSIFICATION

The classification module will incorporate both artificial neural networks and statistical classifiers. The artificial neural network will be implemented using NeuralWorks Professional II/Plus, Version 4.2. The statistical classifiers will be implemented using SPSS® for Windows™, Release 6.1.

An artificial neural network (ANN) is an analytical procedure which can be used to develop nonlinear relationships between known discontinuity types and their corresponding ultrasonic features (Newman and Arcella, 1991). Several artificial neural network paradigms are available in the package, NeuralWorks Professional II/Plus (NeuralWare, 1993), and will be integrated into SCDS via a user-friendly graphical interface. The default neural network available in SCDS will be a three-layer back-propagation network.

SPSS® for Windows™ is a robust package providing extensive statistical capabilities, integrated graphics, and flexible reporting features. The SPSS® Developer's Kit provides a bridge to extend the functionality of SPSS® directly to privately developed applications.

The Developer's Kit will be used to provide SCDS access to the SPSS® Dynamic Link Libraries. Thus, all the statistical classification algorithms and data reduction techniques available in SPSS® will be fully supported by SCDS. In addition, SPSS® will be used to provide graphical representation of the feature parameter space, for example, histograms, scatter plots, box plots, etc.

In typical applications, the classification data set is randomly divided into a training set and verification set. The verification data set is not used in development of the classifier, but simply used as an analysis tool to evaluate the classifier. SCDS will provide full support to separate the data into training and verification data sets.

Source Code Generation

The end objective of SCDS is to provide the complete source code to implement the developed classification algorithm. Once a classifier has been selected the user may request source code generation of the classifier. The C source code will include:

- signal processing, templates, and gates,
- generation of parameter features,
- the classification algorithm.

All processing will be built into a single function call, requiring the signature as the input and returning the classification of the signature as the output. The source code will be inclusive, not requiring access to other library functions or the Windows operating system. The C source code can then provide direct transition of the classification technology to NDE equipment in the field or laboratory.

RESULTS - SCDS IMPLEMENTATION

SCDS is structured around four modules (Classes, Data, Features, Classify) which may be accessed through a main menu as shown Figure 1. The opening screen of SCDS permits the user to select a function **Library** for the classification project. The **Library** defines all signal processing and feature generation routines that available to SCDS. The selected **Library** may be one of the standard Libraries available in SCDS or be a custom Library developed by the user.

Each project has a self contained project file summarizing the data and processing to be performed on the signatures. Along with simple header information, the project file identifies the user's choice of signatures to process, including the true class of each signature and whether the signature should be treated as a training or testing signature. In addition, the project file defines all data processing to be performed, which includes the DSP routines defined by user, the templates used by the gates, definition of all signature gates, and the definition of features to be calculated on each gate.

A SCDS project can be started in one of two ways. The first is to start from scratch and build the entire project, specifying the data and processing routines. The second is to retrieve an existing project for modification using the **Load Project File** menu command.

When defining a new project, the first task is to define the discontinuity classes representative of the data set. This is initiated by selecting the **Classes** menu command. Once the classes have been defined, the next step is select the signatures for classification. Selecting the **Data** menu command brings up the **Signal List** window shown in Figure 2. From the **Signal List** window the user may: 1) add/delete signatures to the project, 2) define the classification of each signature, 3) select signatures for the training and test set, 4) graphically review each signature, and 5) select signatures for interactive evaluation in the **Define Gates and Features** window.

In SCDS Version 1.02, each data file is treated as a single signature. Thus, even though the user may add/define input routines in SCDS to read the raw data, the data must first be organized into separate signature files. In future versions of SCDS, the capability to read single files with multiple signatures may be added.

Selecting the **Features** menu command in the main window opens the **Define Gates and Features** window shown in Figure 3. This window provides interactive analysis of the signatures to set-up the data processing and feature generation routines. Structurally, the **Define Gates and Features** window is comprised of a graphic display and four folders: 1) Signal Processing, 2) Template, 3) Gate, and 4) Feature. The graphic display permits the user to interactively zoom-in on portions of the signature and review the signal processing results, while the four folders contain spread-sheets to define and structure the processing of the signatures.

The Signal Process folder permits the user to select functions from the Library and build processing groups. The signal process group can be as simple as one function or may contain a sequence of functions selected from the Library List. On-line help is available for each Library function to clarify the definition of each process and to define any optional script control parameters for the process.

By selecting the various arrow buttons in the Signal Process Execution panel, the user can immediately review the results of the function on the signature. An executed function is proceed by an "X" in the selected list as shown in Figure 3. The signal processing groups developed by the user are recorded in the database and may to used to preprocess the signatures before execution of a template and to post-process the signature gate prior to calculating a parameter feature.

The Template folder operates in conjunction with the Gate folder. Within this folder the user can select templates routines from the Library to isolate the location (index) of a particular characteristic of the signature. For example, a template may be a routine to determine the starting location or ending location of a discontinuity in the signature or a template may perform a cross-correlation with a reference signature to determine the location of a particular discontinuity type. SCDS supports user defined templates, thus the template routines can be tailored to a specific application. Lastly, while in the Template folder the user can execute each defined template and SCDS will perform the process on the signature and indicate the returned template index by drawing an appropriate vertical line on the graph.

The Gate folder provides a spread-sheet to define various gates for the signatures. In essence the user must define a method to establish the starting and ending location of each desired gate. A gate may be a fixed gate, a variable gate or a combination of both.

For each gate a signal processing group may be selected for post-processing of the gate prior to calculation of the features. For example, the user may define a gate based on template processing of the time signature, and then perform a wavelet transformation of the signature in the gate, or the user could define a similar gate whereas the end process is to take the absolute value of the time-based signature. As with the Template folder, the user may interactively view the execution of the defined gates, including post processing, on the signature in the graphic window.

The last folder in the **Define Gates and Features** window is the Feature folder. In this folder the user can select features available in the Library to calculate on each gate. In addition, on-line Help is provided to describe the features available in the Library and clarify the script control parameters of each feature. By selecting the Calculator Button in the Feature folder, SCDS will process the signature and display the calculated feature in a spreadsheet format. Currently, SCDS is designed to support function calls that calculate only a single parameter for a feature. Lastly, the user may add his/her own feature routines to the Library.

In summary, the **Define Gates and Features** window provides an interactive environment to define all the processing and calculations on the data set. The user can immediately verify the how the signatures will be processed by the routines. Once all the routines have been defined, SCDS can run in a batch mode to process all the signatures in the data set and generate a feature vector file.

FUTURE WORK

At present, the DSP module is nearly complete. Minor modifications are necessary to support batch mode processing and addition of user-defined routines to the Libraries. These modification are scheduled for completion in the Fall of 1995.

Future enhancements scheduled for the Signature Classification Development System include:

1) Artificial Neural Network Module - Integration of SCDS to the neural network package NeuralWare Professional II/Plus. This module will support various feed forward networks and will permit classification of both the raw signatures and feature parameters.

2) Statistical Classifier Module - Integration of SCDS to the statistical package SPSS. This module will provide algorithms to investigate the feature parameter space and to select features for classification. This module will include both parametric and nonparametric statistical classifiers.

3) Source Code Generator - Upon completion of a project this module will build into a single C source code file all the components necessary to perform the signal processing, feature generation and classification of an input signature.

SUMMARY

The SCDS is a development tool to transfer classification technologies to field equipment. The SCDS supports data selection, digital signal processing, generation of pattern vectors, and classification algorithms. The SCDS pulls together the tools necessary to analyze the data, determine significant characteristics of the data, and develop a classifier for field application.

The current version of SCDS supports the data processing module whereas the user may define as processing of the signatures and generate feature parameter vectors for classification. Future versions of SCDS will support the classification module and code generation module.

The SCDS is geared towards the technological fields of nondestructive testing and manufacturing process control, however upon completion the system will support the general analysis of feature vectors. In this regard, this system is truly a generic tool-kit for developing classification algorithms.

REFERENCES

Brown, L.M., Newman, R.W., DeNale, R., Lebowitz, C.A., and Arcella, F.G., 1992, "Graphite Epoxy Defect Classification of Ultrasonic Signatures Using Statistical and Neural Network Techniques," in *Review of Progress in Quantitative Nondestructive Evaluation*, Plenum Press, New York, Vol. 11A, pp. 677-696.

Friesel, M.A., Barga, R.S., Dawson, J.F., Hutton, P.H., Kurtz, R.J., and Lemon, D.K., 1992, "Acoustic Emission Applications on the NASA Space Station," in *Review of Progress in Quantitative Nondestructive Evaluation*, Plenum Press, New York, Vol. 11A, pp. 725-732, 1992.

Hull, B. and John, V., 1988, *Non-destructive Testing*, Springer-Verlag New York Inc., New York, NY.

Kitahara, M., Achenbach, J.D., Guo, Q.C., Peterson, M., Ogi, T., and Notake, M., 1991, "Depth of Surface-breaking Cracks by a Neural Network," in *Review of Progress in Quantitative Nondestructive Evaluation*, Plenum Press, New York, Vol. 10A, pp. 689-696.

Microsoft Corporation, 1991, *Microsoft® C/C++ Version 7.0, Environment and Tools*, Microsoft Corporation, Redmond, WA.

Newman, R.W. and Arcella, F.G., March 1991, "Neural Network Analysis of Ultrasonic NDE Wave Forms," 1991 American Society of Nondestructive Testing Meeting.

Ogi, T., Notake, M., Yabe, Y., and Kitahara, M., 1991, "Application of Neural Network to Classification of Defects: Basic Study of Weights," in *Review of Progress in Quantitative Nondestructive Evaluation*, Plenum Press, New York, Vol. 10A, pp. 683-688.

NeuralWare, Inc., 1993, *Neural Computing, A Technology Handbook for Professional II/Plus and Neural Works Explorer*, NeuralWare, Inc, Pittsburgh, PA.

Schwartz, L.H., 1991, "Nondestructive Evaluation and Material Processing," in *Review of Progress in Quantitative Nondestructive Evaluation*, Plenum Press, New York, Vol. 10A, pp. 35-50.

Song, S.J. and Schmerr, Jr., L.W., 1991, "Ultrasonic Flaw Classification in Weldments Using Neural Networks," in *Review of Progress in Quantitative Nondestructive Evaluation*, Plenum Press, New York, Vol. 10A, pp. 697-704.

Udpa, L. and Udpa, S.S., 1990, "Eddy Current Defect Characterization using Neural Networks," *Materials Evaluation*, Vol. 48, No. 3, pp. 342-347.

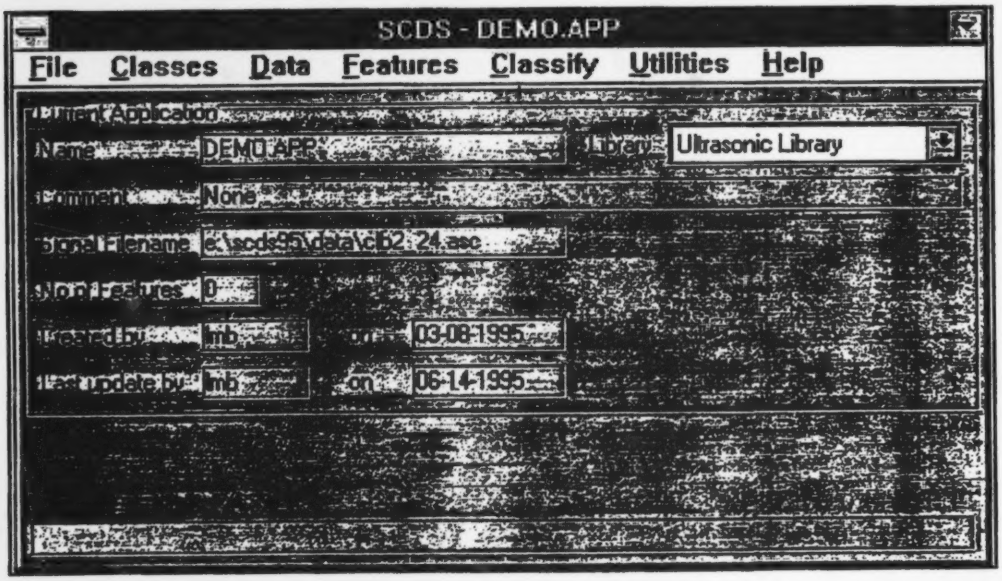
SCDS - DEMO.APP
File
Classes
Data
Features
Classify
Utilities
Help
Current Application

Name DEMO.APP Library Ultrasonic Library
Comment None
Signal Filename e:\scds95\data\clb2_24.asc
No of Features 0
Created by lmb on 03-08-1995
Last update by lmb on 06-14-1995

Figure 1. SCDS main window.

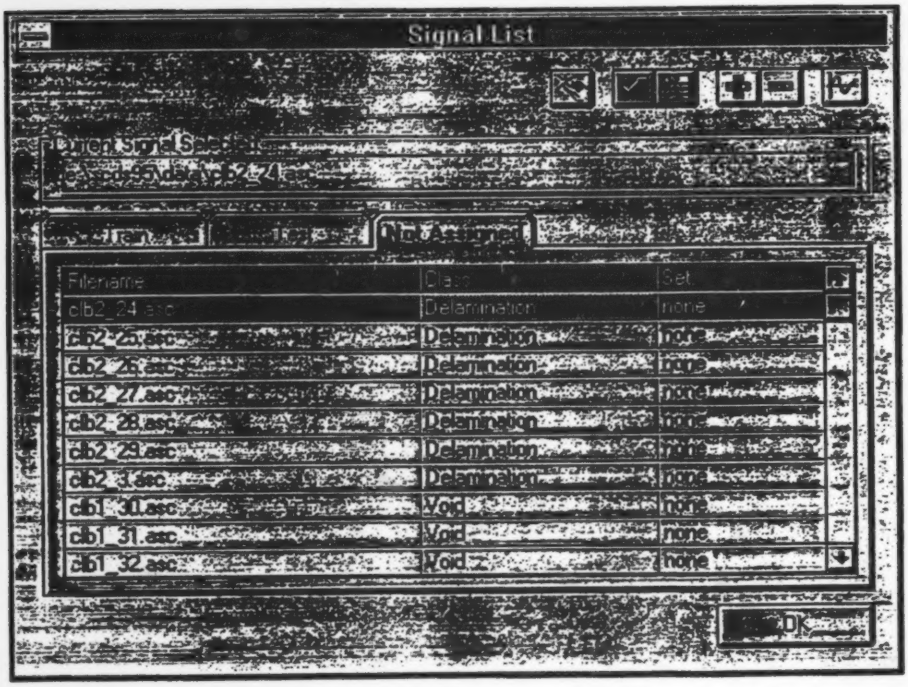
Signal List
Train
Not Assigned
OK

e:\scds95\data\clb2_24.asc

Filename	Class	Set
clb2_24.asc	Delamination	none
clb2_25.asc	Delamination	none
clb2_26.asc	Delamination	none
clb2_27.asc	Delamination	none
clb2_28.asc	Delamination	none
clb2_29.asc	Delamination	none
clb2_3.asc	Delamination	none
clb1_30.asc	Void	none
clb1_31.asc	Void	none
clb1_32.asc	Void	none

Figure 2. SCDS Signal List window.

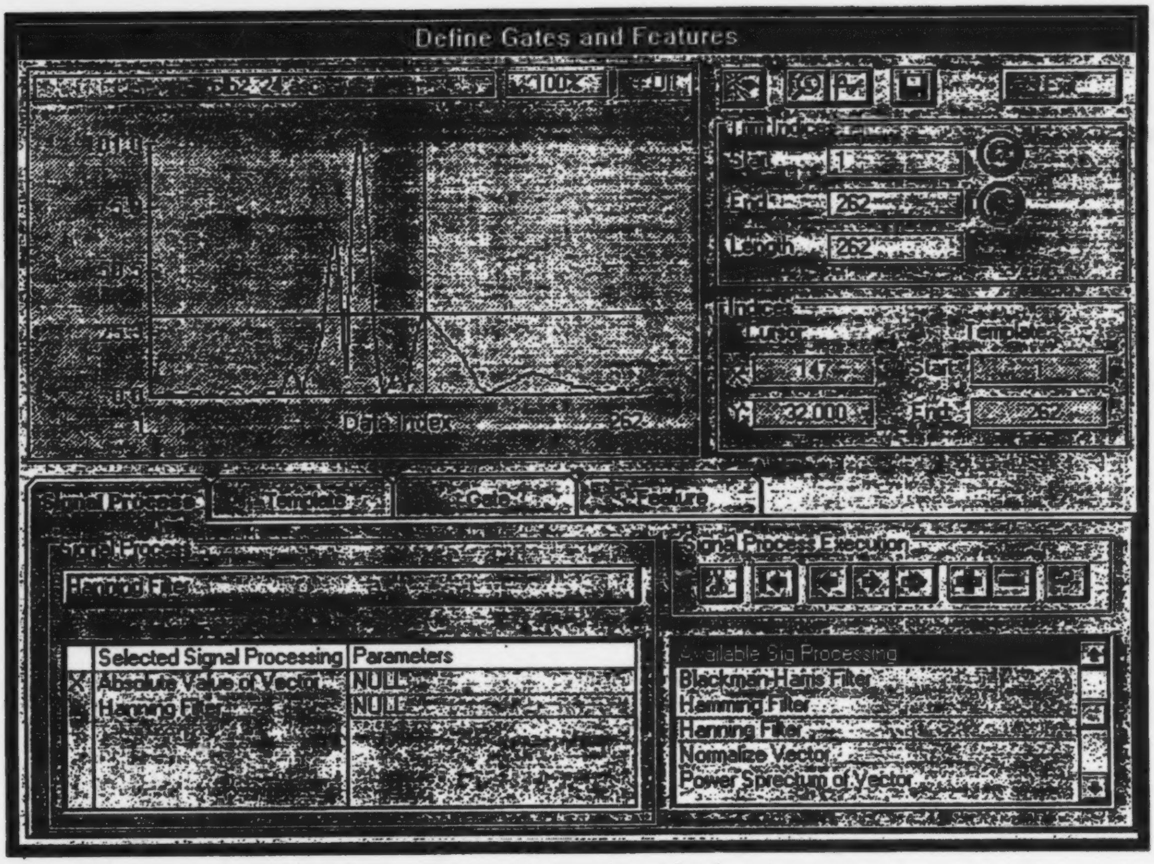
Define Gates and Features
100%
Exit
Trim Indices
Indices
Cursor
Templates
Data Index
1
262
Signal Process
Template
Gate
Feature
Signal Process Execution

Start 1
End 262
Length 262

X 147
Y 32.000

Start 1
End 262

Signal Process: Hanning Filter

	Selected Signal Processing	Parameters
X	Absolute Value of Vector	NULL
	Hanning Filter	NULL

Available Sig Processing
- Blackman-Harris Filter
- Hamming Filter
- Hanning Filter
- Normalize Vector
- Power Sprectum of Vector

Figure 3. SCDS **Define Gates and Features** window showing Signal Process folder.

#510350 C

NDE for Thick Section Composite Laminates

by Carol Lebowitz

Naval Surface Warfare Center, Carderock Division, Annapolis Detachment,
Annapolis, Maryland

ABSTRACT

NDE of Thick Section, Laminated Composites

by Carol Lebowitz

Carderock Division

Naval Surface Warfare Center

2 May 1995

NDE of Thick Section, Laminated Composites

> "The application of fiber-reinforced polymer matrix composites to U.S. Navy surface ships systems offers the potential for significant weight, cost and signature reductions."

Gagorik, Corrodo, and Kornbau
Proceedings of the 36th International SAMPE
Symposium, April 1991

NDE of Thick Section, Laminated Composites

Current applications for composites on submarines and surface ships

- submarine bow sonar domes
- towed array fairings
- sonar windows
- minehunter hulls
- other applications like seawater piping, pumps and ventilation ducting

Gagorik, Corrodo and Kornbau, SAMPE 1991

NDE of Thick Section, Laminated Composites

Potential Composite Ship Structures

Gagorik, Corrodo and Kornbau, SAMPE 1991

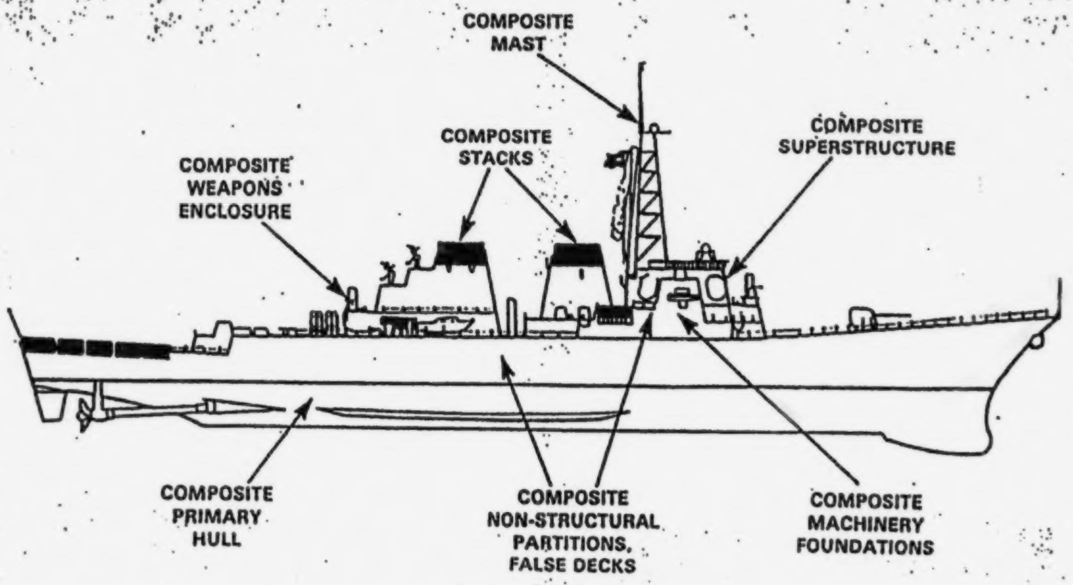
COMPOSITE MAST
COMPOSITE STACKS
COMPOSITE WEAPONS ENCLOSURE
COMPOSITE SUPERSTRUCTURE
COMPOSITE PRIMARY HULL
COMPOSITE NON-STRUCTURAL PARTITIONS, FALSE DECKS
COMPOSITE MACHINERY FOUNDATIONS

NDE of Thick Section, Laminated Composites

Challenges:

- anisotropic, inhomogeneous material
- many potential defect types (i.e., voids, delaminations, inclusions, resin variations, fiber breakage & wrinkles, etc.)
- no predominant failure mode
- presence of “acceptable flaws”
- manufacturing vs. service-induced defects
- large structures
- lack of defect and calibration standards

NDE of Thick Section, Laminated Composites

Classification of Defects in Thick Section Graphite Epoxy Test Blocks

- Objective: To demonstrate the feasibility of using neural networks to classify defect types in thick section gr/ep material
- Approach:
  - construct thick section gr/ep test blocks with known defects at midply and near front surface
  - signal acquisition using immersion UT system
  - select features from power spectrum
  - defect classification using an artificial neural network

NDE of Thick Section, Laminated Composites

Classification of Defects in Thick Section Graphite Epoxy Test Blocks

- Status:
  - 8 specimens examined
  - 6 features from power spectrum selected
  - back propagation neural network analysis resulted in 91% classification accuracy for both training and test sets

COMPOSITE DEFECT CLASSIFICATION

CONSTRUCTION -

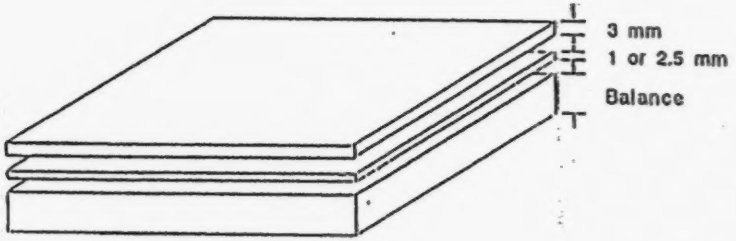

1/8 THICKNESS

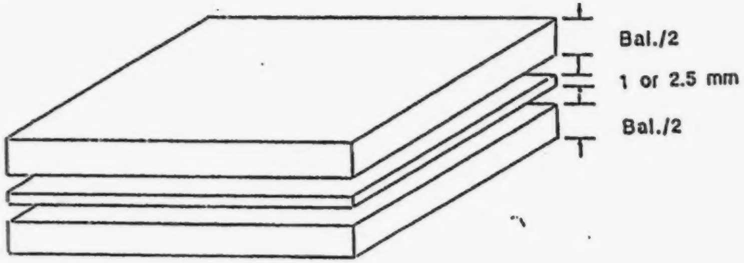

MIDPLANE

ID	PANEL DESCRIPTION	SUB-PANEL THICKNESS	SUB-PANEL PLACEMENT
A1	REFERENCE	NONE	
A2	REFERENCE	8-PLY	MIDPLANE, PLIES 92-99
B1	DELAMINATION	8-PLY	1/8 THICKNESS, PLIES 24-31
B2	DELAMINATION	8-PLY	MIDPLANE, PLIES 92-99
D1	POROSITY[1]	20-PLY	1/8 THICKNESS, PLIES 24-44
D2	POROSITY	20-PLY	MIDPLANE, PLIES 87-106
F1	CONTAMINATION[2]	8-PLY	1/8 THICKNESS, PLIES 24-31
F2	CONTAMINATION	8-PLY	MIDPLANE, PLIES 92-99

[1] Air
[2] Peel Ply

·RESULTS - SAMPLE RF WAVEFORM

F2

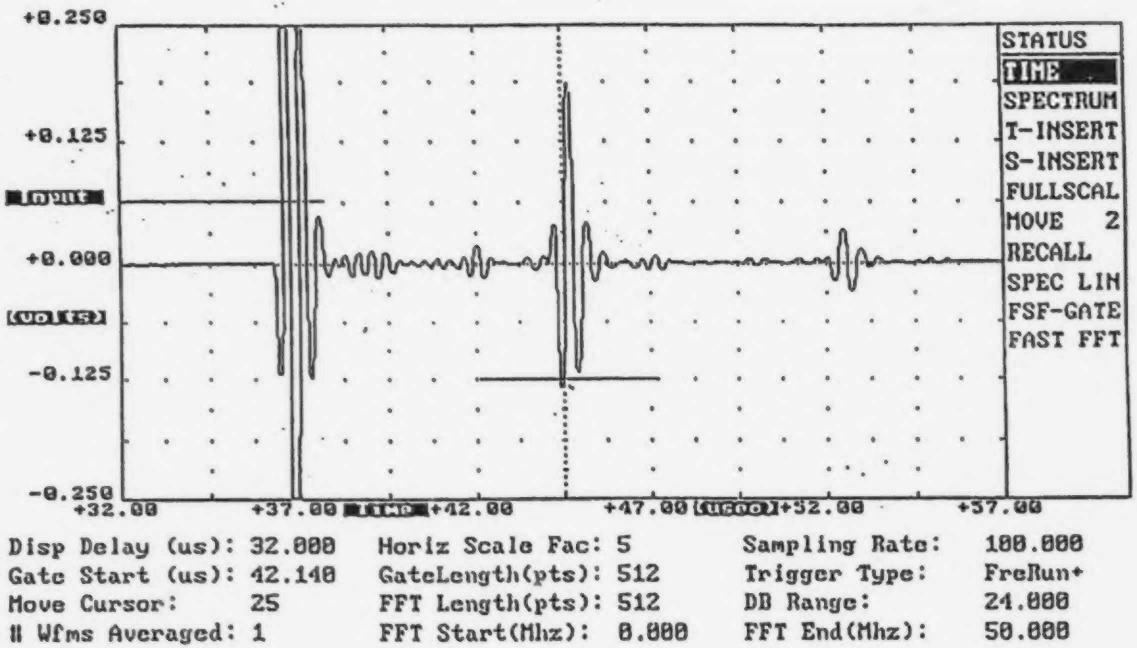
+0.250
+0.125
+0.000
(volts)
-0.125
-0.250
+32.00
+37.00
TIME
+42.00
+47.00
(usec)
+52.00
+57.00
STATUS
TIME
SPECTRUM
T-INSERT
S-INSERT
FULLSCAL
MOVE 2
RECALL
SPEC LIN
FSF-GATE
FAST FFT

```
Disp Delay (us): 32.000   Horiz Scale Fac: 5         Sampling Rate:   100.000
Gate Start (us): 42.140   GateLength(pts): 512       Trigger Type:    FreRun+
Move Cursor:     25       FFT Length(pts): 512       DB Range:        24.000
# Wfms Averaged: 1        FFT Start(Mhz):  0.000     FFT End(Mhz):    50.000
```

COMPOSITE DEFECT CLASSIFICATION

RESULTS - SELECTED FEATURES

- PEAK FREQUENCY, MHz (g)
- BANDWIDTH @ -6dB DOWN (h-f)
- SPECTRAL SKEW @ -6dB DOWN (h-g)/(g-f)
- SPECTRAL ENERGY @ 1.95 MHz
- SPECTRAL FIRST MOMENT, MHz
- SPECTRAL SECOND MOMENT, MHz

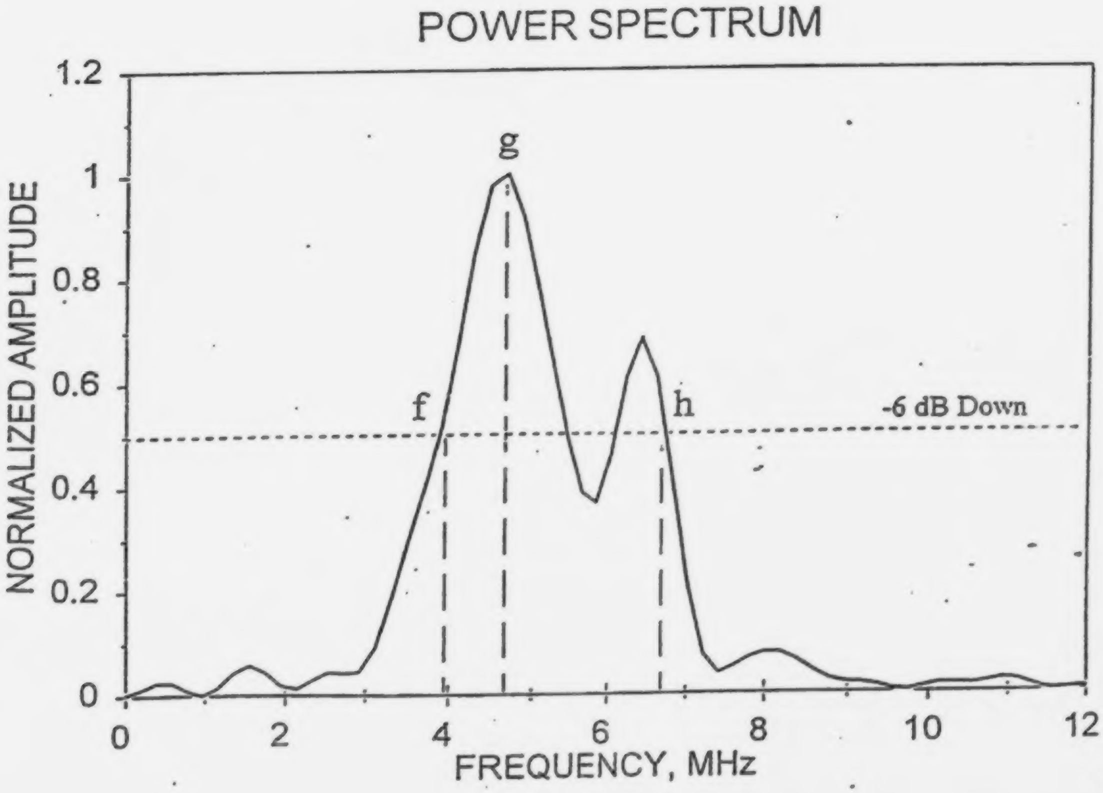

RESULTS - POWER SPECTRA FEATURES

FEATURE SCATTER DIAGRAM

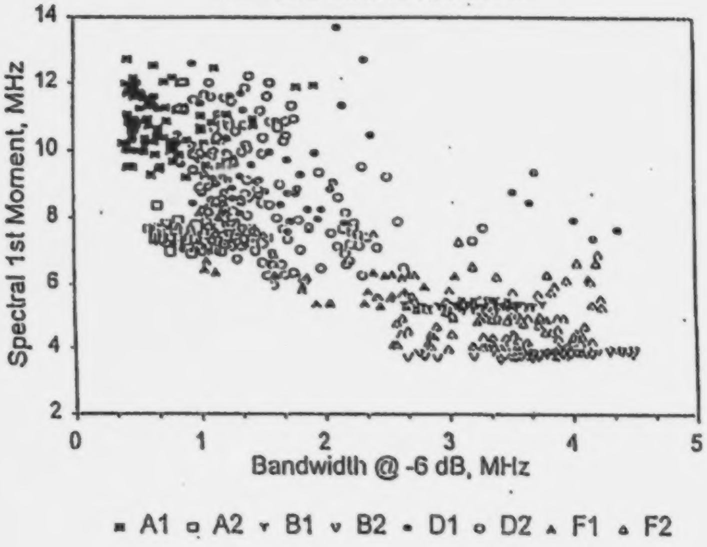

FEATURE SCATTER DIAGRAM

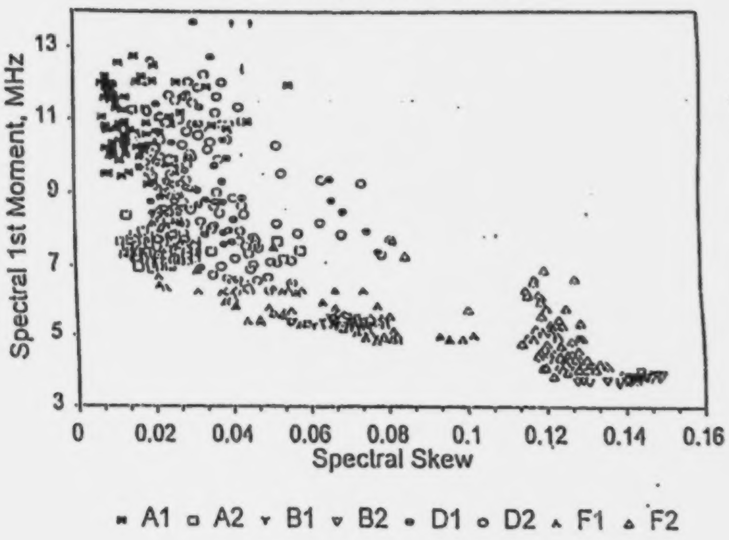

FEATURE SCATTER DIAGRAM

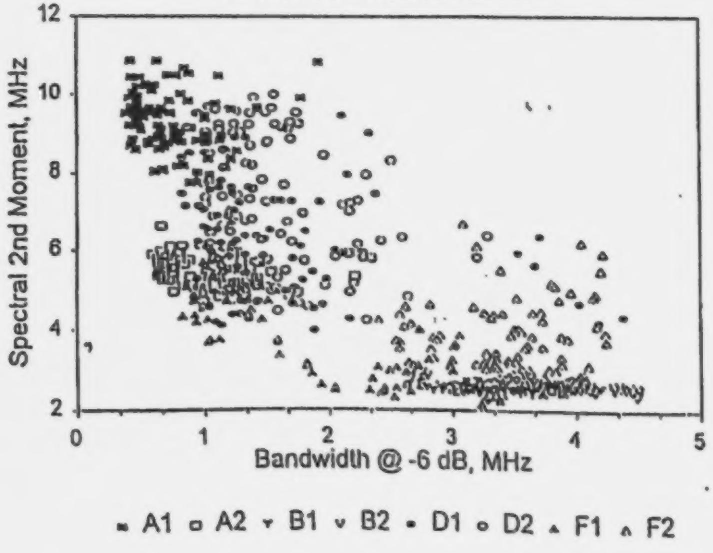

FEATURE SCATTER DIAGRAM

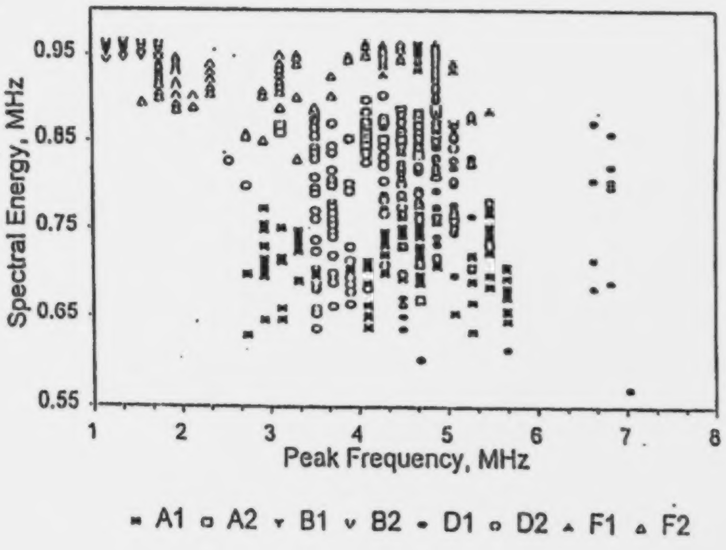

COMPOSITE DEFECT CLASSIFICATION

ARTIFICIAL NEURAL NETWORK -

- BACK PROPAGATION PARADIGM (NEURALWORKS PROFESSIONAL II)
- NORMALIZED CUMULATIVE DELTA LEARNING RULE
- HYPERBOLIC TANGENT TRANSFER FUNCTION
- 6 INPUT NEURONS, 9 NEURONS IN HIDDEN LAYER
- OBSERVATIONS IN CLASSIFICATION DATA (TEST SET RANDOMLY SELECTED BEFORE TRAINING)

CLASS	TRAIN	TEST
A1	90	10
A2	90	10
B1	90	10
B2	90	10
D1	90	10
D2	90	10
F1	69	9
F2	81	9
TOTAL	690	78

POWER SPECTRUM

INPUT FEATURES

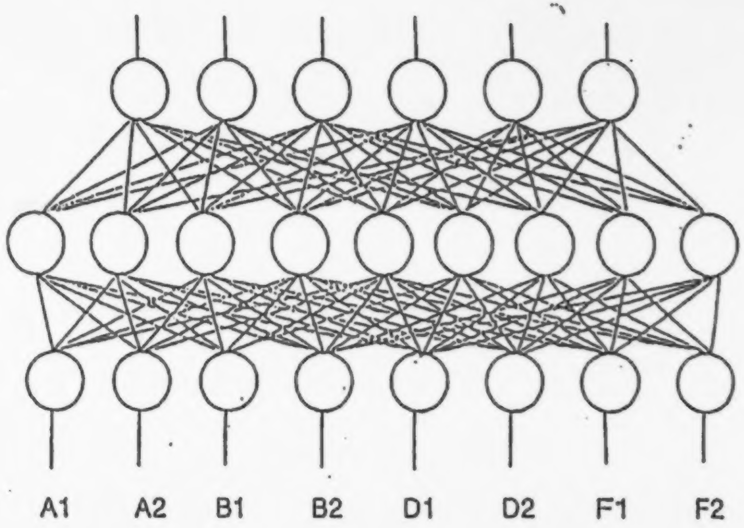

DEFECT CLASSIFICATION

- TRAINING ITERATIONS: 82,807

COMPOSITE DEFECT CLASSIFICATION

CLASSIFICATION RESULTS - TRAINING DATA

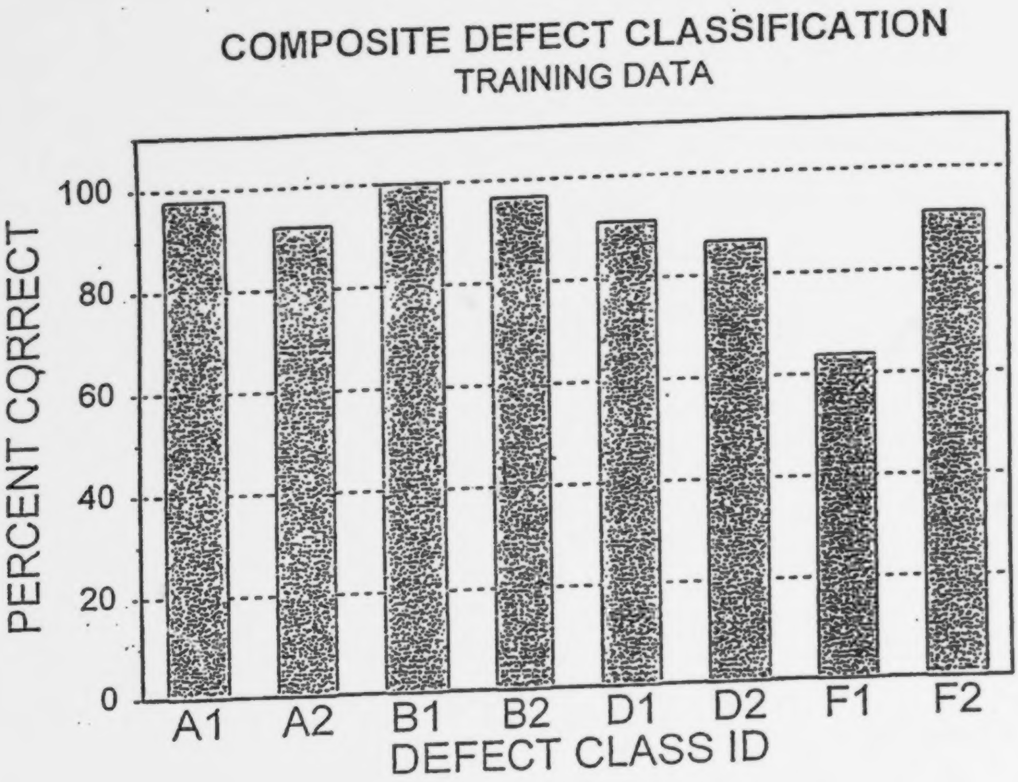

		NEURAL NETWORK CLASSIFICATION*											
		A1	A2	B1	B2	D1	D2	F1	F2	N	NOT CORRECT	CORRECT	PERCENT CORRECT
	A1	88	0	0	0	0	0	0	0	90	2	88	97.8
	A2	0	83	0	0	0	3	0	0	90	7	83	92.2
	B1	0	0	90	0	0	0	0	0	90	0	90	100.0
TRUE CLASS	B2	0	0	0	87	0	0	0	0	90	3	87	96.7
	D1	0	0	0	0	82	0	3	0	90	8	82	91.1
	D2	0	0	0	0	0	78	0	0	90	12	78	86.7
	F1	0	2	0	0	4	0	44	0	69	25	44	63.8
	F2	1	0	0	0	1	0	0	74	81	7	74	91.4
						TOTAL				690	64	626	90.72

*Class assignment for neuron output > 0.6.

COMPOSITE DEFECT CLASSIFICATION

CLASSIFICATION RESULTS - TEST DATA

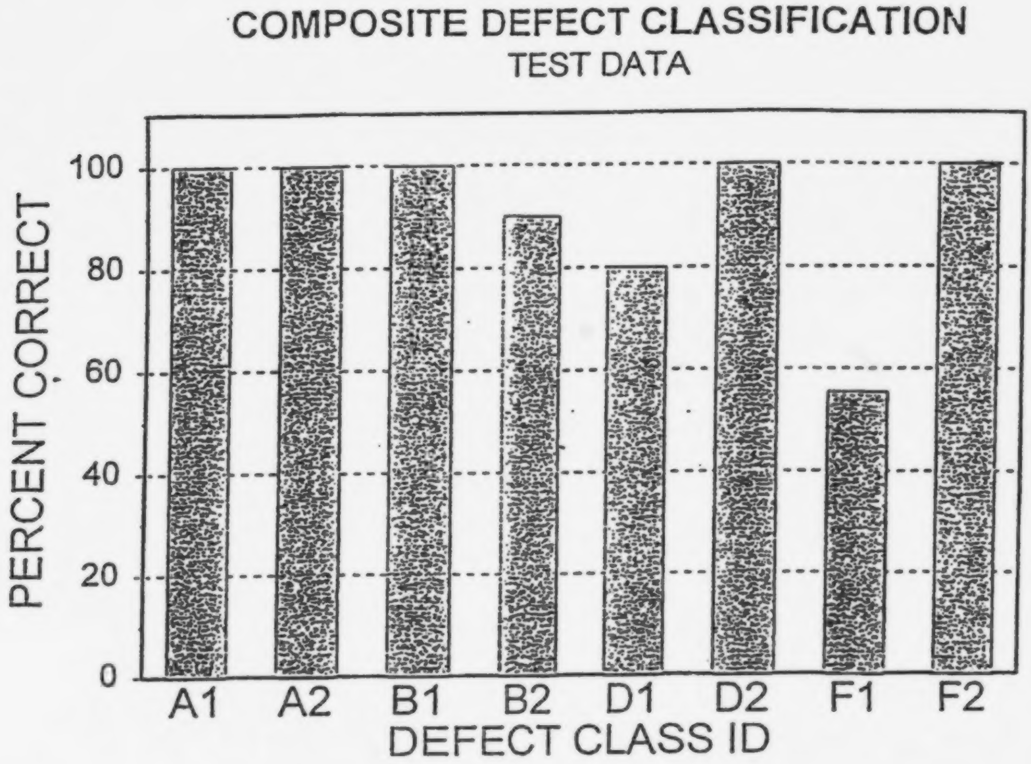

		NEURAL NETWORK CLASSIFICATION*											
		A1	A2	B1	B2	D1	D2	F1	F2	N	NOT CORRECT	CORRECT	PERCENT CORRECT
	A1	10	0	0	0	0	0	0	0	10	0	10	100.0
	A2	0	10	0	0	0	0	0	0	10	0	10	100.0
	B1	0	0	10	0	0	0	0	0	10	0	10	100.0
TRUE	B2	0	0	0	9	0	0	0	0	10	1	9	90.0
CLASS	D1	0	0	0	0	8	0	0	0	10	2	8	80.0
	D2	0	0	0	0	0	10	0	0	10	0	10	100.0
	F1	0	0	1	0	0	0	5	0	9	4	5	55.6
	F2	0	0	0	0	0	0	0	9	9	0	9	100.0
						TOTAL				78	7	71	91.03

*Class assignment for neuron output > 0.6.

NDE of Thick Section, Laminated Composites

Thickness Gaging on a GRP Frame Structure

- Objective: To perform thickness gaging at approximately 175 locations on a GRP machinery cradle.
- Approach:
  - used Krautkramer Branson USD-10 with KB-Aerotech 1”diameter, 500 kHz delay line transducer
  - calibrations performed using:
    - for thicknesses up to 1”, step wedge cut from cradle material
    - for thicknesses from 1” to 2”, used accessible section of known “good” cradle material
  - variety of couplants used - Sonotech High Viscosity Soundclear was selected for this application

NDE of Thick Section, Laminated Composites

Thickness Gaging on a GRP Frame Structure

- Results:
  - at most locations, a backwall was readily discernable, thus permitting thickness measurement
  - A-scans contained obvious evidence of the layered nature of material
  - required approximately 10dB more gain to penetrate the 2” material (vs. 1” material)
  - inspection accuracy approximately +/- 1 mm
- Lessons Learned?????

NDE of Thick Section, Laminated Composites

Thickness Gaging on a GRP Frame Structure

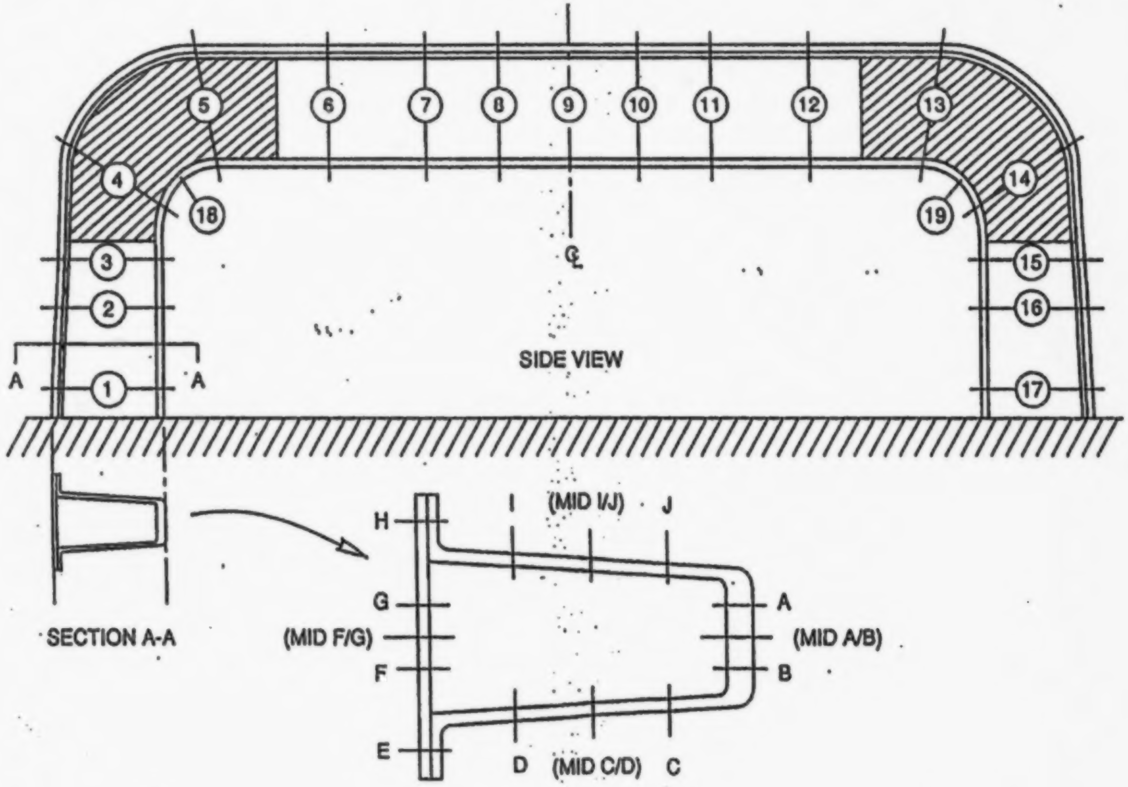

1
2
3
4
5
6
7
8
9
10
11
12
13
14
15
16
17
18
19
℄
SIDE VIEW
A
A
SECTION A-A
H
G
(MID F/G)
F
E
I
(MID I/J)
J
A
(MID A/B)
B
D
(MID C/D)
C

NDE of Thick Section, Laminated Composites

Inspection of a Large GRP Structure

- Objective: NDE of a very thick section (up to 8”), large area, GRP structure
- Approach:
  - identify specific locations to be monitored
  - for UT inspection:
    - independent measure of longitudinal velocity
    - transducer and equipment evaluation
    - calibration standard requirements & design
    - identify limitiations of inspection
  - Identify other potential inspection methods such as visual & microwave

NDE of Thick Section, Laminated Composites

Inspection of a Large GRP Structure

- Independent measure of longitudinal velocity:
  - measurements using point-source/point receiver (PS/PR) ultrasonic technique.
  - two samples evaluated: a plate-like specimen measuring 1” in thickness, and a semi-circular “cut-out” measuring 5.5” thick.
  - resulting measured longitudinal velocities:
    - for 1” sample, V_L= 2.77mm/us
    - for 5.5” sample, V_L = 2.66 mm/us
  - amplitude of signal greatly influenced by thickness

NDE of Thick Section, Laminated Composites

Inspection of a Large GRP Structure

- ➢ independent measure of longitudinal velocity
- ➢ longitudinal wave, pulse echo techniques used to measure time of flight through a 1" thick block of GRP material
- ➢ mechanical thickness measurements made at same locations with a micrometer
- ➢ longitudinal velocity calculated to be 2.66 +/-0.40 Km/s.

NDE of Thick Section, Laminated Composites

Inspection of a Large GRP Structure

- ➢ transducer and equipment evaluation
- ➢ evaluation of the wave penetration capability and influence of transducer frequency and diameter for a thick section of the GRP material (13 cm thick)
  - ➢ frequencies of 0.5 MHz or lower have better penetration capability
  - ➢ large diameter transducers (0.75” - 1”) are more efficient and powerful for generating and receiving ultrasonic signals
  - ➢ dual element transducers provided higher SNR

NDE of Thick Section, Laminated Composites

Inspection of a Large GRP Structure

- transducer and equipment evaluation (cont.)
  - 3 types of UT instruments tried on actual structure with selected transducer
    - analog instrument - penetration depth ~ 0.5”
    - “older” digital instrument - penetration depth ~ 1-1/2”
    - “state-of-the-art” digital instrument - penetration depth ~ 3”

NDE of Thick Section, Laminated Composites

Microwave Inspection

Example: 10 GHz scan of 90 x 53 mm area with defect on a GRP panel. Left image obtained w/ standoff of 1.6 mm, right image w/ standoff of 14.25 mm. Left image shows inclusion; right shows variations in sample thickness.

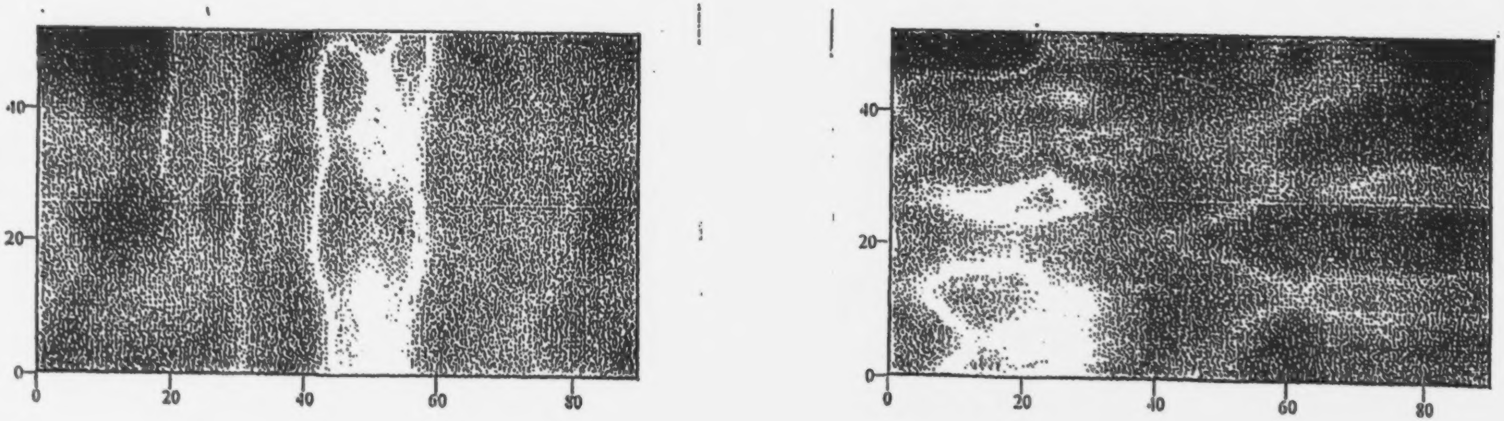

NDE of Thick Section, Laminated Composites

Summary

- Composite usage increasing/many advantages to using composites for shipboard structures
- Many challenges associated with inspecting thick section composites
- Variety of techniques in NDE Toolbox
- Near-term requirement for inspecting a large GRP structure

#510351

NDE for Thick Section, Layered Composite Structures

Johnnie DeLoach

Naval Surface Warfare Center, Carderock Division, Annapolis Detachment

ABSTRACT

OBJECTIVE

EVALUATE/DEVELOPMENT TECHNIQUES TO INSPECT LAYERED AND SANDWICH STRUCTURES

- MANUFACTURING AND IN-SERVICE INSPECTIONS
- MIL-STD-271 AND ADVANCED TECHNIQUES

NDE of Thick Section, Layered Materials

- **INSPECTION THROUGH LAYERED MATERIALS**
- **URETHANE-COATED METALLIC COMPONENTS**
- **THICK, SANDWICH COMPOSITES**

Inspection Through Layered Materials

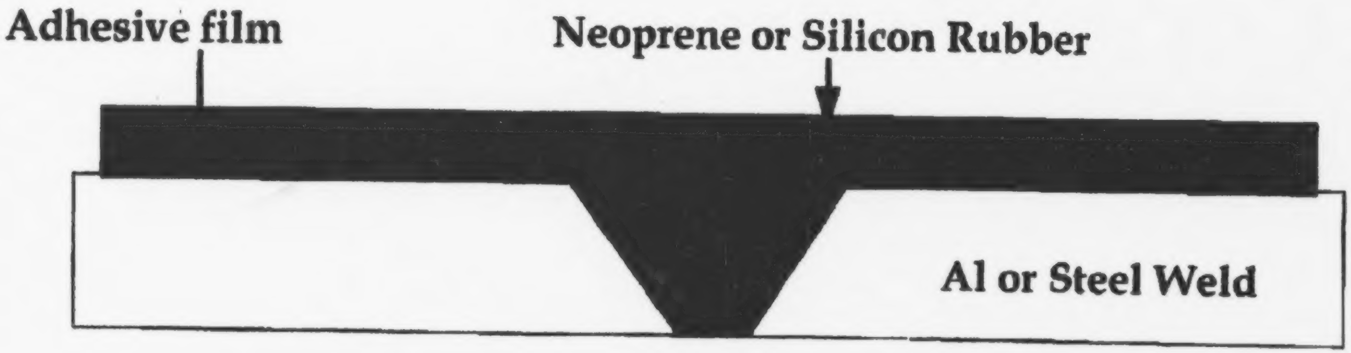
Adhesive film
Neoprene or Silicon Rubber
Al or Steel Weld

- •PREVENTS VT OF WELDS
- •DEGRADES X-RAY RT IMAGE
  - – PENETRAMETER NOT VISIBLE
- •DEGRADES UT SIGNAL
  - – NO RETURN SIGNAL @ 2.25MHz

Inspection Through Layered Materials

EXPERIMENTAL MATRIX

- *Al 5456 Weldments*
  - No defects
  - Lack of fusion
  - Clustered Porosity
  - Scattered Porosity

- *3 Types of Layered Materials*
  - 2 Neoprene rubber foam based
  - 1 Silicon rubber foam based

Inspection Through Layered Materials

C-SCAN SETUP

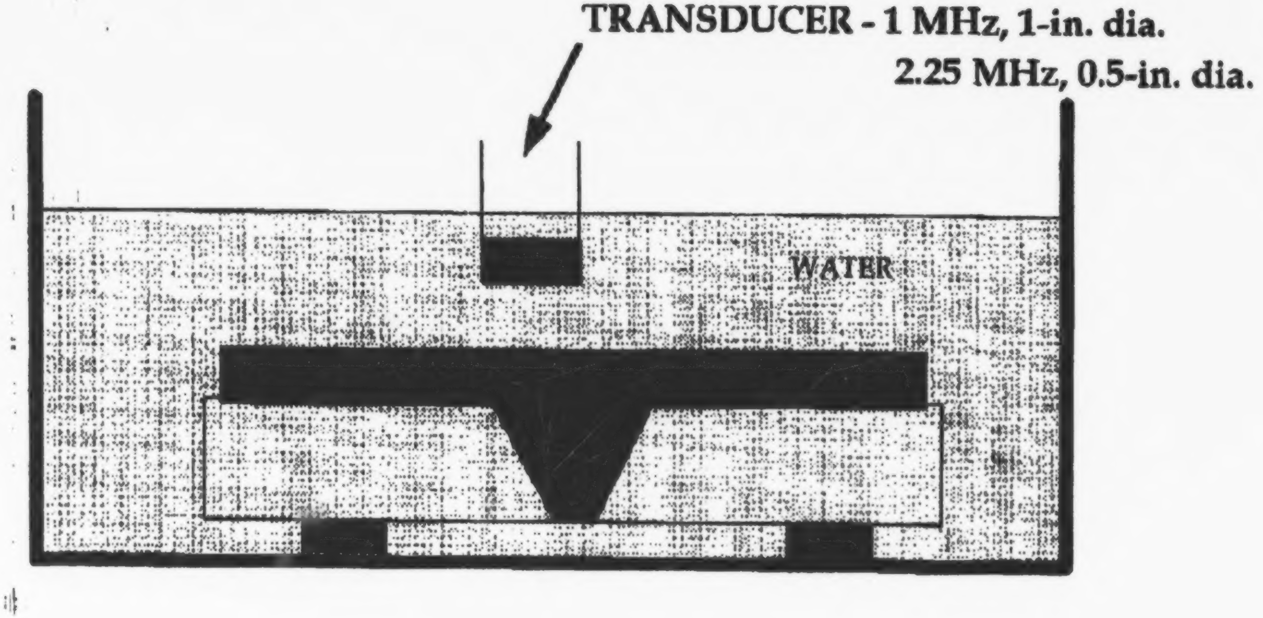
TRANSDUCER - 1 MHz, 1-in. dia.
2.25 MHz, 0.5-in. dia.
WATER

Inspection Through Layered Materials

Ultrasonic Velocity (Longitudinal)

Aluminum	**0.25**
Neoprene 1	**0.046**
Neoprene 2	**0.017**
Silicon	**0.022**

Operator: CAL
Transducer S/N: v306
Nominal Cntr Freq: 2.25
Energy: 2
Gain: 40
Comment1: a/d brd - 500mv
Comment3:

Transducer Type: 2.25MHz,.5",flat
Transducer Mfr: panametrics
Attenuation: 20
Damping: 4
HP Filter: .3
Comment2:
Comment4:

Par File: RD7.CSP **Data Dir:** C:\DATA **Data File:**

Gate Number: 2 AMP

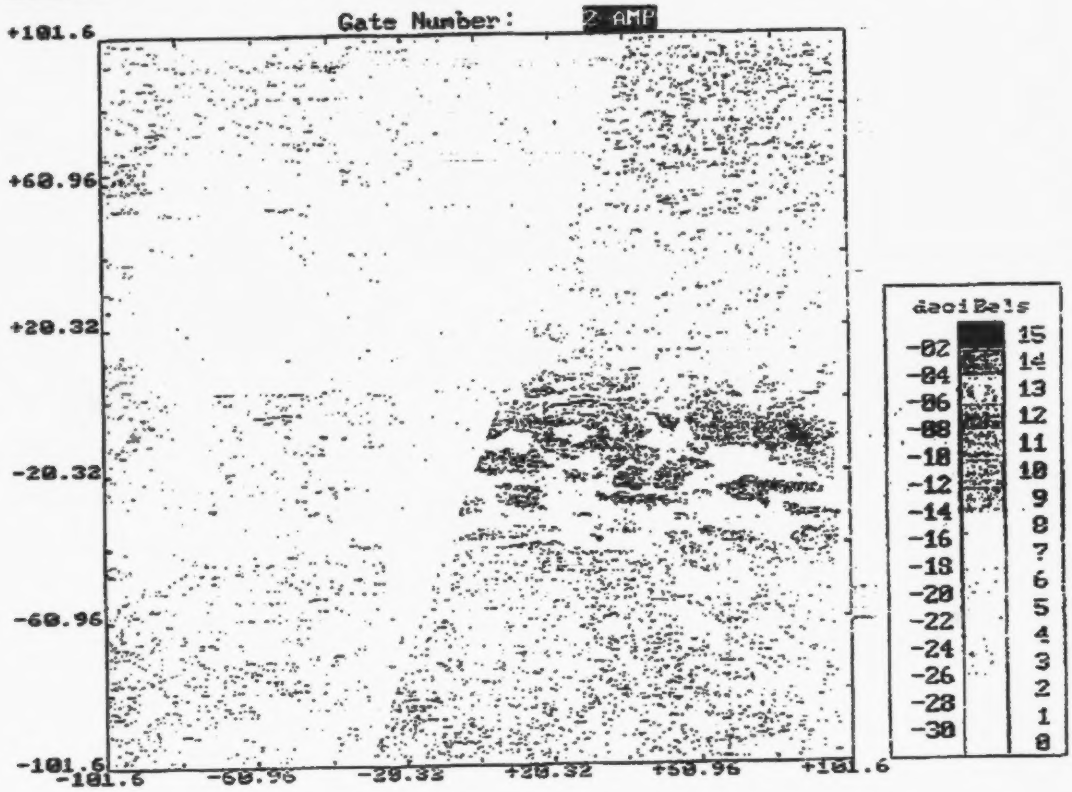

PART I.D. Number:	RD2	PART TYPE:	ST PLT W/TYP 3R CT
Operator:	CAL	Transducer Type:	1MHz, 1"DIA FLAT
Transducer S/N:	A302R	Transducer Mfr:	panametrics
Nominal Cntr Freq:	1	Attenuation:	20
Energy:	3	Damping:	2.75
Gain:	40	HP Filter:	.1
Comment1:	a/d brd - 500mv	Comment2:	
Comment3:		Comment4:	

Par File: RD13.CSF **Data Dir:** C:\DATA **Data File:**

Gate Number: 2 AMP

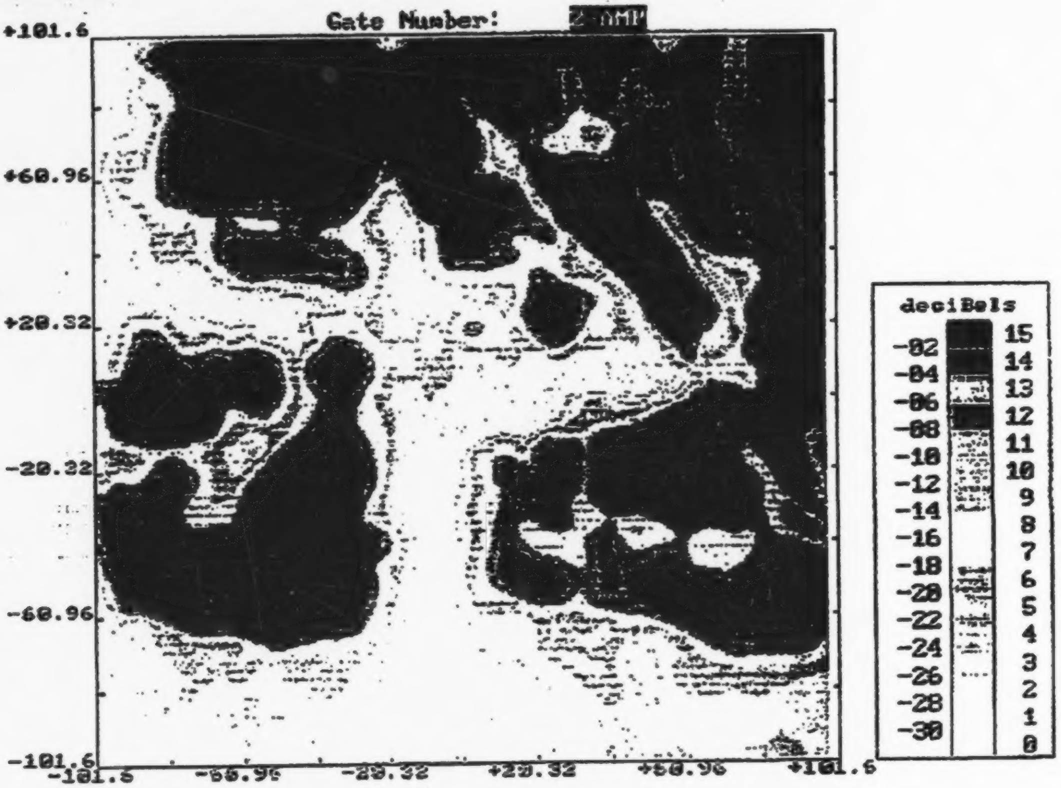

NDE of Urethane-Coated Metals

MORE AFFORDABLE MANUFACTURING
THROUGH REDUCED MACHINING COSTS

MACHINED PART

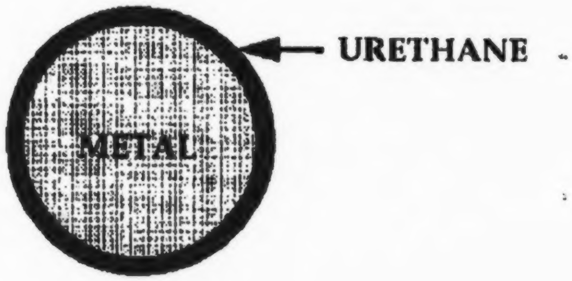

CAST PART COATED W/
URETHANE

NDE TECHNIQUES NEEDED TO MEASURE COATING THICKNESS AND BOND INTEGRITY

NDE of Urethane-Coated Metals

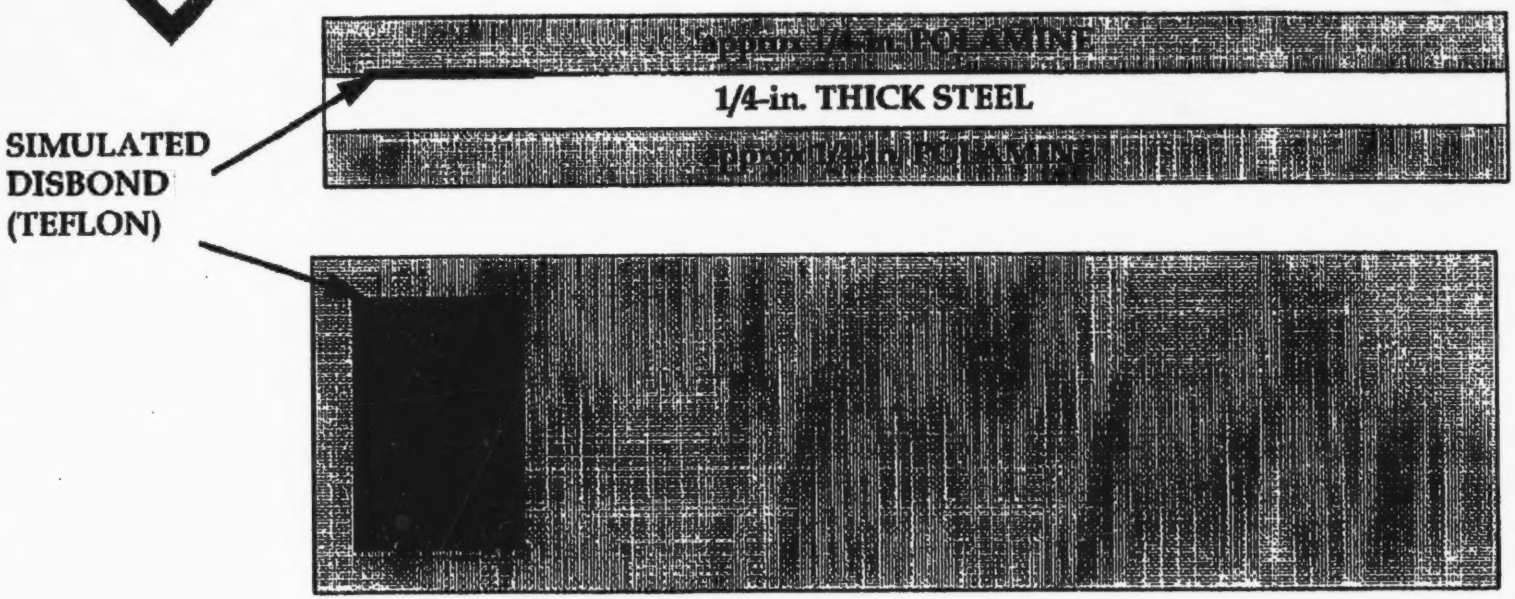
approx 1/4-in. POLAMINE
1/4-in. THICK STEEL
approx 1/4-in. POLAMINE
SIMULATED DISBOND (TEFLON)

NDE Techniques

Ultrasonics - thickness, disbond

Shearography - disbond

Thermography - disbond

NDE of Urethane-Coated Metals

UT RESULTS

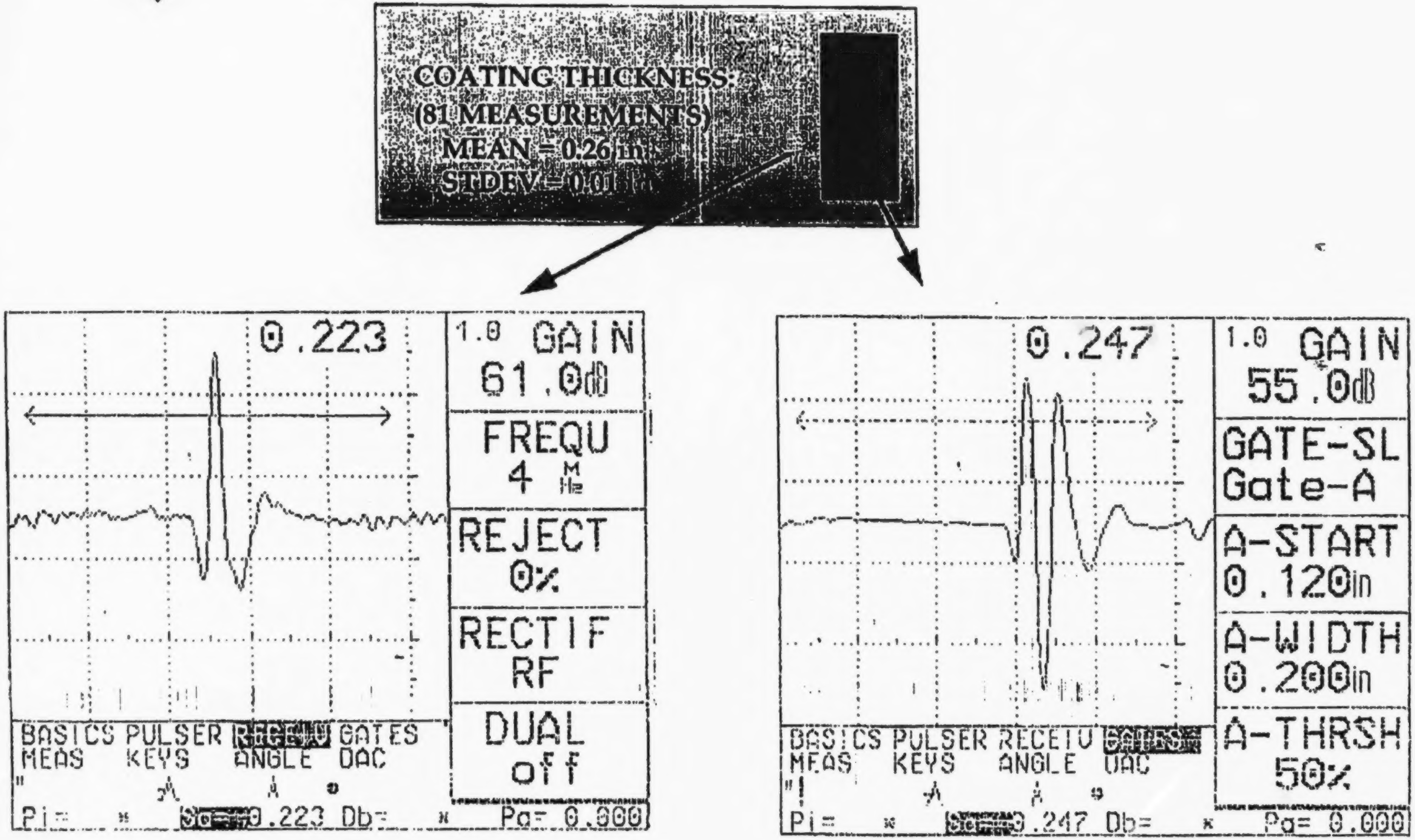

COATING THICKNESS:
(81 MEASUREMENTS)
MEAN = 0.26 in
STDEV = 0.01 in

0.223
1.0 GAIN 61.0dB
FREQU 4 MHz
REJECT 0%
RECTIF RF
DUAL off
BASICS PULSER RECEIV GATES
MEAS KEYS ANGLE DAC
Pi= Sa=0.223 Db= Pa= 0.000

0.247
1.0 GAIN 55.0dB
GATE-SL Gate-A
A-START 0.120in
A-WIDTH 0.200in
A-THRSH 50%
BASICS PULSER RECEIV GATES
MEAS KEYS ANGLE DAC
Pi= Sa=0.247 Db= Pa= 0.000

THEORY OF SHEAROGRAPHY

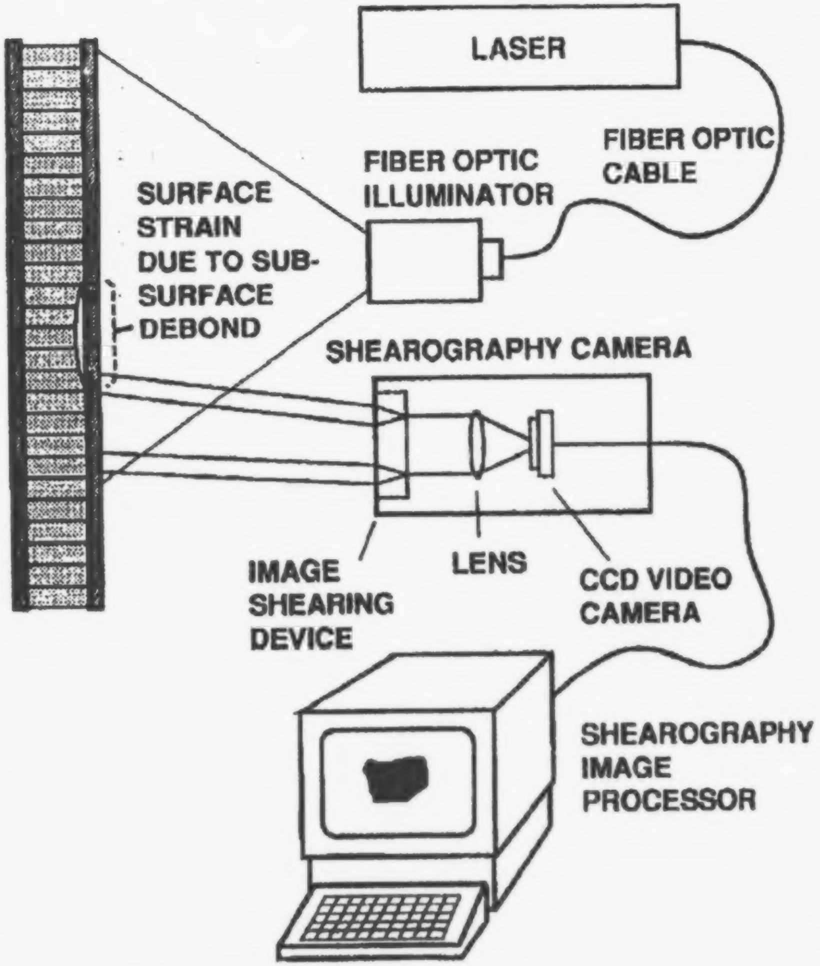
LASER
FIBER OPTIC CABLE
FIBER OPTIC ILLUMINATOR
SURFACE STRAIN DUE TO SUB-SURFACE DEBOND
SHEAROGRAPHY CAMERA
IMAGE SHEARING DEVICE
LENS
CCD VIDEO CAMERA
SHEAROGRAPHY IMAGE PROCESSOR

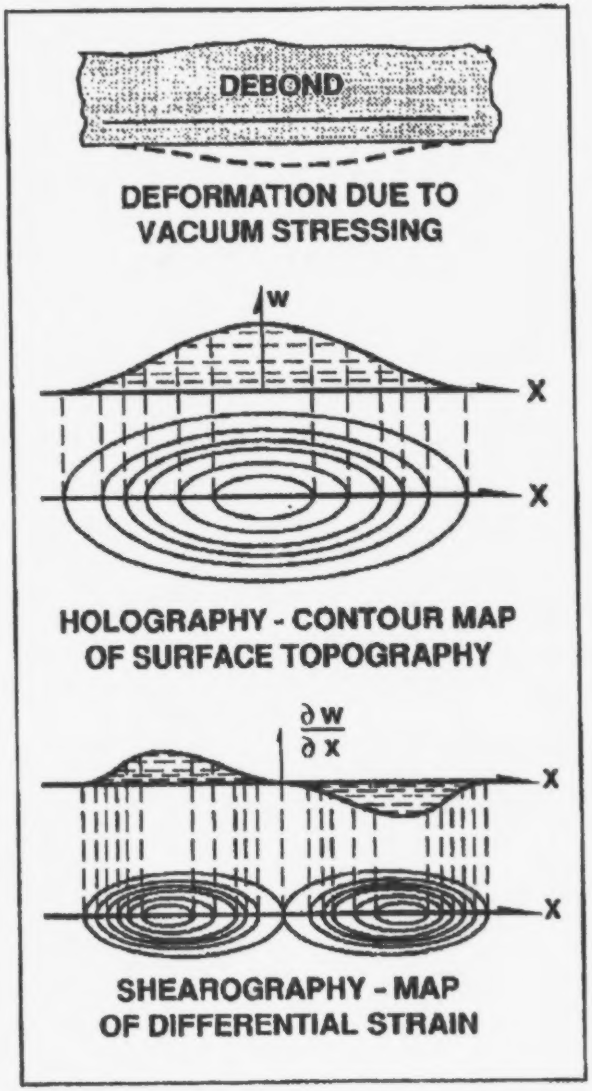
DEBOND
DEFORMATION DUE TO VACUUM STRESSING
w
X
X
HOLOGRAPHY - CONTOUR MAP OF SURFACE TOPOGRAPHY
∂w/∂x
X
X
SHEAROGRAPHY - MAP OF DIFFERENTIAL STRAIN

- Full field video strain gauge
- Uses phase relationship between two light waves
- Sensitive to 1/2λ changes in surface of object → ~1/4 μm

NDE of Urethane-Coated Metals

SHEAROGRAPHY RESULTS

NDE of Urethane-Coated Metals

THERMOGRAPHY RESULTS

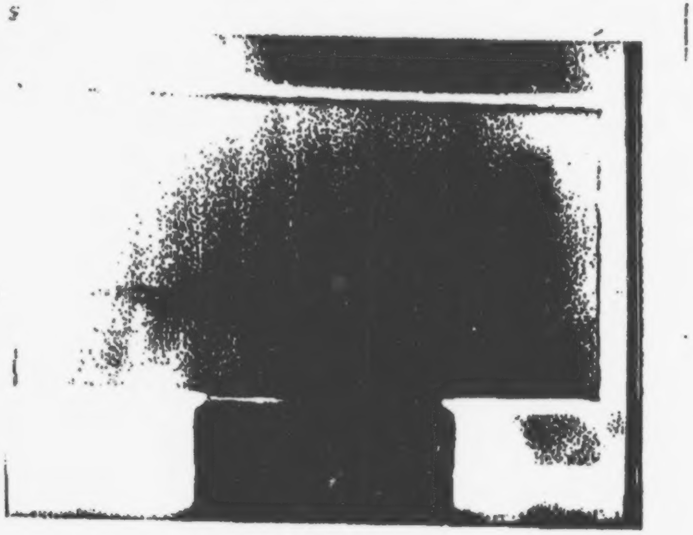

NO DEVELOPER
8-FRAME AVERAGING
NO CONTRAST ENHANCEMENT

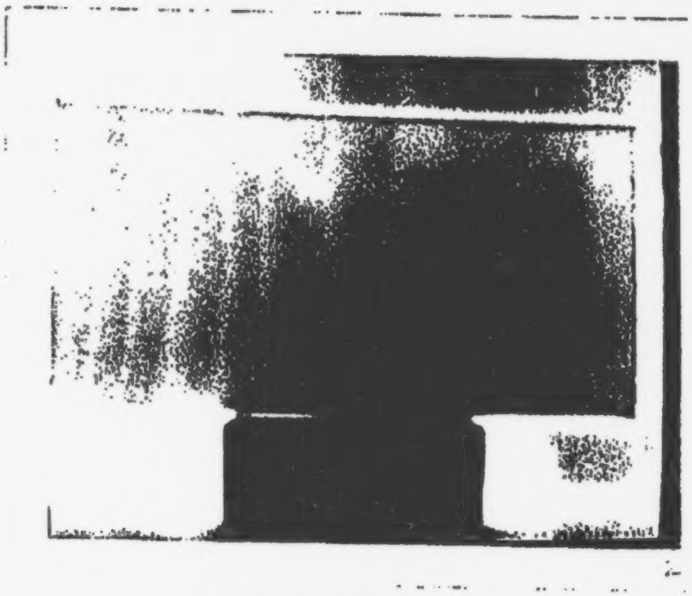

PENETRANT DEVELOPER
NO IMAGE AVERAGING
NO CONTRAST ENHANCEMENT

NDE of Thick, Sandwich Composites

SHEAROGRAPHY RESULTS - IMPACT DAMA

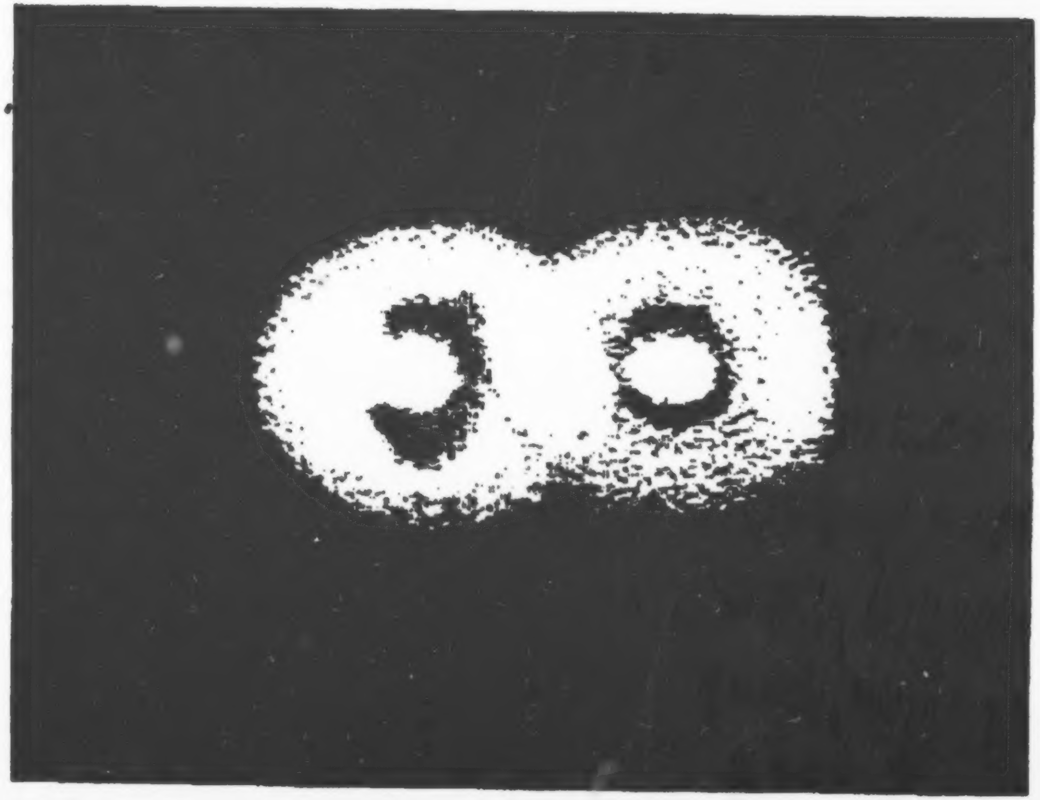

NDE of Thick, Sandwich Composites

COMBINING THIN COMPOSITE LAMINATES
WITH VARIOUS CORE MATERIALS

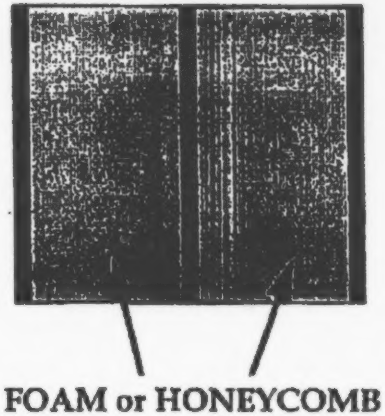
FOAM or HONEYCOMB

WEIGHT SAVINGS

SIGNATURE REDUCTIONS

NDE TECHNIQUES NEEDED TO DETECT DEFECTS IN LAMINATES AND AT BOND LINES

SHEAROGRAPHY NDE, QUARTER SCALE MAST

AFTER 2nd AIR BLAST TEST

FIELD TESTING - LASER TECHNOLOGY INC.

NDE INDICATIONS - SKIN CORE DISBONDS

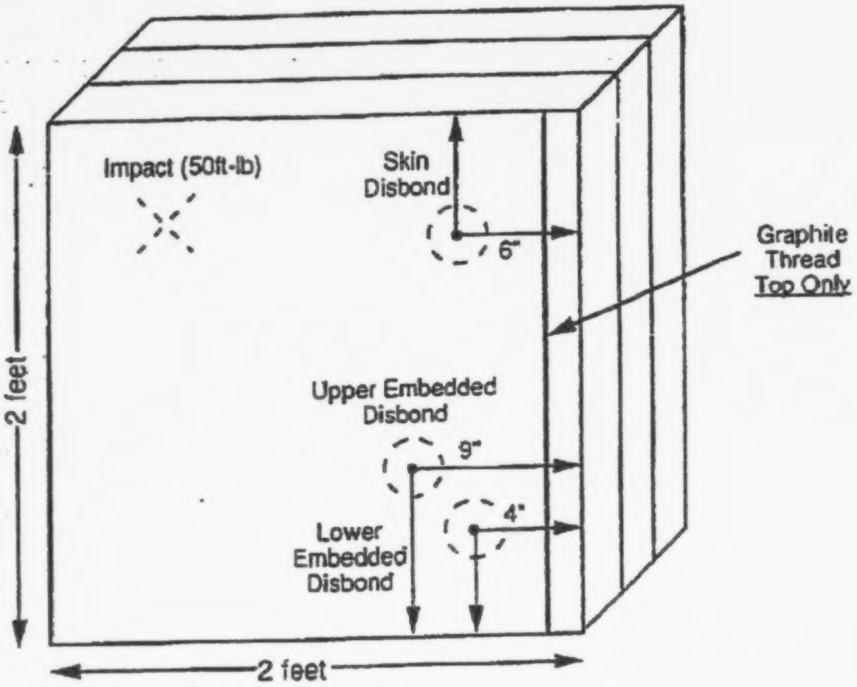
Impact (50ft-lb)
Skin Disbond
6"
Graphite Thread Top Only
Upper Embedded Disbond
9"
4"
Lower Embedded Disbond
2 feet
2 feet

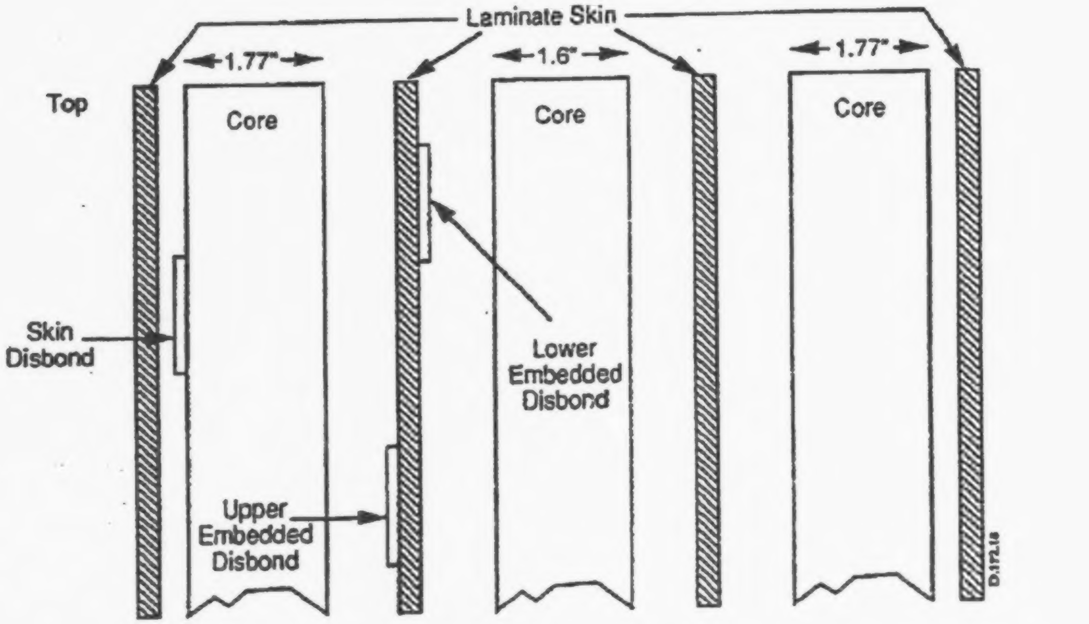
Laminate Skin
1.77"
1.6"
1.77"
Top
Core
Core
Core
Skin Disbond
Lower Embedded Disbond
Upper Embedded Disbond
D.172.18

Exploded View (not to scale)

NDE of Thick, Sandwich Composites

MICROWAVE NDE SETUP

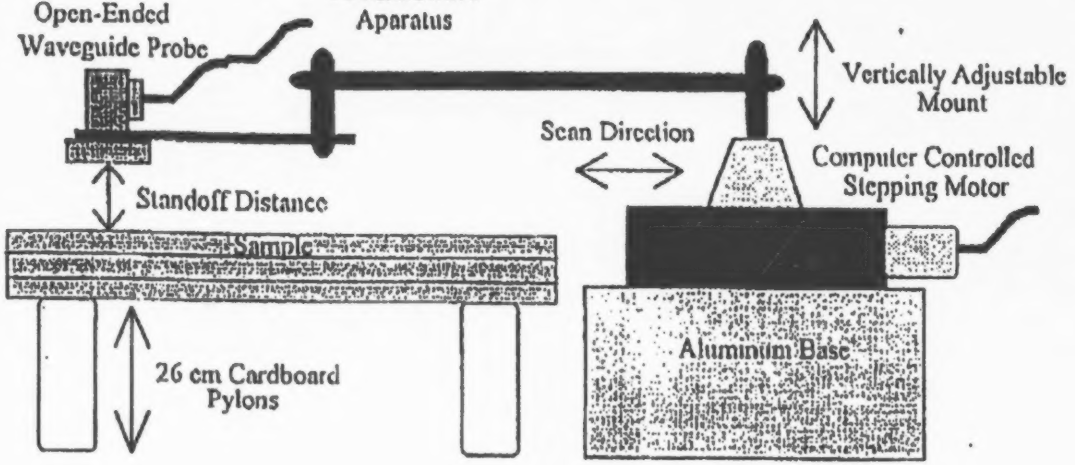
Open-Ended
Waveguide Probe
To Microwave
Apparatus
Vertically Adjustable
Mount
Scan Direction
Computer Controlled
Stepping Motor
Standoff Distance
Sample
26 cm Cardboard
Pylons
Aluminum Base

Figure 2: Scanner using a stepping motor.

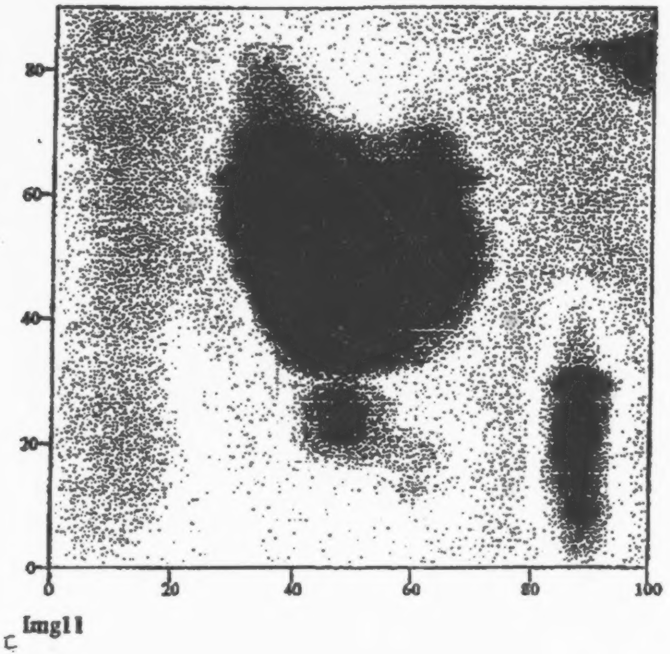

Image 11a: The contour plot of the scan of the upper embedded delamination (Defect 3) for the honeycomb sample at 9.1 GHz at an 17 mm standoff distance.

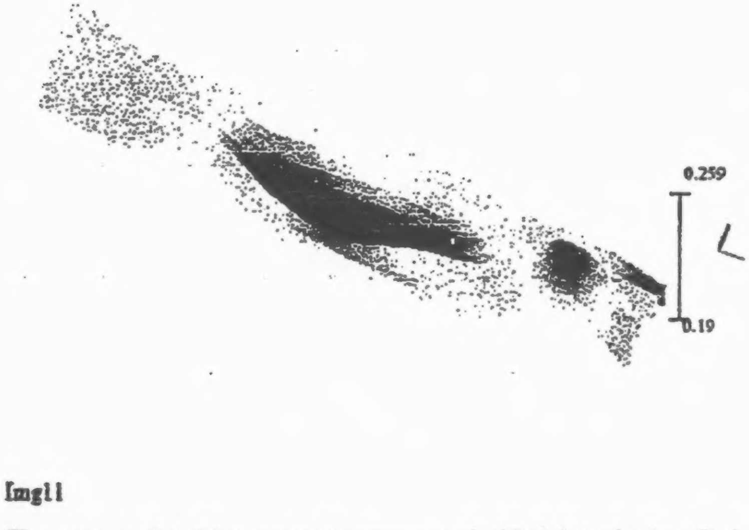

Image 11a: The contour plot of the scan of the upper embedded delamination (Defect 3) for the honeycomb sample at 9.1 GHz at an 17 mm standoff distance.

NDE of Thick, Sandwich Composites

MICROWAVE RESULTS

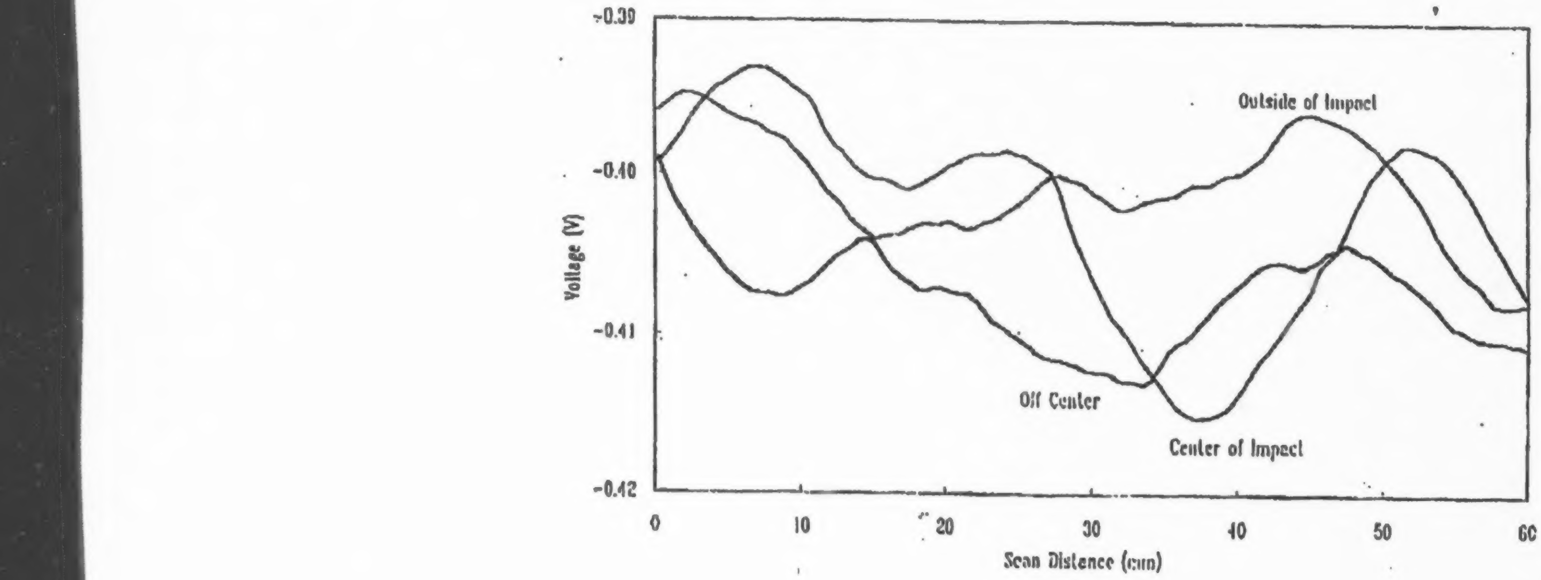

Figure 23: Three line scans of the impact damage of the honeycomb sample from the opposite side at 6 GHz.

NDE of Thick Section, Layered Materials

- INSPECTION THROUGH LAYERED MATERIALS
- URETHANE-COATED METALLIC COMPONENTS
- THICK, SANDWICH COMPOSITES

#510352

Microbiological Contamination of Shipboard Fuel Systems, Causes-Consequences-Control

by

R.D. Haggett

Defence Research Establishment Atlantic
Dockyard Laboratory, FMO Halifax, N.S. Canada, B3K 2X0

ABSTRACT

Microbiological contamination (MBC) of fuel tanks and fuel piping by fungi, yeast and bacteria is a common, but often ignored, cause of fuel system failure. The consequences of MBC range from blocked fuel purifiers, coalescers and filters to catastrophic engine failure resulting in repair costs in the millions of dollars. One such case involved fuel contamination which severely damaged several gas turbine engines with resulting repair expenses exceeding seven million dollars. Laboratory analysis of fuel taken from the contaminated tanks confirmed the presence of salt water, suspended particulate and interfacial fungal mats with the predominant organism being Hormoconis resinae. The TRUMP updated 280 Class destroyers have water ballasted fuel tanks and therefore possess the potential for MBC related fuel problems. In this presentation, the causes and consequences of microbiological contamination (MBC) in shipboard fuel systems will be discussed as well as DREA research efforts for the control and elimination of MBC.

MICROBIOLOGICAL CONTAMINATION OF SHIPBOARD FUEL SYSTEMS
CAUSES -CONSEQUENCES - CONTROL

by
R. D. Haggett
Defence research Establishment Atlantic

Presented at the 2nd Canadian Forces/CRAD Meeting on Naval Applications of Materials Technology, 2-4 May, 1995, Halifax, NS.

Microbiological contamination in hydrocarbon fuels presents a variety of problems to the operators of Naval vessels. The causative organisms are fungi, yeast and bacteria. Free water must be present in a fuel tank for these organisms to grow and proliferate. When water is present conditions are favourable for fungal spores (dormant phase) to become viable. The fungi and yeast grow at the fuel/water interface by extracting oxygen from the water molecules and nutrients from the fuel and water layers. The organisms reproduce by cell division creating branching chains (hyphae) which form an interlocking mat at the fuel/water interface. It is this mat which coats fuel tank walls, plugs filters, poisons coalescers and fouls injectors in diesel engines and causes coking of fuel control nozzles and hot spotting in gas turbine engines. Hot spotting in a gas turbine usually results in catastrophic failure requiring engine replacement.

At present the only effective ways to control MBC if by practicing good fuel husbandry and biocide use. The regular stripping of water bottoms from fuel tanks will help minimize microbiological contamination as organisms can grow only if water is present. Biocidal agents are an effective means for the control and/or elimination of microbiological contamination but, due to the toxicity of the active ingredients and environmental concerns, are used only as a last resort and under strictly controlled conditions.

SLIDE 1 - Micrograph of *H. resinea* showing branching chains (hyphae) forming an interlocking fungal mat.

SLIDE 2 - Cross section of a contaminated fuel tank showing:

- (a) clear upper layer of fuel
- (b) middle layer with moisture haze
- (c) microbial mat at the fuel water interface
- (d) water layer with emulsified oil
- (e) microbial slime coating tank bottom

SLIDE 3 - Water and Sediment Test showing water fungal mat at fuel/water interface and water layer with MBC.

SLIDES 4, 5 and 6 - Photographs of fuel tanks contaminated with microbial growth. Note the clean area on the tank bottom in Slide 5. This is due to vacuuming of the tank bottom by the fuel suction pipe. As fuel is drawn from the tank the microbiological contamination is spread through the fuel system.

SLIDE 7 - Coalescer Filter/Water Separator System contaminated with MBC.

SLIDE 8 - Coalescer/filter elements contaminated and blocked with MBC.

SLIDE 9 - Water separator cartridge which has been poisoned by a MBC produced surfactant.

SLIDE 10 - Fuel control nozzle from a gas turbine engine showing severe coking from MBC in the fuel supply. Coking alters the fuel spray pattern and causes hot spotting in the combustion chamber.

SLIDES 11, 12 and 13 - Gas turbine combustion chamber, injector ring and guide vanes showing the effects of hot spotting from burning contaminated fuel.

Defence Research Establishment Atlantic is currently conducting research into the application of ultrasonic energy for the destruction of microorganisms in shipboard fuel systems. It is envisioned that the system will consist of a flow through ultrasonic chamber with a capacity of up to 6,000 liters per hour. During FY 93/94 Aastra Aerospace, under contract to DREA, carried out a literature review and proof of concept for the use of ultrasonic energy for the destruction of microorganisms. The proof of concept included the construction and testing of laboratory scale prototypes of proposed systems. The next phase of this project, which is sponsored by National Defence Headquarters and will be carried out over a three year period, will be the design, construction and testing of a full scale system

1.

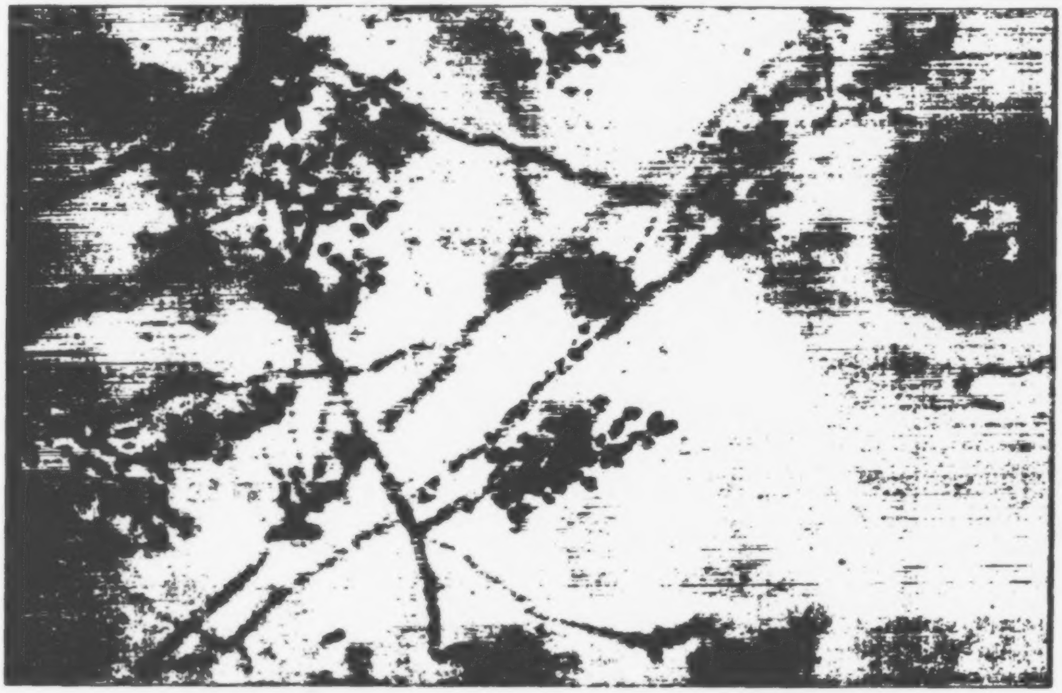

2.

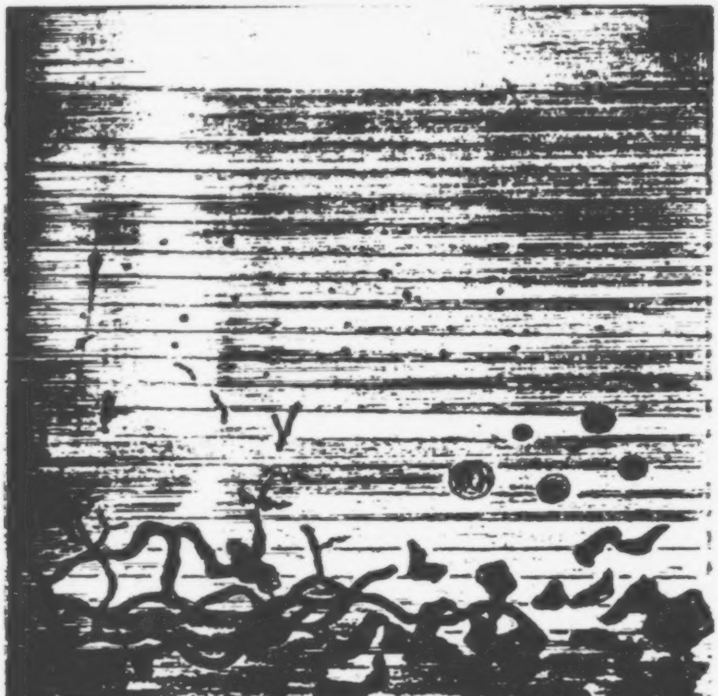

3.

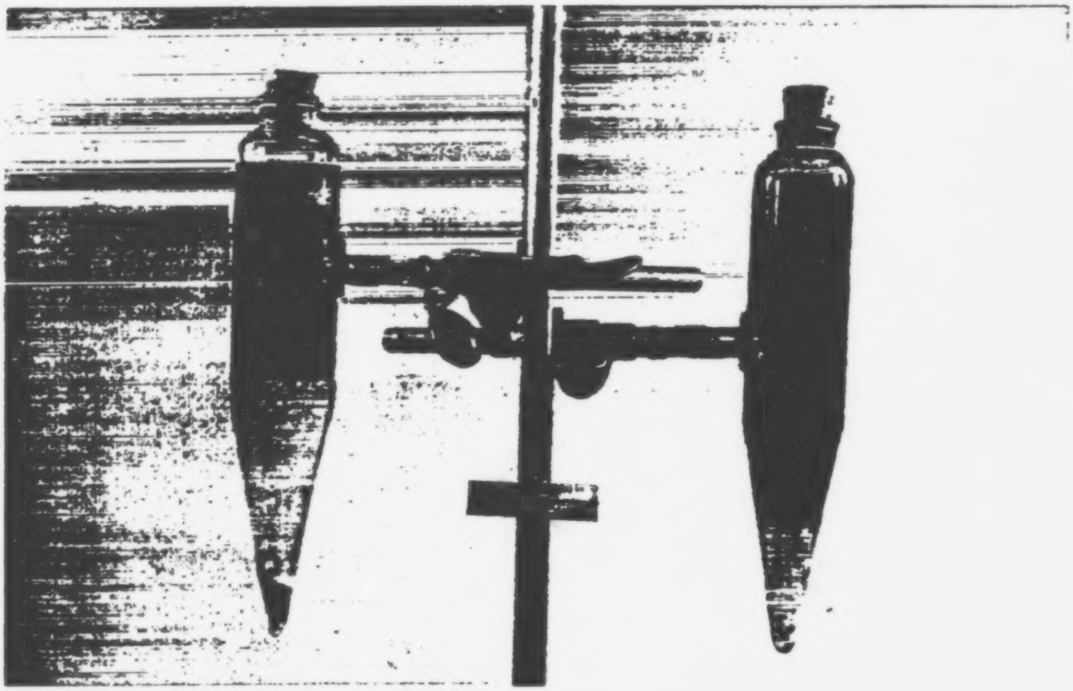

4.

5.

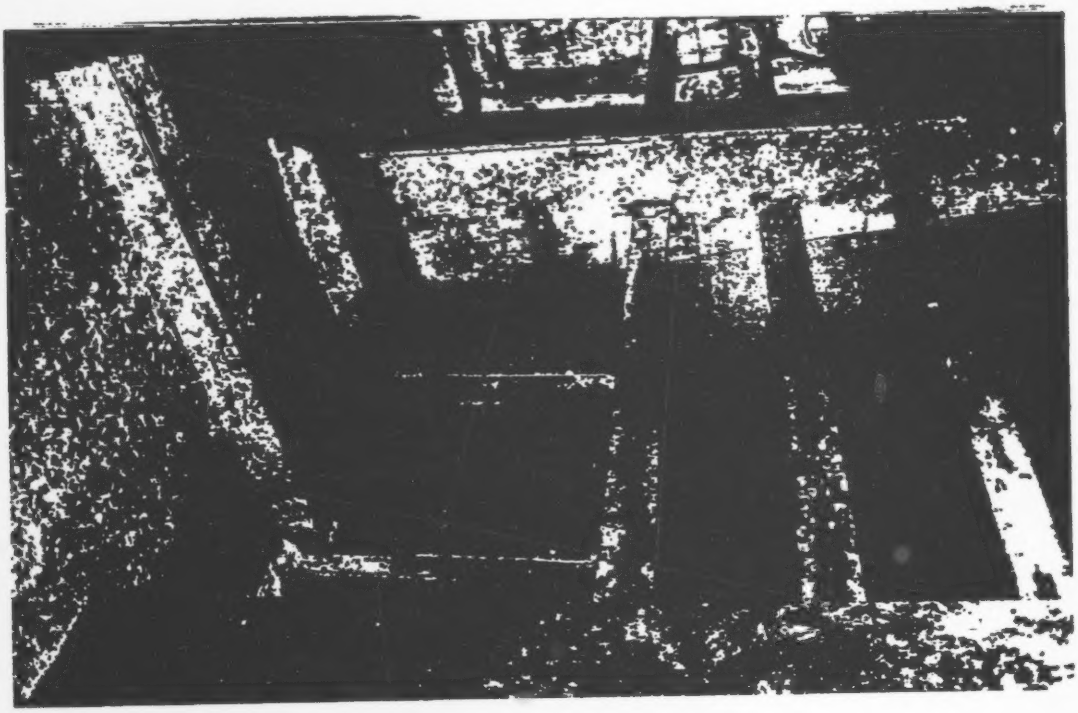

6.

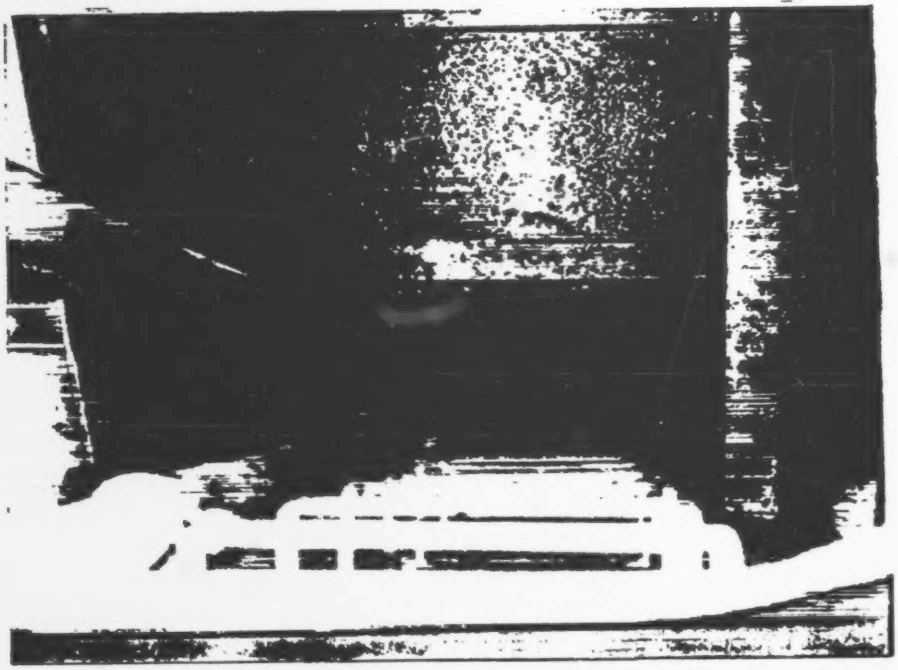

7.

8.

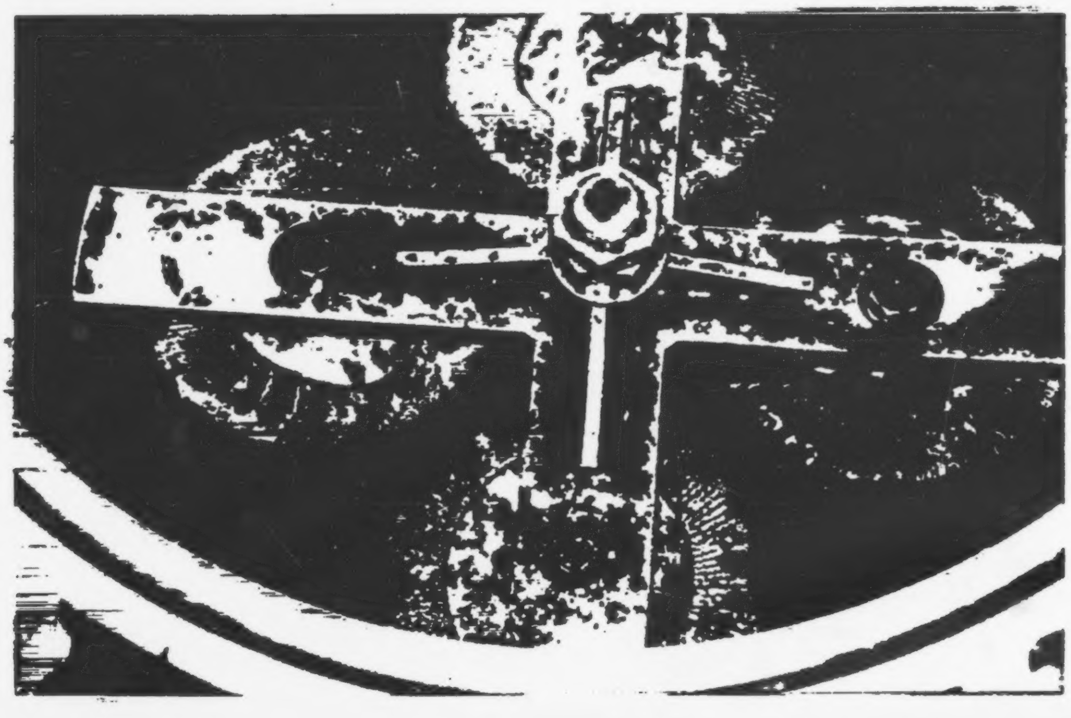

9.

10.

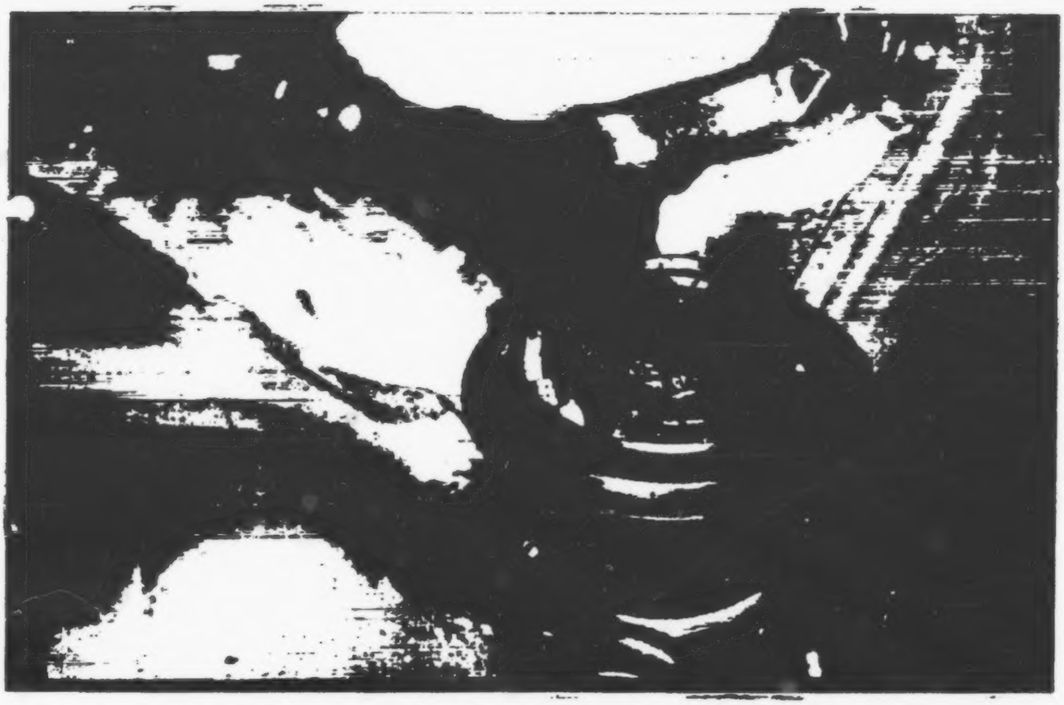

11.

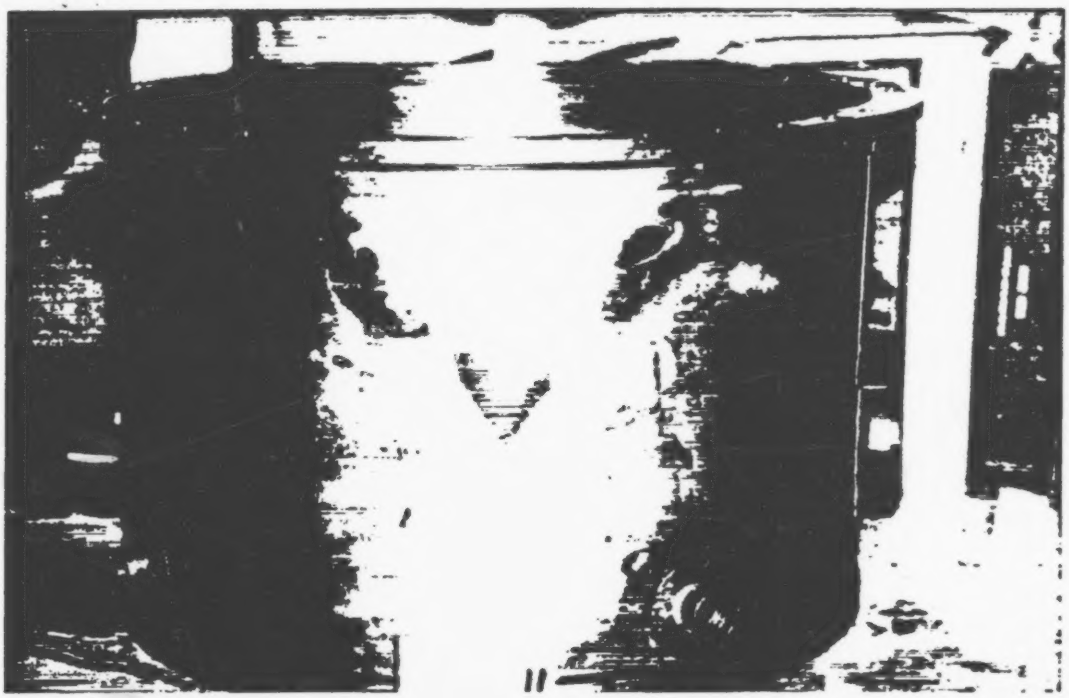

12.

13.

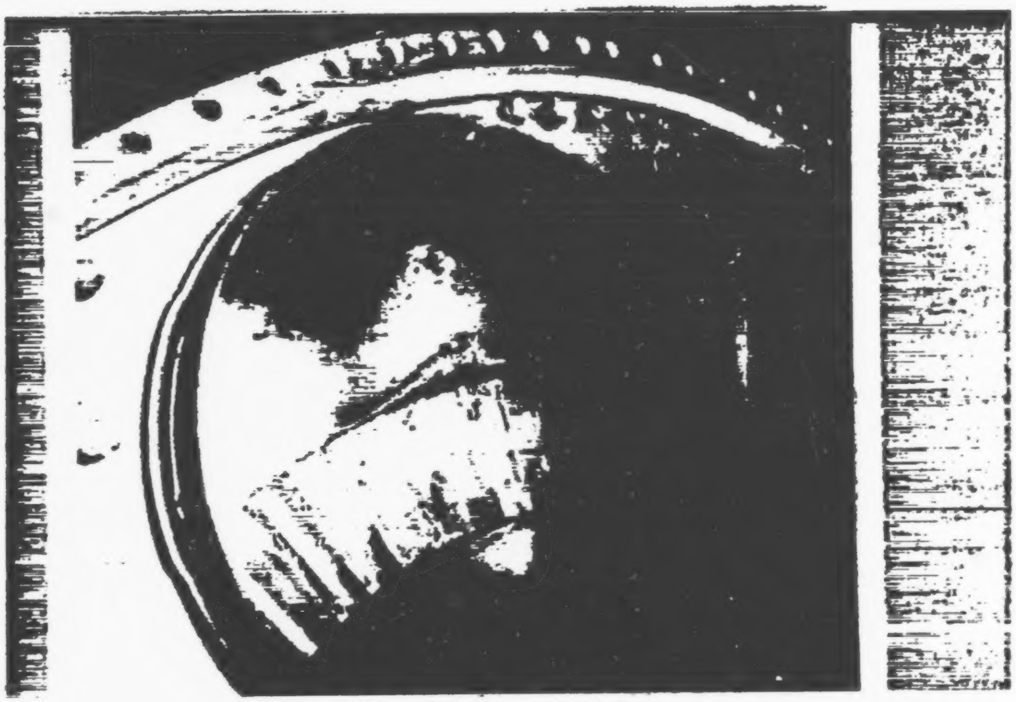

#510353

THE ULTRASONIC DESTRUCTION OF MICROBIOLOGICAL CONTAMINATION IN SHIPBOARD FUEL SYSTEMS

K.M. Valter McConville
Aastra Aerospace Inc.
Downsview, Ontario

ABSTRACT

Microbiological contamination of marine diesel presents an expensive problem for naval operations due to the blockage of filters and nozzles, and the ultimate destruction of the turbine blades. Despite the current use of biocides and the full time use of personnel to replace filters, the contamination problem has led to millions of dollars of equipment damage. Through the support of DREA, Aastra has assessed the feasibility of ultrasonic destruction of microorganisms in marine diesel fuel. This approach to microbiological control represents an environmentally friendly and efficient alternative to the use of biocides.

Two different ultrasonic devices were used in this study. The microorganisms most commonly found in marine diesel were identified and inoculation tests were performed. Results showed that processing in each apparatus can reduce the microbiological contamination levels of marine diesel for both aerobic and anaerobic bacteria, yeast and mold by up to 3 orders of magnitude. Laboratory grown microbial mats were effectively dispersed, and microorganism viability was destroyed. Aastra has proposed that the concepts demonstrated through this work could be developed into a full scale treatment system.

INTRODUCTION

The marine industry is increasingly concerned with the problem of microbial contamination in shipboard fuel. Recent increases in microbial populations and the associated damage to tanks and turbines have led to a heightened awareness of the problem, resulting in several studies on chemical and physical control measures.[1] Alternatives to the use of biocides are being considered to improve the effectiveness of these control measures and to reduce their environmental impact.

Fuel tanks and large scale fuel storage systems have become popular only in the last 60 years. Microbial populations are continually changing and adapting to variations in growth conditions. With fuel formulations constantly changing, it is thought that microbial evolution has yet to run its full course.[2] Since biocides are generally only effective for specific species of microorganisms, they must also be continually adapted to combat the new strains of microbes that may develop.

Physical destruction of microorganisms, such as ultrasonic treatment, may be a feasible alternative to the use of biocides. These physical control measures do not share the above concerns about biocide use. Studies have shown that ultrasonic treatment is an effective means of destroying microorganisms. In order to investigate the applicability of this technology to shipboard fuel systems, this study assessed the ability to destroy microorganisms in marine fuel using ultrasound.

METHODS

Ultrasound destroys microorganisms in liquids via cavitation. An alternating voltage is converted to mechanical vibrations in the ultrasonic transducer. These vibrations give rise to alternating compressions and rarefactions in the liquid surrounding the transducer. Upon rarefaction, vapour-filled cavities are created in the liquid and during compression they are collapsed, or imploded. This cavitation produces the fundamental cleaning action of an ultrasonic cleaner. The shock waves, resulting from cavity implosion, dislodge dirt particles from the item being cleaned. The localized mechanical stresses resulting from cavitation have been shown to be destructive to microorganisms.[3, 4]

The factors affecting cavitation are: frequency, power density, time of exposure and the physical and chemical characteristics of the liquid that is being processed. Ultrasonic frequencies extend from about 20 kHz up to the megahertz range. Power density is a function of the power of the transducer and the size of both the transducer and the container over which the sound waves are distributed. It is generally expressed as watts/cm^2, referring to the surface area of the transducer.

The frequency of the ultrasonic wave influences the size and number of cavities created. The larger the cavities, the greater the force of implosion, and thus the greater the effectiveness of cell disruption. Low frequencies cause a few large cavities which generate stronger shock waves. Higher ultrasonic frequencies require much greater power input to produce cavitation. The cavities that are produced are generally smaller than at low frequencies. High frequencies produce a more directed beam of ultrasonic waves, which does not disperse well throughout the medium. Figure 1 shows the difference between high and low frequency effects schematically.

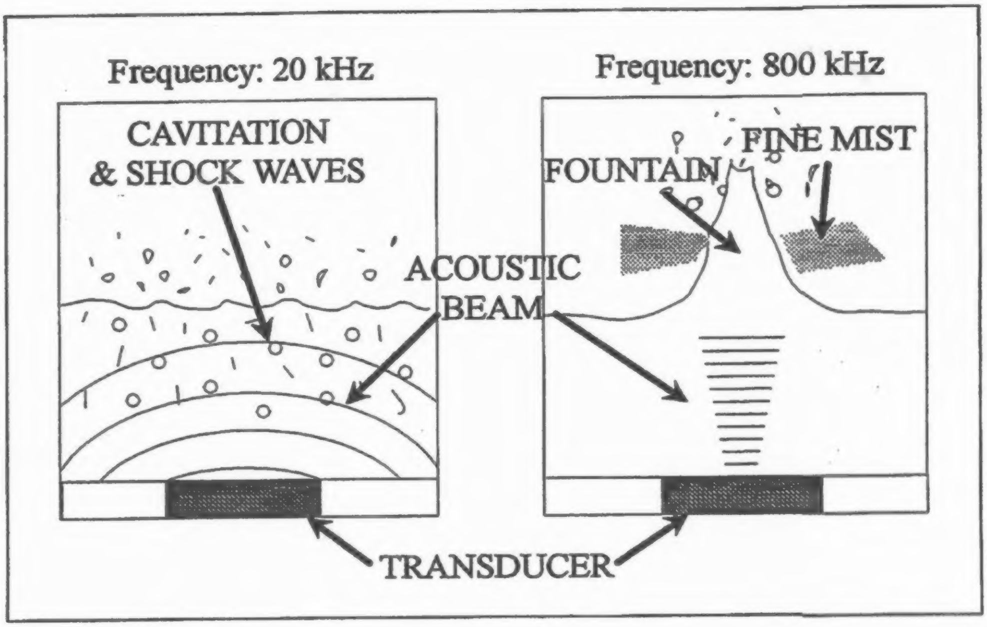
Frequency: 20 kHz
Frequency: 800 kHz
CAVITATION & SHOCK WAVES
FINE MIST
FOUNTAIN
ACOUSTIC BEAM
TRANSDUCER

Figure 1: Low vs High Frequency Ultrasound Waves in Liquid [4]

Two different approaches to ultrasonic treatment of fuel were assessed in this study. One apparatus consisted of the ultrasonic horn system, a treatment cell, and a peristaltic pump. This horn operated at a frequency of 20 kHz, and had a power range of 10 to 175 watts. The tip of the horn had a surface area of 1 cm^2. A schematic of the equipment set-up is shown in Figure 2.

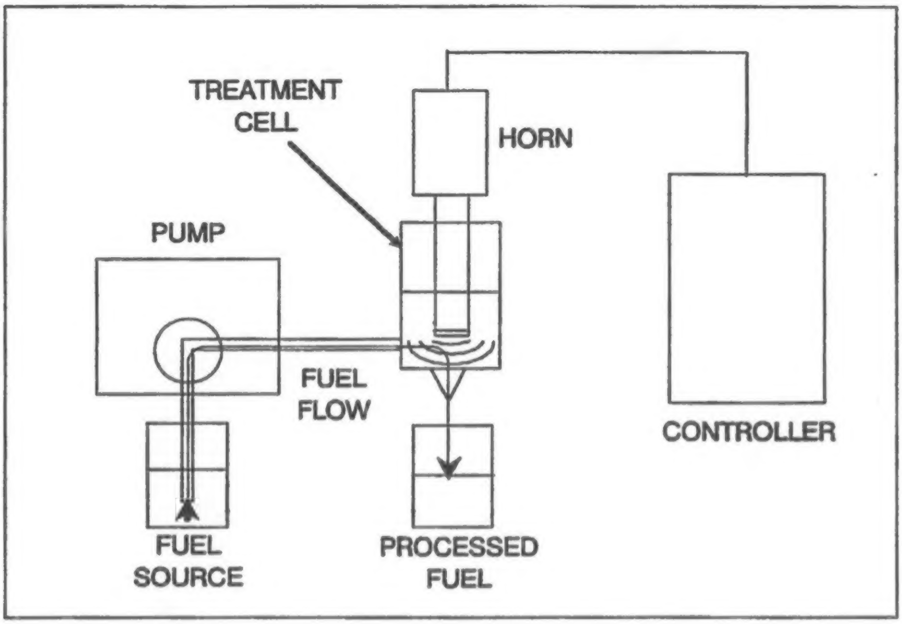
TREATMENT CELL
HORN
PUMP
FUEL FLOW
CONTROLLER
FUEL SOURCE
PROCESSED FUEL

Figure 2: Ultrasonic Horn Equipment Set-up

An industrial cleaner was used as an alternative to the ultrasonic horn flow test. This system operated at 40 kHz. The fuel was pumped through a length of tubing which was immersed in the sonicator bath. The cleaner reservoir had 18 transducers distributed across the bottom. The bottom surface had dimensions 18" x 12". This maximized the length of tubing immersed in the liquid and allowed longer treatment times for a given flow rate. A schematic showing the set-up for this flow test is shown in Figure 3.

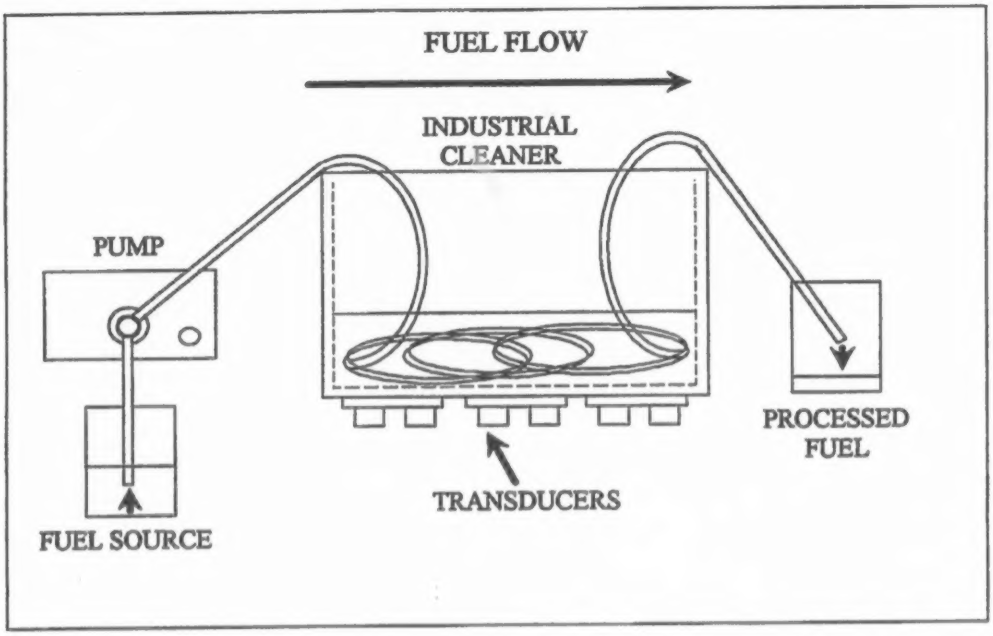

Figure 3: Industrial Cleaner Flow Test Set-up

Field tests were performed with actual contaminated marine diesel. The results of these tests were assessed by counting the number of colonies of microorganisms per millilitre of fuel before and after treatment. The microorganisms were classified as:

- aerobic bacteria,
- anaerobic bacteria,
- aerobic yeast and mold, and
- anaerobic yeast and mold.

Additionally, the most typical microorganisms found in marine diesel were inoculated into sterilized fuel. The following standard microorganism cultures were used:

- Pseudomonas aeruginosa ATCC 15442,
- Candida albicans ATCC 14053, and
- Hormoconis resinae ATCC 18215.

The viability of these microorganisms was also assessed by counting colonies before and after ultrasonic processing for each type.

RESULTS

The results showed that contamination levels were typically reduced by 2-3 orders of magnitude in this preliminary assessment. The microbiological testing was performed by three independent laboratories, all of which were able to show reduced counts after processing.

Figure 4 shows the results of the field tests before and after processing with the ultrasonic cleaner bath. These tests were performed with the fuel immersed in the water bath for the times given in the legend at a power level of 100 watts.

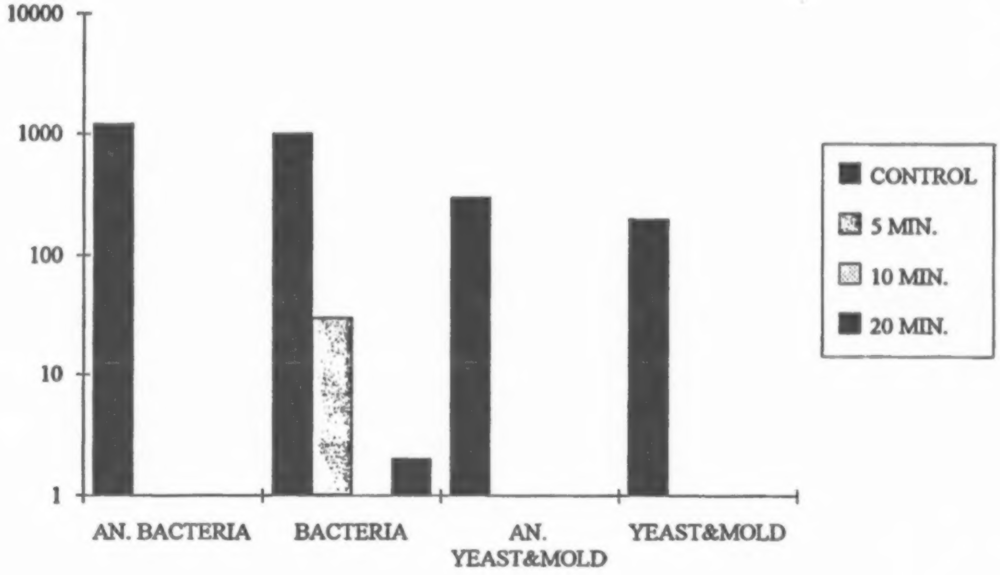

Figure 4: Ultrasonic Cleaner Field Test Results

Figure 5 shows the results from the inoculation tests before and after processing with the ultrasonic horn. These tests were conducted at a medium effective power setting of 55 watts.

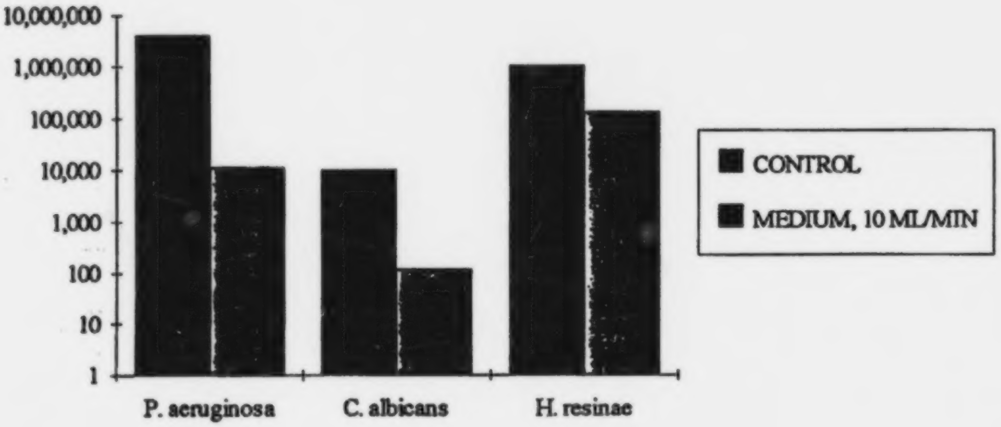

Figure 5: Ultrasonic Horn Inoculation Test Results

DISCUSSION

These preliminary results showed that ultrasonic processing could be a feasible approach to the destruction of microorganisms in marine diesel. Based on the findings from the literature on ultrasonic destruction of microorganisms in other applications, it was found that the frequency, power and geometry of the system can affect the results of this process. For this reason, two alternative configurations were used to evaluate the process with marine diesel. Both field tests and inoculation tests resulted in the reduction of viable colonies of different types of microorganisms that are typically present in fuel.

It was also found that ultrasonic treatment can be useful in disrupting microbial mats that grow at the fuel water interface. Ultrasonic processing can effectively destroy the viability of the microorganisms within the mat, and disrupt the mat to facilitate filtering.

Water reaction tests showed that the quality of the fuel is not degraded by ultrasonic processing. However, it was found that large amounts of water should not be mixed with the fuel during processing. The quality of contaminated fuel as assessed by the water reaction tests was actually improved by ultrasonic processing.

It is recommended that these techniques be adapted for full scale field trials in a marine environment. The proper implementation of large piezoceramic transducers will be critical in the success of scaling up this technology from the laboratory to a marine environment.

REFERENCES

1. Hill, E.C. 1986: Fuels. in: Microbial Problems in Offshore Oil Industry: Proceedings of the International Conference. eds: E.C. Hill, J.L. Shennan and R.J. Watkinson. Inst. Petroleum Microbiology Committee. Aberdeen, U.K.

2. Smith, R.N., Biodeterioration Centre, The Hatfield Polytechnic, Herts., U.K.: Fuels. Informal Report, DREA.

3. Scherba, G. et al. 1991: Quantitative Assessment of the Germicidal Efficacy of Ultrasonic Energy. Applied & Envt. Microbiology. 57(7), 2079-2084.

4. Boucher, R.M.G. 1979: Ultrasonics - A Tool to Improve Biocidal Efficacy of Sterilants or Disinfectants in Hospital and Dental Practice. Can. J. Pharm. Sci. 14 (1), 1-12.

ACKNOWLEDGEMENTS

The author would like to thank the Defence Research Establishment Atlantic for supporting this work.

#510354

High Temperature Firesafe Electrical Cables

by

D.E.Veinot
Defence Research Establishment Atlantic

S. Johar, Z. Wang and S. DasGupta
The Electrofuel Manufacturing Company Limited
Toronto, Ontario

and

Dr. M.K. Murthy
MKM Consulstants International
Toronto, Ontario

ABSTRACT

Electrical cables run fore and aft in tightly packed cable trays on all decks on a warship. During a fire the polymeric coverings on these cables present a high fire load and in addition the fire can progress rapidly throughout the ship along cable runs producing large amounts of fumes and toxic combustion products along the way. Further, many important shipboard systems can be rendered totally ineffective as a result of a loss of electrical power caused by shorting or melting of conductors. Consequently it would be extremely beneficial to have cables that had a high temperature perfomance capability which could remain operative even in a fire situation. It would be a further significant benefit if the sheathing on shipboard cables was non-combustible and did not release fumes and toxic gases when burned.

This presentation will describe the development and testing of an inexpensive, lightweight, flexible ceramic electrical cable sheathing. Details of the materials' development and testing of cable segments for normal and high temperature (1000°C) perfomance will be presented. The presentation will include a video taped summary of the testing of the cable under fire loading relative to a commercially available polymer sheathed cable. In addition a sample of prototype cable will be available for examination.

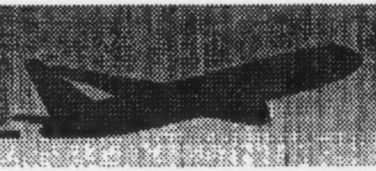

Outline

- background
- technology development
- materials
- process technology
- product development
- evaluation
- videotaped testing and prototype

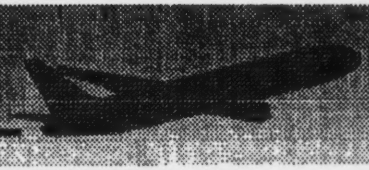

Shipboard Requirements

- fire performance
- no added fuel load
- no toxic smoke or fumes
- comparable performance under normal conditions
- water resistant (no wicking or absorption)
- lightweight and flexible
- connection capability
- comparable cost

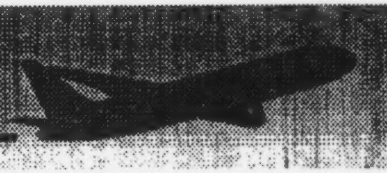

Commercial/Industrial Requirements

- ◆ computers and information technology
- ◆ industrial process control
- ◆ high technology industries
- ◆ alarm and egress systems

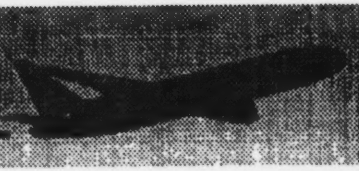

Technology Development

- ◆ cable design
- ◆ ceramic insulation
- ◆ assembly process
- ◆ performance evaluation

Required Properties of Ceramic Insulation

- good electrical resistivity at high temperature
- good mechanical strength
- non-reactive
- hydrophobic
- flexibility
- processibility

Material Development

- boron nitride
- alumina
- silica
- commercial alumino-silicate (Kaowool) and boron nitride in an aqueous slurry

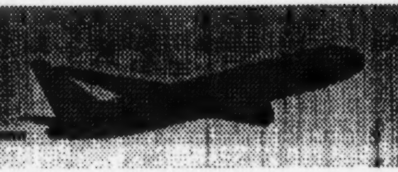

Properties of BN Fibres

- tensile strength 0.8 GPa
- modulus 10 GPa
- melting point ~3000 C
- thermal conductivity 35W/mK @ 1000C
- dielectric constant 4 @ 8.5 GHz
- resistivity(ohm-cm)10E13@ RT, 10E8@1000C

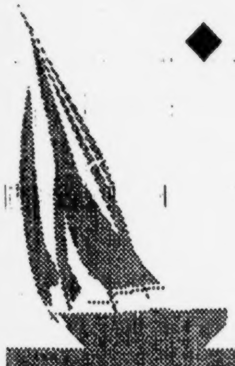

Properties of Kaowool

- 43-47% alumina; 53-57% silica
- melting point 1760C
- tensile strength 1.4 GPa
- modulus 120 GPa
- resistivity(ohm-cm) 10E13@ RT; 10E5 @ 1000C

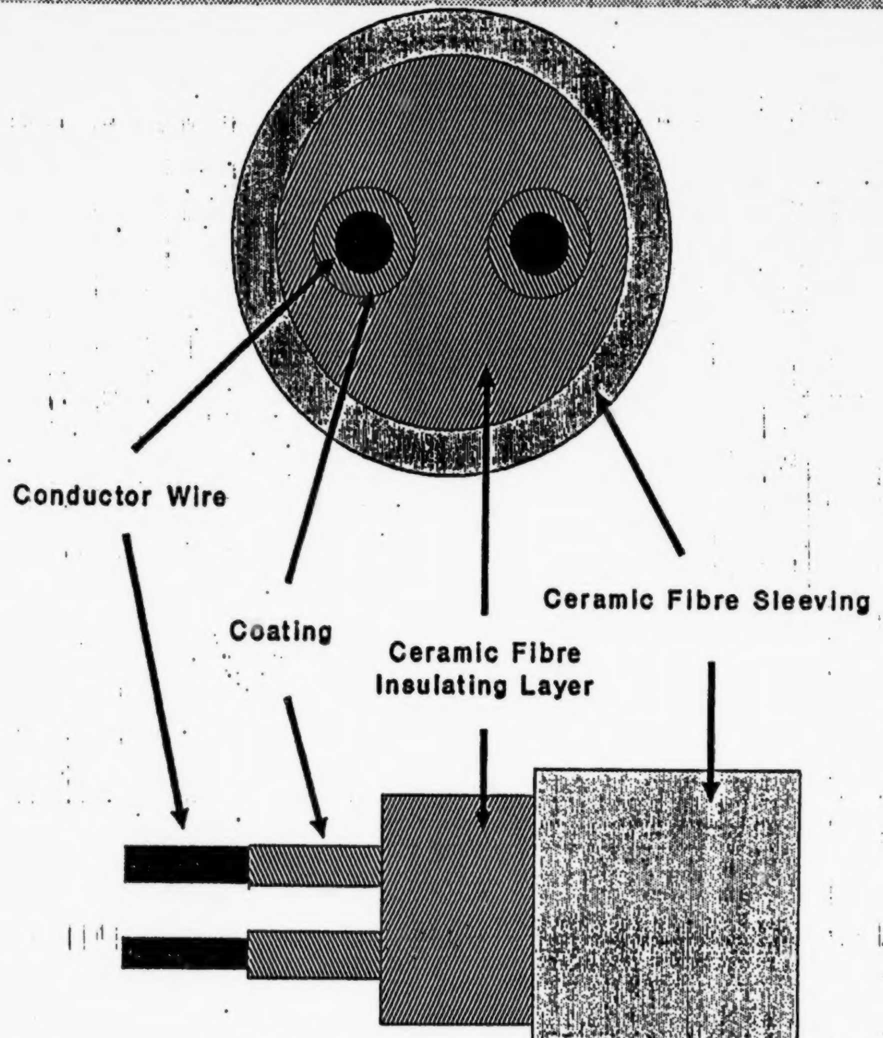

Conductor Wire

Coating

Ceramic Fibre Insulating Layer

Ceramic Fibre Sleeving

cable design concept

1. Gas Cylinder
2. Gas Regulator
3. Gas Flowmeter
4. Control Valve
5. Circular Copper Tube With Holes
6. Plastic Tube
7. Slurry Tank
8. Slurry
9. Slurry Nozzle
10. Felt Making Mold
11. Drive Chain
12. Drive Motor
13. Chain Wheel
14. Microswitchs
15. Water Outlet

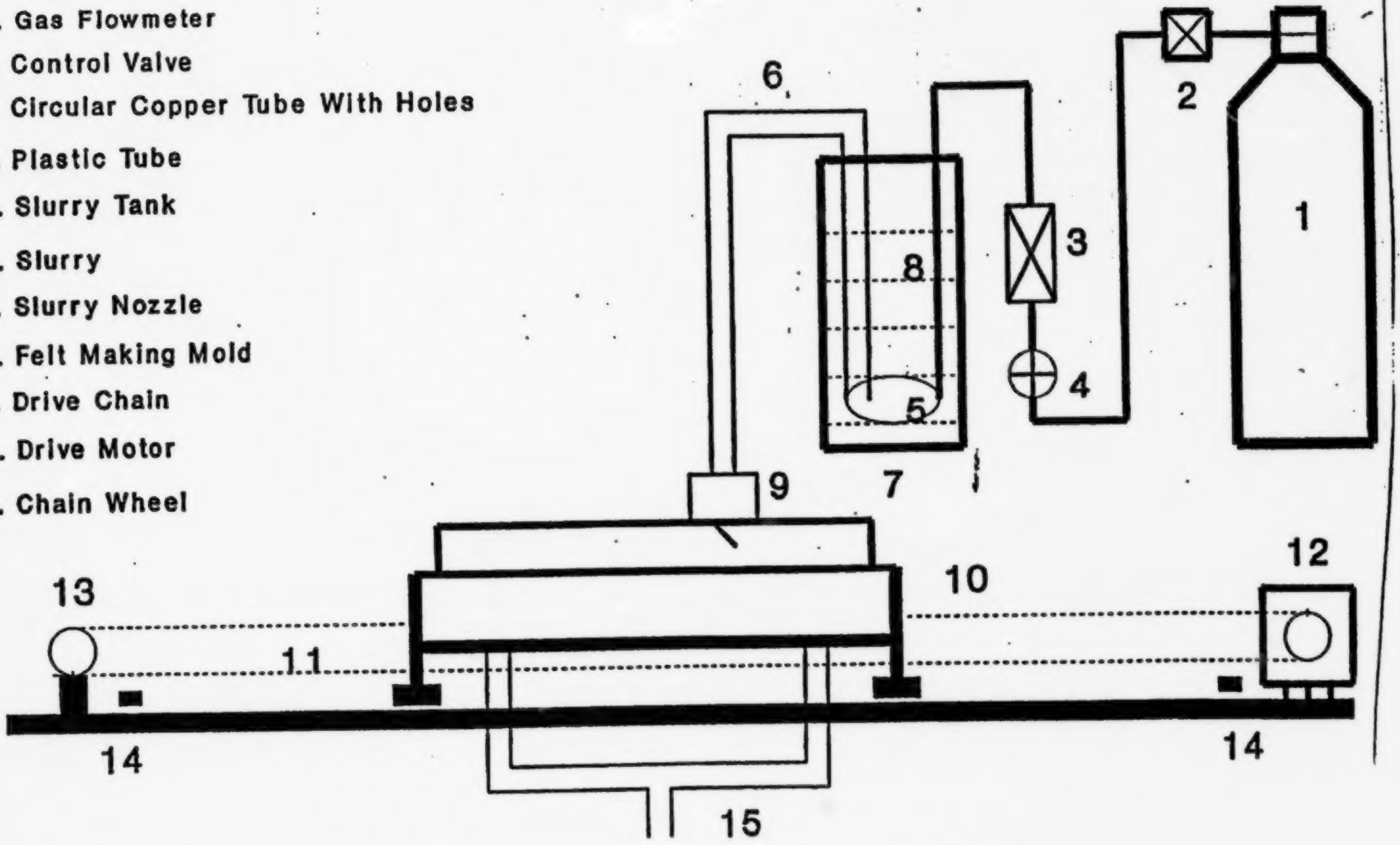

semi-continuous slurry casting apparatus

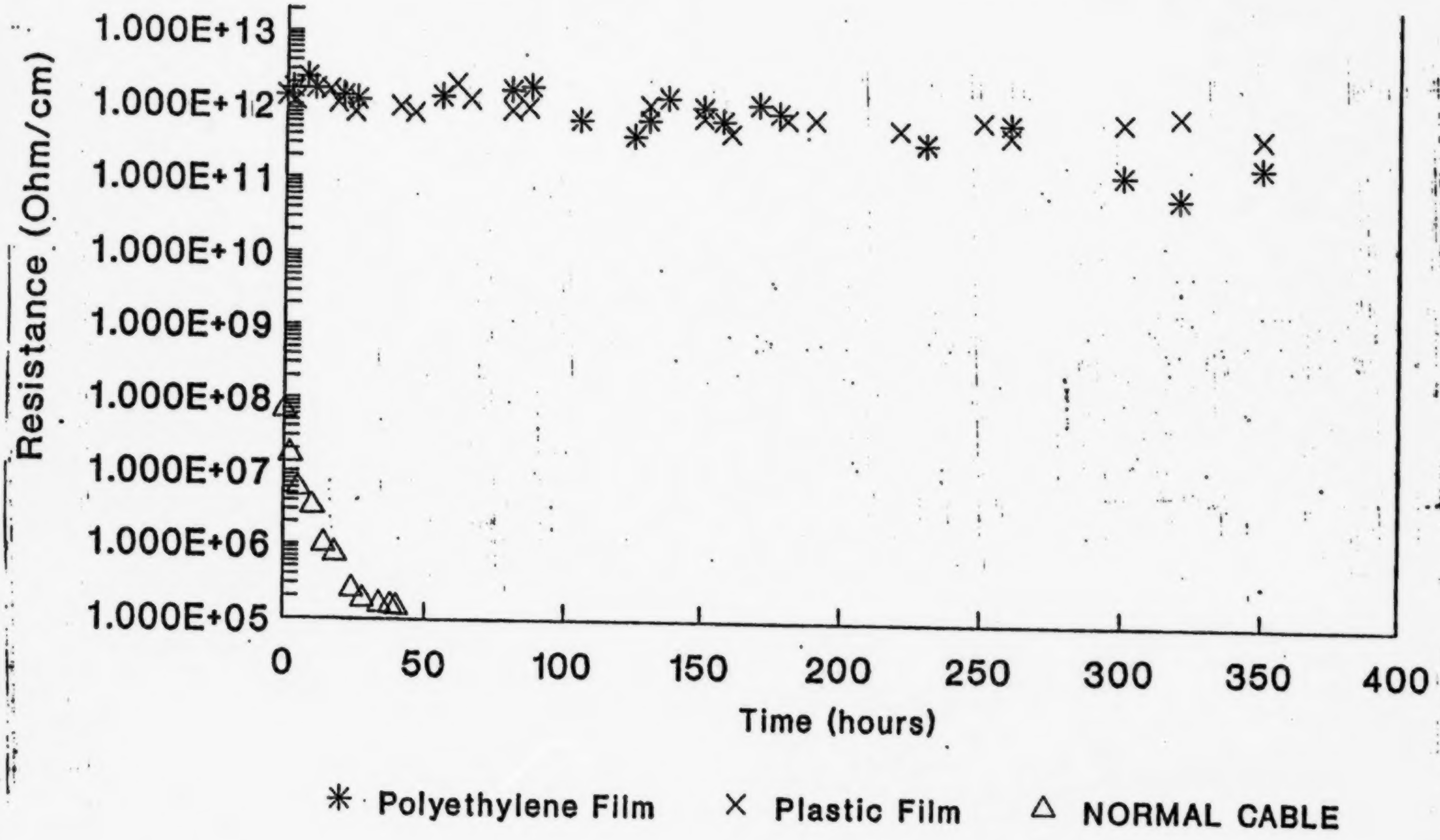

insulation resistance ohm/cm vs time at 85% RH

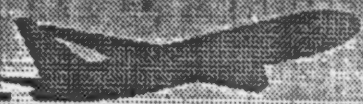

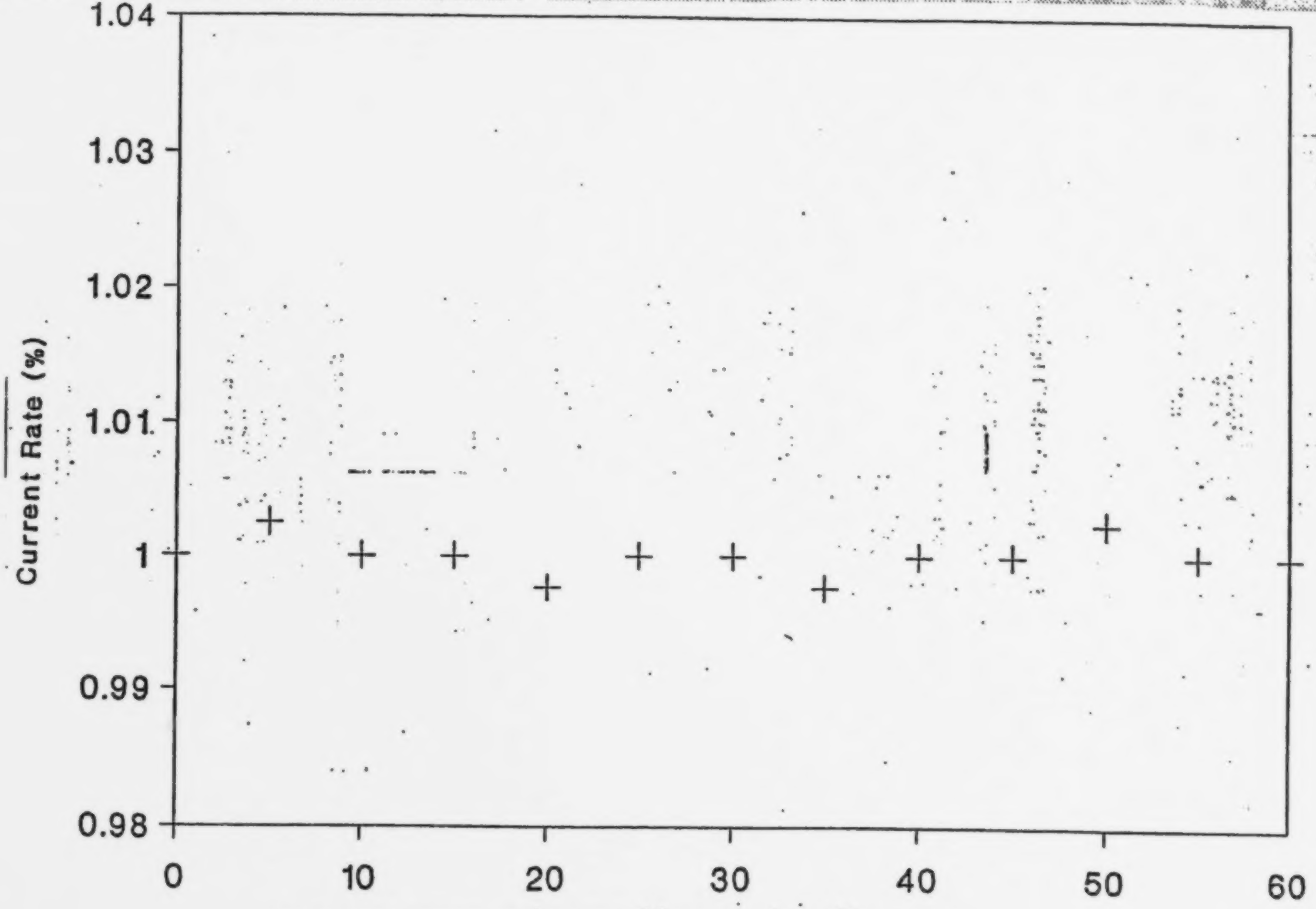

ac current vs time in flame

#510355 (

Laser Processing of Components for Naval Applications

by

T.A. Marsico, P.E. Denney and D.F. Farson

Materials & Manufacturing Division
Applied Research Laboratory
The Pennsylvania State University, P.O. Box 30
State College PA 16804

ABSTRACT

The U.S. Navy has sponsored laser welding and cladding research at the Applied Research Laboratory - The Pennsylvania State University (ARL Penn State) to provide cost effective solutions for fabrication, repair, and refurbishment of components. Laser beam welding has been accomplished on many different alloys, ferrous and nonferrous, and thick (i.e., > 1") and thin (i.e., ~0.008") gauge materials. Carbon dioxide ($C0_2$) and Neodymium Yttrium Aluminum Garnet (Nd:YAG) systems have been used for process development. Beam delivery systems have incorporated transmissive, reflective and fiber optics. Laser beam cladding (LBC) has been used to modify materials surface characteristics in terms of wear resistance and corrosion resistance. In addition, LBC can be used to "build-up" areas where mechanically-induced damage has occurred.

Both LBW and LBC process development for Naval applications will be reviewed. LBC for improved wear resistance will be discussed. And, finally, LBW methods used to fabricate lightweight structures currently in use on the USS *Mt. Whitney* will also be presented.

PRESENTATION OUTLINE

- Introduction
- The Applied Research Laboratory
- High Energy Processing Department
- Research Facilities
- Laser Materials Processing Research Areas
- Laser Materials Processing Examples
- Technology Transfer
- Summary

APPLIED RESEARCH LABORATORY/ THE PENNSYLVANIA STATE UNIVERSITY (ARL PENN STATE)

- Formerly The Harvard Underwater Sound Laboratory
- Established in 1945 at Penn State as the Ordnance Research Laboratory
- One of Four Chartered Office of Naval Research Laboratories
- Traditional Areas of Research Include Acoustics and Hydrodynamics
- During the 1980's, Expanded into Manufacturing and Materials Research to Decrease Life Cycle Costs of Components

HIGH ENERGY PROCESSING DEPARTMENT (HEP)

- Fifteen Full-Time Faculty and Staff
- Nine Graduates/Undergraduates/Hourly Wage
- HEP/University Joint Efforts
  - Industrial Engineering
  - Engineering Science and Mechanics
  - Materials Science and Engineering
  - Computer Engineering

LASER MATERIALS PROCESSING RESEARCH CENTER AT ARL PENN STATE

- ARL was named the US Navy's Center of Excellence in Laser Materials Processing
- Acts as a training and educational center for lasers and laser materials processing
- Performs basic and applied research in the area of laser materials processing for government and private sponsors
- Transfers and implements laser materials processing technology to both government and private sectors

ARL PENN STATE HEP GOVERNMENT SPONSORS

US Navy MANTECH
Navy Joining Center (NJC)
NAVSEA PMS 396
NAVAIR
Army CECOM
NASA
Puget Sound Naval Shipyard
Philadelphia Naval Shipyard
CD-NSWC
DD-NSWC
ID-NSWC
Letterkenny Army Depot
ARPA

ARL PENN STATE HEP
PRIVATE INDUSTRY SPONSORS

General Motors
Martin Marietta
General Electric
Ross Engineering
EPRI
Alcoa
Reynolds Metals
PCC
Cannondale Bicycles
Babcox & Wilcox
Alcan
Stainless Steel Products
Litton Ingalls Shipbuilding
Bath Iron Works

ARL PENN STATE HEP RESEARCH FACILITIES

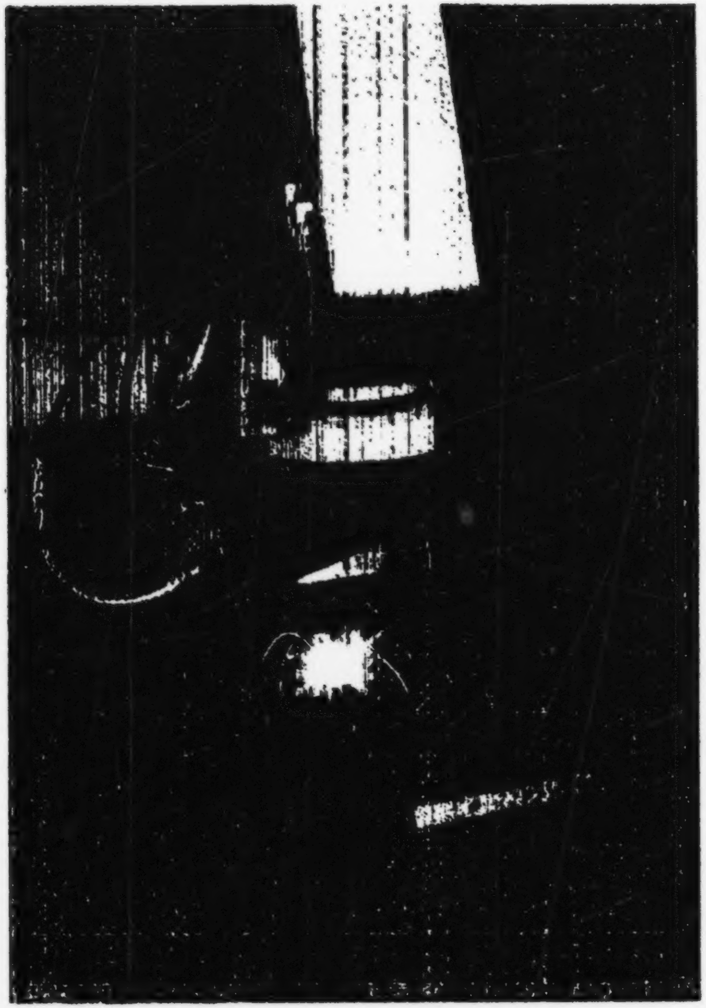

- 14 kW CO_2
- 2 - 1.5 kW CO_2
- 3 kW cw Nd:YAG
- 400 W Nd:YAG
- 110 W Q-Switch Nd:YAG
- 3 W Q-Switch Nd:YAG
- Laser Articulating Robotic System (LARS)
- Large Scale Gantry System
- Up to 150 Meter Fiber Optic Delivery
- Support Equipment

ARL PENN STATE HEP
TECHNOLOGY TRANSFER FACILITIES

- 25 kW CO_2
- LARS
- 1.8 & 3 kW cw Nd:YAG
  @ Puget Sound Naval Shipyard
- 2.4 kW cw Nd:YAG
  @ Philadelphia Naval Shipyard

LASER MATERIALS PROCESSING RESEARCH -ADVANCED WELDED STRUCTURES

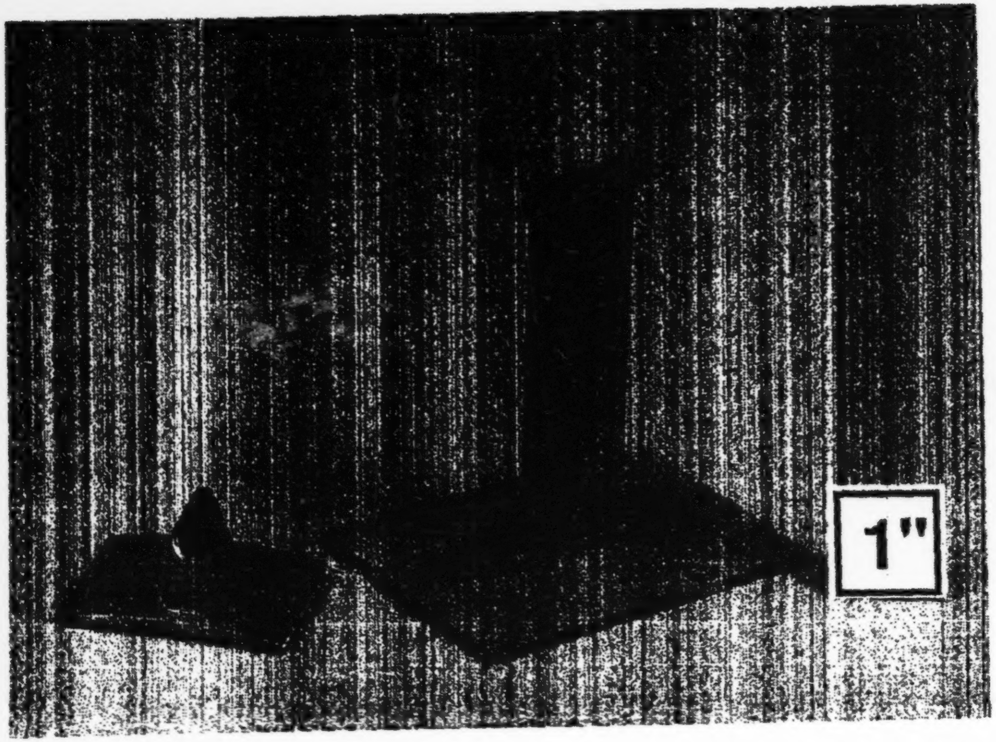

Laser Beam Welded HSLA 80 Tee Section

- **LASCOR**
- **Tee Stiffeners**
- **Double Hull Structures**
- **Titanium Alloys**
- **Automotive Materials**
- **Aluminum Alloy Stiffeners**
- **Metal Matrix Composites**

LASER MATERIALS PROCESSING RESEARCH -LASER SURFACE MODIFICATION

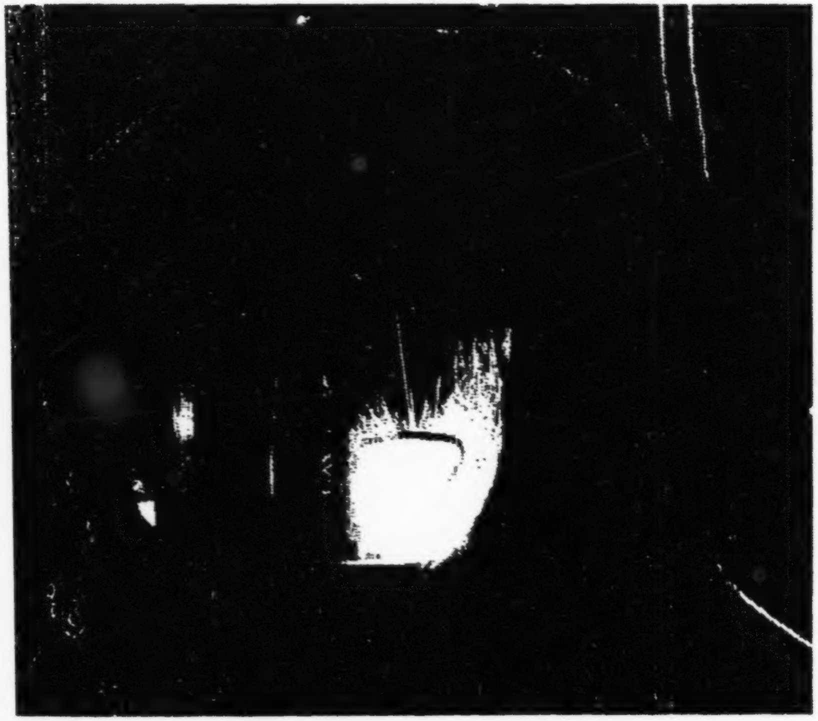

Inside Valve Cladding

- Repair Techniques
- Cladding Material Development
- Surface Re-melting
- Thermal Modelling of Surface Processing
- Qualification of Processing Procedures
- Equipment Development
- Tribology

LASER MATERIALS PROCESSING RESEARCH - HIGH POWER ND:YAG APPLICATIONS

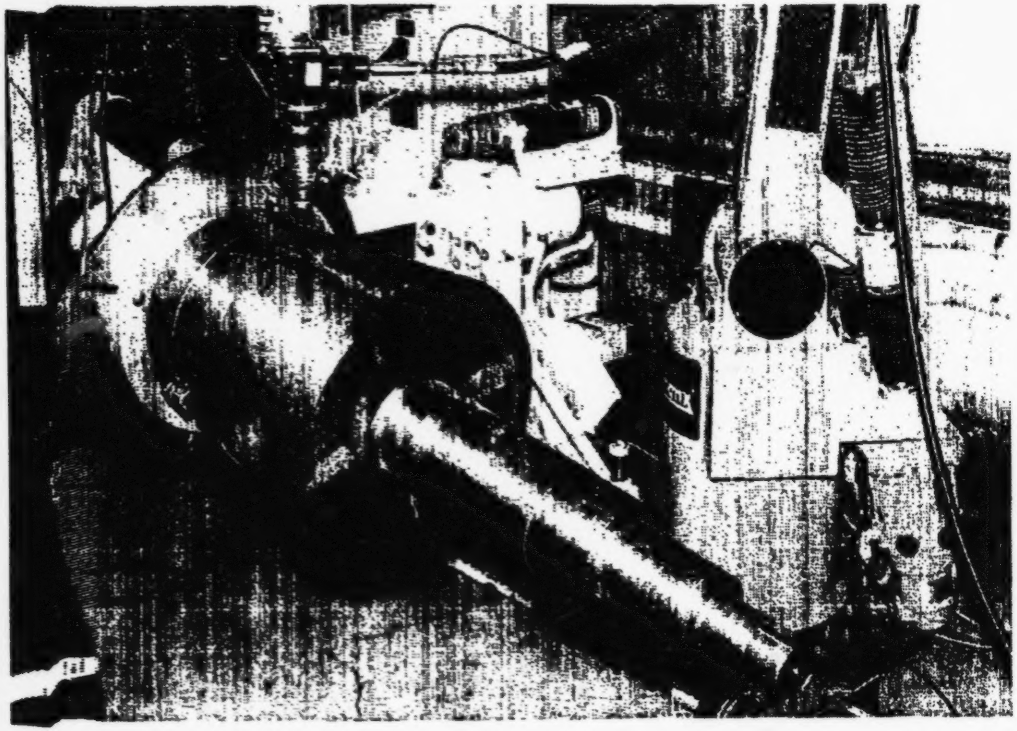

d :YAG Laser Beam Cladding of Launch Valve

- End User for ARPA Program
- Portable Laser Systems for Navy Applications
- "Environmentally Friendly" Processes
- Power Utilities
- Automation

LASER MATERIALS PROCESSING RESEARCH - ENVIRONMENTAL

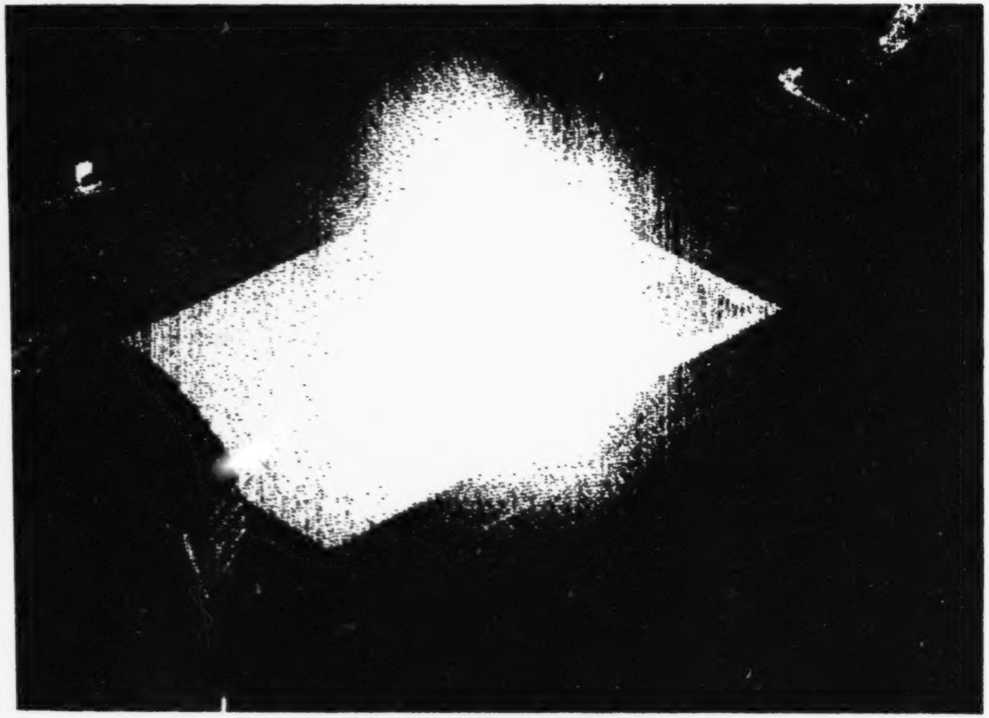

- Cutting of Hazardous Materials
- Cleaning of Contaminated Surfaces
- Cr-Electroplating Replacement
- Paint Removal

Nd:YAG Paint Removal

LASER MATERIALS PROCESSING TECHNOLOGY TRANSFER: LCC - 20 ANTENNAE-SUPPORT PLATFORMS

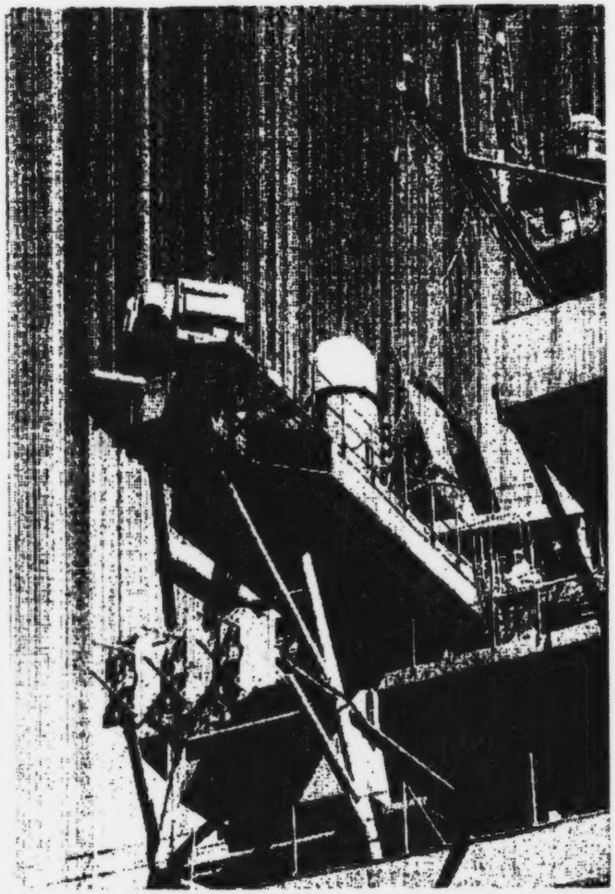

Laser Beam Welded Platform After Installation

- Modification for New Antenna Design
- LASCOR-based Design
- Stiffness Requirement
- Weight Issues
- Saved >20,000 Lbs
- Second Ship Set Completed by Mare Island Naval Shipyard (now Puget Sound Naval Shipyard)

LASER MATERIALS PROCESSING TECHNOLOGY TRANSFER: AIRCRAFT CARRIER COMPONENTS

Laser Beam Clad (Cobalt) Control Valves

- Decreased LifeCycle Cost
- Improved Sliding Wear
- High Temperature Corrosion Resistance
- Welding
- Cladding
- Repair

LASER MATERIALS PROCESSING TECHNOLOGY TRANSFER: AIRCRAFT CARRIER COMPONENTS

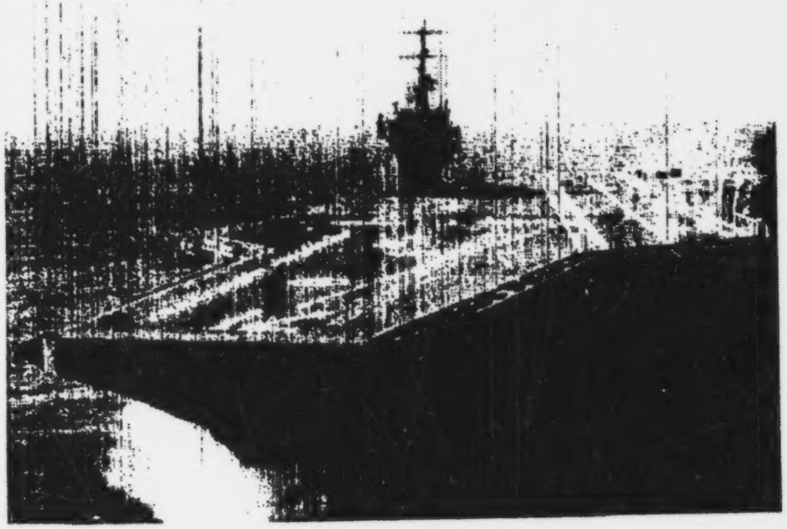

CVN - 71 Theodore Roosevelt

- Al Alloy 2618 Casting
- Improved Sliding Wear
- Reduced Maintenance Costs
- Reduced Replacement Costs

SUMMARY

- ARL Penn State High Energy Processing Department
- US Navy's Center of Excellence in Laser Mterials Processing
- Basic Through Applied Research
- Training and Educational Facility
- Support to both Government and Private Sectors
- Technology Transfer Major Thrust

#570356

LASER WELD CLADDING OF NICKEL ALUMINUM BRONZES[1]

by

C. V. Hyatt
Defence Research Establishment Atlantic

K.H Magee and J. Hewitt
The Laser Institute

and

T. Betancourt
Nova Scotia Research Foundation

ABSTRACT

Procedures for laser cladding nickel aluminum bronzes have been developed and the resulting clad surfaces have been evaluated. A low heat input (400-1200 J/cm) cladding process, which used a specially developed fine wire feeder, and a high heat input laser cladding process which used commercial welding wire, were used. The microstructures produced in this work depended on processing method and conditions, and on material composition. At the lowest heat inputs, deposits were largely martensite. As heat input increased, Widmanstätten and grain boundary α were also observed, as were transformations in the interpass heat affected zones. Experiments indicated laser cladding gives an improvement in resistance cavitation-erosion in seawater. Laser cladding of a number of ship components with complex shapes illustrated the practicality of the process.

---

[1] A first report of this work, which contained no discussion of properties or cladding of complex parts, appeared in *Proceedings of Advanced Methods of Joining New Materials II*, The American Welding Society, Miami, Florida, 1994, 111-126. It is intended that when the long term exposure studies reported in this work are complete, a final report of work on the alloys discussed herein will be submitted to the Welding Journal.

1.0. INTRODUCTION

Laser surface melting and cladding have a number of potential applications for surface texturing, component reclamation, and surface modification for wear, corrosion and erosion resistance. Exploiting this potential requires a basic knowledge about the effect of laser surface melting and laser cladding on alloys of practical interest and the development of cladding procedures. Similarities between many of the copper alloys used to manufacture high value components for use in severe environments mean that procedures and knowledge developed for one class of these alloys will be transferable to another. In this paper, the development of laser surface melting and cladding procedures for nickel aluminum bronze alloys is described. First, the characteristics of these alloys and possible improvements of them by laser treatment are described. Second, some deficiencies in our understanding of laser surface melting and cladding of these alloys are defined. Third, work to overcome these deficiencies is discussed. This work includes development of techniques for cladding nickel aluminum bronze, investigations of the effect of processing variables on deposit or melt microstructure and properties.

2.0. BACKGROUND AND LITERATURE REVIEW

Nickel aluminum bronze castings are used in marine engineering and other applications because of their excellent corrosion, erosion and cavitation performance in sea water and a number of other environments, their good mechanical properties and their acceptable casting and fabrication characteristics (Ref. 1,2). The development of cast microstructures in these alloys has been studied extensively (Ref. 3,4). Briefly, solidification occurs by nucleation and growth of the high temperature β phase, which has a body centered cubic crystal structure. After solidification is complete and, upon cooling, the high temperature β phase transforms to an face centered cubic solid solution designated α, several intermetallic phases, and regions which have traditionally been called retained β. The morphology of the intermetallic phases depends on phase and thermal history. Fine precipitates, spheroidal and dendritic particles, and intermetallic lamellae, the last in a pearlite-like α plus intermetallic eutectoid, are present. Depending on composition an undesirable γ_2 phase may form (5,6). The regions traditionally called retained β, are actually β which has transformed to some type of martensite (Ref. 3), other metastable phase or, possibly, in large castings, a metastable α plus γ_2 eutectoid product like that which gives undesirable corrosion performance in some aluminum bronzes (Ref. 4,7). Regardless of the precise form of the retained β transformation products, the regions where these β transformation products form are generally the last area of as-cast β to transform. Partitioning of alloying elements during earlier transformations leaves these regions with a different composition than the surrounding material (Ref. 3). Heat treatment of nickel aluminum bronze castings is sometimes done to eliminate these regions and to break up the continuous eutectoid regions.

The higher cooling rates associated with welding produce microstructures different than those seen in castings. Data is limited, but, depending on composition and cooling rate, varying amounts of Widmanstätten α in a martensitic matrix are expected to form from the high temperature β phase (Ref. 8,9). Intermetallic precipitates and eutectoid regions may also form in the weld deposit and heat affected zones. The composition and structure of martensites in the weld metal and heat affected zone are, generally, expected to be different than those of the martensite which forms by the transformation of retained β in castings.

Two applications, propellers and valves, illustrate the strengths and limitations of nickel aluminum bronzes. Considering propellers for large ships, applicable standards permit higher stresses on these alloys than on any other common propeller casting alloy (Ref. 1,10). This is a result of the good toughness, corrosion fatigue resistance, and stress corrosion resistance of nickel aluminum bronzes. Nickel aluminum bronze valves also perform well but problems with dealuminification have caused concern and lead to a number of changes in practice (Ref. 7,8,11,12). In contrast to propellers, which are cathodically protected and used in flowing water, valves may see stagnant conditions, receive little deliberate or incidental cathodic protection and have crevices as a result of design or deposits. Such castings are used with the knowledge that corrosion will occur. So long as this corrosion is pitting or impingement attack, nondestructive inspection can be used to identify problems before they become critical. Dealuminification, whether at a crevice or adjacent to a weld heat affected zone is more of a concern because low strength porous copper is redeposited on the affected surface, precluding nondestructive assessment of the depth of attack with acceptable confidence. Rates of attack of 0.25 mm/year at crevices in as cast material and of 1 mm/year in or adjacent to weld heat affected zones have been reported (Ref. 12). In both regions, after an initial transient, a mechanism involving the dissolution of intermetallic lamellae in the eutectoid regions at a more rapid rate than the surrounding α matrix is thought to be active in at least a majority of cases (Ref. 12). While heat treatments have been partly successful in eliminating dealuminification, the problems may still occur in very large castings, which have coarse eutectoid structures and in castings which have insufficient Ni (Ref. 7). It has been suggested that residual stress plays a role in the preferential attack near weld heat affected zones (Ref. 8). Attack of weld metal does not seem to be serious, provided a matching filler metal is selected. On this last topic, however, there is limited information.

There are two reasons why laser surface melting and cladding are expected to improve nickel aluminum bronze castings. First, laser treatment of aluminum bronzes and nickel aluminum bronzes has produced improvements as large as an order of magnitude in resistance to cavitation, erosion, general corrosion and dealloying (Ref. 13-16). In all cases homogenization and refinement of the surface structure are partly responsible for these improvements. Production of a harder martensitic surface also probably contributes to these improvements. Second, conventional heat treatments for nickel aluminum bronzes may not simultaneously optimize the toughness and surface properties. Laser treatment processes offer a mechanism for producing a harder, more homogenous and more corrosion resistant surface on a part whose bulk is treated to have the optimum combination of strength and toughness for a particular application.

Despite the favorable data just presented, some problems remain. For example, most published data has been produced by laser melting processes, often with conditions designed to give very rapid solidification at the expense of depth of melting. As well, previous studies of laser cladding of nickel aluminum bronze used pre-placed powders or pastes and achieved only limited success (Ref. 16,17). Work on laser cladding nickel aluminum bronze onto aluminum has been successfully carried out and investigated in detail (Refs. 18-20). Application of this work to the current case is difficult because the composition of the consumable used is low in iron (2.19 Fe, 5.27 Ni, 9.79 Al) and because of dilution effects with aluminum from the base material under some conditions. Work on autogenous laser welding of a number of nickel aluminum bronzes has also been reported. In general relatively high heat input of 2000 J/cm or more were used. The melt pool geometry's, and thus thermal histories for equivalent heat inputs, are also significantly different than in the cladding case. Finally, only a few compositions of nickel aluminum bronze have been investigated. It is well known, however, that even within the composition ranges permitted by the various standards which specify nickel aluminum bronzes, large variations in continuous cooling behavior, microstructure, and mechanical and corrosion properties are possible. Particularly lacking is data on delaying of laser surface melted or laser clad alloys as a function of heat input and alloying. Work to obtain the required data and understanding is reported in this paper. It includes:

1. developing a better arrangement for laser cladding nickel aluminum bronze;

2. investigating laser surface melting in a regime useful for surface melting of components;

3. performing additional laser surface melting experiments, with lower travel speed and lower power density to investigate one heat input regime in laser cladding;

4. investigating laser cladding in two different heat input regimes;

5. investigating properties such as cavitation erosion, stress corrosion, and dealloying and;

6. demonstrating complex parts can be clad.

3.0. MATERIALS AND METHODS

3.1. ALLOYS

The materials used in this study included: wrought coupons meeting UNS C63200 and UNS C63000, cast coupons meeting UNS C95800 and ERCuNiAl weld wire. Several different sizes and compositions of coupons were used for different purposes. These are summarized in Table 1. A number of nickel aluminum bronze and bronze components were also treated. Both surface melting and cladding experiments were performed. Pretreatment was identical whether materials were intended for cladding or for surface melting. Coupons, were machined flat, glass bead blasted and degreased with acetone immediately before processing.

Table 1. Compositions, dimensions and uses of coupons

Alloy		Thickness	Specimen Composition					Processing	Evaluation
	(UNS)	(mm)	Cu	Al	Ni	Fe	Mn		
a	C95800	~25	80.3	8.75	4.8	4.4	1.4	Substrate for Cladding	Dealloying, Stress Corrosion, bend tests, Cavitation
b	C95800	~25	81.1	8.63	4.8	4.0	1.1	“	“
c	C95800[1]	6.4	79.3	9	4.3	4.9	0.86	“	Dealloying
d	C95800	3.2	81.7	9.1	4.4	3.8	1.2	Surface Melting	“
e	C63000	3.2	81.7	9.8	4.5	2.9	0.7	“	“
f	C63200	3.2	79.4	9.1	4	6.1	1.5	“	“
w	(ER) CuNiAl	0.25, 0.89 (dia)	80.8	9.0	4.6	3.9	1.2	Welding Wire	Dealloying, Stress Corrosion, bend tests, Cavitation

[1] The material was supplied with this designation. Because iron is greater than nickel, it does not satisfy the chemical analysis requirements.

[2] Detailed metallography and microhardness testing was done on all specimens.

3.2 LASER SURFACE MELTING

For laser surface melting experiments, a Mitsubishi 2512HB2 laser capable of roughly 1.6 kW output power in continuous operation was used. A range of travel speeds was achieved with a turntable device. Surfaces were shielded during processing with flowing helium to prevent atmospheric contamination. Power densities at the specimen surface of between 0.76 and 1.1 MW/cm^2 were achieved by placing it at the focal point of a 127 mm focal length lens. With this arrangement, travel speeds between 8 and 80 cm/s were investigated. Because of the relatively high power densities used in these experiments, they will be called the high power density laser surface melting experiments from here on.

Additional surface melting trials were done using the same turntable and a Combustion Engineering CE 5000 laser capable of 5.5 kW output power in continuous operation. Again laser light was focused to achieve appropriate power densities, this time using a 380 mm focal length lens; nominal laser power densities between 0.04 MW/cm^2 and 0.09 MW/cm^2 were achieved by varying laser output power and by placing the specimen 4.7 to 9.4 mm away from the focal point. With these lower power densities, travel speeds between 0.85 and 12.7 cm/s were used. Some preliminary trials were done first to identify the appropriate power level regime. Then, trials, in which overlapping melt beads were produced at a number of scan speeds between 0.85 and 9.3 cm/s, were performed at power densities of 0.09, 0.065 and 0.04 MW/cm^2. A gas flow of either helium or argon was used to shield the specimens from the atmosphere. The experiments with this higher power laser were done under conditions similar to those used for cladding trials; their purpose was partly to optimize process variables—gas shield composition, scan speed, defocus, and laser power—without the complications of adding material by a wire feed. Because the power densities used are lower than in the previous case, these experiments will be called the low power density laser surface melting experiments from here on.

3.3. LASER CLADDING PROCEDURES

The cladding experiments were done with the higher power CE 5000 laser equipped with the two different arrangements to feed wire to the deposit. The arrangement used to feed and position the 0.89 mm diameter wire consisted of a gas metal arc welding torch attached to a commercial wire feeder. Argon or helium shielding was provided through orifices in the torch tip in the normal way. In the arrangement used to feed the 0.25 mm diameter wire, the gas metal arc welding torch was replaced with the tip of a hypodermic needle connected to a custom built wire feeder based on a stepper motor. Precise positioning of the needle tip was possible because it was mounted on a micrometer stage. With the fine wire arrangement, shielding gas was directed at the specimen surface through the primary gas nozzle attached to the laser optics head.

A number of process variables were adjusted by trial and error to produce the best appearing deposit. For both wire sizes, wire was fed from the leading edge of the melt, at an angle of 30° to the specimen surface. In the 0.89 mm wire arrangement, the specimen surface at the start of cladding was located at a position 11.9 mm beyond the focal point and the wire was aimed at the front of the melt pool. In the 0.25 mm wire arrangement, the specimen surface was located at a position 6.4 mm beyond the focal point and the wire was aimed to intersect the specimen surface about 1 mm in front of the melt pool. For almost all preliminary trials, and for many of the specimens upon which detailed metallography was performed, alloy C was used as the base material and helium was used as the gas shield. A range of heat inputs from 400 J/cm to 6000 J/cm were investigated. In this paper detailed metallography on two extremes are reported, one at 650 J/cm and one at roughly 6000 J/cm.

Specimens for cavitation and stress corrosion studies were prepared using the fine wire feeder exclusively. In all cases the base material was either alloy A or alloy B and an argon gas shield was used. Two separate sets of specimens were clad for the cavitation studies. One was produced with a heat input of approximately 700 J/cm and one was produced with a heat input of approximately 3000 J/cm. The stress corrosion specimens were produced with a heat input of 1500 J/cm.

For cladding of complex parts during the demonstration trials, wire feed arrangements, laser parameters and beam polarization were modified. Details are given in Refs. 21 and 22.

3.4 METALLOGRAPHY

Characterization of the laser treated and clad materials was done by optical and scanning electron microscopy, energy dispersive x-ray microanalysis, microhardness testing, and measurement of surface roughness. Etching for optical microscopy was done with either 1 g of CrO_3 in 100 ml of water at 6 V or with 5 g of $FeCl_3$ dissolved in 15 ml HCl and 60 ml methanol. These etchants gave equivalent results for the purposes of black and white micrographs. Etching for examination of cross sections in the scanning electron microscope was done by electrolytic etching at 60 V with 22 g/l of NaCl in water, with pH adjusted to 4.5. An important feature of many of the microstructures examined in this study is the formation of α, during cooling of the high temperature β phase or tempering of the martensite phase. The morphology of the α phase is described using the Dubé classification for ferrite in steel (Ref. 23).

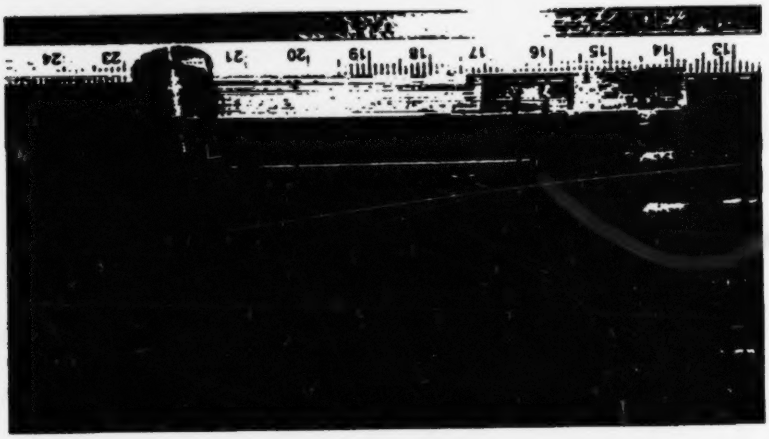

Fig. 1. Stress Corrosion Specimen.

3.5 EVALUATION OF CORROSION PROPERTIES

Evaluation of these materials is ongoing and involves stress corrosion, dealloying and cavitation-erosion tests. Stress corrosion tests are being performed using specimens like those described in Ref. (24). and shown in Fig. 1. These 'tuning fork specimens' allow stresses used to be estimated on the non-laser clad face from strain gage records. Three types of specimens were used. All had been laser clad on the outer face with identical low heat input conditions on the face of one tine. One type had an as laser clad finish. A second type was finished by grinding on metallographic papers to a 600 grit finish. A third type was similarly ground but contained defects in the region of high stress. These defects were either surface breaking porosity or scribe lines. Stresses between 60 percent of the yield strength and 140 percent of the ultimate strength of the base material were induced by closing the tines of the 'tuning fork' specimens. Stresses were estimated from a relationship between surface strain and opening of the tines determined by strain gauging the material on the unclad tine. Following data given in Ref. 25, no bias potential was used. Instead isolated specimens were immersed in flowing Halifax Harbor seawater. Specimens are scheduled to be removed after one, three and nine months, starting in June 1995.

Dealloying tests have been done by immersion of specimens in 50 °C saturated CuCl in water for up to twelve hours and by long term immersion of specimens in Halifax Harbor seawater. In the latter case, alloys of a wide range of specimens, with the compositions shown in Table 1, produced with a range of heat inputs from 25 J/cm to 3000 J/cm were examined. Base materials were also exposed. Following previous workers [5], some specimens were coupled to more noble Ti-6Al-4V and artificial crevices were created on some specimens to reproduce severe service conditions. Specimens are to be removed after three, nine and twenty-one months for weighing to determine weight loss and metallographic examination.

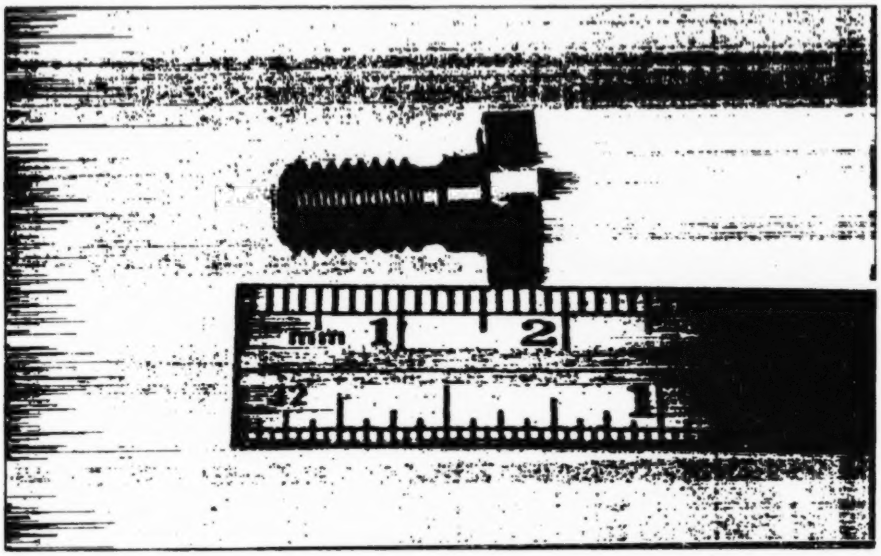

Fig. 2. Photograph of Cavitation Erosion Specimen

Cavitation erosion experiments were carried out according to ASTM standard G-32 [26]. The modified test specimen shown in Fig. 2 was used. The test setup consisted of a piezoelectric vibrator unit equipped with a 12.7 mm diameter horn to which a specimen was attached. Test specimens were machined from material clad with a heat input of 700 J/cm, clad with a heat input of 3000 J/cm and from unclad material. The test surface of each test specimen was ground to a 600 grit finish and the specimen was washed (First in water and then in ethanol in an ultrasonic bath). Following air drying the specimen was weighed to within ± 0.1 mg. The test specimen was attached to the horn with a torque of 35 lbf·in, to avoid premature failure of the threads. The test specimen, mounted on the horn of the ultrasonic unit, was immersed in 1.5 liters of seawater at 25±2 °C and oscillated at a frequency of 20±0.5 kHz and an amplitude of ±50 μm. Periodically the experiment was interrupted, and the specimen was removed, cleaned and weighed so that mass loss as a function of time could be determined. The performance of the test setup was shown to meet the requirements of ASTM standard G-32 by running a test with annealed nickel 200 in distilled water at 20 °C. To ensure consistency, prior to each seawater test, the seawater was sonicated with a Ni 200 specimen for 30 minutes to stabilize waters gas content.

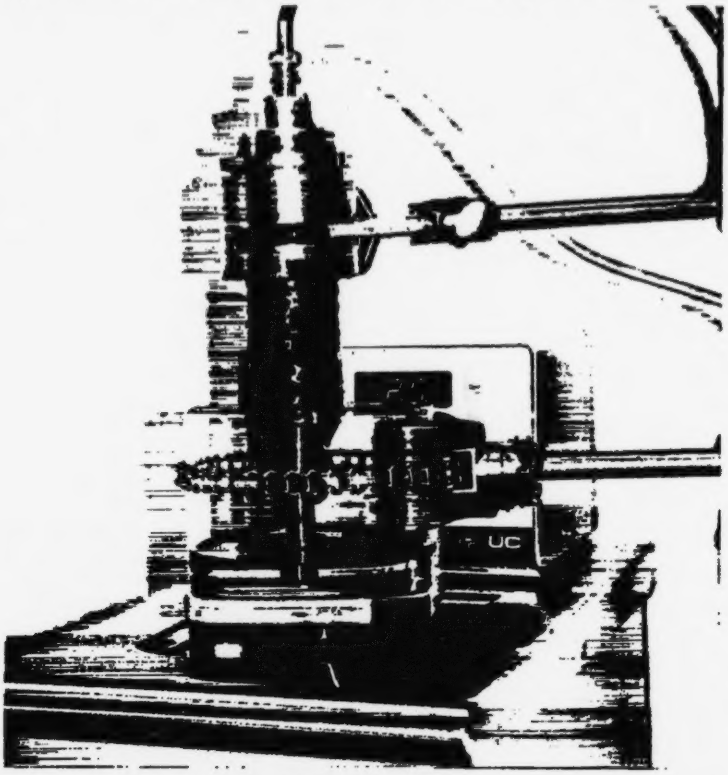

Fig. 3. Photograph of Cavitation Erosion Apparatus

4.0 RESULTS AND DISCUSSION

4.1 LASER SURFACE MELTING

The surface melting trials provided information on the effect of scan speed and power level on melt pool dimensions, surface topography, and deposit and inter-pass heat affected zone microstructures and on the effect of type of gas shield. Two regimes were investigated. The first was a relatively high power density and rapid travel speed regime where surface melting of components might be done. The second was a lower power density and slower travel speed regime with conditions similar to those used in cladding experiments. The two regimes shared one similarity with each other and with the cladding experiments. All of the surface melts, as well as the cladding deposits resolidified epitaxially. The grain boundaries between the columnar prior β grains can be discerned in all surfaces, though their appearance depends on thermal history. In the most rapidly quenched surfaces they are visible only because of orientation differences between transformation products in each prior grain; in more slowly cooled surfaces they are darkened everywhere; in still more slowly cooled surfaces they are outlined with α.

4.11 HIGH POWER DENSITY LASER SURFACE MELTING EXPERIMENTS

Considering the higher power density laser surface melting experiments first, melt pool dimensions at a number of scan speeds for power densities of 0.76 MW/cm^2 and 1.07 MW/cm^2 are summarized in Fig. 4 for alloy UNS C63200. Because of variability in melt pool width, overlaps of 50 % were deemed necessary to produce a uniformly melted surface. Surface topography was strongly dependent on travel speed and also on power level. Above a scan speed of 32 cm/s, breakdown of the regular ripple pattern occurred and produced a rougher surface. Examples are shown in Figure 5. Increases in roughness with decreasing power level and increasing scan speed were also noted. As discussed elsewhere (Ref. 27), this is, in part, thought to be a consequence of prior surface roughness. Surface breaking porosity, both scattered over the melt surface and as porosity chains along the melt pool edges, occurred, as shown in Fig. 5. In contrast with previous work on copper nickel alloys (Ref. 28), porosity chains occurred at the edges of overlapping passes, perhaps because of differences in the high temperature oxide film which forms on the two classes of alloys. The microstructure of the surface melt on wrought alloy UNS C63200 was single phase martensitic, as shown in Fig. 6. Cast alloy UNS C95800 was similar, though what appeared to be small intermetallic particles were observed in specimens produced at the highest travel speed. These are probably incompletely dissolved intermetallics from the prior microstructure (Ref. 28). The hardness of the specimens was dependent primarily on processing. Typical values for microhardness of the as solidified material were HV(100 g) 324 for a specimen surface melted with 1.07 MW/cm^2 at a travel speed of 8 cm/s and HV(100 g) 380 for a specimen surface melted with 0.96 MW/cm^2 at a travel speed of 8 cm/s. Figure 7 shows the inter-pass heat affected zone in a specimen of UNS C63200. While evidence of martensitic decomposition in the heat affected zone could not be detected with optical microscopy, some darkening of prior β high angle grain boundaries was noted.

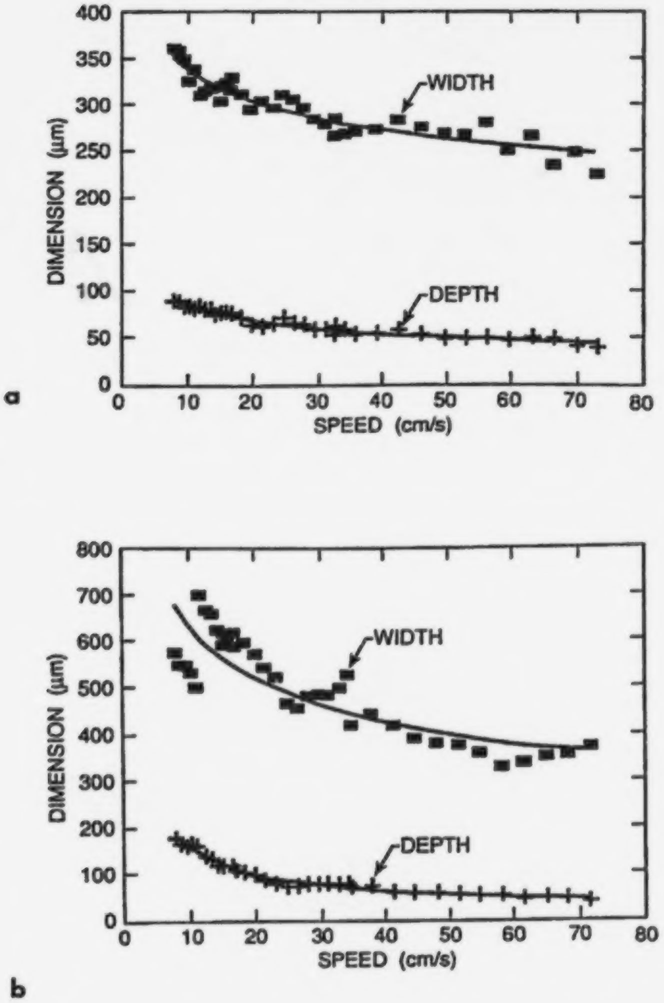

Fig. 4. Effect of scan speed on melt pool dimensions for power densities of a. 0.76 MW/cm^2 and b. 1.07 MW/cm^2.

Comparing these experiments with previous studies, acceptable microstructures and surface topographies have been produced with depths of melting as deep as 190 μm, corresponding to a power density of 1.07 MW/cm² and a travel speed of 8 cm/s. This is four or five times deeper than the depths of melting investigated in previous studies.

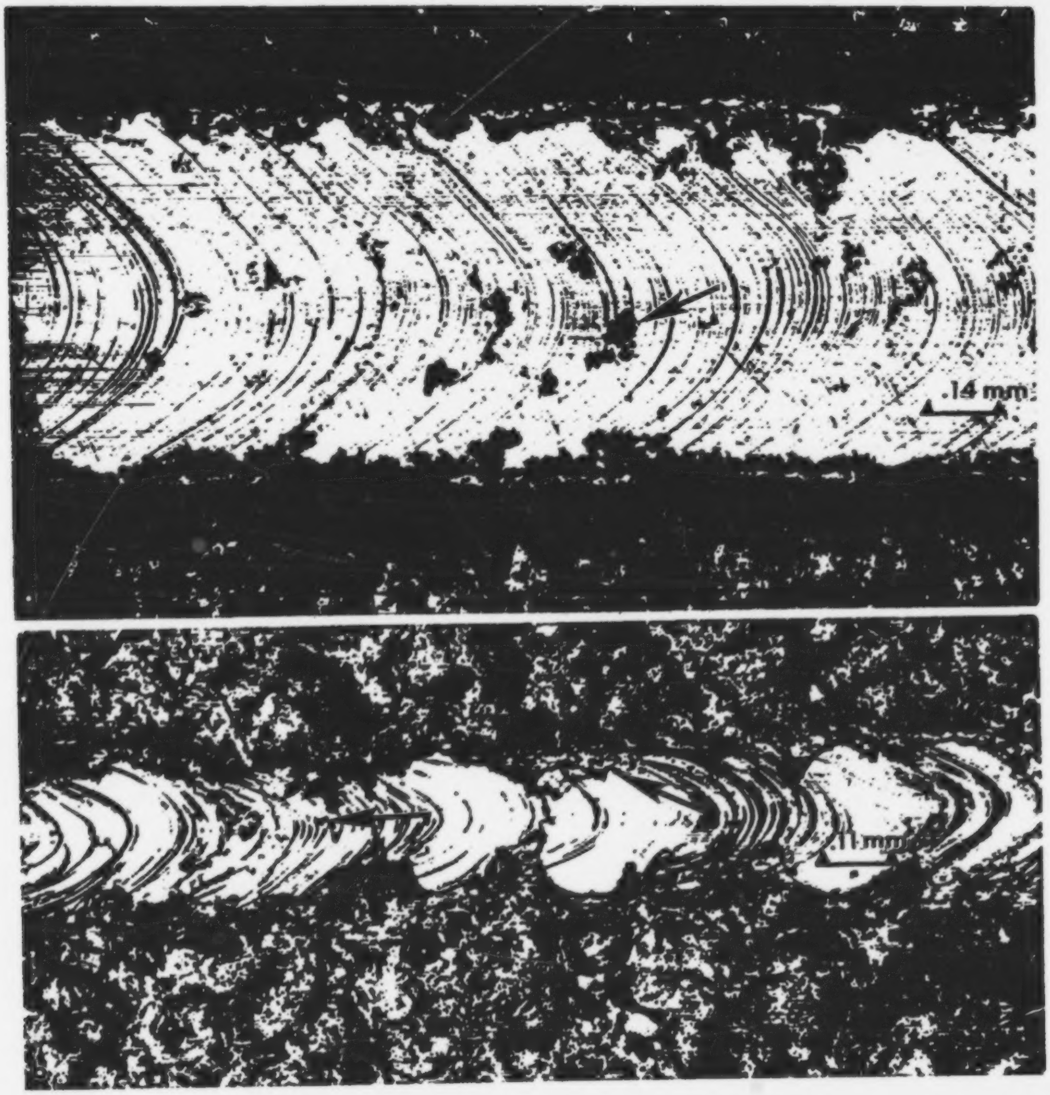

Fig. 5. Single laser passes on alloy UNS C63200. a. 1.07 MW/cm² at 8 cm/s, showing regular ripple pattern. b. 0.76 MW/cm² at 73 cm/s, showing irregular ripple pattern. Surface breaking porosity is marked with arrows on both micrographs.

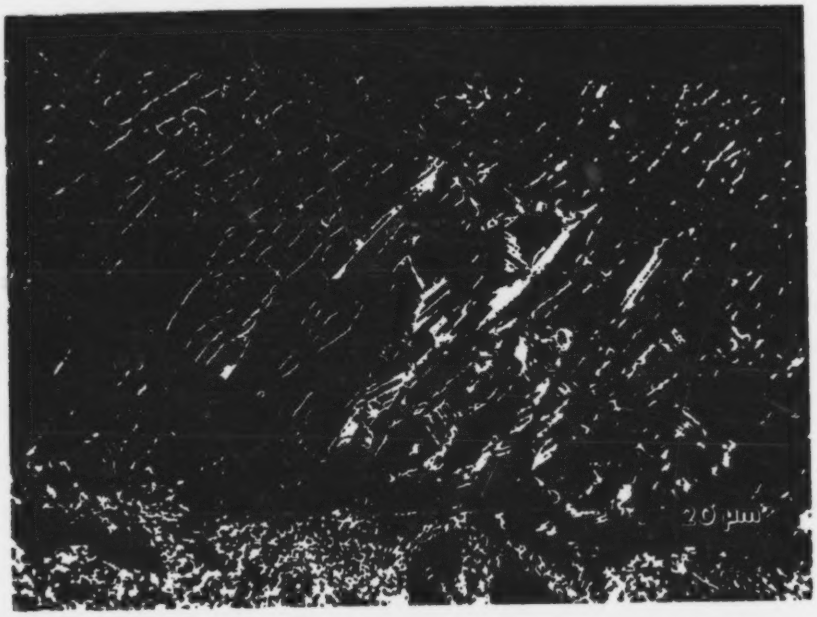

Fig. 6. Martensitic microstructure of alloy UNS C63200 treated using 0.96 MW/cm^2 and 8 cm/s.

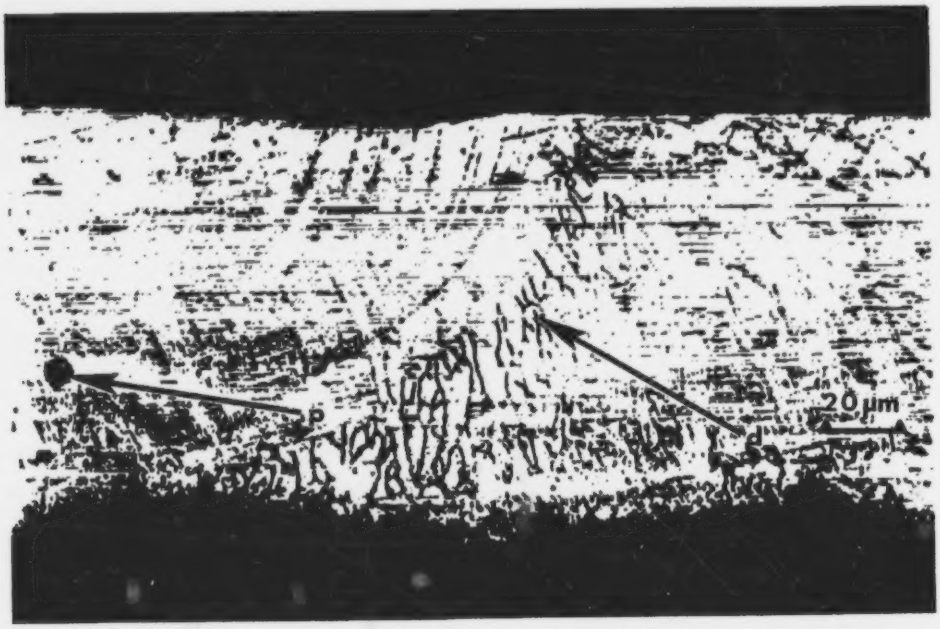

Fig. 7. Typical inter-pass heat affected zone in alloy UNS C63200. Note darkening of prior β high angle grain boundaries(d) and microporosity (p)

4.12 LOW POWER DENSITY LASER SURFACE MELTING EXPERIMENTS

In the lower power density laser surface melting experiments, the as-solidified laser melts were generally martensitic, except for incomplete dissolution of prior intermetallic particles in the specimens produced at higher travel speeds. In contrast to the previous case, after etching, prior β boundaries were more visible, appearing darker than the surrounding martensite. Some α did form within the inter-pass heat affected zones. To make comparisons easier, the heat input used was calculated from the laser power and travel speed. Below a heat input of about 500 J/cm, the heat affected zone α was present only in the grain boundary allotriomorphic form. Above this heat input, α with a Widmanstätten morphology formed in the heat affected zone. With increases in heat input above 500 J/cm, volume fraction α increased rapidly. Because the microstructures produced in these experiments are similar to those produced in the low heat input laser cladding experiments, they are not shown here.

Experiments with both laser setups revealed that the quality of surface was dependent on gas shield type. A flowing helium gas shield increased surface roughness and caused breakdown of the regular ripple pattern compared with a flowing argon gas shield. Presumably, these results are a consequence of oxygen contamination of the helium gas.

4.2 LASER CLADDING EXPERIMENTS

As with the laser surface melting experiments, two distinct regimes were investigated in the cladding experiments. A series of higher heat input trials allowed commercially available wire sizes to be used. A series of lower heat input experiments allowed higher cooling rates to be investigated. Both helium and argon gas shields were used.

4.2.1 HIGHER HEAT INPUT LASER CLADDING EXPERIMENTS

In the higher heat input experiments, both single and double layer deposits were produced. In all cases a helium gas shield was used. Also for all cases alloy b was used as a base material. Considering the single layer deposit first, the areas of interest included the as-deposited material, the inter-pass heat affected zones and the base metal heat affected zone. Fig. 8 shows the relative sizes of these zones on a specimen produced using a travel speed of 8.4 mm/s, 5 kW of laser power, and a laser spot size of about 3 mm. The significance of power density and heat input is unclear in laser cladding, however, these variables give a nominal power density of 0.07 MW/cm^2 and a heat input 5952 J/cm. The microstructure of the as-deposited material developed sequentially. First, β formed by epitaxial solidification. Second, a few volume percent of this β transformed, by nucleation and growth, to α. Finally, the rest of the β phase transformed to martensite. Most prior high angle β grain boundaries are outlined with allotriomorphic α. Some Widmanstätten α is also present. Both types of α can be seen in Fig. 9, which shows both the heat affected zone and the as-deposited weld metal for the same specimen shown in Fig. 8. The volume fraction of both types of α increased with increasing heat input, which was achieved in these experiments by decreasing travel speed for constant power density. In the inter-pass heat affected zone, significant transformation of the martensite occurred. As the optical micrograph in Fig. 9a and the electron micrograph in Fig. 9b show, both grain boundary (allotriomorphic)and Widmanstätten α are present, with total volume fraction as high as 0.7 in some areas. The microstructure of the base metal heat affected zone was similar, although near the unaffected base metal the Widmanstätten α became more random and undissolved and spherodized intermetallic particles were present. The microhardness of the as-deposited material was between HV (100 g) 224 and 280 and that of the heat affected zones was between 240 and 290 on the same scale. The structure of two layer deposits produced with a high heat input was similar to that just described, though some darker etching constituents, which may be intermetallic precipitates, did form.

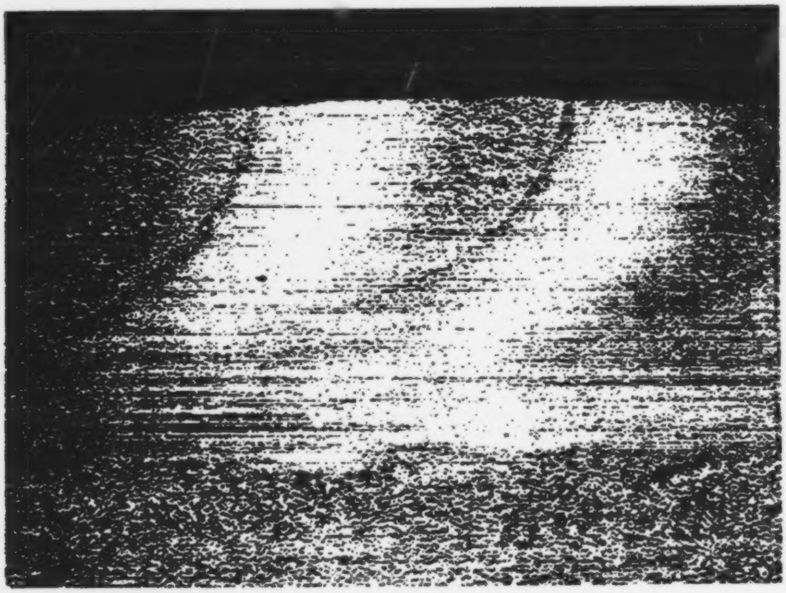

Fig. 8. Single layer laser cladding deposit produced with a travel speed of 8.4 mm/s, 5 kW of laser power, and a laser spot size of about 3 mm (nominal power density of 0.07 MW/cm², heat input 5952 J/cm).

The consequences of having grain boundary allotriomorphic and Widmanstätten α in the as-deposited material and the heat affected zones in the amounts shown are unclear. Some insight comes from related materials and observations. First, in aluminum bronzes, it is the γ_2 phase[2], not the α or β phases, which sensitizes them to preferential corrosion (Ref. 9). Second, in aluminum silicon bronze, decreasing the quench rate used to produce a martensitic microstructure increases the sensitivity to preferential dissolution (Ref. 29). Third, in developing procedures for deep etching (Ref. 30) with NaCl, it was reported that it is generally the β, not the α which is attacked in deep etching over a range of pH levels and etching voltages. This is consistent with data on aluminum bronzes which indicates that the α is generally either at the same potential as or is protected by the β (Ref. 9). Thus, regions of greatest concern are those with a large volume fraction of α and a small volume fraction of martensite, at least from the perspective of preferential dissolution. Finally, these alloys are often used in environments where improvements in their already good erosion resistance could extend their useful lives. Often, increases in surface hardness give improvements in erosion and cavitation resistance (Ref. 1). Because the hardness of the clad surfaces was lower than that of the surface melted layers and the amount of α present in the clad layers was higher than in the surface melted surfaces, lower heat input cladding experiments were carried out to produce microstructures without large amounts of α and with higher hardness.

---

[2] The question of whether of not the γ_2 phase may also form in some laser welds has been raised in related work (Ref. 5). We have seen no clear evidence of it here. It will be addressed in detail in a future study.

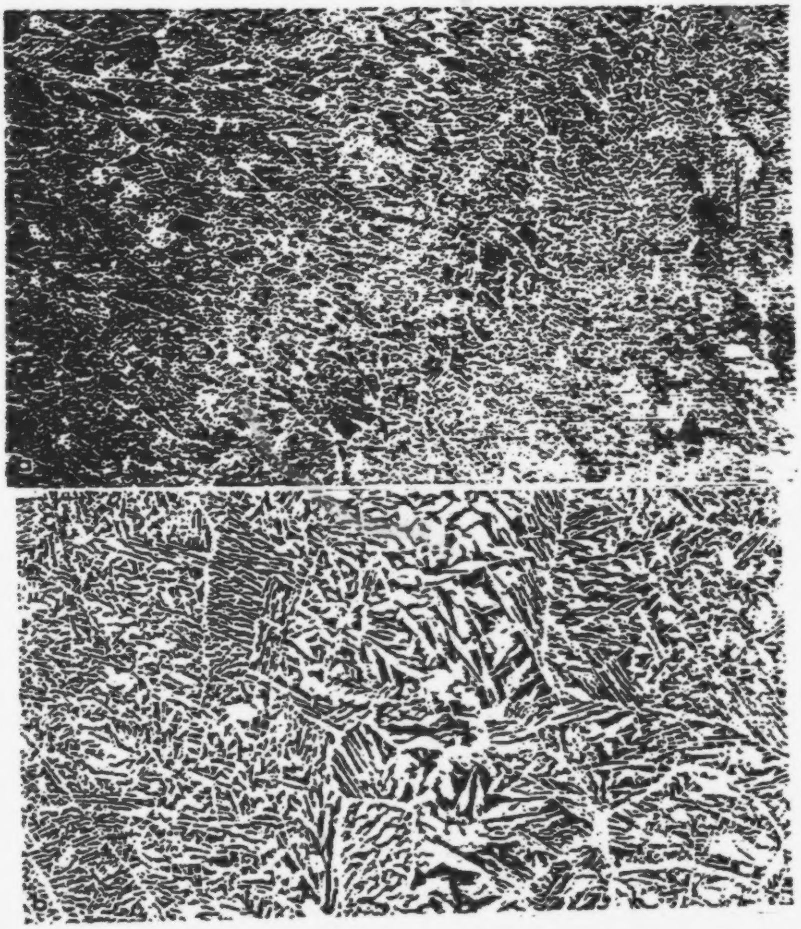

Fig. 9. Deposit shown in Fig. 5 at higher magnification. a. Optical micrograph showing both as-deposited material and an inter-pass heat affected zone. b. Electron micrograph of heat affected zone after deep etching. The α phase is lighter in (a) and unattacked in (b).

4.2.2. LOWER HEAT INPUT LASER CLADDING EXPERIMENTS

In the lower heat input experiments, an appropriate range of heat inputs for investigation was determined from the low power density surface melting experiments. Because of differences between the cladding and surface melting processes, a number of conditions in the regime of interest were investigated. For these experiments base alloy b and a helium gas shield were used. The minimum heat input at which an acceptable deposit shape was possible was about 425 J/cm, corresponding to a laser power density of 0.037 MW/cm^2, a laser power of 1.8 kW and a travel speed of 4.2 cm/s. This produced a deposit which, in the regions in the as-deposited state, was single phase martensitic. In the inter-pass and base metal heat affected zones, some grain boundary allotriomorphic α formed, though it is minimal as Fig. 10 shows. Higher heat inputs of about 650 J/cm, corresponding to a laser power density of 0.095 MW/cm^2, a laser power of 2.7 kW and a travel speed of 4.2 cm/s made the quality of the deposit less sensitive to wire position. These latter conditions were used to produce areas of single and double layer deposits large enough for corrosion, erosion, and cavitation studies. Considering the single layer deposit, the relative sizes of the regions of interest, the as-deposited material and the inter-pass and parent metal heat affected zones are shown in Fig. 11. Figure 12 shows the as-deposited material to be almost wholly martensite, with grain boundary allotriomorphic α forming occasionally at prior high angle grain boundaries. Transformation has, however occurred in the heat affected zones, as Fig. 12 shows. Both grain boundary allotriomorphic and Widmanstätten α are present. In all cases the hardness was significantly higher than that in the high heat input deposit. Within the as-deposited material, the Vickers microhardness was between HV(100 g) 410 and 440 while within the heat affected zones it was between HV 250 and 360. Considering the two layer deposit, microstructural features were quite similar, except where the heat affected zones in the first layer were reheated by the second pass. Here, more significant α formation has occurred, as Fig. 13 shows. In some cases, the effects are as severe as in the high heat input case.

The experiments just described reveal that laser clad layers with minimal Widmanstätten α can be produced, but that slight increases in laser power causes significant precipitation of α in either grain boundary allotriomorphic or Widmanstätten forms, in heat affected zones, and with higher power densities, in the as-deposited material. Where heat affected zone transformation occurs, it is expected to be especially severe where more than one heating cycle is observed.

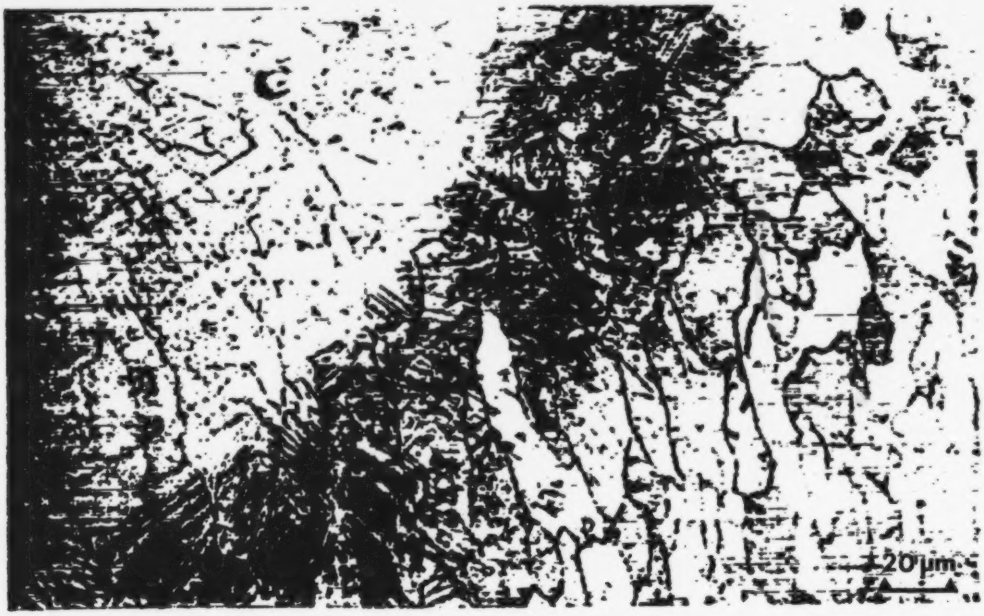

Fig. 10. Heat affected zone in a deposit produced using a heat input of 425 J/cm and a travel speed of 4.2 cm/s.

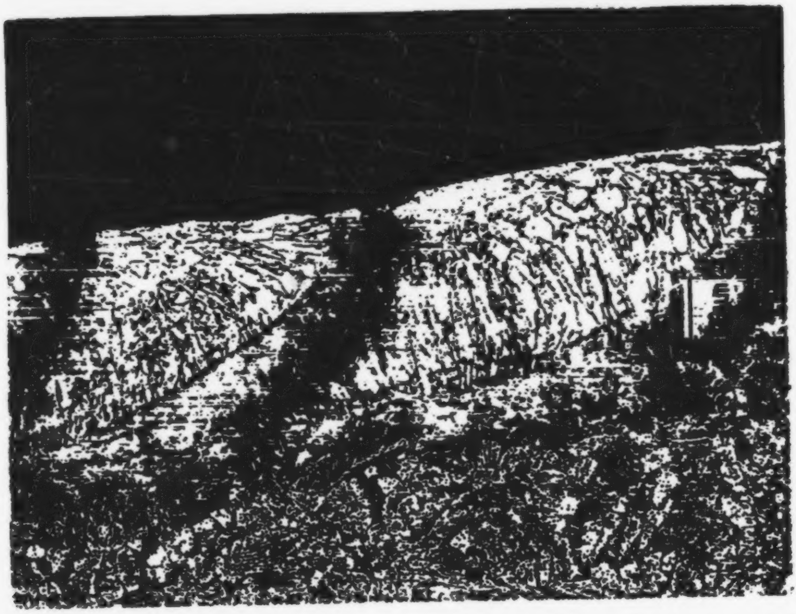

Fig. 11. A deposit produced using a heat input of 640 J/cm and a travel speed of 4.2 cm/s.

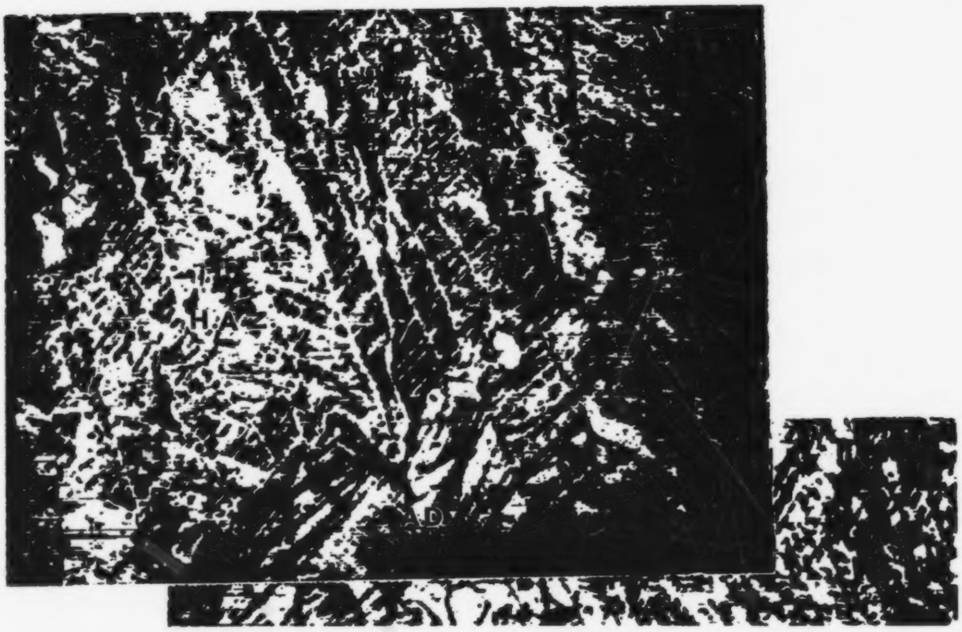

Fig. 12. Same deposit as in Fig. 8 at higher magnification. Both the as-deposited material (A.D) and the heat affected zone (H.A.Z) are shown.

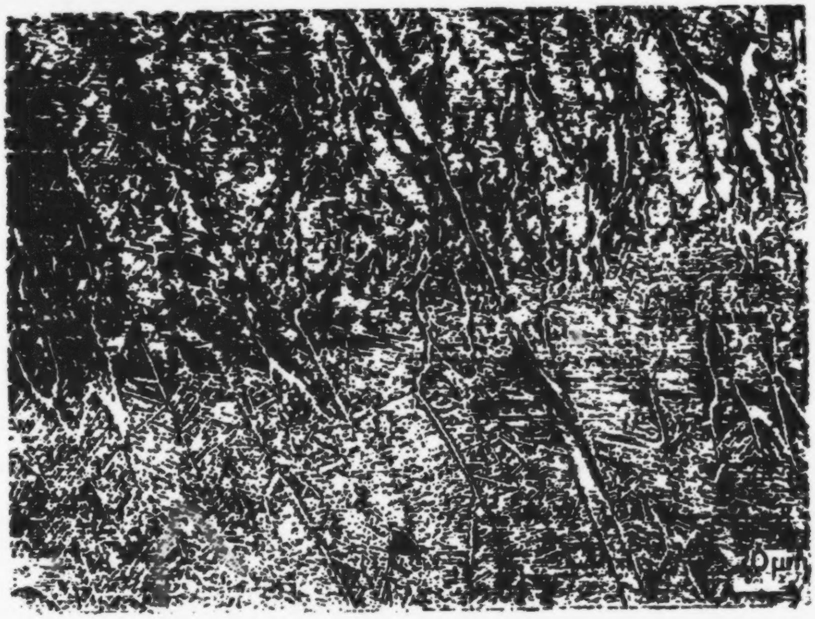

Fig. 13. Heat affected zone reheated during the deposition of a second layer. Deposition conditions are the same as for Figs. 8, 9.

4.3 EVALUATION OF CORROSION PROPERTIES

The microstructure and microhardness data just summarized, along with data on as cast alloys form the basis upon which the approach for evaluation of the laser clad and surface melted alloys was based. Four properties, dealloying, general corrosion, stress corrosion and cavitation erosion resistance have been or are being investigated. Electrochemical behavior is also to be investigated. In evaluating, these different properties, a number of different processing conditions and alloy compositions have been used. In part this was a function of what was available. However, some logical decisions were made. For dealloying studies, as mentioned earlier, dealloying is known to be a strong function of both composition and heat treatment. Thus almost every combination of material and heat treatment condition produced in this work was investigated. The relatively uncomplicated experimental procedures used helped make this possible. Because weight loss as a function of time is to be measured in these experiments, data on general corrosion will also be obtained. As well, metallographic post test examination is expected to give data on pitting. As pitting and dealloying are precursors to stress corrosion cracking, these experiments provide some insight into which alloys are likely to be most susceptible.

Susceptibility to stress corrosion cracking was expected to be low. One composition produced at a heat input of 1500 J/cm was investigated. It was expected that this would provide the widest possible range of microstructures so that a susceptible one, if it existed might be identified. More work will likely be done as an optimum alloy composition evolves and as results from dealloying and electrochemical studies become available.

The hardness and microstructure dependence of cavitation is well known. Thus both high and low heat input clad surfaces were investigated.

4.3.1. DEALLOYING AND GENERAL CORROSION BEHAVIOR

At the time this paper was written, no dealloying specimens had been removed from the seawater immersion tank. Preliminary dealloying experiments in CuCl produced extensive dissolution of the specimen and left a coppery hue on the specimen surface, but metallography revealed no significant dealloying. These results are inconclusive with respect to a seawater service environment. First results from the long term seawater exposure studies will be available in fall 1995.

4.3.2 STRESS CORROSION CRACKING EXPERIMENTS

Three stress corrosion cracking specimens were removed from the seawater immersion tank after one month. Despite stresses in excess of the yield strength of the base material, no evidence of stress corrosion cracking, nor of precrack pitting was noted on either the treated or the untreated tine.

4.3.3 CAVITATION-EROSION EXPERIMENTS

The results of the cavitation erosion experiments are shown in Fig. 14. This Figure shows mean depth of erosion for laser clad material produced with a low heat input (700 J/cm) clad material produced with a high heat input (3000 J/cm) and for base material. The results reveal near order of magnitude improvements in resistance to cavitation erosion are possible by laser cladding.

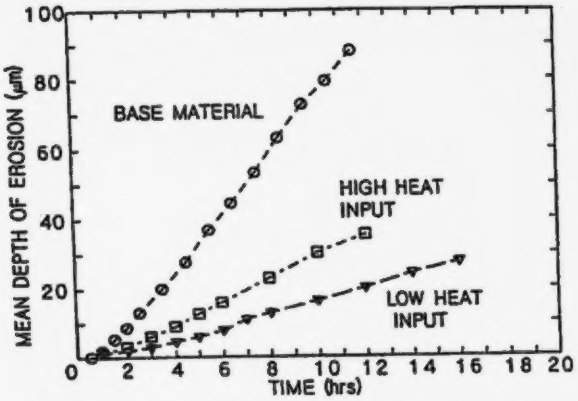

Fig. 14. Cavitation erosion behavior of laser clad and as received materials.

Microstructures of these materials are similar to the high and low heat input clad materials discussed in Sections 4.2, though some differences do exist. The most significant difference is that the high heat input material discussed above was produced at a higher heat input of roughly 6000 J/cm. Another difference is that argon instead of helium gas shielding was used to produce the cavitation specimens. Though the same cladding wire was used in both cases, base metal concentrations were different. As shown in Table 1, the base material, which is alloy a or b, contains less aluminum than the base material (alloy c) discussed in Section 4.2. Dilution of the weld deposit on the clad cavitation specimens likely occurred.

A review of the literature (Ref. 30) reveals that cavitation resistance in nickel aluminum bronze may be weakly affected by aluminum content, all else being equal. Reportedly, resistance increases with aluminum content. Thus these results are thought to be a worst case for the given heat input.

5.0 DEMONSTRATION PROJECTS

A number of demonstration projects have also been performed. Their purpose is to demonstrate that complex shapes and dissimilar metals can be clad. Heat inputs of roughly 1000 to 1500 joules have been used in most cases. Figure 15 shows two nickel aluminum bronze submarine hull valves laser clad on both their seats and pintles. A similarly clad phosphor bronze valve is shown in Fig. 16. Clad bronze and tin bronze impellers are shown in Figure 17. A ball from a nickel aluminum bronze submarine hull valve is shown in Fig. 18. In the as received condition, the ball was damaged by a combination of wear, dealloying and scoring (Fig. 18a). It was clad with several layers of nickel aluminum bronze (Fig. 18b), and machined to final dimensions. Careful dimensional analysis revealed minimal distortion. Dye penetrant inspection revealed no defects. The part was successfully reassembled into the valve and passed a pressure test. It is slated for use in a non-critical application.

The results above show that complex parts can be clad. A cost analysis showed that costs for depositing material on such complex parts is acceptably low, on the order of about 1 and 9 cents/mm^3, depending on complexity.

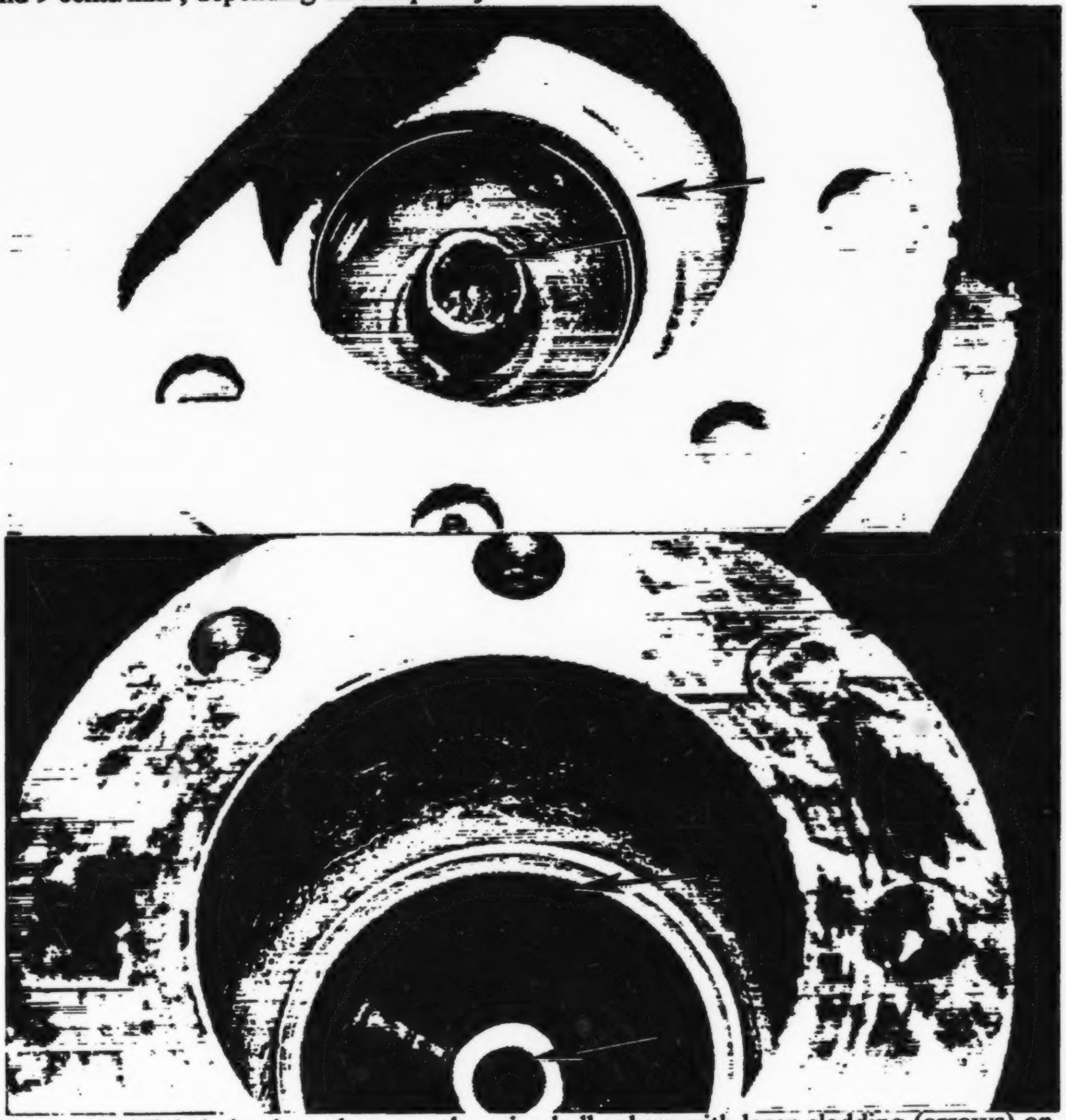

Figure 15. Nickel aluminum bronze submarine hull valves with laser cladding (arrows) on the seats and pintles.

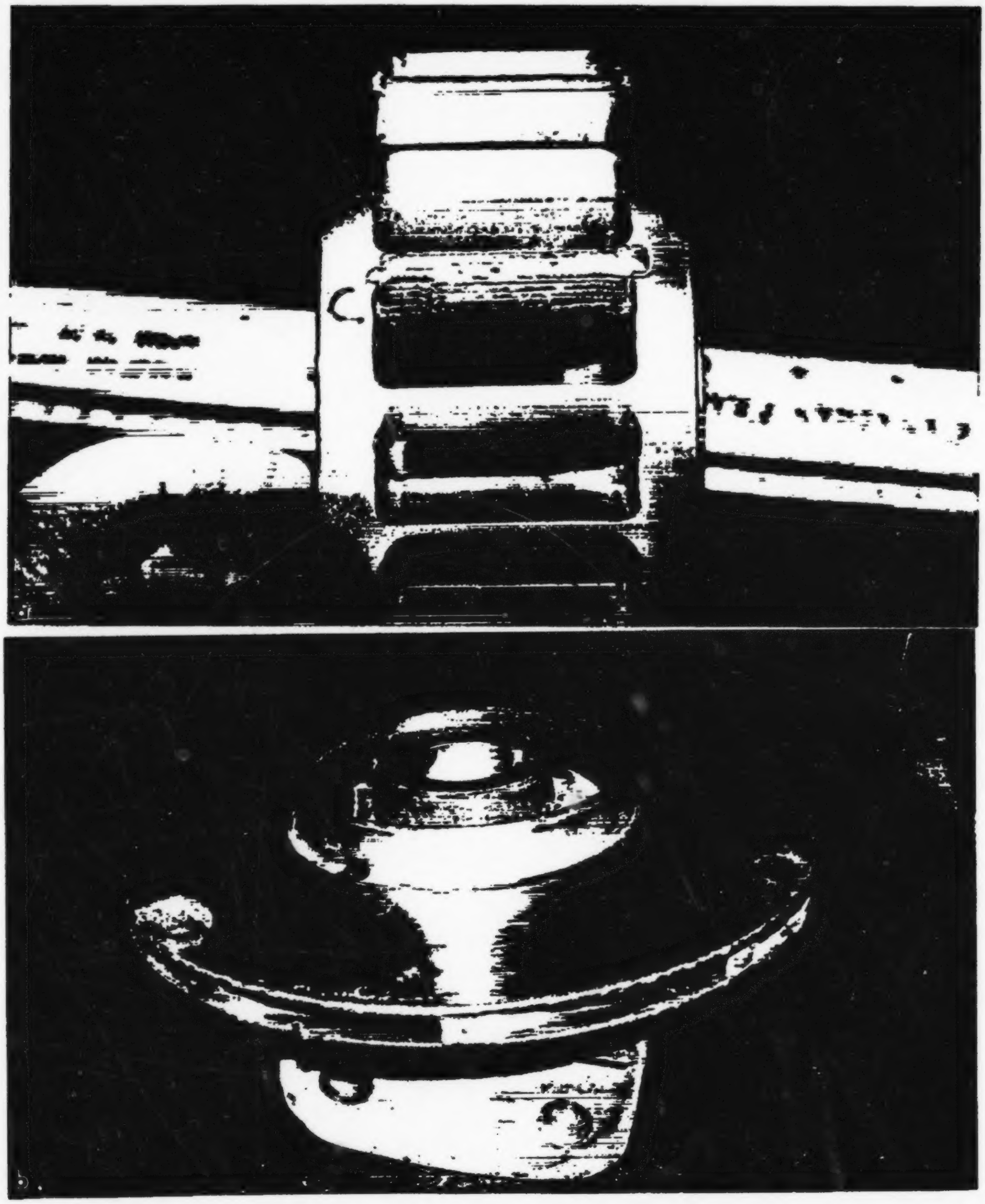

Figure 17. Laser clad aluminum (a) and tin bronze (b) impellers. The blade tips have been laser clad.

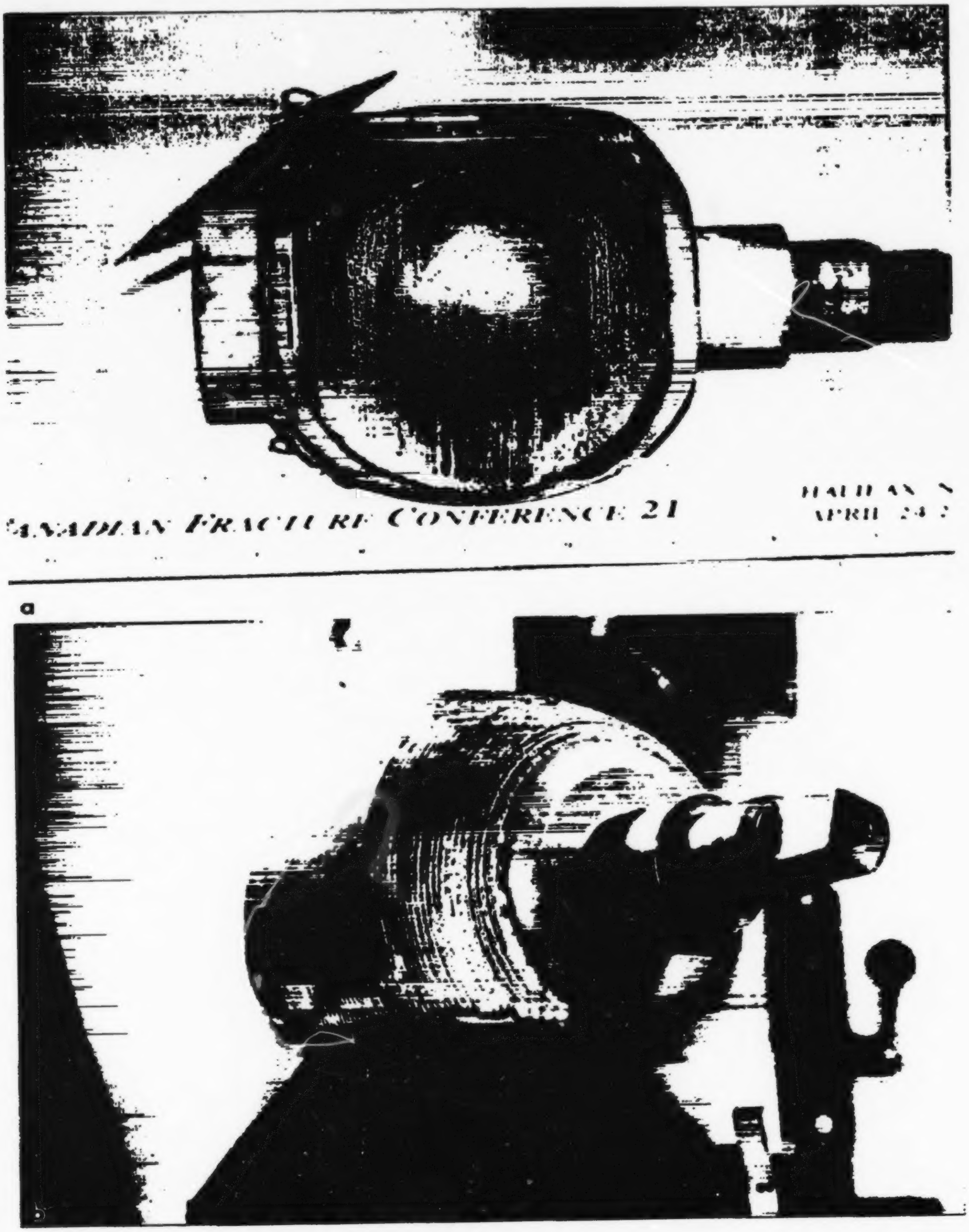
ANADIAN FRACTURE CONFERENCE 21
HALIFAX N
APRIL 24 2
a

Figure 18. Ball from Submarine Valve, before (a) and after (b) laser cladding.

CONCLUSIONS

The laser surface melting and cladding experiments just described reveal that these technologies can be used to produce mainly martensitic layers on nickel aluminum bronzes with hardnesses between HV 250 and 450. In cladding, deposits with high hardness and minimal heat affected zone α formation could only be produced at low heat inputs. Heat inputs between 425 and 650 J/cm, produced reasonable single layer deposits, higher heat inputs produced lower hardness and more α. Double layer deposits produced with a heat input of 650 J/cm, though otherwise similar to single layer deposits produced under the same conditions, exhibited large amounts of α formation in heat affected zones from the first pass which were reheated by the second pass. The materials are still being evaluated, however the laser cladding process does not appear to adversely influence stress corrosion cracking behavior. Cavitation erosion behavior is significantly improved by laser cladding. A number of complex parts have been clad, at costs between 1 and 9 cents/mm^3.

REFERENCES

1. LaQue, F.L. 1975. Marine Corrosion: New York: Wiley.

2. Castings in Nickel-Aluminum Bronze, British Standard 1400-AB2-C, 1948. London: The Mond Nickel Company Limited.

3. Hasan, F.; Jahanafrooz, A.; Lorimar, G.,W.; and Ridley, N. 1982. The Morphology, Crystallography, and Chemistry of Phases in As-Cast Nickel-Aluminum Bronze. Metallurgical Transactions 13A: 1337 to 1345.

4. Sahoo, M.; Edwards, J.O.; and Couture, A. 1983. Forty Years of Investigation, Research and Technology Development on Copper Base Alloys at the Physical Metallurgy Research Laboratories. Canadian Metallurgical Quarterly 22: 247 to 255.

5. J.A. Gianetto, M. Sahoo, M.W. Letts, and C. Bibby. 1995. Microstructural Characterization of NiAl Bronze Weldments, DREA CR/95/435, Defence Research Establishment Atlantic, Dartmouth, Nova Scotia.

6. M. Sahoo. 1983. Foundry Characteristics, Mechanical Properties and Heat Treatment of Nickel Aluminum Bronze Alloys, MRP/PMRL 83-31(OP-J), CANMET, Energy, Mines and Resources, Ottawa, Ontario.

7. Ferrara, R.J. and Caton, T.E. 1981. Review of Dealloying of Cast Aluminum Bronze and Nickel Aluminum Bronze Alloys in Seawater Service. Proc. of Corrosion 81, Paper 198. Houston Texas: NACE.

8. Culpan, E.A. and Rose, G. 1979. Corrosion of Cast Nickel Aluminum Bronze in Sea Water. British Corrosion Journal 14 (3): 160 to 166.

9. Sahoo, M. 1982. Weldability of Nickel Aluminum Bronze Alloy C95800, Transactions of the American Foundrymen's Society 90: 893-912.

10. Rules for Building and Classing Steel Vessels. 1990. Paramus, New Jersey: American Bureau of Shipping Section: 37/2.

11 Rowlands, J.C. and Brown, T.R.H.M. 1976. Preferential Phase Corrosion of Cast Aluminum Bronzes with Complex Microstructure in Seawater. Proc. 4th International Congress on Marine Corrosion and Fouling, 475-479. Juan les Pins, France.

12. Rowlands, J.C. 1981. Studies on the Preferential Phase Corrosion of Cast Nickel Aluminum Bronze in Seawater, Proc. 8th International Congress on Metallic Corrosion 1346-1351. Mainz, Germany.

13. Draper, C.W. 1981. The Effects of Laser Surface Melting on Copper Alloys. Lasers in Metallurgy 21-31. Warrendale, PA: The Metallurgical Society.

14. Draper, C.W. 1981. The Use of Laser Surface Melting to Homogenize Fe-Al bronzes, Journal of Materials. Science 16: 2774 to 2780.

15. Draper, C.W.; Vandenberg, J.M.; Preece, C.M.; and Clayton, C.R. 1982. Characterization and Properties of Laser Quenched Aluminum Bronzes. Rapidly Solidified Amorphous and Crystalline Alloys 529-533. New York: Elsevier.

16. Taylor, R.J.; Weston, D.A.; Wright, G.M.; and Turnbull, B.W. Sept. 1987. Production of Corrosion Resistant Surfaces by Laser Processing. Corrosion Australasia. 12-17.

17. Oakley, P.J. and Bailey, N. 1986. Laser Surfacing of Nickel Aluminum Bronze. Proc. International Conference on Power Beam Technology 301-314. Cambridge, England: The Welding Institute.

18. Y. Liu, J. Mazumder, and K. Shibata. 1994. Transmission Electron Microscopy Study of Martensites in Laser-Clad Ni-Al Bronze on Aluminum Alloy AA333, Metallurgical and Materials Transactions, 25A: 37-46.

19. Y. Liu, M.E. Mochel, J. Mazumder and K. Shibita. 1994. TEM Study of Precipitates in Laser Clad Ni-Al Bronze, Acta Metall. Mater. 42: 1763-1768,.

20. Y. Liu, J. Mazumder, and K. Shibita. 1994. Laser Cladding of Ni-Al Bronze on Al Alloy AA333, Metallurgical and Materials Transactions B 25B: 749-759.

21 J.A. Hewitt, Laser Weld Overlaying of Marine Components and Alloys, DREA CR /95/525, Defence Research Establishment Atlantic, Dartmouth, Nova Scotia.

22. C.V. Hyatt, D.O. Morehouse and J. Hewitt. 1995. Laser Cladding of Nickel Aluminum Bronzes: Dissimilar Metals and Complex Shapes, DREA Technical Communication, in Edit.

23. Sinha, A.K. 1989. Ferrous Physical Metallurgy: Boston: Butterworths.

24 A.W. Loginow and E.H. Phelps. 1962. Stress Corrosion Cracking of Steels in Agricultural Ammonia, Corrosion, 18: 299t-305t.

25. ASTM Standard G32-85, Standard Method of Vibratory Cavitation Erosion Test. 1987 Annual Book of ASTM Standards. 187-194. ASTM, Philadelphia, PA.

26. K.D. Magee and C.V. Hyatt. Laser Surface Melting of Copper Nickel Alloys, to be published.

27. Hyatt, C. V., and MacKay, K. D. 1993, Defects in Laser Treated Copper Alloys. Proc. International Conference on Beam Processing of Advanced Materials 247-257. Warrendale, PA: The Minerals, Metals and Materials Society.

28. Betancourt, T. 1983. Heat Treatments and Corrosion Behavior of 2.1% Si, 7.3%Al Bronze, Dartmouth, N.S., Nova Scotia Research Foundation.

29. P. Brezina. 1982. Heat Treatment of Complex Aluminum Bronzes, International Metals Reviews, 27: 77-120.

#510357

Laser Cladding for Surface Protection

by

J. Hewitt and V.E. Merchant

The Laser Institute
9924-45th Avenue, Edmonton, Alberta, Canada, T6E 5J1

ABSTRACT

The Laser Institute combines technical and economic feasibility studies with routine cutting, welding, case hardening, and cladding jobs at its affiliated Job Shop. Laser weld overlaying, or cladding, is performed on a production basis at The Laser Institute. Filler metal is deposited into the molten pool created by the partially focused beam of a 5 kW carbon dioxide laser on the metal surface. A variety of different powder and wire feed devices have been developed at The Laser Institute, for adding filler material. The application of this technology to repair the seating surface of diesel engine valves, using procedures developed at The Laser Institute, will be described.

The effect of laser processing conditions on the properties of Stellite 6SF deposits has been determined. Fineness of the microstructure, as quantified by the secondary dendritic arm spacing (SDAS), was measured as a function of the deposition conditions, and showed approximate agreement when compared to a calculation based on the known dependence of dendritic arm spacing on cooling rate.

Laser weld overlays of Nistelle C-276 were produced using a 5 kW carbon dioxide laser and a modified plasma transferred arc welding torch as a means of delivering powder metal overlay material to the weld pool. Low dilution, crack free deposits with a minimum of porosity were deposited on mild steel substrates. Electrochemical measurements in a brine solution saturated with H_2S showed the laser coated sample performed in a similar fashion to a sample of bulk C-276 alloy.

Laser Cladding for Surface Protection

INTRODUCTION

This presentation is about laser cladding for surface protection, and in particular describes the properties and applications of laser produced coatings. First, however, The Laser Institute itself shall be briefly described. At The Laser Institute, technology is developed in the Research and Development division and then transferred to Lasertech, the job shop division. Several examples of this technology transfer will be given, with the main example being laser cladding.

The Laser Institute is a wholly owned subsidiary of the University of Alberta, Canada's second largest university. It is located in approximately 5,700 square feet of laboratory, materials processing and office space, in a light industrial area. It has a number of laboratories devoted to laser applications in materials processing, optoelectronics and optical sensing, metrology and inspection. Lasertech, the job shop, occupies a further 6,000-square feet immediately adjacent to The Institute. Research, development, and engineering activities of the Institute are carried out in two fields of activity, optoelectronics and materials processing.

OPTOELECTRONICS RESEARCH AND DEVELOPMENT

The Optoelectronics Division of The Laser Institute investigates and develops the integration of lasers with other electro-optical devices, such as scanners, modulators, detectors, CCD video cameras, and optical elements, such as filters, monochromators, and optical fibres. Recent projects have involved optical time domain reflectometry, differential absorption, laser induced fluorescence, interferometry, and

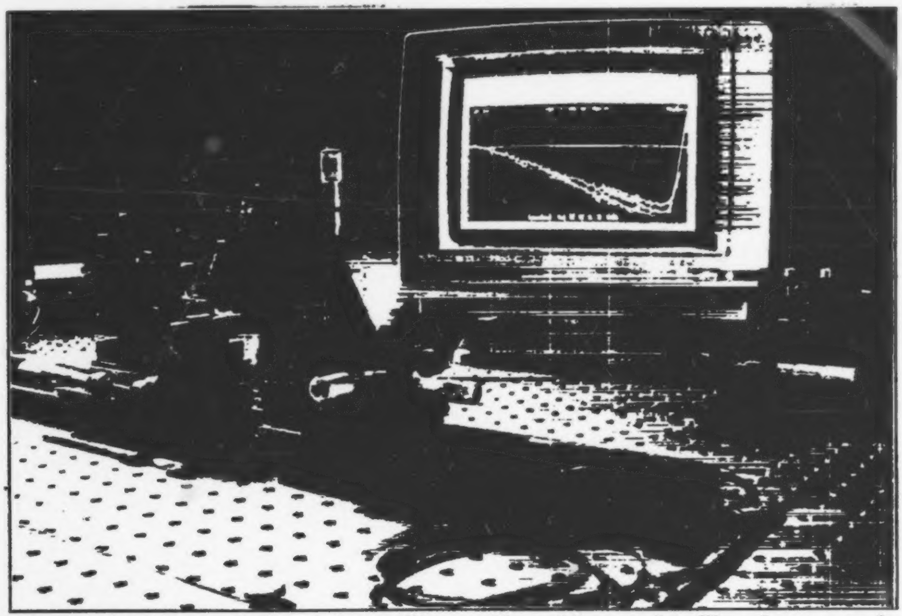

Figure 1 Reflected signal from fibre optic cable, as the fibre is stressed.

fibreoptic sensing, and component inspection using machine vision with feature-enhancing lighting.

In the Optoelectronics area, a recent project was an extensive study for the development of fibre optic strain sensors for sensing of mine wall stability. This study investigated the use of optical time domain reflectometry as a means of sensing reflected signals in the fibre optic as a result of lateral subsurface ground movements to a depth of 50 m with a resolution on a millimetre scale. The method has application to other "smart structures".

MATERIALS PROCESSING

The Materials Processing Department performs two types of activities; one is conducting research, development, and engineering projects for a variety of industrial and government clients. One example of the research and development work in laser materials processing is the contract on processing of Nickel Aluminum Bronze that described earlier in this meeting[1]. Another example is the study of Laser Assisted Arc Welding[2,3,4], a process that has been described at previous CRAD meetings. In this process, the relatively expensive but highly controllable power in a focused laser beam is augmented by the inexpensive power from an arc. Welding procedures using the combined processes were developed at The Laser Institute, and coupons submitted to DREA for testing.

The second type of activity pursued by the Materials Processing department is developing procedures for work being conducted by The Job Shop. One example of this is transformation hardening or case hardening of ball bearing grooves in high pressure swivel joints in piping. The processing conditions for these AISI 4140 steel joints were determined. Figure 2 shows the cross-section of the groove, laser hardened with the beam of a 5 kilowatt carbon dioxide laser partially focused by a beam integrator.

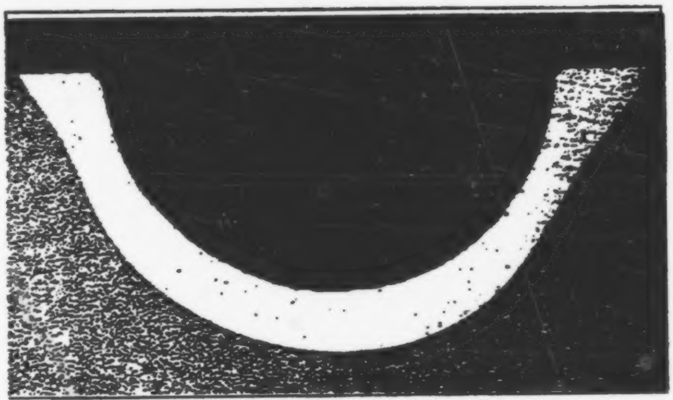

Figure 2 Hardened region in ball bearing race

Laser transformation hardening requires determining the processing conditions such that the material is heated above the phase transition temperature, and held for a dwell period, without melting the material surface. Heat buildup in the material must be controlled, because conduction to the bulk of the material must result in rapid cooling of the surface region, producing a hard Martensitic microstructure. Figure 3 shows how the depth of hardness can be varied by changing the laser processing conditions, in AISI 1070 steel. For these measurements, a 3 kW beam concentrated with beam integrator to a width of 12.5 millimetres, was scanned at speeds ranging from 0.6 to 1.5 meters per minute, producing depth of hardening that varied from 0.75 mm to 1.5 mm. The metal became fully hardened, although a less hard region occurred on the surface due to partial decarburization of the steel during prior treatment.

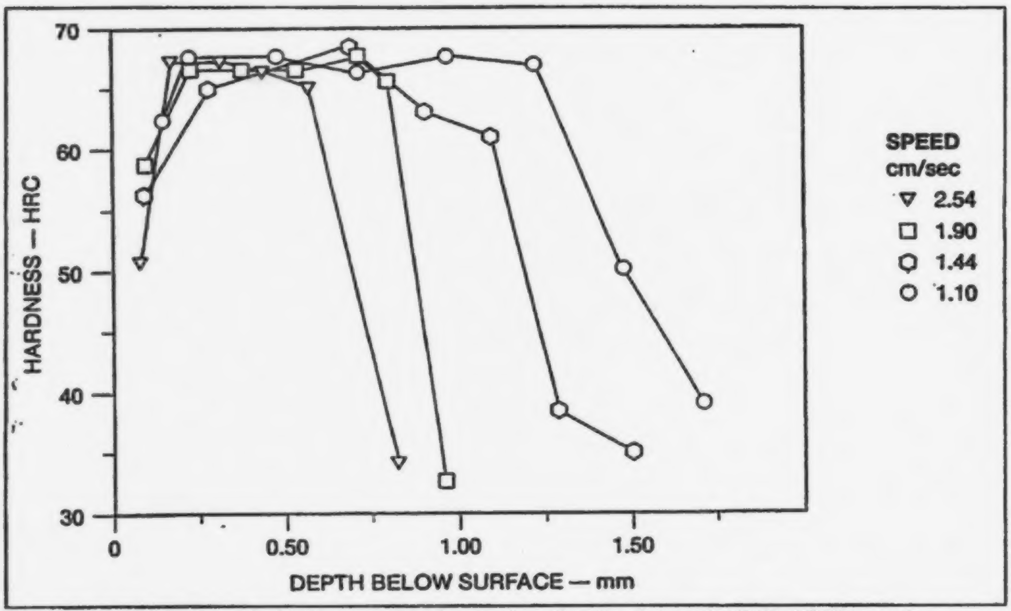

Figure 3 Case Depth in laser transformation hardening of AISI 1070 steel

LASERTECH

Lasertech, a division of The Laser Institute, serves a wide range of industrial clients. In the materials processing area, noteworthy equipment includes:

- a 5000 watt carbon dioxide laser coupled to a 5 axis work-station
- a 700 watt Nd:YAG laser, coupled to the same workstation
- a 1600 watt carbon dioxide laser coupled to a 4x8 foot flatbed cutter,
- a 1700 watt carbon dioxide laser coupled to a rotary cutter. Various pipe sizes, in lengths up to 8 meters, can be cut.
- a 50 watt carbon dioxide laser on a flatbed cutting work-station, used for cutting plastics and other non-metallic materials

All of the CNC work-stations are linked to an AUTOCAD system to facilitate rapid parts programming. The rotary cutter, shown in Figure 4, was used to cut about 60,000 meters of pipe in 1994, with many different hole patterns and spacings, for use in perforating guns. Besides cutting, job shop activities include welding, transformation hardening, and cladding. In a recent welding job, 1250

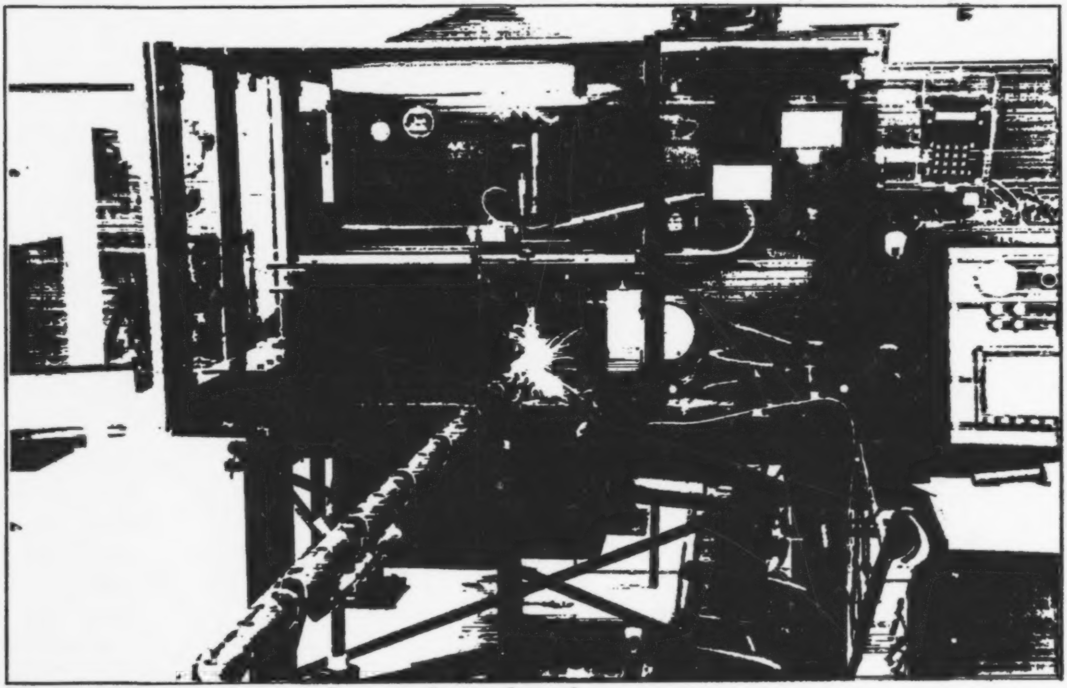

Figure 4 Rotary cutter at Lasertech, cutting pipe

condenser tubes of ASME 310 stainless tubes with wall thickness 0.083" were joined with a welding process approved to the specifications of the ASME Boiler and Pressure Vessel Code, Section IX. The technology for laser Transformation Hardening has been transferred from the R&D Materials Processing group, to LASERTECH, which is now pursuing this activity on a job shop basis. Personnel from the Materials Processing group are available to establish processing conditions on an as-needed basis. Processing of the swivel joints referred to above is one example of an ongoing transformation hardening job.

LASER WELD OVERLAYING, OR CLADDING

The essence of laser cladding is deposition of filler metal into the molten pool created by the partially focused beam on the metal surface. The work at The Laser Institute has used the beam from the 5 kilowatt CE-5000 laser. Filler metal is added using either a powder feed or a wire feed. Wire feed is accomplished using either a Hobart 2210 Wire Feeder or a custom built wire microwire feeder. The Hobart wire feeder was designed for use with gas metal arc welding, but was adapted by using a custom designed torch and integrating the wire feeder controls with the Computer Numerical Control programs of the laser system. The microwire feeder is similar to one designed at Sandia National Laboratory[5] in the United States. This unit uses a high speed stepper motor to drive rubber coated wire drive units, with a hypodermic needle to collect the wire as it is ejected from the drive wheels and guide it into teflon lined tubing. A personal computer is used to program the stepper motor controller, but motion is initiated by a signal from the CNC controller of the laser workstation.

A CCD camera is used with the microwire feeder, to aid in relative positioning of the wire, the seam, and the beam. The camera is mounted off to the side of the focusing column, and views the workpiece through a mirror mounted at 45°. The workpiece can be viewed only during the set-up to welding, with the mirror withdrawn out of the beam path during actual welding. Figures 5 and 6 show the wire feeder and the torch respectively.

Use of the microwire feeder allows control over the rate at which the weld pool cools. A standard wire feeder, using coarser wire, requires higher laser energy input and hence a slower cooling rate. The microstructure of the weld can be controlled because of the range of cooling rates that are accessible. For example, in forming weld overlays of Nickel-Aluminum-Bronze, a weld overlay with a largely single phase microstructure was created, as discussed in Reference 1.

Two different torches have been used to deliver powder to the weld pool. One feeds powder into the leading edge of the weld pool. The other feeds powder collinear with the beam and allows multi-directional operation. This is a modified nozzle for cladding by plasma transferred arc (PTA) welding. The centre electrode of the PTA nozzle has been removed, and the laser beam directed along the centerline of the torch. The laser beam was focused inside the

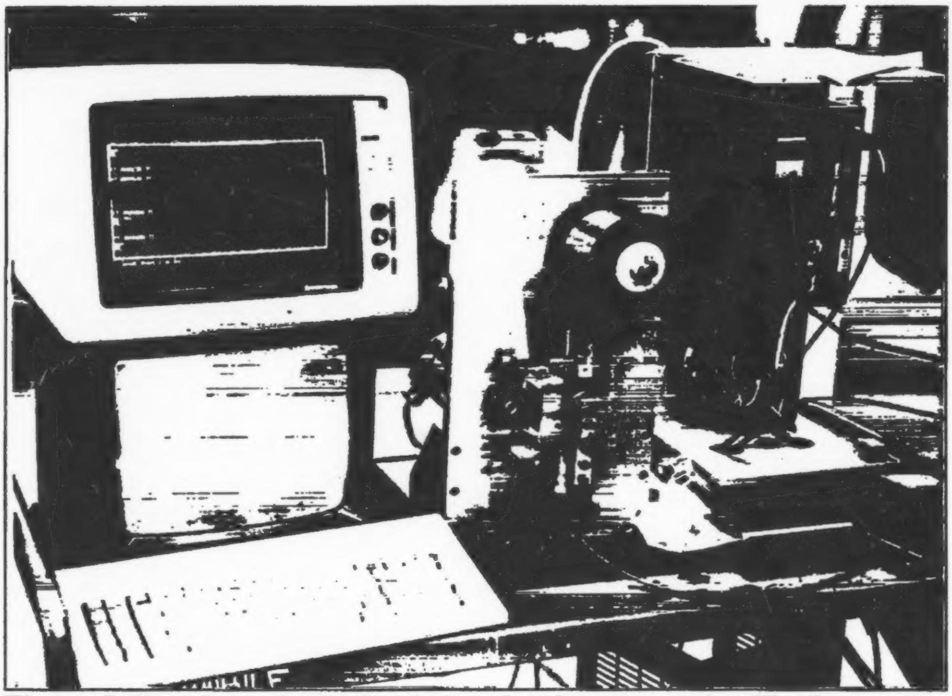

Figure 5 The Microwire feeder designed and constructed at The Laser Institute.

nozzle, so that it diverged as it emerged from the nozzle. This required judicious machining of the inside surface of the nozzle, to match the taper to the conical path of the converging laser beam.

The beam is brought inside overhead beam tubes from the laser to the workstation, then deflected by a 45° mirror downwards through either a 38 cm focal length antireflection coated zinc selenide lens or a 50 cm focal length mirror system. The converging beam passes through the nozzle and is diverging as it strikes the workpiece. An overhead powder feeder, integrated with the CNC control of the laser system, supplies a metered flow of powder into the beam-workpiece interaction area. The position of the workpiece below the nozzle is chosen so that the diameter of the beam approximately matches that of the powder distribution flowing from the nozzle.

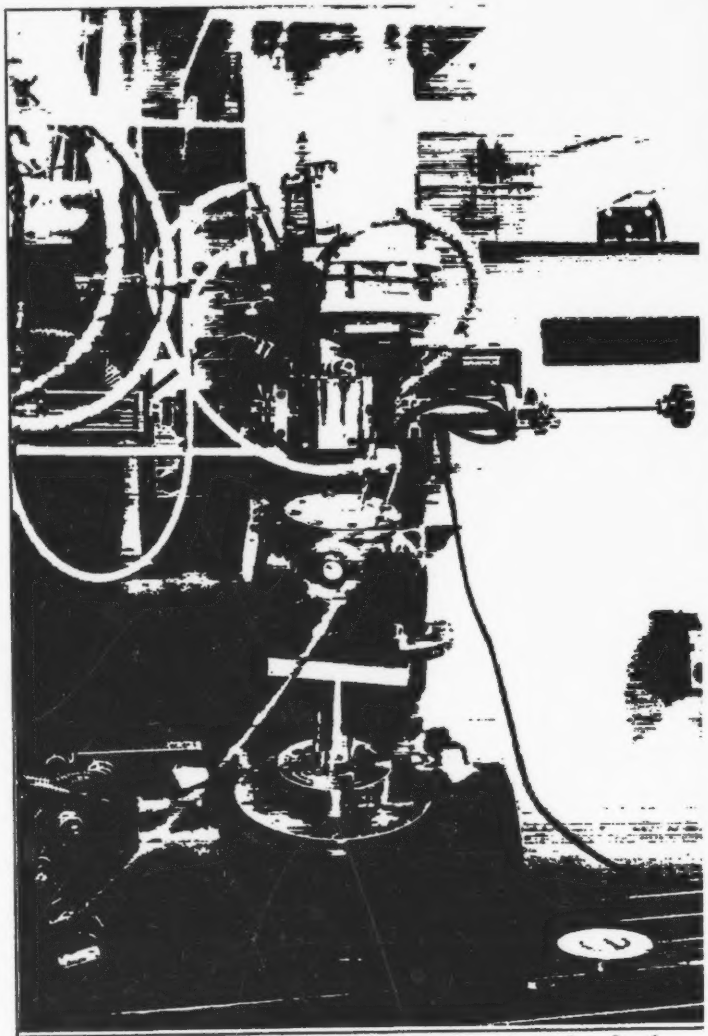

Figure 6 The focussing head, showing the wire feed nozzle attached. The CCD camera is visible to the left o the focusing head; a knob to the right of the focusing head is used to adjust the position of the viewing mirror

The laser beam does not directly impinge on the base metal, but only on the powder being deposited, as shown in Figure 7. The base metal is heated primarily through conducti through the partially solidified build-up, and not directly. This allows control of the dilution, or mixin of the base metal with the deposited material. Figure 8 shows a cross-section, and part of the upper bea of a weld overlaid track on mild steel, in which the low dilution is particularly evident. Figure 9 sho the cross-section and upper bead of a series of side-by-side passes in which C-276 alloy is deposited a coupon of AISI 4140 steel.

Figure 7 Deposition of Powder During Laser Cladding

PROPERTIES OF LASER PRODUCED COATINGS

An extensive study of the microstructure of laser deposited coatings was undertaken. In this work, a partially focused beam was scanned over preplaced powder, rather than using a powder feeder. This experimental procedure resulted in the ability to control the deposit thickness and scanning speed independently. Figures 10 shows the microstructure of a Stellite* 6SF deposit created by a set of parameters producing a low heat input. There is a narrow region in which planar solidification occurs; the dendritic microstructure above this region are much finer than when high heat input was used. The secondary dendritic arm spacing (SDAS) was measured for coatings created under a variety of conditions; the results are plotted against the deposition conditions in Figure 11. Clearly, the linear heat input doesn't uniquely determine the SDAS; there is some dependence on power and speed individually. The cooling rate in deposits created as described above was calculated using the Rosenthal 3-dimensional model[6] for heat flow in the material. The cooling rate was then translated into a predicted SDAS, using the measured[7] dependence of SDAS for Stellite 6; the results are also shown in Figure 11.

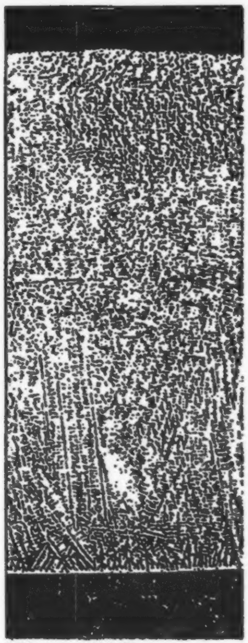

Figure 10 Solidification Microstructure of preplaced powder fused with a heat input of 112 J/mm (400X)

In spite of the approximations inherent in this calculation[8], this approach was shown to result in rough agreement between the calculated values for SDAS and the measured values. The Rosenthal equation assumes a point heat source and results in a cooling rate that

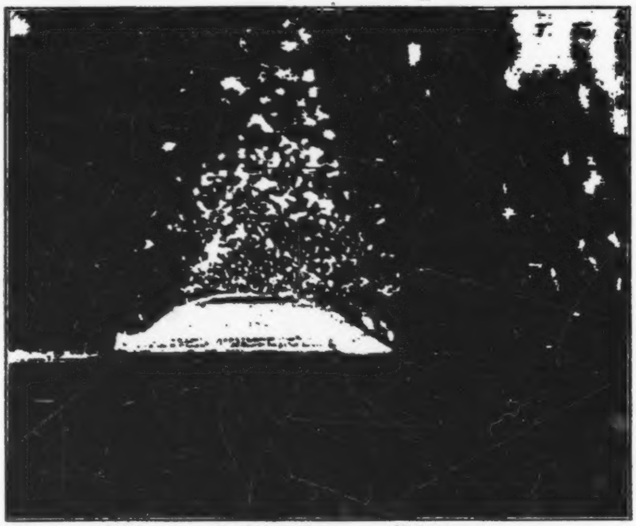

Figure 8 Laser clad track on mild steel

depends only on the linear heat input, not on the power and speed independently. Hence, the calculated cooling rate is a single valued function of the heat input.

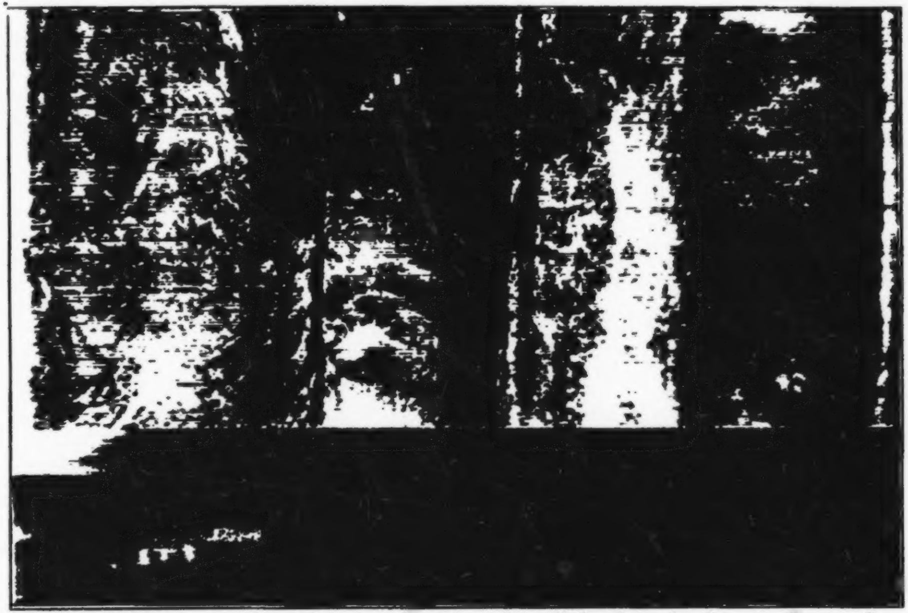
Figure 9 Photographs of upper bead and polished and edge surface of laser clad C-276 alloy.

Electrochemical corrosion tests were conducted on a coupon of weld overlaid C-276 material, and compared to that of bulk material. Slugs were cut from the samples, the surfaces were ground and polished, and corrosion tests were conducted on the overlaid deposits. Electrochemical measurements used a three-electrode configuration within an electrochemical cell containing a brine solution saturated with hydrogen sulphide, at room temperature. The electrodes included the weld overlay sample and a bulk C-276 sample along with a reference electrode, in order to corrode the two sample electrodes under the same conditions. Polarization measurements were obtained with a computer controlled potentiostat. From this, a polarization curve was plotted, as in Figure 12. Corrosion rates for the laser weld overlaid C-276 and the bulk sample were 4.4mpy and 5.8mpy respectively. Although the results from this one test can only suggest a general trend, the hysteresis curve shown in Figure 12 indicates that the laser weld overlayed material appears to react similar to a bulk

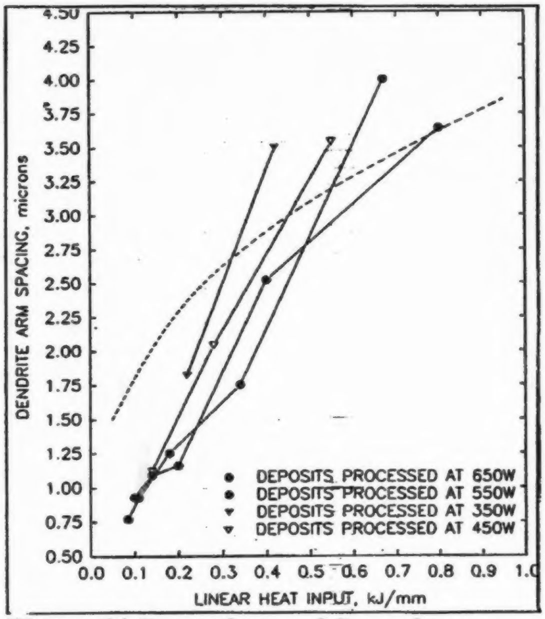

Figure 11 Dependence of Secondary Dendrite Arm Spacing on Linear Heat Input

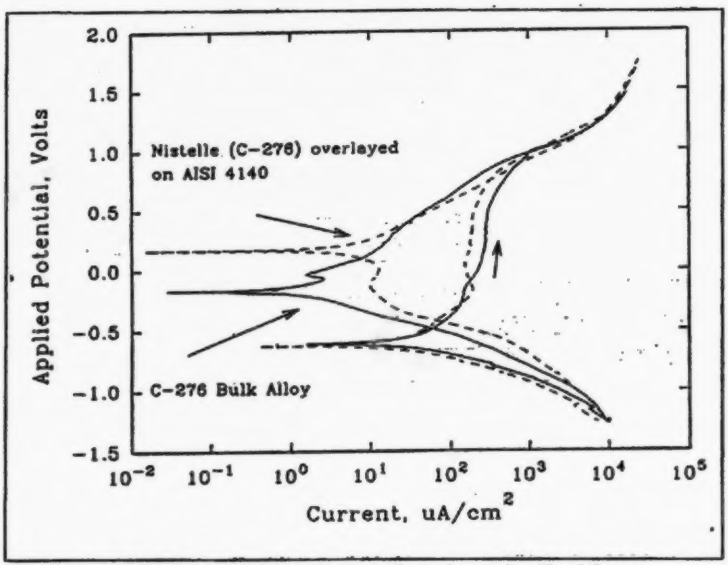

Figure 12 Polarization curves showing similarities between laser weld overlayed and bulk C-276.

C-276 under the given conditions. In other words, the properties of the C-276 material are apparently not altered by using this deposition process, and the low dilution should allow the same corrosion resistance through most of the thickness of the deposit.

APPLICATIONS OF LASER CLADDING

Applications of laser cladding have recently been reviewed, and the results are reproduced in Table 1. The table also indicates the state of the application, whether it is still in a research phase or it is being used in a production environment. Laser cladding is used predominantly either in the aircraft industry, or in valve applications.

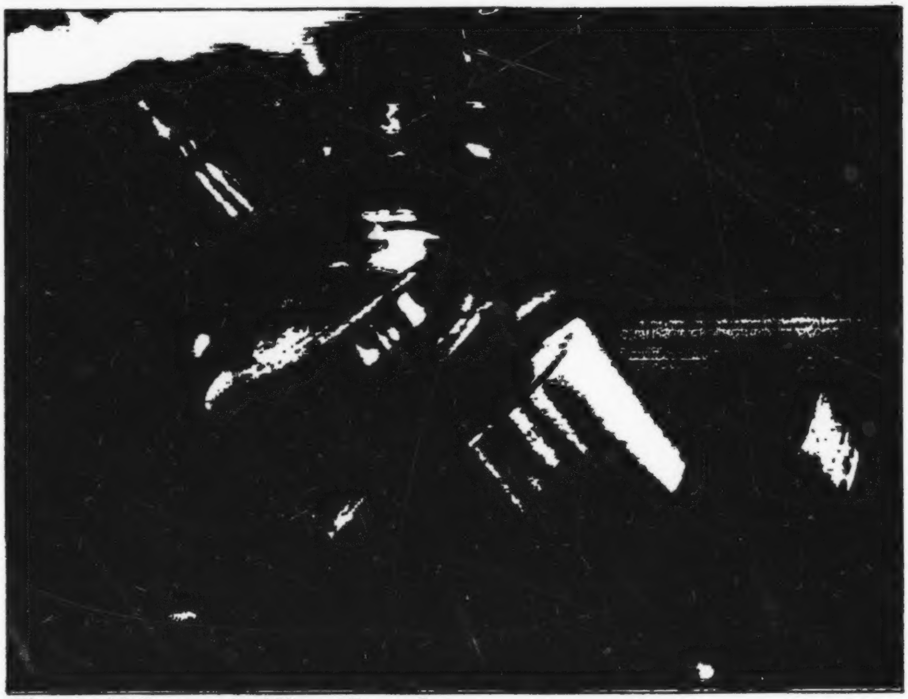

Figure 13 Laser cladding of a valve

An application that has been pursued at The Laser Institute is cladding for reconditioning of diesel exhaust valves. This is another example of technology transfer from the research and development group, in which the processing conditions were developed, to Lasertech, the job shop division. Lasertech is now cladding of the order of 1000 valves per month;

Figure 13 shows a valve being processed.

Each valve is manually preheated by an oxy-acetylene torch prior to cladding; preheating processes more amenable to mass production are currently being investigated. Two side-by-side passes cover the valve sealing area on each of the six different valve sizes that are treated.

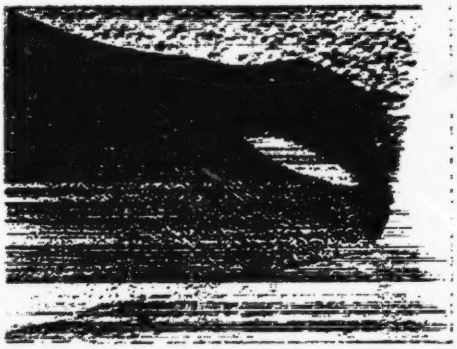

Figure 14 Polished and etched cross section of a clad valve

TLI engineers worked closely with the customer during cladding procedure development to ensure that the clad deposits met his quality requirements. The customer performs pregrinding of the valves prior to material deposition, and postgrinding to ensure the valves have the correct finished profile. Figure 14 shows the cross-section of an as-clad valve, prior to grinding. The customer also chrome plates the valve stems to complete the reconditioning process.

ACKNOWLEDGEMENTS

The corrosion tests were performed by the Linda Gray at the Alberta Research Council in Edmonton. The analysis of the microstructure of laser clad Stellite and its dependence on cladding conditions was performed by Chris Green.

Table I. Laser Weld Overlaying Applications[9]

Organization	Application	Status
Westinghouse R&D	Near net shape casting of cylindrical bosses	Development
Westinghouse	Steam generator blades Internal pipe surfaces	Production Development
Westinghouse	Electrical contactors	Development
General Electric	Gas turbine engine components	Production
Tinkler Air Force Base (USAF)	Turbine blades	Repair
Mare Island Naval Ship Yard/ARL	Submarine steam chests	Development
Stardyne Inc.	Valves Aircraft carrier catapult Turbine engine components Drive shafts	Repair
Quantum Laser	Gas Turbine Parts	Production Repair
Rofin-Sinar Inc.	Die components	Development
Huazhong University	Exhaust valves	Research
Fiat Auto	Exhaust valves	Production
Toyota	Exhaust valves Moulds	Production
Sulzer AG	Exhaust valves	Development
Rolls Royce	Turbine blade interlocks	Production
Pratt and Whitney	Turbine blade interlocks	Production
GEC-Alsthom	Turbine blades	Production
The Welding Institute	Alloying bronzes	Research
Combustion Engineering	Offshore drilling components Boiler firewalls	Research
Komatsu Ltd.	Overlaying copper onto steel	Research
IIT Research Institute	Refractory materials onto steel	Research
Exxon Research and Engineering Co.	Oxidation resistant materials onto steel	Research
Imperial College	ceramic/metal composites onto steel	Research

* Stellite is a registered trademark of Deloro Stellite, Inc.

REFERENCES

1. *Laser Weld Cladding of Nickel Aluminum Bronzes* , C.V. Hyatt, K.H. Magee, and T. Betancourt, presented at The 2nd CF/CRAD Meeting on Naval Applications of Materials Technology, Halifax, Nova Scotia, May 2-4th, 1995

2. *The Potential of Laser Assisted Arc Welding as a Fabrication Technique for Naval Vessels*, V.E. Merchant, presented at The 3rd Canadian Forces/CRAD Meeting on Research in Fabrication and Inspection of Submarine Pressure Hulls, June 6-8, 1989, Halifax, Canada.

3. *Laser Assisted Gas Metal Arc Welding of Thick Steel Plate*, K.H. Magee, Fabrication and Inspection of Submarine Pressure Hulls, 4th Canadian Forces CRAD Meeting, June 5-6, 1991, Halifax.

4. *Laser Assisted Gas Metal Arc Welding of Thick Steel Plate*, K.H. Magee, Naval Applications of Materials Technology, Canadian Forces/CRAD Meeting, Halifax, April 27-29, 1993.

5. *Wire Feeder Developed for Laser Beam Welding*, Welding Journal, Vol 69, no 10, 1990, pp 57-58.

6. *Cooling Rates and Peak Temperatures in Fusion Welding,* C.M.Adams, Jr. Welding Journal Research Supplement, May 1958, Pgs. 2105-2155.

7. *Comparison of the Quench Rates attained in Gas Atomized Powders and Melt Spun Ribbons of Co and Ni Base Superalloys,* F. Duflos and J.F.Stohr, in Rapidly Solidified Amorphous and Crystalline Alloys, B.H.Kear, B.G.Griessen, and M. Cohen, Editors. (Elsevier Science Publishing Co., Inc., 1982) Pgs. 167-171.

8. *Dependence of Microstructure of Laser Weld Overlayed Surfaces on Heat Input during Processing*, C.Green, Internal Report, The Laser Institute, 1992.

9. *The Applications and Technology of Laser Weld Overlaying*, K.H. Magee, DREA Report CR/92/419

#510358

Current US Navy Welding Consumables Research

by

P.W. Holsberg, J.J. DeLoach, J.M. Blackburn,
G.L. Franke, R.J. Wong, and R. DeNale

Naval Surface Warfare Center, Carderock Division,
Annapolis Detachment, Annapolis, Maryland, USA 21402

ABSTRACT

The affordable construction of U.S. Naval Ships is dependent on the ability to weld high strength steels using the most desirable process for a specific application. Typically, construction of ships includes gas metal arc welding, submerged arc welding, and shielded metal arc welding. While the use of the HY series of base materials and consumables have served the U.S. Navy well, the impetus towards more affordable, highly weldable steels is a major thrust of ships to be fabricated in the 1990's and beyond.

The development of high strength, high toughness steel welding consumables, the understanding of the introduction and role that hydrogen plays in the establishment of multipass gas metal arc welding procedures in these high strength steel weld metals and modeling of weld metal microstructure of gas metal arc welds which incorporates multiple thermal cycles and different peak temperatures will be discussed.

The effects of Ti content between 0 and 250 ppm on the strength and impact toughness are described for SMAW. The effects of MnO content in the flux will be discussed in relation to the amount of Mn transferred to the weld metal and the effect on weld metal strength and impact toughness. Ultra low carbon bainitic weld metals produced by GTAW and GMAW and the resulting differences will be addressed. The development of a multipass weldability test and comparison to single pass WIC test will be discussed. The status of modeling of the GMAW process will also be presented.

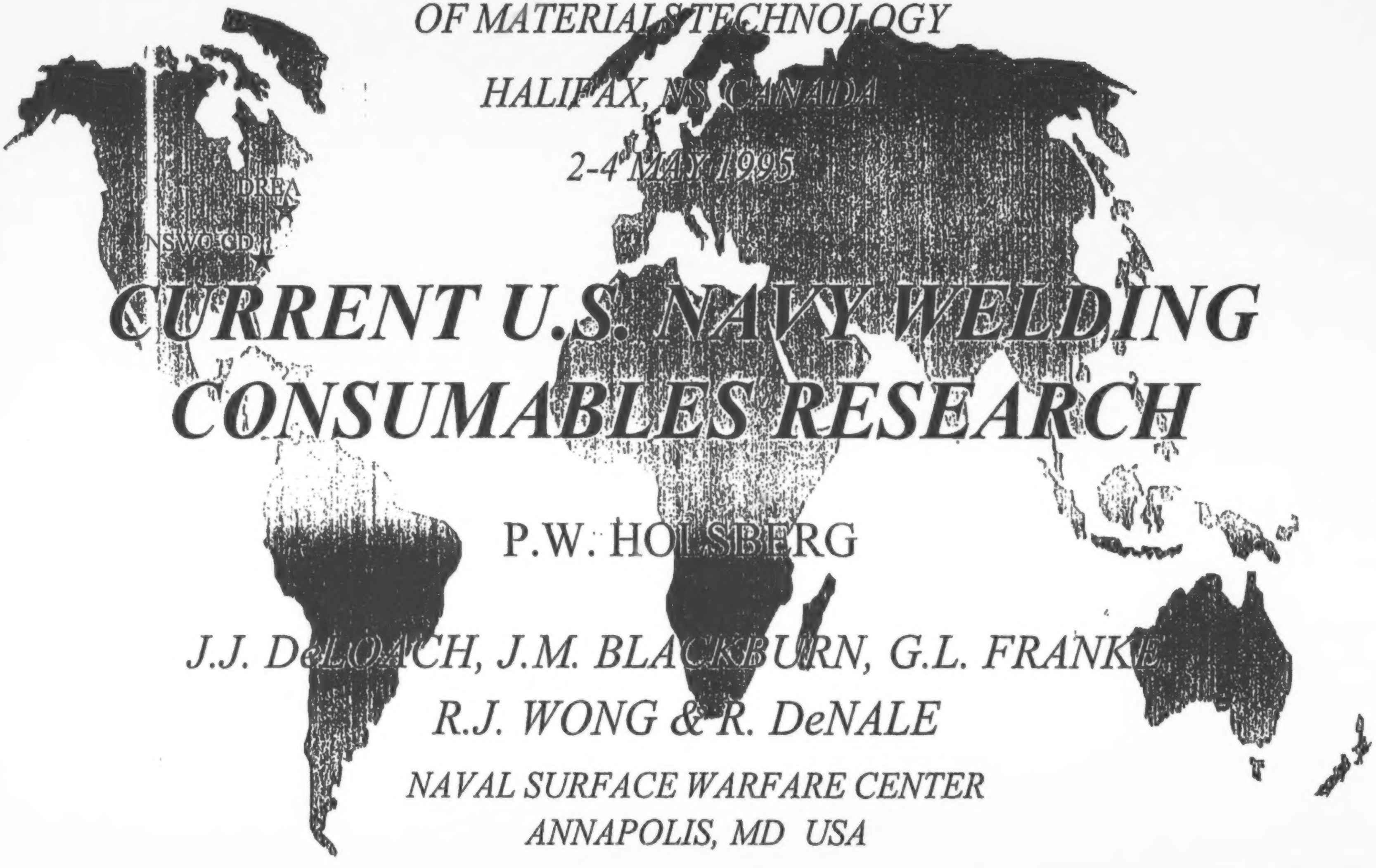

2nd CF/CRAD MEETING -- NAVAL APPLICATIONS
OF MATERIALS TECHNOLOGY

HALIFAX, NS CANADA

2-4 MAY 1995

CURRENT U.S. NAVY WELDING CONSUMABLES RESEARCH

P.W. HOLSBERG

J.J. DeLOACH, J.M. BLACKBURN, G.L. FRANKE
R.J. WONG & R. DeNALE

NAVAL SURFACE WARFARE CENTER
ANNAPOLIS, MD USA

NSWC-CD

WELDING 690 MPa STEELS

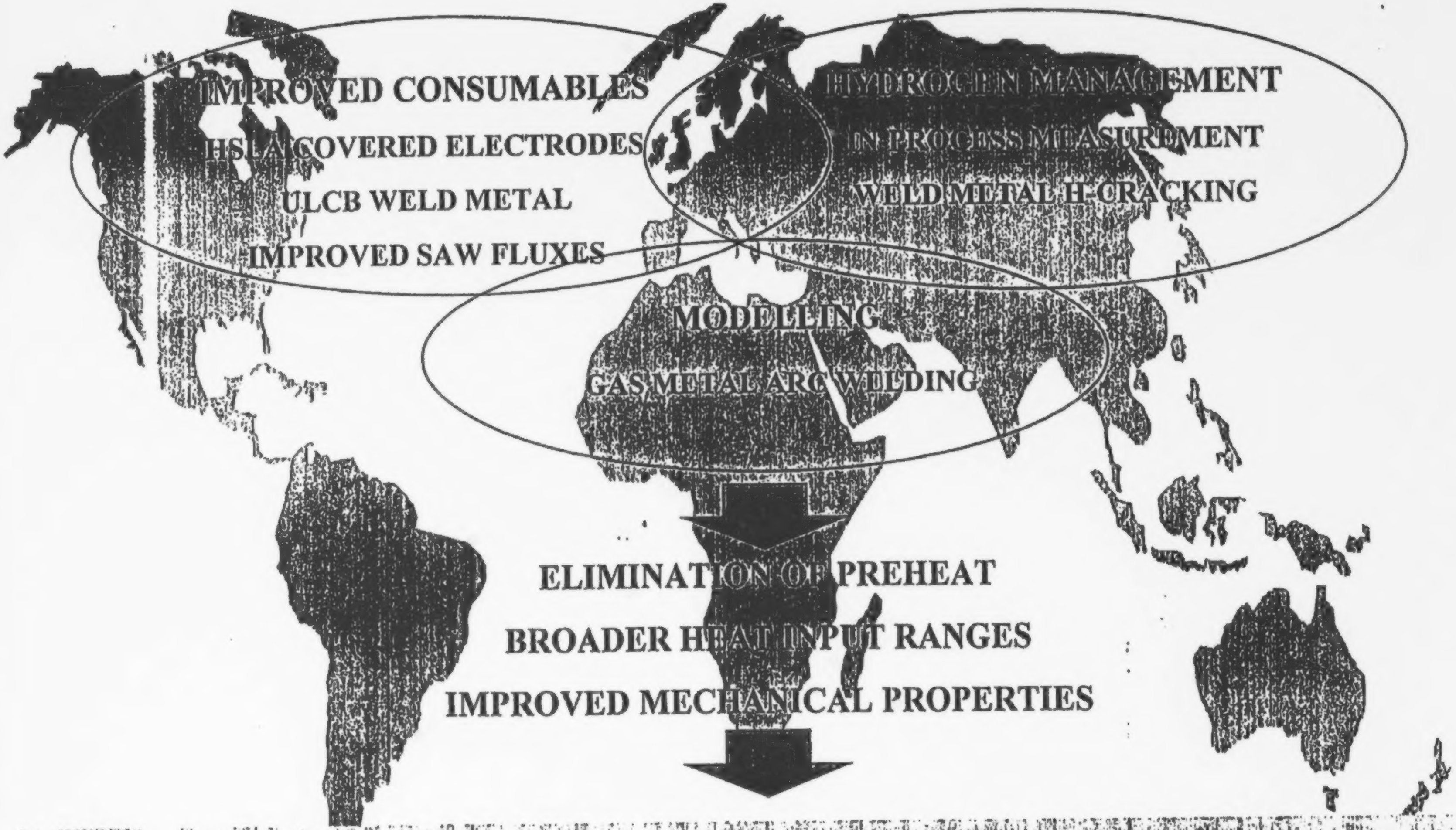

IMPROVED CONSUMABLES

HSLA COVERED ELECTRODES

ULCB WELD METAL

IMPROVED SAW FLUXES

HYDROGEN MANAGEMENT

IN PROCESS MEASUREMENT

WELD METAL H-CRACKING

MODELLING

GAS METAL ARC WELDING

ELIMINATION OF PREHEAT

BROADER HEAT INPUT RANGES

IMPROVED MECHANICAL PROPERTIES

DECREASED COSTS AND BETTER PERFORMANCE

NSWC-CD

EFFECT OF Ti ON MMA WELD TOUGHNESS

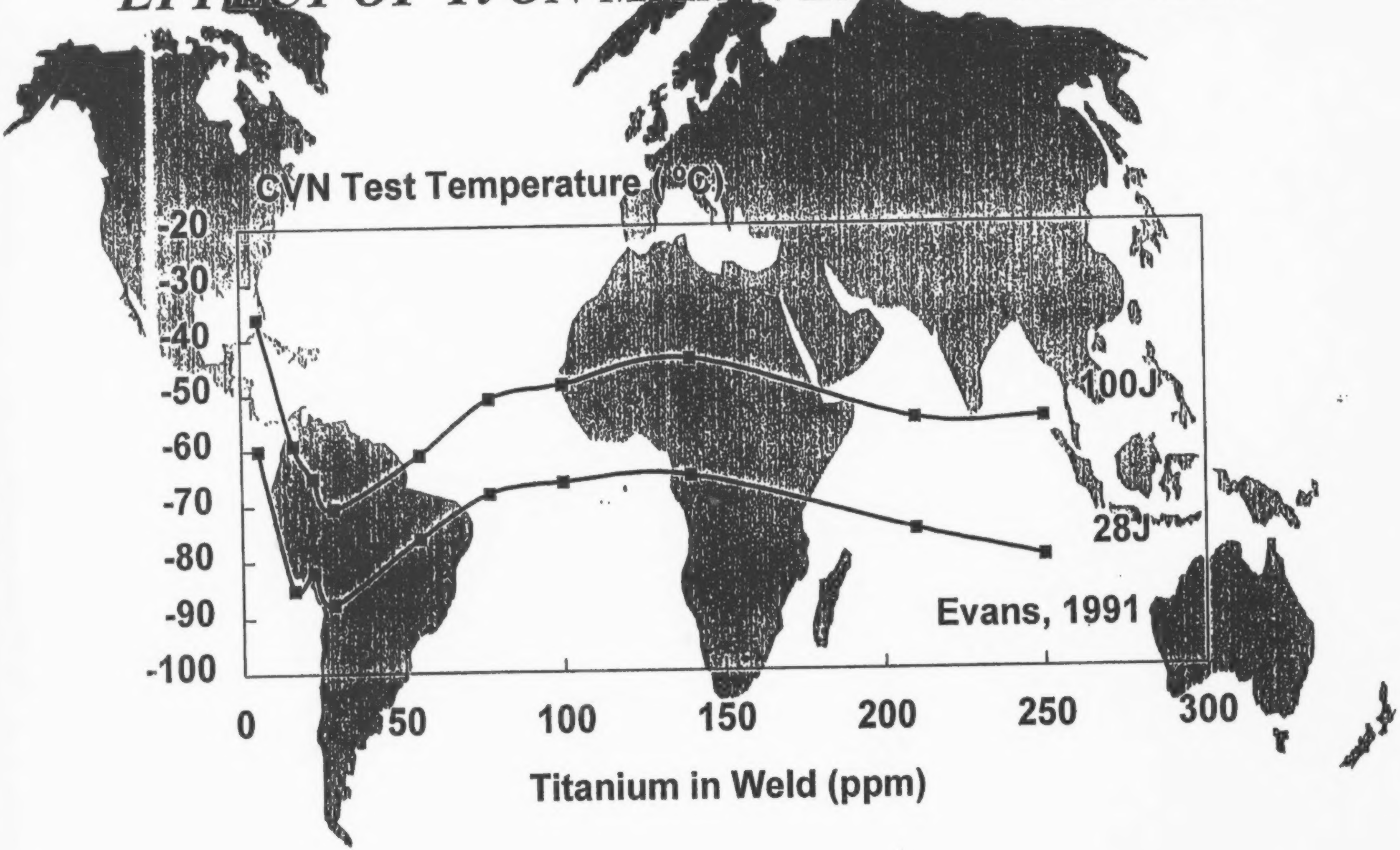

EFFECT OF Ti ON IMPACT TOUGHNESS

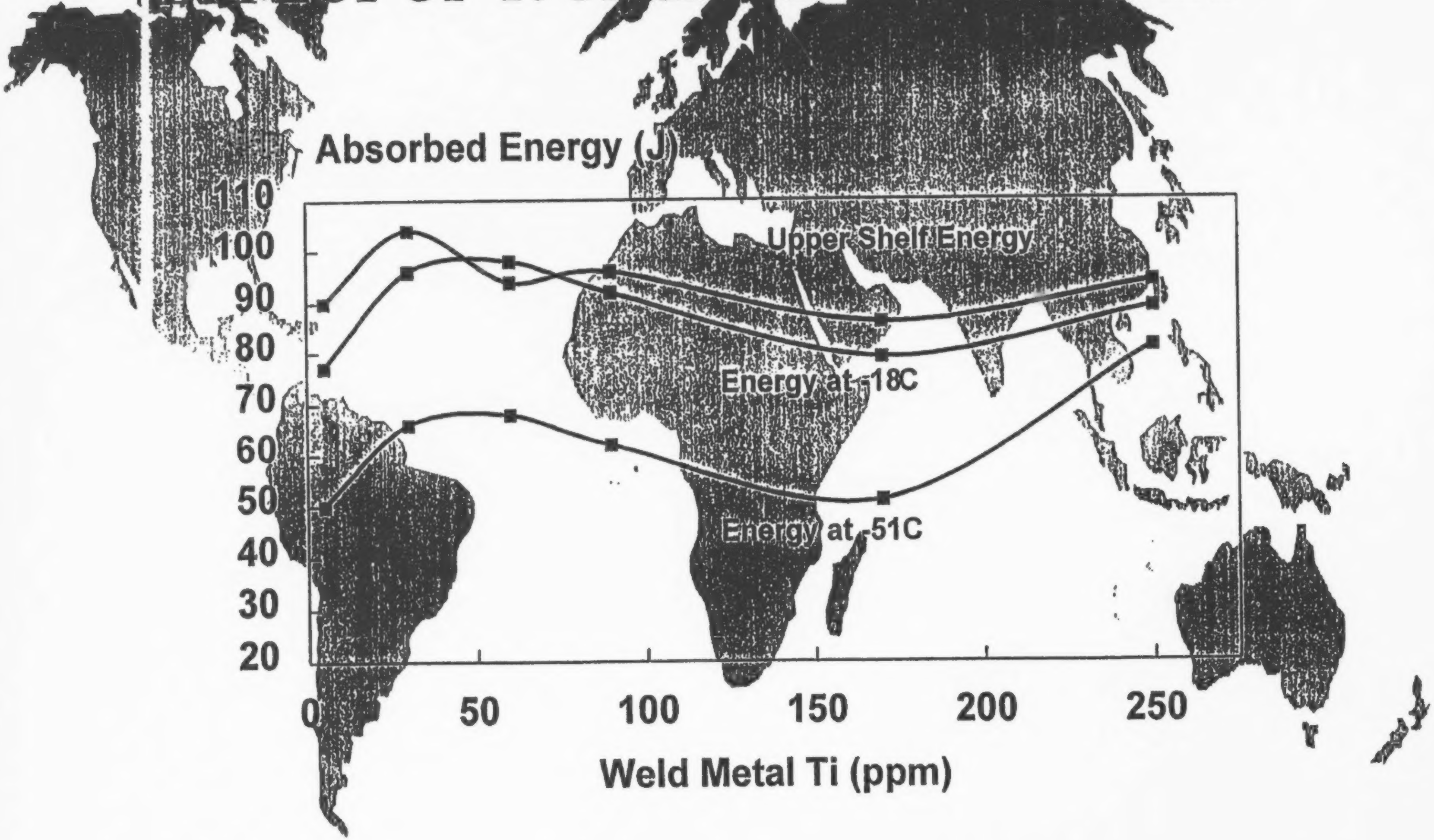

ANN and Statistical Models of Toughness in SMAW

1.4% Manganese

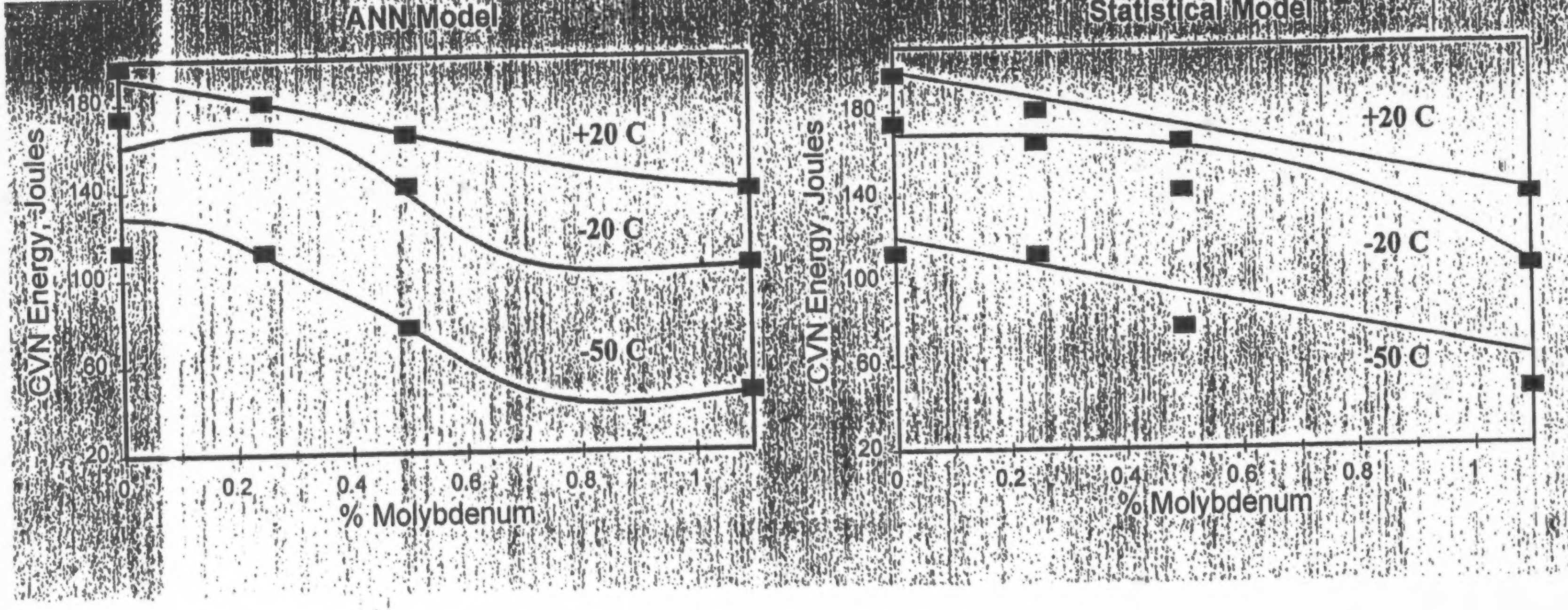

Error Standard Deviation for ANN and Statistical Models of SMAW Properties

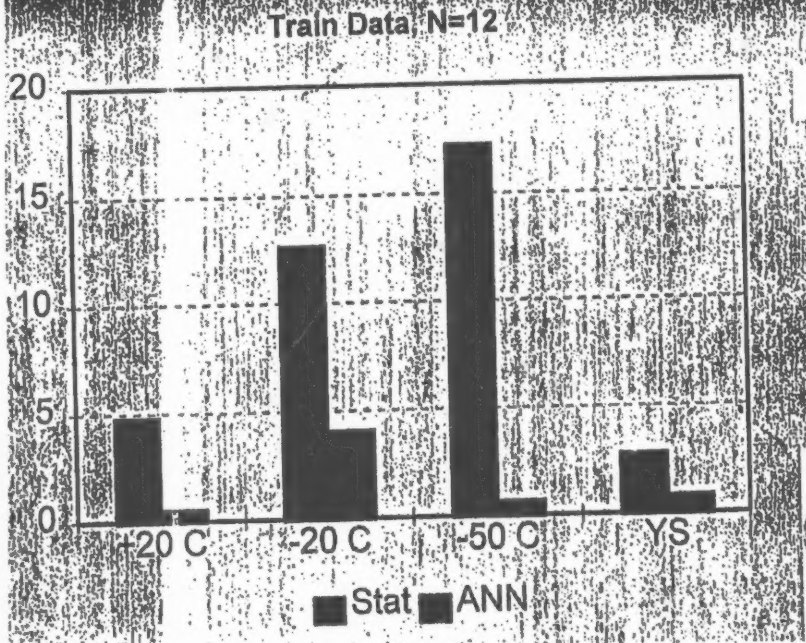

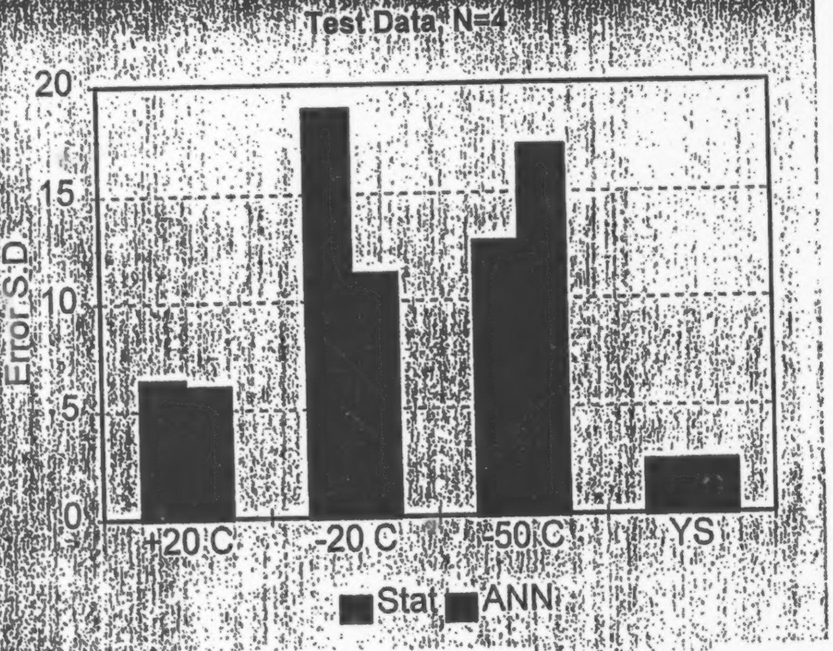

EFFECT OF COOLING RATE SENSITIVITY

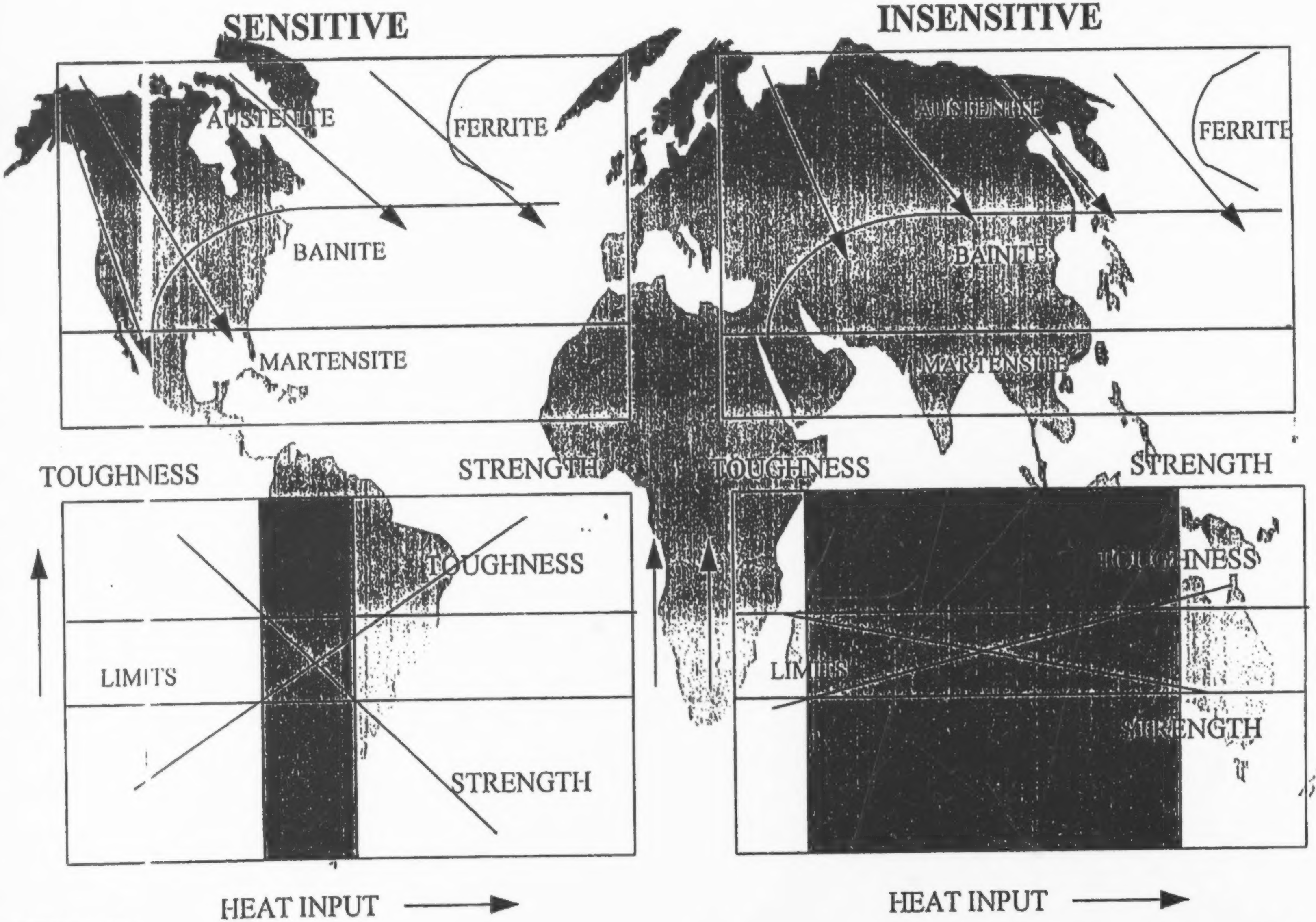
SENSITIVE
AUSTENITE
FERRITE
BAINITE
MARTENSITE
TOUGHNESS
STRENGTH
TOUGHNESS
LIMITS
STRENGTH
HEAT INPUT
INSENSITIVE
AUSTENITE
FERRITE
BAINITE
MARTENSITE
TOUGHNESS
STRENGTH
TOUGHNESS
LIMITS
STRENGTH
HEAT INPUT

NSWC CD

EFFECT OF COOLING RATE ON ULCB STRENGTH

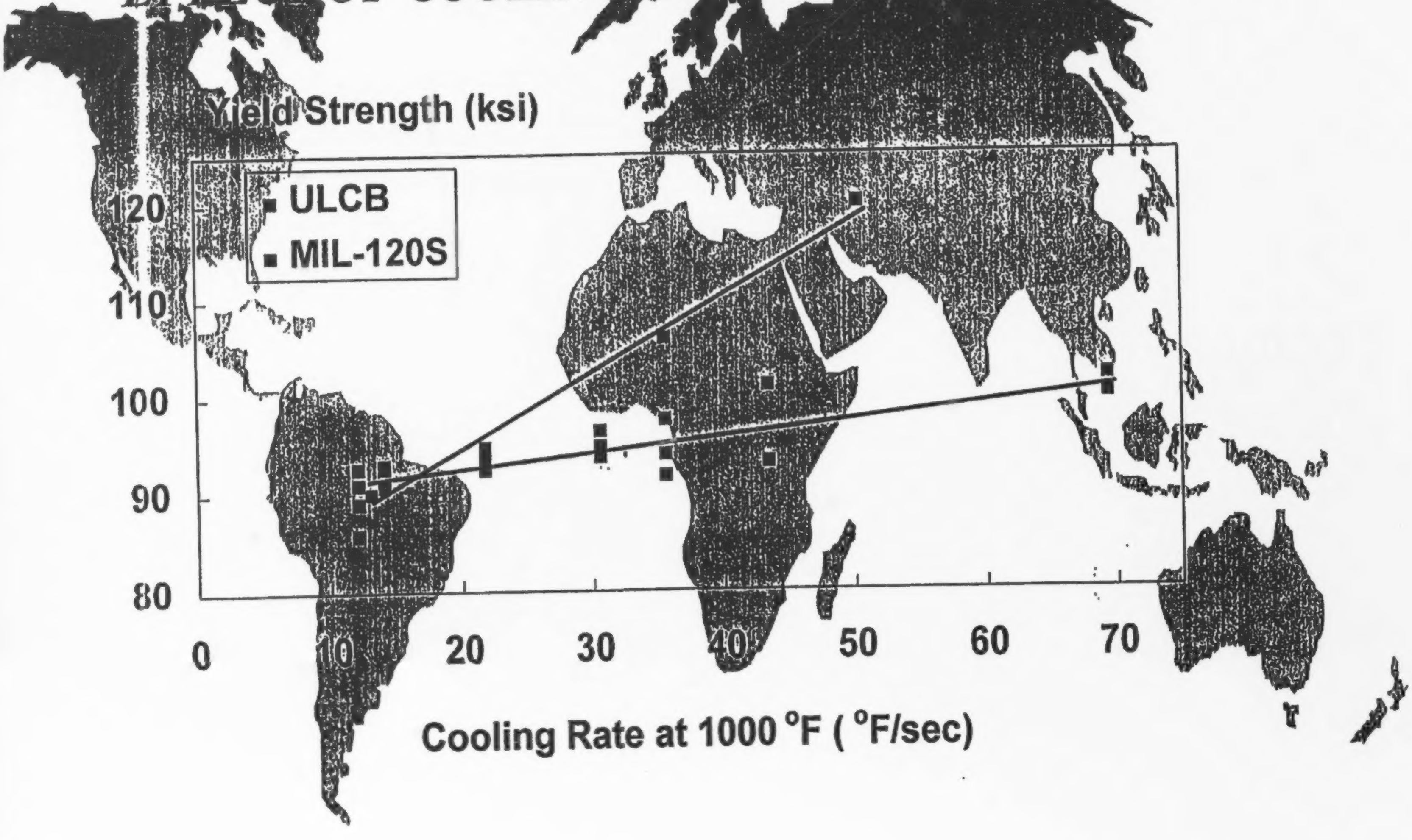

CVN PROPERTIES OF ULCB WELDS

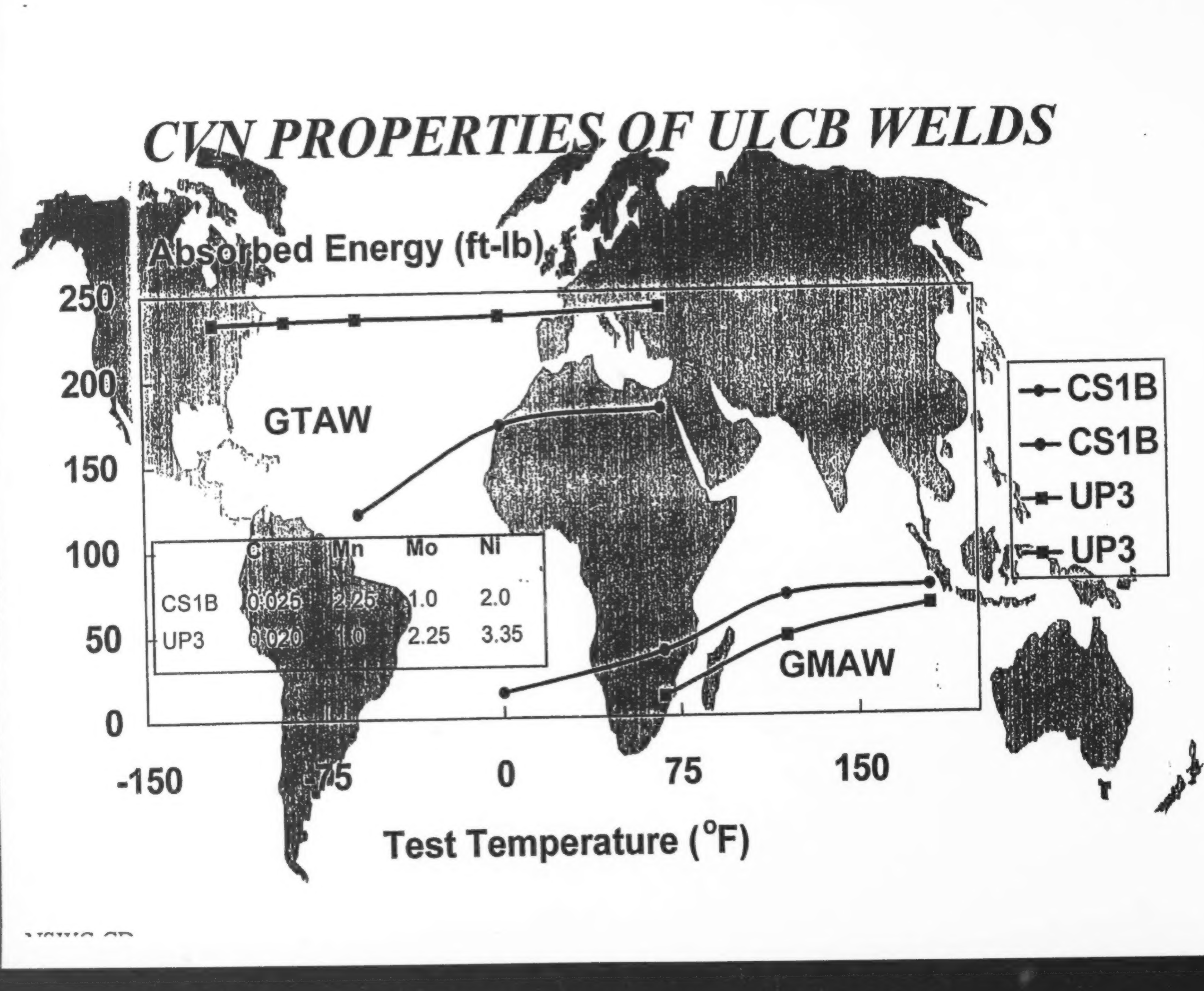

	C	Mn	Mo	Ni
CS1B	0.025	2.25	1.0	2.0
UP3	0.020	1.0	2.25	3.35

EFFECT OF HEAT INPUT ON ULCB TOUGHNESS

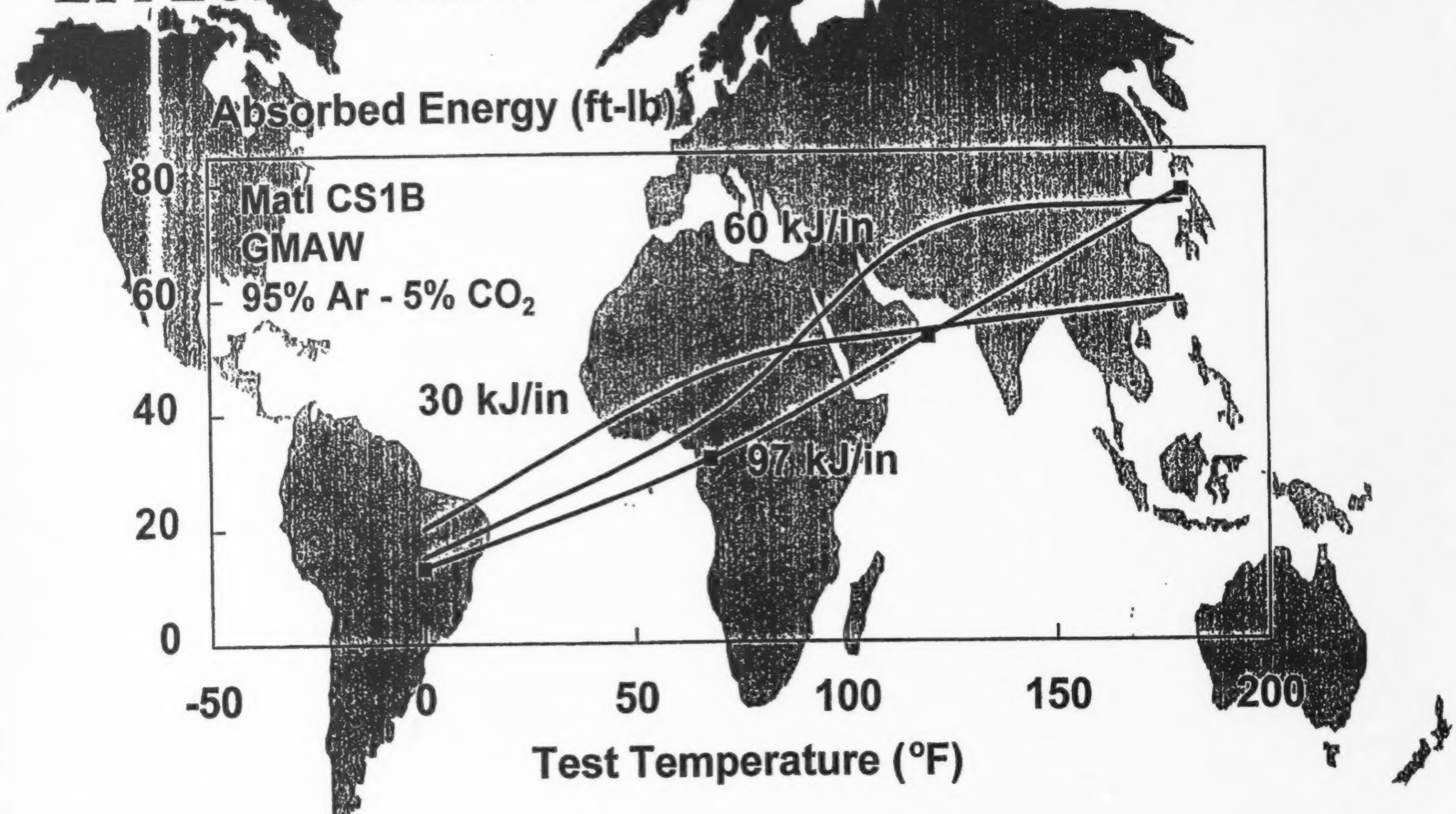

EFFECT OF SHIELDING GAS ON ULCB TOUGHNESS

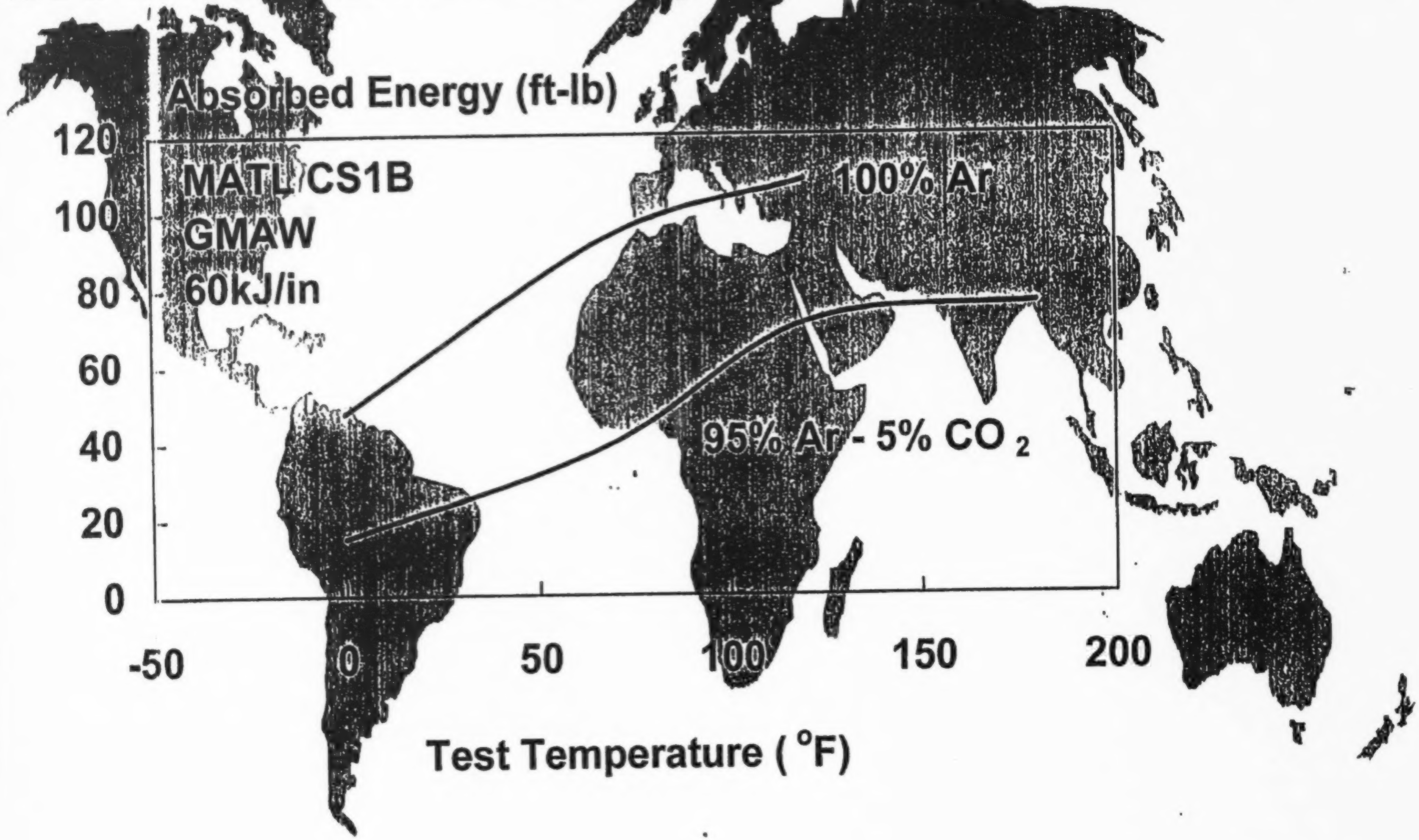

ULCB WELD METAL

Gleeble Thermal Cycles Performed on GMA Weld Metal

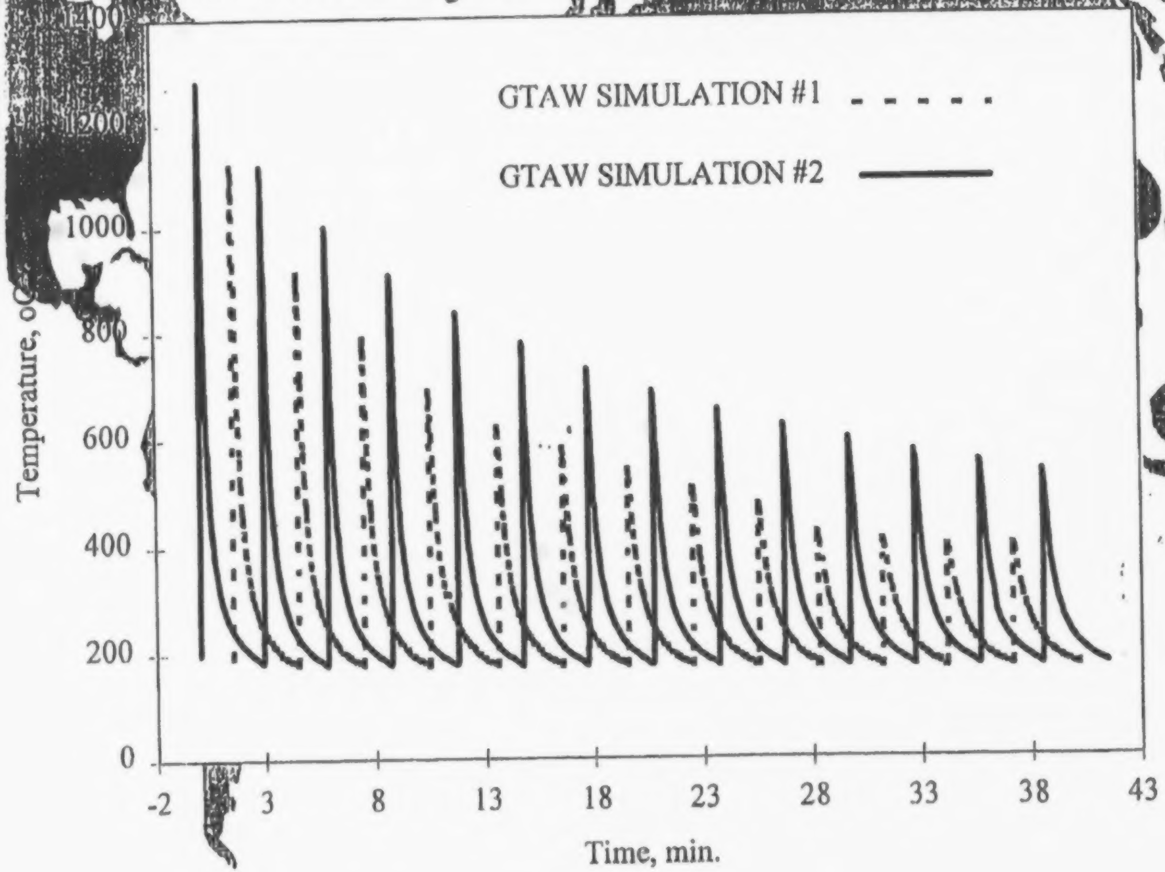

ULCB WELD METAL

Inclusion Study Results

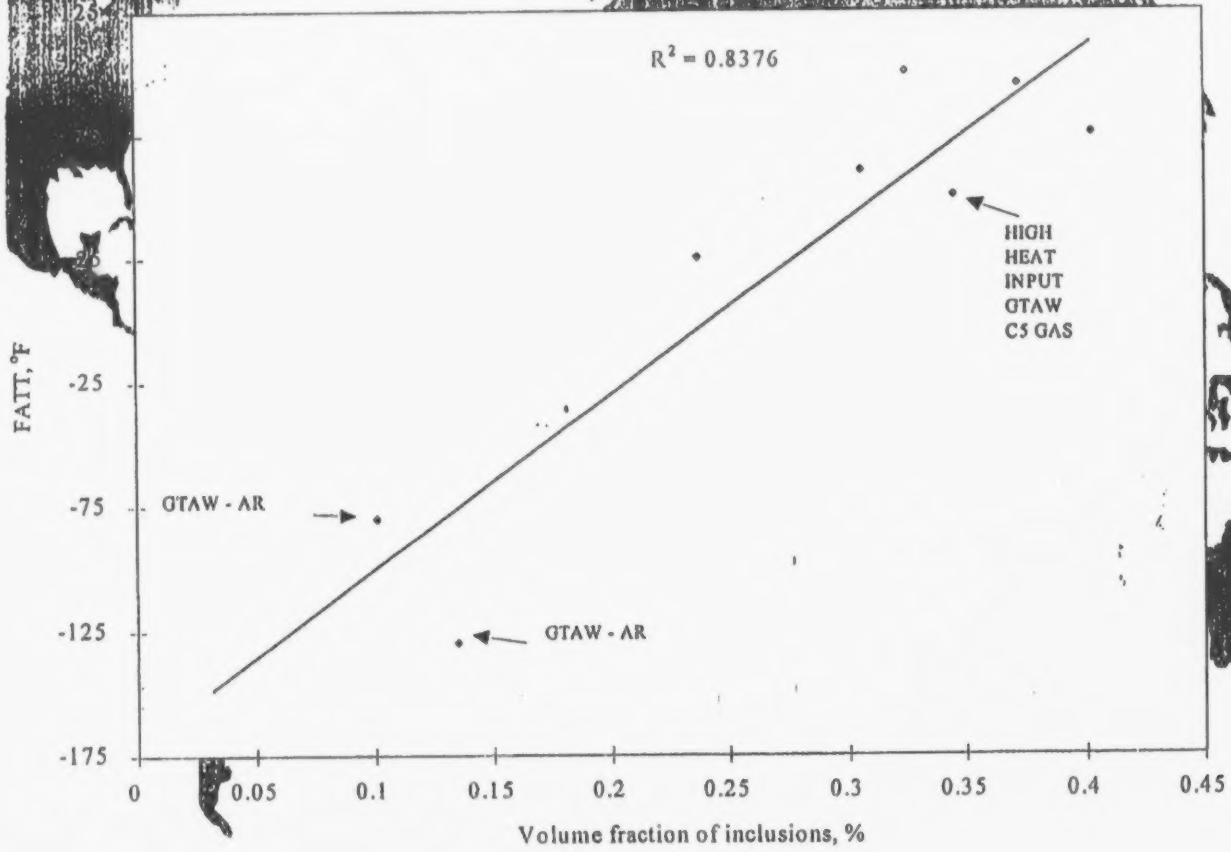

ULCB WELD METAL

Inclusion Study Results

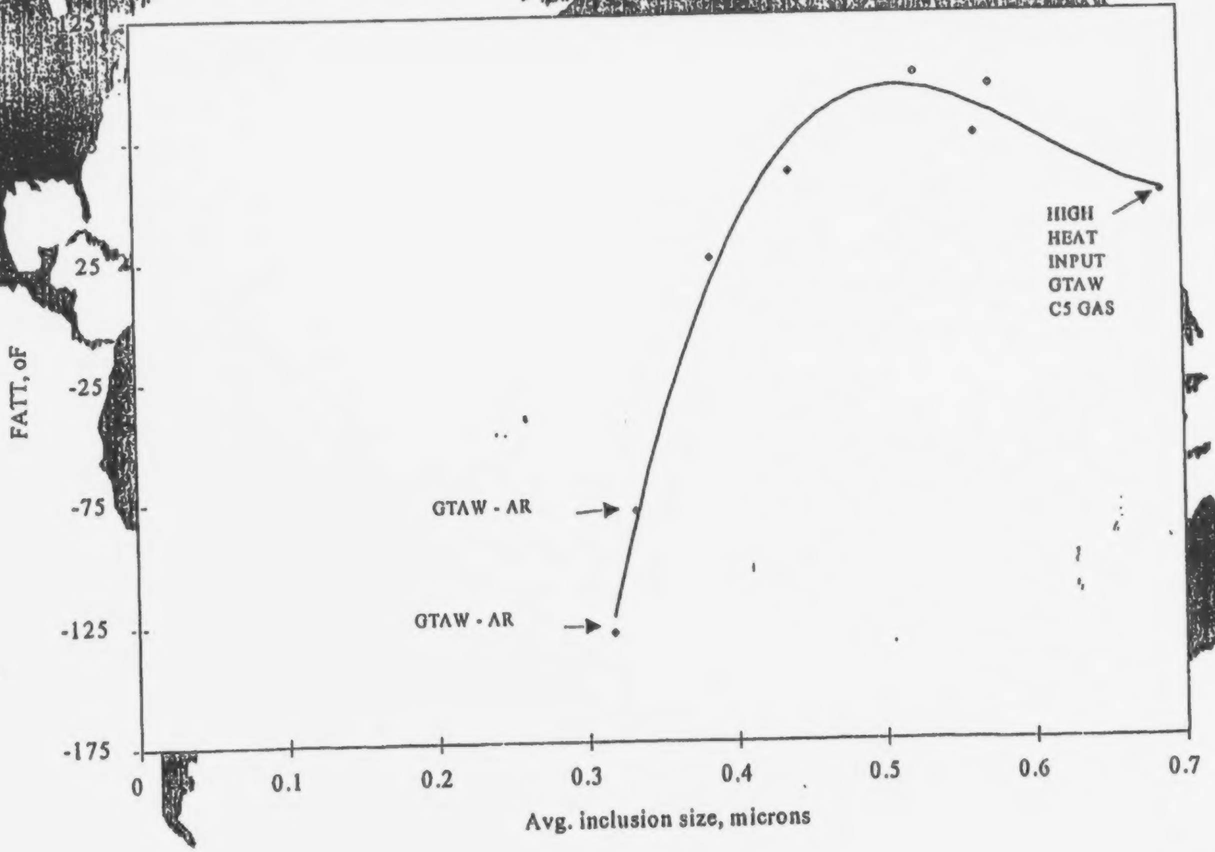

ULCB WELD METAL

The Effect of Thermal Cycles on CVN Impact Performance

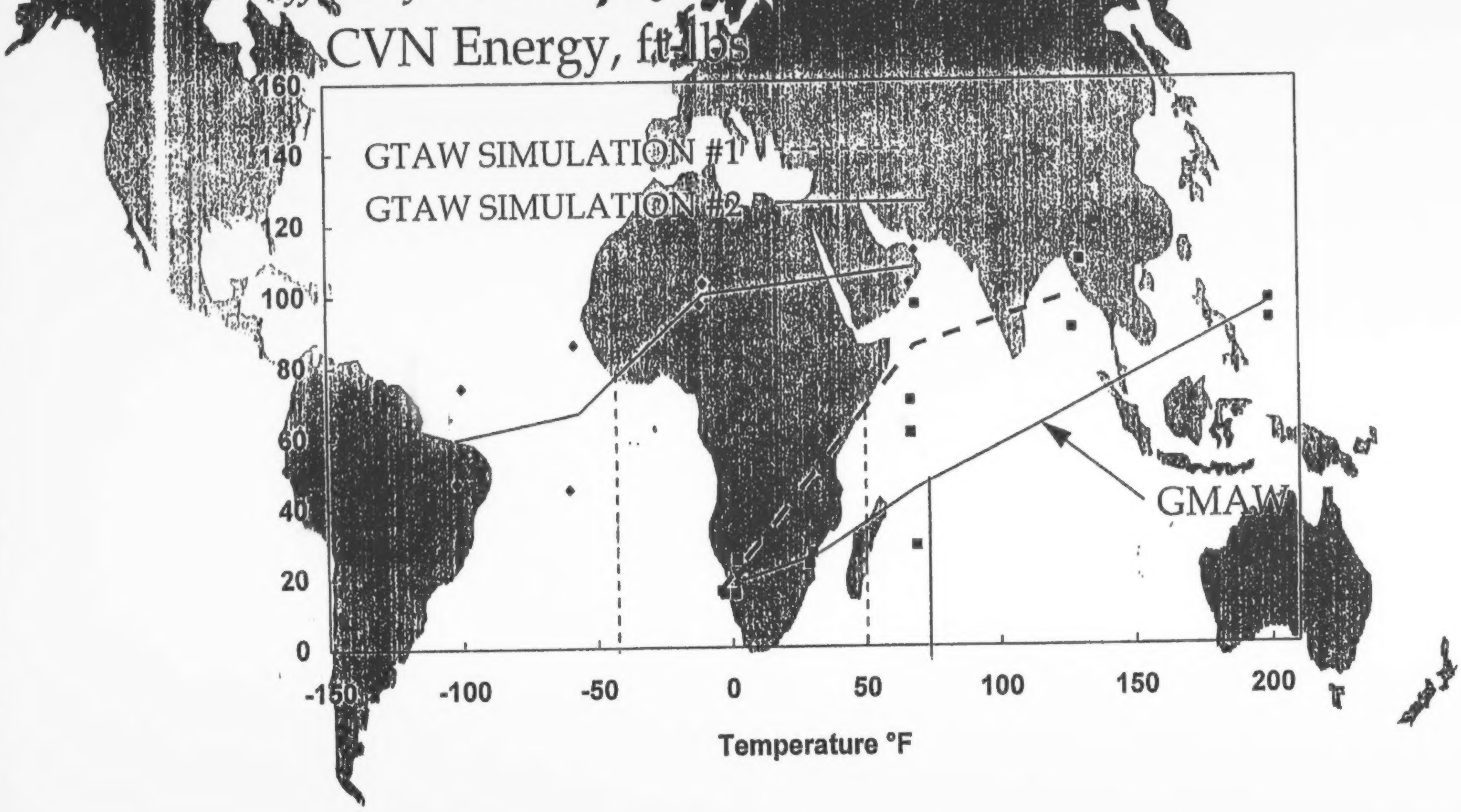

EFFECT OF FLUX MnO ON WELD METAL Mn

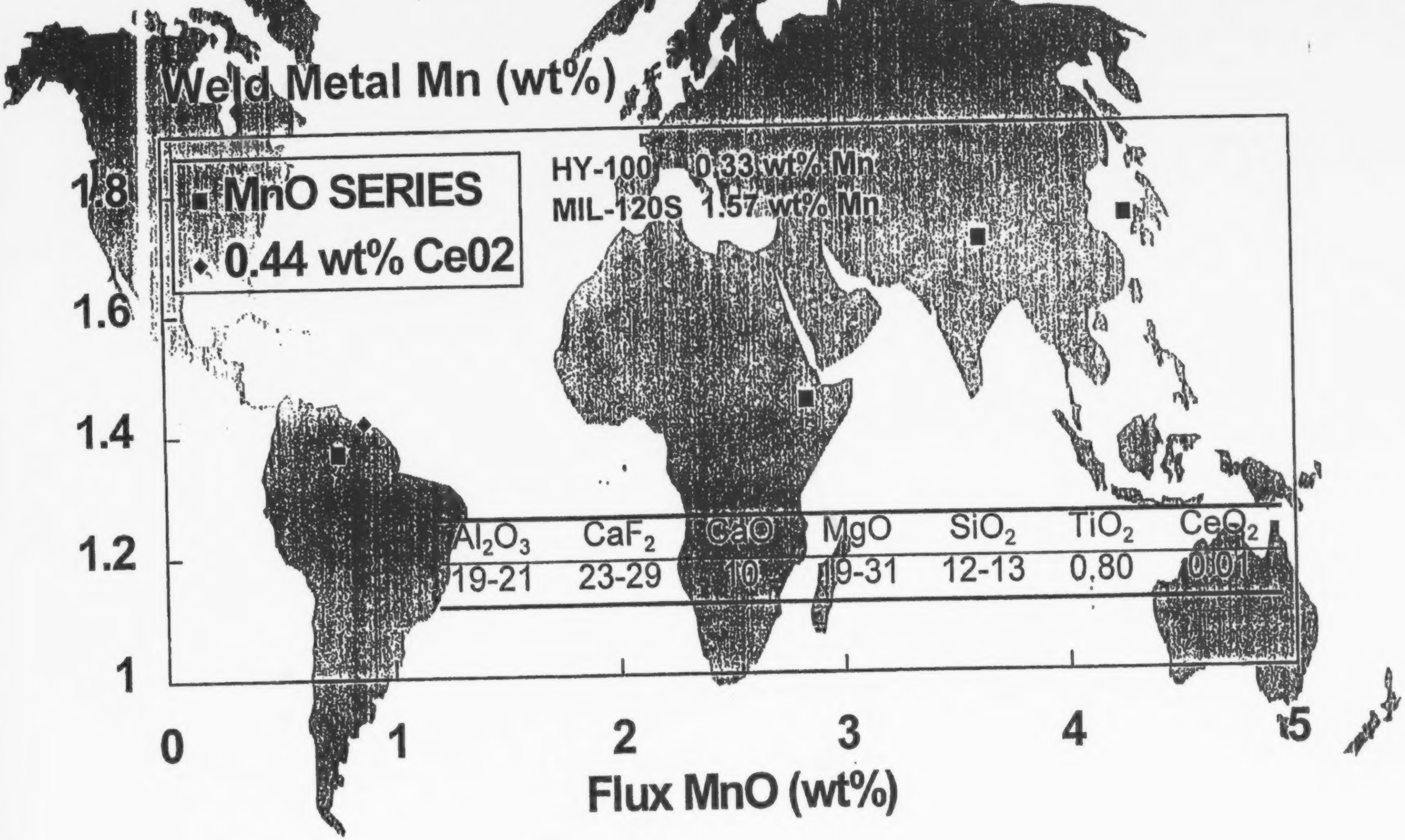

Al_2O_3	CaF_2	CaO	MgO	SiO_2	TiO_2	CeO_2
19-21	23-29	10	19-31	12-13	0,80	0.01

EFFECT OF FLUX MnO ON FATT

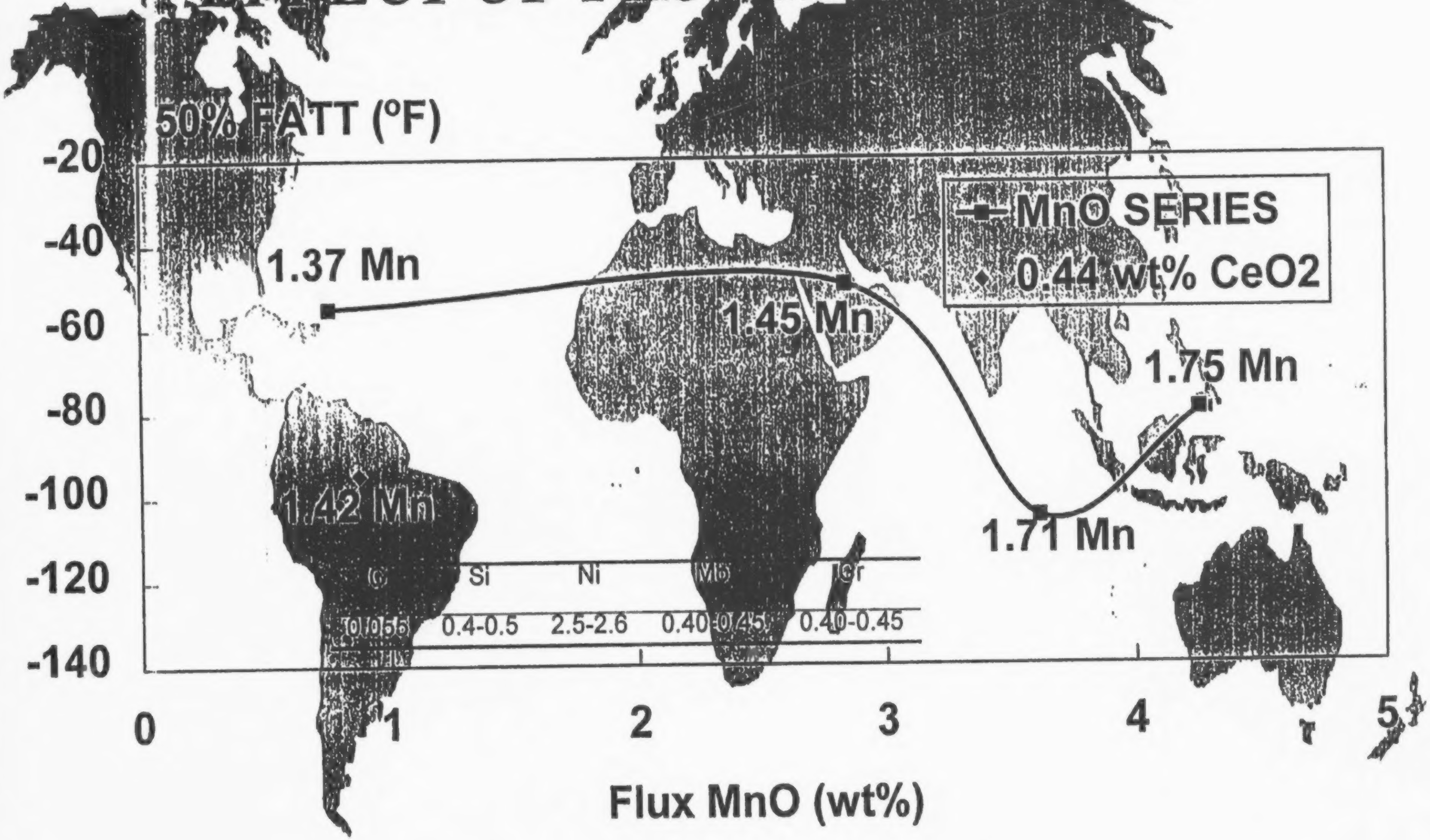

C	Si	Ni	Mo	Cr
0.055	0.4-0.5	2.5-2.6	0.40-0.45	0.40-0.45

MEASUREMENT OF ARC HYDROGEN

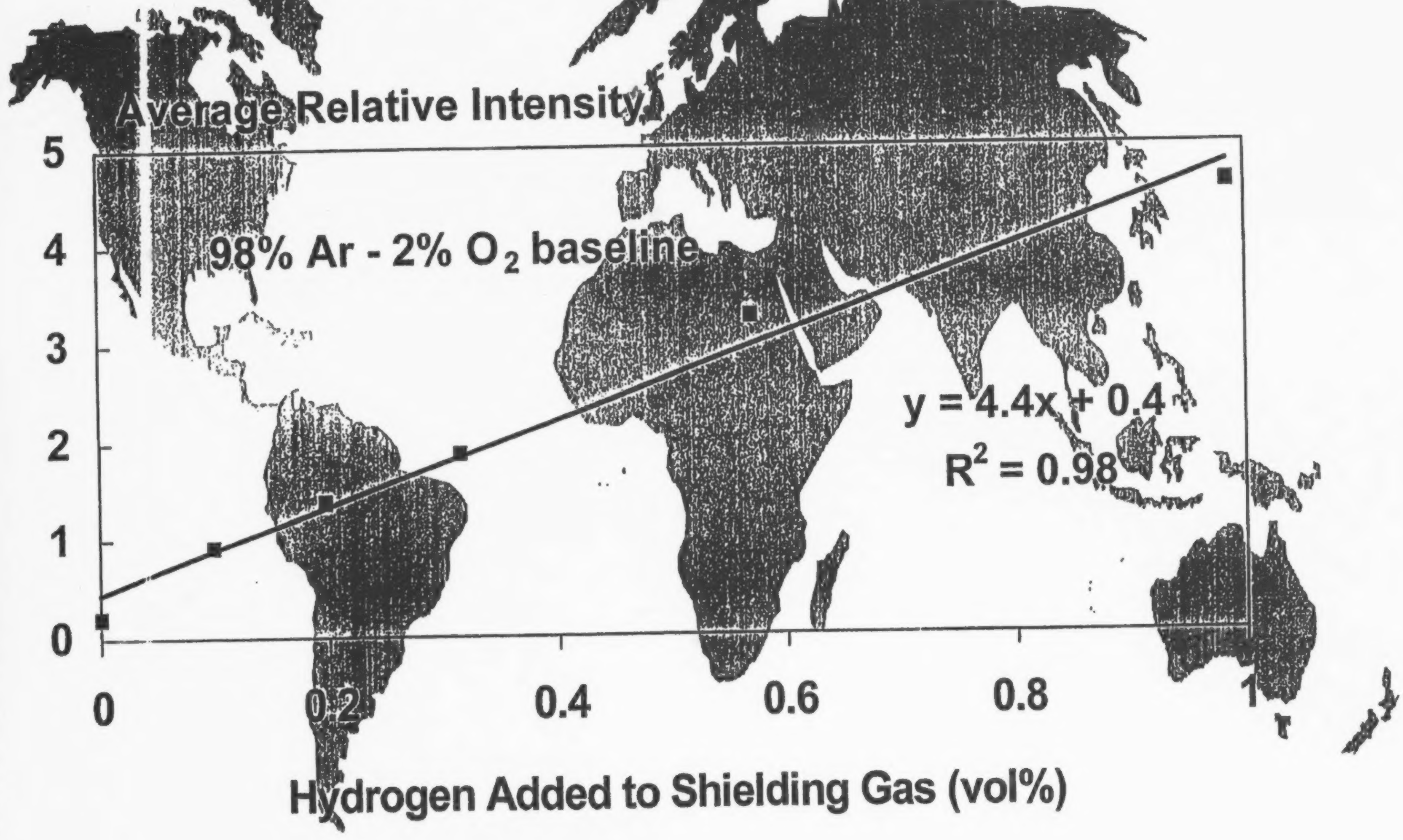

HYDROGEN SENSOR - H_D CORRELATION

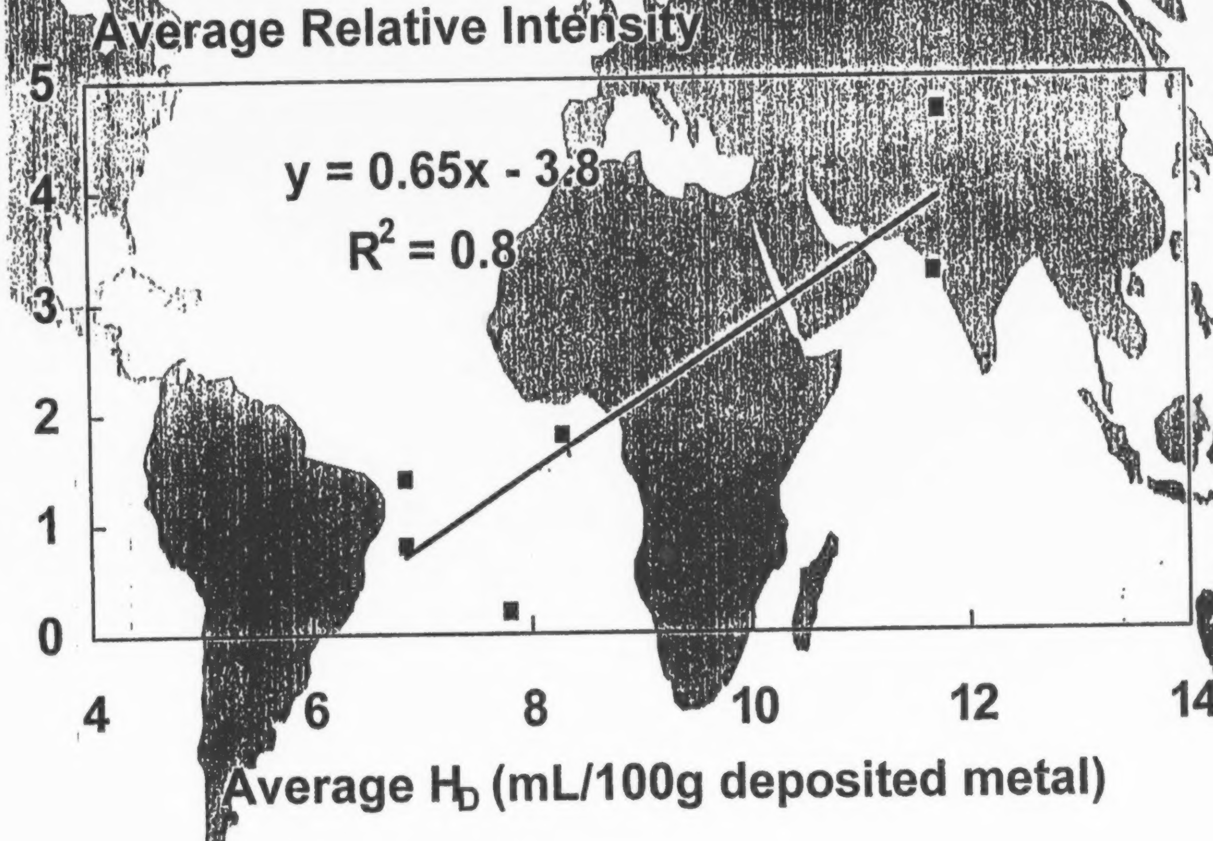

Modified Cruciform Test

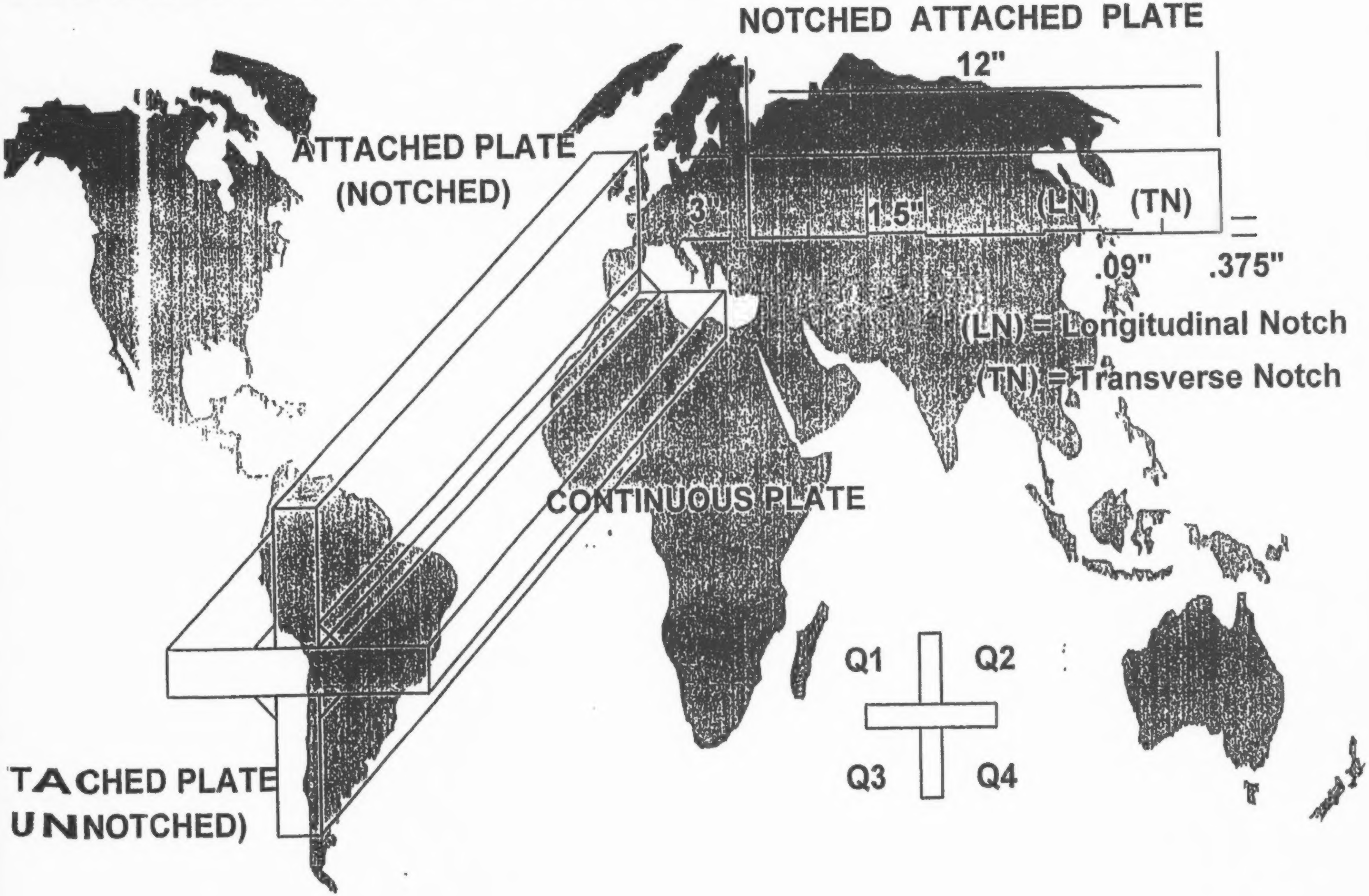
NOTCHED ATTACHED PLATE
12"
ATTACHED PLATE
(NOTCHED)
3"
1.5"
(LN)
(TN)
.09"
.375"
(LN) = Longitudinal Notch
(TN) = Transverse Notch
CONTINUOUS PLATE
Q1
Q2
Q3
Q4
TACHED PLATE
UNNOTCHED)

Multipass Cruciform Radiographic Results

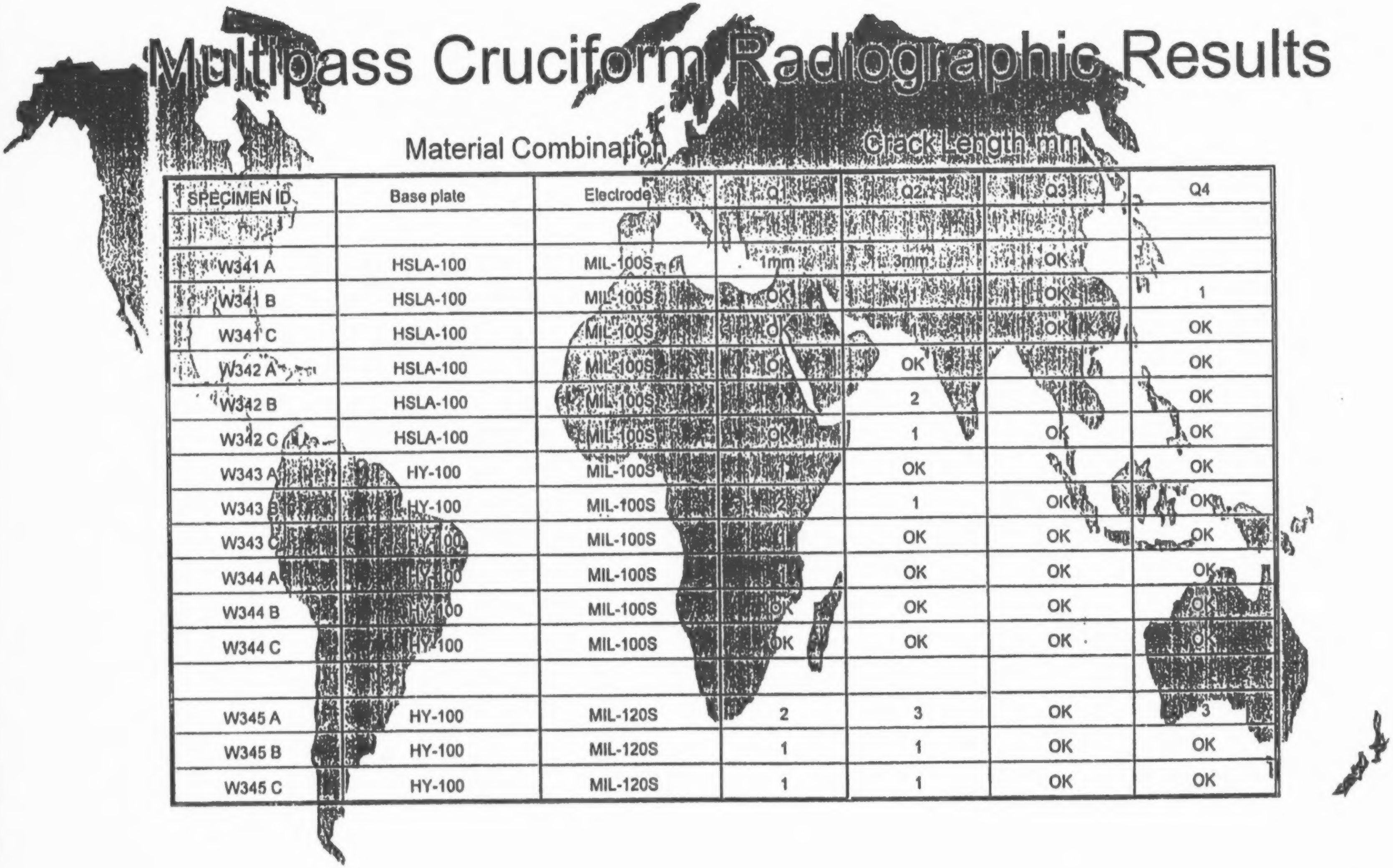

Material Combination			Crack Length mm			
SPECIMEN ID	Base plate	Electrode	Q1	Q2	Q3	Q4
W341 A	HSLA-100	MIL-100S	1mm	3mm	OK	
W341 B	HSLA-100	MIL-100S	OK	1	OK	1
W341 C	HSLA-100	MIL-100S	OK	1	OK	OK
W342 A	HSLA-100	MIL-100S	OK	OK	1	OK
W342 B	HSLA-100	MIL-100S	1	2		OK
W342 C	HSLA-100	MIL-100S	OK	1	OK	OK
W343 A	HY-100	MIL-100S	1	OK		OK
W343 B	HY-100	MIL-100S	2	1	OK	OK
W343 C	HY-100	MIL-100S	1	OK	OK	OK
W344 A	HY-100	MIL-100S	1	OK	OK	OK
W344 B	HY-100	MIL-100S	OK	OK	OK	OK
W344 C	HY-100	MIL-100S	OK	OK	OK	OK
W345 A	HY-100	MIL-120S	2	3	OK	3
W345 B	HY-100	MIL-120S	1	1	OK	OK
W345 C	HY-100	MIL-120S	1	1	OK	OK

ROOM-TEMPERATURE WIC & CRUCIFORMRESULTS

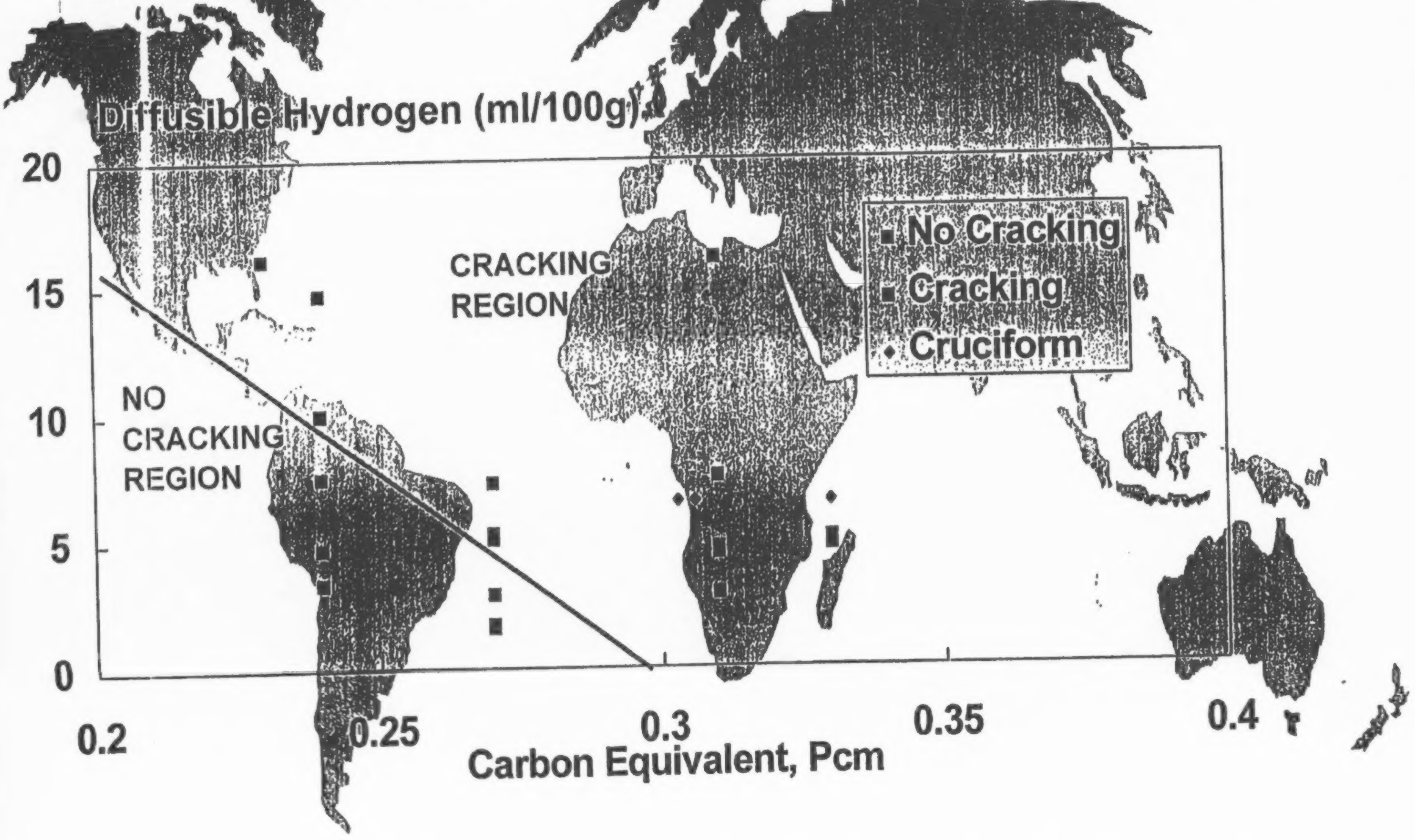

GMAW MODELLING

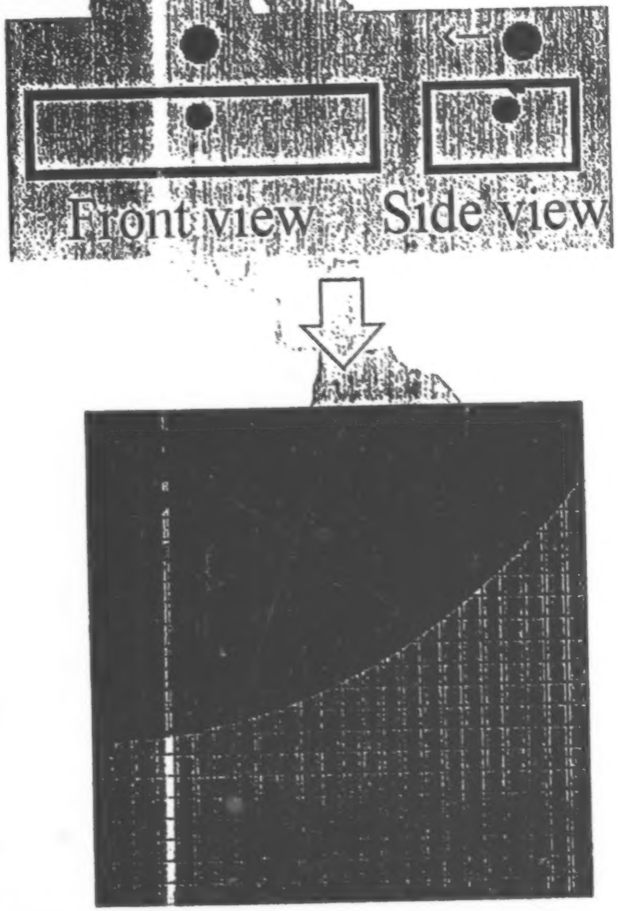
Front view
Side view

- Modified Rosenthal Equation
- Two Point Sources
  - Above surface
  - Below surface
- Total Energy Partitioned Between Sources

MODELLING GMAW

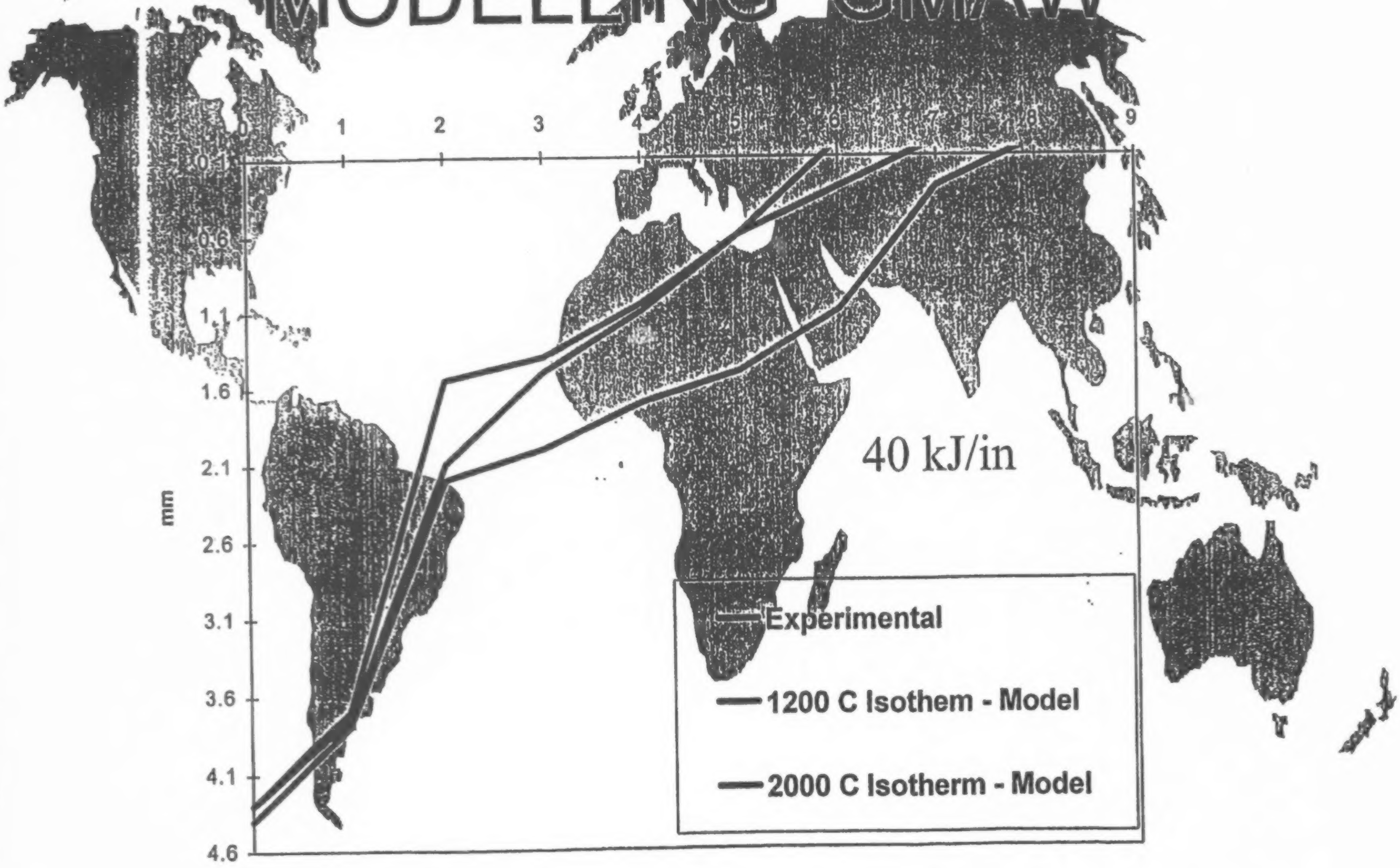

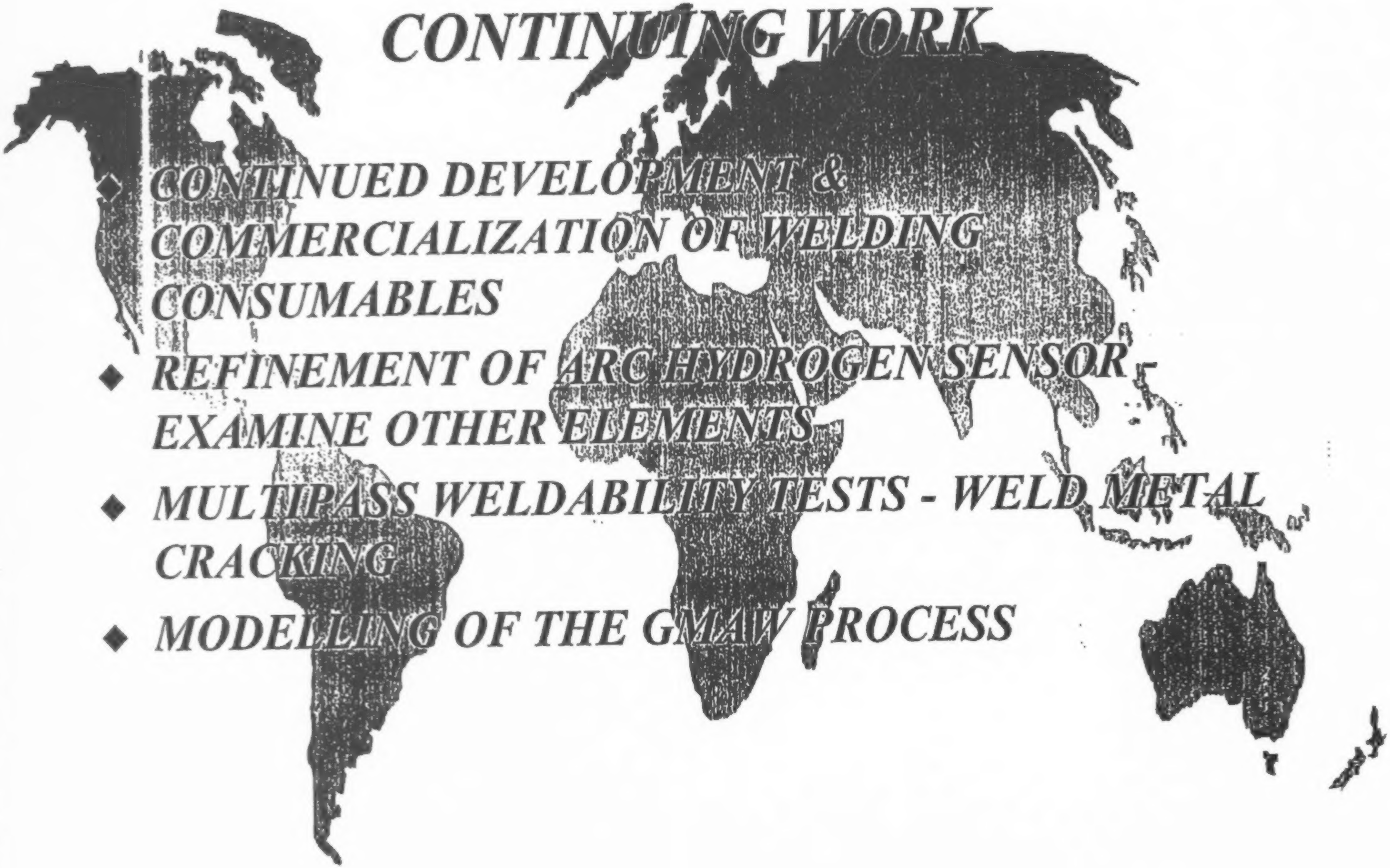

CONTINUING WORK

- ◆ *CONTINUED DEVELOPMENT & COMMERCIALIZATION OF WELDING CONSUMABLES*
- ◆ *REFINEMENT OF ARC HYDROGEN SENSOR - EXAMINE OTHER ELEMENTS*
- ◆ *MULTIPASS WELDABILITY TESTS - WELD METAL CRACKING*
- ◆ *MODELLING OF THE GMAW PROCESS*

#510359 ⑯

Computational Evaluation of Shipboard Cathodic Protection Systems

by V. G. DeGiorgi, E. D. Thomas III and K. E. Lucas

Mechanics of Materials Branch and Environmental Effects Branch
Naval Research Laboratory, Washington, DC, 20375, USA

A. Kee

Geo-Centers
Ft. Washington, Maryland, 20744, USA

ABSTRACT

Impressed current cathodic protection (ICCP) systems and computer modeling using boundary element techniques are independent established technologies. The application of boundary element methods to the design of ICCP systems will result in the development of more effective and more efficient ICCP systems. Three analyses are highlighted in the presentation. In two analyses, detailed comparisons are made between physical scale modeling (PSM) and computer modeling results. PSM results are defined as the baseline that computer modeling results are compared with to determine the applicability and accuracy of the technique. The first analysis performed uses U. S. Navy CG Hull Class and examines issues of mesh refinement and material characterization accuracy. In the second analysis, PSM and computer analysis for the CG Hull Class are directly compared with sea trial data. In the final analysis presented issues of scale and material characterization are examined using a model of a U. S. Navy CVN Hull Class ship.

Computational Evaluation
of
Shipboard Cathodic Protection Systems

NAVAL RESEARCH LABORATORY
WASHINGTON, D.C.

Dr. Virginia G. DeGiorgi
Mechanics of Materials Branch

Mr. E. Dail Thomas III
Mr. Keith Lucas
Environmental Effects Branch

Mr. Anthony Kee
Geo-Centers, Ft. Washington, MD

The Naval Research Laboratory

Washington, DC

The Naval Research Laboratory (NRL) is the direct result of a proposal made in 1915 by Thomas Edison to the United States Government for the establishment of a government laboratory for research and development of military technologies. NRL was officially founded in 1923. In 1992 NRL was designated as the U. S. Navy's Corporate Laboratory. The research staff at NRL consists of nearly 1500, primarily civilian employees of the Navy. The main campus is located along the Potomac River at the southern tip of the District of Columbia.

Research is conducted at NRL in general science and technology, warfare systems and sensors, materials science, ocean and atmospheric sciences and space science and technology. The diversity of expertise available at NRL is an important asset in the formation of research teams. Access is provided by NRL to multiple super-computer facilities for state of the art computational analyses. Fully equipped fatigue and fracture laboratories, corrosion testing laboratories, a vacuum arc melting furnace for reactive metals, hot isostatic press and ultrasonic non-destructive testing laboratory are only a few of the facilities available at NRL.

More information on NRL may be obtained from it's World Wide Web Home Page at:

http://www.nrl.navy.mil/

Cathodic Protection

GOAL: Maintain material to be protected at electrical charge level which minimizes corrosion.

*Makes use of natural electrochemical response

*Sacrificial Anodes
    Zinc
    Aluminum
    Impractical for large ships

*Impressed Current
    External power source
    Electrical current source points - anodes
    Voltage read at reference cells
    Simple feedback loop
    -reference cell readings control power input

Approach/Description

Application of computer modeling capability to determine geometric, spacial and electrochemical interactions for use in system design and evaluation

Approach has been verified for a ship hull ICCP system

Using a Boundary Element Method (BEM) a ship hull ICCP system has been reproduced as a Computer Model:

- * Precisely Duplicates Complex Geometries
- * Precisely Duplicates Major Alloys
- * Includes ICCP System Anodes as Part of Computer Model

Method Verification by comparison to:

- * Physical Scale Model Tests
- * Ship Trial Data

Physical Scale Modeling

Scale Dimensions

Scale Conductivity

Reproduce Design as Scale Model
Precisely Duplicate Complex Geometries
Precisely Duplicate All Metal Alloys

Validated by Comparison with Sea Trails Data
USS Princeton
(CG-59)

Partial Coating System Applied to Princeton
Conditions Between Minimum and Maximum Damage Conditions

Physical Scale Model Data
Distal vs Side

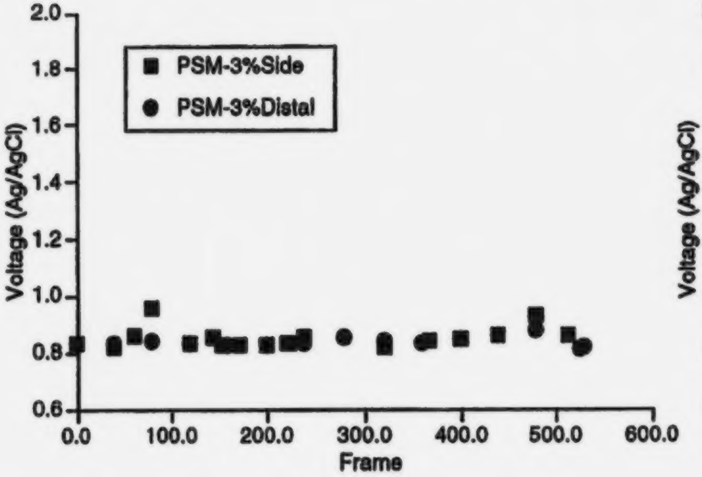

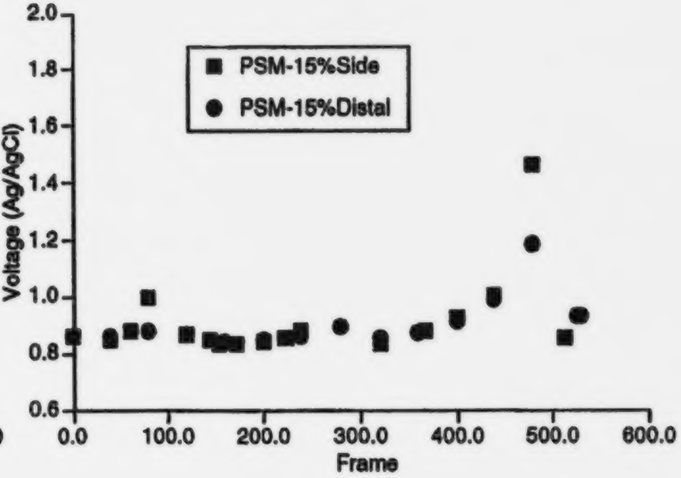

Demonstrates the similarity in readings. Distal readings correspond to real ship data. Side readings correspond to computer model data.

Comparison of Ship Data and Physical Scale Model Data

Beginning of Life Conditions for Modeling Results

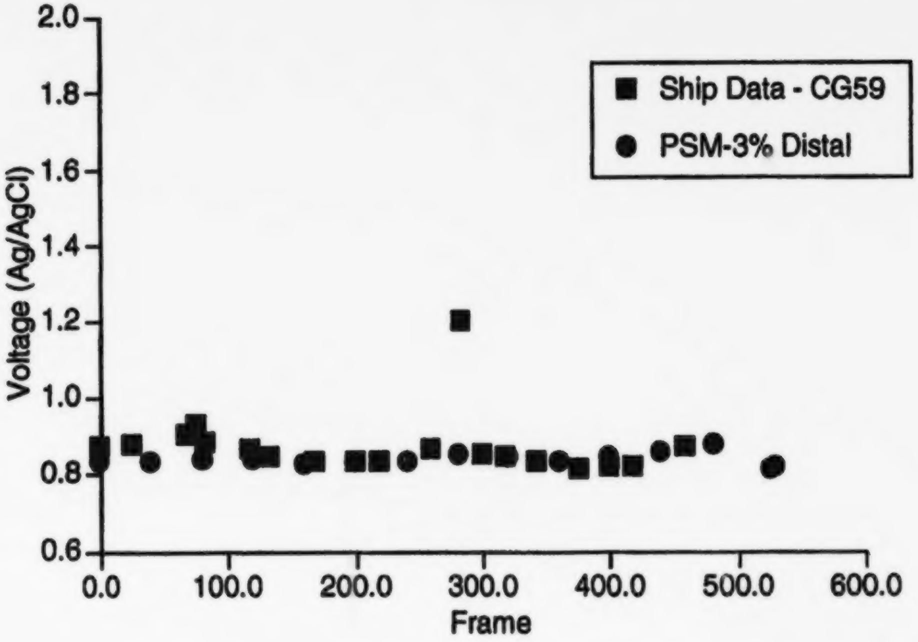

Comparison of Ship Data and Physical Scale Model Data

End of Life Conditions for Modeling Results

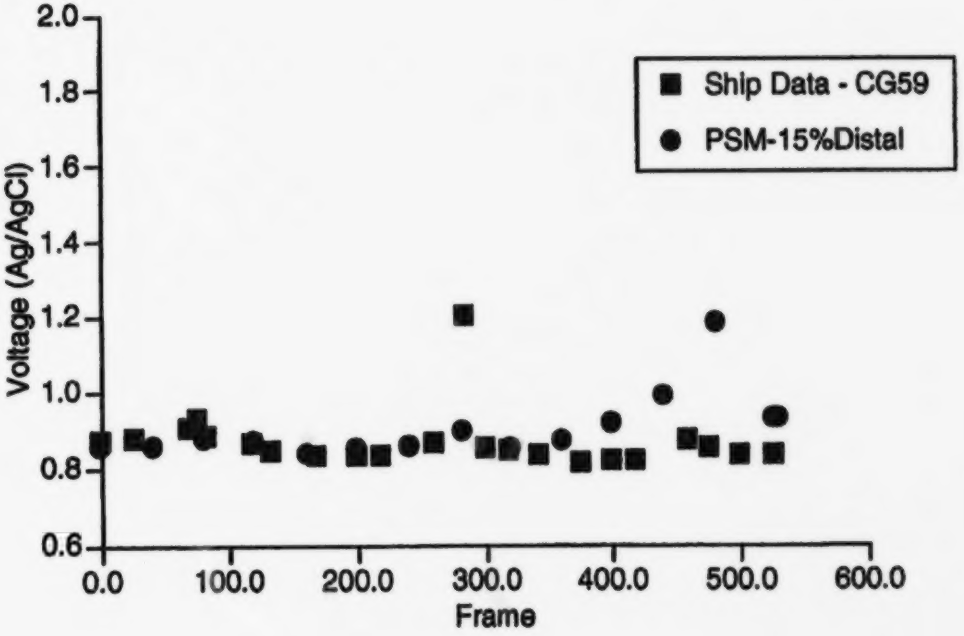

Computer Modeling Approach

Boundary Element Method

LaPlace's Equation

$$\nabla^2\Phi = 0$$

Nonlinear Material Polarization Response

Constant Potential (i.e. Anode)

$$\Phi = c$$

Constant Current (i.e. Anode)

$$\frac{\partial\Phi}{\partial n} = c$$

Insulated (i.e. Painted Surface)

$$\frac{\partial\Phi}{\partial n} = 0$$

Results from Computer Modeling

* Potential Map of Entire Surface

* Current Density Map of Entire Surface

* Potential Map of Surrounding Electrolyte

* Access to Potential and Current Density Values at Point Locations

* Current Balance

Ship/System Geometry

CG-59 (6 anode/2 power supply zones)
CG-66 (7 anode/2 power supply zones)

Conditions Considered

Static -
Minimum (3%) Damage
Maximum (15%) Damage
Dynamic -
Minimum (3%) Damage
Maximum (15%) Damage

Open Water Polarization Response

Plate Velocity Polarization Response Study
NAB
Steel
20 Ohm-cm Seawater

CG Model Details

BEASY-CP Version 1.1
(revision date 22 July 1988)

Linear Elements

1583 Elements

1876 Mesh Points

1 CPU Hour Cray YMP

8 Megawords Memory

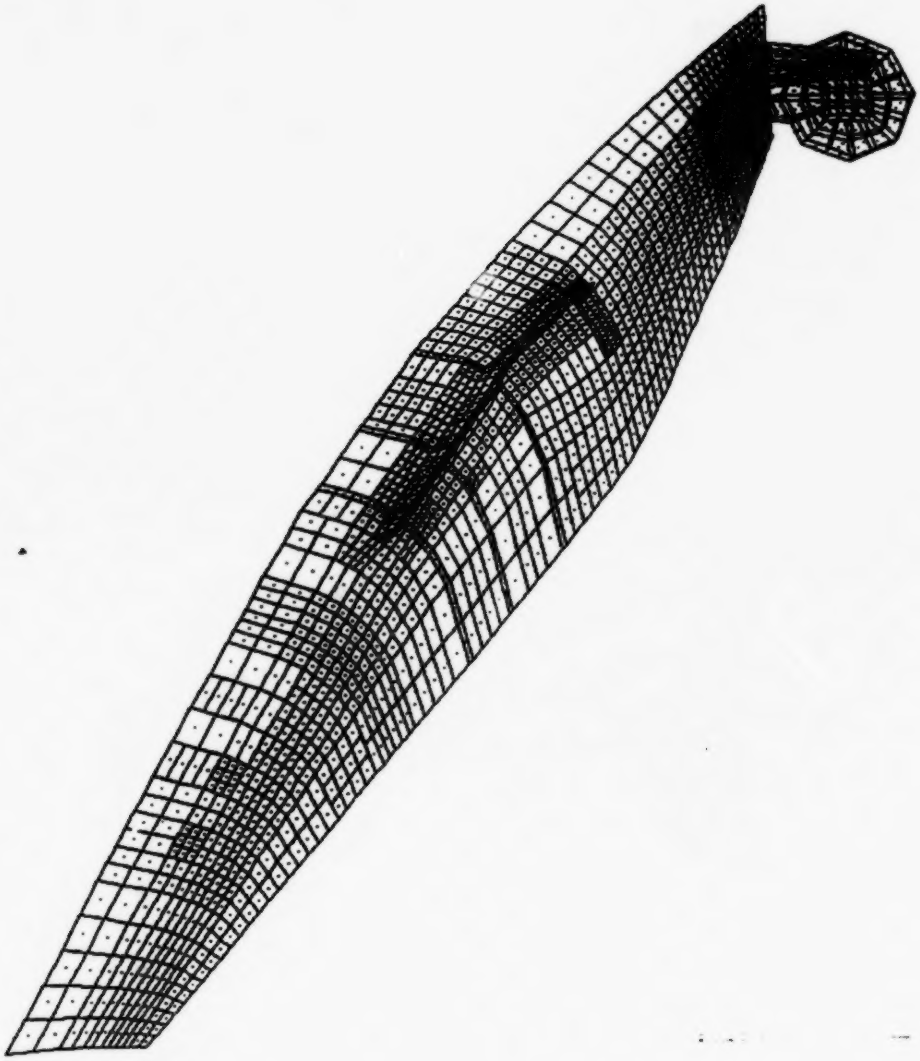

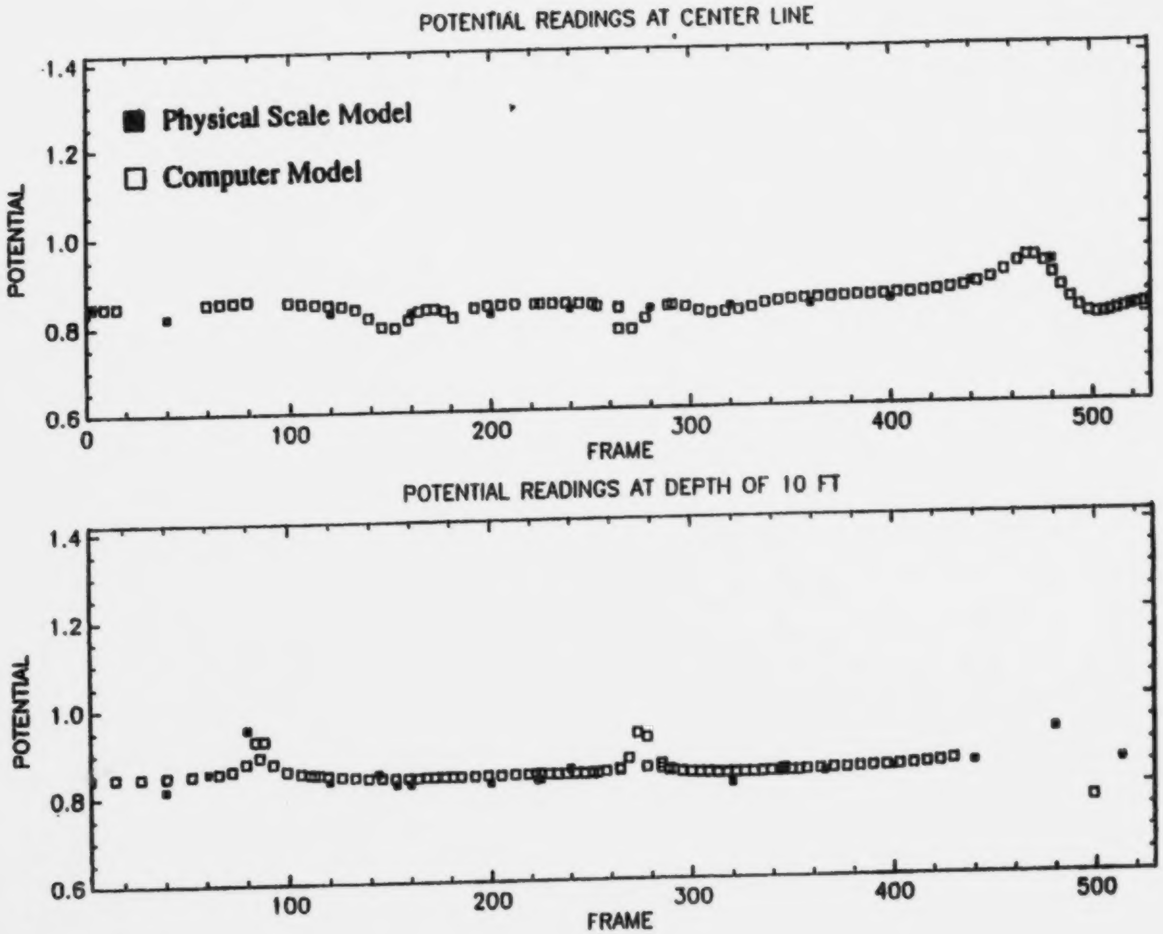

CG-59, Static - Minimum Damage

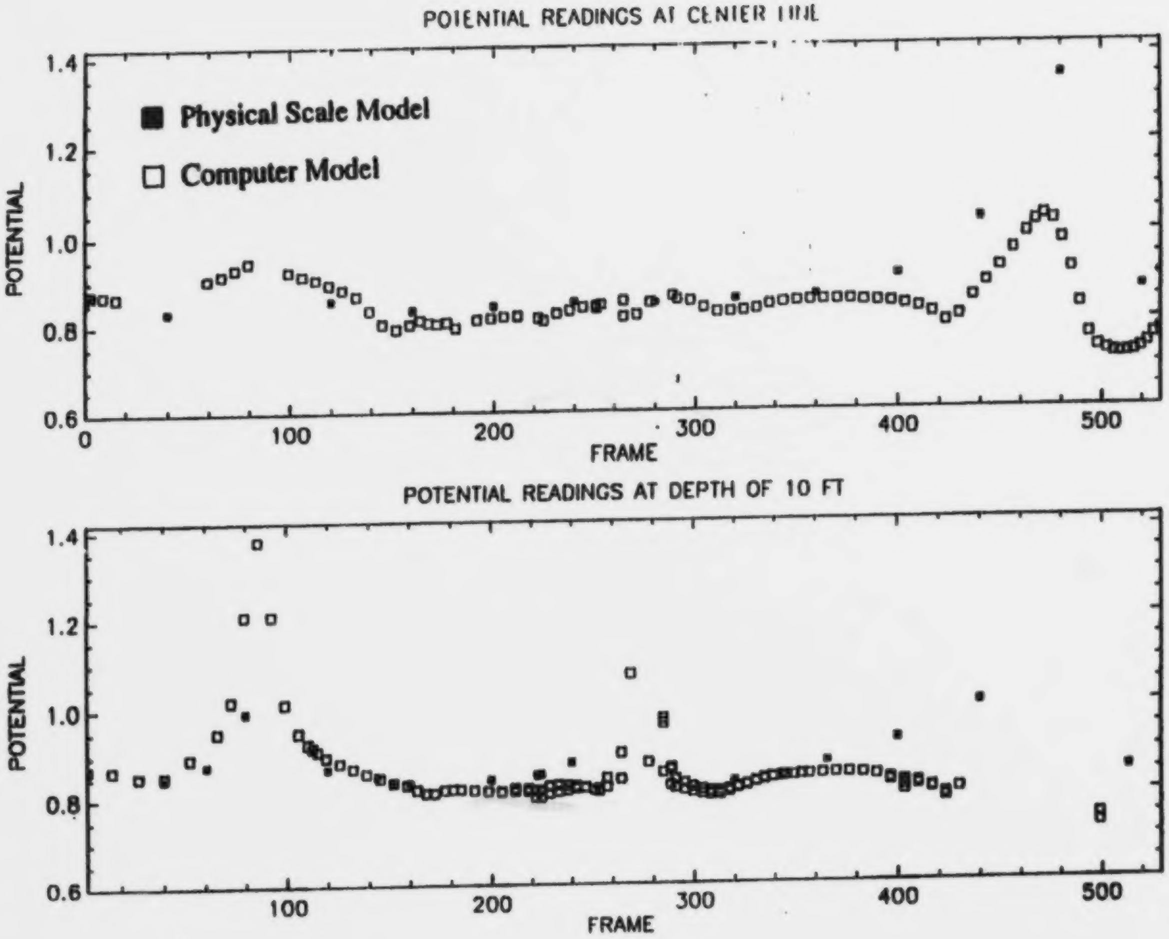

CG-59, Static - Maximum Damage

CG-59 Current Summary
6 Anodes/2 Power Supply Zones
Reference Cell = -0.85 V Ag/AgCl
(Amps)

	Total	Steel	NAB
Static -			
Minimum (3%) Damage			
Computer	35.7	8.0	27.7
Physical Scale Model	33.6	7.3	26.3
Maximum (15%) Damage			
Computer	181.1	8.6	26.2
Physical Scale Model	172.6	7.6	22.0
Dynamic -			
Minimum (3%) Damage			
Computer	60.0	13.2	46.8
Physical Scale Model	52.6	9.5	44.1
Maximum (15%) Damage			
Computer	553.0	24.4	69.3
Physical Scale Model	604.2	15.7	112.3

Comparison of Ship Data, Physical Scale Model Data and Computer Analysis Data

Beginning of Life Conditions for Modeling Results

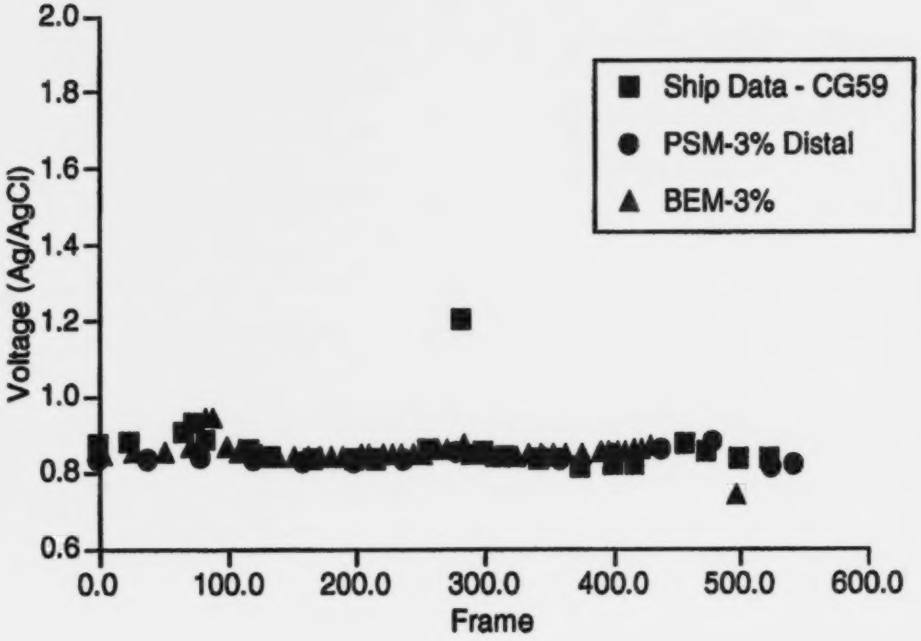

Comparison of Ship Data, Physical Scale Model Data and Computer Analysis Data

End of Life Conditions for Modeling Results

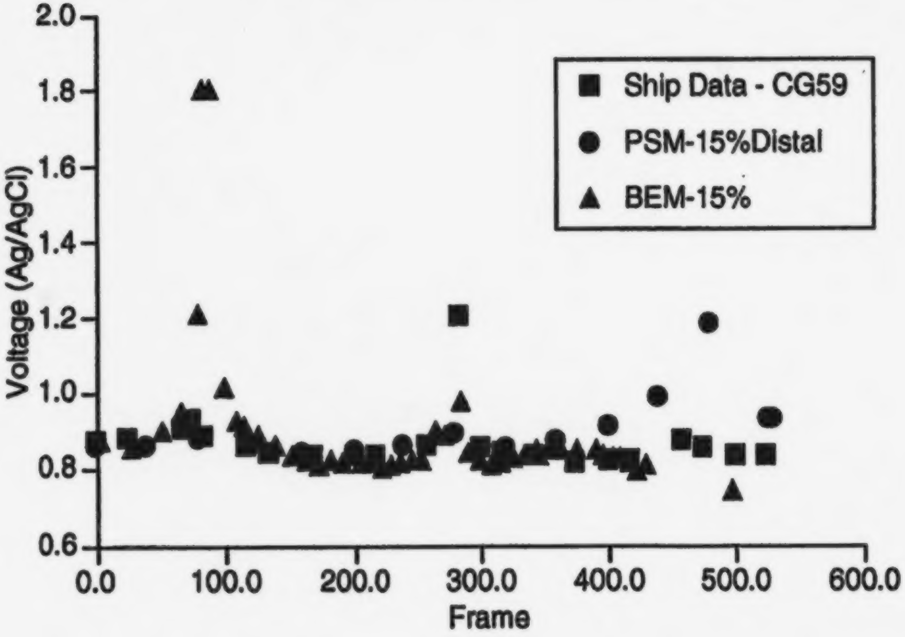

Ship/System Geometry

CVN
Upgrade System Design
(17 anodes/3 power supply zones)

Conditions Considered

Static -
Minimum (3%) Damage
Maximum (15%) Damage
Dynamic -
Minimum (3%) Damage
Maximum (15%) Damage

Tank Water Polarization Response

NAB
Steel
20 Ohm-cm Seawater

CVN Model Details

BEASY-CP Version 5.0_DEVELOP
(release date 15 Nov. 1992)

Linear-Quadratic Elements

1884 Elements

7996 Mesh Points

2 + CPU Hours Cray YMP

12 Megawords Memory

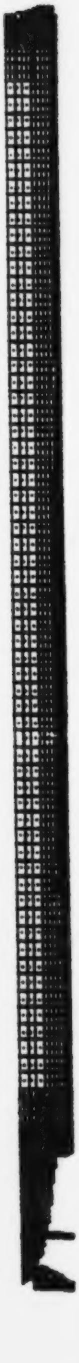

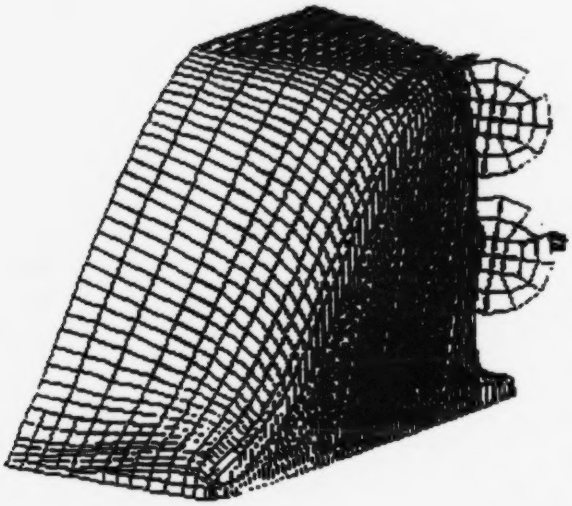

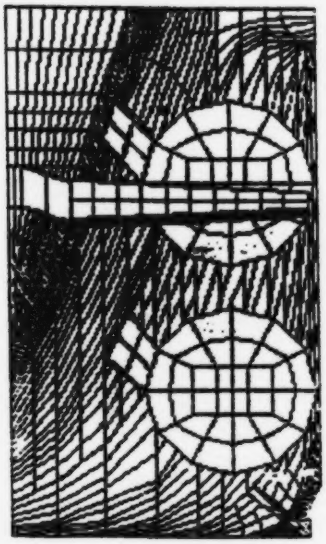

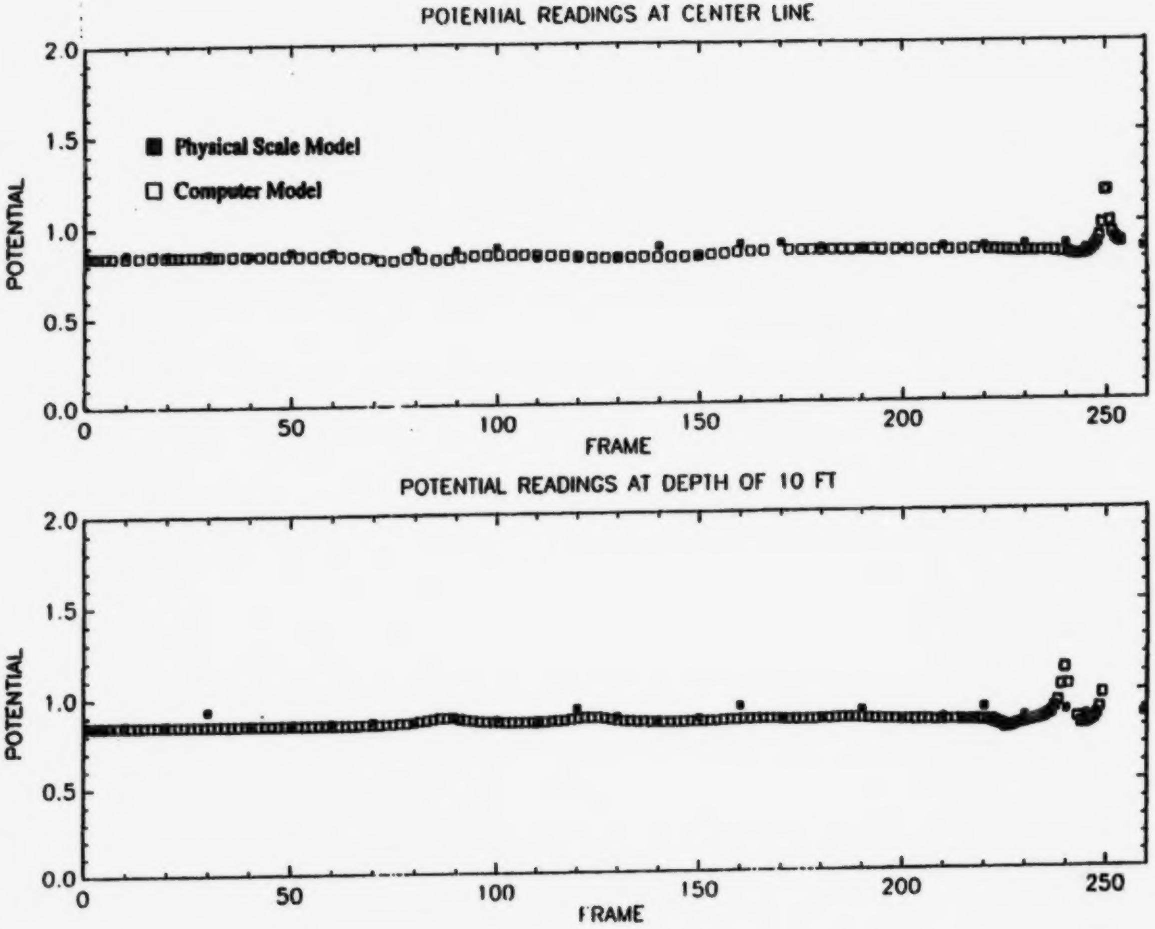

CVN-68, Static - Minimum Damage

POTENTIAL READINGS AT CENTER LINE

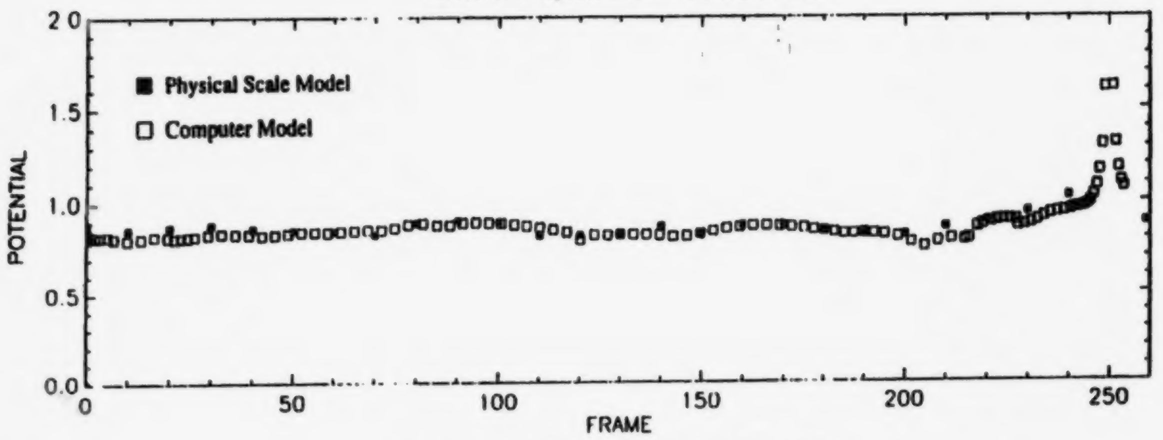

POTENTIAL READINGS AT DEPTH OF 10 FT

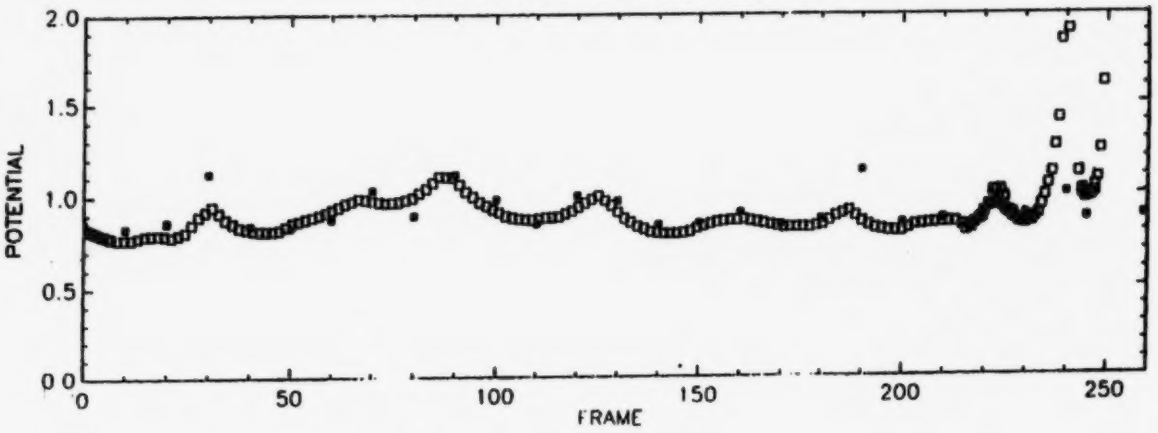

CVN-68, Static - Maximum Damage

CVN Current Summary/Upgrade System
17 Anode/3 Power Supply Zones
Reference Cell = -0.85 V Ag/AgCl
(Amps)

	Total	Steel	NAB
Static -			
Minimum (3%) Damage			
Computer	91.6	29.8	61.8
Physical Scale Model	81.9	31.8	50.1
Maximum (15%) Damage			
Computer	605.1	527.7	77.3
Physical Scale Model	704.1	650.0	54.0
Dynamic -			
Minimum (3%) Damage			
Computer	190.6	71.7	118.9
Physical Scale Model	314.7	110.6	204.1
Maximum (15%) Damage			
Computer	1718.0	1528.2	189.8
Physical Scale Model	1837.7	1609.5	228.2

Mesh Refinement

Element Type
Computer Time/Cost

Element Size
Selective Refinement

Driving Forces
Size of Electrolyte Volume
Features to be Modeled

Material Properties/Polarization Response

Current Density vs. Potential
Nonlinear
Duplicate Service Conditions
Accuracy in Area Representation
Material Interactions

Proposed Design Procedure

Utilizes both Physical Scale and Computer Modeling

Computer Modeling -
Preliminary design
Able to perform many iterations in cost effective manner
Takes advantage of nature of computer modeling

Physical Scale Modeling -
Final design verification
Takes advantage of nature of physical scale modeling

Shipboard ICCP System Design Process

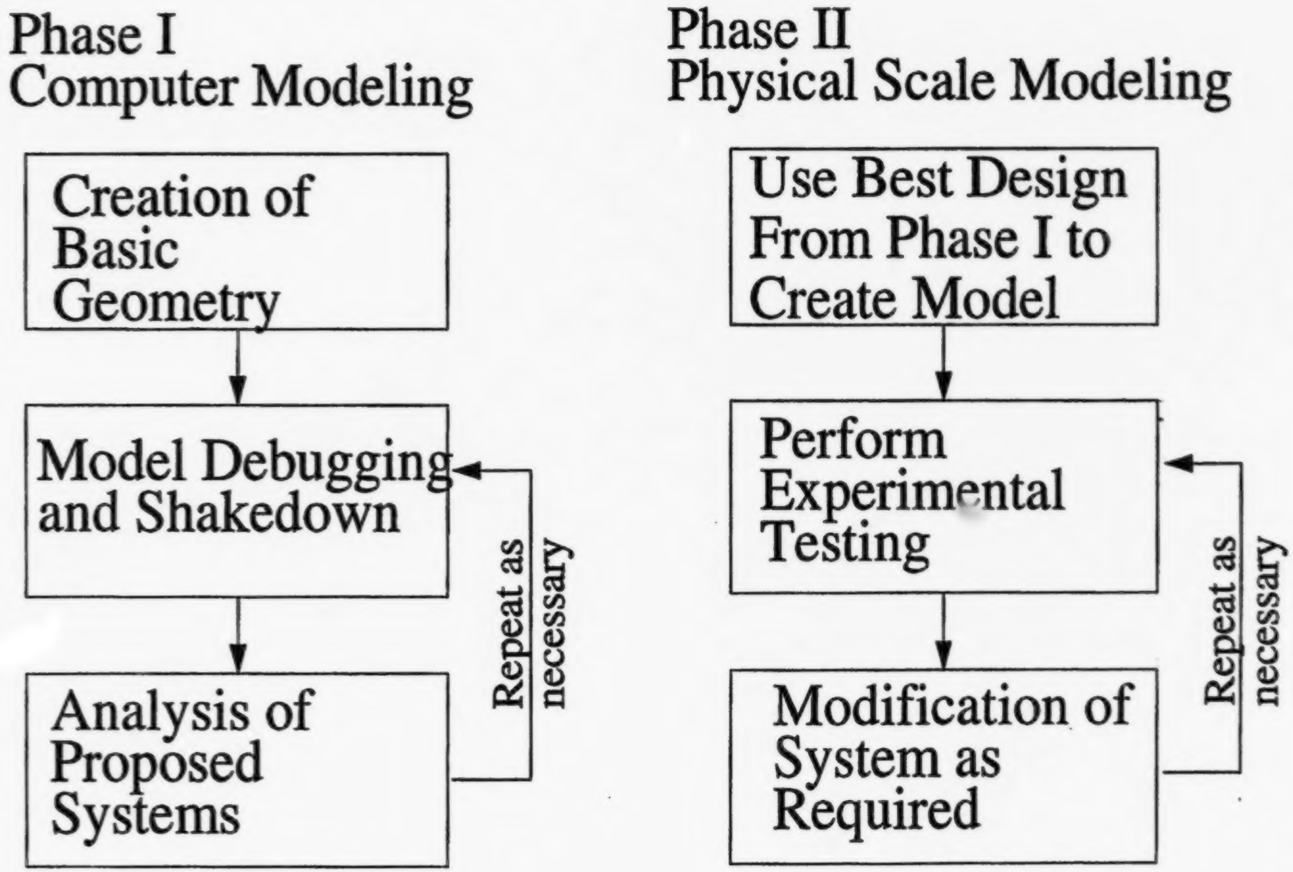
Phase I
Computer Modeling
Creation of Basic Geometry
Model Debugging and Shakedown
Analysis of Proposed Systems
Repeat as necessary
Phase II
Physical Scale Modeling
Use Best Design From Phase I to Create Model
Perform Experimental Testing
Modification of System as Required
Repeat as necessary

Summary

Completed detailed investigation into the feasibility of use of computer modeling for design and evaluation of shipboard ICCP systems

Identified sensitivity to and quantified modeling parameters: mesh refinement, material characterization, geometry sensitivity, spatial sensitivity and convergence criteria

Have successfully predicted shipboard ICCP system performance using a commercial boundary element code

Verification of physical scale modeling techniques by comparison with full size ship data

Developed design methodology which combines computer modeling and physical scale modeling methods for the design and evaluation of ICCP systems

#510360 ⑰

CPBEM Program Suite For The Design Of Cathodic Protection Systems For Ships

by

D. Brennan*, J. Wallace*, K. KarisAllen^, M. Chernuka*, and M. Palmeter*

* Martec Ltd., Suite 400, 1888 Brunswick St., Halifax, Nova Scotia, B3J 3J8
^ Facts Engineering, Halifax, Nova Scotia, PO Box 20039,
Halifax, Nova Scotia, B3R 2K9

ABSTRACT

A computer program that would assist DND engineers in the design and optimization of suitable cathode protection systems for surface ships has been developed. The resulting program suite CPBEM was built around the existing cathodic system analysis program CPBEM. Included in the suite is the analysis program (CPBEMHS), a model generator (CPBGEN), a graphical plotting program (CPBEMG), and a shell program (CPBSHL). The graphical model generator program was designed to simplify the task of creating CPBEM boundary element models. These models include refined meshes at each anode location, and a cathode that is boundary element mesh of an actual propeller. The thinness of the propeller blades necessitated the use of a hypersingular boundary integral formulation in the analysis program. The ability to plot CPBEM models, as well as contour plots of both hull potentials and current densities, was incorporated into the graphical plotting program. The entire suite was designed to be run under the shell program.

#510361 (18)

Fracture Control for Surface Ships

by

Ken KarisAllen

Facts Engineering
Halifax, Nova Scotia, Canada

and

Dr. J.R. Matthews

Defence Research Establishment Atlantic, Dockyard Laboratory
FMO Halifax, Halifax, Nova Scotia, Canada, B3K 2X0

ABSTRACT

Determining susceptibility of structural steels and weldments to transgranular cleavage instabilities is of primary importance in the safe design of any structure. Gaining acceptance during the Liberty Ship failures during the Second World War, the Charpy V-notch test (ASTM E23) has since dominated material transition curve testing in the nuclear, pipeline, pressure vessel, shipping and offshore industries. Acceptance has been in part derived from the inexpensive and simplistic nature of the test. It was recognized early on that there were a number of serious problems associated with the interpretation of the data realized from such a test. Of these perhaps the most significant was the fact that because of the notch detail and small size of the specimen, the transition curve obtained may not reflect actual structural performance of the material. Debate on the magnitude of the transition curve shift still continues (especially with the increasing use of thermo-mechanically controlled rolled steels).

DREA has been developing alternative testing procedures which provide directly transferable, structurally relevant temperature transition data. These tests will be described with respect to their applicability to fracture control issues of CF surface ships.

SUMMARY

Why Qualify Minimum Notch Toughness Levels for Surface Ship Structural Steels and Weldments?

What Small Scale Specimen Geometry Should be Utilized to Generate Notch Toughness Information?

What Test Parameters Accurately Describe the Fracture Characteristics of Structural Steels and Weldments?

MATERIAL FAILURE MECHANISMS

Plastic Collapse (flow stress)

Fracture (over the service life of a ship cracking will occur)

- **a) Ductile Tearing**
- **b) Brittle Crack Propagation**

Important Variables

- **a) Temperature**
- **b) Loading Rate**
- **c) Constraint Effects**

Classification Societies (Loyds, ABS) Allow the Use of Structural Steel Components Which Have No Minimum Material Notch Toughness Requirements

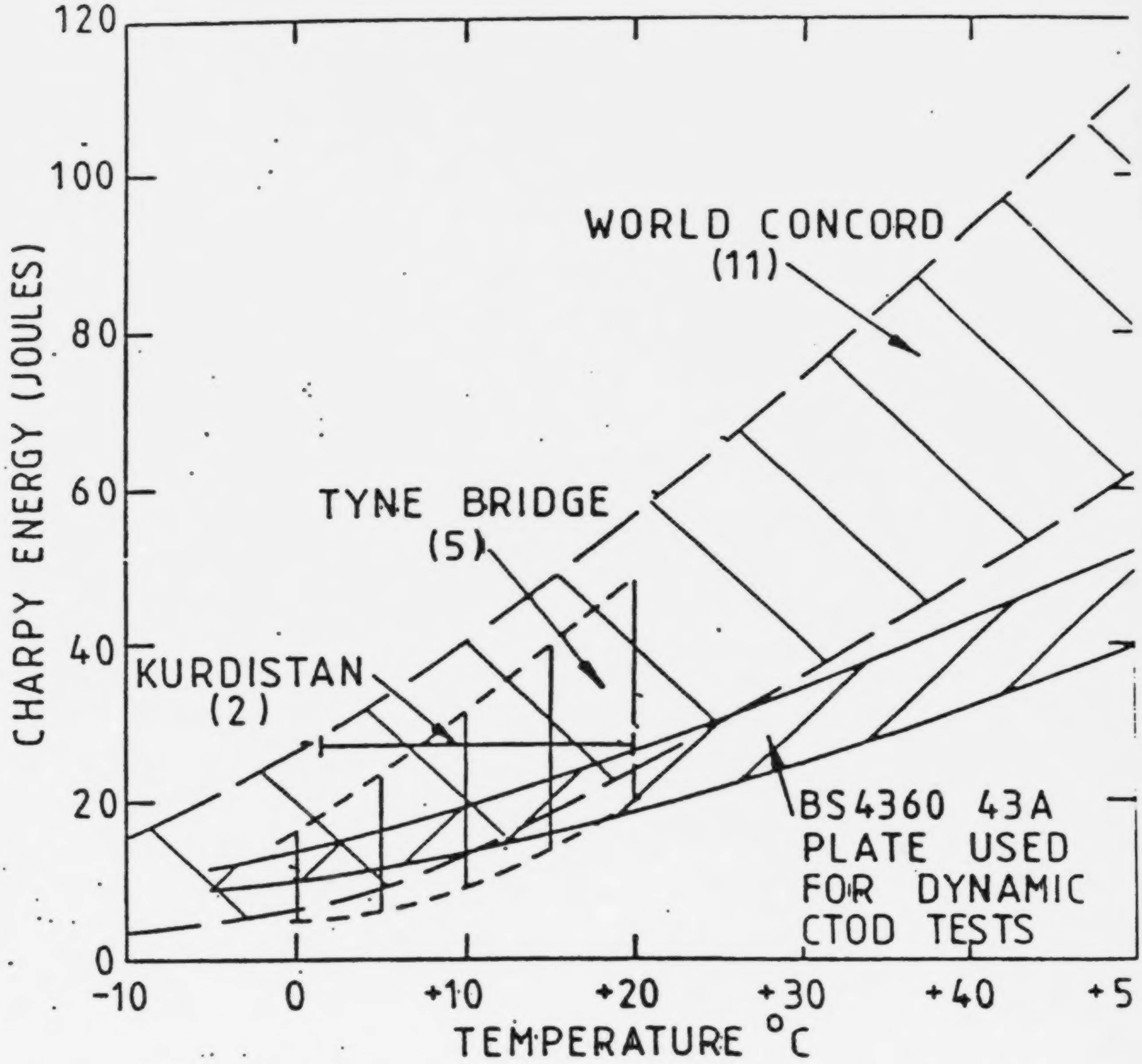

(J.D.G. Sumpter et al, 1989)

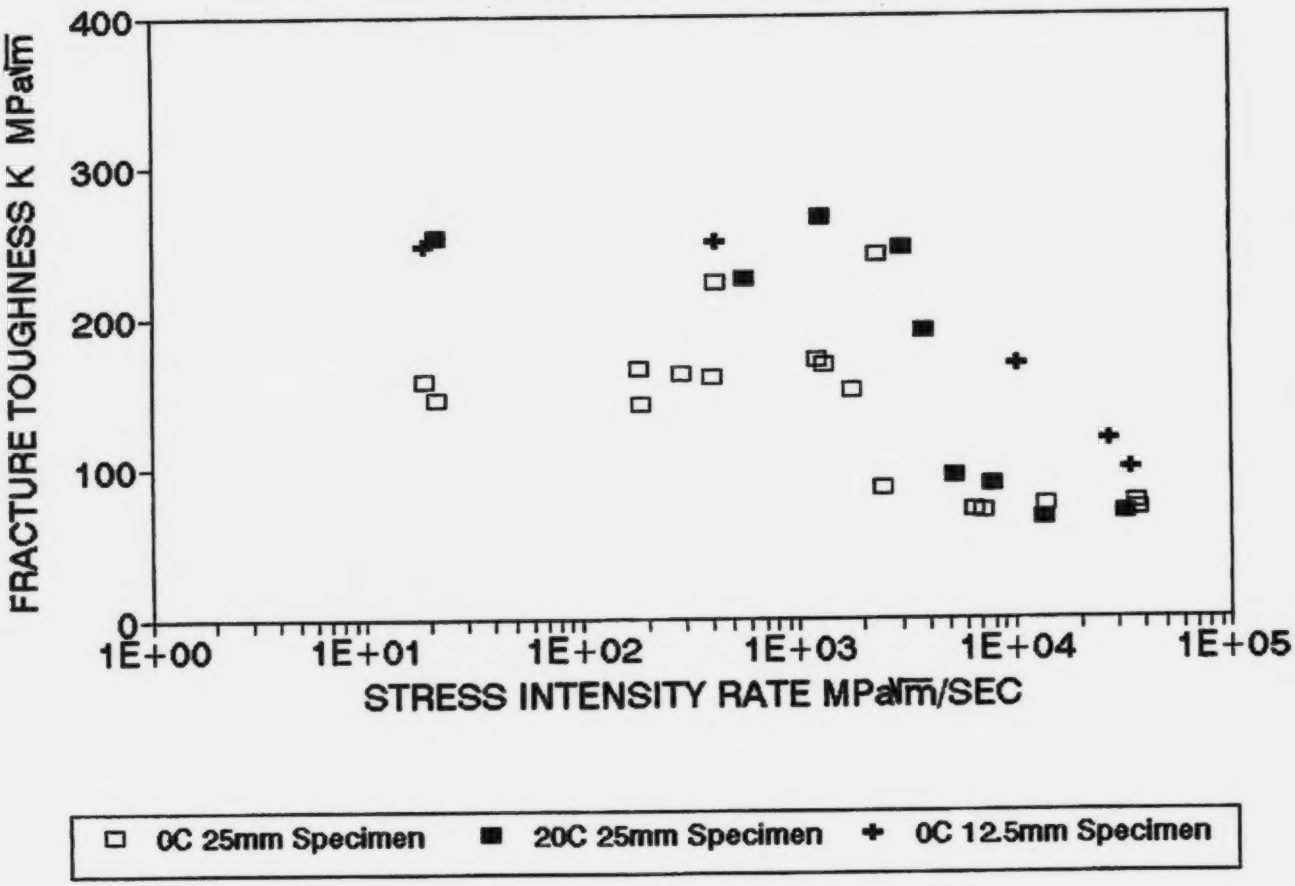

TOUGHNESS DATA for a BS4360 43A PLATE
(J.D.G. Sumpter et al, 1989)

SOURCES OF DYNAMIC LOADING

Slamming (global stress, intermediate rate)

Side Shell Impact (local stress, high rate)

Collision (local & global stresses, high rate)

Grounding (local & global stresses, high rate)

Weapons (local & global stresses, high rate)

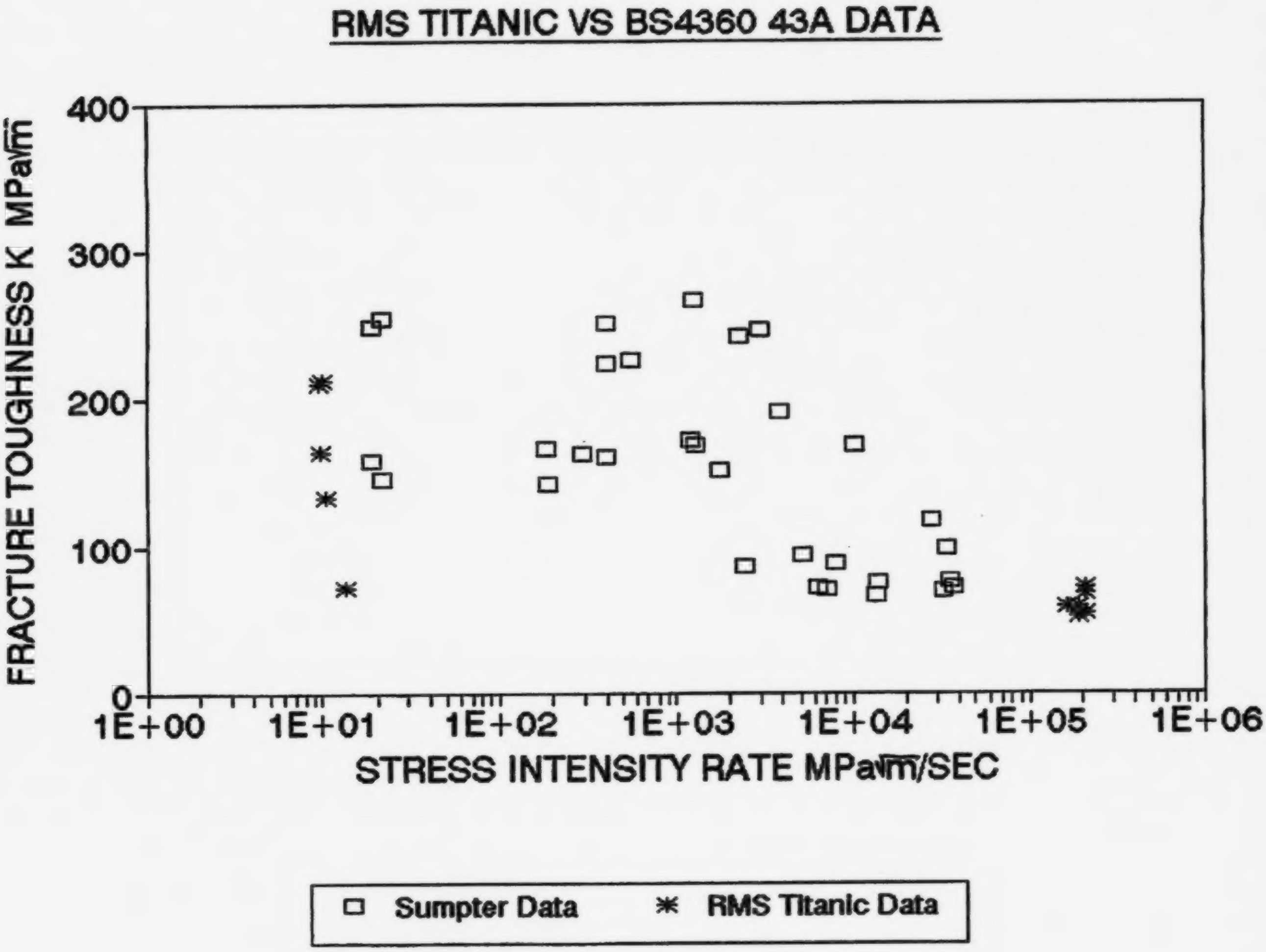
RMS TITANIC VS BS4360 43A DATA
FRACTURE TOUGHNESS K MPa√m
400
300
200
100
0
1E+00
1E+01
1E+02
1E+03
1E+04
1E+05
1E+06
STRESS INTENSITY RATE MPa√m/SEC
□ Sumpter Data
✱ RMS Titanic Data

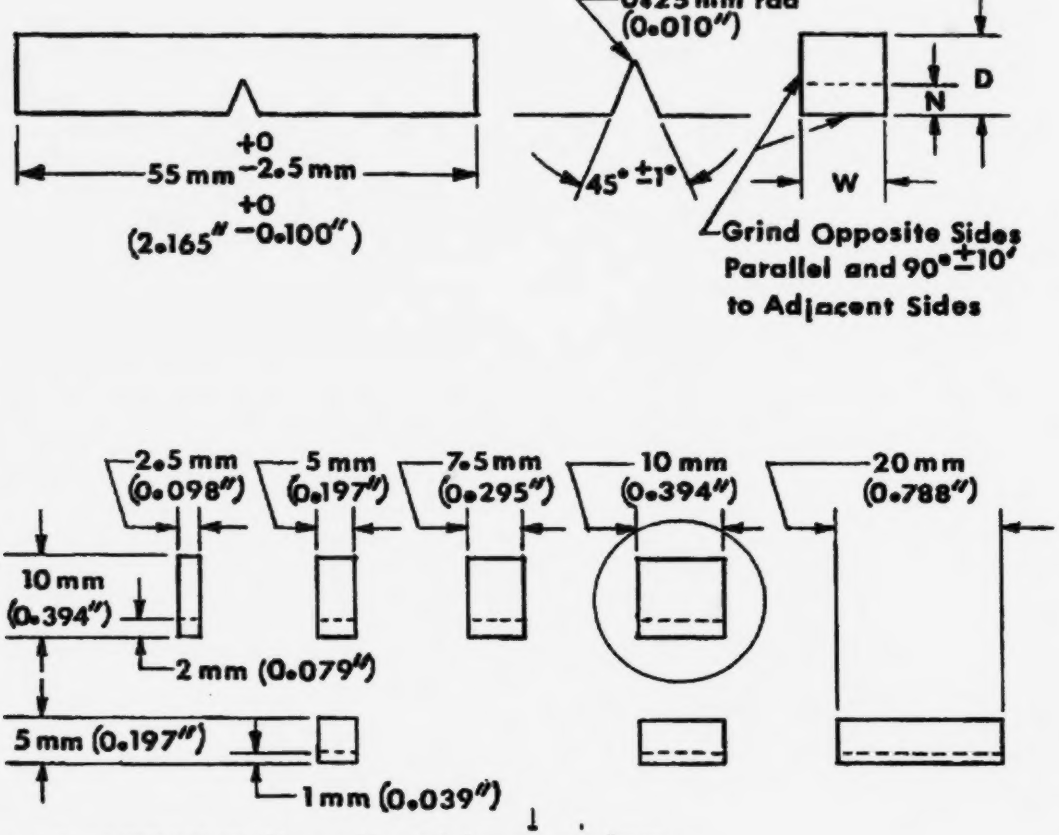
0.25 mm rad
(0.010")
D
N
W
+0
55 mm -2.5 mm
+0
(2.165" -0.100")
45° ±1°
Grind Opposite Sides Parallel and 90° ±10' to Adjacent Sides
2.5 mm (0.098")
5 mm (0.197")
7.5 mm (0.295")
10 mm (0.394")
20 mm (0.788")
10 mm (0.394")
2 mm (0.079")
5 mm (0.197")
1 mm (0.039")

Figure 3 - ASTM E-23 Charpy V-notch impact specimen

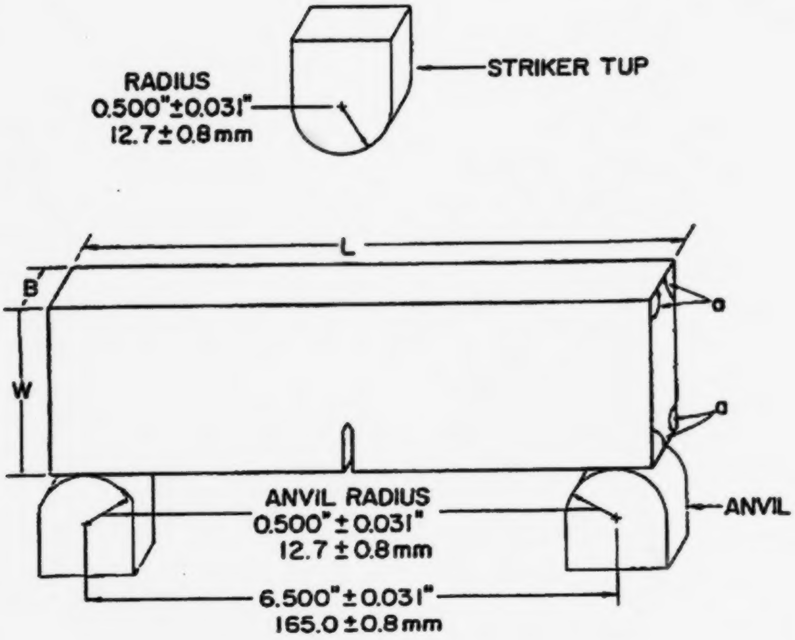
RADIUS
0.500"±0.031"
12.7±0.8mm
STRIKER TUP
L
B
W
α
α
ANVIL RADIUS
0.500"±0.031"
12.7±0.8mm
ANVIL
6.500"±0.031"
165.0±0.8mm

Dimensions and Tolerance for Specimen Blank

Parameter	Units	Dimension	Tolerance
Length, *L*	in.	7.125	±0.125
	mm	181	±3
Width, *W*	in.	1.60	±0.10
	mm	41	±2
Thickness, *B*	in.	0.625	±0.035
	mm	16	±1
Angularity, α	deg	90	±1

NOTE—See 9.1 for specimens less than ⅝-in. (16 mm) thick.

FIG. 1 Dynamic Tear Test Specimen, Anvil Supports, and Striker

Figure 4 - ASTM E604 dynamic tear impact specimen.

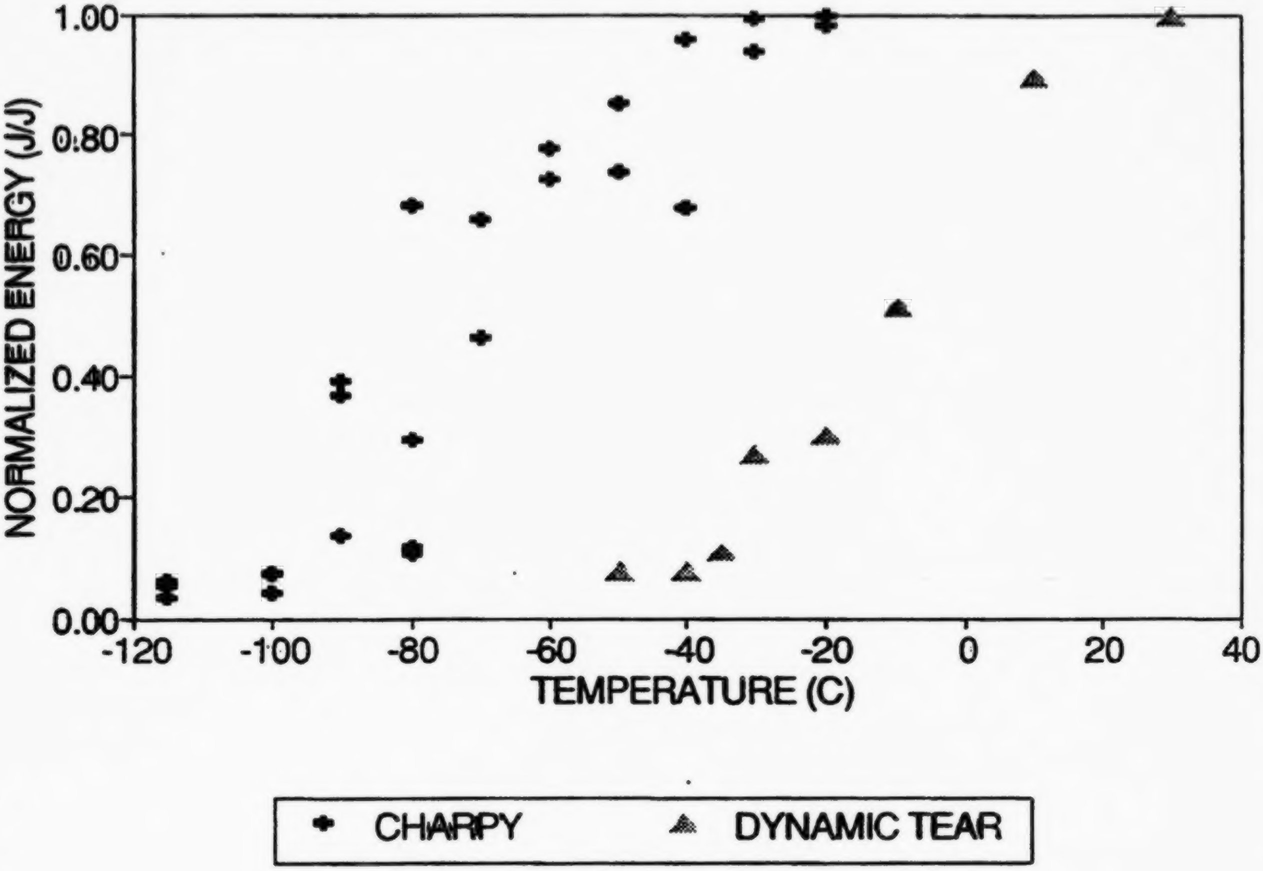

HSLA80 TRANSITION CURVES

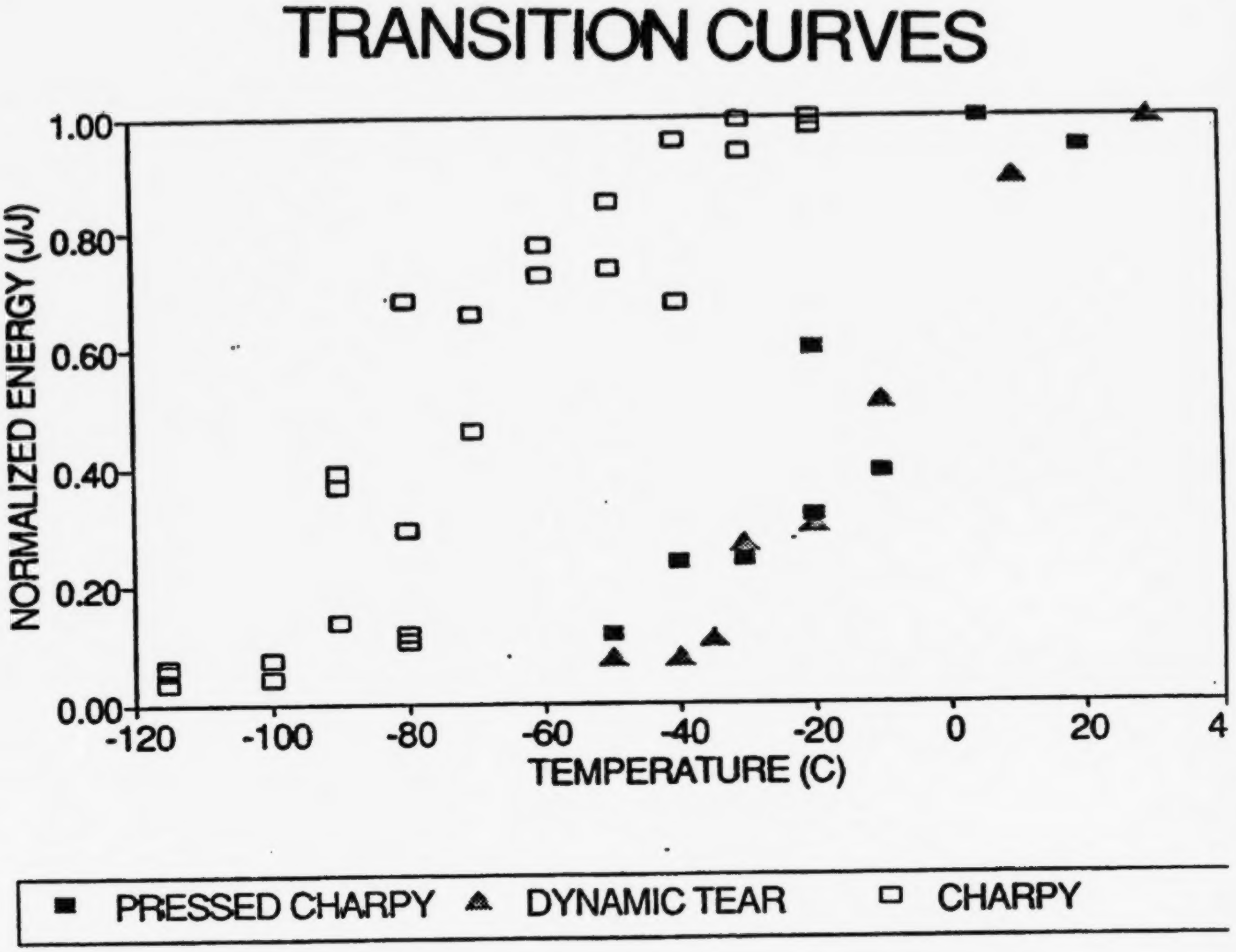
TRANSITION CURVES
NORMALIZED ENERGY (J/J)
1.00
0.80
0.60
0.40
0.20
0.00
-120
-100
-80
-60
-40
-20
0
20
4
TEMPERATURE (C)
■ PRESSED CHARPY
▲ DYNAMIC TEAR
□ CHARPY

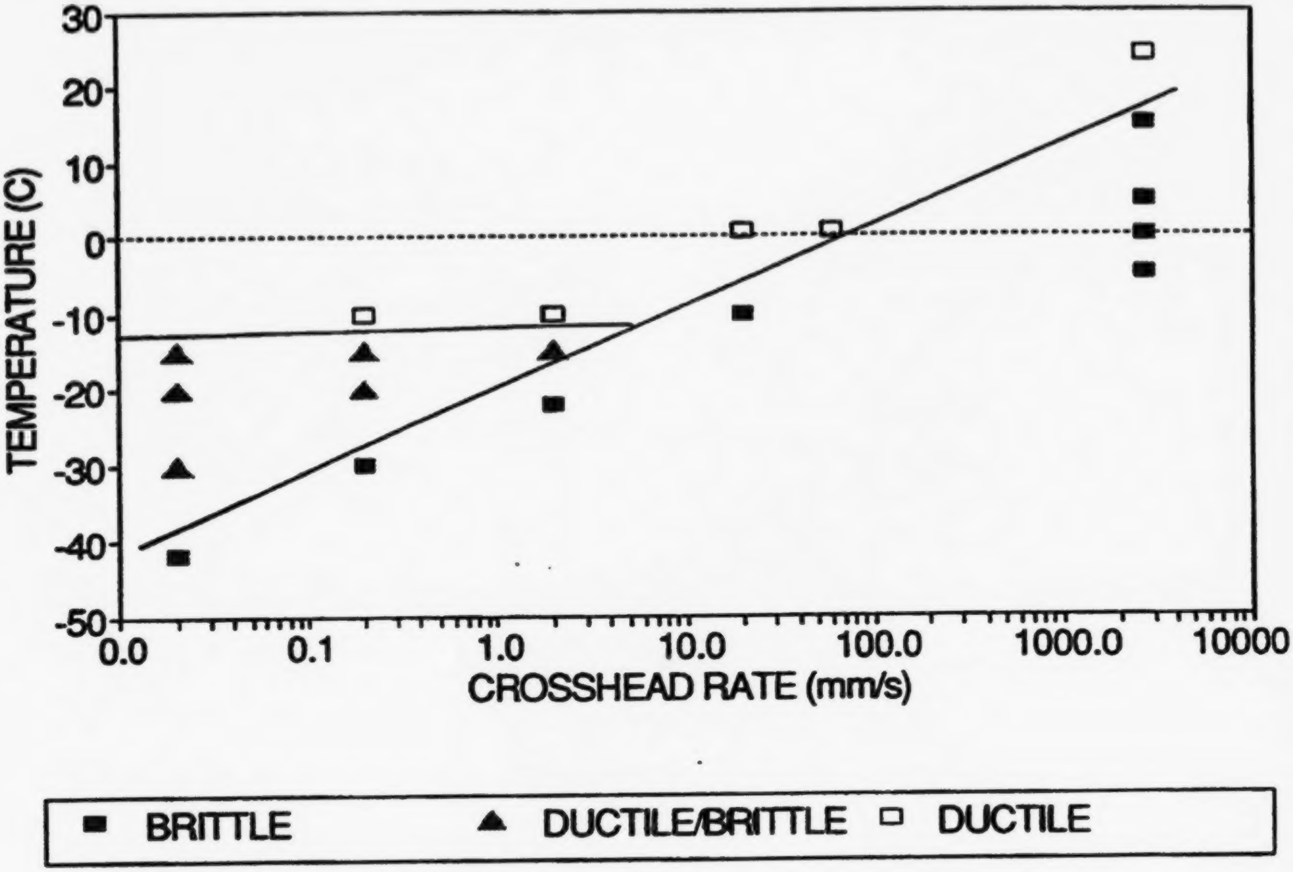

TEMP/RATE DIAGRAM HSLA80 (T-L)

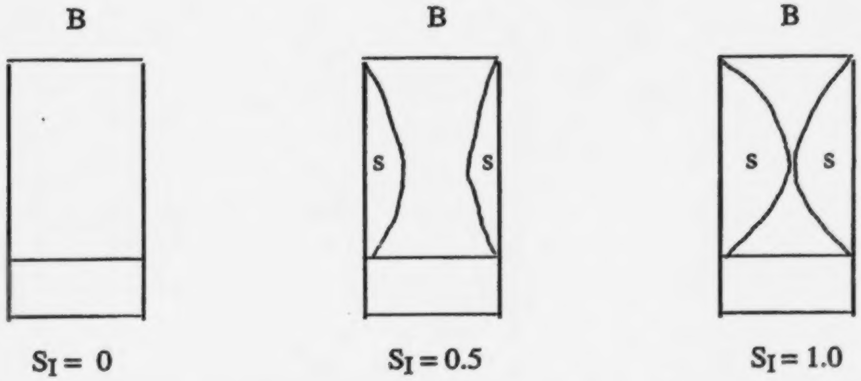
B
B
B
s
s
s
s
$S_I = 0$
$S_I = 0.5$
$S_I = 1.0$

Fig. 1. Typical morphologies for dynamic tear impact samples (shear index is measured at the point of the closest contact between the two shear lips: $S_I = 2s/B$).

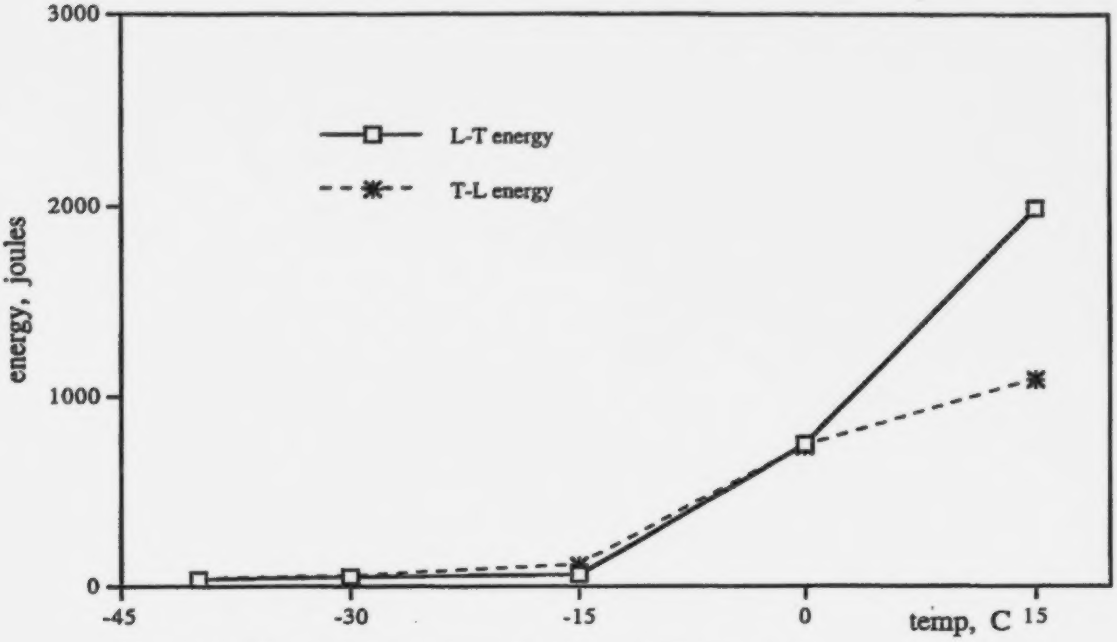

Figure 1a: Dynamic tear energy for 15 mm 350 WT steel.

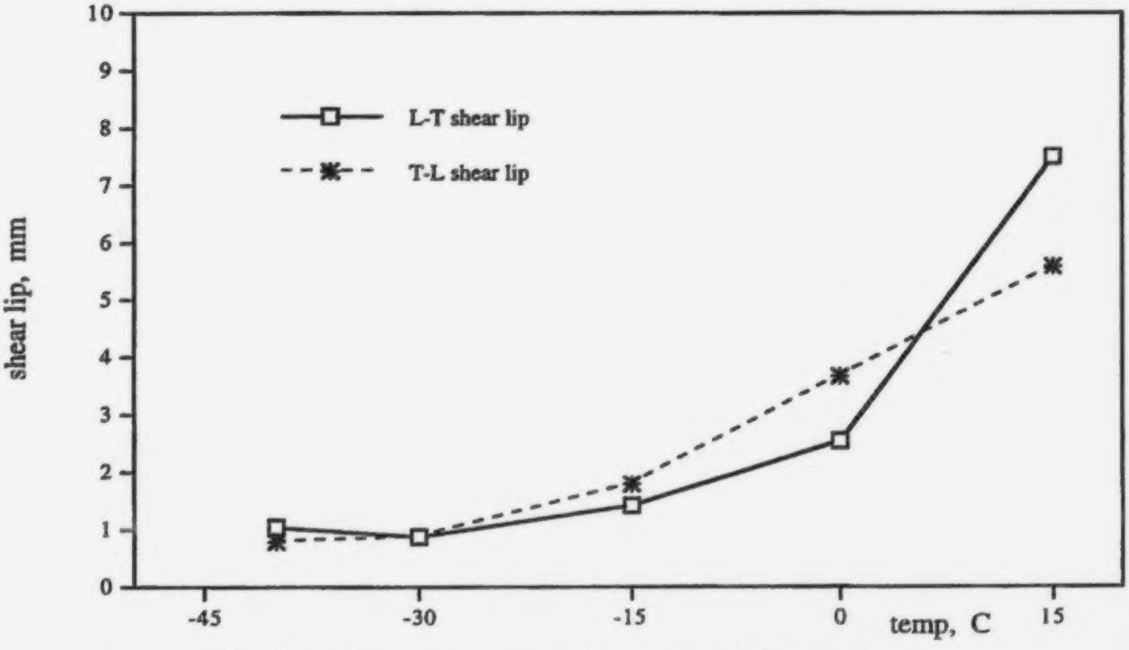

Figure 1b: Shear lip transition curves for 15 mm 350 WT steel.

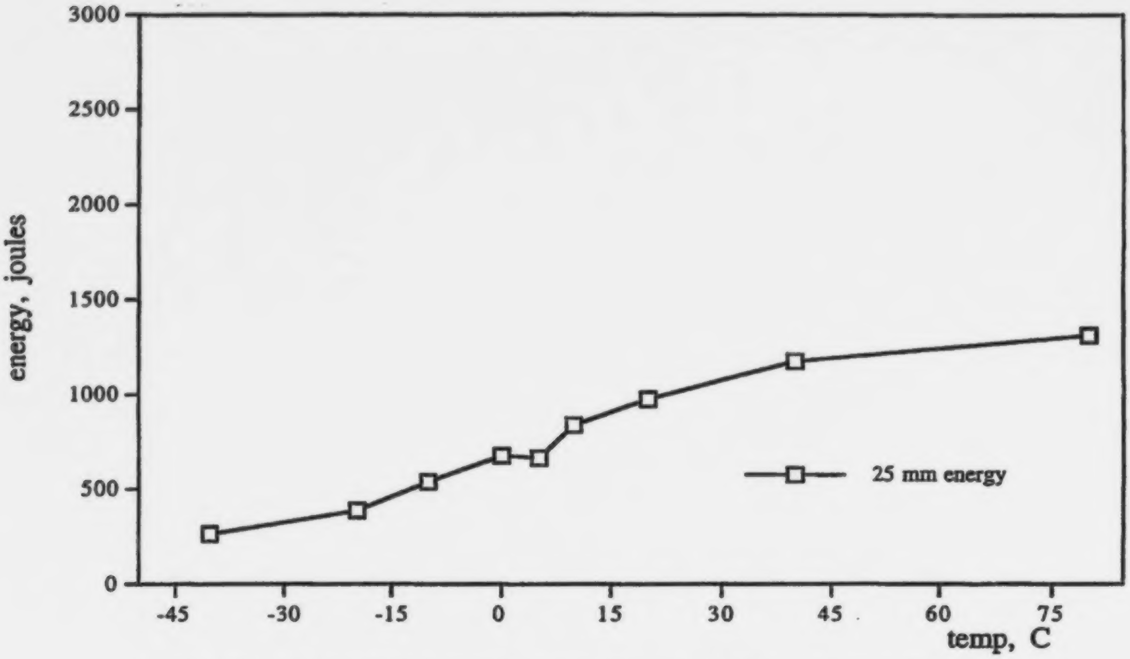

Figure 2a: UK produced marginal toughness GMAW weldment (2-4 kJ/ mm). Marginal toughness was intentionally produced for TTCP Op Ass.

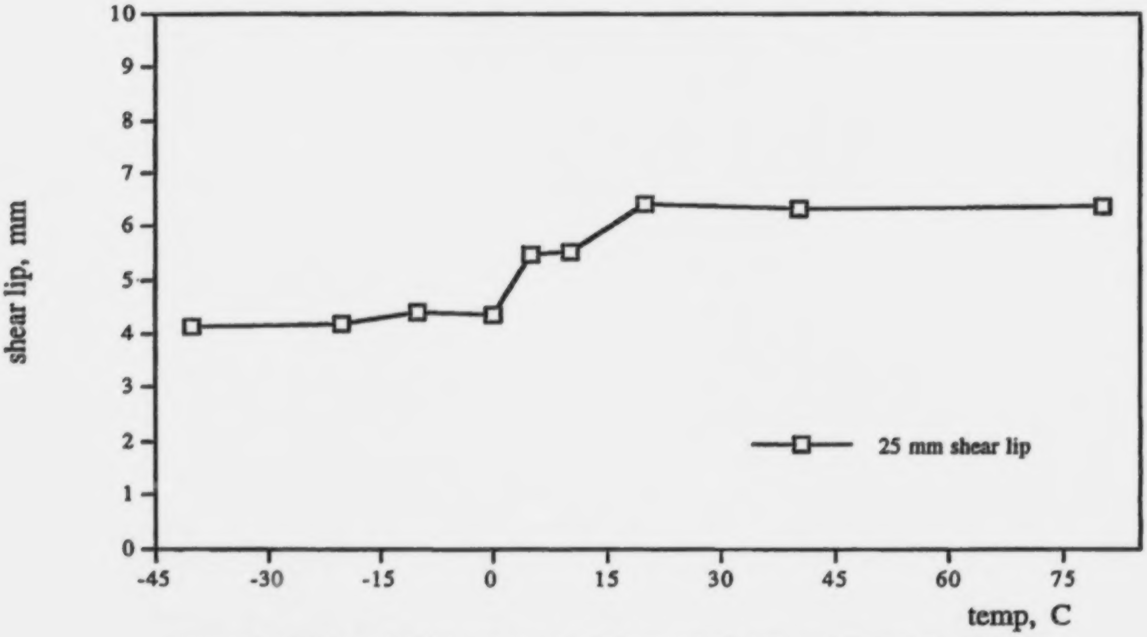

Figure 2b: UK produced marginal toughness GMAW weldment (2-4 kJ/mm). Marginal toughness was intentionally produced for TTCP Op Ass.

CONCLUSIONS

In conclusion, by not specifying minimum notch toughness requirements for steel and weldments we've ignored fracture as a possible failure mechanism in the design process.

Investigations into surface ships which have suffered structural failure indicate that the absence of notch tough steel leaves these structures susceptible to failure under dynamic loading.

The Dynamic Tear specimen geometry and procedure provides transition temperature information which is directly transferable when predicting structural response.

Transition curves generated using the shear lip measurement procedure outlined correlates well to transition curves developed from fracture energy measurements.

#510362 ⑲

Crack Arrest Toughness of a Heat Affected Zone Containing LBZ

by

L. Malik*, L.N. Pussegoda*, B.A. Graville** and W.R. Tyson***

* Fleet Technology Limited, 311 Legget Drive, Kanata, Ontario

** Graville Associates Inc., Georgetown, Ontario

*** MTL, CANMET, 568 Booth Street, Ottawa, Ontario

ABSTRACT

The awareness of the presence of local brittle zones (LBZs) in the heat affected zone (HAZ) of welds has led to the requirements for minimum initiation toughness for the HAZ for critical applications (API RP 2Z, CSA S473). Such an approach however is expensive to implement and limits the number of potential steel suppliers.

A fracture control philosophy that is an attractive alternative to the prevention of initiation is the prevention of propagation. This is implemented via crack arrest requirements. In the Canadian offshore code (CSA S473), arrest requirements are imposed on base plate for critical applications. If it could be demonstrated that cracks initiated in LBZs will be arrested without causing catastrophic fracture, then requirements for initiation toughness could be relaxed. Unstable propagation of a crack initiating from an LBZ requires the rupture of tougher microstructural regions surrounding the LBZ in the HAZ, and therefore the CTOD value reflecting the presence of the LBZ is unlikely to provide a true indication of the potential for fast fracture along the heat affected zone.

One possible uncertainty related to crack arrest is whether the presence of LBZs promotes propagation within the HAZ, i.e., whether a crack can run parallel to the weld within the HAZ causing fracture by avoiding arrest in the base plate. To investigate the likelihood of fast fracture within the HAZ, a test program has been carried out that involved performing compact plane strain (ASTM E1221) and plane stress crack arrest tests on a heat affected zone that contained LBZs and thus exhibited unacceptably low CTOD toughness for brittle fracture initiation.

The results indicated that in contrast to the initiation toughness (CTOD toughness), the crack arrest toughness was little influenced by the presence of the local brittle zones. Instead, the superior toughness of the finer grain HAZ surrounding the LBZ has a greater influence on the crack arrest toughness, mainly because of its larger proportion present along the crack path. It further seems that there may be potential to estimate the HAZ crack arrest toughness from more conventional smaller-scale, laboratory tests such as the conventional or the precracked, instrumented Charpy specimen.

INTRODUCTION

Toughness requirements for structural steel in North American standards for offshore structures are based on providing certain capabilities for *crack arrest* at the design temperature (API RP2Z and CSA S473). These are specified indirectly through the drop weight test for nil ductility transition temperature (NDTT) or through correlations with the Charpy V notch (CVN) transition temperature. The goal here is to arrest unstable cracks that might initiate in a low toughness or defective region such as a weld.

For the weld region itself, however, it is considered sufficient to ensure that unstable cracks would not initiate from flaws from a certain minimum reliably detectable flaw size. The recognition of the existence of local brittle zones (LBZs) in the heat affected zone (HAZ) and the possibility of a crack running parallel to the weld and remaining in the HAZ has led to requirements of *initiation* toughness in the HAZ and weld metal for critical applications which in turn are specified through the crack tip opening displacement (CTOD) test. The CTOD test is good at detecting LBZs because the fatigue crack tip can be accurately placed in the heat affected zone and only a small fraction (>15%) of the crack front need intersect a brittle region for the test to record a low value. Consequently, CTOD requirements, typically 0.25 mm at the design temperature for thick plates, are difficult to meet, thus restricting the sources of steel supply for offshore structures. For design temperatures less than -15°C, for example in Arctic applications, the supply sources will be even more limited.

Local brittle zones (grain coarsened or intercritically reheated grain coarsened HAZ, grain diameter typically greater than 80 μm) are generally small, usually only a few grains wide and often limited to the HAZ's of a few passes in a multipass weld. Except in a single pass groove weld, these are unlikely to extend completely through the plate thickness. In order for a crack initiating in a local brittle zone to lead to fracture of the member, a macroscopic crack front must be established which involves fracturing the material surrounding the LBZ. Thus, whereas the initiation toughness is determined by the most brittle 15% of a through thickness crack front, the continued propagation of the crack is largely determined by the toughness of the remaining 85% and this may render the *initiation* prevention requirement more onerous than the crack *arrest* one.

Unstable fractures oriented transverse to the weld axis or parallel to the weld but perpendicular to the surface can not propagate very far before running out of the LBZ which increases the potential for their arrest. The case of surface fatigue cracks interacting with LBZ's was in fact explored in a series of wide plate fatigue/fracture tests [Pussegoda et al, 1992] which showed that while the probability of such interaction is low, it can still lead to brittle crack initiation. However, in all the tests in this study, the cracks once initiated were arrested immediately on running out of the LBZ and no complete fractures of the specimens took place.

Through-thickness cracks parallel to the weld, however, could encounter a continuous band of brittle material along the HAZ. Maintenance of a crack front through the thickness and continued propagation should therefore depend on the toughness of the material adjacent to the LBZ as well the LBZ itself (**Figure 1**). The case of most significance is a 3 to 7 pass weld where the LBZ occupies 15 to 30% of the thickness. This is enough to cause failure in the CTOD initiation test but leaves 70 to 85% of the surrounding material to influence crack propagation. This is the case studied in the present investigation.

A second aspect of the study has been to evaluate the application of recently developed compact crack arrest (CCA) test procedures (plane strain and plane stress type) to heat affected zones and thus apply the crack arrest philosophy in a more direct manner rather than through an arbitrary temperature shift with respect to the nil ductility transition (NDT) temperature to ensure adequate arrest toughness.

OBJECTIVE AND APPROACH

The broad objective of the present program was to demonstrate the conservatism of the "initiation prevention" approach for the heat affected zone in relation to the "prevention of propagation" approach. Specifically, this required the measurement of the crack arrest toughness of the heat affected zone in a steel that showed typical LBZ behavior in HAZ CTOD testing.

The main feature of the approach followed was to select a steel and develop a multipass welding procedure that would give a reasonably straight heat affected zone that would not meet the CTOD requirements in documents such as API RP 2Z and CSA S473 at a temperature where the base material still shows a reasonable level of crack arrest toughness, i.e., at a temperature corresponding to the steel's NDT temperature plus 15 to 20°C.

The experimental program thus comprised:

- selecting a steel, developing a welding procedure to give the appropriate HAZ properties and then welding the panels for the required tests;
- characterization of the heat affected zone containing grain coarsened regions (LBZs) by performing standard tests (CVN, CTOD, and drop weight tests);
- performing plane strain and plane stress compact crack arrest (CCA) tests for the heat affected zone containing grain coarsened regions.

EXPERIMENTAL PROCEDURES AND RESULTS

Steel and Welding Procedure

The steel selected for making the welds was a controlled rolled steel, having the following chemistry (wt.%): 0.17 C, 1.07 Mn, 0.23 Si, 0.018 P, 0.012 S, 0.13 Cr, 0.1 Ni, 0.2 Cu, 0.043 Al, 0.055 V and 0.007 N. Its yield and ultimate tensile strengths were 373 and 543 MPa respectively. In the longitudinal orientation, the steel had a 40 J CVN transition temperature of about -40°C, and the NDTT was -10°C.

Based on the NDT temperature, the main test temperature for the investigation was selected to be +10°C, 20°C above the NDTT for the steel. (At +10°C, the CVN toughness of the steel in the longitudinal direction was 130 J [Malik et al, Jan. 1991].)

For the welding procedure development, the aim was to obtain a reasonably straight heat affected zone that would give unacceptably low HAZ CTOD results at +10°C. This required the use of a K groove and complete welding of the joint in four submerged arc weld passes. All welds were made perpendicular to the steel's rolling direction. A typical cross section of the weld as obtained from post-CTOD test metallography is shown in **Figure 2**, and it can be noted that most of the grain coarsened heat affected zone (GCHAZ) is associated with the 1st pass deposited from the 2nd side at a 4.6 kJ/mm heat input.

HAZ CTOD Tests

Standard B x 2B, through thickness notched CTOD specimens were machined and tested at +10°C at a quasistatic loading rate following the procedures and guidelines in British Standard BS 5762. The notches were placed next to the fusion boundary after macroetching the specimens with the objective of maximizing the amount of grain coarsened HAZ sampled by the fatigue precrack. Prior to fatigue precracking of the specimens, both surfaces of the ligament ahead of the machined notch were compressed 0.5%.

The results of all the CTOD tests as well as of post-test metallography are summarized in **Table I**. All the test results met the validity criteria in BS 5762, and in every specimen, the fatigue precrack sampled more than 15% grain coarsened (> 80 μm grain size) HAZ. It is therefore not surprising that of the ten specimens tested, nine had their fracture initiation site in the grain coarsened HAZ next to the fusion boundary. Further, while the average HAZ CTOD toughness is 0.233 mm, three of the valid HAZ CTOD toughness values are less than 0.1 mm, signifying that for a design temperature of +10°C, the steel would not be acceptable according to the requirements of documents such as API RP 2Z or CSA S473. In comparison, the CTOD toughness of the base material at -5°C was found to be 0.86 mm (average of three specimens) [Malik et al, Jan. 1991].

Standard CVN and Drop Weight Tests

Through thickness notched, standard 10 mm x 10 mm, CVN specimens were machined from a near half thickness location such that the V notch could sample as much of the grain coarsened HAZ as possible. The fracture path orientation in the CVN and CTOD specimens was thus identical. The specimens were tested over a range of temperatures to obtain the CVN transition curve for the grain coarsened HAZ. However, from the fracture surface appearance (shiny coarse facets or dull grey), the results could be segregated into two groups, one with fracture path predominantly in the GCHAZ, and one with path outside the GCHAZ. These results are shown plotted in **Figure 3**. The 40 J transition temperature for the GCHAZ is about -20°C, and it is about -40°C for the surrounding HAZ, the latter being similar to that for the base material.

For determining the NDTT of the GCHAZ, P-2 size specimens were employed and ASTM E 208 procedures for unwelded steel followed except for two minor deviations. First, the surface had to be skim machined to remove the test weld reinforcement and place the brittle weld bead. Secondly, a V notch was machined in the brittle bead instead of a square groove to facilitate the injection of the crack into the region of interest, viz., the GCHAZ. The NDTT obtained for the

GCHAZ was -15°C, essentially the same as for the base material (NDTT = -10°C).

Compact Crack Arrest (CCA) Tests

Plane Strain CCA Tests

The test procedures for plane strain CCA tests were essentially the same as described in ASTM Standard E1221. The dimensions of the specimens tested are shown in **Figure 4.** The EDM notch in the brittle bead at the root of the notch and the side grooves on the specimen surfaces were placed such that the plane between the side grooves contained as much of the coarse grained HAZ next to the fusion boundary as possible.

These tests were performed at -10°C, 0°C and +10°C, and appropriate post-test metallography was carried out to confirm that the crack front during the run and arrest events had indeed sampled the GCHAZ in these specimens. The results obtained are shown in **Table II.** It should be noted that in most cases, run-arrest event was not obtained within the first five loading cycles. In these cases, a sixth loading cycle was employed and the loading continued until a run-arrest event occurred or the test was discontinued as a result of ductile tearing at the notch root indicated by a plateau in the load-crack mouth opening displacement.

Of all the specimens tested, only one test (specimen 28-1) conducted at 0°C met all the validity criteria given in ASTM E1221 and it yielded a plane strain crack arrest toughness (K_{Ia}) value of 85 MPa.$m^{0.5}$. Two other specimens (27-1 at -10°C and 28-3 at +10°C) can be deemed to provide useable crack arrest values. In one of these tests (27-1), the remaining ligament after arrest was 23 mm instead of the 25 mm minimum required for a valid test (**Figure 5(a)**), and in the second case (specimen 28-3), the invalidities were related to not meeting the plane strain requirements. The crack arrest toughness (K_a) values computed from these two tests are 78 MPa.$m^{0.5}$ at -10°C and 133 MPa.$m^{0.5}$ at +10°C, respectively. The crack path in these three samples typically comprised 30% or more of GCHAZ (**Figure 5(b), for example**).

(b) Plane Stress CCA Tests

Procedures for performing a plane stress CCA test for quality assurance purposes have been suggested by Crosley and Ripling [1990]. The main objective in this approach is to establish if the material complies with a pre-established minimum level of crack arrest toughness. The specimen does not employ side grooves and uses a chevron notch, which may be artificially embrittled, for crack initiation. The specimen dimensions (see **Figure 6**) are based on the minimum specified or the expected crack arrest toughness K_v, and the specimen becomes larger as the expected plane stress crack arrest toughness value increases. If the arrest of an initiated crack occurs within 0.5W and 0.8W from the load line, then a plane stress crack arrest toughness value can be calculated. Arrest locations less than 0.5W and more than 0.8W signify crack arrest toughness values that are respectively greater than or lower than the target value.

In the present project, the material at the chevron notch in the specimens was embrittled by compressing this region (10% reduction in thickness) prior to machining followed by strain aging at 230°C for 2 hours. The expected values for the plane stress crack arrest toughness were inferred from the plane strain test results reported in the previous section, and these along with the dimension W of the specimens tested and the calculated plane stress crack arrest toughness values are shown in **Table III**. The largest specimens, tested at +10°C, had a W dimension of 285 mm.

Four specimens were tested at -10°C (see **Figure 7**) and plane stress crack arrest toughness values could be calculated from two of these. In both these specimens, a running crack was initiated across the full specimen thickness and it intersected the GCHAZ as well; however, the arrest location was in the GCHAZ for specimen 34-1 only and the corresponding K_a value was 76 $MPa.m^{0.5}$. In the other specimen, the arrest location was the parent material adjacent to the HAZ resulting in a higher value for K_a (112 $MPa.m^{0.5}$).

At 0°C, a K_a value could be calculated for one of the two specimens tested (31-1). In this specimen, the crack was injected across the full thickness, adjacent to the fusion boundary and within the GCHAZ, and the arrest occurred in the fine grained HAZ right next to the GCHAZ. In the other specimen tested at this temperature, the crack did not enter at the desired location and did not follow the GCHAZ.

Finally, at +10°C, three specimens were tested but in none of the cases did the injected crack go beyond the 0.5W location. In specimen 35, the injected crack sampled only a small amount of the GCHAZ. However, in the two remaining specimens (31-3 and 33), cracks initiated from the embrittled region and the fracture path was next to the fusion boundary and included the GCHAZ (see **Figure 8**), however, the crack propagated only about 6 mm into the test material after initiation. These two tests indicate that at +10°C, the K_a value for the HAZ containing low toughness, grain coarsened region is greater than 101 and 133 $MPa.m^{0.5}$, respectively.

DISCUSSION

Crack Arrest Toughness of the HAZ

In all, twenty compact crack arrest tests (plane strain and plane stress) have been performed in this study; however, only seven of these can be considered as valid based on the requirements of the ASTM Standard and the requirement that both, crack entry and arrest in the test material should sample the GCHAZ. These results are shown in **Figure 9** along with results from a previous investigation [Malik et al, Sept. 1991] which was similar to the present one in that it also studied HAZ crack arrest toughness for a weld made in the same steel as that in the present investigation. The main differences were that only the plane strain compact crack arrest tests had been employed and that the welding procedure comprised a two pass weld deposited at a higher heat input (5.5 kJ/mm); none of the tests had given a completely valid K_{Ia} value for the higher heat input HAZ containing LBZs. However, in four of the tests, the only invalidity was related to the remaining ligament being marginally smaller than the minimum required. The computed K_{Ia} values thus provide an upper bound estimate [Crosley and Ripling, 1990]. Also included were plane strain compact crack arrest tests on the base material, which provided a greater number of valid results over a range of temperatures (filled points in Figure 9).

The results in Figure 9 suggest that;

- the somewhat lower heat input and the greater number of passes in the welds in the present study have resulted in a slightly better crack arrest performance of the HAZ containing LBZs;
- above the NDT temperature, the crack arrest toughness rises quite rapidly;
- both (plane strain and plane stress) types of specimens provided valid results at -10°C and 0°C,. The crack arrest toughness values are also similar indicating minimal influence of the side grooves on the crack arrest toughness at these temperatures. At +10°C, both types of specimens provided lower bound values only [Crosley and Ripling, 1990], and one can infer that with larger specimens than those employed, the 'plane stress' specimens would provide higher crack arrest toughness values.
- the crack arrest toughness of the base metal and the heat affected zone are very similar. This is not particularly surprising in light of their similar NDT temperatures. This observation also confirms the relatively minor role of the local brittle zones and a predominant role of the remaining HAZ microstructure in determining the crack arrest toughness of the HAZ containing LBZs.

Influence of Local Brittle Zones on Crack Arrest Toughness

The present tests were designed to guide the crack in the plane of the HAZ giving maximum opportunity to sample the local brittle zones. The metallography reported above confirmed that in seven of the compact crack arrest tests, the crack stayed in the correct plane throughout the complete propagation and arrest event. There were other tests where the crack was injected in the correct plane to sample the local brittle zones but the crack did not propagate very far or deviated into surrounding tougher HAZ or base material.

Focusing on the results at +10°C (3 tests), the crack planes did sample the material with low CTOD (initiation) toughness and yet high crack arrest toughness (K_a) was recorded. It can be inferred from the results that to obtain a running crack, the toughness along the entire crack front must be sufficiently low. The presence of a small brittle zone is not enough to support crack propagation with low K_a.

It is also useful to compare the experimentally determined HAZ crack arrest toughness values to those estimated from HAZ CTOD (initiation toughness) values which are the basis of steel qualification in CSA S473 and API RP 2Z. CTOD values (δ) may be converted to K values using the relationship:

$$K_I^2 = m \sigma_y \delta E$$

where m is a dimensionless constant that is about 1 for plane stress and 2 for plane strain, and standard notations apply for the other symbols. Thus, if the average of the three δ_c values for GCHAZ in Table I (0.055mm) represents the initiation toughness of the GCHAZ, then the equivalent quasistatic K_I toughness value for plane stress and plane strain situations would be 69 and 97 $MPa.m^{0.5}$, respectively. On the other hand, if the CTOD values from all specimens that sampled GCHAZ are considered, then the average CTOD of 0.233 mm would correspond to a quasistatic K_I toughness value of 140 $MPa.m^{0.5}$ under the plane stress condition expected at +10°C. Since the crack arrest toughness is usually less than half the initiation toughness, the average HAZ CTOD will imply a crack arrest toughness of no more than 70 $MPa.m^{0.5}$. The fact that the actual crack arrest toughness is considerably larger confirms that the low toughness GCHAZ has little influence on the crack arrest behavior and is in fact governed by the surrounding microstructure.

It is worth noting that in all three CTOD specimens that showed δ_c behavior with initiation in the GCHAZ, the brittle crack advance was limited to a small region and did not spread to the specimen surface. The maximum brittle crack advance from the fatigue crack in these specimens was less than 12 mm and the associated load drop was less than 25%. According to Arimochi and Isaka [1986], in a CTOD test, the stored energy is sufficient to drive the crack at the same toughness level as long as the crack advance associated with the load drop is less than 6% of the loading span, which for the CTOD tests performed is 12 mm. This presents further support that these arrests in CTOD tests were a result of the higher toughness of the adjacent HAZ.

The above results do not indicate how the distribution of toughness along the crack front (i.e., through the thickness) influences the effective crack arrest toughness. It is easy to imagine that a brittle zone exposed to the surface could extend along the surface (particularly if bending components were present) more easily than a brittle zone at the mid-thickness. For small brittle regions it is reasonable to assume the effective toughness for through thickness cracks is the average of the through thickness toughness distribution. Since the small brittle regions have very low toughness, the effective value will be determined largely by the extent and toughness of the higher toughness regions. It is of interest to explore whether the effective toughness can be estimated from small scale tests on local regions through the thickness.

To investigate this further, sub-size (5mm) Charpy tests were undertaken in an attempt to obtain some information on the toughness distribution through the thickness. [It should be noted that initiation tests such as CTOD do not provide suitable data as the outcome of the test is determined by the lowest toughness region along the crack front.] Because of sawcut allowances, only three positions could be sampled but at the middle position, the specimen notch was almost entirely in the coarse grained HAZ. From the transition curves (see **Figure 10**) the sub-size Charpy energy at +10°C was:

Position	Microstructural Region	Energy
Side 1	Fine grain HAZ	>80J
Centre	Grain Coarsened HAZ	38J
Side 2	Fine grain HAZ	>80J

Assuming the energy is proportional to area of the fracture ligament, the average energy for an equivalent full size CVN specimen is >132J. Using the Barsom correlation [Rolfe and Barsom, 1977] with K_{Id} data:

$$K_{Id}^2 / E = 0.64 \text{ CVN} \qquad \text{(GPa, m, J)}$$

gives an estimated value of $K_{Id} > 132$ MPa.m$^{0.5}$. This is close to the value for K determined from CCA tests which gave lower bound estimates at this temperature. It should be noted, however, that the correlation used is not necessarily reliable and also that K_{Id} values are usually lower than K_{Ia} values. Nevertheless the reasonableness of the answer suggests the possibility of estimating effective crack arrest toughness from simple laboratory tests by averaging the through thickness toughness distribution.

SUMMARY AND CONCLUSIONS

Crack arrest toughness of a heat affected zone containing local brittle zones and therefore not meeting the CTOD toughness requirements of documents such as API RP 2Z and CSA S473, has been evaluated using plane strain (ASTM E1221) and plane stress compact crack arrest tests. The arrest behavior has been discussed primarily at +10°C, because this temperature was about 20°C above the steel's nil ductility transition temperature; therefore, this steel can be considered to have reasonable crack arrest toughness and be suitable for service at +10°C design temperature except for its low HAZ CTOD toughness at this temperature. The objective of the work was to confirm that a heat affected zone containing local brittle zones and thus exhibiting low CTOD toughness can still exhibit adequate crack arrest toughness, thereby demonstrating a high degree of conservatism in the HAZ CTOD requirements.

The main conclusions of this investigation can be summarized as follows:

1. Based on the steel NDT temperature (-10°C), the steel tested is considered suitable for service for design temperature of +10°C but would be rejected on account of the low HAZ CTOD toughness at this temperature which was far lower than that of the base

metal at the same temperature. Further, assuming that the crack arrest toughness is about half the crack initiation toughness, the average CTOD toughness of the HAZ based on all the specimens tested would imply a crack arrest toughness of no more than 70 MPa.m$^{0.5}$ at +10°C.

2. Compact crack arrest tests (both plane strain and plane stress type) have been employed successfully to sample the HAZ containing coarse grain brittle regions and to obtain valid crack arrest toughness values at the NDT temperature and (NDT+10°C), i.e., at -10 and 0°C. At +10°C (NDTT + 20°C), only a lower bound estimate (133 MPa.m$^{0.5}$) could be obtained.

3. Clearly, the crack arrest toughness of the HAZ containing low toughness grain coarsened HAZ is superior to that inferred from the HAZ CTOD tests. In fact, at +10°C, the above HAZ crack arrest toughness is comparable to that of the base metal and it suggests that the steel and the HAZ are suitable for service at +10°C.

4. The above evidence supports the postulate that initiation is a "weakest link" event dependent on minimum properties, while arrest is a "collective" event reflecting average properties.

5. It is therefore concluded that in contrast to the initiation toughness (CTOD toughness), the local brittle zones in the amounts usually present have little influence on the crack arrest toughness. Instead, the toughness of the finer grain HAZ surrounding the local brittle zones has a greater bearing on the crack arrest toughness, probably because of its greater proportion along the crack path.

6. The investigation therefore has demonstrated that brittle crack are likely to be arrested after initiation from local brittle zones in multipass welds. Therefore, the requirements for minimum HAZ CTOD toughness based on the need to prevent crack initiation from local brittle zones, may be unduly conservative.

7. It is instead suggested that crack arrest toughness of the HAZ determined using the compact crack arrest test is a viable and adequately conservative alternative for the qualification of steels. The success rate for obtaining valid results for heat affected zones using the plane strain compact crack arrest specimens is rather low; however, it could be used to provide an approximate value which can then be verified using the plane stress compact crack arrest specimens. An approximate calculation of the crack arrest toughness may also be possible, subject to a further investigation, based on standard small scale laboratory tests such as standard or precracked Charpy test.

Acknowledgements: The authors are grateful to Fleet Technology Limited, Graville Associates Inc., Amoco Corporation and Panel for Energy R & D (Natural Resources, Government of Canada) for joint funding of the project.

REFERENCES

Arimochi, K., and Isaka, K.; 1986, *"A Study of Pop-In Phenomenon in CTOD Test for Weldment and Proposal of Assessment Method for Significance of Pop-In"*; IIW Document X-1118-1986.

Crosley, P.B., and Ripling, E.J.; 1990, *"A Quality Control Test for Selecting Materials to Arrest Fast Running, Full Thickness Cracks"*; J. of Test. & Eval.; V18 1990; pp 396-400.

Malik, L., et al; Jan. 1991, *"Evaluation of Toughness of Conventional Ship Steels at Intermediate Loading Rate, and Its Implications"*; Fleet Technology Contract Report 23440-7-9227/01-SQ submitted to CANMET/DSS; January 1991.

Malik, L., et al; Sept. 1991, *"Study of Wide Plate Testing of Structural Steels for Arctic Ships"*; Fleet Technology Contract Report 23440-9-9014/01-SQ submitted to DSS/CANMET; September 1991.

Pussegoda, L.N., et al; 1992, *"Significance of Local Brittle Zones in Weld Heat Affected Zones-Wide Plate Tests"*; OMAE Conference 1992, Calgary; Vol III-A, Materials Engineering; pp 41-51.

Rolfe, S.T., and Barsom, J.M.; 1987, *"Fracture and Fatigue Control in Structures - Application of Fracture Mechanics"*; 2nd edn., Prentice-Hall Inc., N.J. (1977).

Table I: HAZ CTOD (at 10°C) Test Results at 10°C

Specimen No.	Fracture Initiation Site	a/W Ratio	B (mm)	W (mm)	CTOD (mm)	Mode of Failure	% GCHAZ @ Fatigue Crack
22-1	GCHAZ	0.49	24.17	48.31	0.269	u	38
22-2	GCHAZ	0.49	24.25	48.38	0.016	c	34
22-3	GCHAZ	0.49	24.27	48.40	0.227	u	24
22-4	GCHAZ	0.50	24.26	48.32	0.161	u	26
22-5	GCHAZ	0.50	24.21	48.34	0.516	u	19
23-2	GCHAZ	0.49	24.57	49.56	0.468	u	30
23-3	GCHAZ	0.50	24.89	49.78	0.061	c	27
23-4	GCHAZ	0.49	24.82	49.63	0.088	c	18
23-5	GCHAZ	0.49	24.89	49.87	0.291	u	23
23-6	Outside GCHAZ	0.49	24.87	49.87	0.173	c	20

Table II: Results of Plane Strain (Side Grooved) CCA Toughness Tests

Specimen No.	Test Temp (°C)	Cycles to Failure	Initiation Stress Intensity K_o(MPa/√m)	Crack Arrest Toughness K_a(MPa√m)	Invalidity Criterion* (ASTM E 1221)	Sampled GCHAZ
25-3	10	5	387	206	C,B,E+crack dev	no
26-1	10	6	721	273	C,B,E + tunnel	crack dev
26-2	10	6	353	298	C,B,E + tunnel	crack dev
27-2	10	6	593	398	C,B,E + tunnel	crack dev
28-3	10	6	356	133	C,B,E	yes
27-3	10	6			no crack initiation	
26-3	0	6	305	179	C,B,E + tunnel	crack dev
28-1	0	6	219	85		yes
28-2	-10	2	129	104	D,C	yes
25-2	-10	2	123	99	D	yes
27-1	-10	6	246	78	A	yes

* (A) $W-a_a \geq 0.15W$
(B) $W-a_a \geq 1.25\ (K_a/\sigma_{yd})^2$
(C) $B \geq (K_a/\sigma_{yd})^2$
(D) $a_a-a_o \geq 2N$
(E) $a_a-a_o \geq (K_o/\sigma_{ys})^2\ /2\pi$

Table III: Results of Full Thickness Plane Stress CCA Toughness Tests

Specimen No.	Test Temp (°C)	W (mm)	a_o/W	Estimated K_a, i.e., K_v*(MPa√m)	Full Thickness Crack Arrest Toughness, K_a(MPa√m)	GCHAZ Sampled
33	10	285	0.382	133	>133	yes
33-3	10	171	0.392	101	>101	yes
35	10	285	0.360	133	>133	no
31-1	0	171	0.645	101	91.9	yes
31-2	0	172	0.475	103	>103	no
32-1	-10	147	0.685	97	111.6	crack dev
32-2	-10	147	0.839	97	<97	no
34-1	-10	145	0.664	97	75.6	yes
34-2	-10	145	0.839	97	<97	no

(* K_v is the initial assumed value of K_a for specimen design)

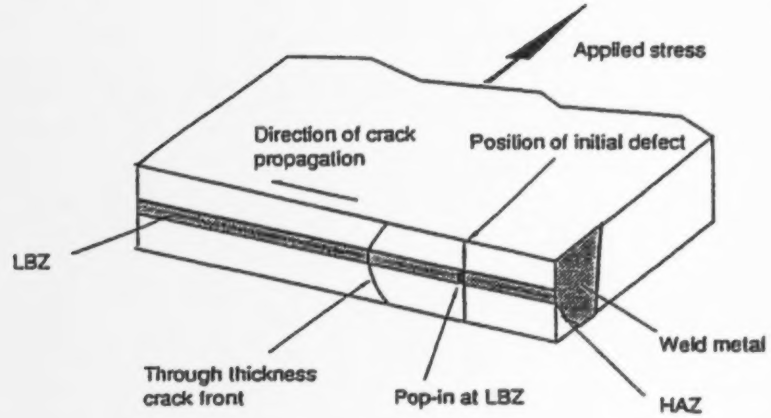
Applied stress
Direction of crack propagation
Position of initial defect
LBZ
Weld metal
Through thickness crack front
Pop-in at LBZ
HAZ

Figure 1: **Illustration of a crack front following a local brittle zone.**

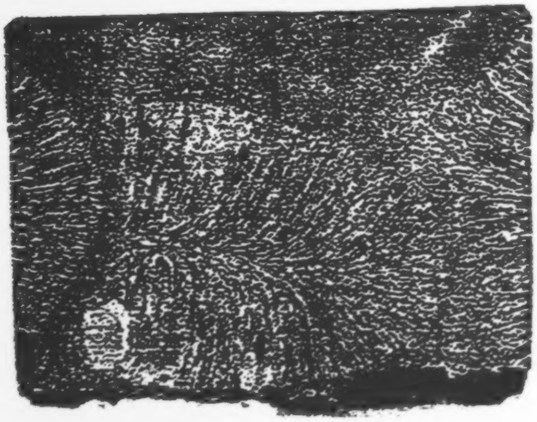

Figure 2: **Cross section of the test weld as observed during post CTOD test metallography. (Mag. X3).**

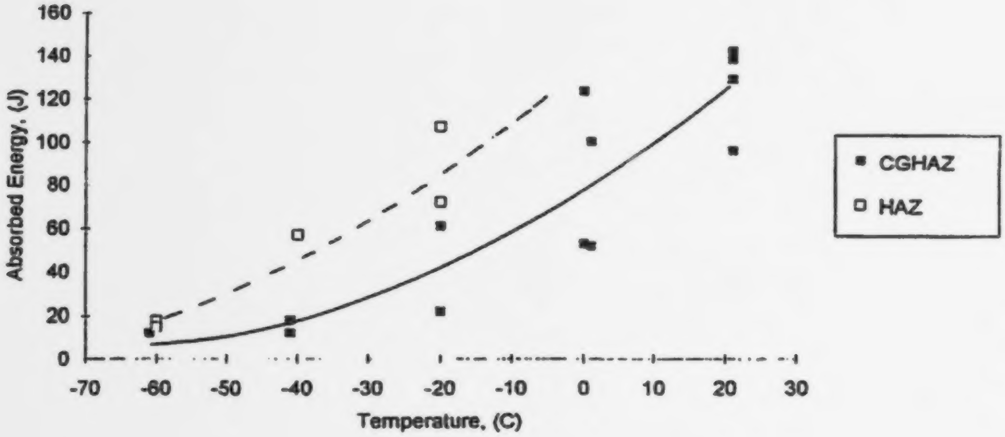

Figure 3: Standard CVN transition curves for GCHAZ and the remainder of the HAZ.

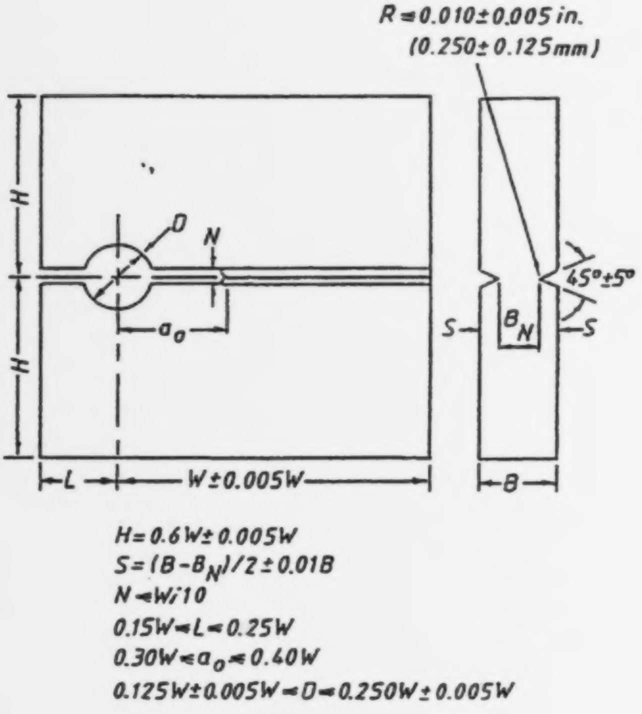
R = 0.010 ± 0.005 in.
(0.250 ± 0.125 mm)
H
H
D
N
a_0
45° ± 5°
S
B_N
S
L
W ± 0.005W
B
$H = 0.6W \pm 0.005W$
$S = (B - B_N)/2 \pm 0.01B$
$N \leq W/10$
$0.15W \leq L \leq 0.25W$
$0.30W \leq a_0 \leq 0.40W$
$0.125W \pm 0.005W \leq D \leq 0.250W \pm 0.005W$

B = 25; W = 168; H = 101; N = 12.7; L = 33.6;
D = 31.5; S = 3.2 and a_o = 60 (all dimensions in mm)

Figure 4: Dimensions of plane strain CCA test specimens.

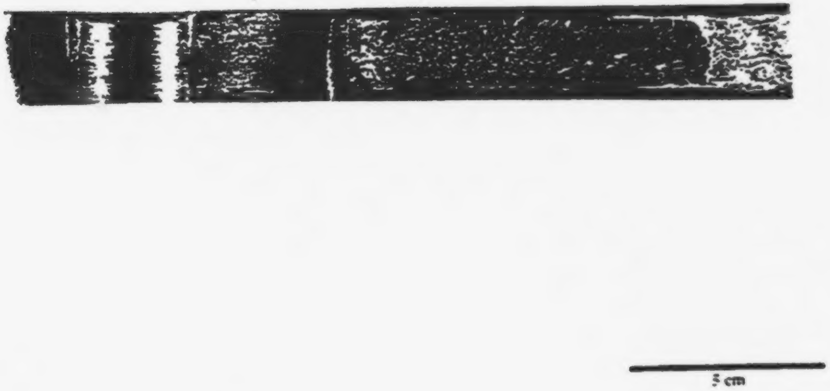

Figure 5(a): **Fracture surface showing crack arrest location inplane strain CCA specimen 27-1 tested at -10°C.**

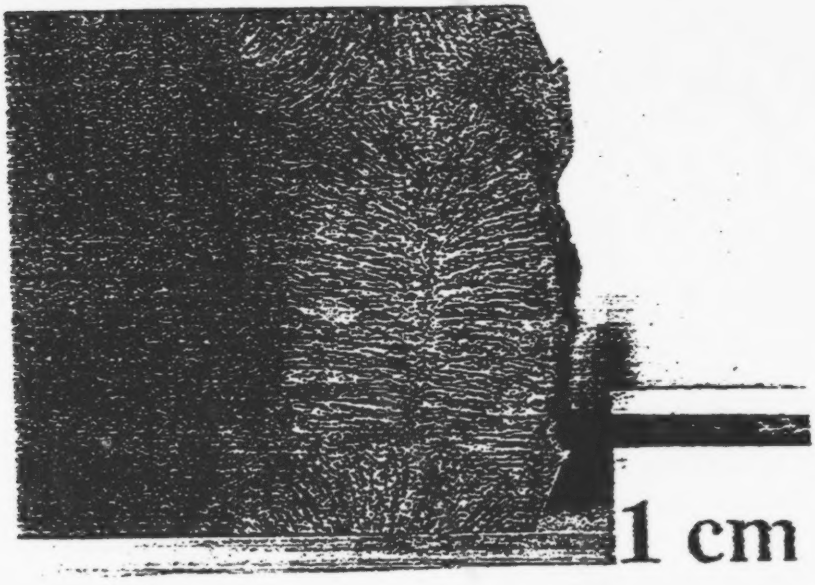

Figure 5(b): **Cross section at the crack arrest location in plane strain CCA specimen 28-1 tested at 0°C.**

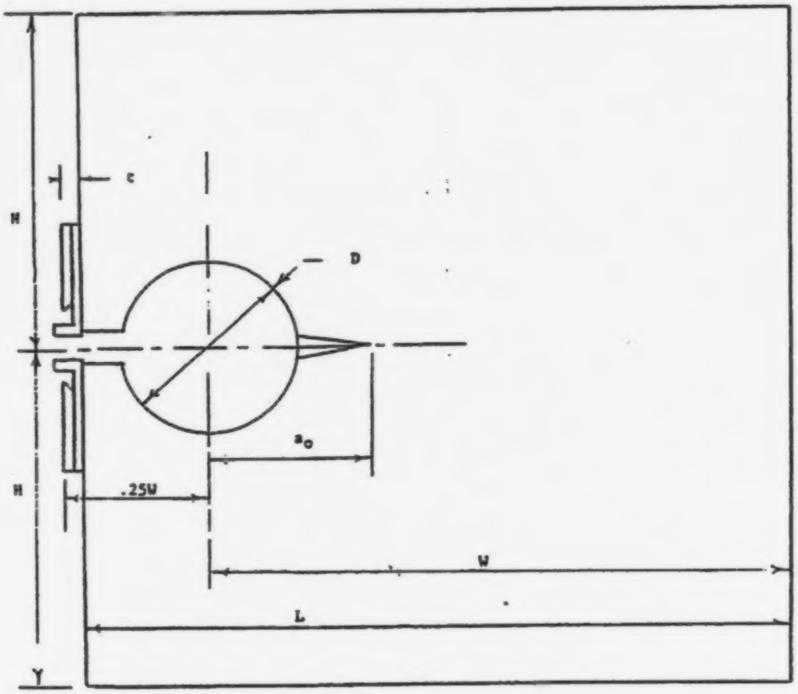

$H = 0.6W \pm 0.005W$

$L = 1.25W - c$

$0.30W \leq a_o \leq 0.40W$

$0.3125W \leq D \leq 0.375W$

(Notice that D is much larger than it is in ASTM E1221. The reason for this is to be able to reach the chevron tip with a torch in order to embrittle it.)

Figure 6: Dimensions of plane stress CCA test specimen.

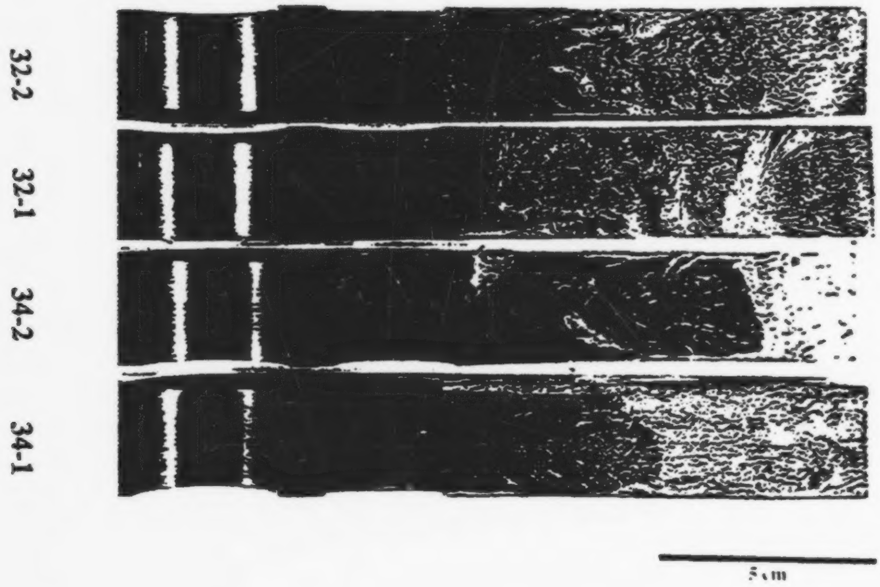

Figure 7: Fracture surfaces of the four plane stress CCA tests carried out at -10°C; however, arrest location in the GCHAZ in only one specimen (34-1, the fracture surface at the bottom).

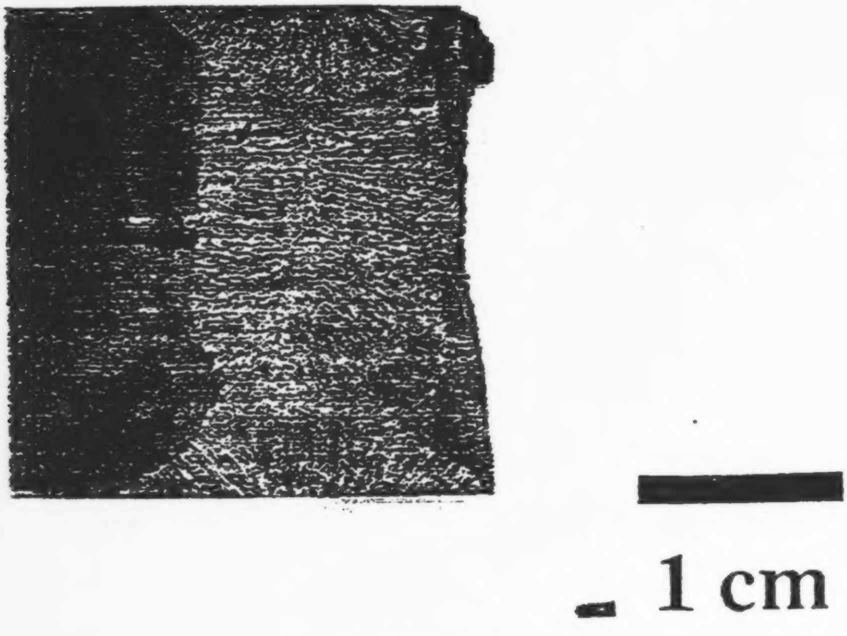

Figure 8: Cross section at the crack arrest location in plane stress CCA specimen no. 33 tested at +10°C.

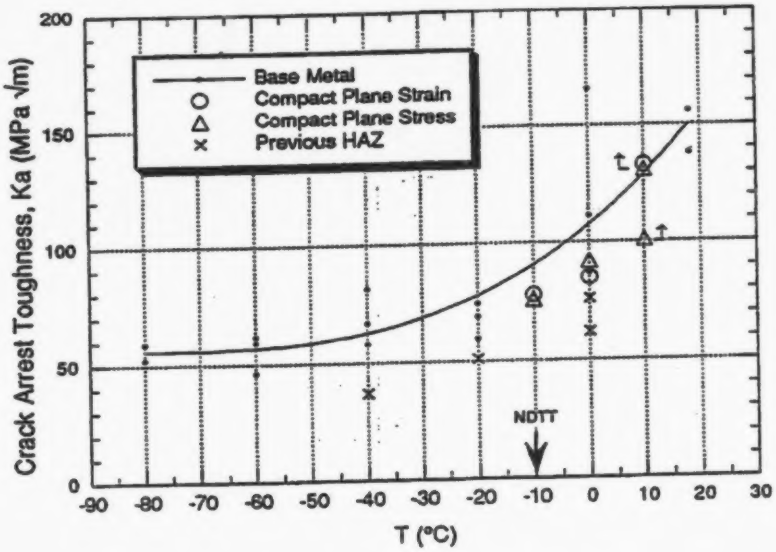

Figure 9: HAZ Crack arrest toughness values from all the tests from this and a previous study shown as a function of test temperature in relation to the base metal crack arrest toughness.

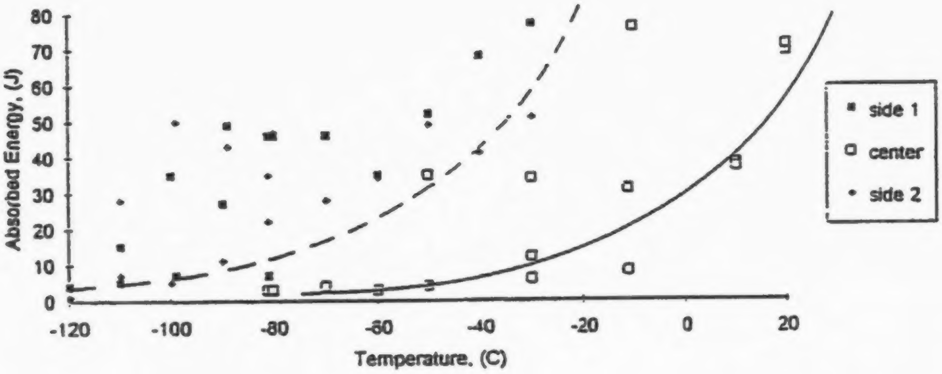

Figure 10: CVN transition curves (subsize specimens) showing the toughness distribution through the thickness.

#510363

(

Effect of Undermatching Weld Metal on the Measured Fractures Toughness of HSLA 100 Joints

by

R. Yee+, L. Malik+ , and J. Morrison++

+ Fleet Technology Limited, Kanata, Ontario

++ Esquimalt Defence Research Detachment, Victoria, B.C.

ABSTRACT

Modern high strength steels such as HSLA 100 have excellent toughness and resistance to cold cracking in the heat affected zone, even when they are welded without pre-heat. Unfortunately, welding consumables with comparable strength, toughness, and resistance to cold cracking are not yet commercially available. As a result, fabricators are unable to fully exploit the cost advantages of welding such steels at this time. A potential solution to this problem is to weld the steels with undermatching consumables that have a lower tensile strength but higher intrinsic fracture toughness than the base metal. It is assumed that the higher intrinsic fracture toughness of the undermatching weld metal is sufficient to counter the higher crack driving force resulting from strain concentrations in the undermatching weld metal.

Although the effect of undermatching weld metal on measured fracture toughness has been inferred from numerical studies of the crack driving force in undermatching weld metal, there has been little experimental investigation of this effect. In the present study, HSLA steel plate was heat-treated to four lower yield strengths. Butt joints were subsequently made from these four steels as well as steel in the as-received condition. These joints were subsequently made from these four steels as well as steel in the as-received condition. These joints were fabricated with the same shielded metal arc welding procedure and consumable. Therefore, the weld metals in these joints were nominally identical with the same dilution, composition, microstructure, strength, and intrinsics toughness. Three-point bending specimens with standard deep notches and shallow notches were machined from each joint, and CTOD tests with these specimens were performed at various sub-zero temperatures. Traces of load versus load line displacement (LLD) and load versus crack mouth opening displacement (CMOD) were collected during these tests. This paper presents CTOD and J values calculated from both sets of traces, and examines the effect of undermatching weld metal on these values.

1.0 INTRODUCTION

Modern high strength steels such as HSLA 100 have excellent toughness and resistance to cold cracking in the heat affected zone, even when they are welded without pre-heat. Unfortunately, welding consumables with comparable strength, toughness, and resistance to cold-cracking are not yet commercially available. As a result, fabricators are unable to fully exploit the cost advantages of welding such steels at this time. A potential solution to this problem is to weld the steels with undermatching consumables that have a lower tensile strength but higher intrinsic fracture toughness than the base metal. It is assumed that the higher intrinsic fracture toughness of the undermatching weld metal is sufficient to counter the higher crack driving force resulting from strain concentrations in the weld metal. However, the magnitude of the required increase in fracture toughness cannot be reliably quantified at this time because of uncertainties in the calculation of crack driving force in the undermatching weld metal in real structures and standard fracture mechanics specimens.

The following sets of equations are commonly used to calculate the crack driving force (**CTOD** and **J**) in standard Single Edge Notch Bend (**SENB**) specimens for fracture toughness tests of steels:

Set 1 (BS 5672 [1] and BS 7448 [2])

$$CTOD_{standard} = \frac{K^2(1-\nu^2)}{2\sigma_{YS}E} + \frac{.4(W-a_o)\,CMOD_p}{.4(W-a_o)+.6a_o+z}$$

$$J_{standard} = \frac{K^2(1-\nu^2)}{E} + \frac{2A_{LLD}}{B(W-a_o)}$$

Set 2 (Wang and Gordon [3])

$$CTOD_{CMOD} = \frac{K^2(1-\nu^2)}{2\sigma_{YS}E} + \frac{\eta_{C-C}A_{CMOD}}{\sigma_{YS}B(W-a_o)}$$

$$J_{CMOD} = \frac{K^2(1-\nu^2)}{E} + \frac{\eta_{J-C}A_{CMOD}}{B(W-a_o)}$$

where

$$K = \left(\frac{4F_{c,\ u,\ or\ m}}{BW^{5}}\right) \times \frac{3\left(\frac{a_o}{W}\right)^{.5}\left[1.99 - \frac{a_o}{W}\left(1 - \frac{a_o}{W}\right)\left(2.15 - \frac{3.93a_o}{W} + \frac{2.7a_o^{2}}{W^{2}}\right)\right]}{2\left(1 + \frac{2a_o}{W}\right)\left(1 - \frac{a_o}{W}\right)^{1.5}}$$

$$\eta_{J\text{-}C} = 3.5 - 1.4167\left(\frac{a_o}{W}\right)$$

$$\eta_{C\text{-}C} = 4.292 - 1.667\left(\frac{a_o}{W}\right) + .304\left(\frac{\sigma_{UTS}}{\sigma_{YS}}\right)^{2} - 2.0\left(\frac{\sigma_{UTS}}{\sigma_{YS}}\right)$$

K is the elastic stress intensity factor, **a_o** is the depth of the fatigue pre-crack and its starter notch; **F** is the applied load; **$CMOD_p$** is the plastic component of the crack mouth opening displacement; **A_{CMOD}** is the area bounded by the applied force versus crack mouth opening displacement curve up to **F** and the elastic unloading line from **F**; **A_{LLD}** is the area bounded by the applied force versus load-line displacement curve up to **F** and the elastic unloading line from **F**; **W** is the width of the specimen; **z** is the distance from the mouth of the starter notch to the point of attachment between the extensometer and its knife edges; **ν** is the Poisson ratio of the material; **E** is the material's modulus of elasticity; **σ_Y** is the material's yield strength, and **σ_{UTS}** is the material's ultimate tensile strength.

Both sets of equations are empirical and have been calibrated against experimental data for homogeneous test specimens. The first set of equations is only intended for **a_o/W** ratios between .45 and .55, whereas the second set of equations is applicable to **a_o/W** ratios between .1 and .6. For the same base metal, specimen geometry, and applied load, the plastic strain distribution and the limit load of test specimens with either undermatching or overmatching weld metal differ from that in homogeneous test specimens, Therefore, in principle, the equations should not be applied to test specimens with mis-matched weld metal. However, recent elasto-plastic finite element analyses by Kirk and Dodd [4] have indicated that the strain concentration effect and limit load effect in **SENB** test specimens with mis-matched weld metal tend to offset each other and that the aforementioned equations are sufficiently accurate for test specimens with up to +/-20% mis-match between the yield strengths of the weld metal and base metal.

This paper presents fracture toughness data (**CTOD** and **J**) for shallow notch and deep notch **SENB** specimens that were machined from HSLA 100 steel butt joints with the same weld metal but base metal heat-treated to different tensile strengths. These measured fracture toughness values provide an indirect indication of the effect of weld mis-match on calculated driving force force since the specimens had the same weld metal and therefore the same intrinsic fracture toughness.

2.0 EXPERIMENTAL PROCEDURE

Standard crack tip opening displacement (CTOD) tests were conducted with 94 Single Edge Notch Bend (SENB) specimens. These specimens were machined from five series of butt joints (18 to 20 specimens from each series). Each series of butt joints were fabricated from the same weld metal but different base metals, viz., HSLA 100 steel heat treated to different yield strengths (FIgures 1 and 2). The latter strengths were chosen to achieve five levels of mis-match between the yield strength of the weld metal (YS_{weld}) and the yield strength of the base metal (YS_{base}): $(YS^{weld}-Y_{base})/YS_{base}$ = -.295, -.165, -.088, -.019, and +.156. The dimensions of these specimens and the orientation of the weld metal in these specimens are shown in Figure 3. A 12 mm deep notch was machined in the weld metal of half of the specimens from each series, while a 3 mm deep notch was machined in the weld metal of the remaining specimens from each series. These through-thickness notches were machined with a slitting wheel which produced the notch tip geometry shown in the inset of Figure 3.

A 2 to 3 mm deep fatigue crack was initiated at the notch tip of each specimen by cyclically loading the specimen in three-point bending. This pre-cracking was performed in a Pegasus servo-hydraulic test machine at an R-ratio of .1. Prior to this operation, the notch tip was plastically compressed in the through-thickness direction (1% plastic strain) with a 12.7 mm diameter platen. The maximum applied loads for the shallow notch specimens and deep notch specimens were initially maintained at 24.7 kN and 10.4 kN, respectively, until a .5 mm deep fatigue crack was visually detected at the edges of the starter notch. The maximum applied loads for the shallow notch specimens and deep notch specimens were then reduced to 19.1 kN and 7.9 kN, respectively, for the next .5 to 1.0 mm of fatigue crack growth[1]. The maximum applied loads for the shallow notch specimens and deep notch specimens were maintained at 13.6 kN and 5.4 kN, respectively, for the final 1.0 to 1.5 mm of fatigue crack growth$_1$. The latter loads produced a maximum stress intensity factor of 700 $MN/mm^{3/2}$ at the final crack tip.

The CTOD tests were conducted with the SENB specimens immersed in an alcohol bath. These tests were performed under displacement control in a Baldwin servo-hydraulic test machine with the three-point bending fixture. The load-line displacement rate (quasi-static) was approximately .5 mm per minute. The deep notch specimens were tested at -10°C, -30°C, -40°C, and -60°C, while the shallow notch specimens were tested at -40°C and -60°C (see Table 1 for test matrix). These temperatures were obtained by cooling the alcohol bath with dry ice to a temperature 3°C below the desired test temperature.

---

[1] visually measured at the edges of the starter notch

Table 1: Matrix of specimens for fracture toughness tests.

Deep notch specimens

$\frac{YS_{weld}-YS_{base}}{YS_{base}}$	-10°C	-30°C	-40°C	-60°C
-.295		3	3	3
-.165	3		3	3
-.088	3	1	3	3
-.019		4	3	3
+.156	1	2	3	3

Shallow notch specimens

$\frac{YS_{weld}-YS_{base}}{YS_{base}}$	-10°C	-30°C	-40°C	-60°C
-.295			5	4
-.165			5	4
-.088			5	5
-.019			5	5
+.156			5	4

Three quantities were monitored during each test: applied force (**F**), crack mouth opening displacement (**CMOD**), and load-line displacement (**LLD**). Load-line displacement, which was defined as the vertical displacement of the notch mouth relative to a comparator bar, was measured with a proximity probe. Crack mouth opening displacement was measured with an extensometer that was attached to knife edges at the mouth of the starter notch. Applied force was measured with a load cell in series with the loading ram and hydraulic actuator. Data from these transducers was collected with a 16 bit data acquisition system at a sampling rate of 3 Hz. Each test was terminated when the applied force reached a maximum plateau or abruptly decreased by more than 5%. In every case, a plateau or peak in the applied force was reached before a pop-in occurred, where a pop-in was defined as a less than 5% drop in the applied force followed by an increase in the applied force to a level at least as high as the applied force at the start of the load drop.

Once the **CTOD** tests were completed, the specimens were soaked in liquid nitrogen and broken apart by rapidly loading them in the Baldwin's three-point bending fixture. The final fracture surfaces of the specimens were then examined under a stereomicroscope. These examinations identified three basic modes of failure during the **CTOD** tests:

1. arrested unstable cleavage,

2. stable ductile tearing followed by arrested unstable cleavage, and

3. stable ductile tearing.

These three modes are herein referred to as **Mode c**, **Mode u**, and **Mode m** failures, respectively.

As stated earlier, each test was terminated when the applied force reached a maximum plateau or peaked and then abruptly decreased by more than 5%. In every case, a plateau or peak in the applied force was reached before a pop-in had occurred, a pop-in being defined as a less than 5% drop in the applied force followed by an increase in the applied force to a level at least as high as the applied force at the start of the load drop. The peak forces coincided with the onset of unstable cleavage in **Mode c** and **Mode u** failures, whereas the force plateaus were reached in **Mode m** failures. The force peak in a **Mode c** or **Mode u** failures is herein referred to as $\mathbf{F_c}$ or $\mathbf{F_u}$, respectively, while the maximum force in a **Mode m** failure is herein referred to as $\mathbf{F_m}$.

Equations 1 and 3 were used to independently calculate the **CTOD** value at $\mathbf{F_c}$, $\mathbf{F_u}$, or $\mathbf{F_m}$ for each specimen, while Equations 2 and 4 were used to independently calculate the **J** value at $\mathbf{F_c}$, $\mathbf{F_u}$, or $\mathbf{F_m}$ for each specimen. As indicated earlier, Equations 1 and 2 are only intended for $\mathbf{a_o/W}$ ratios between .45 and .55. Nevertheless, these equations were applied to the shallow notch specimens as well as the deep notch specimens. For the purposes of this project, all calculations were based on material properties at room temperature. The average crack depth of the fatigue pre-crack and its starter notch was based on nine equally-spaced measurements across the crack front with a travelling microscope. A Simpson's rule algorithm (1% convergence tolerance) was used to numerically evaluate the areas under the applied load versus crack mouth opening displacement curves and applied load versus load-line displacement curves, while the areas under the elastic unloading lines were calculated analytically. The slopes of the elastic unloading lines were derived from empirical solutions for the elastic compliances of the **SENB** specimens in their initial configuration.

Fracture toughness values could not be derived for Specimens AR-2, 2-7, 6-2, 6-7, and 72-1 because the raw data for these specimens was not properly stored by the data acquisition system. In addition, $J_{standard}$ values could not be derived for Specimens AR-1, 1-1, 1-4, 2-1, 2-2, 6-1, and 6-3 because the proximity probe for measuring load-line displacement was improperly mounted.

3.0 RESULTS

The measured fracture toughness values for the shallow notch specimens are plotted against temperature in Figures 4-7, while the measured fracture toughness values for the deep notch specimens are plotted against temperature in Figures 8-11. The failure mode of each specimen is identified in these figures.The following observations were made from the aforementioned figures:

1. The fracture toughness values for the shallow notch specimens tended to increase with increasing temperature. The majority of these specimens failed by **Mode u**. Of the remaining specimens, only one failed by **Mode m** and only three failed by **Mode c**. This indicates that the two test temperatures for the shallow notch specimens (-40°C and -60°C) were well within the ductile-brittle transition for these specimens.

2. The measured fracture toughness values for the deep notch specimens tested tested at -30°C, -40°C, and -60°C tended to increase with increasing temperature, while the measured fracture toughness values for the deep notch specimens tested at -10°C were similar to the measured fracture toughness values for the deep notch specimens tested at -30°C. All of the deep notch specimens that were tested at -10°C failed by **Mode m**, whereas the deep notch specimens that were tested at -30°C failed by either **Mode u** or **Mode m**. Furthermore, most of the deep notch specimens that were tested at -60°C failed by **Mode c**; the remainder of these specimens failed by **Mode c**. This indicates that the start of the *upper shelf* for the fracture toughness of the deep notch specimens was somewhere between -10°C and -30°C while the lower part of the ductile-brittle transition region for these specimens was located near -60°C.

3. For a given temperature, the fracture toughness values for the shallow notch specimens were generally higher than the fracture toughness values for the deep notch specimens. This geometry dependence is related to the lower constraint in the shallow notch specimens, which promoted crack initiation by ductile tearing tearing rather than brittle cleavage.

4. The fracture toughness values for the shallow notch specimens were much more variable than the fracture toughness values for the deep notch specimens. In addition, the fracture toughness values in the upper ductile-brittle transition region of the deep notch specimens appeared to be more variable than the *upper shelf* fracture toughness values for these specimens. These differences can be attributed to two factors. First, the dominant mode of failure in these specimens was ductile crack initiation followed by brittle cleavage (i.e., **Mode u**). The measured fracture toughness values were associated with the onset of brittle cleavage. Second, cleavage in a **Mode u** failure occurs when the stress field ahead of the initial growing crack samples a critical particle. Therefore, the onset of cleavage is influenced by statistical sampling effects.

4.0 DISCUSSION

The mean, maximum, and minimum fracture toughness values for different notch depths and test temperatures are plotted against mismatch in Figures 12 to 16. None of these figures show an obvious relationship between measured fracture toughness and degree of weld mis-match, and statistical analyses of variance (ANOVA) failed to isolate any such relationship from the experimental scatter. This implies that the crack driving forces predicted by the equations were essentially independent of weld metal mis-match over the range of mis-match considered in this test program (-29.5% to +15.6%[2]), since all the test specimens had the same weld metal and therefore the same intrinsic fracture toughness. This is consistent with Kirk and Dodd's finite element analyses which show that the crack driving forces predicted by Equations 1-4 are essentially independent of the degree of weld metal mis-match in SENB specimens with up to +/- 20% weld metal mis-match.

According to Kirk and Dodd's finite element analyses, the equations based on the area underneath the applied load versus displacement (load-line or crack mouth opening) curve (i.e, Equations 3 and 4) are the most accurate for predicting the cracking driving force in SENB specimens with up to +/- 20% weld mis-match. However, Figures 17 to 20 indicate that Equation 1 is sufficiently accurate for predicting CTOD values greater than .1 mm and .2 mm in shallow notch specimens and deep notch specimens, respectively, while Equation 3 is sufficiently accurate for predicting J values with no lower bound. Figures 17 and 18 are plots of $(\mathrm{CTOD}_{\mathrm{standard}}-\mathrm{CTOD}_{\mathrm{CMOD}})/\mathrm{CTOD}_{\mathrm{CMOD}}$ versus $\mathrm{CTOD}_{\mathrm{CMOD}}$ for the shallow notch specimens and deep notch specimens, respectively. Figures 19 and 20 are plots of $(J_{\mathrm{standard}}-J_{\mathrm{CMOD}})/J_{\mathrm{CMOD}}$ versus J_{CMOD} for the shallow notch specimens and deep notch specimens, respectively. Figure 18 shows that the $\mathrm{CTOD}_{\mathrm{standard}}$ values for the deep notch specimens were 4% to 6% lower than their corresponding $\mathrm{CTOD}_{\mathrm{CMOD}}$ values when $\mathrm{CTOD}_{\mathrm{CMOD}}$ exceeded ≈.3 mm, while Figure 17 shows that the $\mathrm{CTOD}_{\mathrm{standard}}$ values for the shallow notch specimens were about 6% to 8% lower than their corresponding $\mathrm{CTOD}_{\mathrm{CMOD}}$ values when $\mathrm{CTOD}_{\mathrm{CMOD}}$ exceeded ≈.6 mm. Below these critical $\mathrm{CTOD}_{\mathrm{CMOD}}$ values, the $\mathrm{CTOD}_{\mathrm{standard}}$ values for both types of specimens exceeded their corresponding $\mathrm{CTOD}_{\mathrm{CMOD}}$ values with the differences increasing exponentially with decreasing $\mathrm{CTOD}_{\mathrm{CMOD}}$. In contrast, no exponential relationship was found between the J_{standard} and J_{CMOD} values for either the shallow notch specimens or the deep notch specimens. Figure 19 shows that the majority of J_{standard} values for the shallow notch specimens were within +/- 20% of their corresponding J_{CMOD} values, while Figure 20 shows that the majority of J_{standard} values for the deep notch specimens were 2% to 10% less than their corresponding J_{CMOD} values.

---

[2] $(YS_{\mathrm{weld}}-YS_{\mathrm{base}})/YS_{\mathrm{base}}$

5.0 SUMMARY

HSLA 100 steel plate was heat-treated to four lower yield strengths, and butt joints were subsequently made from these four steels as well as steel in the as-received condition. These joints were fabricated with the same shielded metal arc welding procedure and consumable. Therefore, the weld metals in these joints were nominally identical with the same dilution, composition, microstructure, strength, and intrinsic toughness. 94 SENB specimens with deep and shallow notches were machined from the joints, and CTOD tests were performed at various sub-zero temperatures. Two sets of equations were used to calculate crack driving force: (1) the standard equations for deep notch SENB specimens and (2) recommended equations for shallow notch SENB specimens. There was no obvious effect of weld metal mis-match on the measured fracture toughness values. This implies that the crack driving forces predicted by the equations were essentially independent of weld metal mis-match over the range of mis-match considered in this test program (-29.5% to +15.6% with respect to yield strength), since all the test specimens had the same weld metal and therefore the same intrinsic fracture toughness.

6.0 REFERENCES

[1] BS 5762:1979,"Methods for Crack Opening Displacement (COD) Testing".

[2] BS 7448: Part 1: 1991,"Fracture Mechanics Toughness Tests. Method for the Determination of K_{IC}, Critical CTOD and Critical J Values of Metallic Materials."

[3] Wang, Y.Y. and Gordon, J.R., "The Limits of Applicability of J and CTOD Estimation Procedures for Shallow-Cracked SENB Specimens", Proc. of Conf. on Shallow Crack Fracture Mechanics, Toughness Tests, and Applications, Sept 23-24, 1992, The Welding Institute, Paper 28.

[4] Kirk, M.T. and Dodds, R.H.,"Effect of Weld Strength Mismatch on Elastic-Plastic Fracture Parameters", University of Illinois, Civil Engineering Studies, Structural Research Series No. 570, Report UILU-ENG-92-2008, Aug., 1992.

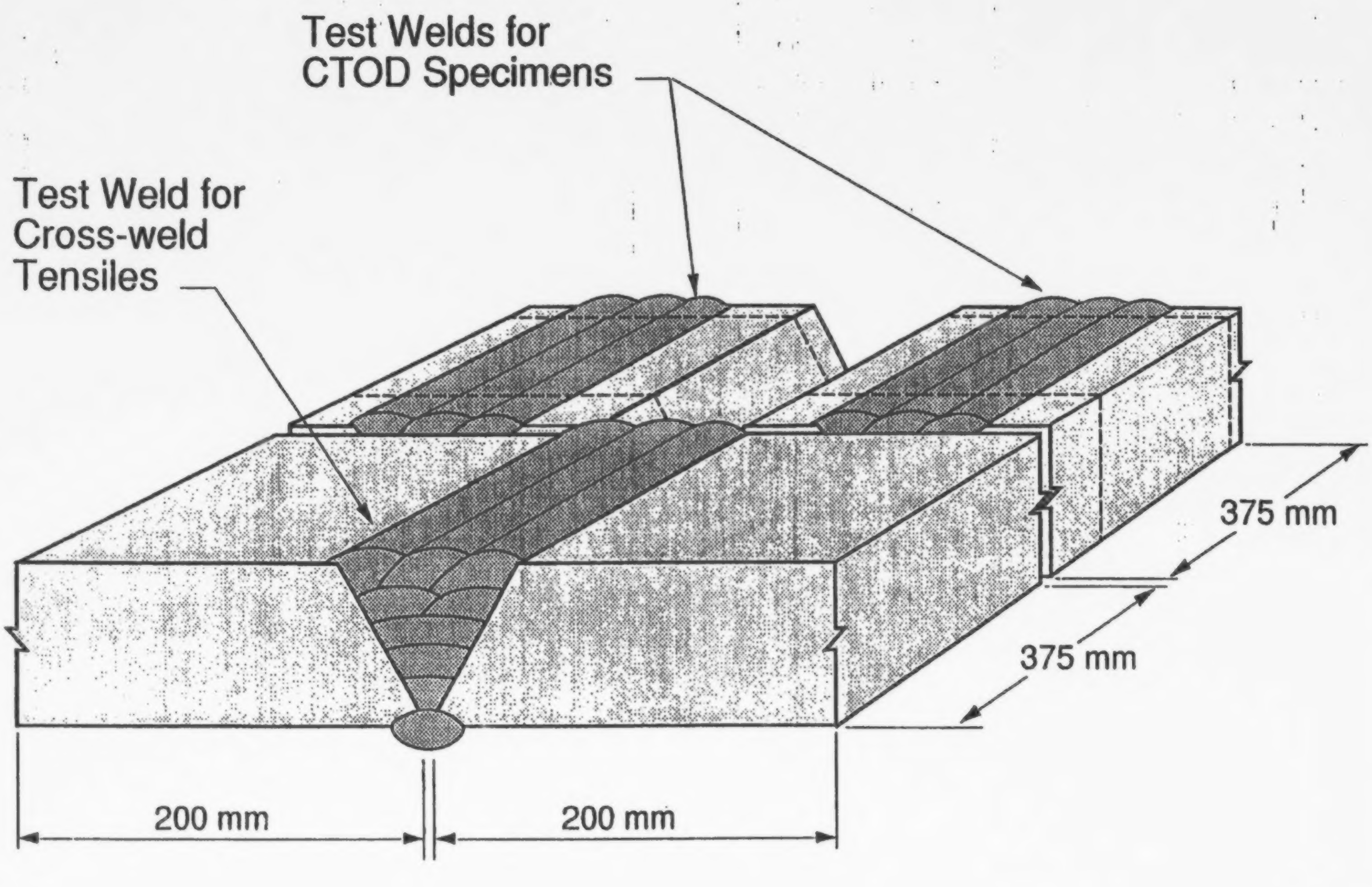
Test Welds for
CTOD Specimens
Test Weld for
Cross-weld
Tensiles
375 mm
375 mm
200 mm
200 mm

Figure 1: Cutting pattern for SENB specimens from test welds.

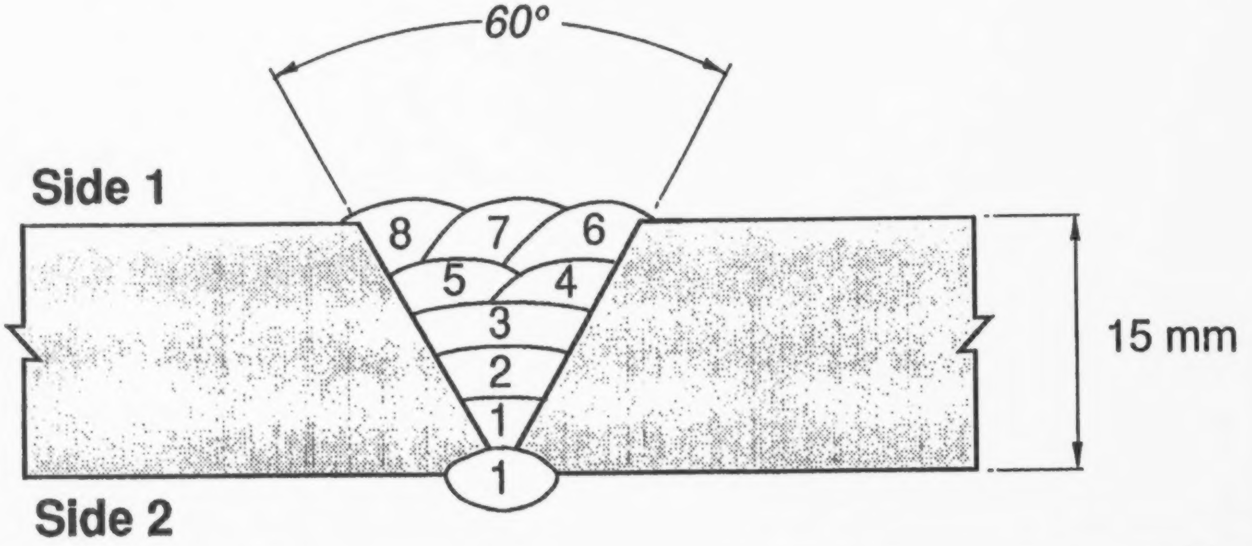

Material Specification: HSLA 100
Welding Process: Manual SMAW
Position of Welding: 1G
Filler Metal: E10018M-1 Alloy Rods, 4 mm Dia.
Single or Multipass: Multipass
Single or Multiple Arc: Single (170 Amps, 22 Volts)
Preheat Temperature: 66° C
Interpass Temperature: 100° C
Preheat Method: Propane Torch
Travel Speed: 130 - 200 mm/min.

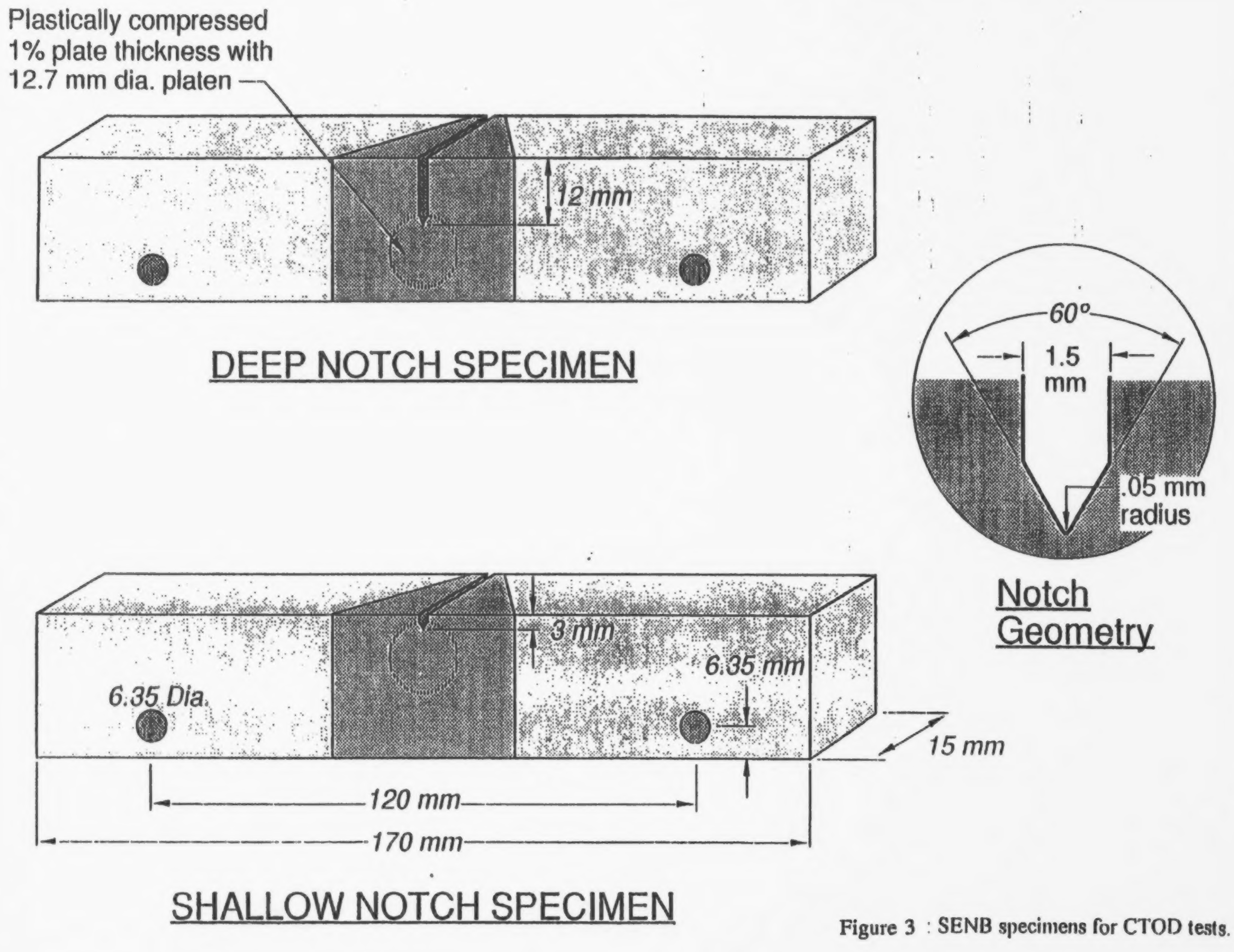
Plastically compressed
1% plate thickness with
12.7 mm dia. platen
12 mm
DEEP NOTCH SPECIMEN
60°
1.5
mm
.05 mm
radius
Notch
Geometry
3 mm
6.35 mm
6.35 Dia.
15 mm
120 mm
170 mm
SHALLOW NOTCH SPECIMEN

Figure 3 : SENB specimens for CTOD tests.

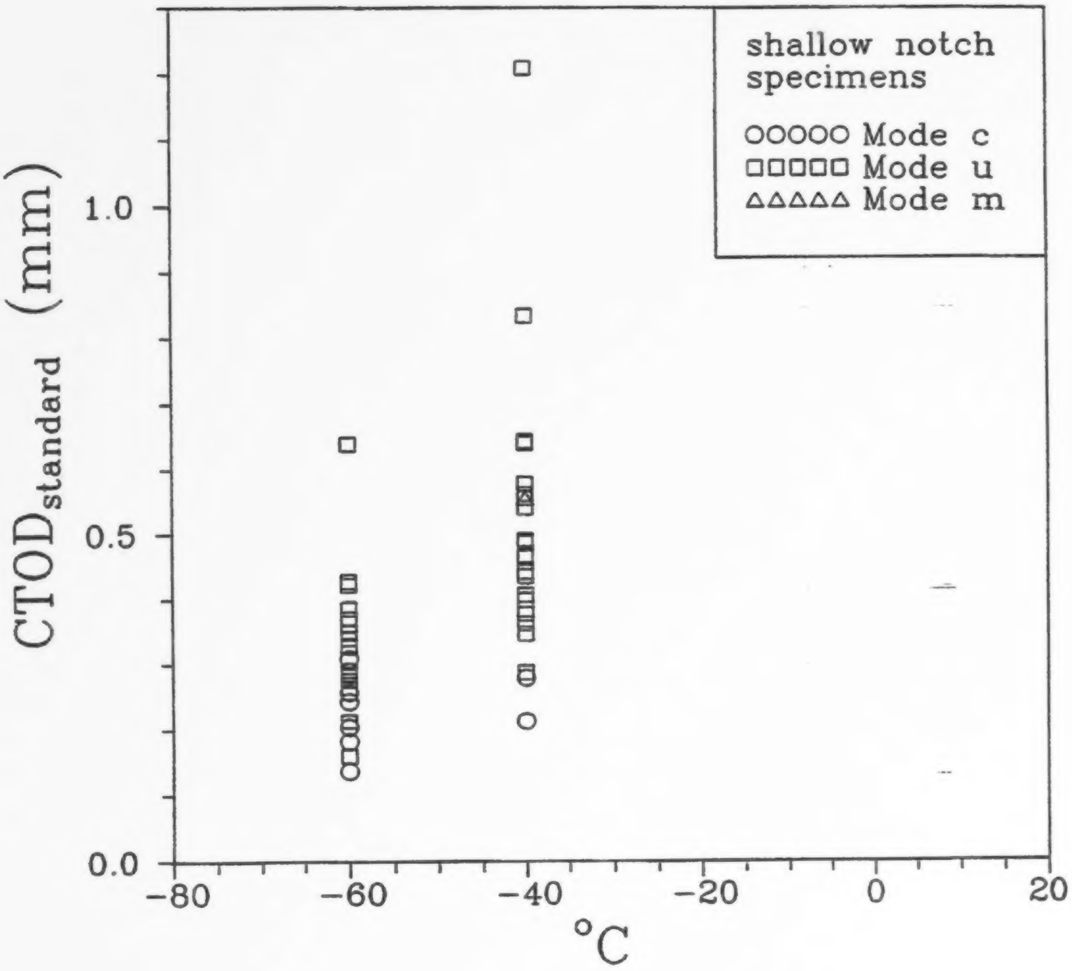

Figure 4: CTOD$_{standard}$ versus test temperature for shallow notch specimens.

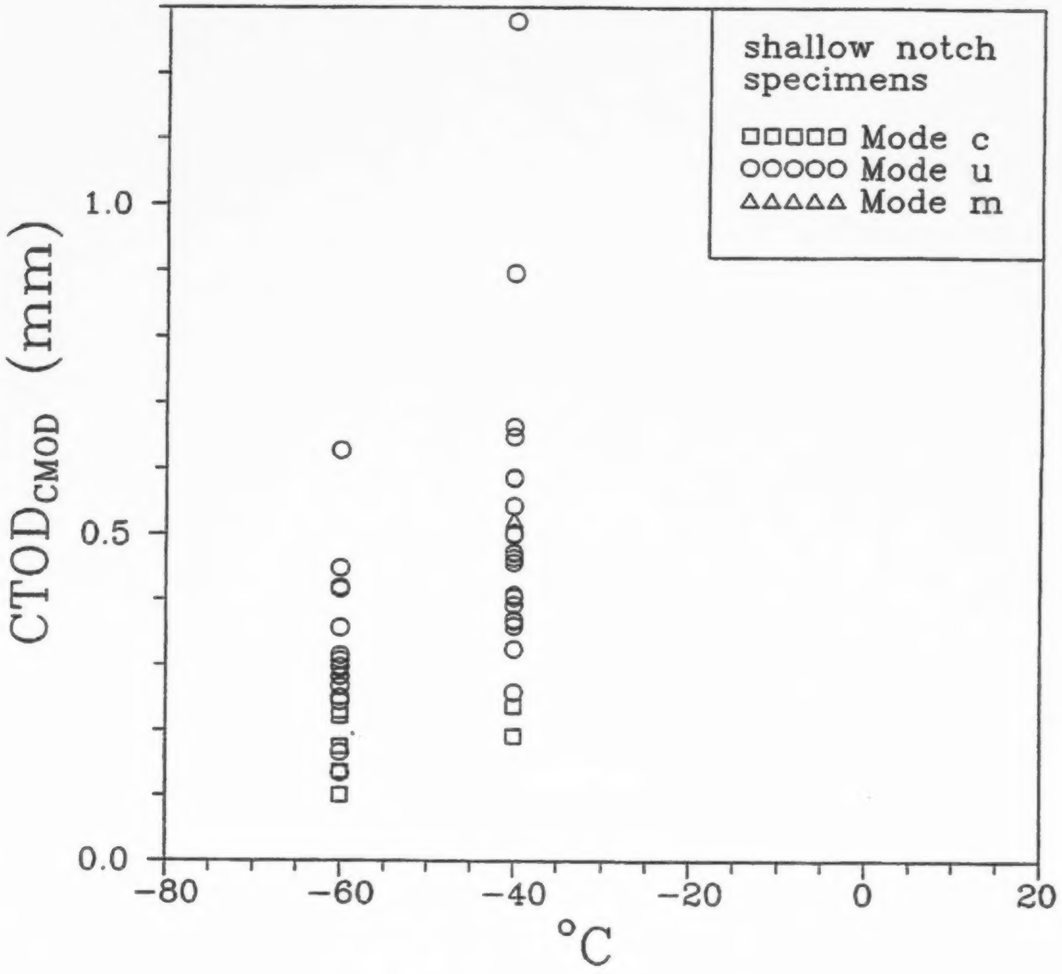

Figure 5: CTOD$_{CMOD}$ versus test temperature for shallow notch specimens.

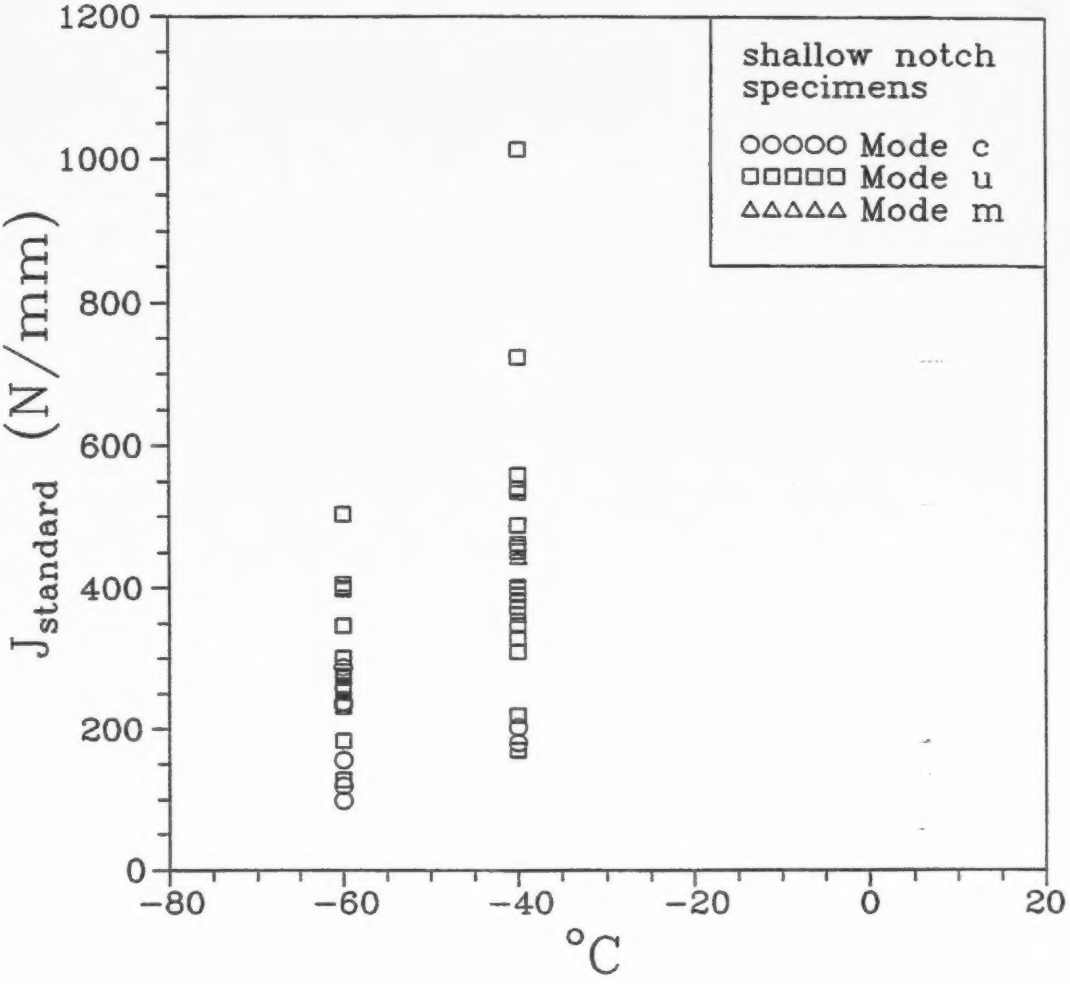

Figure 6 : $J_{standard}$ versus test temperature for shallow notch specimens.

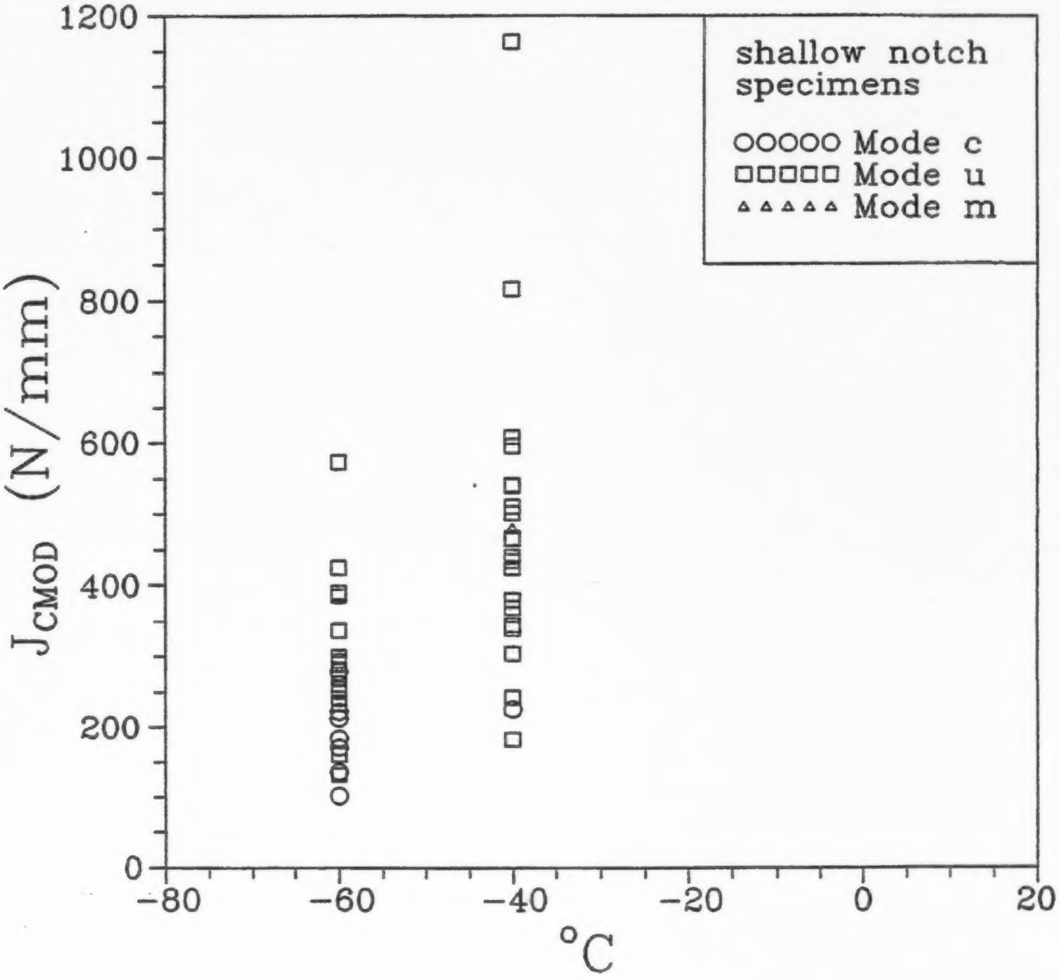

Figure 7: J_{CMOD} versus test temperature for shallow notch specimens.

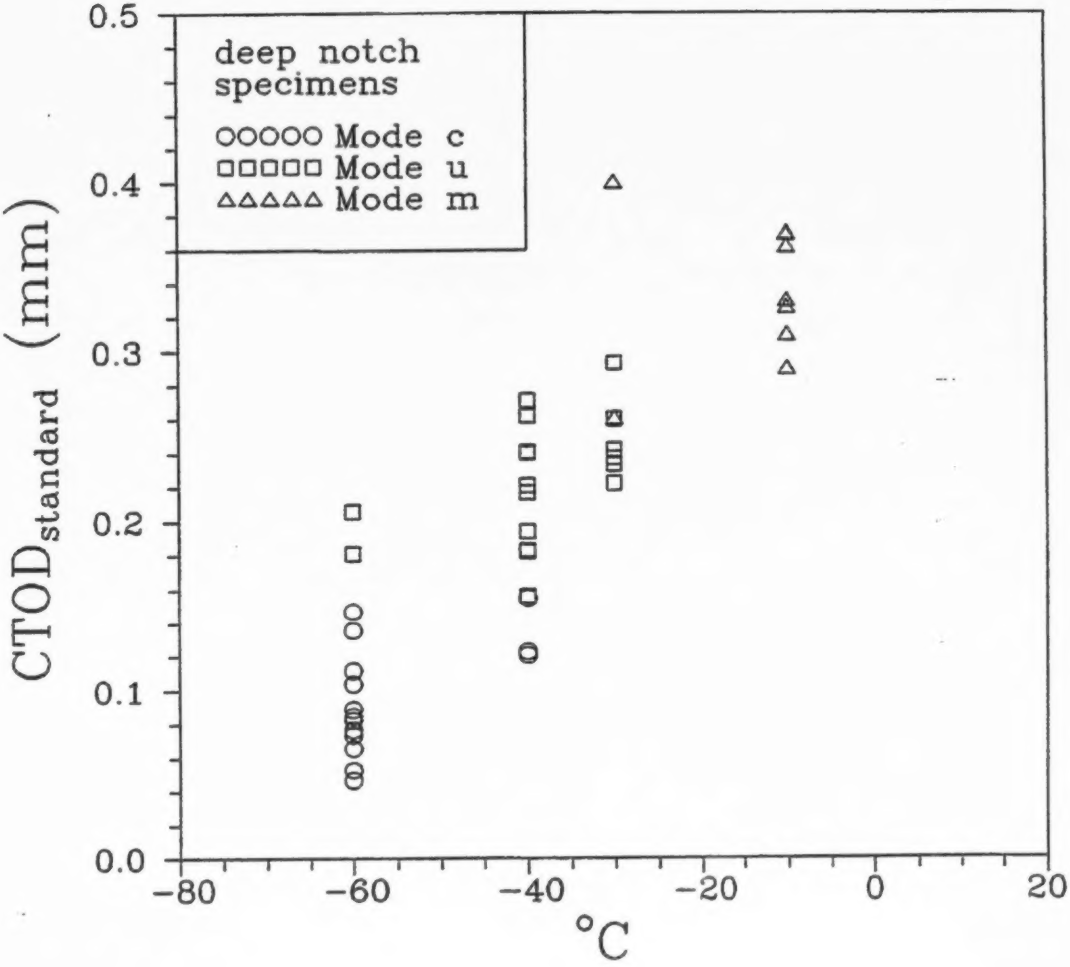

Figure 8 : CTOD$_{standard}$ versus test temperature for deep notch specimens.

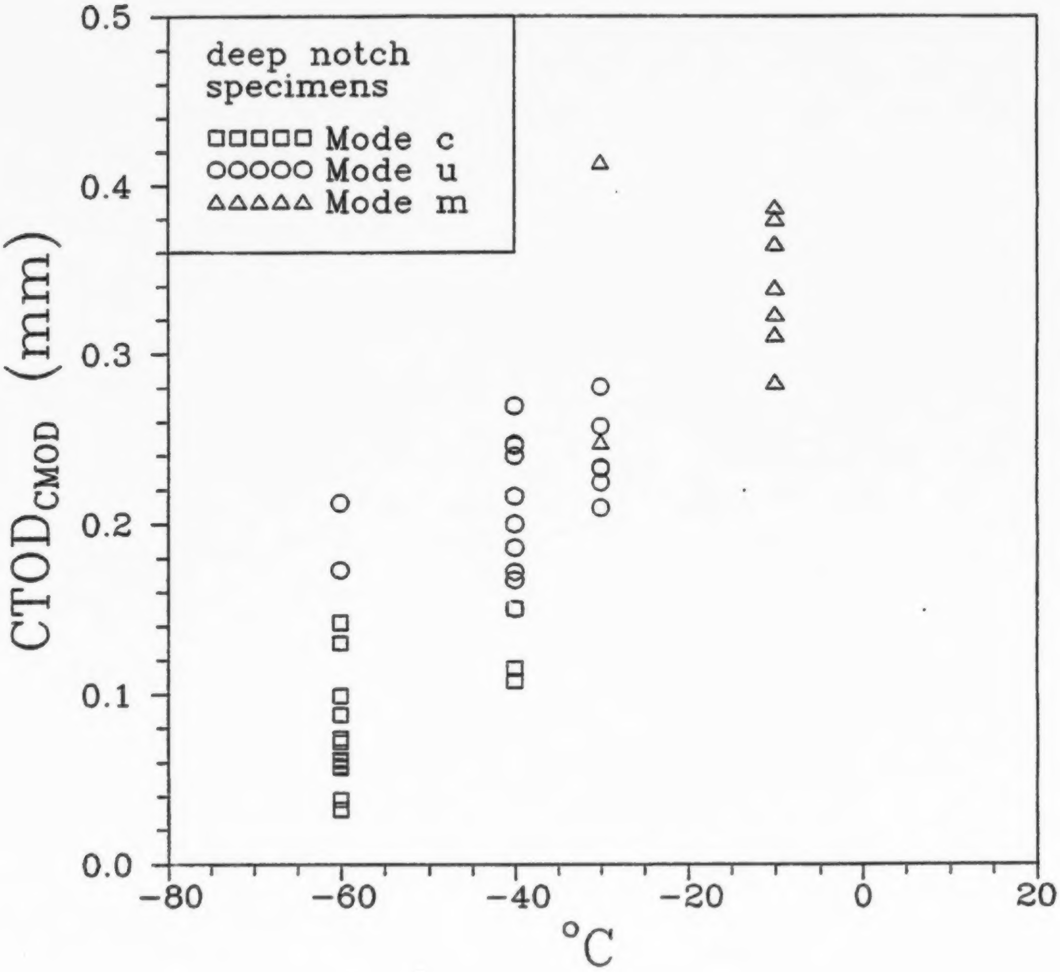

Figure 9 : CTOD$_{CMOD}$ versus test temperature for deep notch specimens.

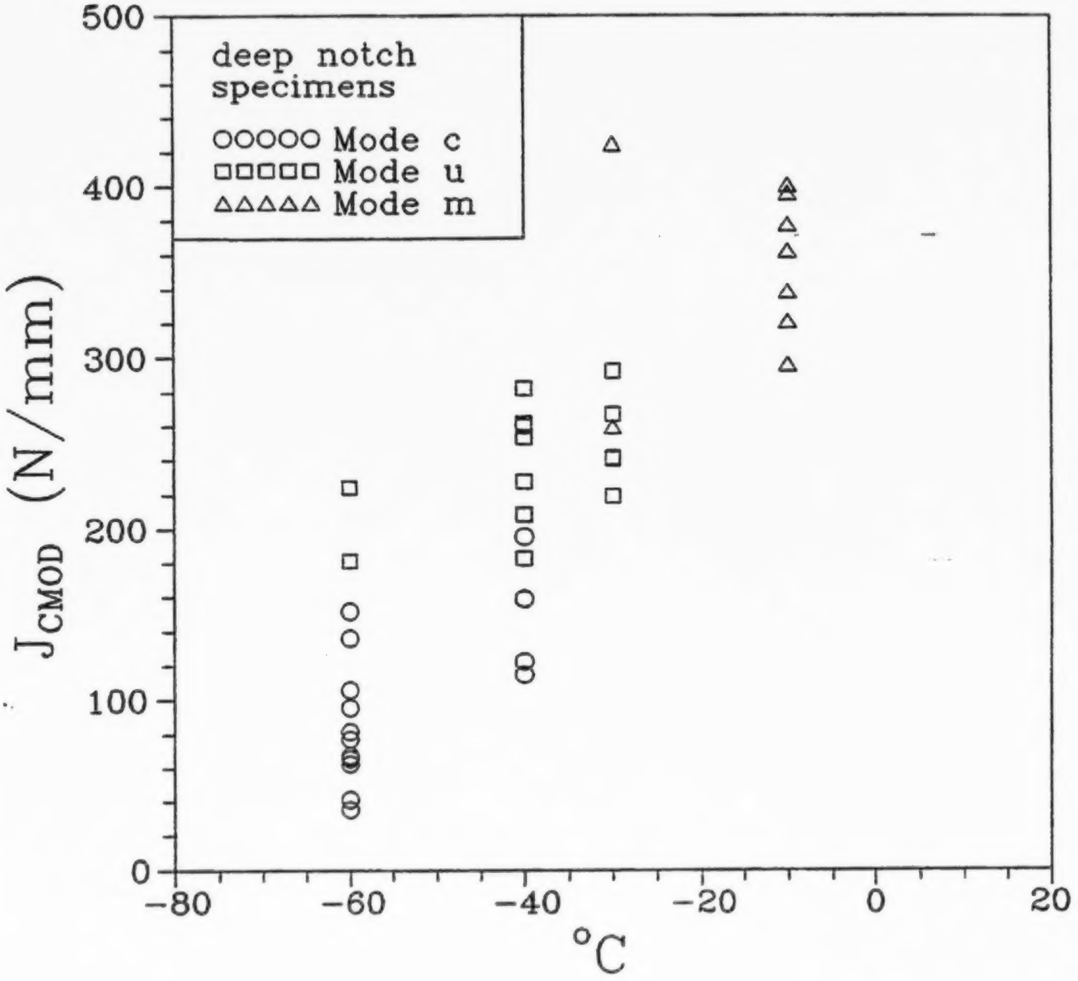

Figure 10: J_{CMOD} versus test temperature for deep notch specimens.

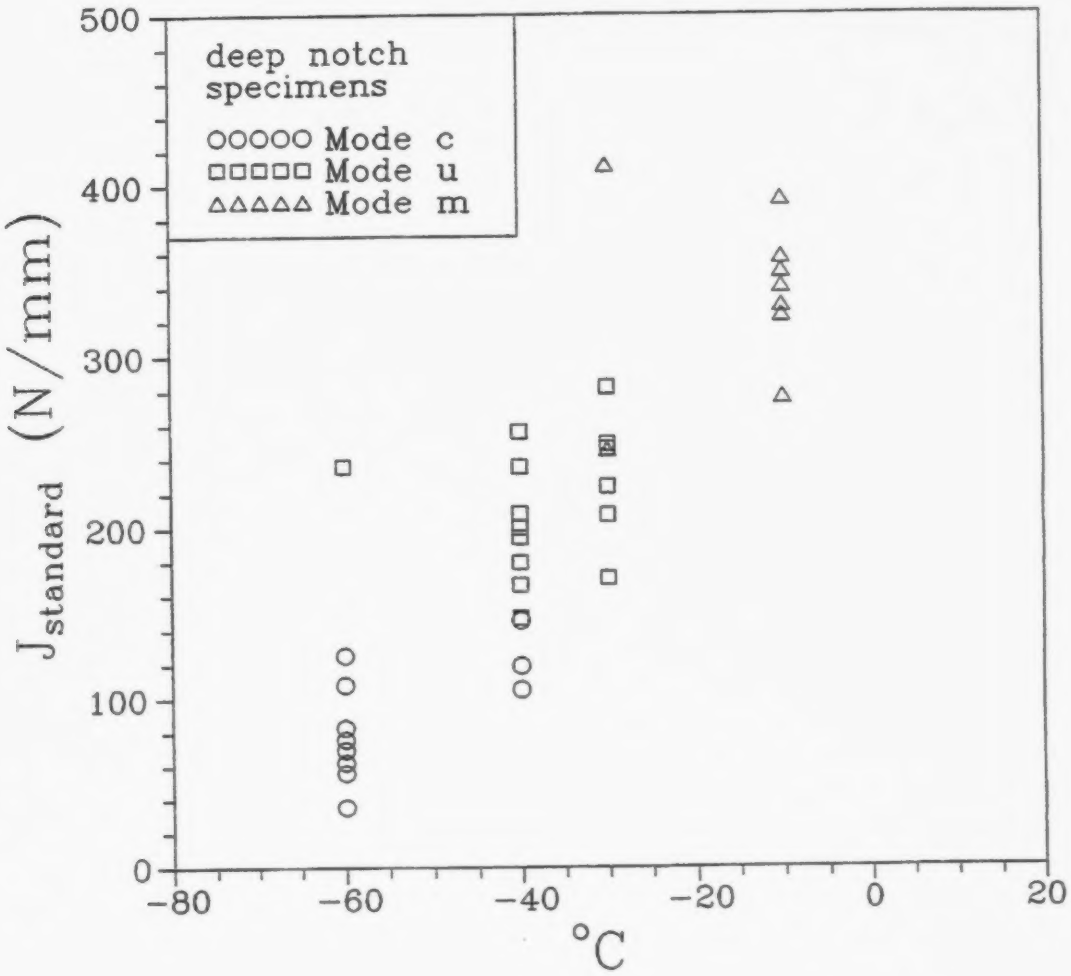

Figure 11: $J_{standard}$ versus test temperature for deep notch specimens.

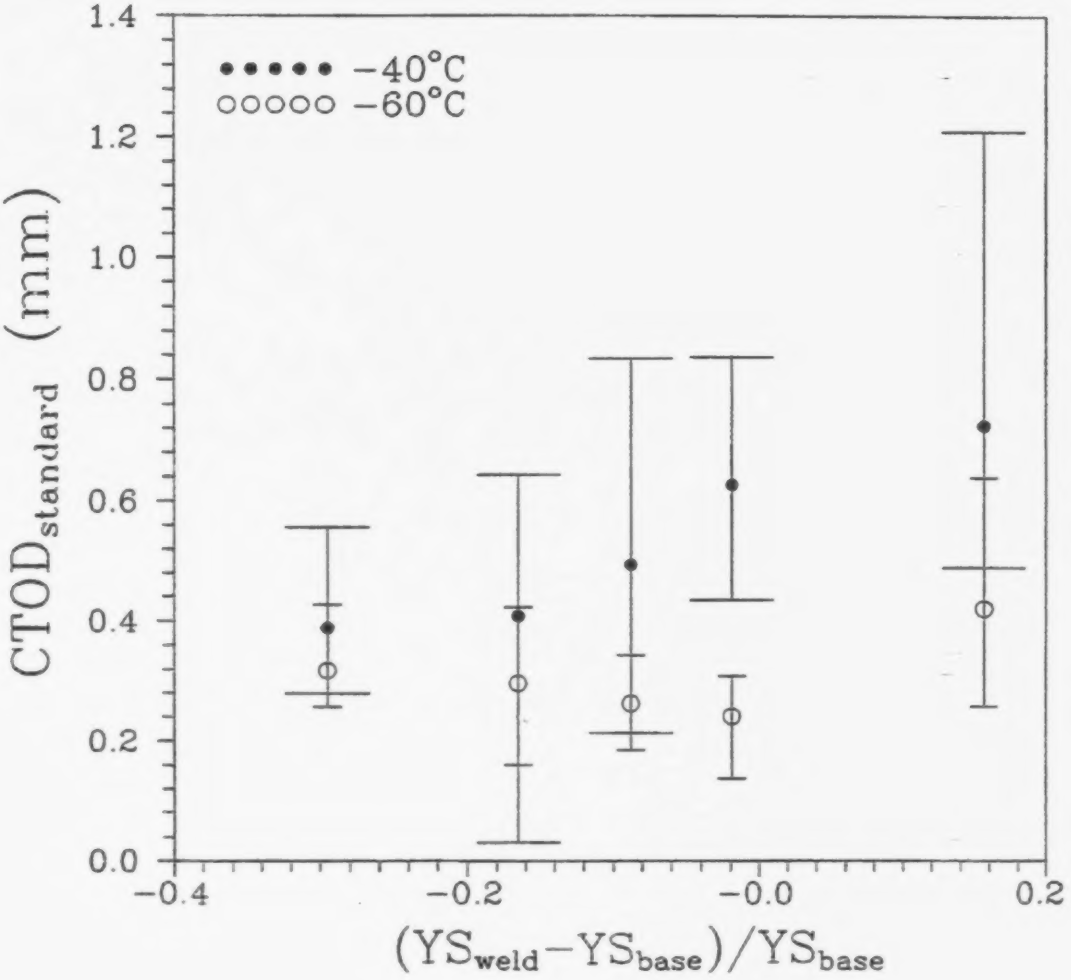

Figure 12: CTOD$_{standard}$ versus (YS$_{weld}$-YS$_{base}$)/YS$_{base}$ for shallow notch specimens tested at -40°C and -60°C.

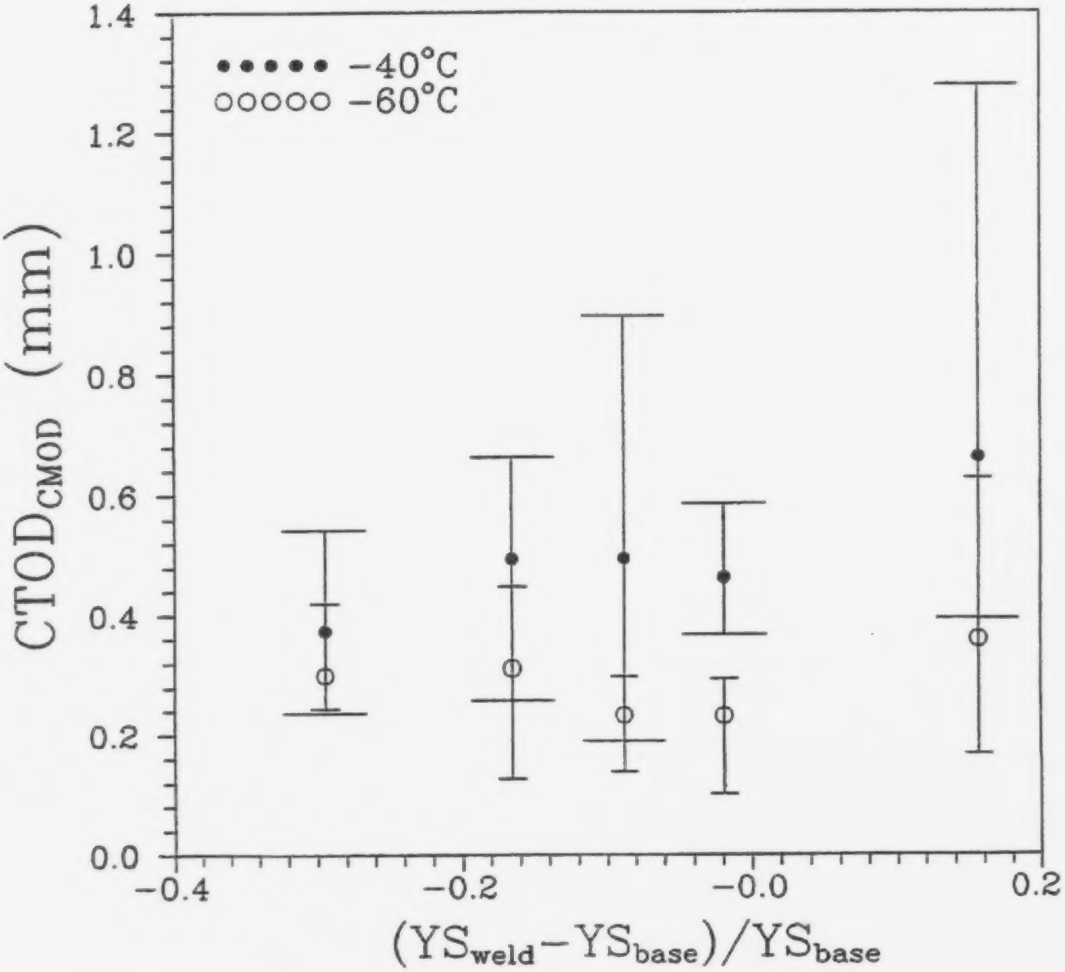

Figure 13: CTOD$_{CMOD}$ versus (YS$_{weld}$-YS$_{base}$)/YS$_{base}$ for shallow notch specimens tested at -40°C and -60°C.

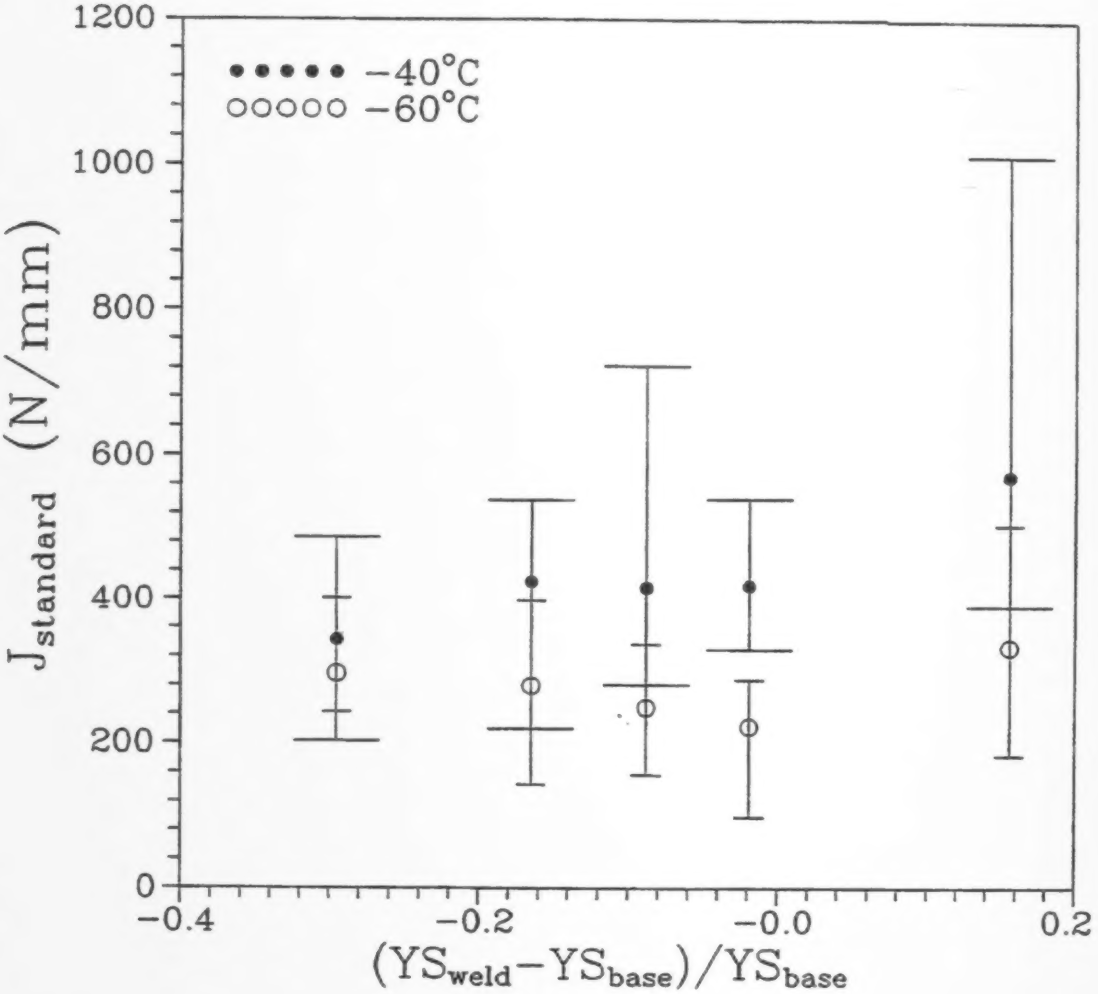

Figure 14: $J_{standard}$ versus $(YS_{weld}-YS_{base})/YS_{base}$ for shallow notch specimens tested at -40°C and -60°C.

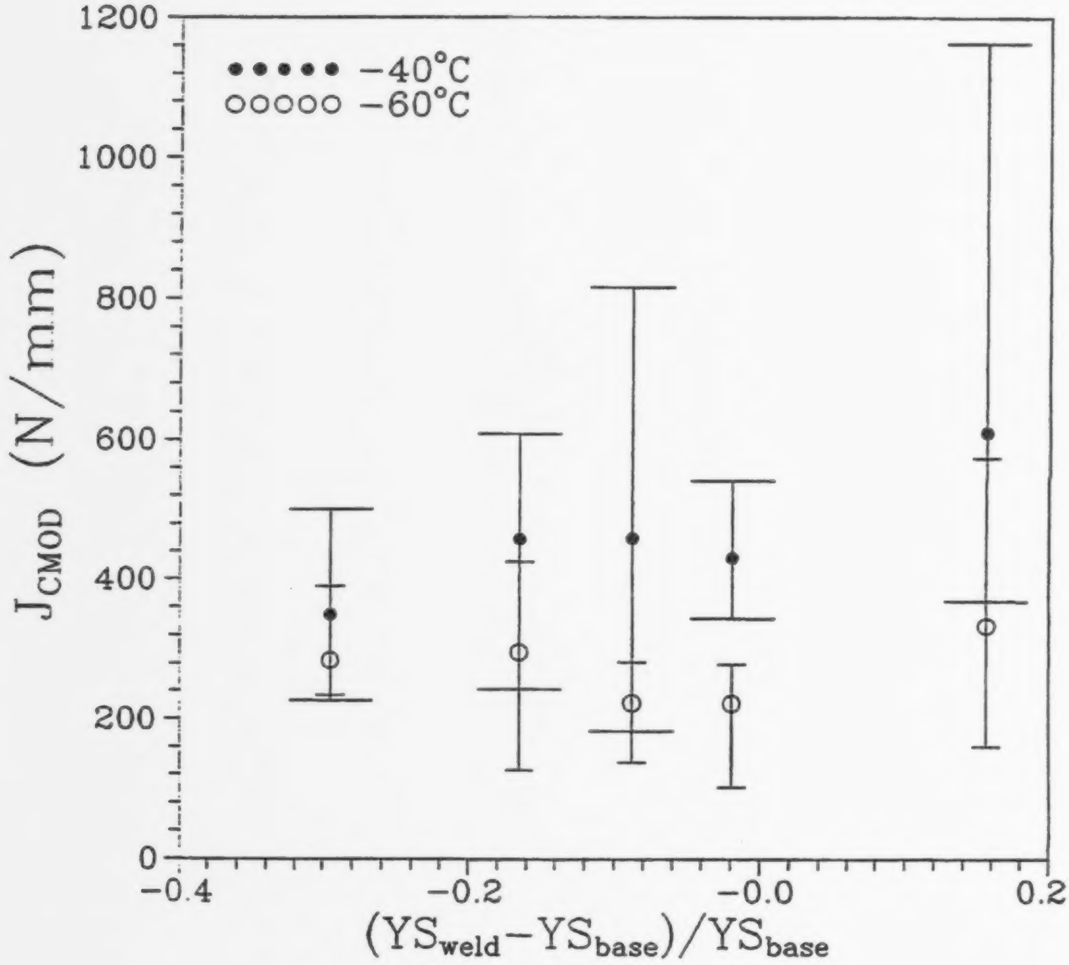

Figure 15: J_{CMOD} versus $(YS_{weld}-YS_{base})/YS_{base}$ for shallow notch specimens tested at -40°C and -60°C.

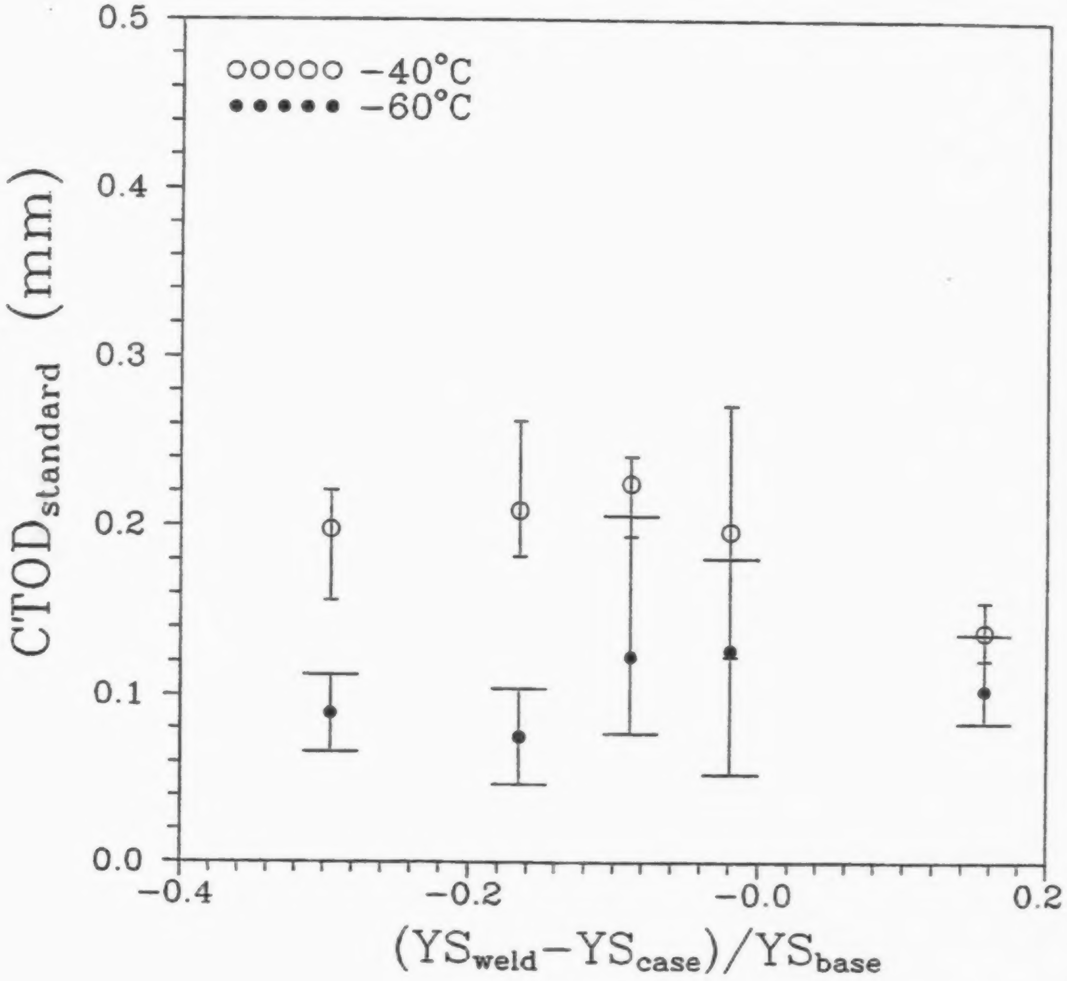

Figure 16: CTOD$_{standard}$ versus (YS$_{weld}$-YS$_{base}$)/YS$_{base}$ for deep notch specimens tested at -40°C and -60°C.

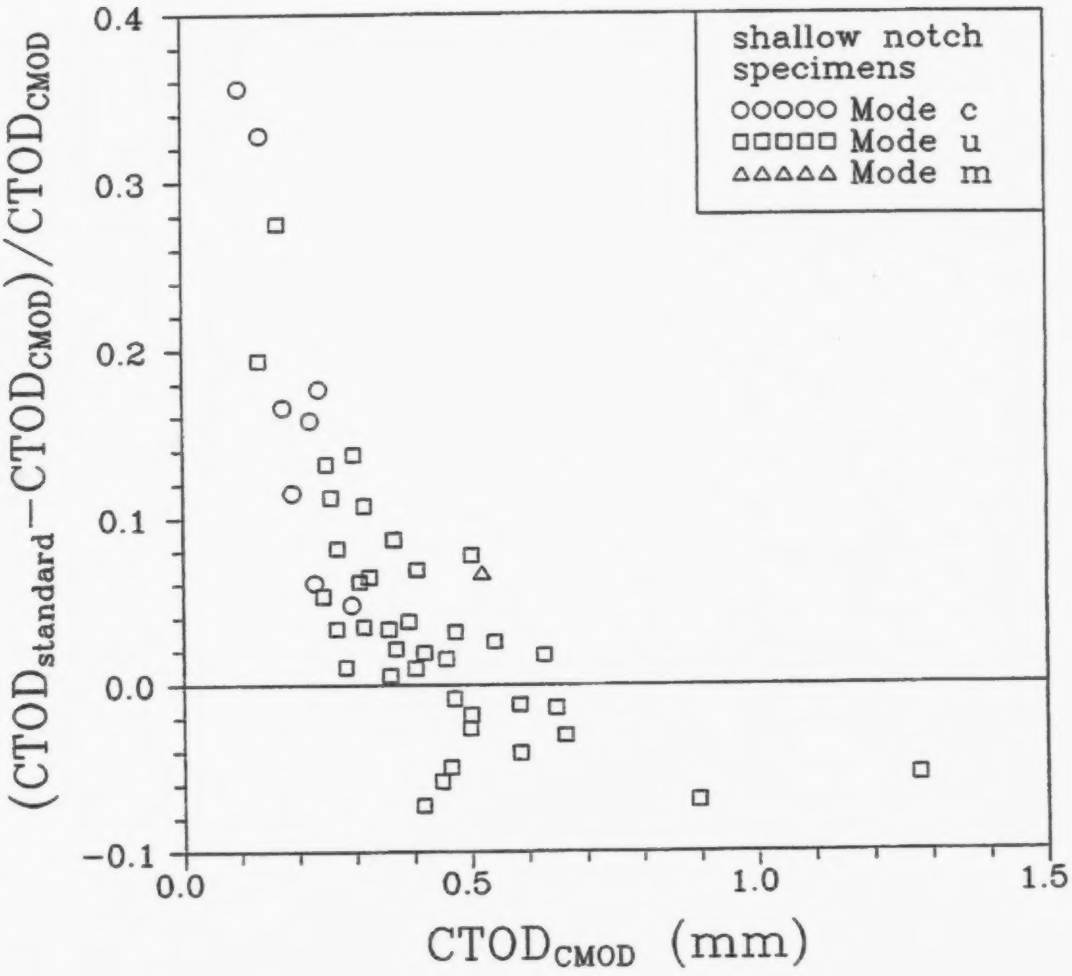

Figure 17: $(CTOD_{standard}-CTOD_{CMOD})/CTOD_{CMOD}$ versus $CTOD_{CMOD}$ for shallow notch specimens.

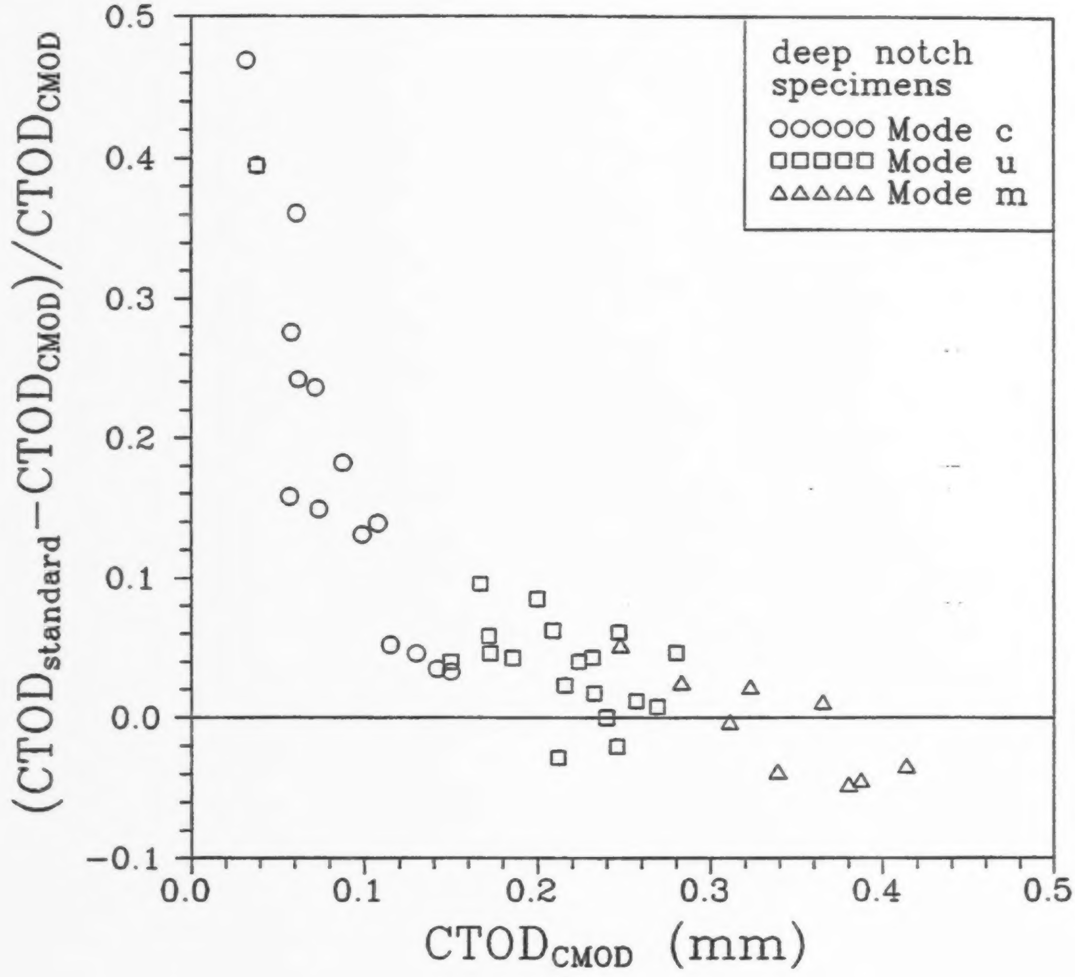

Figure 18: $(CTOD_{standard}-CTOD_{CMOD})/CTOD_{CMOD}$ versus $CTOD_{CMOD}$ for deep notch specimens.

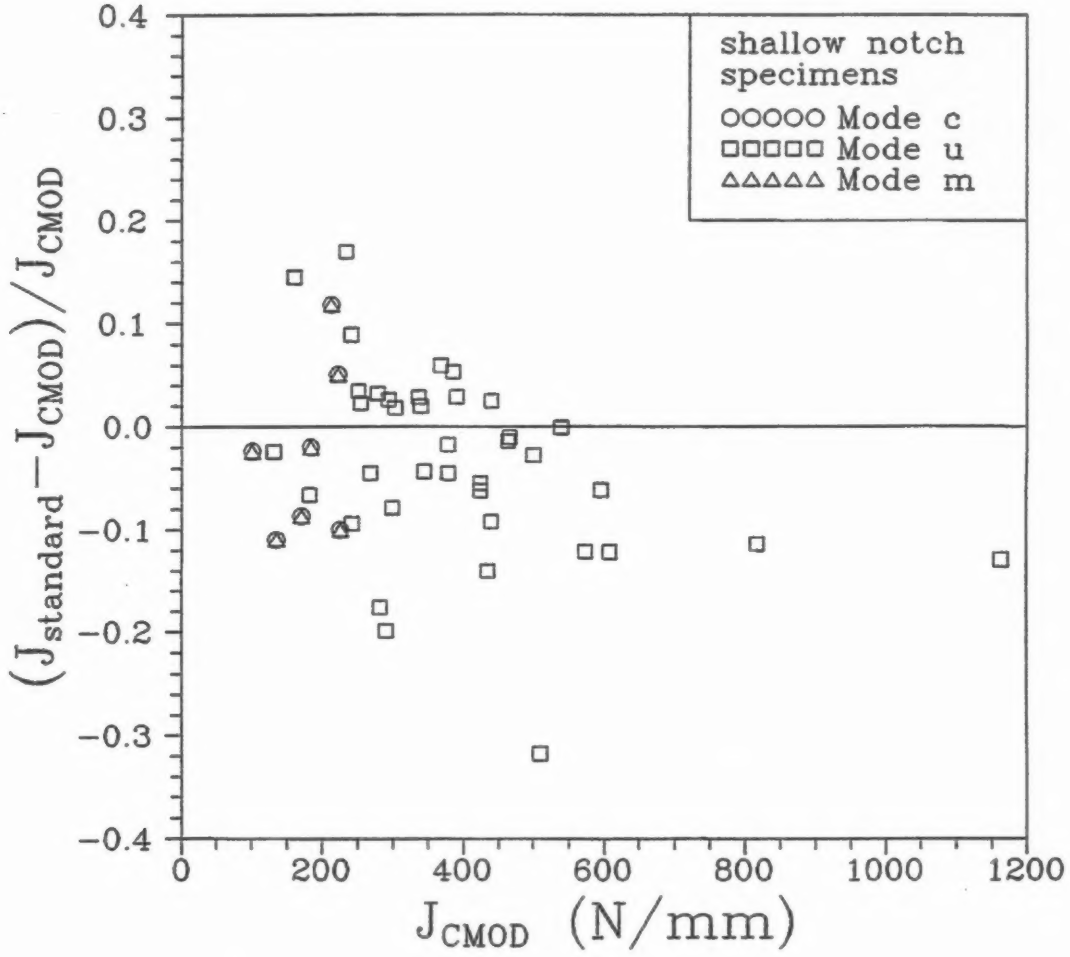

Figure 19 : $(J_{standard}-J_{CMOD})/J_{CMOD}$ versus J_{CMOD} for shallow notch specimens.

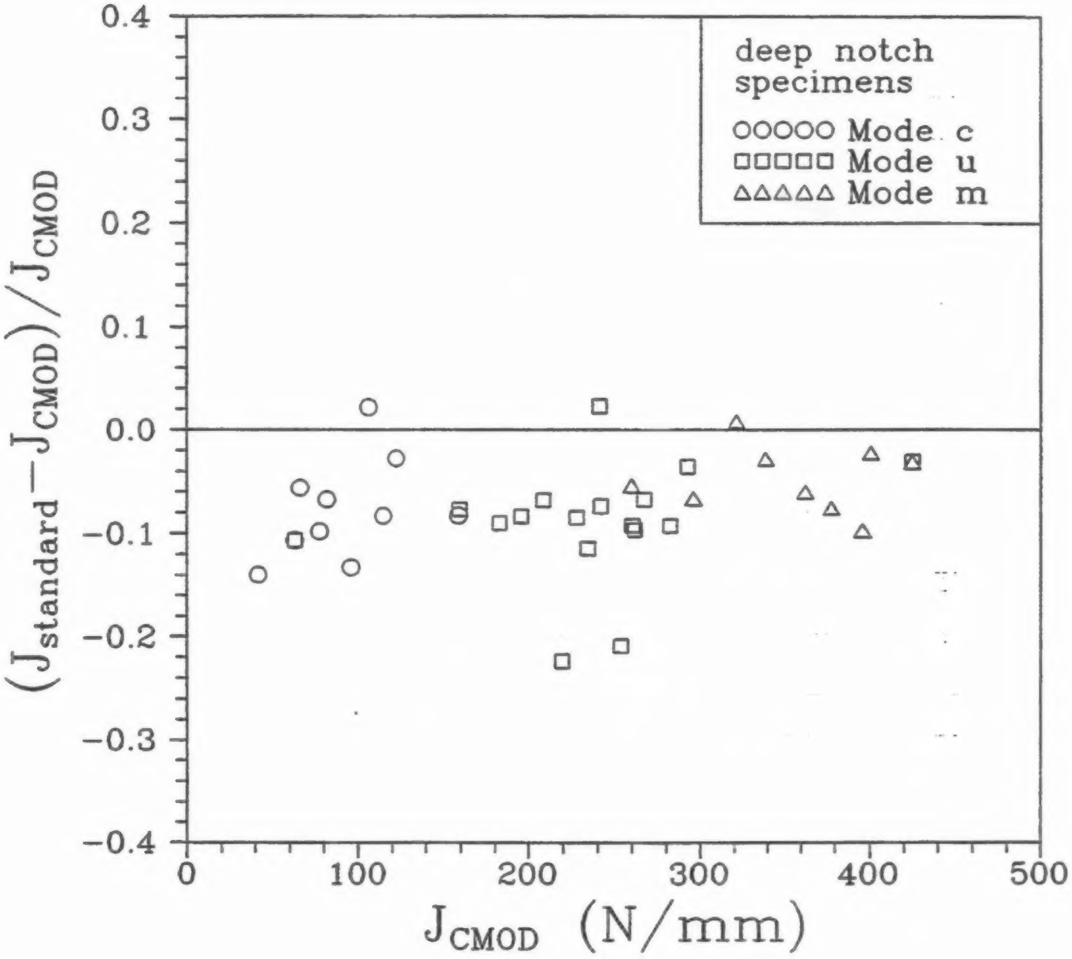

Figure 20: $(J_{standard}-J_{CMOD})/J_{CMOD}$ versus J_{CMOD} for deep notch specimens.

#510364 (21)

PRESERVATION AND PAINTING - MEETING THE ENVIRONMENTAL CHALLENGE

BY DAVID M ALLISON C ENG, MRINA, RCNC, DIRECTORATE OF NAVAL ARCHITECTURE, MINISTRY OF DEFENCE (UK) PROCUREMENT EXECUTIVE

INTRODUCTION

The twin objectives of reducing Unit Production Cost (UPC) and Life Cycle Cost (LCC) are of long standing within the Ministry of Defence (MOD). The reduction of LCCs has assumed particular importance within the Royal Navy as it is intertwined with the need to reduce the maintenance effort required from ships' companies and to increase availability. Thus, in the field of preservation and painting improved and longer lasting coatings are constantly sought. Some of these coatings primarily provide protection against corrosion while others provide operational attributes eg anti-fouling or non-skid properties.

The technological challenges have been increased by the increasing requirements of environmental and occupational hygiene legislation. The Ministry of Defence is, of course, committed to the protection of the environment and of its workforce. This paper will only address occupational hygiene matters where they coincide with environmental issues.

Taking a positive approach, the challenge has also presented the opportunity to increase the pace of modernisation in products, processes and working practices and to achieve rationalisation of products. MOD's role has been 'proactive' as MOD is, arguably, the major shipowner having painting undertaken in the UK, and is especially affected by the impact of environmental legislation on the painting process.

THE LEGISLATIVE FRAMEWORK

It will be helpful to list here the major pieces of legislation which have required responses from the MOD and from the Marine Painting Industry at large. These are:

1. The Control of Pollution Act (COPA) 1974.
2. The Food and Environment Protection Act 1985.
3. The Water Resources Act 1989.
4. The Eighth Amendment to the European Commission Marketing Directive 76/769/EEC, 21 December 1989.
5. The Environment Protection Act (EPA) 1990.

There is also a proposal from the Commission of the European Communities for a Council Directive concerning the placing of biocidal products on the market, COM(93)351 final SYN 465.

The various UK Acts are 'parents' to Regulations and Orders which implement the requirements perceived to be necessary for the achievement of the desired environmental objectives. The MOD has been fully engaged in discussions between the 'users' and the regulators in many cases. The objective is, of course, to maximise environmental protection at an affordable cost without crippling operational capability.

All the legislation listed has imposed restrictions upon the marketing and use of anti-fouling paints, principally, but not exclusively, upon those containing Triorganotin compounds. The EPA 1990 also allows for the regulation of Volatile Organic Compounds (VOCs) in paints and for controls upon painting processes. The principal regulations affecting painting and preservation processes are briefly set out at Annex 1.

ANTI-FOULING PAINTS

Under the Control of Pesticides Regulations (Food and Environment Protection Act 1985) the Advisory Committee on Pesticides (ACP) makes recommendations to Ministers concerning the continuing registration of biocidal products. As part of this process, the Health and Safety Executive (HSE) is conducting a progressive review of non-agricultural biocidal products. Of particular interest to MOD is the Review of the Environmental Effects of Triorganotin Compounds and the Review of Copper Compounds Used in Antifouling Products. These reviews are being conducted by the ACP's Environmental Panel, ad hoc meetings of which the author attends as an 'invited specialist'. Much of the reviews' data concerning the effects of shipyard operations upon the environment is provided by MOD from the results of its own environmental monitoring programmes.

The measures taken to contain shipyard effluents (the Royal Yards have lead the way in this) and the programmes to monitor the long-term levels of Tributytin (TBT) in the environs of the Royal Yards and to monitor the effects of individual shipyard operations have been extensively reported (references 1 and 2 are examples). The monitoring of shipyard operations now includes analysis for dissolved copper. Work to identify the most efficient and economical means of monitoring 'integrated' levels of copper in the marine aquatic environment is being undertaken for MOD by the Defence Research Agency (DRA) and CAPCIS (a University of Manchester Institute of Science and Technology company).

MOD's long-term TBT monitoring programme is designed to demonstrate the trends in levels of TBT in the environment through the use of bioaccumulation techniques. The levels of TBT measured in the flesh of the oyster spat used for this work can only be approximately related to average concentrations in the water. However, the author considers the technique to provide a valuable indication of trends and of the efficiency (or otherwise) of the package of measures taken to reduce levels of TBT in the marine environment. Summary reports for the levels of mean tissue TBT content measured in Crassostrea Gigas (C Gigas) in esturial sites 'remote' from Rosyth Royal Dockyard (RRD), Devonport Royal Dockyard and Her Majesty's Naval Base Portsmouth are shown in Figures 1, 2 and 3 respectively. Figures 4 and 5 give summary reports for levels in the non-tidal and tidal basins in RRD. General trends are encouraging.

However, the statutory Environmental Quality Standard (EQS) for TBT in controlled seawaters is 2 ng/litre. An approximate bioaccumulation factor of 10,000 can be used to estimate average levels. Thus, in 1993, the last year for which a complete set of data is available, levels in the Forth were in the order of 5 ng/litre.

The National Rivers Authority (NRA) and Her Majesty's Inspectorate of Pollution (HMIP) cannot grant consents for discharges which will cause the EQS to be exceeded. It is readily apparent that consents are difficult to obtain, even though the concept of a mixing zone in the vicinity of a shipyard could allow consents to be issued for certain discharges at a concentration of 200 ng/litre. However, controls exercised by HMIP will be site specific and the dispersion of discharges may need to be modelled. The controls imposed upon shipyard operations involving TBT-Copolymer anti-fouling paints (the only type of TBT anti-fouling products used by MOD for some years) result in additional costs: some selected figures relating to the wash down of the anti-fouling paint on the hull of a typical frigate are given in Table 1.

Treatment of the effluent and subsequent discharge is an option. MOD sponsored the development of a pilot plant with a capacity to treat 250 litres of effluent: a schematic layout of this plant is at Figure 6, while Table 2 shows results typically achieved during the trials. Flocculation and settling of the suspended solids removes significant quantities of TBT. The liquor treated in the plant was run-off water collected immediately beneath the hull, whereas the liquor to be treated following a typical shipyard operation could be expected to have a lower concentration, levels of 1.9×10^3 - 7.3×10^4 ng/litre having been measured in samples taken from dock culverts.

The contractor who developed the plant has been licensed to market the technology. No plant has yet been sold, although Devonport Management Ltd (the operators of Devonport Royal Dockyard) have purchased a plant from Sweden, and have obtained a discharge consent from the NRA.

While the greatest potential sources of TBT pollution are perceived to be shipyard operations (hydro-washing, coating removal, paint application), the EQS can be exceeded eg at Sullum Voe where there is significant shipping activity but no shipyards. Hence, as part of the overall package of measures to protect the environment there are moves to seek international agreement on maximum permissible leaching rates - a figure of 4 $\mu g/cm^2$/day is frequently quoted. If there is to be agreement on any figure, there must be an internationally recognised, repeatable and reproducible, laboratory method to determine leaching rates. The ASTM SMT 56B method is generally held to produce inconsistent results but is often advanced as, at least, the basis of a standard method of determination. As the availability of anti-fouling paints giving the performance required by the Royal Navy is considered to be essential, the rectitude of any regulatory procedure is of more than passing interest. Accordingly, the Defence Research Agency (DRA) has been tasked to conduct an extensive laboratory programme to evaluate the ASTM procedure and any modifications which will ensure repeatability. The HSE is sponsoring similar work which will be undertaken by the Ministry of Agriculture, Fisheries and Food and by the Plymouth Marine Laboratory. Thus, reproducibility will also be assessed. As considerable replication of samples and determinations are necessary to assure statistically acceptable results, the DRA's programme is not expected to complete before the end of 1995.

As responsible ship owners, MOD would wish to limit its use of TBT-Copolymer paints to those with the minimum TBT content and leaching rate consistent with assured performance. Although the paint companies' literature would suggest that for the speeds appropriate to Destroyers and Frigates ie 18 knots and upwards the 'slow polishers' should be used to reduce the leaching rate and to extend the life of the coating, the normal pattern of usage of our ships results in periods of "inactivity" during which faster polishing rates are required to achieve protection. These faster polishing rates are also considered to be beneficial in accelerating the removal of any fouling when the ship gets underway. In fact, the most reliable of the TBT-Copolymer paints used has a leaching rate of some 2.7 to 27 µg/cm^2/day at speeds from 1 to 20 knots (manufacturers figures).

TBT is an EC 'Red List' substance and a 'Schedule 1' substance under the EPA 1990. Copper, principally in the form of Cuprous Oxide, is generally considered to be the most immediately practical alternative to TBT as an anti-fouling biocide. It is, however, a List 2 substance under Council Directive 76/464 EEC and both the North Sea Conference of Ministers 1990 and the Paris Commission for the Prevention of Pollution from Land Based Sources seek the reduction of discharges of, inter alia, copper into the aquatic environment. The EQS for copper in the marine environment is 5 µg/litre (dissolved copper). The use of copper as an anti-fouling biocide is now the subject of a review by the HSE.

Copper, principally in the form of cuprous oxide, is present as a biocide in all anti-fouling paints used on ships of the Royal Navy - this is readily apparent from an examination of Figure 7, which lists the biocides present in a number of anti-fouling paints either in use or approved for use. Thus, the change in copper burden in the environment resulting from any moves to eliminate the use of TBT should not be great. For example, a "five year" TBT copolymer scheme from one manufacturer will, on a typical frigate's underwater area of 2,300 m^2, have a mass of some 1400 kg of CU_2O. A three year "tin free" system from the same manufacturer will contain about 930 kg CU_2O. The leaching rates quoted for Copper by the manufacturer are broadly similar. Ignoring differences in lengths of refit arising from changes in docking cycles, it will be apparent that a change from TBT-Copolymer paints to Erodible "tin free" paints should not result in a significant increase in the input of copper to the marine environment. The relative importance of anti-fouling paint as a source of copper pollution has yet to be established, but is thought to be minor.

A modification of ASTM SMT56B is being considered for determination of leach rates for copper. Quite apart from refinements - the method was developed by one manufacturer to suit his particular requirements and laboratory facilities - required to enable the method to be advanced as a standard, determination of the leaching rates of organic biocides need to be developed. Once analytical techniques which will detect and measure these organic biocides have been found, experimental techniques will need to be assessed. Techniques which produce concentrations of TBT or copper amenable to accurate analysis might not give the same results with organic biocides.

Initial Assessment of Anti-Fouling Coatings

Tin-free erodables are, in one major respect, a retrograde step in technology. The TBT-Methacrylate "back bone" in TBT-Copolymer paints hydrolyses reliably and predictably, releasing biocide at a rate dependent, inter alia, upon the ships speed. Most, if not all, "tin free" erodables use a soluble resin (natural or synthetic) technology. Reliable erosion is, in some cases, questionable or non-existent. Hence, laboratory methods to assess erosion and distribution of biocides through the paint film, are being sought. Anti-fouling performance will be assessed on the exposure raft.

The DRA and CAPCIS have been giving consideration to the techniques needed to examine the paint films. To date, the DRA has undertaken defect analysis of a failed "tin free" coating and analysis of a successful (4 years life) "tin free" coating using various microscopic analysis techniques. Scanning Electron Microscopy (SEM) was used to map individual coats of paint, while qualitative elemental analysis was undertaken using Energy-Dispersive X-Ray microanalysis (EDX) to determine the composition of the material in each of the coats of paint. Analysis of the cross-section of the coating using X-Ray Photoelectron Spectroscopy (XPS/ESCA) determined the presence and chemical state of elements - organic biocide was 'tracked' by the sulphur molecule - and X-Ray linescanning and mapping was carried out to plot the spatial distribution of selected elements across the whole paint scheme.

It is planned that a large number of replicates of anti-fouling coatings should be 'rotored' in sea-water for 3 months. Some samples will be examined by micro-analytical techniques to determine erosion, depth of leached layer, and distribution of biocides, while others will be placed on the exposure raft to assess subsequent anti-fouling performance. The scope of this programme is currently being revised - early ambitions exceeded the capacity of the anti-fouling exposure raft - and analytical options assessed.

VOLATILE ORGANIC COMPOUNDS

The UNECE Protocol setting a target of cutting emissions of volatile organic compounds (VOCs) by 30% from 1988 figures by the year 1999 was ratified by the UK in June 1994. Under the EPA 1990, a number of Secretary of State's Process Guidance Notes setting targets for VOCs in products and placing controls on processes have been issued, setting out the contributions to be made by sections of industry. Process Guidance Note PG6/23 sets requirements and procedures for, inter alia, manufacturing industry.

Shipbuilding is held to be 'manufacturing' whereas ship repair and conversion are not. Strictly speaking, therefore, the Royal Navy's maintenance operations could be claimed to be outwith the regulations. However, quite apart from it being difficult to envisage this situation continuing in perpetuity, it is difficult to envisage a situation where one range of products is used at new build and a further range of very different products is used for maintenance. Moreover, the Expert Panel on Air Quality Standards has recommended an Ozone standard which would require a 75-80% cut in VOC emissions rather than the current 30% commitment. Accordingly, the Directorate of Naval Architecture (DNA) has established a target for 85% of coatings specified to be 1998 VOC compliant by the end of 1995.

Table 3 records the principal VOC definitions for 1996 and 1998 compliance. It can be seen that the 1998 figures have been altered from time to time following discussions between the British Coating Federation (BCF) and the Department of the Environment (DOE). The most recent proposals are still the subject of discussion, and DNA's objective remains a VOC level of 250 gm/litre for primers and 420 gm/litre for 'top coats' - the term 'top coat' is taken to include anti-fouling paints.

In fact, in some areas, such as ballast tanks and reactor compartment finishes, products with a VOC content of less than 250 gm/litre have already been introduced and are being used in the later boats of the VANGUARD Class.

A typical ballast tank coating has a declared VOC content of 175 gm/litre and may be applied at temperatures down to 10°C. These products are intended for application by airless spray, and are not so easy to use in situations requiring brush application.

Weatherwork finishing paint and interior finishing paint are high usage products and reduction of VOCs in these products will make a major contribution to the reduction of airborne pollution. Water-based products are under evaluation for these applications, and a further aim is to achieve commonality between weatherwork, surface ship interior and submarine interior systems. Hence, suitable products are evaluated for all three applications, requiring that the paints meet requirements for fire characteristics and submarine atmospheric control. Not all water based products are suitable for all three applications, however. The submarine interior application is of considerable importance: the principal solvent in the two pack epoxy currently used is 1-Methoxypropan -2-ol (1, 2, 4 - Trimethylbenzene, Xylene, and a mixture of isomers are also present) which has an Occupational Exposure Limit (OEL) of 300 ppm for a 15 minute (average) exposure and an OEL of 100 ppm for an 8 hour time weighted average. These OELs are very difficult to achieve in a submarine interior when paint is applied at a practical rate. In service maintenance is virtually impossible.

One acrylic product has been in use in Royal Fleet Auxiliaries for some years, and is being evaluated as a weatherwork finish, although its comparatively low sheen (approximately 50 units using an Erichsen 60° gloss meter) could be a drawback. This product has also been applied to 2 compartments in HMS GRAFTON and is about to be tried on various areas of the internals of SSBN 07.

By no means all problems are solved by a change to water-based products, of course. Although the ventilation requirement for occupational hygiene reasons is greatly mitigated, air flow is required to enable water to evolve from the curing coating at an optimum rate. Obviously, humidity is critical but air flow is considered to be more important than temperature alone. Surface cleanliness is more critical than for the application of the existing alkyd products.

The museum ship HMS PLYMOUTH has been used a test vehicle for the application of water based weatherwork finishes. This ship is moored at Wallasey, near the mouth of the River Mersey, and the initial application trials were conducted in March 1994. Approximately 10% of the trial area allocated for each product was cleaned to an ST3 standard using power tools. Remaining areas were detergent washed. As the ship was downwind of an unloading berth, it proved necessary to wash the surfaces with fresh water daily to remove surface contamination. The weather was as might have been expected for the time of year - the air temperature varied from 6-15.5°C, the steel temperature from 5.5-15°C, and the Relative Humidity from 55-94%.

At high humidity and with little air flow, coatings took up to 1½ hours to become touch dry. Rain within ½ hour of application proved to have a detrimental effect. Neither brush nor roller application could achieve the required dry film thicknesses for the water based primers, and some rust staining was evident. It was concluded that, for weatherwork, a low VOC primer would be preferable. Not all the finishing coats had reasonable brushing properties: some coatings were, of course, at an earlier stage of development than others.

Levels of gloss achieved were lower than those achieved on initial application of the current silicone alkyd weatherwork finish. However, measurements of colour and gloss some 4 months later indicated good gloss retention. The four products applied in the Autumn of 1994 showed higher initial levels of gloss. Some selected gloss levels from the PLYMOUTH trials are shown in Table 4, together with some selected figures for silicone alkyd paint on the superstructure of HMS NORFOLK: these latter readings were taken before and after a deployment to the South Atlantic.

A full-scale trial of water-based finish in an operational ship is under consideration. An earlier trial in HMS COVENTRY was of limited success only, the constraints of surface cleanliness and weather conditions not being fully appreciated at that time.

VOC compliant weather and flight deck coatings are under initial evaluation in HMS BRISTOL, a harbour training ship. Certain products show promise, and it should soon be possible to proceed to an initial trial in an operational ship.

One paint evaluation programme of particular interest is that to find a VOC compliant replacement for the chlorinated rubber finish used in the reactor compartments of nuclear submarines for the past 30 years or more. VOC compliance was merely one of a lengthy list of requirements, but this requirement, together with severe limitations on trace elements and certain pigments, limited the number of candidate coatings offered for evaluation. The most severe test requirement was the evaluation of the paints in a "Design Basis Fault (DBF) Simulation" test - also referred to as the Loss of Coolant (LOCA) test. The terms were undertaken to a commercial standard for the Nuclear Power Generating Industry as this was (relatively) conveniently available. The test profile is shown in Figure 7. Only one candidate paint passed this test - it was, in fact, a ballast tank coating already in use, overcoated with a water-based epoxy to improve the decontamination characteristics.

The most scientifically challenging requirement was the determination of the thermal conductivity of the coating, especially as it was required to be determined at 200°C, in a steam atmosphere at 5 bar pressure. There is no standard method for determining the thermal conductivity of thin films, and the technique found to be available does not use a steam atmosphere. The technique used was the determination of thermal diffusivity using the heat pulse or laser flash technique. The thermal conductivity is calculated from the relationship

$$k = \alpha \rho C_p$$

where k is the thermal conductivity, α is the thermal diffusivity, ρ is the density and Cp is the specific heat at constant pressure. The specific heat is determined using Differential Scanning Calorimetry (DCS).

Determination of thermal conductivity in air has been determined and the thermal conductivity calculated. A test rig is being modified to measure thermal diffusivity in a steam atmosphere at 200°C and 1 bar pressure. Measurements will also be made in argon, a more usual-and cheaper-method, to establish whether or not the steam atmosphere affects the results obtained.

POWDER COATINGS

This environmentally friendly process cannot -yet- be used to coat a ship! The use of Fire Retarded Polyester powder coatings for component parts is an option now incorporated in the appropriate Naval Engineering Standard. Epoxy powder coated components are often to be found in equipments procured from industry.

SURFACE PREPARATION

Coating removal and surface preparation present further environmental challenges, and merit a paper in themselves. Suffice it to say that MOD, in close co-operation with industry, is constantly assessing the cost effectiveness and environmental credentials of all the techniques which are evolving.

SUMMARY

Meeting the environmental challenge to the painting process in a cost effective manner while continuing to deliver the performance required of the coatings of warships and submarines has provided, and will continue to provide, a stimulus to the development of new products and processes.

REFERENCES

1. D M ALLISON AND L J SAWYER, OCEANS '87, HALIFAX, NOVA SCOTIA, VOLUME 4, pp 1392-1397.

2. D ALLISON, N GUEST, AND J F D STOTT, MONITORING AND CONTROL OF DOCKYARD ACTIVITIES INVOLVING TBI-CONTAINING PAINTS, 3RD International Organotin Symposium, Monaco, April 1990.

Any views expressed are those of the author and do not necessarily represent those of the Ministry of Defence or HM Government.

© British Crown Copyright 1995/MOD: Published with the permission of the Controller of the Britannic Majesty's Stationery Office.

ANNEX 1 - THE LEGISLATIVE FRAMEWORK

THE CONTROL OF POLLUTION ACT 1974

In 1986, regulations made under COPA restricted the retail sale of TOT paints to copolymer paints containing less than 7.5% tin in the dry film and free association paints containing less than 2.5% tin in the dry film.

In 1987, regulations made under COPA banned the retail sale of all anti-fouling paints containing TOTs and the sale of TOT anti-fouling treatments for aquaculture applications.

THE FOOD AND ENVIRONMENT PROTECTION ACT 1985

The Control of Pesticide Regulations (COPR) were made under this Act in 1986. On 1 July 1997, under the aegis of COPR, the full control on sale, supply, storage, advertisement and restrictions of use of TOTs to vessels over 25 metres in length came into operation. Anti-fouling products, even "non-toxic" low surface energy products, must be registered with the HSE.

THE WATER RESOURCES ACT 1989

Section 85 (Offence of Polluting Waters) states that "a person contravenes this section if he causes or knowingly permits any poisonous, noxious or polluting matter or any solid waste matter to enter any controlled waters." Controlled waters include dockyard basins and water within 3 miles of the shoreline.

Discharges require consents to be issued by the NRA.

THE EIGHTH AMENDMENT TO THE EC MARKETING DIRECTIVE, 76/769/EEC, 21 DECEMBER 1989

The Eigth Amendment introduced an EC wide ban on the application of TOT anti-fouling paints to vessels less than 25 metres in length.

THE ENVIRONMENT PROTECTION ACT 1990

EPA 1990 is wide ranging and requires, inter alia, the keeping of records of substances, and quantities thereof, discharged. Processes using Schedule 1 substances are subject to Integrated Pollution Control (IPC) by Her Majesty's Inspectorate of Pollution (HMIP). TBT is a Schedule 1 substance.

HMIP are due to issue, following discussion of draft versions, a "Chief Inspectors Guidance to Inspectors, Environment Protection Act 1990, Process Guidance Note IPR 6/1, The Application or Removal of Tributyltin or Triphenyltin Coatings." This will require operators to apply to HMIP for authorisation - a distinction is made between "existing processes" and "new processes". IPC is exercised on all aspects of shipyard operations involving TOT coatings, including VOC emissions and waste disposal. The aim in upgrading existing processes is to attain the appropriate control parameters by, generally, no later than 31 January 2000. The operator will be required to implement a compliance monitoring programme.

Waste Management Regulations, imposing a Duty of Care, have been introduced.

Secretary of State's Guidance Note PG6/23(92) introduces controls on VOC emissions for most painting processes (some, eg road vehicle finishing, are covered by separate Guidance Notes). Only users of 5 tonnes or more solvent or 20 tonnes or more of paint per annum are affected (at present). Basically, to comply with the requirements users will have to demonstrate that solvent emissions are less than 50 mg Carbon per cubic metre of air or use compliant coatings.

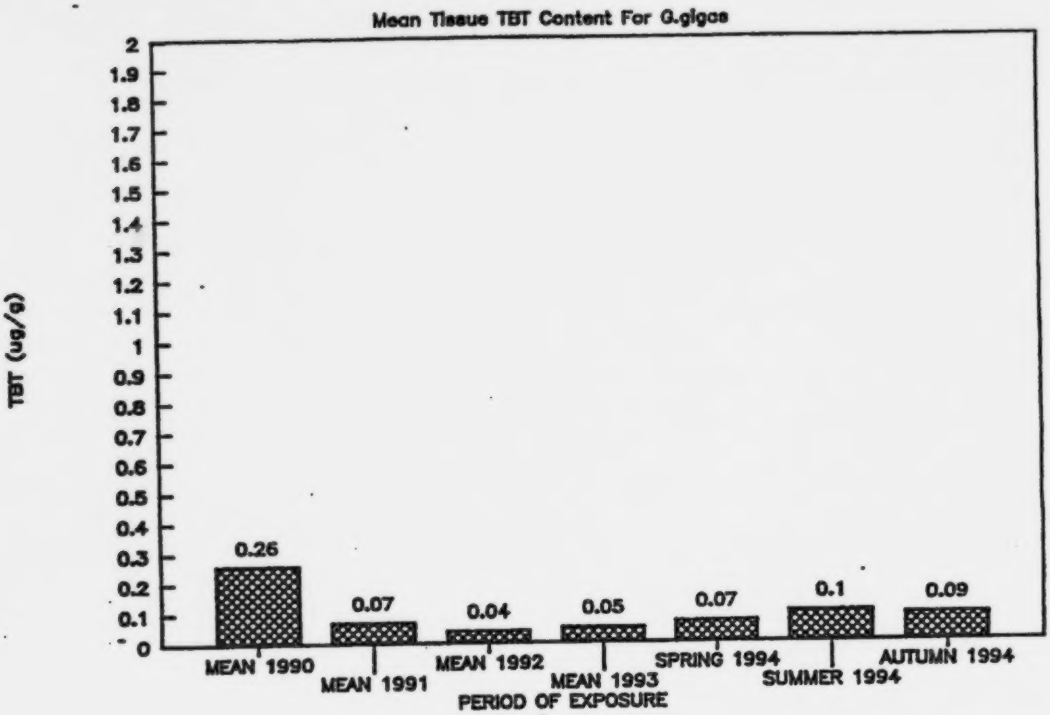

FIGURE 1

Rosyth Royal Dockyard - Integrated TBT Levels, Esturial Areas

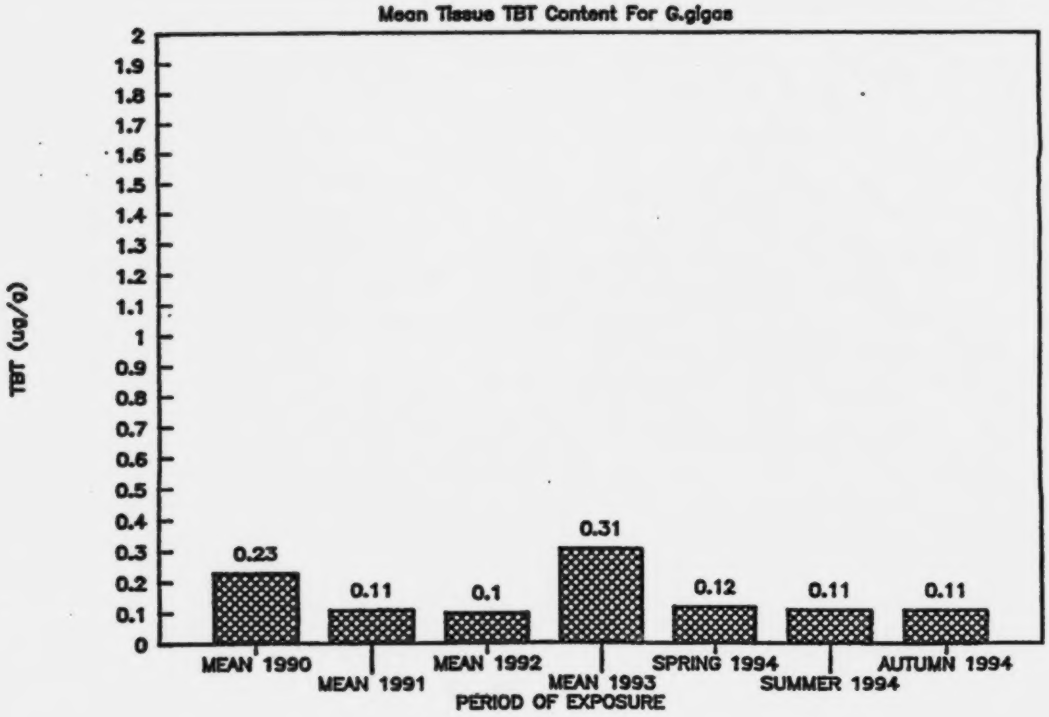

FIGURE 2

Devonport Royal Dockyard - Integrated TBT Levels, Esturial Areas

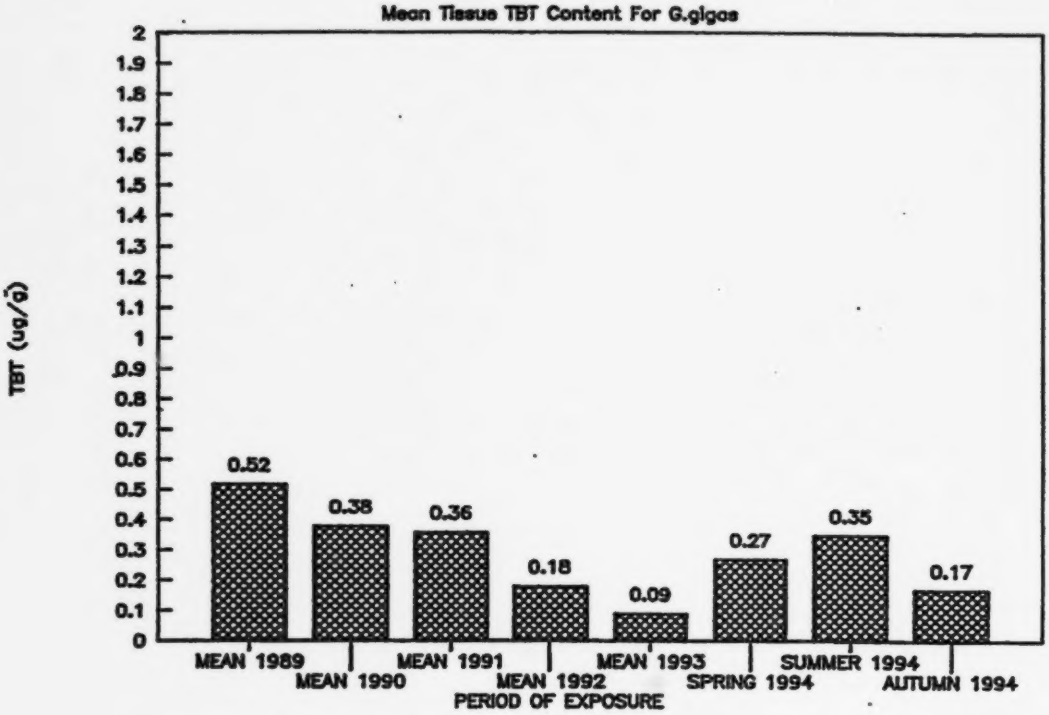

FIGURE 3

HM Naval Base Portsmouth - Integrated TBT Levels, Portsmouth Harbour

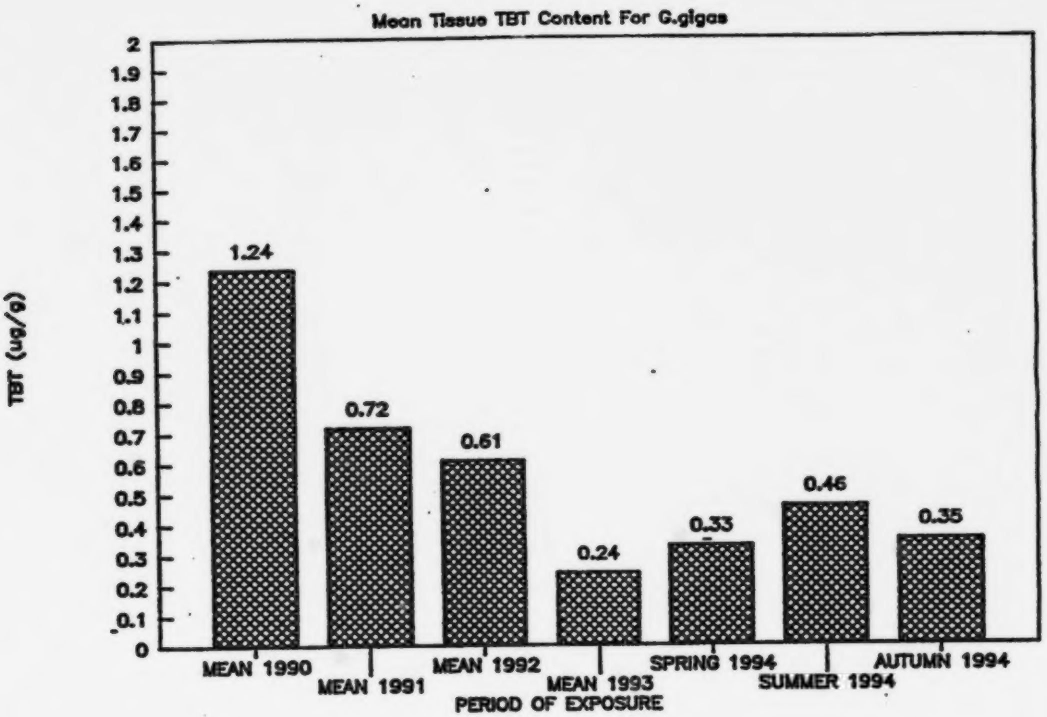

FIGURE 4

Rosyth Royal Dockyard - Integrated TBT Levels, Dockyard Basin

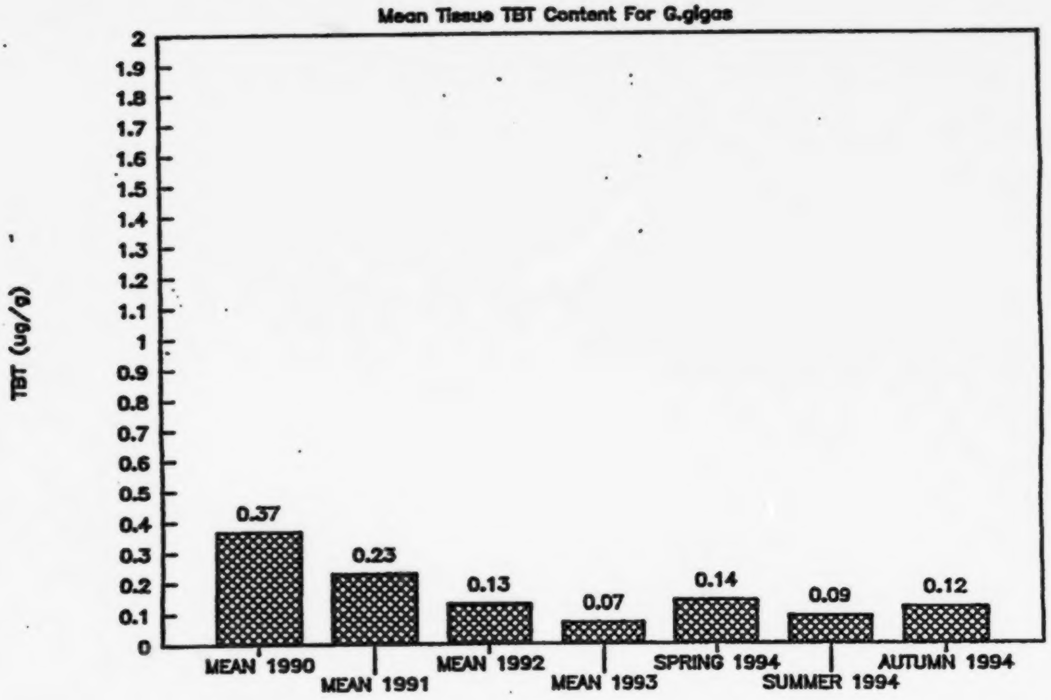

FIGURE 5

Rosyth Royal Dockyard [illegible]

DOCK PREPARATIONS FOR CONTAINMENT	2.5 MANWEEKS
SENTRIES, ETC, DURING WASHDOWN	2.5 MANWEEKS
FRESH WATER USED	60,000-75,000 litres
DAILY HIRE OF 20 TONNE ROAD TANKER	£1000-£3000 Approximately
NOTE: Actual cost of road tankers is dependent upon the distance of the disposal site from the yard, and hence the number of trips per day, or days per trip, involved.	

TABLE 1

SOME ADDITIONAL COSTS INVOLVED IN CONTAINING THE EFFLUENT FROM THE WASH-DOWN OF THE HULL OF A TYPICAL DESTROYER OR FRIGATE

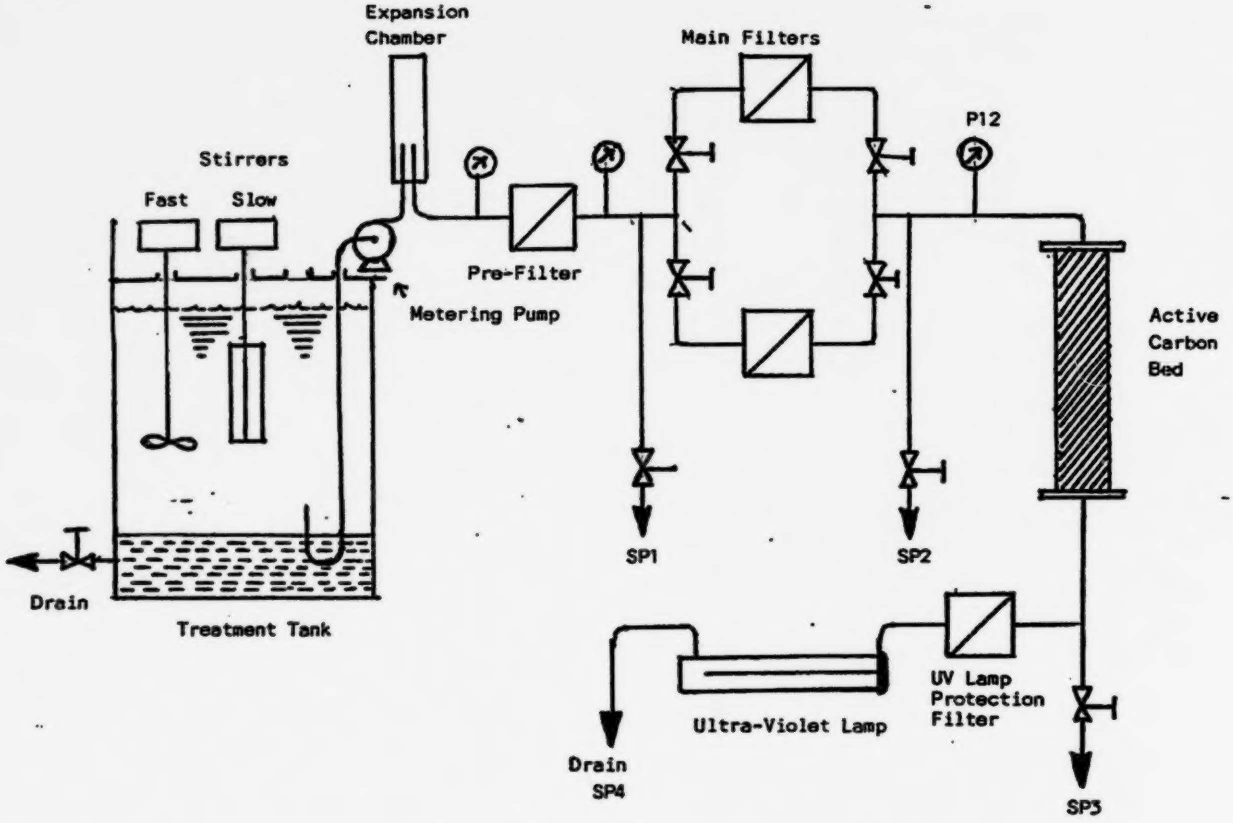
Expansion Chamber
Main Filters
P12
Stirrers
Fast
Slow
Pre-Filter
Metering Pump
Active Carbon Bed
SP1
SP2
Drain
Treatment Tank
UV Lamp Protection Filter
Ultra-Violet Lamp
Drain SP4
SP3

FIGURE 6

Pilot Scale TBT Removal Plant - Schematic Arrangement

SAMPLE POINT	TOTAL TBT ng/ltr	SUSPENDED SOLIDS PPM
RAW	2420500	380
SP1	1044300	0.8
SP4	49	3.6

TABLE 2

Typical Results from Pilot Scale Plant

FIGURE 7 SOME ANTI-FOULING PRODUCTS AND THEIR CONSTITUENT BIOCIDES

ANTI-FOULING PRODUCT BIOCIDE	SEAMATE HB66	SEAVICTOR 50	SEAGUARDIAN	NAUTIC H1 7690	OLYMPIC-H1 7661	GRASSLINE M396	GRASSLINE ABL M349	ENVOY TF400 & TF500	SEAFLO Z-100LE -HS	TFA 10	INTERSMOOTH HISOL BFA 954/956	INTERSMOOTH BGA 530
CUPROUS OXIDE	●	●	●	●	●	●	●	●	●	●	●	●
ZINC OXIDE	●	●						●		●		
4,5-DICHLORO-2-N-OCTYL -4-ISOTHIAZOLIN-3-ONE		●										
2,3,5,6-TETRACHLORO-4-(METHYL SULPHONYL) PYRIDINE						●		●				
2,4,5,6-TETRA CHLORO ISOPHTHALONITRILE										●		
DICHLOROPHENYL DIMETHYLUREA										●		●
2-METHYLTHIO-4-TERTIARY-BUTYLAMINO-6-CYCLOPROPYLAMINO-5-TRIAZINE					●			●				
CUPROUS THIOCYANATE								●				
TRIBUTYLTIN ACRYLATE							●					
TRIBUTYLTIN OXIDE	●			●			●		●		●	
TRIBUTYLTIN METHACRYLATE	●			●					●		●	
ZINEB											●	

PRODUCT TYPE	VOC COMPLIANCE LEVEL, gm/litre				
	INITIAL PROPOSALS		1ST REVISION	2ND REVISION	MARCH 1995 PROPOSALS
	1996	1998	1998	1998	1998
METAL AIR DRYING COATING	400	250			
SHOP/HOLDING PRIMER				780	780
PRIMER			250	250	
TOPCOAT			400	420	
UNDERWATER ANTI-CORROSIVE, ONE PACK					560
UNDERWATER ANTI-CORROSIVE, TWO PACK					450
ANTI-FOULING TIE COATS					550
ANTI-FOULING TBT-COPOLYMER					450
ANTI-FOULING TIN FREE POLISHING					400
NON POLISHING TRADITIONAL ONE PACK ANTI-FOULING					450
BALLAST TANK COATINGS					400
BALLAST TANK COATINGS, WINTER WORKABLE					450
CARGO TANK COATINGS					475
POTABLE WATER TANK COATINGS*					350*
ONE PACK ABOVE WATER PRIMERS					520
ONE PACK ABOVE WATER FINISHES					560
HIGH TEMPERATURE RESISTANT COATINGS					600
TWO PACK ABOVE WATER PRIMERS					350
TWO PACK ABOVE WATER FINISHES					420
* LIMIT REPRESENTS AVERAGE FOR PRIMER (250) + TOP COAT (420) SYSTEM					

TABLE 3

PROPOSALS FOR VOC LEVELS IN COMPLIANT COATINGS

SHIP AND PRODUCT	60° GLOSS LEVEL			
	NOV 93	JUN 94	OCT 94	DEC 94
HMS PLYMOUTH				
LEAST GLOSSY MATERIAL		13.8	13.2	
ACRYLIC MATERIAL, STARBOARD		15.9	18.2	
ACRYLIC MATERIAL, PORT		49.5	52.0	
SILICONE ALKYD, LAUNDRY		39.5	#	
SILICONE ALKYD, BOMB ROOM		60.4	60.4	
WATER BASED SILICONE ALKYD		NA	50.0	
WB PAINT, SPRAYED		NA	80.2	
WB PAINT, BRUSHED		NA	47.6	
WATER BASED EPOXY		NA	67.4	
NOTE: # OVER-PAINTED				
HMS NORFOLK				
SILICONE ALKYD, LOWEST INITIAL GLOSS	34.0			29.1
SILICONE ALKYD, HIGHEST INITIAL GLOSS	78.0			58.0
SILICONE ALKYD, LEAST CHANGE	52.1			52.0

TABLE 4

GLOSS LEVELS MEASURED IN HMS PLYMOUTH AND HMS NORFOLK

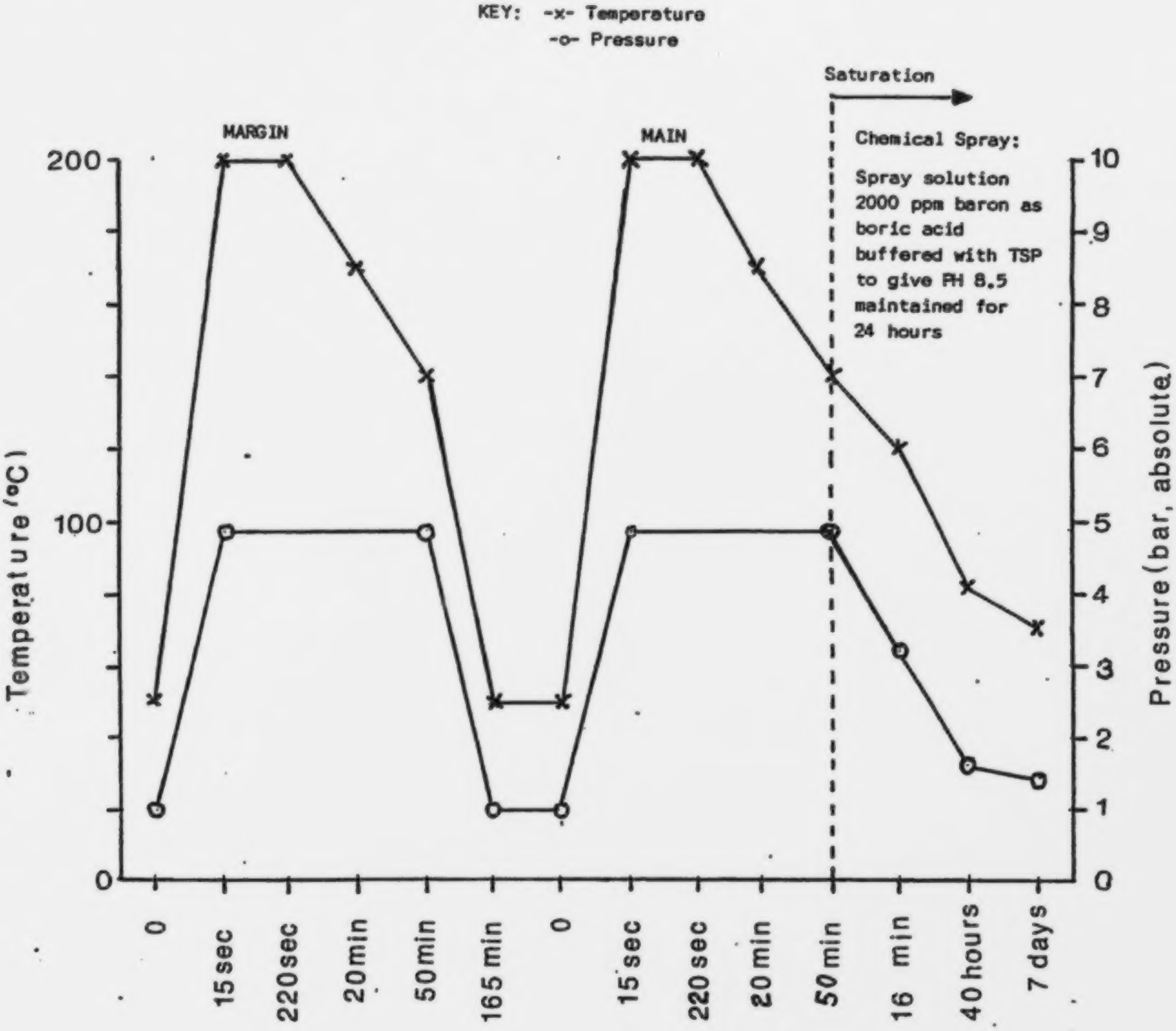

Chemical Spray:

Spray solution 2000 ppm baron as boric acid buffered with TSP to give PH 8.5 maintained for 24 hours

FIGURE 7

Temperature/Pressure Profile for Design Fault Basis (DBF) Environment Simulation

#510365

(22)

Evaluation of Noise Reduction Coatings

by

C.A. Hamm[1] and J.P. Szabo[2]

[1]Guigné International Ltd
82 St.Thomas Line, Paradise, Newfoundland, Canada, AIL 1C1

[2]Defence Research Establishment Atlantic
Dockyard Laboratory, FMO Halifax, Halifax, Nova Scotia, Canada, B3K 2X0

ABSTRACT

The use of exterior hull tiles can have a significant impact on the noise signature of surface ships and submarines as demonstrated by trial on HMCS ANNAPOLIS. At this point, DND cannot compare the effectiveness of various commercial noise reduction tiles, except through large scale tests. This paper describes current work on developing small scale evaluation tests for noise reduction coatings. To partially simulate the radiation of acoustic energy from hulls, mechanically driven 2' x 2' x 3/8" steel plates were fluid-loaded on one side. Two water tanks of significantly different volume ($5.8 m^3$ and $80 m^3$) were used to see what role reverberation plays in the data interpretation. Radiation from non-tiled plates was measured and compared to the radiation from plates with damping tiles. Tiles of several thicknesses were used. Noise reduction spectra were also compared for plates of different shape to separate the effects of flexural damping and velocity reduction (decoupling).

Objective

- Develop a small scale evaluation test for underwater noise reduction materials.
  - damping and decoupling materials
  - free field versus reverberent field
  - analysis framework (size, shape)

Motivation

- Noise reduction materials are currently used on CF ships (interior and exterior). Can often be used to solve noise problems.
- Direct experimental data needed for cases where modelling is not possible:
    - no material data available
    - complex structure (voids)
- Small scale tests are more rapid, less expensive than full scale tests.

Definition

- A noise reduction coating reduces the radiated noise signature of a naval vessel when applied to the exterior or interior of the ship hull.
- The coating may affect the radiated noise by
  - decoupling (exterior only)
  - mass damping
  - free layer damping
  - constrained layer damping
  - changes in radiation efficiency

Decoupling

Surface velocity reduction due to soft coating. Ignoring wave effects:

$$\mathrm{VR} = 20\log\left|\frac{v_1}{v_2}\right|$$

$$\frac{v_1}{v_2} \approx 1 + \frac{i\omega\rho_o c_o d_2}{L_2}$$

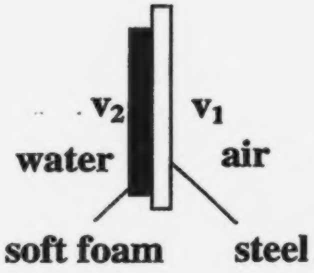
v₂
v₁
water
air
soft foam
steel

where L_2 is dialational modulus of coating.

Damping

- Consider single DOF system:

$$\mathbf{v} = \frac{\mathbf{F_{in}}}{\mathbf{i\omega m} + \frac{\bar{\mathbf{k}}}{\mathbf{i\omega}}(\mathbf{1} + \mathbf{i\eta})}$$

Coating will alter substrate velocity through changes in

•mass	m
•system loss factor	η

Free Layer Damping

- System loss factor η :

$$\eta = \frac{3\eta_2 \overline{E}_2 d_2}{\overline{E}_1 d_1}\left(1 + \frac{d_2}{d_1}\right)^2$$

Substrate = 1 Coating = 2

η_2 = coating loss factor

E_1, E_2 = substrate, coating Young's moduli

d_1,d_2 = substrate, coating thicknesses

Radiation Efficiency

Acoustic power radiated, W_{ac}, depends on radiation effieciency, σ,

$$W_{ac} = \rho_o c_o A \left\langle v^2 \right\rangle \sigma$$

$\left\langle v^2 \right\rangle$ is mean squared velocity over plate

- Coating may alter σ

Materials

- Substrate: Steel, 3/8" x 2' x 2'
- Coatings:
  - Decoupling: Foamed Neoprene

    Lossy material, energy conversion to heat
  - Damping: Isodamp EAR C-1002

    Impedance mismatch, energy reflection

Experimental Design

- **Acoustical Considerations**

  - free-field conditions hard to achieve at low frequencies

  - reverberant tank tests necessary (2 tank sizes)

  - far-field measurements difficult in tanks of limited size

  - homogeneous / isotropic sound field

- **Mechanical Considerations**

  - emulate hull via steel plates fluid loaded on one side

  - different plate shape/mass change modal characteristics

  - reduce energy loss to supporting structure

  - reduce energy radiated from supporting structure

  - monitoring sensors and locations

Experimental Requirement

- Should in some way emulate hull damping (fluid loaded plates).
- Monitor the radiated sound power.
- Evaluate the coating material for damping purposes.
  (Do not want to evaluate the substrate).

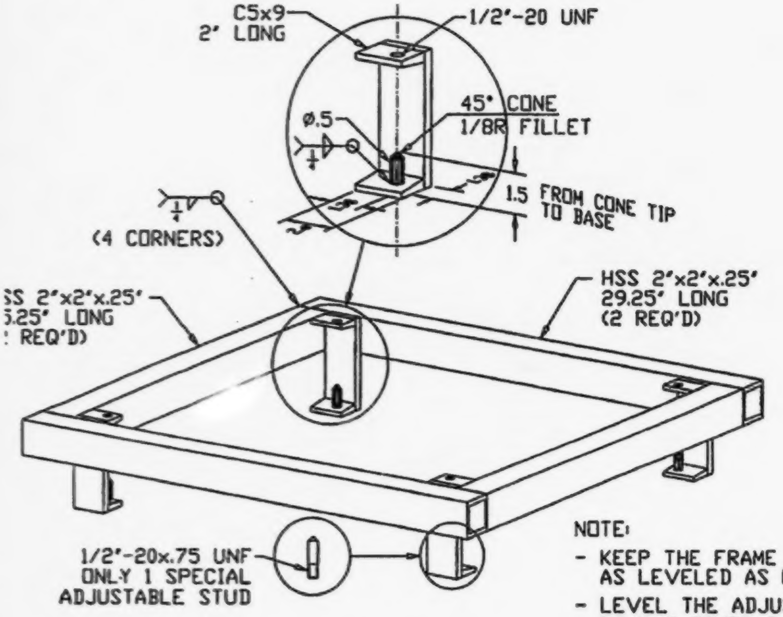
C5x9
2' LONG
1/2'-20 UNF
45° CONE
1/8R FILLET
Ø.5
1.5 FROM CONE TIP TO BASE
(4 CORNERS)
SS 2'x2'x.25'
5.25' LONG
REQ'D)
HSS 2'x2'x.25'
29.25' LONG
(2 REQ'D)
1/2'-20x.75 UNF
ONLY 1 SPECIAL
ADJUSTABLE STUD

NOTE:
- KEEP THE FRAME AND STUDS AS LEVELED AS POSSIBLE
- LEVEL THE ADJUSTABLE STUD TO THE OTHER 3 STUDS WITH LOCTITE APPLIED

Apparatus for plate support

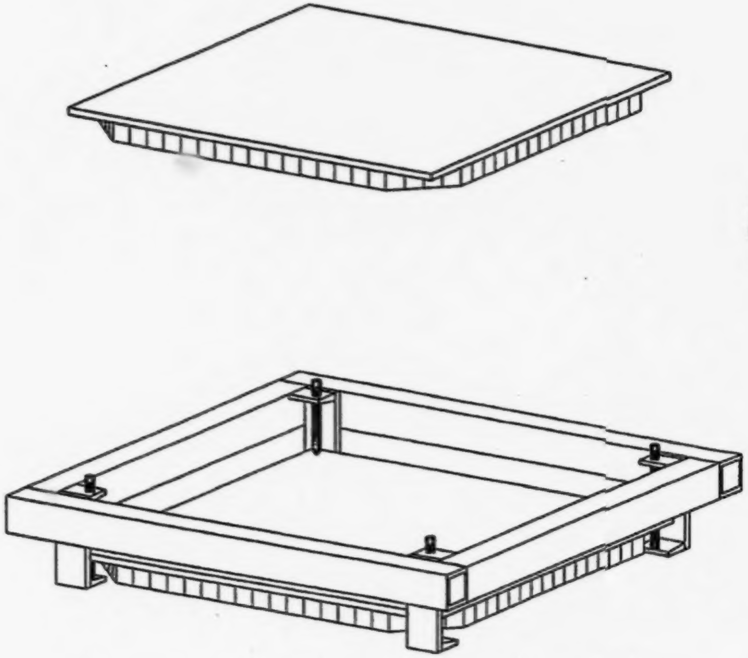

Apparatus shown with plate and damping material

Detail of plate support with plate and damping material shown

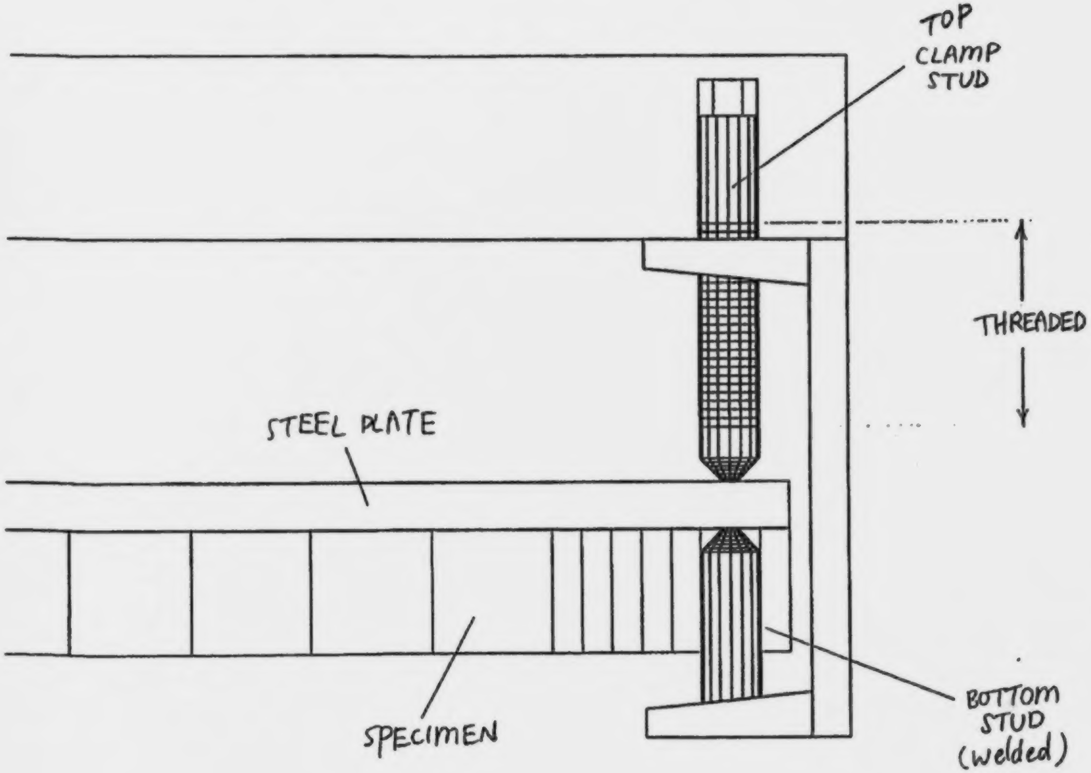
TOP
CLAMP
STUD
THREADED
STEEL PLATE
SPECIMEN
BOTTOM
STUD
(welded)

NOTE:

- STUD POINTS ARE 90°
- DIMPLES ON THE STEEL
  PLATE ARE 118° (STD. DRILL BIT)

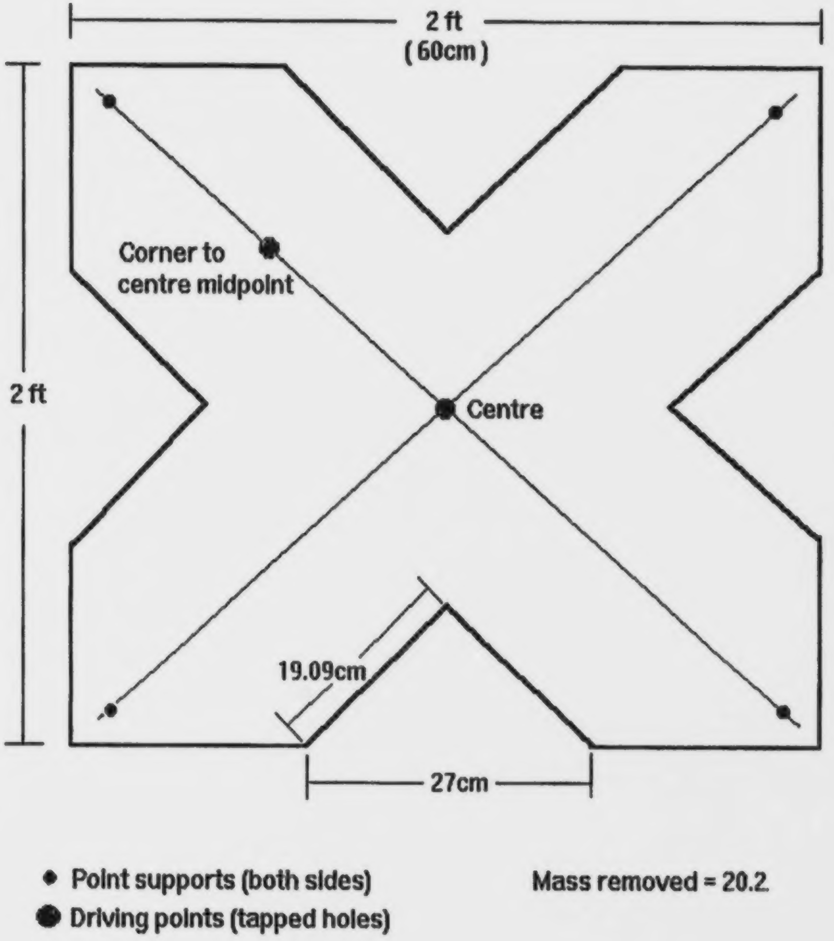
2 ft
(60cm)
2 ft
Corner to
centre midpoint
Centre
19.09cm
27cm
● Point supports (both sides)
● Driving points (tapped holes)
Mass removed = 20.2

Detail of X-Plate showing driving and support points

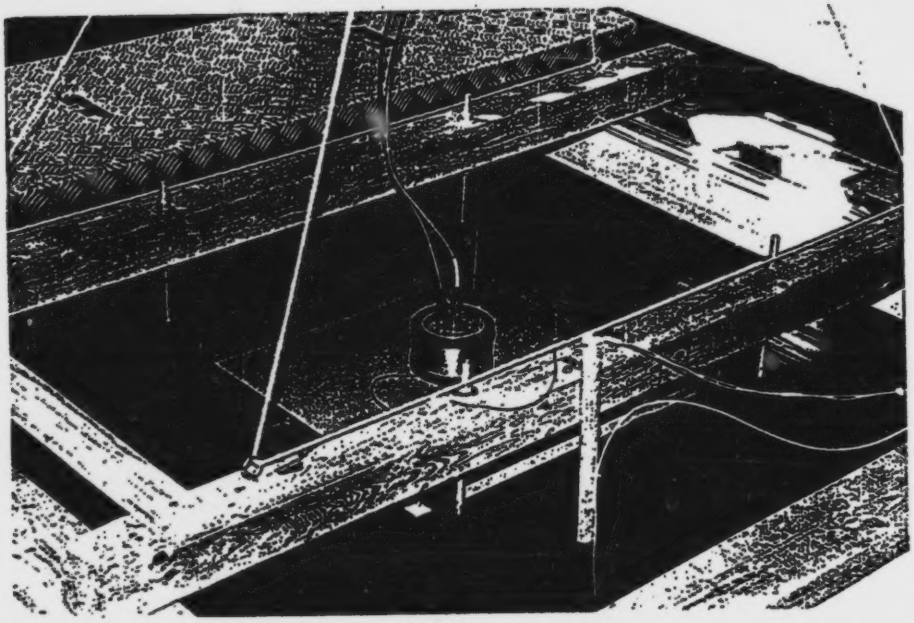

Top: Fluid-loaded square plate shown in small tank with shaker
Bottom: Fluid-loaded X-plate shown in small tank with shaker

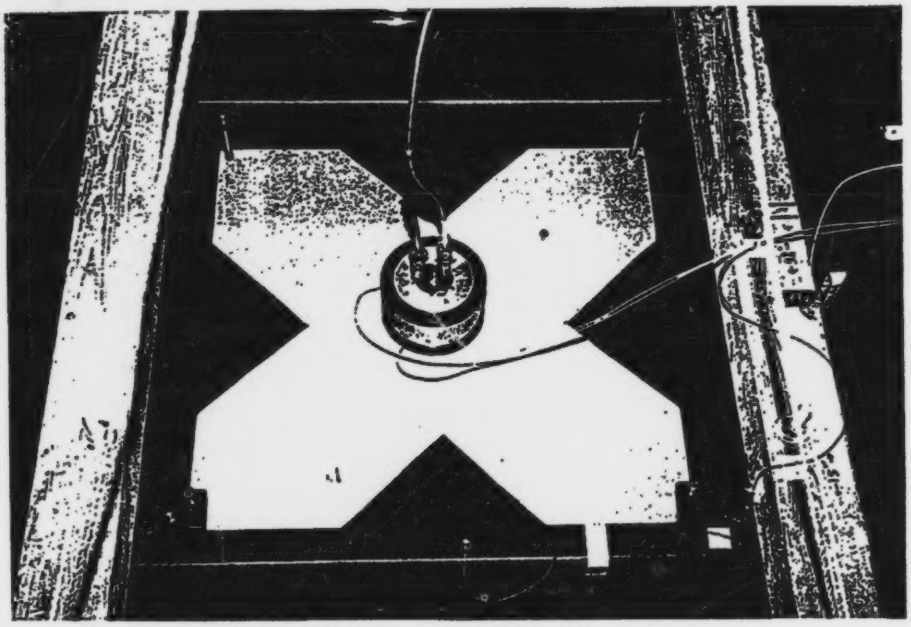

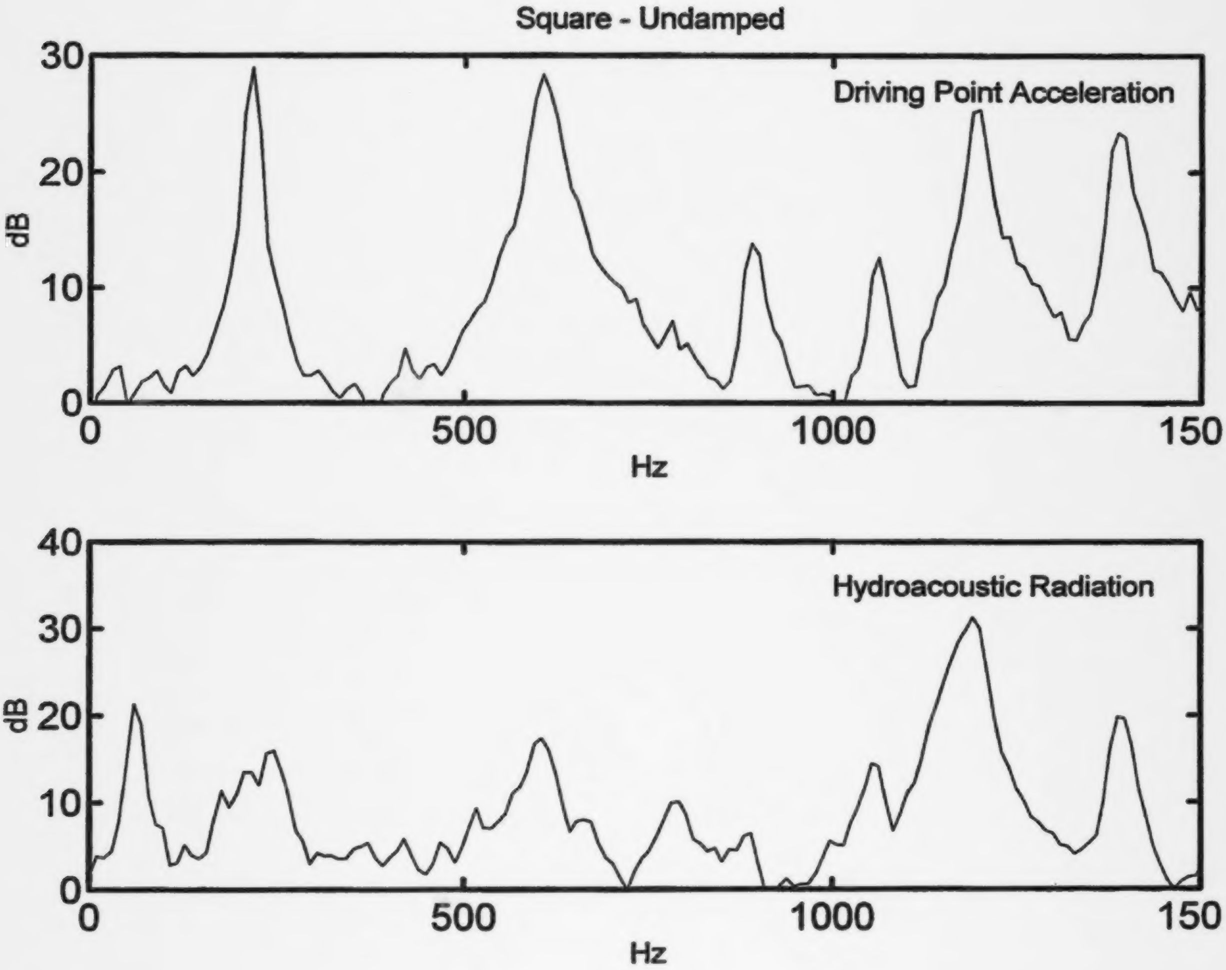
Square - Undamped
Driving Point Acceleration
30
20
10
0
dB
0
500
1000
150
Hz
Hydroacoustic Radiation
40
30
20
10
0
dB
0
500
1000
150
Hz

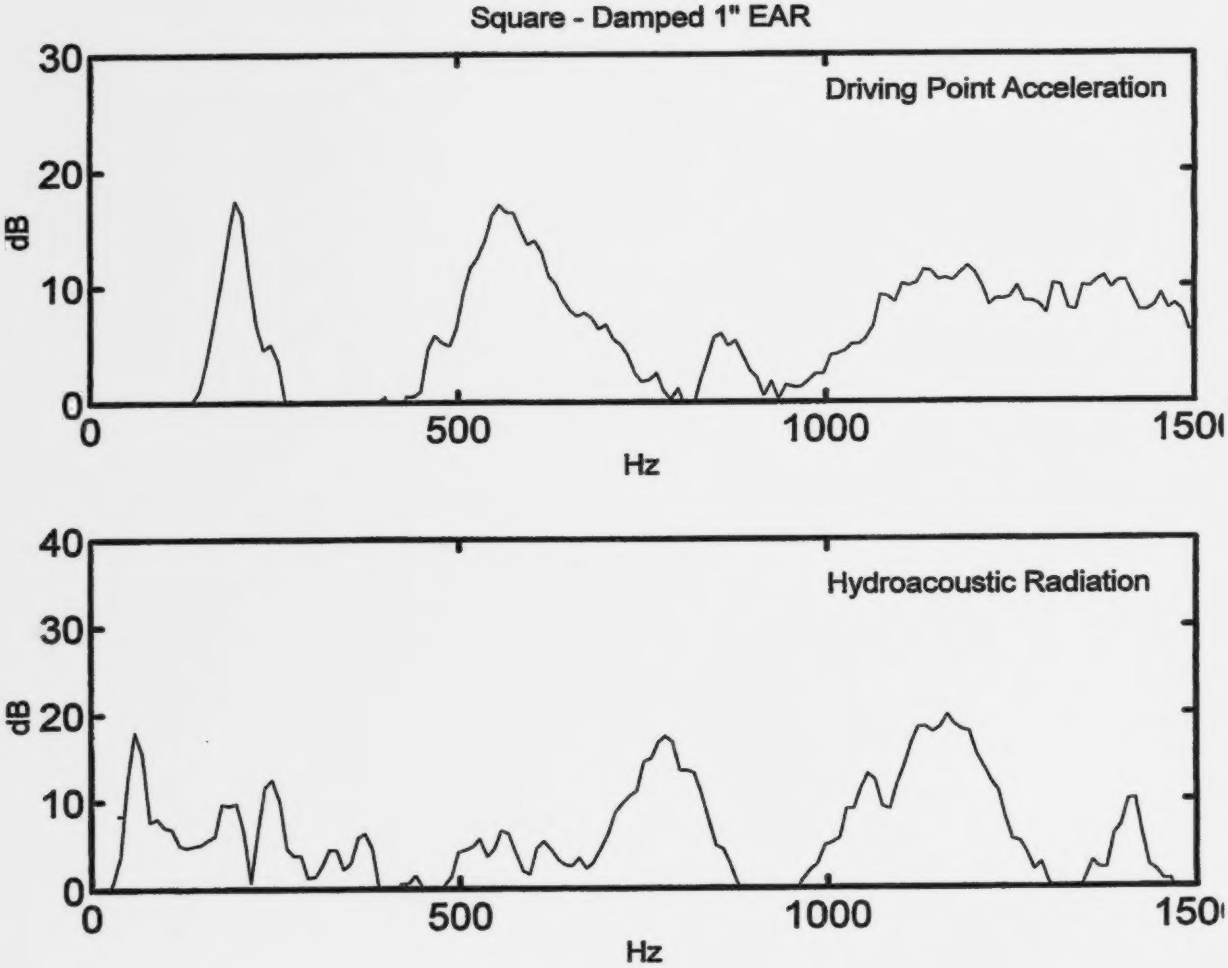
Square - Damped 1" EAR
Driving Point Acceleration
30
20
10
0
dB
0
500
1000
150
Hz
Hydroacoustic Radiation
40
30
20
10
0
dB
0
500
1000
150
Hz

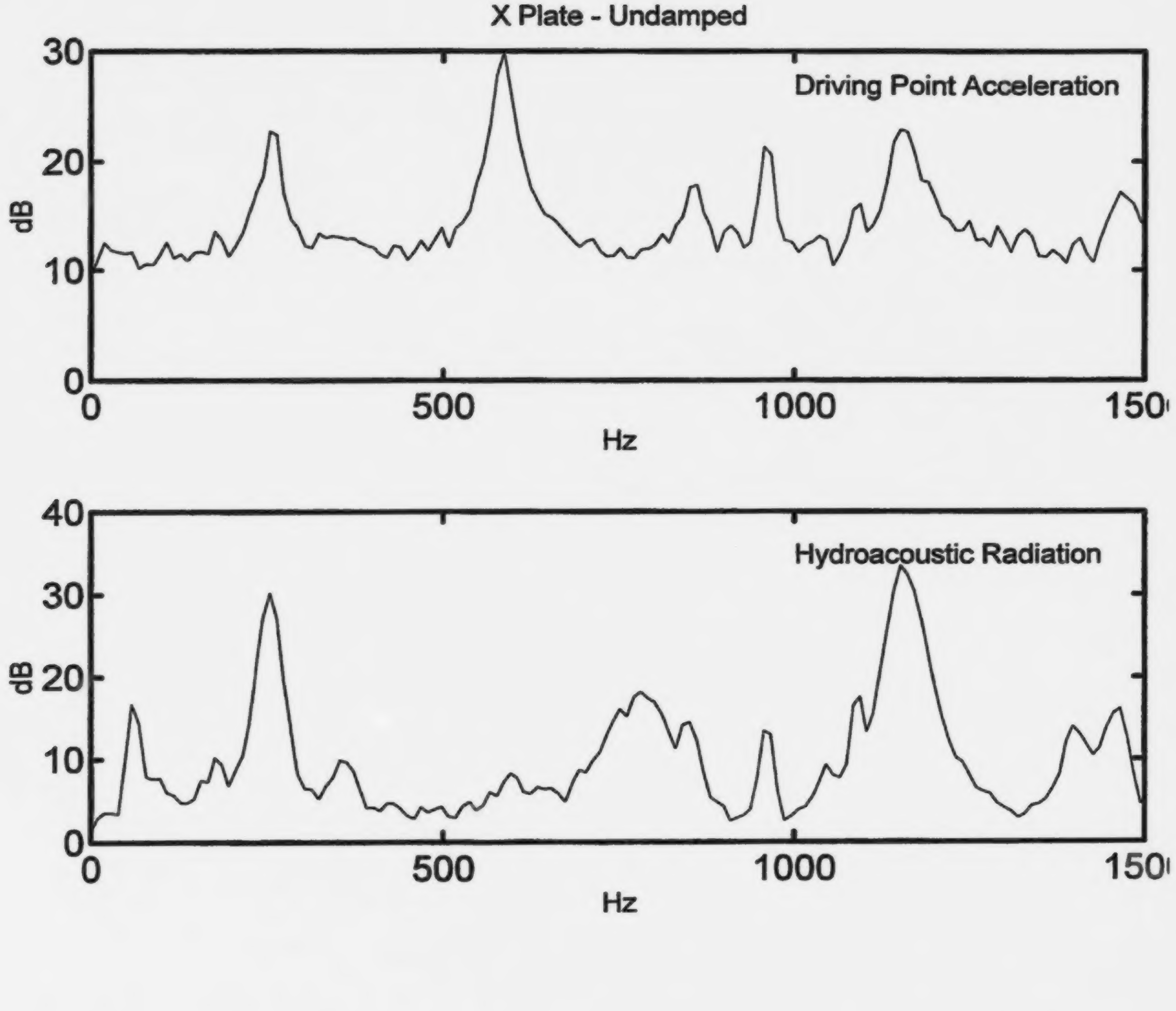
X Plate - Undamped
Driving Point Acceleration
30
20
10
0
dB
0
500
1000
150
Hz
Hydroacoustic Radiation
40
30
20
10
0
dB
0
500
1000
150
Hz

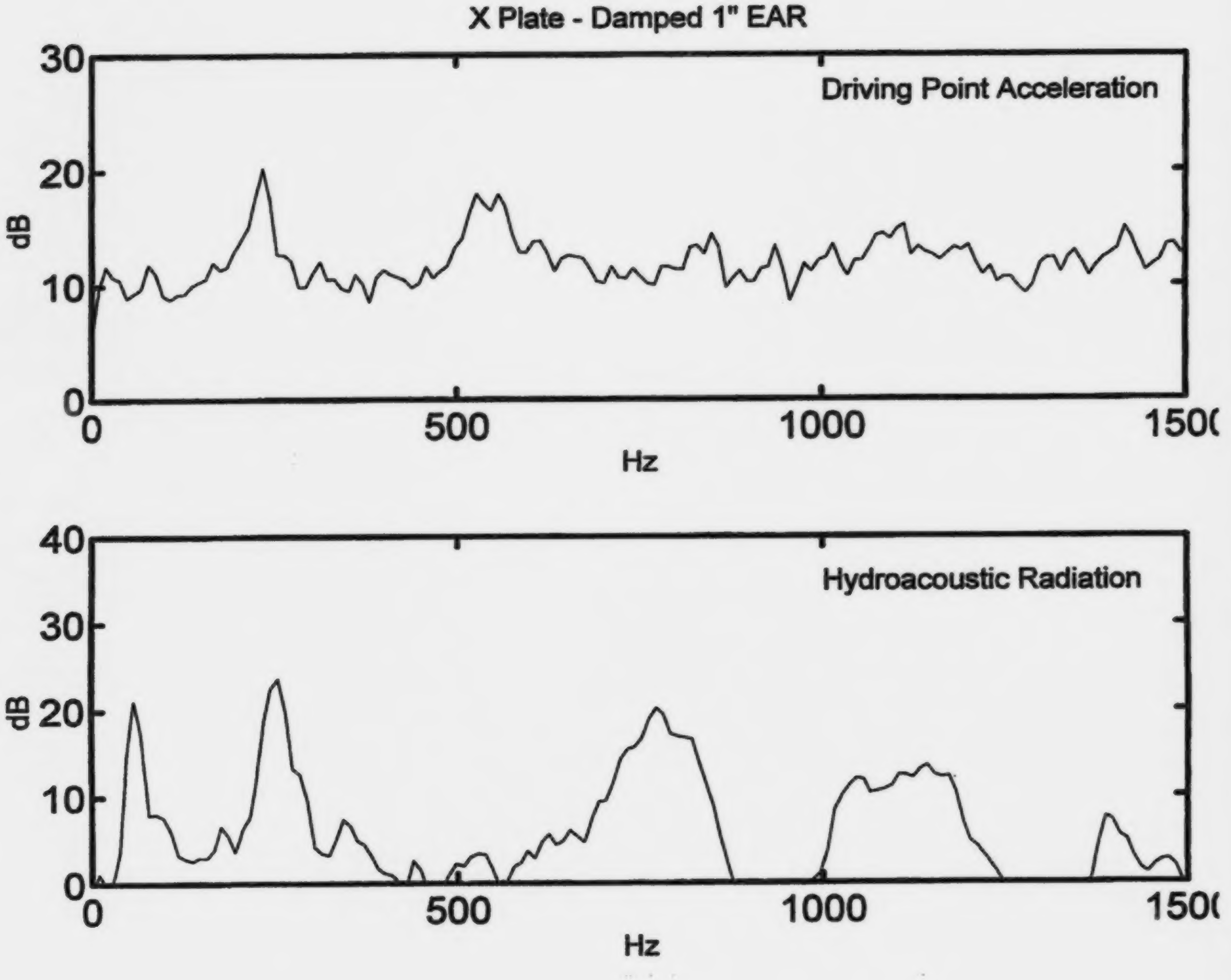
X Plate - Damped 1" EAR
Driving Point Acceleration
dB
30
20
10
0
0
500
1000
150(
Hz
Hydroacoustic Radiation
dB
40
30
20
10
0
0
500
1000
150(
Hz

Summary

- Early data shows expected trend
- Trying different figures-of-merit to evaluate effectiveness of coatings
- Approximately 10-20 dB reduction in radiated sound power observed

#510366 ㉓

Inorganic Intumescent Fire Protective Coatings For Marine Use

by

D. E. Veinot
Defence Research Establishment Atlantic

and

D. Nguyen
J. O. Bernt and Associates Limited
Mississauga, Ontario

ABSTRACT

Fire at sea has been called "the ultimate nightmare" and ships' damage control teams have little choice but to respond rapidly and get the situation under control as soon as possible. Fire can spread rapidly throughout a ship by many paths including direct thermal energy transfer through bulkheads and deckheads and along burning electrical cable pathways spreading smoke and toxic fumes which are released from burning materials as the fire grows. The use of materials which are inherently "fire resistant" in ship construction or in retrofitting installed substrates which are vulnerable to fire would provide an added measure of safety during a shipboard fire. This would also reduce the rate of fire growth thus increasing the damage control team response time.

This presentation will describe some of the materials' development work, the results of both small and large scale testing, and the potential applications and commercial spin-spinoffs of a non-toxic, non-combustible, inorganic inorganic intumescent fire protective coating that has resulted from the DREA/CRAD R&D effort in firesafe materials. The presentation will include a video taped summary of small and large scale testing of the coating. Some prototype samples of potential commercial products will also be shown.

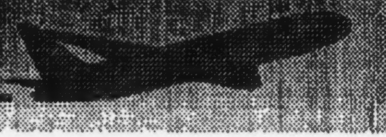

Outline

- ◆ Background to the problem
- ◆ Organic vs Inorganic systems
- ◆ Compositional development
- ◆ Small and large scale evaluation
- ◆ Video of large scale test
- ◆ Tech transfer/commercial opportunities
- ◆ Summary and discussion

Background

- ◆ Fire at sea
- ◆ Falklands conflict
- ◆ Minimize spread and buy time
- ◆ Protection of vulnerable substrates
- ◆ Use non-toxic, non-combustible coatings
- ◆ Cost and commercialization

Organic Intumescent Coatings

- ◆ add to fire load
- ◆ uncontrolled release of blowing agent
- ◆ ablation of surface char
- ◆ smoke and toxic gas
- ◆ expensive

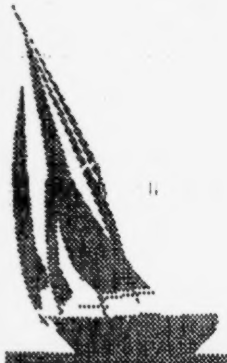

Inorganic Intumescent Coatings

- ◆ no added fire load
- ◆ no toxic gases or smoke released
- ◆ strong rigid intumesced structure
- ◆ inexpensive

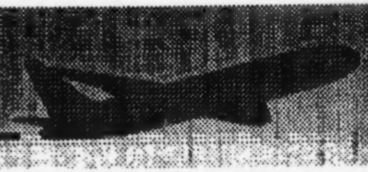

Silicate Compositions Studied

- sodium silicate
- potassium silicate
- lithium silicate
- sodium/potassium/lithium phosphosilicates
- mixtures of the above

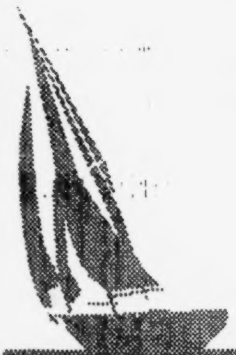

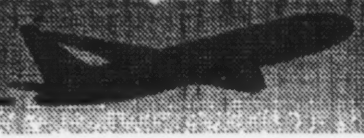

Formulations Studied

- silicate solutions
- powdered silicate granules in silicate solution binders
- powdered silicate granules in latex binder

Small Scale Tests

- ◆ degree of intumescence
- ◆ water solubility
- ◆ hygroscopicity
- ◆ efflorescence
- ◆ flexibility
- ◆ thermal analysis

Large Scale Testing

- conducted at fire research section at NRC
- 2.5m x 2.5m x 2.5m room
- all welded 0.25 in. thick Al alloy 6061 T651
- ASTM E 119 time-temperature profile
- propane burners

SUMMARY RESULTS OF THE FIRE TESTS

(COATED AND UNCOATED ALUMINUM COMPARTMENTS)

Themorcouples Locations		Time (min.) to reach the temperature on the cold side (average of upper half Thermocouples)		% of improvement
		COATED Al	UNCOATED Al	
Ceiling (Average of the three Tc at front)	300°C	13.5	7.5	80%
	400°C	16	8.5	88%
South Wall (right side, looking in)	300°C	12.75	8.75	46%
	400°C	18	9.25	95%
North Wall (left side, looking in)	300°C	13.75	8.5	62%
	400°C	19.25	9.25	108%
East (back wall)	300°C	14	10	40%
	400°C	20	11.75	70%

Ceiling melted & failed - uncoated Aluminum panels: 10.5 minutes

Ceiling melted & failed - coated Aluminum panels: 21 minutes

Temperature Control

(COATED Al)

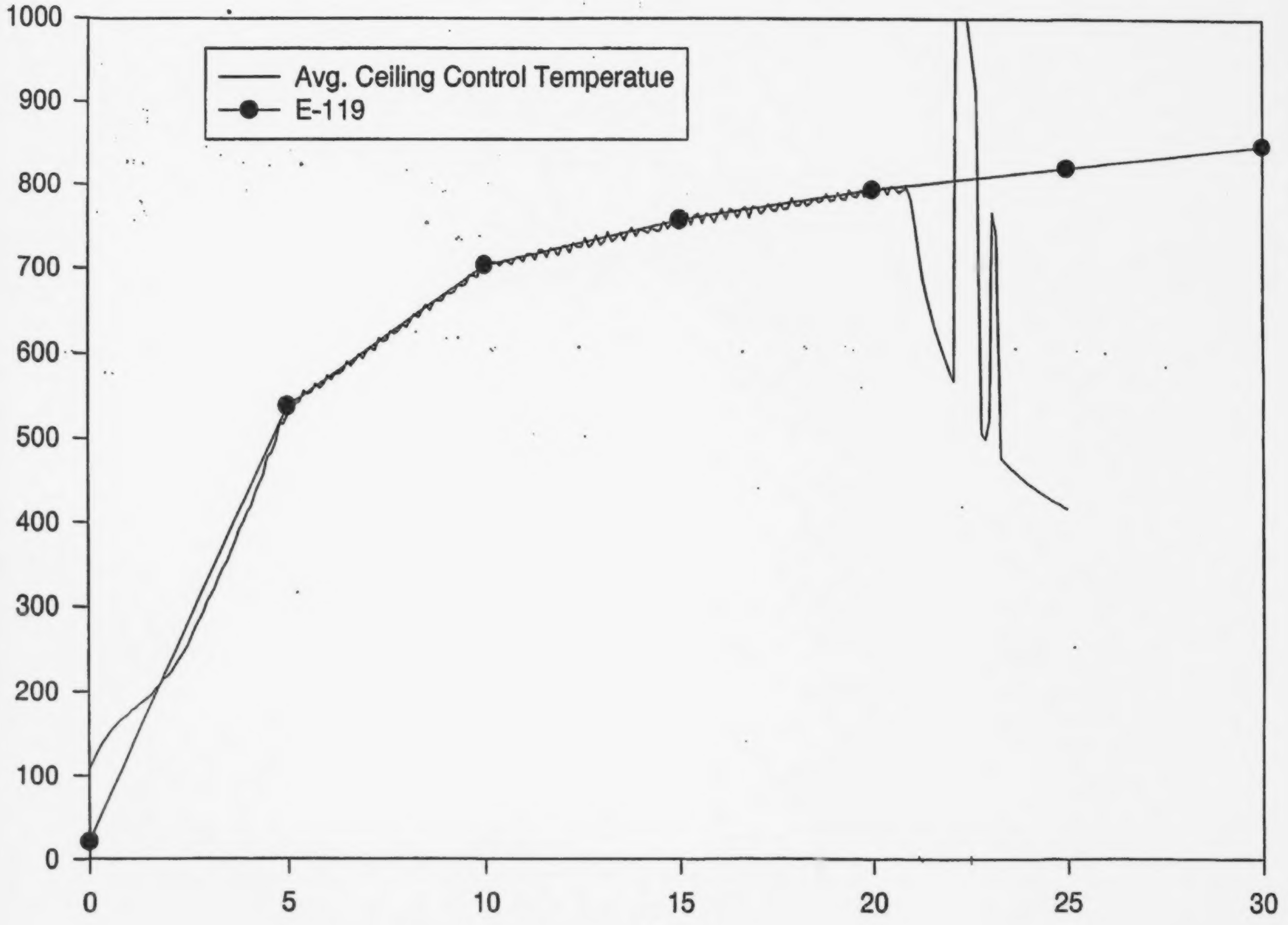

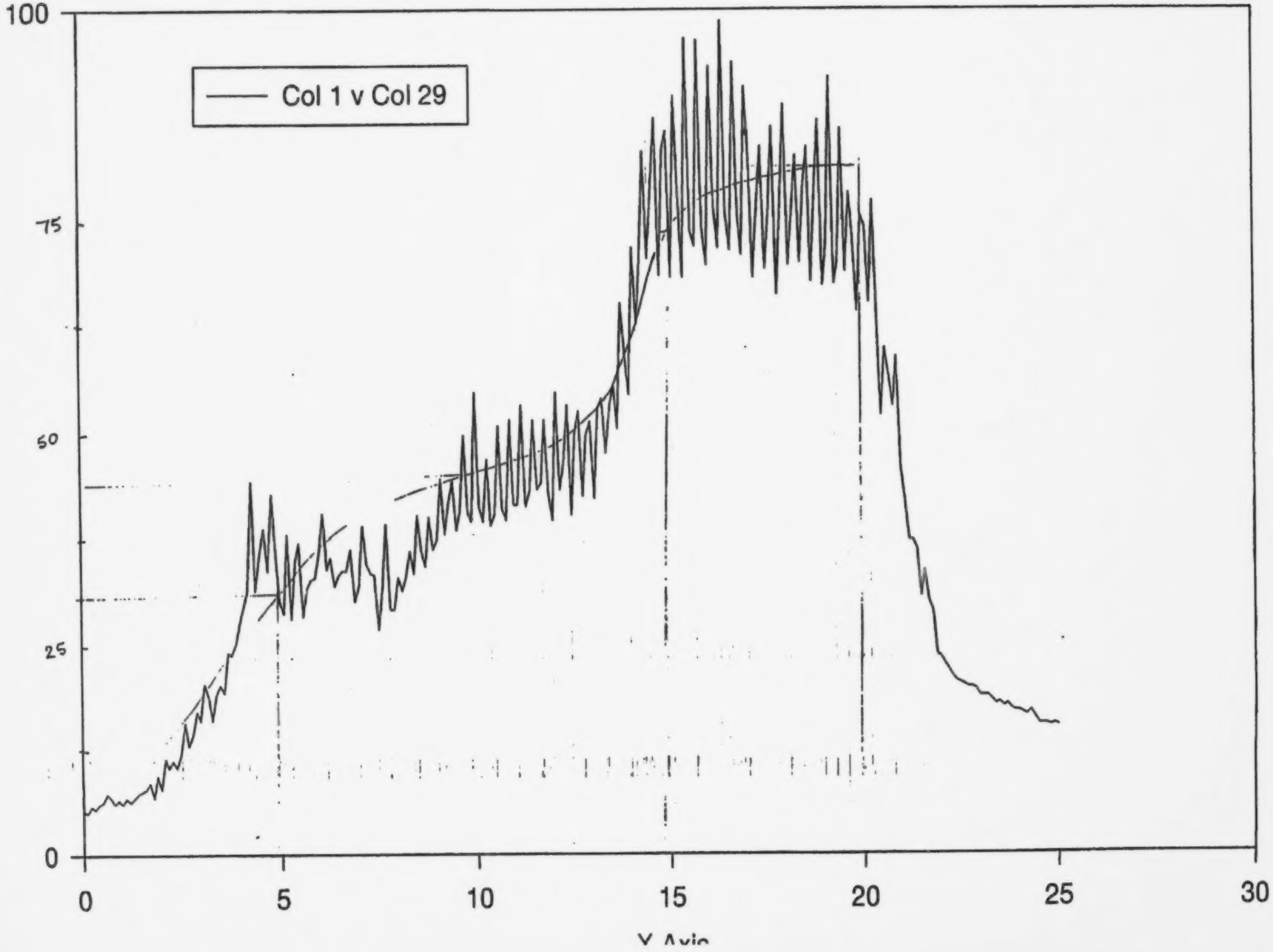

Heat Flux
(COATED Aluminum)

#510367 (25

DDH 205 CLASS
STRUCTURAL INTEGRITY HISTORY
1951-1994

by D.J. Hussey[1], C.D. Roushorn[1], D.G. Smith[2], LCDR K.B. Holt[3], Lt(N) K. Kirkov[3]

[1] Donelad Hydronautics Limited
Suite 720, 1550 Bedford Highway, Bedford, Nova Scotia
Canada B4A 1E6

[2] Command Paint and Preservation Officer (retired)
Naval Engineering Unit Atlantic
FMO Halifax, Nova Scotia B3K 2X0

[3] Surface Ship Structures, Naval Architectural Services
Directorate of Ship Engineering
National Defence Headquarters
Ottawa, Ontario, Canada K1A 0K2

Presented at the Canadian Forces/Chief Research and Development Meeting on "Naval Applications of Materials Technology", Halifax, May 1995.

ABSTRACT

The keel for the first Canadian designed destroyer escort (DDE), HMCS ST. LAURENT was laid down 22 November 1950, launched November 1951 and completed 1955 followed in quick succession by six more ships of the DDE 205 Class. The 2900 ton DDEs were converted to DDHs commencing in 1962 with the fitment of a large hangar/flight deck complex for an operational 22,000 lb. Sea King helicopter. The last ship, HMCS FRASER, ended over four decades of reliable service by the 205 Class ships in 1994.

This paper addresses the structural integrity of the DDH 205 Class over forty-three years in five distinct periods:

a) Eight years as a DDE, 1955-1963;
b) First thirteen years as a DDH, 1963-1976;
c) Two years prior to Destroyer Life Extension (DELEX), 1976-1978;
d) DELEX at twenty-seven years average age post launch, 1979-1982; and
e) Twelve year life after DELEX, 1982-1994.

It is believed this is the first factual public record of the corrosion and structural problems experienced by a naval ship class over an entire ship class lifetime and life extension. Techniques developed to eliminate or at least retard such problems are presented.

TABLE OF CONTENTS

PAGE

TITLE i
ABSTRACT i

1.0 INTRODUCTION 1

2.0 BACKGROUND TO THE NOVEL ST. LAURENT HULL FORM 1

3.0 STRUCTURAL PROBLEMS 5

- 3.1 Failure Mechanism 5
- 3.2 DDE 205 Class Structural Defects, 1955-1963 6
- 3.3 DDH 205 Class Structural Defects, 1963-1976 12
- 3.4 Midship Defects, 1976-1978 20
- 3.5 Destroyer Life Extension (DELEX), 1979-1982 24
- 3.6 Life after DELEX, 1982-1994 24

4.0 CORROSION PROBLEMS 36

- 4.1 State-of-the-Art circa 1948-1958 36
- 4.2 Corrosion Mechanism 37
- 4.3 Corrosion on DDE/DDH 205 Class, 1951-1981 (and DDH 265 Class, 1961-1981) 37
- 4.4 Corrosion on DDH 205 Class, 1981-1994 45

5.0 HIGH COST OF STRIPOUT, INSPECTION, REPAIR AND REPLACEMENT 45

TABLE OF CONTENTS
(Continued)

SECTION	TITLE	PAGE
6.0	**COMPARISON OF DDE/DDH 205 WITH DDH 265 AND DDH 280**	48
7.0	**CONCLUSIONS**	52
8.0	**RECOMMENDATIONS**	57

LIST OF FIGURE CAPTIONS

2-1	Framing Section - Midship	3
3-1	Summary of Charpy C_v Valves for Ship Fracture Initiation, Propagation, and Arrest Plates	6
3-2	Rough Profile of a DDH 205/265 Class Destroyer	13
3-3	Junction of the Transverse Watertight Bulkhead Frame 36 Forward Boiler Room Bulkhead and the Longitudinal Bulkheads Forming the Boundaries of No. 3, 4 and 5 Fuel Tanks	15
3-4	View of Starboard After End of Bridge Superstructure Looking Forward and Toward the Centreline	16
3-5	"Original" Pillar Head Arrangement Port and Starboard	17
3-6	"Redesigned" Pillar Head Arrangement Port and Starboard	17
3-7	Typical Pillar Head Connection 3 Deck Frame 27 (Modification to each Pillar is Custom Designed)	18
3-8	Knuckle Frame 27	19
3-9	HMCS FRASER & SKEENA: 1976-77 No.1 Deck at Amidships Frames 37-47	30
3-10	HMCS SAGUENAY - 1978 No.1 Deck at Amidships Frames 37-47	31

TABLE OF CONTENTS
(Continued)

SECTION TITLE PAGE

LIST OF FIGURE CAPTIONS (CONT'D)

3-11 HMCS ASSINIBOINE - 1978 No.1 Deck at Amidships Frames 37-47 32

3-12 HMCS MARGAREE - 1978 No.1 Deck at Amidships Frames 37-47 33

3-13 HMCS FRASER - 1979 No.1 Deck at Amidships Frames 37-47 34

3-14 DELALT 51 - NO. 1 Deck, Midships and Area "After Modification" 35

LIST OF TABLES

3-1 DDE 205 Class - Structural Defects 1955-1963 10-11

3-2 DDE/DDH 205 Keel and Deck Stresses Before and After Conversion 14

3-3 Principal Events in Life of DDE/DDH 205 Class Related to Midships Structural Failures 27

3-4 DDH 205 Class - Structural Defects Post DELEX Refit 1982-1994 28-29

6-1 Charpy V-Notch Steel Impact Test Results, HMCS GATINEAU, DDE 236 49

6-2 Steel Mechanical Properties, Canadian Naval Ships, 1950-1955 50

LIST OF ILLUSTRATIONS

i-1 DDH 205 Incident Board Showing Corrosion Areas in Green and Fractures in Red for the Period 1951-1981 v

i-2 HMCS ASSINIBOINE Before Conversion vi

i-3 HMCS FRASER After Conversion with its Sea King Helicopter vi

ACKNOWLEDGEMENTS 59

REFERENCES 60

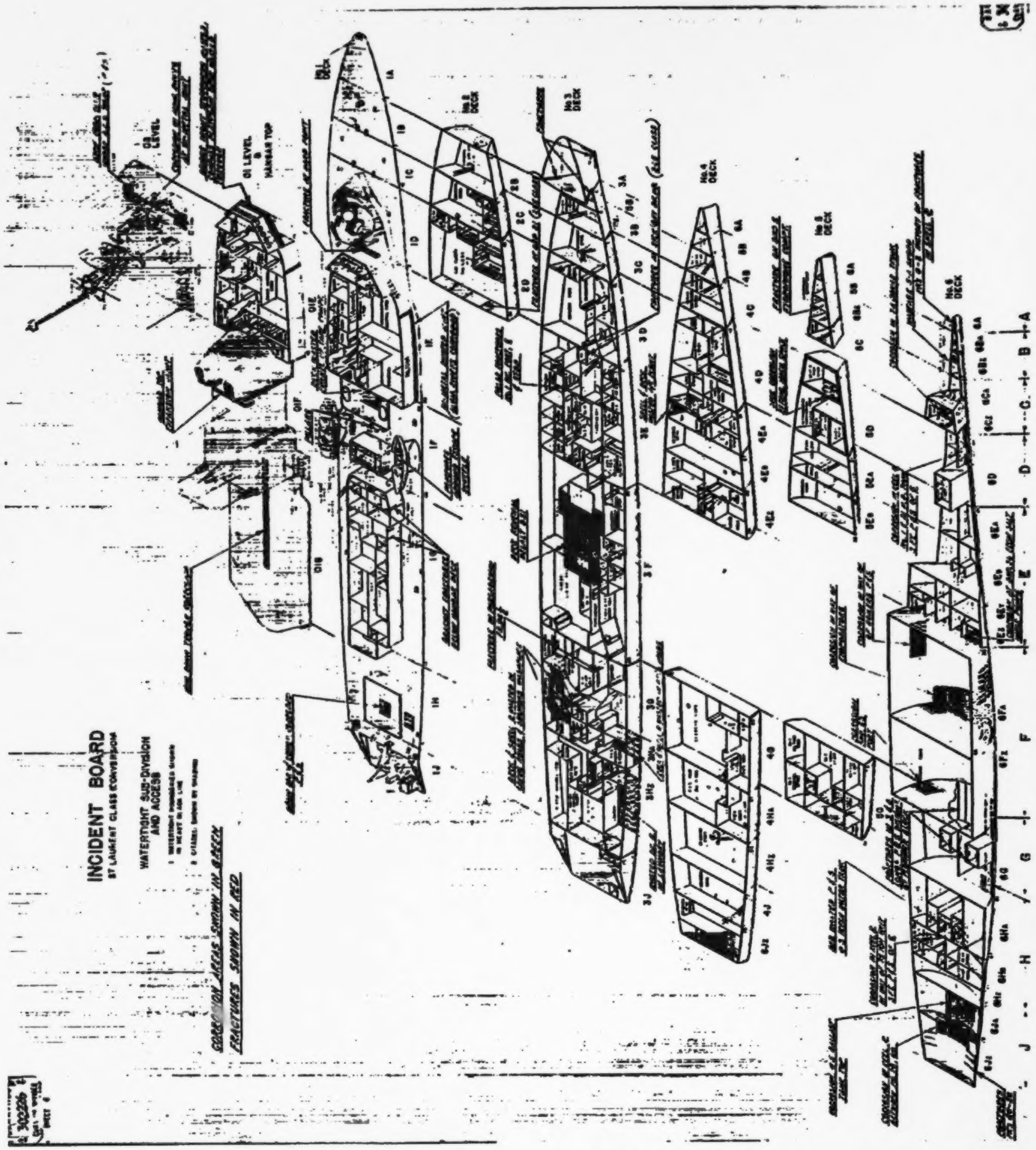
INCIDENT BOARD
ST LAURENT CLASS CONVERSION
WATERTIGHT SUB-DIVISION AND ACCESS
CORROSION AREAS SHOWN IN GREEN
FRACTURES SHOWN IN RED
No.3 DECK
No.4 DECK
No.5 DECK
No.6 DECK
A
B
C
D
E
F
G
H
J

Illustration i-1 DDH 205 Incident Board Showing Corrosion Areas in Green and Fractures in Red for the Period 1951-1981

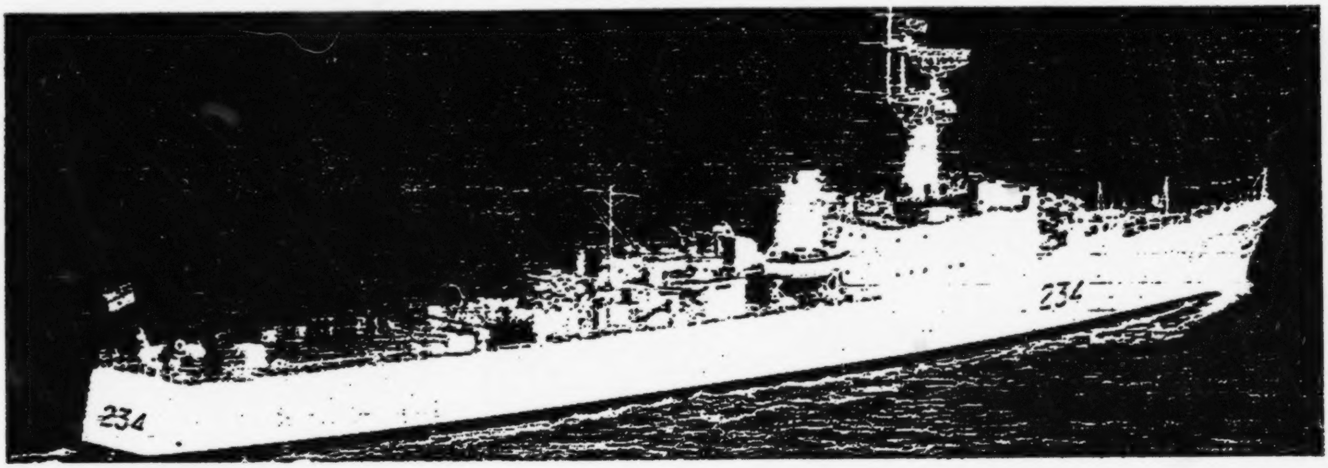

Illustration i-2 HMCS ASSINIBOINE Before Conversion

Illustration i-3 HMCS FRASER After Conversion with its Sea King Helicopter

1.0 INTRODUCTION

DDE/DDH 205 Class ships have stood the test of time providing quite satisfactory service with an excellent utilization rate. As these ships aged, failures occurred. Most structural failures may be attributed to deficiencies in detail design and/or a less than optimum fabrication quality in specific areas. The large Flight and Hangar complex fitted during the conversion from a DDE to a DDH had an impact on the structural integrity of these ships. This paper describes the structural failures, giving:

a. location and description of failure;
b. probable cause of failure; and
c. proposed or adopted method of repair.

By 1981 the DDH 205 Class steam driven destroyers, 25 years of age since initial commissioning, had extensive localized corrosion over various parts of the hulls. This paper describes most areas of corrosion, giving:

a. location and description of corrosion;
b. probable cause of corrosion;
c. proposed or adopted repair method; and
d. action taken to prevent or retard further corrosion.

The loss of operational capability because of structural integrity reduction due to cracking and/or corrosive attack is illustrated. A comparison is made of the structural history of the DDH 205 with the newer DDH 265 and DDH 280 Classes. Conclusions are drawn from the structural integrity history of these magnificent ships with the hope that lessons learned will be considered for integration into future ship design specifications, drawings and in-service maintenance policies.

2.0 BACKGROUND TO THE NOVEL ST. LAURENT HULL FORM

Reference Illustrations i-1 to i-3

During World War II the Royal Canadian Navy (RCN) became the third largest allied force at sea, after the Royal Navy and United States Navy, by building over 300 ships of British design. Although the RCN anti-submarine warfare (ASW) capability was standardized with the British during the war, there was no British (or American) destroyer designs available which met Canadian requirements for a renewed post war navy. An all Canadian design was commenced in 1948 with the intention that the ship should be of the size of the Wartime Destroyers, but modified so as to make the ASW weapons the main armament, intentionally sacrificing the anti-air role to that of anti-submarine.

Despite the fact that Canada had very little previous warship design experience, the RCN established a new concept of stability, a new hull construction (including a NBC pre-wet and contaminant wash down system, an enclosed citadel, within an air conditioned hull, isolated from the external atmosphere and a ship which eventually sailed for 43 years), a new shipbuilding engineering and electrical industry, a new propulsion plant manufacturing industry, new RCN standards of furniture, valves and piping (CuNi), etc., commonality of equipments, and a new concept of habitability as an integral part of the development of a new class of ship. This was a fair achievement for a nation of only 12 million people at the time.

The Canadian DDE 205 hull form had unique stability and structural hull features. The hull form, rise of floor and midship section, and the watertight subdivision of the DDE 205 St. Laurent is such that the ship would not sink by capsizing but by remaining upright as flooding progressed to the Upper Deck. The escape scuttle was located in the deckhead rather than the ship's side, a proportion of the life rafts on the middle line on the Pilotage Deck (Bridge top), etc. The hull structure erection sequence and structural design was organized to allow the ships to be prefabricated in units, which in an emergency could be put together far from water, and shipped to assembly berths. These units weighed about 20 tons each and were fitted together in such a manner to ensure accurate adjustment of the ship and alignment of the plating. Adopting British practice, framing in way of amidships generally consisted of deep main transverse frames at 4 feet 6 inches or 5 feet frame spacing with smaller half frames placed between the main frame stations for extra support in critical panting and berthing regions. Lighter longitudinals provided the longitudinal strength required for a large length/beam ratio, characteristic of a modern monohull warship. The longitudinals were "eggboxed" with the transverse frames to form a rigid grid to which the plating was moulded to form the unit. See Figure 2-1.

Unique features of the DDE 205 hull construction were the rounded deck edge and the "turtle back" Forecastle which extended to Fr. 27. Although aesthetically pleasing, naval architects incorporated these features for improved strength, less foc'sle deck wetness, and to facilitate washdown of nuclear, biological and/or chemical (NBC) contaminants in a hostile environment. The break of the Foc'sle had long been a serious stress concentration in a rivetted ship needing careful attention in a welded ship. The St. Laurent form achieves an extra deck height forward (2 Deck which ends at the Bridge Front Fr. 21 or about 1/3 of length of the ship) while at the same time ensuring continuity of strength in the highly stressed region. During the early life of this class, the Naval Constructor-in-Chief (NCC) emphasized the serious nature of any welding or cutting on the hull without, it was hoped, frightening anyone.

The fine fore end shape with V-shape hull sections and high freeboard over the forward one-third of the ship's length greatly reduced panting and slamming loads and was responsible for the outstanding seakeeping performance in the rough waters of the North Atlantic. The ability to maintain high speeds in a rough seaway before the onset of slamming required greater attention to detailed structural design and the need for increased scantling in the panting region of the hull forward.

Improved high speed manoeuvrability, to combat the modern high speed submarine, was achieved by incorporating a longer "cut-up", greater rudder area by fitting twin rudders in the race of twin screws and improved rudder design.

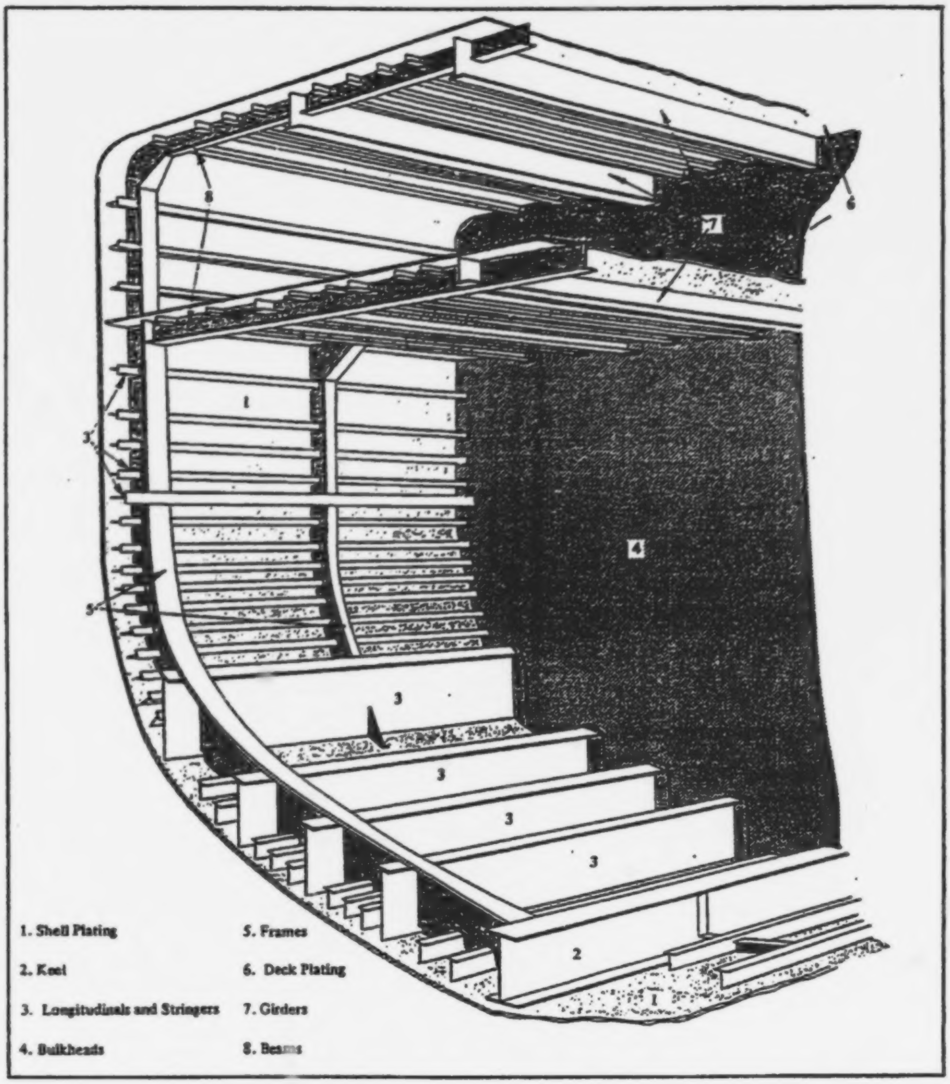
8
6
7
1
3
4
5
3
3
3
3
2
1
1. Shell Plating
2. Keel
3. Longitudinals and Stringers
4. Bulkheads
5. Frames
6. Deck Plating
7. Girders
8. Beams

Figure 2-1

Framing Section - Midship

The Weather and Pilotage Decks, at one time astonishingly free of obstruction in preparation for the nuclear age, continued to be comparatively clean with the Anchor Windlass and the ASW Mortar below decks. The enclosed Bridge/Command Position was an inevitable step which the RCN took at the same time as the RN but ahead of the USN. Most Weather Deck fittings were of aluminum to reduce the chipping and painting workload caused by corrosion of steel fittings.

The RCN was in the forefront of state-of-the-art developments in Cathodic Protection. The St. Laurent Class was fitted with a steel anode impressed current system commencing about 1960 developed from experimental installations on the original WWII Tribals. Similarly, the RCN under water paint systems attracted considerable attention in the RN and USN.

The beam of the DDE 205 Class at 42 feet was one foot wider than the original 1948 RN Type 12 design of similar hull size otherwise. This feature and the fitment of an aluminum superstructure, with a steel Bridge Front to counteract sea slap and gun blast overpressure, allowed the Canadian Navy to eventually convert the DDE 205 to a DDH without having to fit a salt water displacement fuel system. These design features permitted the operation in Sea State 5 conditions of a large 22,000 lb. Sea King ASW helicopter from a relatively small 2900 ton destroyer revolutionizing ASW warfare in the mid 1960s.

The following lists the four classes, 20 ships, of the St. Laurent hull form and its derivatives with displacement 2900 tons, length overall 366-373 feet, beam 42 feet and draft 14.5 feet.

CLASS	PENNANT NUMBER	NO. OF SHIPS	LAUNCHED
St. Laurent	205	7	1951-54
Restigouche	257	7	1954-57
Mackenzie	261	4	1961-62
Annapolis	265	2	1961-63

3.0 STRUCTURAL PROBLEMS

3.1 Failure Mechanism

Two general methods of structural failure which are significant in the case of the DDE/DDH 205 Class ships are:

a. **Fracture** is an unstable, rapid propagation of a crack in the presence of an applied stress; and

b. **Fatigue failure** is the stable propagation of a crack in the presence of a cyclic stress.

Ships in a seaway are continually experience cyclic stress due to hogging and sagging, and on occasions, racking. With few exceptions the characteristics of fatigue failure eventually become evident. However, because initiation of cracks frequently occurs at so few cycles it becomes a moot point as to whether the initial crack resulted from true fatigue or from a very high stress during a few cycles. In most cases it is better in a dockyard environment, where time is of the essence, to look for the source cause in terms of stress concentrations, such as: inadequate use of materials; inappropriate fabrication techniques such as faulty welding, rough plate edges, misalignment of structure, incorrect selection and use of welding rods; and generally poor detail design in high stress areas causing abrupt structural changes or hard points.

Before describing examples of structural failure in some detail, it is pointed out that there is a materials engineering factor which affects the susceptibility of the steel structure to fail. As the temperature of the sea water and air drops, the probability of a brittle fracture initiation increases. Canadian ships regularly operate in such an environment as, for example, the Fishery Patrols in the cold eastern North Atlantic off the Newfoundland coast. Since 1965, commencing with the AOR 509 and DDH 280 Classes, the Canadian Navy has specified the hull structure be constructed of a notch tough steel incorporating good weldability characteristics with a steel manufacturer's guaranteed impact test.

To combat in-service brittle fracture in new construction ships, conversion/modernization or after a large repair job, all heavily loaded structural members should be periodically inspected for early warning signs of fatigue failure. This is a health monitoring type of inspection which is part of the conditional maintenance performed over the years by experienced Canadian Naval Hull Inspectors. Hussey wrote in 1982, Reference 1, that ship designers should be cognizant of the importance of providing accessibility for hull surveys and hull maintenance/ship husbandry, especially in machinery and/or damp spaces. A ship design which is "too tight" may be prohibitably expensive to life extend and/or convert at normal mid-life -- it has happened to other navies! Ship detail designers are prone to neglect such mundane things as access for ease of inspection, maintenance and repair.

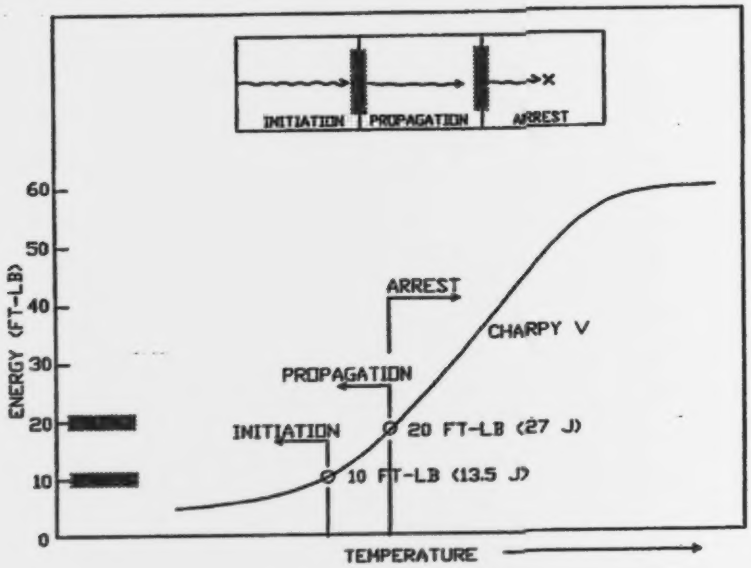

Figure 3-1

Summary of Charpy V (C_v) Energy Values for Ship-Fracture Initiation, Propagation, and Arrest Plates (Ref. 11)

Having said all of the above, there is one particular condition which repeatedly occurs in ship construction and has been the cause of several failures in our ships and that is the hard point "knife-edge intersection". In this case as the ship "works" in a seaway and the structure moves relative to other structure except at the point where they meet or cross. This crossing forms an unyielding "hard" point and one or the other of the deck or bulkhead will crack. The cure is to spread out the attachment point by brackets in one or both structures or to slot one of the unyielding structures to eliminate the hard point. One thing is for certain, hard spots are easy to design in, and pure hell to design out. Examples will be shown to illustrate this failure.

3.2 **DDE 205 Class Structural Defects, 1955-1963** Reference Illustration i-1

The DDE 205 Class was constructed during the period 1951 to 1957, all being commissioned during the period 1955 to 1957. Seven ships of the class were built, HMCS ST. LAURENT was the lead ship, and as a result, it has features which are slightly different than the follow-on ships. Several refinements to the design were made as a result of the lessons learned during the early construction of the ST. LAURENT.

DDE 205 Class were constructed in several different shipyards with different overseeing staffs involved. Even though the ships were constructed to the same set of drawings with the exception of ST. LAURENT, perhaps because of the lead ship aspects, it is clear that each builder did not fabricate the ships in precisely the same way, and as a result, there are differences in the details of how they are constructed.

In the early life of these ships there were a number of structural defects identified and repaired. The structural cracks may fall into one of three basic categories:

a. fundamental design;
b. detail design, drawings, or specifications; and
c. fabrication deficiencies in the form of:

    (1) not meeting the intent of the design;
    (2) undercut weldments;
    (3) incomplete penetration of weldments; and
    (4) plate forming "thins".

Fundamental design deficiencies would normally require a re-examination of the design with a probable modification to rectify the deficiency. Load concentrations beyond those anticipated during the design, or the inadequate assumption of the load configuration associated with the particular design configuration, may be the source cause of some design deficiencies.

Most common is the matter of structural discontinuities and hard points, both causing stress risers locally in the structural configuration. These may be a result of detail design or drawing development showing these features in the structural configuration. More than 40% of the structural cracks may be attributed to detail design and/or drawing detail inadequacies. Fabrication deficiencies will also cause stress risers in the form of misalignment of adjoining structure, undercut or incomplete penetration weldment deficiencies or plate "thins" from forming. Often these are stress risers in the proximity of the weldments.

At Table 3-1, is a listing of a number of known structural defects that occurred in the first eight years of the DDE 205 Class ships. These defects all occurred prior to the conversion to the DDH Class, commencing with the ASSINIBOINE and ST. LAURENT in 1963.

A fundamental design deficiency is apparent in the after end of the Engine Room in way of oiltight bulkhead 53 in the 4th longitudinal, see Table 3-1. All ships of the class cracked in the web plate in way of the rider plate to the longitudinal frames below the shaft bearings. A design modification was implemented early in the life of these ships. This was the only known fundamental design deficiency in the DDE 205 Class during the first eight years of operational life that could have had a consequence leading to safety of the ship.

The intersection of the forward superstructure bulkhead with the No. 1 Deck in way of Frame 21 1/2 may be taken as a fundamental design fault or a detail design fault. All ships of the class were constructed with the forward edge of the forward superstructure at Frame 21 1/2 at the centreline. Four ships were fitted with angled brackets on the centreline and at No. 1 longitudinal, port and starboard. HMCS ST. LAURENT was fitted with a bracket at centreline initially and subsequently fitted with brackets at No. 2 longitudinal, port and starboard. Two ships, HMCS SKEENA and ASSINIBOINE, had no brackets at all. There were differences between the respective ships in regards to this particular area.

It is interesting to note that of all the ships that were differently fitted, only the two ships with no brackets at all had no history of cracking at the intersection of the superstructure bulkhead and the No. 1 Deck. All other ships experienced cracking at the intersection in the vicinity of the No. 1 Deck and forward superstructure bulkhead and/or in the bulkhead No. 21 in way of the lower periphery of the brackets. On each occasion of a crack occurring in No. 1 Deck, clearly it was a major inconvenience with water coming into the Sick Bay, and of course, quite unacceptable for an operational ship. At no time was the safety of the ship of concern.

Each of these ships, with the exception of ST. LAURENT, was fitted with structural modifications in the way of the Frame 21 1/2 to 21 in the form of a structural cruciform following the curvature of the forward superstructure and running downwards from No. 2 longitudinals, port and starboard side, to No. 3 Deck. With this structural modification the forward superstructure load was distributed downward through Nos. 1, 2 and 3 Decks. ST. LAURENT did not have this alteration fitted throughout its entire life. It is also noted that the ST. LAURENT was the only ship of the Class that had the brackets fitted at No. 2 longitudinal. After the modifications to the fitment of the bracket at bulkhead No. 21, by the installation of insert plates in the bulkhead, there were no further cracks, hence there seemed to be no reason to fit the cruciform configuration as in the other ships.

All other structural defects that occurred in the early life of the DDE 205 Class may be attributed directly to detail design or to fabrication inadequacies. Examples of the detail design deficiencies may be attributed to the Boiler Room Intake cracking at Frame 43 1/2 which was a problem with all ships of the class and directly related to a detail structural corner as the source of the cause of the cracking. Elimination of this structural discontinuity rectified the problem.

An example that may be attributed to either detail design or a combination of detail design and fabrication detail is related to the breast plate cracking and forepeak shell plate cracking below No. 5 Deck, between the stem and watertight bulkhead No. 2 in the forepeak. Clearly ASSINIBOINE, ST. LAURENT and MARGAREE had breast plates fitted without face plates. The resultant was a series of cracks located in the vicinity of Frames 0, 1 and 2, propagating through the breast plates and ultimately into the shell of the forepeak causing flooding of the forepeak of course. These breast plates were repaired or replaced in part with the additions of 3/8" x 3" face plate fitted around the periphery of the inner edge of the breast plates in these three ships. SAGUENAY had the face plates already fitted, however, there was a fault in the weldment in such a way that cracks were initiated and propagated similar to the other ships in way of Frame No. 1. The remaining ships of the class had the face plates already fitted and no known cracking occurred.

Examples of fabrication deficiencies could be related to the foremast at No. 2 Platform inadequate welding, the cofferdam at oiltight bulkhead No. 64 to watertight bulkhead No. 65, the steering gear compartment watertight bulkhead 78 to the stern in MARGAREE, all of which were related to welding deficiencies and fabrication.

The cracking in the keel approximately 1 foot aft of the forefoot in HMCS MARGAREE was a direct result of the forming of the plate that caused a "thin" or weak spot in the plate. Also of interest, the MARGAREE was fabricated with a known misalignment of the forefoot from stem to Fr. 1.

Summary 1955-1963

In the first eight years of operational life of the DDE 205 Class there were several nuisance structural failures in the form of cracking in some form or another. Not all ships were built identically and the quality of the fabrication differed between the shipyards. It is not surprising that at that time in the history of the shipbuilding industry in Canada in regards to warship construction, differences would occur and detailed problems would arise. It is noted, in particular, that the largest portion of the structural defects were clearly related to detail design or fabrication matters of one form or another.

With the exception of the crack in the 4th longitudinal in way of OTB 53, none of these structural defects could be taken as being a threat to the safety of the ship or the persons therein at any point in time during the early eight years of the ships life. Of course, the matter of bulkhead 21 where the water was being taken on in the Sick Bay area was quite unacceptable in any sense of the word, however it was not a cause of concern to the safety of the ship, per say. Where the crack propagation was relatively slow and could be observed easily because of the specific location, a drill hole at the ends of the crack effectively stalled progress of the crack for an extended period of time.

TABLE 3-1

DDE 205 CLASS - STRUCTURAL DEFECTS
1955-1963

LOCATION		NAMES OF SHIPS AFFECTED	DEFECT	ACTION TAKEN
Area	Frame Space, etc.			
Forepeak below #5 deck	Stem - WTB 2	ASSINIBOINE ST. LAURENT MARGAREE SAGUENAY	(a) Cracks in shell plating adjacent to Frame #1. (b) Breast plates cracked.	(a) Cracks veed and welded. (b) Welded or renewed according to severity of fractures. 3/8" x 3" faceplate fitted (negative SAGUENAY).
Forepeak below #5 deck	Stem - WTB 2	MARGAREE	Crack in keel at 1 foot aft of forefoot (crack occurred twice).	Crack veed and welded.
Steering Gear Compartment	WTB 7 - Stern	ST. LAURENT SAGUENAY	Cracking and weld failure at junction of rider plates and steering bridge table, Frames 80, 81, 81 1/2 and 82 port and starboard.	Veed and welded in ST. LAURENT. SAGUENAY to be taken in hand at refit.
Sick Bay	WTB 21	ST. LAURENT FRASER SAGUENAY OTTAWA	Cracks at deckhead on C/L and on port and starboard C/L bracket stiffeners.	To be repaired during conversion in accordance with CANAVHED instructions.
Fore end of Superstructure at weather deck.	Frame 21 1/2	SAGUENAY FRASER MARGAREE	Crack in weld joining deck and front of superstructure at centre line.	Veed and welded. Exterior doubler fitted to deck about 12" x 6".
Boiler Room Intakes	Frame 43 1/2	ST. LAURENT FRASER SAGUENAY SKEENA OTTAWA ASSINIBOINE	Hairline cracking of welds at #3 deck level in passage and Crew's Dining Hall.	To be repaired during conversion in accordance with CANAVHED instructions
Foremast	#2 platform	SAGUENAY FRASER SKEENA	Weld failure at tripping brackets of AN/SPS 12 pedestal.	Veed and welded.

TABLE 3-1

DDE 205 CLASS - STRUCTURAL DEFECTS
1955-1963

LOCATION		NAMES OF SHIPS AFFECTED	DEFECT	ACTION TAKEN
Area	Frame Space, etc.			
Cofferdam	OTB 64 - WTB 65	MARGAREE ST. LAURENT SAGUENAY	Welding cracked at WTB 65 from #3 F.W. tank.	Veed and welded.
3"/50 Gun Support	Frame 16 - Frame 19	SKEENA SAGUENAY MARGAREE FRASER	Crack in weld at #2 deck, Frame 18 on port and starboard sides at deckhead.	Crack veed and welded. 3" x 12" x 10 lb. doubler fitted on face of standing flange.
Fog Oil Tank	OTB 73 - OTB 75	MARGAREE SAGUENAY	Weld crack at OTB 75 at corner (port or starboard).	Veed and welded.
Engine Room	OTB 53, 4th longitudinal	All Ships	Cracks in plating in way of rider plate to longitudinal frames below shaft bearings.	Modified and repaired in accordance with Esquimalt drawing #8535.
Steering Gear Compartment	WTB 78 - Stern	MARGAREE	Cracks in shell plating and at welds of internal framing in vicinity at WTB 78. Cracks were both longitudinal and athwartships and were 3 in number.	Veed and welded.

3.3 DDH 205 Class Structural Defects, 1963-1976 Reference Illustrations i-1 to i-3

The original designers of the DDE 205 Class assumed the ships would have a life of about 20 years after commissioning. It was no surprise that the seven ships of this class would complete midlife conversion/modernization to DDHs during the period 1963-65. During conversion the ships underwent a major reconfiguration which changed the appearance of the ships and the structural arrangements to accommodate an operational helicopter and facilities and the Variable Depth Sonar (VDS) system.

At the conversion of the DDE 205 Class to the DDH 205 Class, the after superstructure was removed and the uptakes from the Boiler Room were split Port and Starboard sufficiently to allow the nose of the helicopter to be located between the uptakes in the new hangar. The new hangar and flight deck after superstructure was installed with the flight deck material of Lukens T1 steel (100,000 psi yield stress) to keep weight as low as possible and with the hangar and supporting superstructure of marine grade aluminum. The hangar has an expansion joint aft of the funnel uptakes which allowed for the flexing of the ship in seaway. Three inch longitudinal movement of the expansion joint at the top of the hangar was witnessed on occasions in sea states greater than five. Very little change was made to the main weather deck structural configuration during this conversion other than the modifications to accommodate the twin uptakes and the cut away stern for the VDS. In other words, the scantlings at #1 deck prior to the DDH conversion were essentially the same as they were afterwards. The aft portion of the ship was reconfigured substantially to accommodate the installation of the variable depth sonar and the reconfiguration of the tankage for a change in the fuel tank capacities including the additions of the JP5 Tank and Pump Room.

The stability margin of the DDE 205 ships was such that the Flight Deck could be placed one deck height above the uppermost continuous hull deck (No. 1 or Weather Deck). The Flight Deck had to be robust enough to handle the landing loads and the inertial parking loads of a 22,000 lb. helicopter in Sea States 5 to 7! The "Beartrap", a Canadian innovation, is a constant tension device for recovery of the helicopter from its hovering position, securing the helicopter in the trap and transversing the helicopter into the hangar. The hangar deck was constructed of steel.

There were two main factors which affected the location of the Flight Deck on the DDH 205 Class:

a. It must be high enough in the ship to prevent the take-off and landing pattern being obstructed by the ship's superstructure and environmental conditions;

b. It should be as low as possible in the ship to minimize the effects of pitch and roll, and to minimize the impact on ship stability.

In the face of these conflicting requirements, life's usual compromise was reached. An obstruction-free area approximately 78 feet long and 40 feet wide was provided (at the expense of the after gun turret and one set of mortars) one deck above the forecastle deck and abaft the main superstructure and hangar. For the record, the Flight Deck is only 6 feet longer than the aircraft! The after part of the fuselage can overhang the after end of the Flight Deck, effectively increasing the length of the deck by some 10 feet.

No major changes were made to #1 Deck midships region of the steel hull, Fr. 39-45 except that necessary to accommodate the twin funnel openings, port and starboard of the ship's centreline (as opposed to the single C.L. funnel of the DDE) to permit the nose of the helicopter to fit between the uptakes in the hangar. The outboard strake of plate at 1 Deck Fr. 39-45 was 17 lbs. (7/16 inch, 11mm, 17.85 lbs.) while the inboard plate was 12 lb. and the centreline strake was 10 lbs. (1/4 inch or over 6mm). It appears there was no appreciation of the large vertical loads which would be transmitted to the 1 Deck midships area from the large hangar (and parked helicopter) cantilevered from the flight deck, supported only by the structure surrounding the Boiler air intake(s), see Figure 3-2.

The conversion designers thought this was unnecessary because their calculations, using the 1954 Muckle Method of balancing the ship on a standard trochoidal wave height equivalent to L/20, revealed the following (after conversion):

Sagging Maximum B.M. = 31,130 tons ft., 8 feet aft amidships
Hogging Maximum B.M. = 43,581 tons ft., 7 feet off amidships
I = 111, 613 in^2ft^2
y (1 Deck) = 14.07 ft.; I/y = 7940 in^2ft.
y (Keel) = 14.43 ft.; I/y = 7720 in^2ft

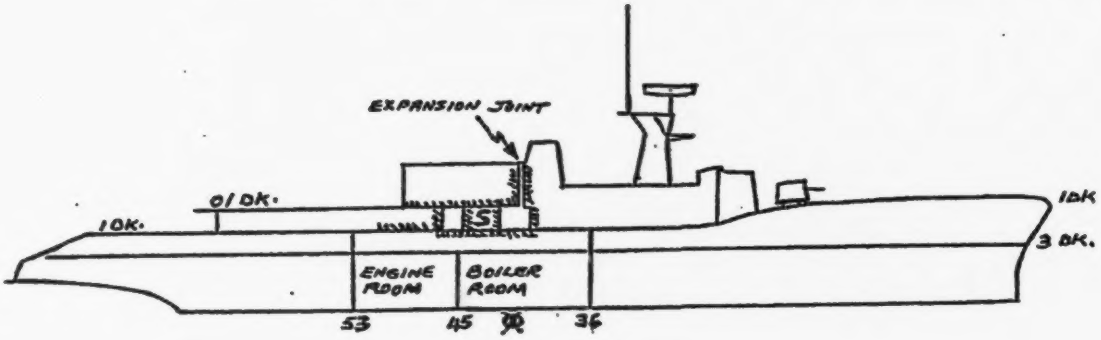

Figure 3-2

Rough Profile of a DDH 205/265 Class Destroyer

Hence, the following stresses (B.M. divided by I/y):

TABLE 3-2

DDE/DDH 205 KEEL AND DECK STRESSES BEFORE AND AFTER CONVERSION

	AFTER CONVERSION			BEFORE CONVERSION		
	tons/in²	PSI	MPa	tons/in²	PSI	MPa
Sagging						
Deck (compression)	3.92	8780	61	4.03	9030	63
Keel (tension)	4.03	9030	63	4.14	9270	64
Hogging						
Deck (tension)	5.49	12300	85	4.99	11180	78
Keel (compression)	5.65	12660	88	5.12	11470	80

Assuming a nominal yield strength, σ_y, of 32,000 psi, these hogging and sagging primary stresses were comfortably less than 0.5 σ_y. For comparison purposes the primary deck stress for HMCS NIPIGON, DDH 266, was calculated to be 14,240 psi (98.2 MPa) after her mid-life modernization in 1987-89.

During the period 1963 to 1976, the DDH 205 Class the ships experienced the following structural failures:

3.3.1 OTB Fr. 36 Discontinuity + Hard Point

The cracking occurred at the junction of the transverse watertight bulkhead Frame Station 36, forward Boiler Room bulkhead and the longitudinal bulkheads forming the boundaries of No. 3, 4 and 5 fuel oil tanks. The cracking typifies the knife edge intersection problem and was compounded by the fact that several ships showed misalignment between the longitudinal bulkhead and the web of the longitudinal. Repairs were affected by carrying the longitudinal rider plate through the main transverse bulkhead 36 to the first vertical stiffener of the longitudinal FFO tank bulkhead, lining up the web of the longitudinal with the plate of the longitudinal FFO tank bulkhead, installing insert plates in both bulkheads (where the cracks had occurred) and fitting a beam end type bracket shown at Figure 3-3.

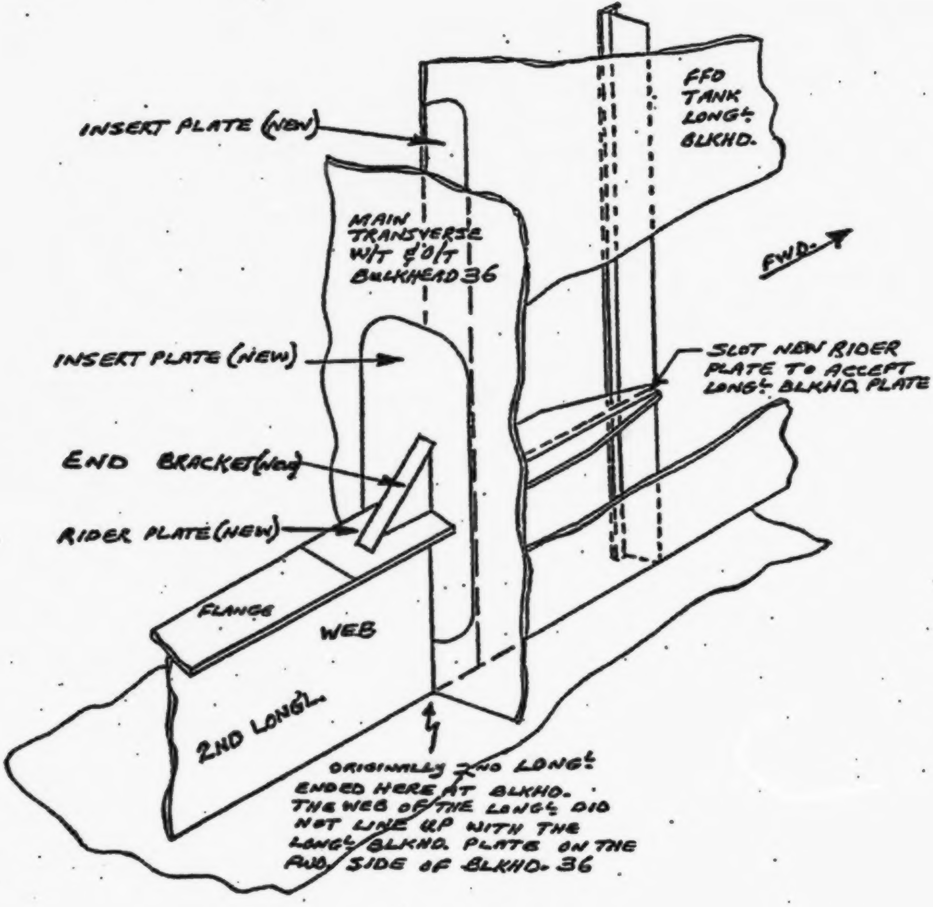
INSERT PLATE (NEW)
FFO TANK LONG'L BLKHD.
MAIN TRANSVERSE W/T & O/T BULKHEAD 36
FWD.
INSERT PLATE (NEW)
SLOT NEW RIDER PLATE TO ACCEPT LONG'L BLKHD. PLATE
END BRACKET (NEW)
RIDER PLATE (NEW)
FLANGE
WEB
2ND LONG'L.
ORIGINALLY 2ND LONG'L ENDED HERE AT BLKHD. THE WEB OF THE LONG'L DID NOT LINE UP WITH THE LONG'L BLKHD. PLATE ON THE FWD. SIDE OF BLKHD. 36

Figure 3-3

Junction of the Transverse Watertight Bulkhead Frame 36
Forward Boiler Room Bulkhead and the Longitudinal Bulkheads
Forming the Boundaries of No. 3, 4 and 5 Fuel Tanks

3.3.2 Superstructure Fr. 36 Hard Point

This crack occurs at the connection between the aluminum funnel casing port and starboard and the aluminum bridge structure at approximately 01 Deck level. DDH's which have rivetted superstructures have not exhibited this failure.

In welded construction a hard point exists at the location of funnel casing/01 Dk which again typifies the "knife edge intersection". Two repairs have been tried to relieve the hard spot, adding insert plates and addition of a gusset plate inside the funnel casing in line with 01 Deck.

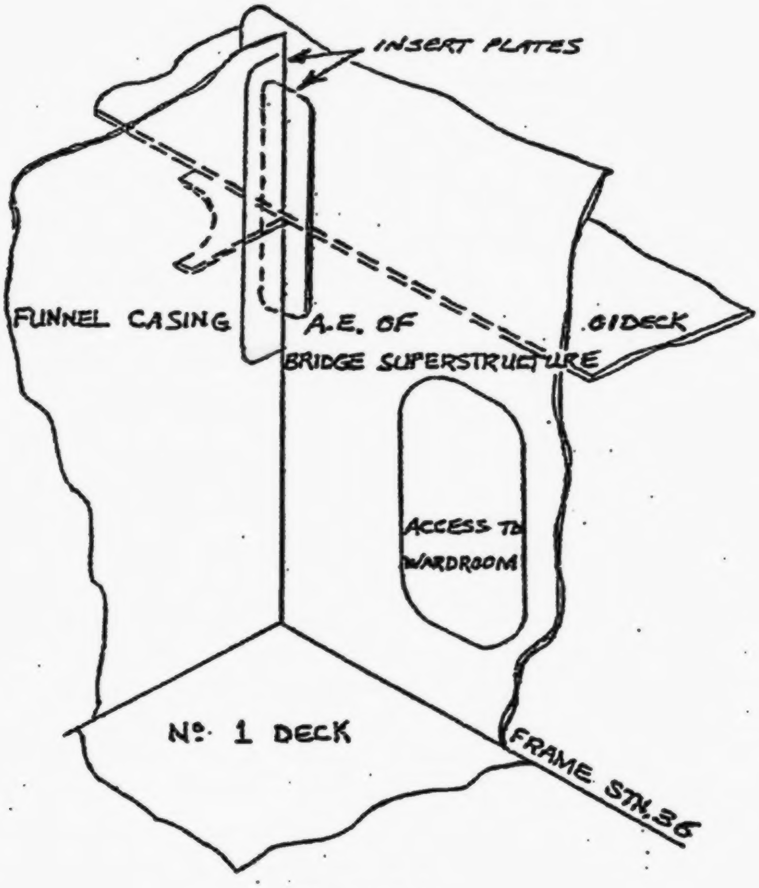
INSERT PLATES
FUNNEL CASING
A.E. OF
BRIDGE SUPERSTRUCTURE
01DECK
ACCESS TO
WARDROOM
Nº. 1 DECK
FRAME STN.36

Figure 3-4

View of Starboard After End of Bridge Superstructure
Looking Forward and Toward the Centreline

3.3.3 Pillars (No. 1 Deck Midships Frame 41 and No. 3 Deck Frame 27)

There are basically two pillar head connection methods: floating free such as pillars located on 1 Deck midships supporting the hangar deck and fixed such as pillars located at Frame 27 between 1 and 3 Decks.

(1) No. 1 Deck Midships Frame 41. The failure occurs at head of pillars, No. 1 Deck, which supports hangar structure. The crack results from the relative movement of the hangar deck with No. 1 Deck. In effect, the pillar is being subjected to tensile forces for which it was never designed. Two alternatives exist: strengthen the connection with the use of gusset plates or allow the hangar to move relative to the pillar. The latter has been adopted for this area because of the relatively large movement in the area. See Figure 3-5 and 3-6.

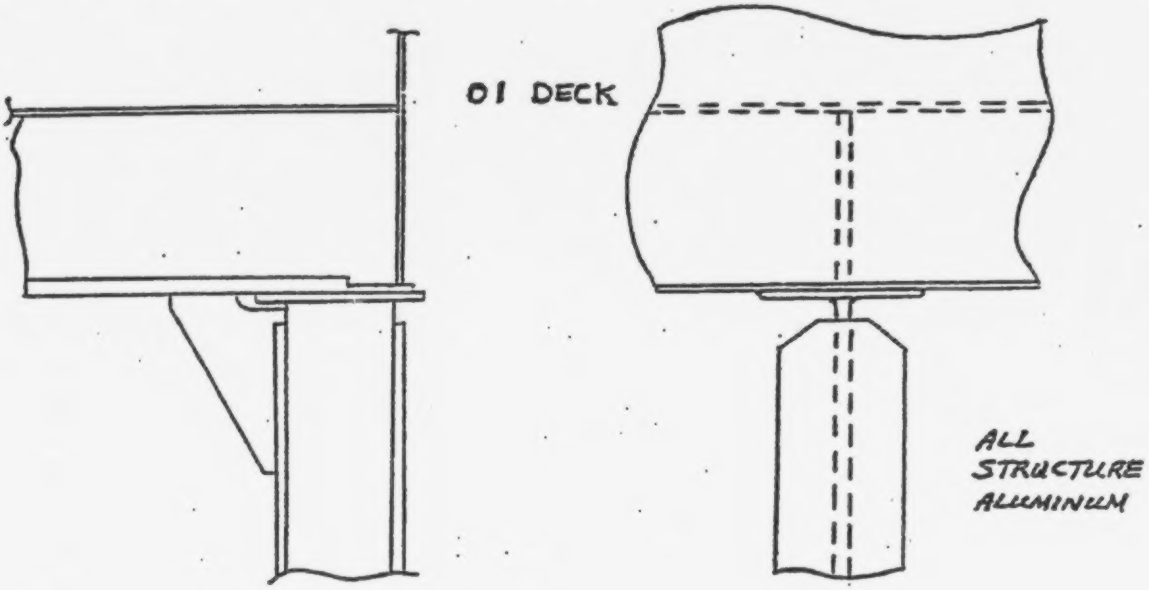
01 DECK
ALL STRUCTURE ALUMINUM

Figure 3-5

"Original" Pillar Head Arrangement
Port and Starboard Midships Frame 41

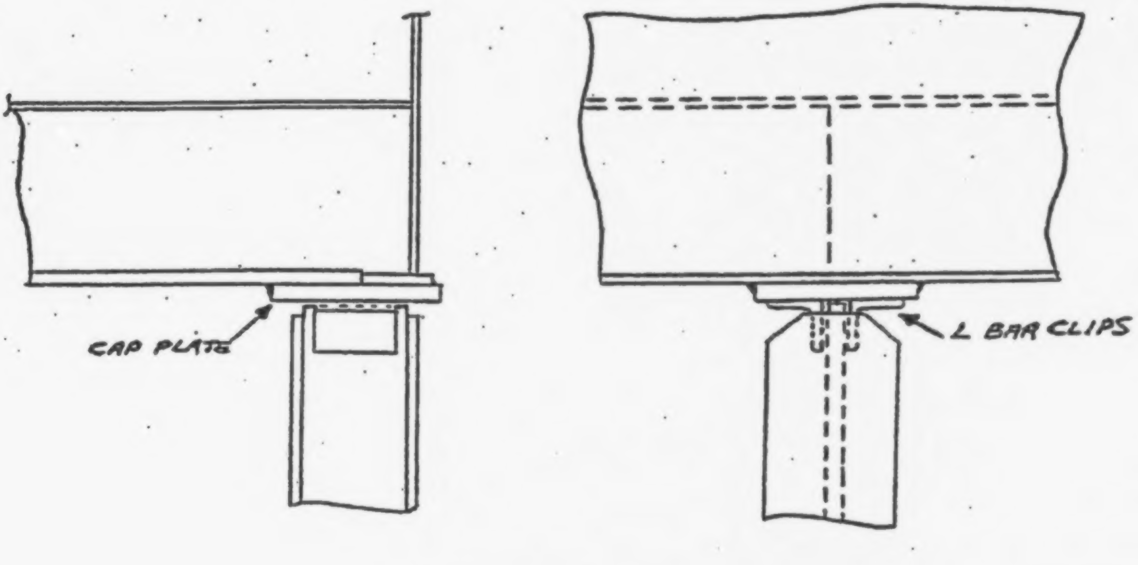
CAP PLATE
L BAR CLIPS

Figure 3-6

"Redesigned" Pillar Head Arrangement
Port and Starboard Midships Frame 41

(2) No. 3 Deck Frame 27. Three (3) in number pillars exist at Frame 27 to resist compressure loading forces between 1 Deck and 3 Deck. As stated previously, pillars are not normally designed to withstand tensile loadings of any great magnitude. In this case it was decided to restrain vertical movement between the pillar head and the 1 Deck supporting longitudinal structure to alleviate stresses from minor bulkheads which would hopefully prevent cracking and noises caused by the relative movement of minor bulkheads, boundary bars, etc. This problem was not considered so much as a structural one as it was psychological in that the cracks and noises were readily visible and audible to the ship's company. It also kept the officers awake in their cabins and created an abundance of volunteers for the morning watch!

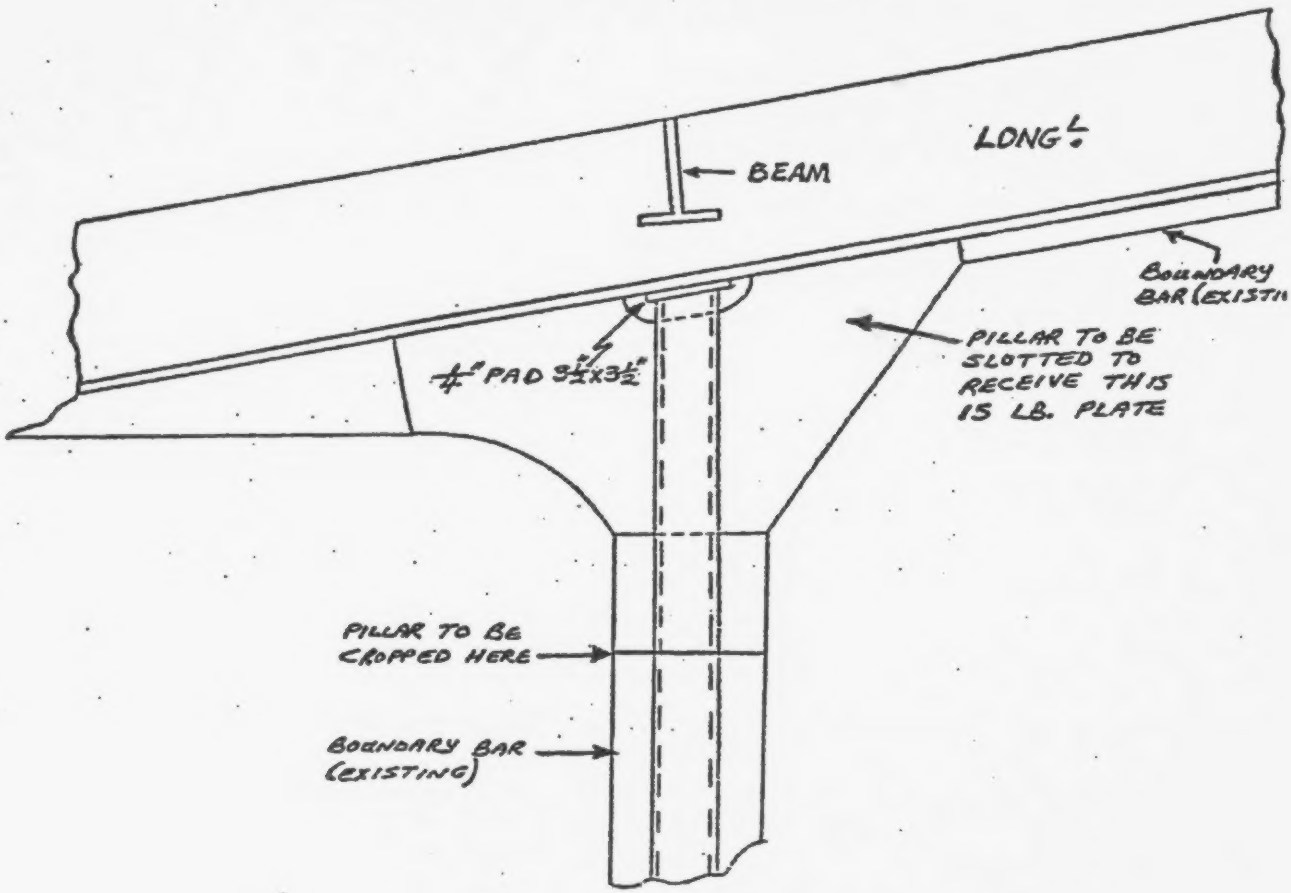
LONG'L
BEAM
BOUNDARY BAR (EXISTI
¼" PAD 3½"x3½"
PILLAR TO BE SLOTTED TO RECEIVE THIS 15 LB. PLATE
PILLAR TO BE CROPPED HERE
BOUNDARY BAR (EXISTING)

Figure 3-7

Typical Pillar Head Connection 3 Deck Frame 27
(Modification to each Pillar is Custom Designed)

3.3.4 Cracks at Knuckle, Frame Station 27 1/2

Almost all ships have experienced cracks on 1 Deck at the knuckle. The problem appears to result from the panting of the panel in a seaway with the stiffeners being too rigid because of the knuckle bend and not being able to follow the motion in a seaway. Longitudinal cracks develop along the welds of the stiffeners and by 1979 on SAGUENAY, OTTAWA, SKEENA, and MARGAREE cracks have also developed in the deck plate in way of the longitudinals. The repair is to either relieve the hard points at the knuckle by cutting slots in the longitudinals or stiffening the panels by running a flat bar across between the longitudinals. The latter to restrict panel panting has proved to be more economical. Section 5.0 uses this fracture to demonstrate the high cost of stripout, inspection, repair and replacement.

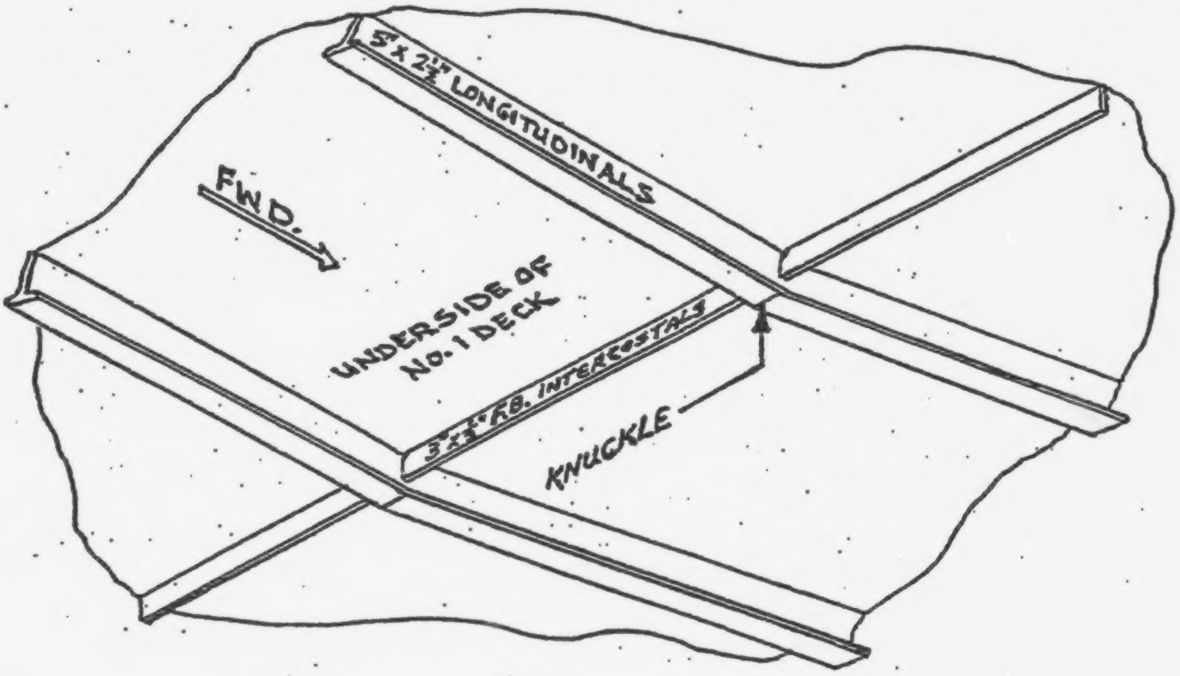

Figure 3-8

Knuckle
Frame 27 1/2

3.4 **Midship Defects, 1976-1978** Reference Illustration i-1

3.4.1 Background History

The seven DDE/DDH 205 Class ships spanned a lifetime between 1951 (HMCS ST. LAURENT) 1st launching to 1994 (HMCS FRASER) last decommissioning. Table 3-3 provides "Principal Events in the Life of DDE/DDH 205 Class 1951 to 1994 Related to the Midships Structural Failures". The conversion to DDH was completed between 1963 and 1966.

The first occurrences of fatigue like failures in the midships area of the ships of the DDH 205 Class were detected in 1976. All structural defects in whatever form could be encompassed in an envelope between Frame 38 and 46 longitudinally, and just outboard of longitudinal #3 Port, to and including, longitudinal #3 Starboard. The failure pattern in each ship tended to be unique, the details of which are illustrated in the associated figures, Figures 3-9 to 3-13 inclusive.

Commencing in 1976, with HMCS SKEENA, through 1979 several occurrences of midships structural cracking occurred. In 1978 three ships of the Class had debilitating structural failures in the midships area between Frames 38 1/2 to 45 1/2 which were cause to remove the ships from the scheduled operational programs until such times as they could be repaired to make them safe for future operations. Clearly there was a midships structural class problem of fatigue and/or fracture failures notwithstanding that each of the ships were uniquely different from each other in the pattern of the failures. Interim repairs or emergency repairs were undertaken to put the ships back into operational programs simultaneously with the development of Destroyer Life Extension Alteration, DELALT D51 for the replacement of all plating and longitudinals between Frame 38 1/2 and 45 1/2 and just outboard of longitudinals # 3 Port and Starboard. Figure 3-14 illustrates the renewals and reconfiguration in the area of concern implemented by DELALT D51.

The specifics of the structural failures and the emergency repairs or interim repairs are discussed and illustrated by ship in the following sections.

3.4.2 Midships Structural Cracking DDH 205 Class

Prior to 1976 there is no known structural cracking in the midships area of #1 deck except for the 1960 occurrence of HMCS ST. LAURENT centreline longitudinal cracking immediately forward of Frame 45. This particular defect appears to have been a fabrication inadequacy in the form of incomplete penetration or undercutting of the weldments.

3.4.3 **HMCS SKEENA and FRASER** Reference Figure 3-9 Interim Repair

In 1976 HMCS SKEENA had some structural cracking in the vicinity of Frame 43, Starboard side under the after superstructure. Similar structural cracking occurred in HMCS FRASER in late 1976 or early 77 (Figure 3-9 refers). Both of these ships were repaired during their respective refits in 1976/77 by cropping out the defective area and replacing with a 17 lb. insert plate. These two ships were the first to show a significant structural failure in the midships area which could be interpreted as being a fatigue failure.

3.4.4a **HMCS SAGUENAY** Reference Figure 3-10 Temporary Emergency Repair

HMCS SAGUENAY was given a check survey in early autumn of 1977 and was found to be free of any cracking in the midships portion of the ship. It is known the ship was called to an emergency rescue mission in the North Sea approximately November of 1977 in which the environmental conditions were Sea State 6 and the ship had full power on to execute the emergency. In the January to March time frame HMCS SAGUENAY served in the Fishery Patrol off the Grand Banks area in some rather significant sea conditions and very cold temperatures. In March 1978 HMCS SAGUENAY reported unusual structural noises and entered St. John's, Newfoundland harbour for an on-site inspection. Several longitudinals were fractured or in the progress of cracking. These included failure of longitudinal #2 Port and Starboard side in way of Frame 40; a crack had initiated in longitudinal #3 Starboard; partial cracking of longitudinal # 1 Port and Starboard; and centreline longitudinal crack in way of Frame 43 1/2. It is interesting to note that the line of the failures was approximately a "V" with the apex at the forward end of the Boiler Room air intakes branching outwards approximately 30° to the centreline to Frame 39 1/2 in way of longitudinal #3. An operational restriction was placed on the ship to sail from St. John's to Halifax in Sea State 4 or less.

Temporary emergency repairs were undertaken to ensure the safety of the ship for its deployment through the remaining operational commitments until August of 1978. Clearly, the emergency repairs were essential to ensure the ship's safety. Also it was clear that the proper interim repairs would take several weeks cutting into an operational commitment for Fisheries Patrols. The emergency repairs implemented in March 1978 included the installation of inverted "T"s above the line of #2 longitudinal Port and Starboard side spanning two frames either side of the #2 structural failures. The centreline longitudinal was repaired temporarily by "veeing out" and re-welding the area of the crack in the longitudinal member. The remaining known cracks were not touched at this time. Each time the ship returned to port between its Fisheries Patrols, the opportunity was taken to inspect the ship to ensure no progress in the area of structural failures.

3.4.4b HMCS SAGUENAY - Reference Figure 3-10 Interim Repair

In August 1978 the interim structural repairs were implemented by replacing a length of #2 longitudinal and modifying it to remove the structural discontinuity in the proximity of Frame 39. A section of the centreline longitudinal was also replaced just forward of the Boiler Intakes. All other repairs consisted of "veeing out" the defected area and rewelding the #3 and #1 longitudinals. No plate replacement was undertaken at this time. A minor crack was "veed out" and welded.

3.4.5 HMCS ASSINIBOINE Reference Figure 3-11 Interim Repair

In the spring of 1978 HMCS ASSINIBOINE reported taking on water in the proximity of the Galley ventilation trunk, Port side, Frame 42. Upon inspection it was discovered that there was a continuous crack through the #1 Deck plating and the longitudinals from #3 longitudinal Port, across the Galley exhaust, #1 longitudinal Port, up the Boiler Intakes coaming, shearing all rivets in the bimetallic connection, down the coaming into the deck, across #1 and #2 longitudinals and was progressing towards #3 longitudinal. The centreline longitudinal was fractured in three locations in the proximity of Frame 43 1/2 just forward of the Boiler Intake in way of Frame 42 and just forward of Frame 45. It is significant that this ship had a continuous crack in #1 Deck midships from outboard of #3 longitudinal Port to just inboard of #3 Starboard. This is over half the width of the ship. The ship was removed from operational programs until such time as full interim repairs could be implemented. Extensive examinations of the area immediately forward and aft of the identified crack in No. 1 Deck area was undertaken to ensure there were no further failures occurring. It was this inspection procedure that discovered the centreline longitudinal failure near Frame 42. Interim repairs undertaken included a replacement of the centreline longitudinal from Frame 41, to and including, 45 1/2. A short section of #1 longitudinal Port and Starboard side was also replaced and an insert plate was installed in the proximity of the cracked area.

3.4.6 HMCS MARGAREE Reference Figure 3-12 Interim Repair

In the late summer of 1978 HMCS MARGAREE had structural failures of the centreline longitudinal in two locations, forward of Frame 45 and in the proximity of Frame 43. Cracking of the numbers 1 and 2 longitudinals was in progress and deck plate cracking had initiated between Frame 42 and 45. None of the cracks seemed to be in a specific pattern nor were they indicating that they were about to progress as a continuous crack across the ship. Of particular interest is the details of the centreline longitudinal passing through the Boiler Room inlets. The centreline longitudinal on all other ships of the Class was fitted with a "T" and rider plate configuration with flange top and bottom. In the case of MARGAREE it was a "T" with no rider plate on top.

The interim repair for this ship included replacement of the centreline longitudinal from approximately Frame 42 to Frame 45 1/2, with the section 43 1/2 to 45 being now an "H" section. A short section of #2 longitudinal Starboard was replaced in the proximity of Frames 42 to 43 and a small insert plate was installed in this general area. All other detected cracks were "veed out" and welded without replacement of the section or the plating involved.

3.4.7 **HMCS FRASER Midships Fracture** Reference Figure 3-13 Emergency Interim Repair

Subsequent to the interim repairs identified above at 3.4.3, an instantaneous fracture occurred forward of the Boiler Room emergency escape hatch on the boundary of the new insert plate and old plate weldment. The point of initiation of this fracture was at the weldment of the insert where 3 beads of weldment were positioned diagonally across the insert weldment. The reasons for these three beads of weldment are unknown but could be related to a holding bracket for the insert plate positioning. The fracture occurred off the coast of Halifax in a Sea State 4 stern quartering sea. The ship reported an "odd" wave hitting them at the time of fracture. The fracture had radiated out in two directions in a random, irregular pattern, one inboard and one outboard from the point of inception. The total length of the crack was about 20 feet. The noise created was heard throughout the ship and because of the weather conditions at the time, water immediately started to enter the ship through the fracture crack. The ship returned to Halifax Harbour as soon as possible thereafterwards for an evaluation and appropriate repairs.

The inspection of the area indicated that a fracture had occurred and the inception was, as indicated above, at the very point of the intersection of the short beads across the insert weldment. A beautiful chevron pattern on the plate edge was quite obvious. The plate had some distortion (buckling) characteristics and the fracture crack had opened up a fraction of an inch. The total length of the fracture occurred in both directions through the existing old plate. By inspection it appeared that the locale of the fracture initiation was a source of high stress concentration, probably in the form of residual stresses which, when combined with longitudinal stresses and the stresses due to the racking of the ship in the stern quartering sea, was sufficient to cause the stress levels to be beyond the ultimate strength of the structural members. The interim repair in this case was to replace a substantial panel of plating with slightly heavier plate from just inboard the centreline to outboard of #3 longitudinal, between Frame 43 and Frame 41. The longitudinals affected by the fracture were "veed out" and rewelded except #2. A section of the #2 longitudinal was replaced between Frame 41 1/2 to aft of 43.

3.4.8 HMCS ST. LAURENT and HMCS OTTAWA

No known midships structural cracking or failures occurred with the exception of that mentioned in 3.4.2 above pertaining to the ST. LAURENT. HMCS ST. LAURENT was decommissioned in 1974 and had not quite reached 20 years since the commissioning of the ship. So far as is known by anyone knowledgable of the subject, HMCS OTTAWA had no midships failures or cracking of any form through its life prior to the implementation of DELALT D51.

3.5 Destroyer Life Extension (DELEX), 1979-1982 Reference Figure 3-14 DELALT D51 and Illustration i-1

1978 saw the removal of three DDH 205 Class ships from operational status pending completion of structural repairs in order to ensure the safety of the ship and personnel therein. Prior to this time, two ships had structural failures of lesser nature in a similar area of the ship. It was quite apparent there was a Class problem in the midships structure of #1 deck between Frames 39 and 45, and longitudinal #3 Port to longitudinal #3 Starboard. Peacemeal repairs and/or replacements of the plate and/or longitudinals would not ensure the tenure of life for these ships other than of relatively short duration, simply because the replacement of either plate or longitudinal members would move the failure site further along the structural configuration. The whole of the area affected in all ships was examined and it was concluded that the replacement of the #1 deck plating and the replacement of all longitudinals between Frames 39 and 45 was essential as a minimum to ensure an extended further life of the ships beyond the next refit cycle. DELALT D51 was initiated in conjunction with the DELEX Project and appropriately funded through the DELEX Project. Figure 3-14 shows the extent of those structural replacements. In the development of the D51 some areas of plating were increased in thickness and some longitudinals in specific locations were increased in size. The inception of DELALT D51 took place in October of 1978 and the first off installation was specified in HMCS ASSINIBOINE and integrated into the refit specifications closing 7 January 1979. Each ship of the Class going to refit thereafter included the DELALT D51 structural replacement. There is no known occurrence of structural failures in the No. 1 Deck midships areas of these ships subsequent to the implementation of the DELALT D51.

3.6 Life After DELEX, 1982-1994

3.6.1 Background History

During the period 1980-1982 each of the ships had completed their Destroyer Life Extension Refits. Each ship was operational for an additional eight to as many as twelve years in the case of HMCS FRASER after 1982. With the exception of

HMCS ST. LAURENT all ships saw a life of 36 to 43 years from launch. At Table 3-4 is a summary of the defects occurring from 1982 to the decommissioning of the respective ships. Specific observations and comments will be made on the more important defects during this period of the life of the ships.

3.6.2 Centreline Vertical Keel Distortions

Between 1982 and 1985 HMCS FRASER, OTTAWA and MARGAREE showed signs of the inception of centreline vertical keel buckling. In all three of these ships the locations were at Frame 67-68 and at Frame 33-36. In each case the centreline vertical keel was fitted with diagonal stiffeners, Port and Starboard side of centreline vertical keel web. These ships completed their life without further progress of the buckling phenomena.

In addition to the three ships mentioned, HMCS ASSINIBOINE had centreline vertical keel distortion at Frames 71-73. A similar stiffening was adopted for this particular case. It should be noted however, that ASSINIBOINE was subjected to a grounding situation prior to this occurring in which substantial deformations of the centreline vertical keel occurred in way of Frame 45 and the adjoining bulkhead between the machinery spaces. The principal part of the grounding was repaired during a refit in 1984/85.

3.6.3 Longitudinal Bulkheads and Associated Shell Plate and Tank Top Cracking

All ships of the Class experienced longitudinal bulkhead failures at Port and Starboard No. 1 Diesel Oil Tank, No. 5 Fuel Oil, bulkheads between Nos. 1 and 2 Fresh Water Tanks and Nos. 6 and 7 FFO Tanks. These failures occurred as cracks in the structural members and plating or as distortions to the bulkhead panel. Many of the stiffeners on the bulkheads were cracked near the top or bottom. In the case of the lower boundary cracking, some cracks propagated into the shell plating causing a significant leakage and a pollution problem. In the case of the failures near the top of the bulkhead stiffeners some cracks propagated into the tank tops causing fumes and oil leakage to the interior of the ship. Most longitudinal bulkheads that were subjected to this failure were fitted with additional horizontal stiffening in addition to the appropriate detail repairs made in the vicinity of the damaged plating or stiffeners.

HMCS FRASER, and one other ship, which cannot be confirmed at this writing, showed signs of shell buckling in the vicinity of Frame 67 and moving upwards diagonally towards the stern and also in the vicinity of Frame 36 and moving upwards diagonally towards the bow. No attempt to repair this was undertaken and the two ships involved concluded their operational life without incident.

3.6.4 Bulkhead 53 Cracks

All ships of the Class experienced cracking in bulkhead 53 in way of the shell longitudinals within the Fuel Tank area. No. 2 longitudinal had failures in each ship. Some ships had additional cracking in way of further outboard longitudinals. The machinery seating and longitudinal configuration as it approached and passed through bulkhead 53 was modified to reduce the structural discontinuity which appeared to be the source of the problem.

3.6.5 Pillars Distorted

Various pillars were found distorted in FRASER, MARGAREE and OTTAWA with little commonality of the failure in the Class. Nothing more needs to be mentioned about the pillars overall, with one exception. HMCS ASSINIBOINE had several pillar distortions and failure problems in way of the Galley Frame 41 and 43; Diesel Compartment Frame 14; Gunner Room Frame 18; No. 10 Mess Frame 64; No. 3 Mess Frame 16 and 19. It is important to note that all of these pillar distortions in HMCS ASSINIBOINE occurred in the time frame after the grounding. There was no similarities in the pattern or specific failures in other ships of the class.

TABLE 3-3

PRINCIPAL EVENTS IN LIFE OF DDE/DDH 205 CLASS RELATED TO MIDSHIPS STRUCTURAL FAILURES

Ship	Pennant Number	Launch	Commiss.	Conversion Completion DDE to DDH	1st Documented Midship Defect	Interim Midship Repairs	Related Figures	DELALT D51	Decommis.	Life from Comm.	Life from Launch	Life from DELALT D51
		Year	Year	Year	Year	Year		Year	Year	Years	Years	Years
ST. LAURENT	205	1951	1955	1963	1960[1]	--	--	--	1974[3]	19	23	--
SAGUENAY	206	1953	1956	1965	1978	1978	Fig. 3-10	1979	1990	34	37	11
SKEENA	207	1952	1957	1965	1976	1976/77	Fig. 3-9	1981	1993	36	41	12
OTTAWA	229	1953	1956	1964	--	--	--	1982	1992	36	39	10
MARGAREE	230	1956	1957	1965	1978	1978	Fig. 3-12	1980	1992	35	36	12
FRASER	233	1953	1956	1966	1977[2]	1977 1979	Fig. 3-9[2] Fig. 3-13[2]	1981	1994	38	41	13
ASSINIBOINE	234	1954	1956	1963	1978	1978	Fig. 3-11	1979	1988[4]	32	34	9

[1] HMCS ST. LAURENT centreline longitudinal cracked immediately forward of bulkhead # 45. The longitudinal was not continuous through bulkhead 45 but welded to bulkhead forward and aft respectively. Ship decommissioned prior to implementation of DELALT D51.

[2] HMCS FRASER initial centreline area cracking occurred in 1977 starboard, forward of BR inlets. See Figure 3-9. Instantaneous fracture initiated at boundary of repairs in 1977 and original plating propagating through old plating and longitudinals. See Figure 3-13.

[3] The lead ship, HMCS ST. LAURENT, was paid off into reserve in 1974 and subsequently cannibalized for parts until the decision to scrap her in 1979.

[4] HMCS ASSINIBOINE, the first DDE to be converted to DDH, effectively broke her back during a 1983 grounding. Repairs were effected during a 1984-5 refit prior to the decision to pay her off in 1988.

TABLE 3-4

DDH 205 CLASS - STRUCTURAL DEFECTS
POST DELEX REFIT 1982-1994

LOCATION		NAMES OF SHIPS AFFECTED	DEFECT	ACTION TAKEN
Area	Frame Space, etc.			
Centreline Vertical Keel (CVK)	Fr. 33-36	FRASER, OTTAWA MARGAREE	Centreline vertical keel distortion Fr. 33-36 and Fr. 67-68 - inception of buckling 1982-85	Added a diagonal stiffener Port & Stbd. side of Centreline Vertical Keel (CVK) web. Arrested buckling for remainder of operational life.
	Fr. 67-68	FRASER, OTTAWA MARGAREE (+ANNAPOLIS)		
	Fr. 71-73	ASSINIBOINE	Inception of buckling 1984	Added a diagonal stiffener Port & Stbd. side CVK
Centreline Girder between Boiler Uptakes	Fr. 37-41, 3 Dk.	MARGAREE, FRASER & OTTAWA (+ ANNAPOLIS)	Centreline long'l distorted and fractured 1984-85	Centreline long'l replaced Fr. 36 1/2 - 42 1/2
Fuel Tanks in way of (IWO) shell long'ls	Fr. 53-54	ALL SHIPS	Blkd. cracked IWO shell long'ls at #2 long'ls Port and Stbd, all ships, #3 long'ls some ships 1983-85	Modified the transition from machinery seat to long'l and intersection of blkd. 53 to eliminate structural discontinuities.
Longitudinal Bulkheads	- No. 1 Diesel Oil Tank Port & Starboard -No. 5 FFO Tank Port & Starboard - Blk. between No. 1 & 2 FW Tanks - Blk. between No. 6 & 7 FFO Tanks	ALL SHIPS OF DDH 205 CLASS (+ ANNAPOLIS NO. 5 FFO TANK)	- Blkd plate distortions and stiffener cracking near top and bottom of long'l blkds - Shell plate cracking in some ships (see below) - Tank top cracking in some ships 1982-85	Added horizontal stiffening on long'l bulkheads, repaired or replaced defective plate and stiffeners.
Boiler Room Escape Hatch Dk. Insert	No. 1 Dk. Fr. 43-44	MARGAREE ASSINIBOINE SAGUENAY	Cracked IWO hatch hinge recess	Veed out and welded.
No. 1 Dk. IWO Knuckle	No. 1 Dk. Fr. 27-28	ASSINIBOINE OTTAWA	Cracked IWO Knuckle 27-28	Veed out and rewelded plus addition of intercostal stiffener between long'ls

TABLE 3-4

DDH 205 CLASS - STRUCTURAL DEFECTS
POST DELEX REFIT 1982-1994

LOCATION		NAMES OF SHIPS AFFECTED	DEFECT	ACTION TAKEN
Area	Frame Space, etc.			
Pillars Distorted or Cracked	Boiler Room Capstan Compt.	MARGAREE	Pillar head cracked	Veed out and rewelded plus minor modifications.
	Capstan Compt.	FRASER	Pillar head cracked	Replaced some pillars that buckled.
	Fr. 26 under No. 1 Dk.	OTTAWA	Pillar head cracked	
	Galley Fr. 41 & 43 Diesel Compt. Fr. 14 Gunner Room Fr. 18 No. 10 Mess Fr. 64 No. 3 Mess Fr. 16 & 19	ASSINIBOINE	Various failures in ASSINIBOINE pillars including buckling and/or crack top or bottom	
Bilge Keels		MARGAREE OTTAWA SAGUENAY	Bilge keel plate cracked	Veed out and rewelded some small insert plates.
Forepeak Tank Shell Plate	Fr. 0-2	OTTAWA ASSINIBOINE MARGAREE	Shell plate in forepeak tank cracked	Veed and rewelded.
Shell Plate Various	No. 8 FFO Tank Fr. 61-62	MARGAREE	Shell plate cracked IWO No. 11 long'l	Veed out and rewelded minor modifications in detail.
	No. 1 Diesel Oil and No. 5 FFO	FRASER (+ ANNAPOLIS)	Shell plate cracked IWO vertical blkd. stiffeners and propagated to shell	
	Bilge Keel IWO shell	OTTAWA	Shell plate cracked in way of bilge keel crack propagation	
No. 6 Longitudinal Stbd. Side	Fr. 36 No. 1 Deck Stbd. Side	SKEENA FRASER	No. 6 longitudinal cracked less than two feet forward Fr. 36	Replaced a three foot section of #6 long'l vicinity of construction unit boundary - a fabrication defect.

FIGURE 3-9

H.M.C.S. FRASER & SKEENA - 1976-77

PLAN VIEW BENEATH NO.1 DECK - FRAMES 37 TO 47

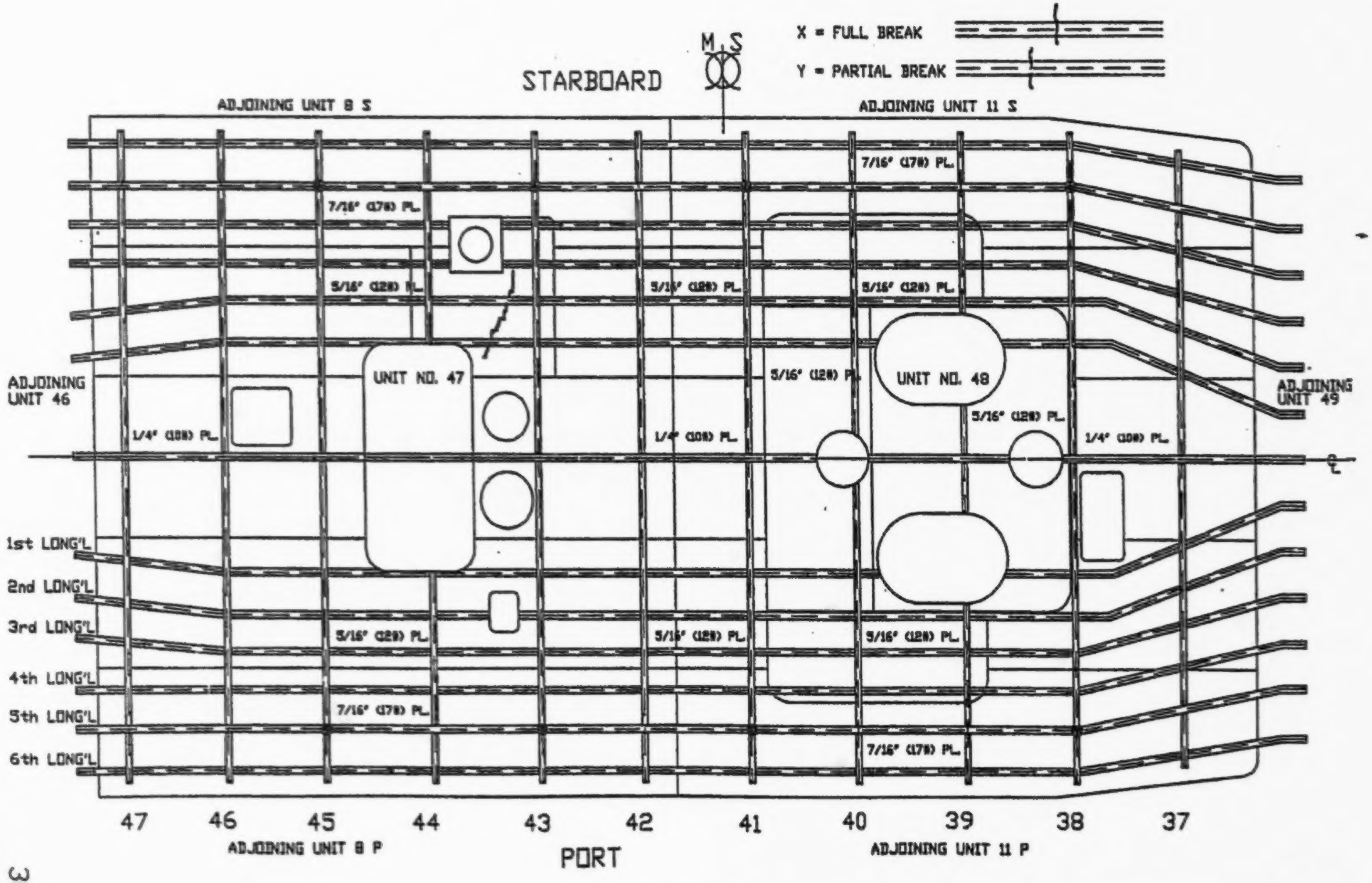
M.S
STARBOARD
X = FULL BREAK
Y = PARTIAL BREAK
ADJOINING UNIT 8 S
ADJOINING UNIT 11 S
7/16" (17#) PL.
5/16" (12#) PL.
1/4" (10#) PL.
UNIT NO. 47
UNIT NO. 48
ADJOINING UNIT 46
ADJOINING UNIT 49
℄
1st LONG'L
2nd LONG'L
3rd LONG'L
4th LONG'L
5th LONG'L
6th LONG'L
47
46
45
44
43
42
41
40
39
38
37
ADJOINING UNIT 8 P
ADJOINING UNIT 11 P
PORT

FIGURE 3-10

H.M.C.S. SAGUENAY - 1978

PLAN VIEW BENEATH NO.1 DECK - FRAMES 37 TO 47

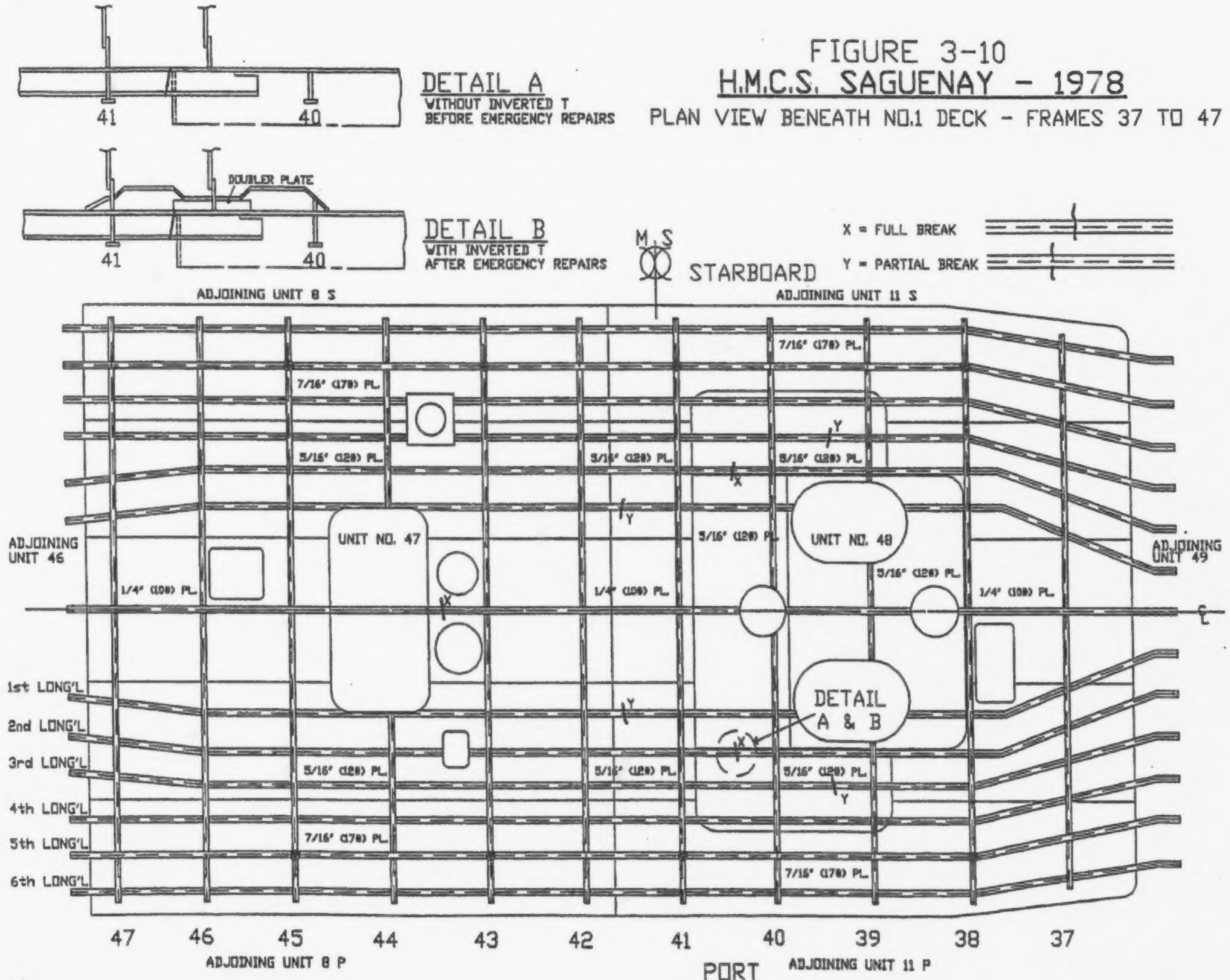
DETAIL A
WITHOUT INVERTED T
BEFORE EMERGENCY REPAIRS
41
40
DETAIL B
WITH INVERTED T
AFTER EMERGENCY REPAIRS
DOUBLER PLATE
41
40
M.S
STARBOARD
X = FULL BREAK
Y = PARTIAL BREAK
ADJOINING UNIT 8 S
ADJOINING UNIT 11 S
7/16" (17Ø) PL.
5/16" (12Ø) PL.
1/4" (1ØØ) PL.
UNIT NO. 47
UNIT NO. 48
DETAIL
A & B
X
Y
ADJOINING UNIT 46
ADJOINING UNIT 49
℄
1st LONG'L
2nd LONG'L
3rd LONG'L
4th LONG'L
5th LONG'L
6th LONG'L
47
46
45
44
43
42
41
40
39
38
37
ADJOINING UNIT 8 P
PORT
ADJOINING UNIT 11 P

FIGURE 3-11
H.M.C.S. ASSINIBOINE - 1978
PLAN VIEW BENEATH NO.1 DECK - FRAMES 37 TO 47

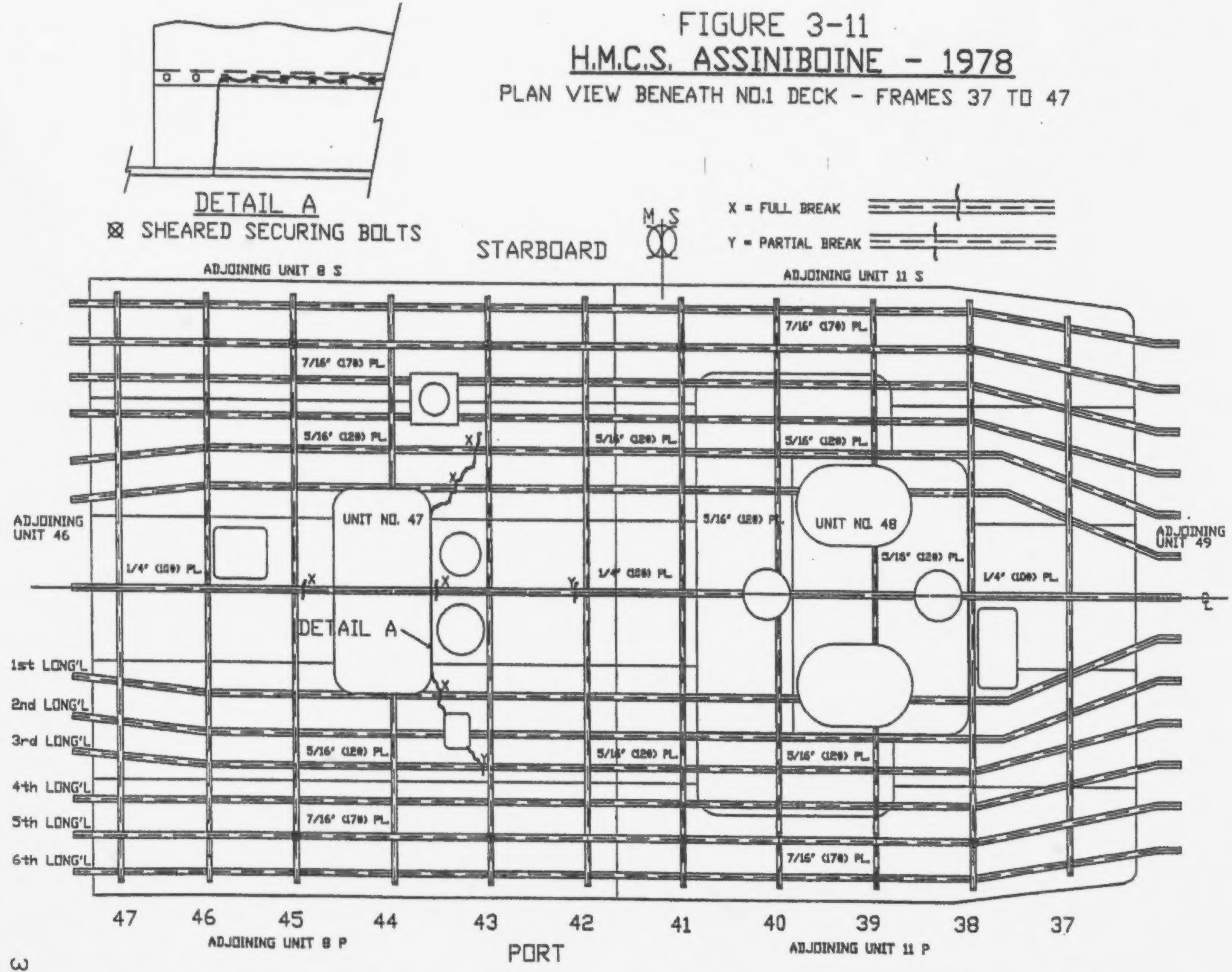
DETAIL A
⊠ SHEARED SECURING BOLTS
STARBOARD
M.S
X = FULL BREAK
Y = PARTIAL BREAK
ADJOINING UNIT 8 S
ADJOINING UNIT 11 S
7/16" (170) PL.
5/16" (120) PL.
1/4" (100) PL.
UNIT NO. 47
UNIT NO. 48
DETAIL A
ADJOINING UNIT 46
ADJOINING UNIT 49
℄
X
Y
1st LONG'L
2nd LONG'L
3rd LONG'L
4th LONG'L
5th LONG'L
6th LONG'L
47
46
45
44
43
42
41
40
39
38
37
ADJOINING UNIT 8 P
PORT
ADJOINING UNIT 11 P

FIGURE 3-12

H.M.C.S. MARGAREE - 1978

PLAN VIEW BENEATH NO.1 DECK - FRAMES 37 TO 47

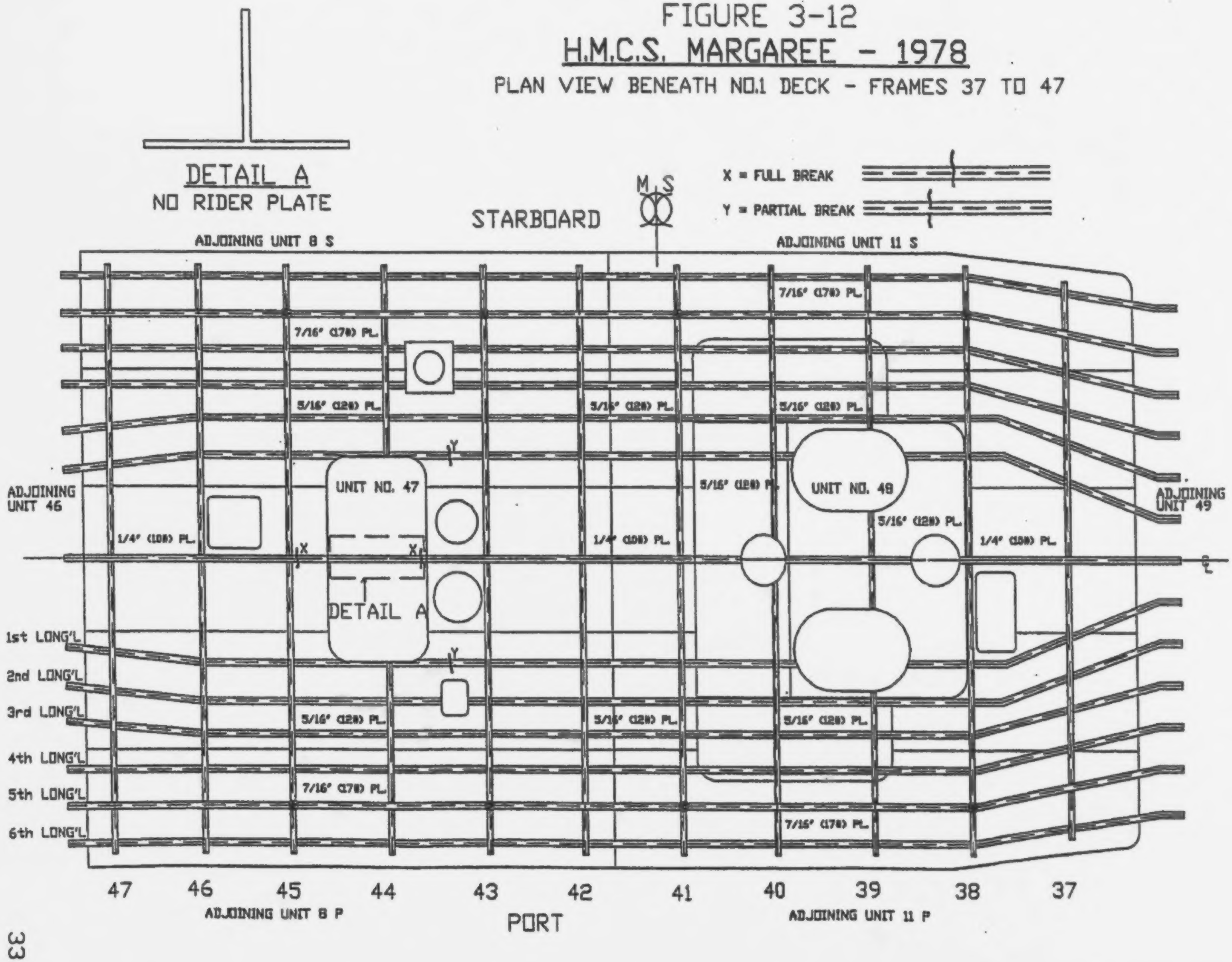
DETAIL A
NO RIDER PLATE
STARBOARD
M.S
X = FULL BREAK
Y = PARTIAL BREAK
ADJOINING UNIT 8 S
ADJOINING UNIT 11 S
7/16" (17#) PL.
5/16" (12#) PL.
1/4" (10#) PL.
UNIT NO. 47
UNIT NO. 48
DETAIL A
X
Y
ADJOINING UNIT 46
ADJOINING UNIT 49
℄
1st LONG'L
2nd LONG'L
3rd LONG'L
4th LONG'L
5th LONG'L
6th LONG'L
47
46
45
44
43
42
41
40
39
38
37
ADJOINING UNIT 8 P
PORT
ADJOINING UNIT 11 P

FIGURE 3-13

H.M.C.S. FRASER - 1979

PLAN VIEW BENEATH NO.1 DECK - FRAMES 37 TO 47

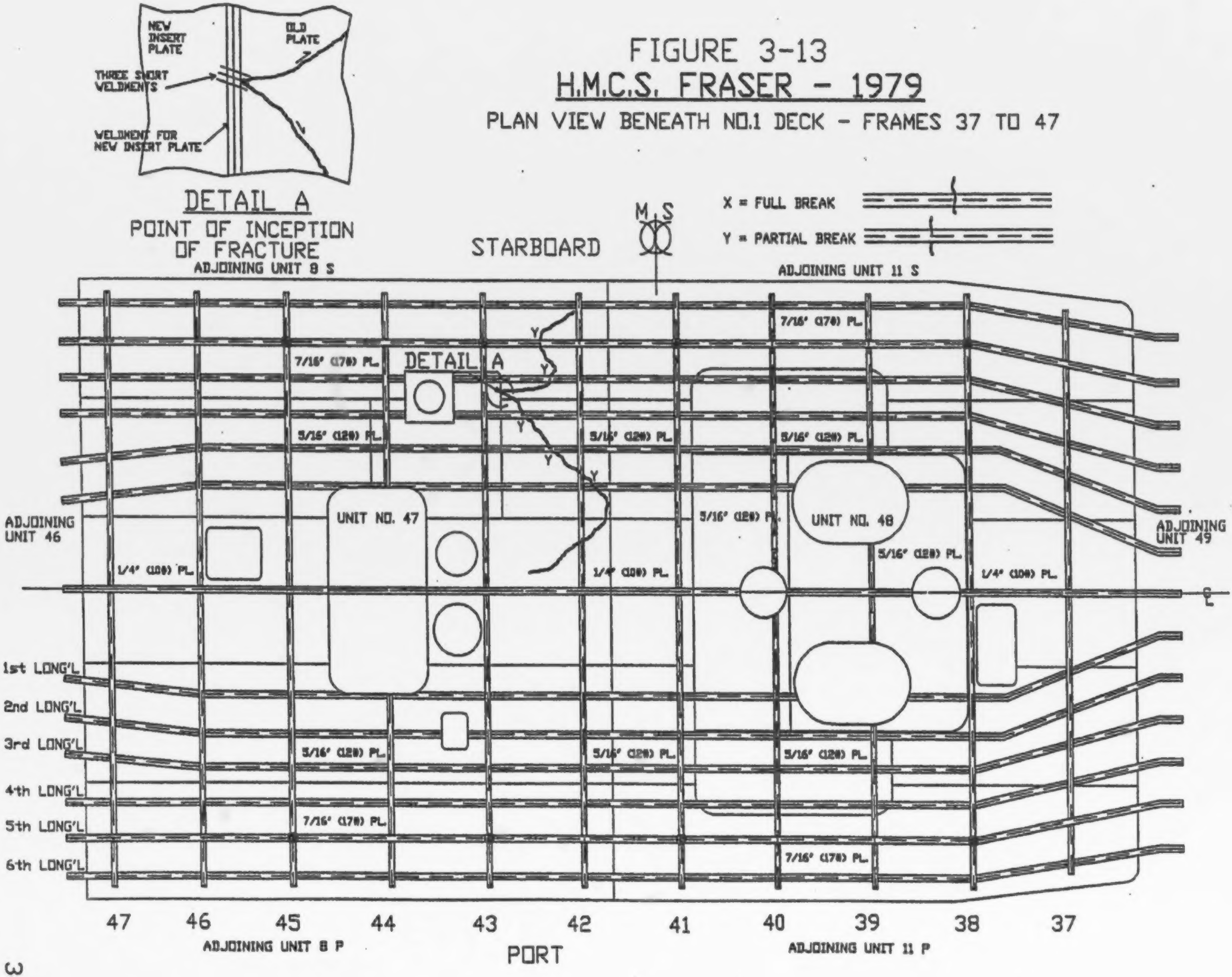
NEW INSERT PLATE
OLD PLATE
THREE SHORT WELDMENTS
WELDMENT FOR NEW INSERT PLATE
DETAIL A
POINT OF INCEPTION OF FRACTURE
STARBOARD
M.S
X = FULL BREAK
Y = PARTIAL BREAK
ADJOINING UNIT 8 S
ADJOINING UNIT 11 S
7/16" (17Ø) PL.
7/16" (17Ø) PL.
DETAIL A
Y
Y
Y
Y
Y
5/16" (12Ø) PL.
5/16" (12Ø) PL.
5/16" (12Ø) PL.
ADJOINING UNIT 46
UNIT NO. 47
5/16" (12Ø) PL.
UNIT NO. 48
5/16" (12Ø) PL.
ADJOINING UNIT 49
1/4" (1ØØ) PL.
1/4" (1ØØ) PL.
1/4" (1ØØ) PL.
℄
1st LONG'L
2nd LONG'L
3rd LONG'L
4th LONG'L
5th LONG'L
6th LONG'L
5/16" (12Ø) PL.
5/16" (12Ø) PL.
5/16" (12Ø) PL.
7/16" (17Ø) PL.
7/16" (17Ø) PL.
47
46
45
44
43
42
41
40
39
38
37
ADJOINING UNIT 8 P
PORT
ADJOINING UNIT 11 P

FIGURE 3-14

DELALT 51 - NO.1 DECK, MIDSHIPS AND AREA "AFTER MODIFICATION"

PLAN VIEW BENEATH NO.1 DECK - FRAMES 37 TO 47

1. 3 1/2 x 7 C.L. LONG'L RENEW
2. 2 1/2 x 5 2nd LONG'L REPLACED WITH 3 1/2 x 7
3. 3 1/2 x 7 3rd LONG'L RENEW
4. 1st LONG'L RENEWED WITH 3 1/2 x 7 FROM FR. 41 1/2 TO 45

▨ REPLACEMENT PLATE

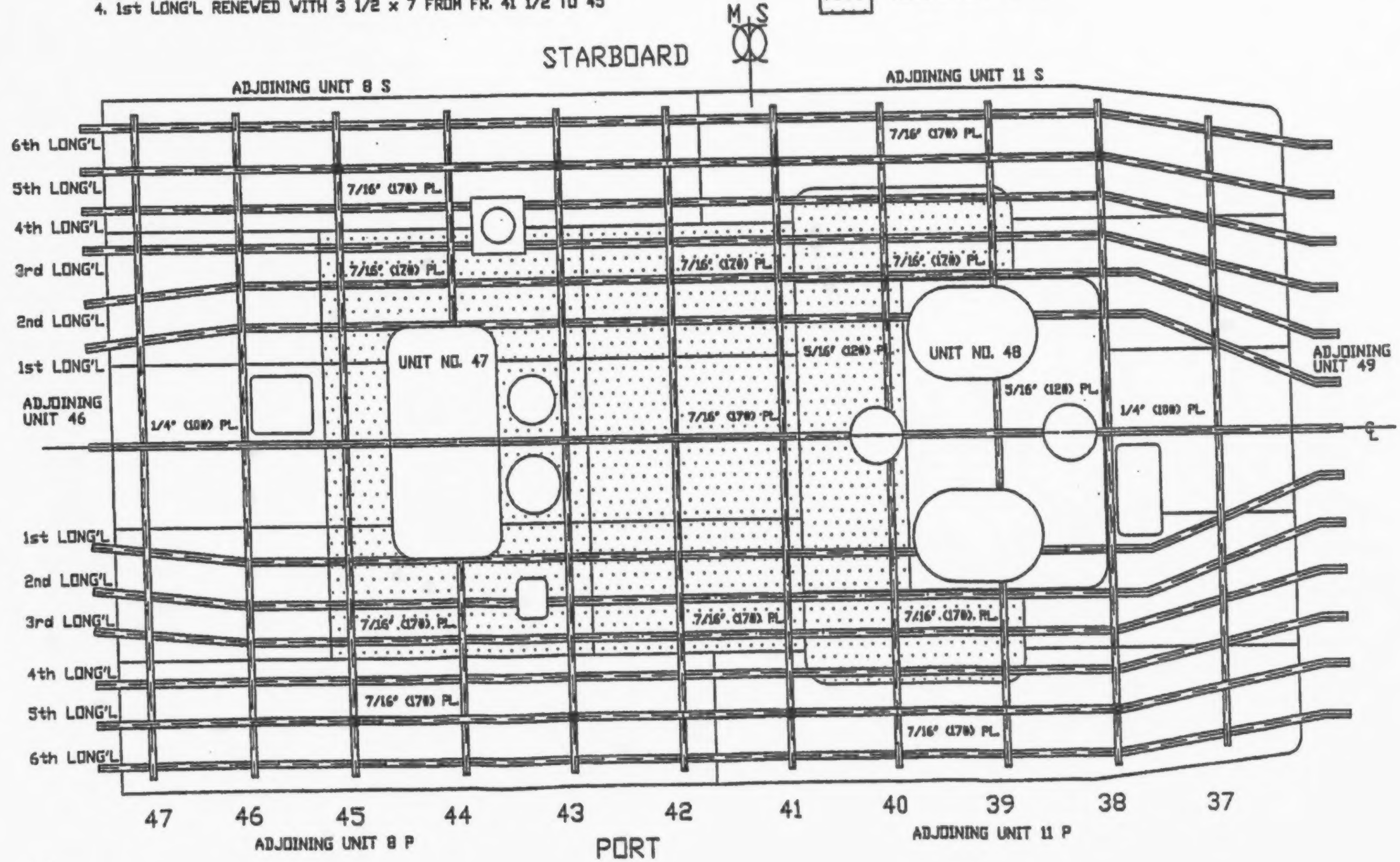
M.S
STARBOARD
ADJOINING UNIT 8 S
ADJOINING UNIT 11 S
6th LONG'L
5th LONG'L
4th LONG'L
3rd LONG'L
2nd LONG'L
1st LONG'L
ADJOINING UNIT 46
1st LONG'L
2nd LONG'L
3rd LONG'L
4th LONG'L
5th LONG'L
6th LONG'L
7/16" (170) PL.
7/16" (170) PL.
7/16" (120) PL.
7/16" (120) PL.
7/16" (120) PL.
5/16" (120) PL.
UNIT NO. 47
UNIT NO. 48
5/16" (120) PL.
1/4" (100) PL.
7/16" (170) PL.
1/4" (100) PL.
ADJOINING UNIT 49
℄
7/16" (170) PL.
7/16" (170) PL.
7/16" (170) PL.
7/16" (170) PL.
7/16" (170) PL.
47
46
45
44
43
42
41
40
39
38
37
ADJOINING UNIT 8 P
PORT
ADJOINING UNIT 11 P

4.0 CORROSION PROBLEMS Reference Illustration i-1

4.1 State-of-the-Art circa 1948-1958

During 1948 Constructor Captain A.N. Harrison, O.B.E., R.C.N., Director of Naval Construction, formulated the Royal Canadian Naval Committee on Corrosion and Fouling and served as its first Chairman. It was at this time that the R.C.N. began its post-war new design and construction program. Although much has been learned about corrosion during W.W. II, the experiences had to be properly recorded and consolidated for future use and reference.

In 1950 Constructor Commodore R. Baker, O.B.E., R.C.N. (R) arrived in Canada to commence the design and construction of the St. Laurent Class of destroyer escorts and the Bay Class of coastal minesweepers. He succeeded Captain Harrison as Chairman of the Corrosion Committee and with considerable flair and dynamic leadership brought considerable recognition to the Committee and its members.

Coincident with these first ventures by Canada into advanced naval ship design and construction was the formation of the Defence Research Board. The Naval Research Establishment Dockyard Laboratory (now Defence Research Establishment), developed advanced techniques for the painting, preservation, dehumidification, cathodic protection and selection of materials for marine vehicles. Much of the research found its way into R.C.N. Specifications and Books of Reference.

Under the leadership of Mr. T. Howard Rogers the Dockyard Lab contributed much to the British Non-Ferrous Metals Research Association by putting its research on copper-nickel-iron alloys into practical use on the new class of Canadian destroyers. He also conducted much of the investigations into "The Uses and Abuses of Aluminum in "Bay" Class Minesweepers". He is best known, however, for his book, The Marine Corrosion Handbook, which is a collection of all the marine corrosion knowledge available up to 1959, Reference 4. He wrote a second updated version in 1968, Reference 6.

By 1958 the research effort on cathodic protection and paint systems had reached such a high level of success that D.R.E. Dartmouth terminated research in these fields. It was now time for HMC Dockyards to hone the practical implementation of this research. One of the D.R.E. Dartmouth scientists, Donald G. Smith, joined the R.C.N. as a Sub-lieutenant and became the Command Paint and Preservation Officer. For over thirty years LCDR Smith, O.M.M., C.D., C.F., helped the Canadian Navy save hundreds of millions of dollars and greatly enhanced the operational capability of our ships and submarines by continuously pioneering the practical development and operational use of advanced cathodic protection and paint systems. The result has been progressive increase of intervals between refits from 18 months to two years to four years, and now, to even greater intervals of time. The structural repair/replacement necessary because of corrosion related wastage to sustain operations at sea is somewhat less than would have been the case without these developments and practical applications. Several of LCDR Smith's papers have been published internationally and he, like others before him, has helped to keep the Canadian Navy in the forefront as world leaders in cathodic protection and ship preservation coating systems.

4.2 Corrosion Mechanism

Marine corrosion engineering like ship structural engineering is a very complex subject to master and apply. Classic reference texts are References 4 and 6. Successful ship structural engineers have a good grasp of corrosion mechanisms, corrosion defense and wastage allowances. The reader is encouraged to study an excellent 49 page summary of the subject by Professor J. Harvey Evans written in 1972. See Reference 9, Chapter 16, pages 382-431. There is little doubt that successful warship structural design is highly dependent on a thorough understanding of corrosion mechanisms, especially where relatively thin skinned warships are expected to be operationally effective beyond 20-25 years of service and at a reasonable cost.

4.3 Corrosion On DDE/DDH 205 Class 1951-1981 (and DDH 265 Class 1961-1981)

There was evidence of corrosion on the **internal** DDE 205 Class hulls after four years of operational experience (1959-60). The problem continued into the early sixties as the conventional paint systems used in the bilges continued to break down exposing the plate and welds. The resultant pitting was randomly dispersed over the more anodic exposed plates and welds. The R.C.N. which had been experimenting with many anode types during the fifties decided to fit MK 5 magnesium anodes in the bilges. Zinc anodes worked well in oil-free environments such as ballast and fresh water tanks but would become coated in oily bilges and not function properly. Magnesium anodes worked satisfactorily in machinery space bilges.

During 1967-68 the keel plates in the Engine and Boiler Rooms of the 10 year old DDE 257 Restigouche Class were replaced and anodes fitted in the wet bilges. During survey it was discovered that these ships had suffered extensive pitting 450 thousands of an inch deep. The original plate thickness was one-half inch.

Probably the single most contributing factor to the early corrosion problems on these ships was the use of 1-GP-48 oil based iron oxide primer which was used to cover the complete interior hull including water ballast tanks, machinery bilges and so on. The 1-GP-48 iron oxide primer was applied before and during construction as a standard anti-corrosion coating in most, if not all, shipyards. Because 1-GP-48 broke down easily, research was carried out to find an overcoat barrier coat which could be applied over the iron oxide to give better protection. During 1959-60 an attempt was made to reinforce the GP-48 with another oil based coating, 1-GP-93 which did not work very well. The structure was coated with 2 more coats of GP-48 primer followed by 2 barrier top coats of the aluminum 93. The sad result was this did not work well either. Inorganic zinc, first applied in controlled test areas in 1960-61, was used on new construction commencing in 1968. The inorganic zinc provided much better corrosion control service. During the late 1970s much more persistent coatings such as coal tar epoxies for use on the S.W. ballast tanks and non-toxic epoxy enamels in potable F.W. tanks were applied at the first available opportunity. The Command Paint and Preservation Officer was initially restricted from using these wonderful epoxy coatings in tanks because they required clean, bare metal only achieved with sandblasting steel. This was rectified in 1978-79 by permitting holes to be cut in the tank bottom allowing other spaces in the ship to be sealed off from sand dust. Men and hoses simply entered the ship from the dock floor rather than from inside the ship. Although the coal tar epoxy based coatings provided excellent corrosion control due to their permeability properties, their use was later disallowed because of potential carcinogenic problems to applicators.

Anodes can only work well as a cathodic protector when immersed in a good electrolyte such as salt water. This means that anodes are basically ineffective above the sloshing line in machinery space bilges. Since there is no sloshing up the turn of the bilge when the ship is alongside a jetty, the anodes are basically ineffective above the normal still bilge water level. So a good paint system is needed over the entire machinery space including wet bilges because there are many areas under or behind machinery and structural seatings, etc., where it is difficult to survey and maintain a paint system. Bilge areas should be given a proper application of protective coatings before the machinery and piping is installed making the area difficult to access. It should be mandatory that properly qualified and experienced Naval Overseers, knowledgeable in protective coatings and structure, be present in the machinery spaces during paint and preservation operations. This is discussed briefly in Section 4.3.1 on DDH 280 corrosion.

There is no requirement to fit anodes in FFO, W.B. (except AORs) or F.W. tanks. Anodes do not work well in F.W. tanks because F.W. is such a poor electrolyte, unless a lot of anodes are installed. In addition, F.W. tanks do not suffer from very much corrosion activity since they are coated with a thick, specially designed and specially approved Fresh Water Tank Coating (usually epoxy based); are easily accessible and are usually of such a size that men can work in them without any problems. The Canadian Navy does not normally fit anodes in salt water W.B. tanks because again, they are readily accessible and easily maintained. An exception to this practice is the 22,000 ton AOR ships. During the late 1970s anodes were fitted in the very large AOR S.W. tanks because they are difficult to maintain as well as costly to paint due to their size. Ballasting for trim and stability is a common occurrence on these ships. The anodes are to be renewed as they are consumed. For completeness, it should be noted that a new approach was also being used on the AOR 509 Class forepeak. These forepeaks have corroded and are very difficult to sandblast and properly clean out preparatory to painting because of inaccessibility. The forepeak tank sides and bulkheads are not now painted but are fitted with a zinc anode cathodic protection system to the point of over protection to be sure to retard or eliminate further corrosion. The only area of the forepeak tank painted is the tank top.

With the exception of the machinery space bilge problem there were really no other major problems on the 20 steam-driven destroyers until the decision was made in 1976 to life extend these ships beyond twenty-five years of service. When HMCS ST. LAURENT was decommissioned in 1974, 23 years after launching of 19 years after commissioning, her hull was considered to be in good shape.

Using the colour-coded incident board located at the beginning of this paper, major areas of corrosion discovered by survey just prior to and during the destroyer life extension (DELEX) refits of HMCS ASSINIBOINE, SAGUENAY and MARGAREE during 1979-80 are now described by deck level.

4.3.1 No. 6 Deck

Sonar 5A sword shipbuilder's tube was very inaccessible making the hanging of anodes and the coating of the structure with a protective coating virtually impossible during normal refits. The original shipbuilder's tube was galvanized and with the deterioration of coating over time and dissimilar metals at the Sonar 5A housing, active pitting occurred.

Sonar 7A trunk is also inaccessible and difficult to maintain. During normal refits the structure was hand-cleaned as well as possible. Even if this space were reasonably accessible, the equipment was too delicate to allow sandblasting.

The keel plates of No. 1 and 2 W.B. tanks had to be renewed indicating anodes probably should have been placed in the bilges of these tanks years ago. In the future anodes may not be necessary because the W.B. tanks are coated with multi-coats of polyamide cured epoxy finish which have provided excellent adhesion and curing properties.

Boiler Room corrosion was quite extensive which is not surprising when all the factors are considered. These ships were all coated during construction with oil based iron oxide primer, 1-GP-48, without the benefit of anodes. Many of the areas around boilers, under and around machinery and blind bilges were inaccessible to survey and maintain. The normal atmosphere in a B.R. was very conducive to the acceleration of corrosive attack. Also over the years, rust was painted over repeatedly in difficult to access areas of structure.

The main areas of corrosion on the first two DELEX ships, ASSINIBOINE and SAGUENAY, were the forward end of the B.R. under and around the S.W. pumps in way of the boilers and aft end of the B.R. in way of the evaporators. The MARGAREE survey found the ship to be badly wasted in so many large areas (approximately 90%) of the B.R. that the only practical solution was to replace the entire B.R. structure from longitudinal 8 to 17, i.e., from turn of the bilge to 3 Deck and from forward of Bulkhead 36 to aft of Bulkhead 45 in order to pick up sound structure - a two month job. The main lesson learned from this is **accessibility** for survey and maintenance is a must if a ship is expected to be operationally effective after 20 years. It should be specified that all ships (in service 18-22 years) due for a life extension should have all machinery fitted against the ship side or covering blind bilges stripped out for survey of adjoining structure. In MARGAREE's case, it was noted that the undersides of the webs of the longitudinals were corroded as well. There were no anodes fitted in the blind bilges, but the remaining accessible bays had MK5 magnesium anodes fitted. There was much evidence of successive painting over corrosion products which just absorbed more condensation to make matters worse.

There is a striking difference between the corrosive attack in the machinery bilges of the old DDH 205 Class ships and the newer gas turbine driven DDH 280 Class, launched almost two decades later in 1972. On the 205 ships the pitting and corrosion was not localized to the weld but spread, more or less, randomly over the entire plate and weld surfaces. It appears that the electrodes used with the post W.W. II relatively low notch tough plate on the 205 Class were fairly compatible. During 1980 it was discovered that the potential difference between the low hydrogen E7018 electrodes and the notch tough G40.21 "T" quality steel used on the 280 Class was more pronounced causing the attack on weld material in the machinery bilges. This leads one to conclude it would be a good idea prior to new construction to take a couple of pieces of the steel chosen for that design, weld them together with the correct welding rods and measure the potential difference in order to determine the cathodic protection properties.

Engine Room Bulkhead 53 port is inaccessible for maintenance. The E.R., which is much dryer than the highly humid atmosphere of the B.R., was in very good condition overall. Over the years the main condenser inlet tubes had deep pitting over an area one foot from the valve. This deep pitting of the inlet tube was caused by the bimetal coupling of the bronze alloy valve and the adjacent mild steel inlet tubes in an area very difficult to maintain due to its inaccessibility. A SHIPALT for a top hat and anode was implemented. During SAGUENAY's 1979 DELEX refit, however, both tubes had to be remanufactured at great expense. It is understood one other ship, (ST. CROIX), had this problem some years previously.

No. 7 FFO tank top and margin plate is the only oil fuel tank to have a major problem. The tank top margin plate is inclined downwards, at approximately 45 degrees in this case, to be perpendicular to the ship's side. All such margin plates corrode because they are such natural catch basins for water. The answer to this problem is to use a different detail design in future ships to eliminate the catch basin and to pay more attention to the maintenance of this area on existing ships.

The nonstructural bulkheads, port and starboard, of No. 3 F.W. tank - a black non-toxic and not very effective bituminous coating was used on F.W. tanks until the late 1970s. The Canadian and American navies then changed to epoxy enamels suitable for potable water. Since 1978, sandblasting has been allowed in F.W. tanks. Men and equipment enter tanks through holes cut in the ship's bottom.

The relatively inaccessible area under the 75 ton A/C Refrigeration Machinery plant aft of Fr. 67 was surveyed in HMCS SKEENA in 1976. The hull inspector lost his hammer in the skeg. A similar experience occurred a few months later in HMCS FRASER when the hull inspector's hammer went through the bottom aft of Fr. 67 ending up on the dock floor. These two ships had the affected bottom plating, structrual members and skeg reconstructed to as-built condition in their respective refits, probably as arisings. All ships of the class had some structural reconstruction in way of Fr. 67-69 and skeg included in the refits immediately following 1976.

Tank top of No. 5 W.B. tank - it is not possible to cathodically protect a tank top, so the replaced tank top was coated with epoxy based materials which is a much better material than the old oil based iron oxide primer.

Keel plate in the forward end of the Tiller Flats in way of the bilge suction found the paint coating around the bilge suction would deteriorate allowing the first two bays to corrode freely. Over the years the corrosion spread outward from the bilge section. Fitment of an anode in the vicinity arrested this active corrosion.

4.3.2 No. 5 Deck

Refrigeration machinery space deck corroded. It was not anticipated during design that auxiliary machinery spaces would be continuously damp because of leaky gaskets. It is particularly bad when a S.W. pump is also located in the space. The use of better coatings, such as inorganic zinc or zinc rich epoxies, provided much more long-time service than oil based iron oxide used originally.

4.3.3 No. 4 Deck

Shell and deck wasted in A/C plant - see comments in Section 4.3.2 and Section 4.3.1 with respect to the 75 ton A//C Refrigeration Machinery Plant aft of Frame 67.

4.3.4 No. 3 Deck

Crews Heads Aft, After Seaman's Washplace, P.O.'s Heads, and Laundry Deck had "nice looking". boxes fitted to house the brass fittings. The boxes would fill up creating a bimetallic couple with the deck plate. The boxes were never cleaned properly because they were so small. These spaces were usually kept warm and were continuously damp aiding the corrosion mechanism.

Mortar well sumps were inaccessible and continuously exposed to the corrosive S.W. environment.

4.3.5 No. 1 Deck

The funnel uptake compartment deck was originally coated with iron oxide GP 48 primer. This very hot (when steaming) relatively inaccessible compartment was usually filled with air which is quite acidic. It is possible that this deck would have to be replaced after 20 years no matter what deck coating was used, but it is thought that a modern epoxy coating would stand up well. Inorganic zinc is not recommended because of the acidic content of the atmosphere in this space and the residue would dissolve the zinc based finishes.

4.3.6 Superstructure

The steel bridge front and part of the bridge deck has had to be replaced on several ships including NIPIGON (16 years after commissioning). The original drains from the bridge window wells were only one-half inch diameter making them prone to blockage from cigarette and other debris. The water would back up and find its way under the bridge front insulation and under the deck tile. This repair is quite expensive because there are quite a variety of "black boxes" attached to the bridge front bulkhead. Although a SHIPALT was engineered a number of years previously to replace these small drains by one and one-half diameter lines, it was implemented on only a couple of ships.

There is a bimetal riveted joint just forward of Fr. 29 superstructure girth where the steel superstructure front and the aluminum superstructure meet and at one deck level where the 1 Deck steel boundary bar and the aluminum superstructure are joined. The boundary between the aluminum and steel was originally coated with zinc chromate and carton flannel to prevent bimetallic corrosion. After a long period of time this becomes brittle and leaks setting up a bimetal couple which causes the aluminum rivet to waste and shear off. When the rivets were replaced a more flexible polysulphide epoxy alumilastic embedding compound was used.

Deck under the A.L.O. sights on top of the superstructure had an accessibility problem as well as heat from the unit's heating coils. This same problem occurred under the boat winch amidships which also has a heating coil fitted.

4.3.7 Aluminum Hangar

Naval Architects and ship structural engineers interested in expansion joint design are encouraged to seek out the solution developed by C1HT J. Osborne, MMM. A SHIPALT was raised, to be implemented on an as-required basis when the expansion joint was corroded or worn sufficiently to justify replacement. Osborne's solution is simple in design using neoprene type rubber, much quicker to implement than repairing the old design and is extremely easy to maintain.

4.3.8 Flight Deck

The original hauldown troughs fitted on the DDH 205 Class were inaccessible and subject to the extremely harsh S.W. environment. These troughs are very difficult to re-align when tampered with so maintenance was minimal over the years. The troughs were covered with zinc rich coatings as they are cleaned out and repaired. The newer troughs fitted on the DDH 280 and 265 Classes are much easier to maintain and align.

4.3.9 External Hulls and Appendages

The Canadian Navy has had outstanding success keeping **external** hulls in a very high state of preservation. Unlike hull internals, access is very easy for survey and sandblasting, permitting the proper application of preservation materials. The problem is to develop and apply a good material in the first instance.

A vinyl paint system for the underwater hull was introduced by S/LT D.G. Smith (later LCDR, Command Paint and Preservation Officer) during 1958 and 59. At first there were teething problems because it was found that if the appropriate thickness of paint film was not used during application, the paint would strip. Painters were used to applying 1 1/2 mils of conventional coatings in one application. Vinyl has a low solid content and at least two coats are required to give a 1 1/2 mil thickness. A minimum of 6-8 mils is required to withstand current density when impressed current cathodic protection was installed.

During 1968 the Jungle Deck and hull above the water line, on AOR 508, were a mass of corrosion. PROVIDER was treated to a new above-water inorganic zinc paint system which lasted until 1978 when it had to be redone. NIPIGON followed later in 1968 when her complete above-water hull was sandblasted to the bare hull and treated during a refit at Sorel, P.Q.

The internal structure of the skeg in way of the after cut up, bilge keels and rudders are filled up with a bituminous coating and drained. No problems have been experienced to date.

The permanently fitted impressed current external hull cathodic protection system has been secured to bilge keels since the early sixties. This steel anode system would be more effective if it were fitted alongside the ship but this is not practical. Later, several ships were fitted with a small lead silver anode system which is still giving good results. The newer 280 Class use dinner plate-size platinum anodes. They basically consist of a little tungsten wire covered with inert platinum. These anodes give very good noise and drag signatures compared to the sacrificial zinc anodes fitted on the much larger Operational Support Ships. The zinc anodes have also given excellent results but do need replacement periodically.

The results of the vinyl paint system for underwater hulls used in conjunction with the impressed current system plus the above-water inorganic zinc system have meant that Canadian destroyer hulls are in excellent shape externally. It is not necessary to send sailors over the side to chip paint any more. Experience has now demonstrated that after 9 or 10 years the hulls have to be sandblasted to bare metal and recoated because the paint tends to delaminate from the weight of the many cosmetic coats applied over the years and perhaps from the difference of thermal expansion rates of multi-coats of alkyds and the base steel plate.

External hull corrosion has been kept to a minimum as pointed out above except for a localized area where there was cavitation erosion and pitting on the DDH 205/265 rudders and "A" brackets. A jury rig fix using DEVCON and spot welding was quickly thrown off from the parent metal re-exposing the deep pits which simply continued to grow. During the early 1980s, the Command Paint and Preservation Officer trialed two very promising but expensive materials - INERTA 160 on ASSINIBOINE and ZEBRON on MARGAREE. Both are excellent high build solventless materials. INERTA 160 is a black epoxy and ZEBRON is a polyurethane. Exotic equipment is required for application. A complete underwater hull of a 590 class tug was also coated for trial purposes. These materials are used by the Canadian and U.S. Coastguards on icebreakers because they are highly abrasive resistant and should be excellent in the slush ice water our navy and auxiliary vessels often work in. If the trials went well, it was planned to cover complete underwater hulls, including the boot topping, with these materials. In the interim, boot tops were coated with high build vinyl black which are only partially satisfactory because they are not particulary abrasion resistant to rubbing of ships side by fenders, etc. Unfortunately, all of the above coatings did not solve the cavitation/erosion problems on the rudders despite the potential coating abrasion resistance, flexibility properties and so on.

Rudder cavitation erosion was a problem on the twin screw/twin rudder DDH 205 and its derivatives where the rudder was placed in the race of the propeller. The DDH 280 which had twin screws and a single centreline rudder did not appear to have rudder problems prior to the TRUMP modernization commenced in 1987.

4.4 Corrosion on DDE/DDH 205 Class, 1981-1994

After the DDH 205 Class ships completed their destroyer life extension refits, there were no startling or eventful corrosion problems for the remaining thirteen years, 1981-1994. The proper application and maintenance of the preservation materials developed, trialed and perfected during the previous thirty years, as discussed in Section 3.4, have provided very positive results.

5.0 HIGH COST OF STRIPOUT, INSPECTION, REPAIR AND REPLACEMENT

Stripout, repair and replacement takes much more time than most people realize. An example of the involvement to implement a relatively minor structural repair should illustrate the point.

The repair described in Section 3.3d. and by Figure 3-8, "Fractures at Knuckle, Frame Station 27", covers the original deck plating fractured in way of eleven in number longitudinals. The Ship Repair Unit Atlantic took 1000 manhours or 16 working days to supply, fit and weld in place a new 3/8" x 18" x 26' steel insert plate, plus thirty linear feet of 1/2 inch by 3 inch flat bar intercostals installed between the longitudinals to stiffen the plate panels.

The lead shop was the Plate and Boiler Shop with 13 other shops assisting plus hire/fire brush hands. To facilitate repairs, the following items were removed or released, and replaced (or renewed) on completion of repairs:

Space	Description	Shop(s) Involved
Captain's Pay Office	10 sq. ft. deckhead insulation.	Shipwright
	14 ft. D.O. transfer line.	Pipe Shop & Laggers & Riggers
	14 ft. firemain & lagging.	Pipe Shop & Laggers & Riggers
	6 ft. electrical cable.	Electrical
Passageway - No. 1 Dk.	All electrical cable incl. trays and hangars, FS 26-29.	Electrical & Riggers & & Shipwrights
	16 ft. F.W. pipe.	Pipe Shop

Space	Description	Shop(s) Involved
No. 10 Cabin - No. 3 Dk.	Stowage rack & 2 lockers.	Riggers & Boilermaker (unbolt it)
	5 ft. pipe.	Pipe Shop & Laggers & Riggers
Lobby 3 Dk.	All electrical cables incl. hangars FS 27-29.	Electrical & Pipe Shop (hangars)
	14 ft. vent trunking.	Sheet Metal Ship & Lagger
Quad Cabin 3 Deck	3 ft. curtain plate incl. rivets coated with alumilastic.	Platters & Boilermakers & Shipwright U/W Repair
	8 ft. electrical cable .	Electrical (only remov screws not bolts & clamp (Boiler Shop)
	4 pipes 10 ft. long incl. lagging.	Pipe Shop & Laggers & Riggers
	Inboard bunks incl. lights.	Electrical & Shipwright (unbolt) & Riggers
Communications Control Room 1 Deck	2 desks incl. 4 deck pads; 1 cabinet; Safe & seat.	Boilermakers & Platters & Riggers & Burners
	Seat for stateboard.	Platters
	1 pedestal chair.	Boilermakers & Platters & Welders & Chippers
	84 deck tiles and underlay; 1 ft. of tile boundary flat bar.	Paint Shop & Shipwright U/W Repair (tile) & Burne Shop & Welders & Burner & Chippers
Passageway 1 Deck	4 ft. ground bar plus 15 all rivets and aluminastic.	Boiler Shop & Shipwrights U/W Shop & Burners & Chippers & Welders
	4 sq. ft. tile underlay and 5 ft. ground bar.	Shipwrights U/W Repair & Paint Shop
	1 non-skid thread.	Shipwright U/W Repair
	Tile fairing plate.	Boiler Shop

Space	Description	Shop(s) Involved
Radar 3, 1 Deck	12 deck tile plus underlay.	Shipwrights U/W Repair & Paint Shop
	5 ft. tile boundary bar.	Boiler Shop
	39 inches steel angle for radar set base.	Boiler Shop & Welders & Burners & Chippers
Miscellaneous	Protect electrical cables during hot work.	Laggers
	Reposition cables where they interfere with new flat bar stiffeners.	Electrical & Riggers
	Disturbed pipe joints - new gaskets plus function test.	Pipe Shop
	Staging.	Shipwrights
	Cleaning, etc.	Brush hands
	Misc. removals.	Determined by lead shop who discusses the matter with the NEUA Hull Inspectors

1000 manhours to remove the cracked plate, replace it with a new 39 square foot insert plate(s) and 30 linear feet of new 1/2 by 3 inch flat bar! 600 pounds of steel! Clearly the removals, replacements and renewals of non-steel materials was by far the largest percentage of manhours and of cost. In this case the actual structural repairs were about 20 to 25% of the total manhours and less than 20% of the material costs. It is not unusual to find that the removals, renewals and replacements necessary to effect a structural repair is three times to as much as ten times of the actual structural repair. Prevention of the need for structural repairs is the best cure and most economic solution. The trick is to be clever enough with structural detail during the design and building stages to eliminate the necessity for such repairs years later. A continum of knowledge and experience, passed downwards through the organizational hierarchy, is necessary to gain the advantages of improved detail design, minimize structural defects and hence, minimize the cost of structural maintenance. Without building on practical knowledge and experiences the same mistakes and same problems will be repeated every 15 to 20 years and, unfortunately, new and more difficult problems may also be introduced.

6.0 COMPARISON OF DDE/DDH 205 WITH DDH 265 AND DDH 280 CLASSES

Although there is eight years difference between the DDH 265 and DDH 205 Classes (31 years of service versus 39 years by 1994), they exhibited similar structural and corrosion problems. Both classes had the same amount of sea time as DDHs which explains some of the structural similarities. This leads one to hypothesize that it generally takes 10 or 15 years for major structural (and corrosion) problems to surface. When one considers the fact that these designs are well over 40 years of age; and it was the first major warship designed in Canada for operations off the East coast of Canada in the harsh environment of the North Atlantic, these ships have performed beyond reasonable expectation. As these ships grew older, the amount of time they spent at sea appeared to increase.

Many of the structural defect problems encountered by the steam-driven destroyers were apparently designed out of the DDH 280 Class. The drawing and specification configuration control program used during the DDH 280 design has paid great dividends and is justification for implementing such a program for follow-on programs. In the first nine years of service, 1972-1981, these ships only had four detail design problems rectified with no loss of operational time. The one major corrosion problem in the machinery space bilges was discovered before any great embarrassment but it did mean the unscheduled docking of three ships and disrupting their operational schedules for a couple of weeks. Overall, the 280 Class has performed magnificently well during the first half life prior to the recent TRUMP update and modernization.

The attachment of the large hangar and stiff flight deck on the DDH 205 and 265 Classes has had a significant effect upon the midship hull structure in way of the Boiler Room Air Intake and the Funnel Exhaust No. 1 Deck openings. The resulting large vertical loadings did not exist in the same manner on the DDH 280 Class because the Flight Deck is integral with No. 1 Deck. On the other hand, the DDH 280 suffers from a "deckhouse end problem" at the after quarter point.

A recent analysis of the DDH 265 and DDH 280 structural integrity databases, Reference 12, showed that the:

a. DDH 265 had about 2.5 times more defects than the DDH 280;

b. Number of corrosion defects was almost the same for both Classes; and

c. Ratio of crack/corrosion defects was 1:1 for DDH 265 compared to 1:3 for DDH 280.

The above numbers were compiled for a 26 year period (1964-89) for DDH 265 and 21 year period (1972-92) for DDH 280. It is reasonable to assume the DDH 265 record is similar to the older DDH 205 Class.

These statistically based structural databases are interesting, however, conclusions or actions can very easily be misdirected. It is the impact of each structural defect as it affects the safety of the ship or the crew therein, and the operational program of the ship that is important. However, it does point out that the DDH 280 has had a smaller number of structural defects than the DDH 205/265 Classes because of superior detail design and welding sequences, better quality assurance, and the use of much better notch tough steel. The DDH 280 design had the benefit of mature research and development, design, overseeing and in-service support teams. Corrosion, despite better paint systems, is still a major problem, except ships are now paid off well after 20 years of service and refit intervals have increased from 18 months to 48 months with the potential for longer intervals. As determined by experience during a 1980 study, the practical effective life of Inorganic Zinc Silicates and Zinc Rich Epoxies is about seven years after commissioning (or nine years from the construction application).

A major contribution to structural integrity health is the notch toughness (sensitivity of the material to brittle fracture) and yield strength characteristics of the steel used in construction. The hull of the DDE 205 and DDE 257 Classes, launched between 1951 and 1957, were constructed of a commercially available mild steel with the added requirements of 0.21% carbon content maximum and silicon killed; ASTM designation is unknown. The DDE 261 and DDH 265 Classes, launched 1961 to 1963, used steel to ASTM A-131 Grade C with maximum carbon content of 0.21%, fully killed and made to fine grain practice. The nominal yield stress is believed to be 32,000 psi (220 MPa). During 1992 the Defence Research Establishment Atlantic/Dockyard Laboratory determined the steel mechanical properties of HMCS GATINEAU, a DDE 257 Class ship launched in 1957, Table 6-1. This steel was not very notch tough; 3 ft. lb. (4J) at -40°F but it was the best available at the time.

TABLE 6-1
CHARPY V-NOTCH STEEL IMPACT TEST RESULTS
HMCS GATINEAU, DDE 236

TEST TEMPERATURE °C	ENERGY, J	
	T-L	L-T
-40	4	8
-20	11	34
0	20	52
20	27	N/A

TL = CRACK RUNNING **with** ROLLING DIRECTION of PLATE
TL = CRACK RUNNING **against** ROLLING DIRECTION of PLATE (i.e. ORTHOGONAL)

Mr. Marc LeMarsh, the Canadian Naval Material Design Authority, specified steel for complete hull structure in 1960 to be a notch tough steel incorporating good weldability characteristics with a steel manufacturer's guaranteed impact test of 40 ft. lb. (54J) at -40°F (-40°C). Due to metric conversion factor confusion this value became 25 ft. lb. (34J) at -40°F! In 1965 Mr. LeMarsh finally convinced Canadian steel mills to roll notch tough steel to Canadian Standards Association specification CSA G40.8 Grade B normalized (later changed to CSA G40.21 38T) for the construction of the 22,000 ton operational support ships, AOR 509 Class.

In 1969 a similar steel was used in the construction of the DDH 280 Class but with the slightly higher yield stress of 40,000 psi. This higher nominal yield strength was 25% or 8,000 psi higher than that of the mild steel used in the DDE/DDH 205 Class permitting lighter scantlings. For comparison, CPF steel was over 56% or 18,000 psi higher than the 205 Class.

Table 6-2 gives the minimum average energy impact test values and the nominal yield strength of the steel used for construction of Canadian frigates/destroyers since 1951 including that for the Canadian Patrol Frigate contract announced in June 1983.

TABLE 6-2

STEEL MECHANICAL PROPERTIES
CANADIAN NAVAL SHIPS
1950-1995

LAUNCH	CLASS	CHARPY V-NOTCH IMPACT TEST (LONG'L)				
		TEST TEMP.	AVERAGE ENERGY MINIMUM		YIELD STRESS	
		°C °F	J	FT. LB.	PSI	MPa
1951-63	DDH 205/265	-40	4	3	32,000	220
1969	AOR 509	-40	34	25	38,000	260
1970-71	DDH 280	-40	34	25	40,000	275
1989-	CPF	-40	40	29.5	50,000	350

A minimum impact test value for the DDH 205 is only 3 ft. lb. compared to 25 ft. lb. for the DDH 280. It is worth noting that the Boiler Room air intakes, located just aft of midships, is the primary location of the major midship fractures during the 1976-78 time frame and the atmosphere can be very cold off Canada's east coast during winter. Further, there has been a tendency to use steels with increasing yield strength values to save weight by using thin plate and/or small stiffeners. This could spell trouble for newer ship classes when this is combined with unrealistic corrosion allowance in machinery space bilge areas and at the lower area of thin bulkheads.

Although the case of higher yield notch tough steels is encouraged for obvious reasons, considerations should be given in future design calculations to limit the "design" yield strength to about 30,000 psi maximum for 3000 ton frigates and 40,000 psi for 4000 to 5000 ton frigates to ensure the hull is robust enough to withstand unforeseen corrosive attack and structural failures.

The DDH 205 and 265 Class hulls were not coated with inorganic zinc when constructed because this marvellous material was not available until the late 1960s when it was specified for the DDH 280 Class. The best time to coat a machinery space is before the machinery is first fitted on its seats. Everything is down hill from that time. On the other hand, the re-coating of the 205/265 external hull with inorganic zinc, commencing in 1968-9 was a much easier proposition. In any event, a rigorous hull survey of the main machinery spaces should take place every 12 to 15 years and any unacceptable structure replaced. An examination of the refit interval period for the newer ships by experienced naval architects, paint and preservation officers, and hull surveyors would reveal if a refit or extended work period should be planned for 6, 7 or 8 years from commissioning (new ships) or recommissioning (modernized ships). The effective life of machinery space anode systems in combination with an inorganic zinc preservation system will be a major factor in the determination of a practical refit interval from a structural integrity point of view. Certainly a corrosion protection effectiveness curve drops off very quickly after six or seven years from initial coating application.

7.0 CONCLUSIONS

7.1 A Tolerant Structural Design

Canadian Naval Engineers can be very proud of their achievements in advanced warship design since the commencement of the St. Laurent design in 1948-49. The St. Laurent design was innovative since conception and tolerant of structural defects. The design was flexible enough to allow a major midlife conversion without reverting to a compensated fuel system. This midlife conversion transformed surface ship ASW warfare into a new dimension. The life of these ships was increased during an extended refit of only 7 to 8 months at a very reasonable cost. The original designers of the St. Laurent Class would be surprised and pleased to know these hulls would still be operational over two decades beyond their expected life of 20 years.

7.2 Milestone Years 1976 to 1979

As the life of the DDH 205 Class approached and exceeded 20 years since commissioning, serious structural and corrosion failures needed immediate attention. Structural restoration was essential to extend the operational life of these ships. Through the foresight of the initiation of the DELCA project, the DELEX program became the vehicle by which most of these ships had a nine to twelve year life extension. Some highlights are summarized:

7.2.1 Structural failures amidships in No. 1 Deck included both longitudinal members and deck plating - the worst case being HMCS ASSINIBOINE (1978) with a continuous crack through all structural members, extending 60% of the width of the upper deck. Any one of these amidships failures could have resulted in catastrophic consequences if not discovered early enough. Immediate interim repairs followed by the implementation of DELALT D51, commencing in 1979 refits to replace all deck plating Frames 39 to 45 and longitudinals #3 port to #3 starboard, restored these ships amidships to equal or better condition than at the time of conversion to a DDH.

7.2.2 Corrosion failures aft of Fr. 67 in way of the skeg and under the 75 ton A/C plant were first discovered in 1976 and 1977 in HMCS SKEENA and FRASER. These areas of corrosion were very close to a penetration of the underwater hull with the potential resultant flooding of the watertight compartment and damage to machinery. Prompt reconstruction of the affected area of plating, structural members and skeg restored the ships to as-built condition. All ships of the class had this repair implemented in refits immedately following 1976.

7.2.3 The financial approval and decision to implement the DELEX (Destroyer Life Extension) program in 1976 and 1978, respectively, provided a sound basis for extending the life of the DDH 205 Class ships in terms of both: a. safe to navigate;

and b. operational capability restored. The Destroyer Life Cost Analysis (DELCA) project was initiated in late 1974 on the full realization that the DDH 205 Class could not be replaced in a timely manner and something had to be done to maintain at least a safe to navigate capability and an operational capability. The DELCA project results were the basis for the DELEX approval.

7.3 The Post DELEX "Golden" Years 1982 to 1994

Late in the operational life of the DDH 205 Class after the DELEX life extension, the DDH 205 ships showed signs of getting "tired". All ships had buckling or shear failures in the longitudinal bulkheads between No. 4, 5 and 6 fuel tanks forward of Frame 36. All of these required repairs. At least three ships, HMCS FRASER, MARGAREE and OTTAWA showed the initiation of centreline vertical keel (CVK) buckling forward of Frame 36 and aft of Frame 67. In each case the CVK was fitted with diagonal stiffening both port and starboard without incident for the remainder of operational life.

7.4 Factors Affecting Amidships Structure

There are four contributing factors affecting the No. 1 Deck amidships structure. These include:

a. stress due to the vertical loads on No. 1 Deck from the hangar and helicopter;

b. stresses due to longitudinal loading;

c. stresses due to secondary and tertiary loads; and

d. stresses due to inappropriate detail design and fabrication, i.e. hard points.

The combination of these stresses were sufficient to cause serious structural failures in No. 1 Deck plating and longitudinals amidships. These failures occurred approximately 12-14 years after conversion to DDH.

7.5 Detail Design and Fabrication Techniques

The DDE/DDH 205 Class ships had a number of structural failures over the years. The vast majority of these structural failures can be traced to inadequate detail design resulting in structural "hard points" and localized high stress concentrations; or, inappropriate fabrication techniques such as faulty welding practices, rough plate edges and misaligned structure in the more highly stresses areas. None of these structural failures, except as may have been contributing in the amidships of No. 1 Deck resulting from detail design or fabrication technique deficiencies, were catastrophic in character or greatly affected the operational capability of the ships for any significant period of time.

7.6 Machinery Bilges and Other Wet Spaces

Accessibility, preparation of surfaces, application of preservation materials and installation of anodes are factors directly related to how well machinery bilges and wet spaces stand up in an operational ship. Brief amplification of these points follow.

7.6.1 Accessibility to locations under and behind machinery and confined structural configurations is essential to facilitate structural surveys and proper maintenance. Those locations that are difficult to access frequently are the most corrosive prone because of the difficulty of surface preparation and preservation application. Experienced hull inspectors and naval architects are in the best position to identify these areas of the ship.

7.6.2 Preparation of surfaces in difficult to access locations can be dealt with in new construction more readily as part of the unit construction and the fact the machinery is not yet fitted. The surface preparation in an operational ship is much more difficult and often far more troublesome and often not inspected adequately prior to preservation application.

7.6.3 Preservation application in difficult to access locations can be accomplished during new construction with reasonable assurance the specification can be met. In an operational ship some six to nine years after commissioning the adequacy of the preservation will be directly related to the quality of the surface preparation and the degree of difficulty to access the locations. Far too often corrosion products and dirt are overpainted in these difficult to access locations.

7.6.4 Anodes should be installed in machinery bilges and other wet spaces in way of the CVK and "A" strake up to the slosh line no matter what paint system is used.

7.6.5 Design for accessibility is an essential key to shipboard flexibility, lower life cycle costs and enhanced operational availability of the ships.

7.7 Corrosion Allowances

A ship is a collection of corrodible items sitting in salt water. The combination of the barrier coatings of preservation and the cathodic protection system(s), under ideal circumstances, prevent the corrosion of these items. Preservation coatings deteriorate with time, 4 to 8 years depending upon the system, and do have surface breaks from abrasion and other causes. Cathodic protection systems do not cover all areas equally. Will a 6mm plate corrode any less than a 15mm plate under the same environmental conditions? Probably not. A corrosion of 1mm in a 6mm plate is 16.7%, whereas a corrosion of 1mm in a 15mm plate is 6.7%. Furthermore, the higher strength steels are more susceptible to stress corrosion cracking which in turn has an impact on the fatigue strength of the plate.

In some of the more difficult to access locations that are continually damp, corrosion allowances of the order of 20% are reasonable. Clearly, an in-depth examination of corrosion prone areas with the objective to identify appropriate corrosion allowances is a study that should be undertaken by experienced hull inspectors and naval architects for specific ship classes.

7.8 Ship Structural Maintenance and Repair Cycle

The structure must be protected and maintained to ensure the operational availability of the ship. Structural hull surveys will be required regardless of the preservation coatings and cathodic protection systems. The frequency of, and scope of, these hull surveys needs to be addressed with the objective to establish a practical plan for the maintenance of the newer ships, in short, extended work periods and refits.

7.9 Materials Selection

The proper selection of structural materials in the first instance will eliminate many future problems and substantially reduce costs associated with the ship's structure. The present structural design Canadian Forces Technical Orders and associated welding, painting, etc. CFTOs do not present the "judgement" knowledge required to make the proper material selections. The preparation and addition of a material selection standard to the available CFTOs would be of appreciable technical benefit and probable cost savings.

7.10 Structural Data Base

This paper has essentially assembled the structural record of the DDE/DDH 205 Class ships from the first launch in 1951 to the last decommissioning in 1994. Insofar as is known, this is the only ship class with the structural defects history documented with the repairs and the rationale for the repair method discussed, and with the probably cause of the defect offered.

7.11 Moving from In Service Support by Inspections, Maintenance, Repairs (IMR) to Reliability, Availability, Maintainability (RAM)

Throughout the life of the DDE/DDH 205 Class ships the structure was inspected in a planned way, maintained primarily at refits subject to the inspection findings and repaired when there was evidence of a need for repair, again primarily at refits. A team of experienced hull inspectors, a paint and preservation specialist and naval architects provided continuity of knowledge about, and familiarity with, the ship class structure. The structural history was recorded in hull survey reports, special hull structure reports of unusual occurrences and in the familiarity and memory of the knowledgeable and experienced individuals involved.

With the current restructuring of both National Defence Headquarters and the Maritime Command there will be a direct impact on the human resource concerned with ship structure. Some changes may be necessary to ensure quick response action to structural problems and predict potential problem areas before they become a problem. Will the RAM methodology achieve the intended objective? It is beyond the scope of this report to answer this question.

Perhaps the structural history of the DDE/DDH 205 Class can be used in some constructive way to test any RAM techniques or other techniques against a known data base. Clearly there is no merit in adopting new techniques and methodologies at considerable expense in terms of time and dollars unless there is a meaningful benefit derived.

8.0 RECOMMENDATIONS

8.1 Recommended Success Criteria

The following success criteria are recommended to minimize structural failure in monohull frigates and destroyers:

8.1.1 Avoid long deckhouses/superstructures and discontinuous (shortened) uppermost main hull deck ship configurations which increase the probability of major structure failure;

8.1.2 Construct the complete hull structure using notch tough steel incorporating good weldability with the manufacturer's guaranteed minimum impact test results. Suggest CSA WT Steel with minimum impact results of 40 Joules at -40°C (29.5 ft. lb. at -40°F). Notch tough steels should be specified for repairs on older ships;

8.1.3 Select steels with a yield strength consistent with the design of minimum acceptable plate thicknesses and stiffener sizes to avoid fatigue failures in the form of "oil can" effect and from corrosion problems;

8.1.4 Provide accessibility for structural survey and maintenance with particular attention to machinery spaces and above and below 1 Deck Amidships;

8.1.5 Use realistic corrosion allowances especially for difficult to access locations and in damp spaces. Corrosion allowances as high as 20 to 35 per cent may be appropriate for higher strength steels;

8.1.6 Use superior preservation coatings and anodes in wet spaces. Completely coat the interior and exterior hull with approved inorganic zinc silicates or better at new construction; and

8.1.7 Use superior detail design practices to ensure structural continuity and avoidance of structural hard points; and, fabrication techniques to ensure quality weldments without undercutting or incomplete penetrations. Construction should not commence until the Owner is satisfied with the Contract Design or ideally the Detail Design of the ship structure.

8.2 Recommended for Development or Further Study

The following subjects are recommended to enhance the present knowledge and quantify the theoretical and practical facts to the benefit of ship structural design and maintenance.

8.2.1 Develop a "Materials Selection Standard for New Construction and Maintenance" for use by commercial shipyards and naval ship repair units;

8.2.2 Conduct a study and analysis of ship structural maintenance and repair cycle by ship class to establish the most cost effective ownership; and

8.2.3 Conduct a study by ship class to determine the practical corrosion allowances by zones of the ship (i.e. machinery bilges and damp spaces, difficult to access locations hidden behind equipment or panelling, etc.). In the case of new construction these would be corrosion allowance additions to structural members additional to design requirements. In the case of existing ships the margin for corrosion on an existing design can be established.

ACKNOWLEDGEMENTS

The authors wish to acknowledge the following who were very generous with their expertise, advice and "corporate memory" during the preparation of this Paper:

Mr. Gerry LeBlanc, Chief Hull Inspector (retired)

Mr. Ed McSweeney, Senior Hull Inspector (retired)

Mr. Ron Chisholm, Senior Hull Inspector,
Naval Engineering Unit Atlantic,
Halifax, Nova Scotia

REFERENCES

1. CDR D.J. Hussey, "DDH Structural and Corrosion Problems 1951-1981", presented at a joint meeting of the Eastern Canadian Section of SNAME and the Canadian Institute of Marine Engineers, Ottawa, February 1982.

2. Captain C.D. Roushorn, various documents and personal papers on DDE/DDH 205 structural integrity held by the Donelad Hydronautics Limited library. In particular, "DDE/DDH 280 Class Midship Cracking History and Details 1976-1981", and "DDE 205 Class Hull Defects, Commissioning to 28 January 1963 (pre-conversion).

3. LCDR D.G. Smith, several papers and personal communications with CDR D. Hussey on the preservation of Canadian naval ships and submarines, Command Paint and Preservation Officer, Maritime Command, Halifax, 1964, 1969, 1972, continuously 1977-1981 and 1995.

4. Howard T. Rogers, Officer-in-Charge, Naval Research Establishment (Dockyard Laboratory) Halifax, The Marine Corrosion Handbook, BRCN 6376, McGraw-Hill Canada, 1960.

5. Professor Amelio M. D'Arcangelo, A Guide to Sound Ship Structures, Cornell Maritime Press, Inc., Cambridge, Massachusetts, 1964.

6. Howard T. Rogers, Marine Corrosion, George Newness Limited, London W.C. 2, 1968.

7. Dr. Gordon W. Bigg, "Stress Concentrations Existing Around Large Openings in a Highly Stressed Ship's Deck", Carleton University, DDP Contract 760122/0018/203-60-30-601, April 15, 1968.

8. LCDR D.A. Henley, "DDE's DDH's - Most Common Structural Failures Experienced from Sep 1967 - Jul 1970", Naval Architect Ship Services, Ship Repair Unit Atlantic, July 1970.

9. Professor J. Harvey Evans, Editor, Ship Structural Design Concepts, Cornell Maritime Press, Inc., 1974.

10. I.F. Glen, "Report on St. Laurent Hull Inspection, 11900-DDH/SL-15 (DMEM 3-2-6), October 1976.

11. William S. Pillini, Principles of Structural Integrity Technology, National Technical Information Service, U.S. Department of Commerce, 1976.

12. "Analysis of Annapolis and Iroquois Class Structural Defect Histories - Final Report", MSEI Project 1727-0013 prepared for Directorate of Ship Engineering, Ottawa, March 1994.

#510368 (25)

An Overview of Fatigue Assessment and Control in Naval Welded Details

by

Dr. A.M. Abdel-latif

Materials Engineering & Applied Physics
Quality Engineering Test Establishment
Ottawa, Ontario, Canada, K1A 0K2

ABSTRACT

QETE surveyed the current literature on fatigue design procedures, analytical methods and fatigue control in welded structural details in surface ships. The survey addressed the issues of material selection, geometry of fabricated detail, post fabrication processes and availability of fatigue design data for specific steels on the CPF. Most of the reported Canadian tests had been conducted on thick steel plates for offshore structural platforms to improve weld profiles and corrosion protection. QETE found that the US Coast Guard had published an extensive materials data Handbook which contained data from thousands of tests on eleven structural steels commonly applied in surface ship construction. The databases include tensile strength and Charpy impact values, DT energies, NDTT and J_{Ic} values for a limited number of critical design details. The US Handbook contains fatigue design data for two steels which match the composition and constituents of two Canadian steels. It was concluded that there is a need to generate fatigue design and durability data for susceptible structural details manufactured from ASTM A715, ASTM A570 and CSA CAN3-350WT steels.

QETE Tasking on Fatigue of Welded Ship Details

- ◆ Determine the feasibility of generating material database for CPF steels.
- ◆ Review fatigue control approaches and life assessment of weldments.
- ◆ Review the current developments on application of Marine Structural Integrity Program (MSIP).

Considerations

- ◆ The majority of accidents are unrelated to the ship structures.
- ◆ Corrosion and fatigue cracking are responsible for structural failure,
- ◆ Fatigue cracking is generally associated with welds and stress concentrations in the critical joints.

Points to Remember

- Management of corrosion and fatigue are of paramount importance.
- Economic pressures have forced reductions in the time allocated for design, inspection, QA and maintenance.
- Most of ship structural problems are associated with durability design considerations and/or maintenance procedures.

Steels In The CPF

- HIGH STRENGTH STEEL for ballistic protection: ASTM 715 gr. 70.
- HIGH STRENGTH STEEL for No. 1 plating & flight decks: ASTM 517* gr F
- MEDIUM STRENGTH STEEL for primary and superstructures: CSA CAN 3- G40.21-350 WT*
- (ASTM A 570 gr 50) & ASTM 572* gr.50
- REGULAR STRENGTH STEEL: for other applications.

CPF Material Systems of Interest

- CSA CAN 3- G40.21-350 WT
- ASTM A517 Grade F
- 350 WT/E7018/350 WT (Weldment)
- A517 / E11018M /A517 (Weldment)
- 350WT / E7018M /A517 (Weldment)
- 350 WT / E11018M / A517 (Weldment)

Available Fatigue Data in the Marine Structural Hdbk

- Data were generated from 10000 tests of 11 steels including : ABS EH-32, ABS-36, A36, A572, A588, A710/ A710A, HY 80, HY100 and BS 4360. The following properties are listed:
- Fracture toughness (J1c).
- Tensile strength (UTS & yield).
- Charpy impact values.
- Dynamic Tear DT energy and NDTT.

Classification of Marine Steels

- HSLA Steels containing Ni, Cr, Mn & Mo: (A 514, HY 80 & HY100)
- HSLA Steels containing Cu, Ni, Cr & Mo: (A710 & HSLA 80).
- Medium/high strength Steels containing Mn: (A537, A656, A737 & ABS-EH36)
- Medium/low strengthSteels containing Mn: A36, A572, A588, A633 & BS4360.

Steels for Marine Applications

- The specifications and properties of marine steels overlap;
- Steels of close composition may not be completely equivalent for the same application due to heat treatment and/or fabrication practices; and
- A great amount of information is required for building useable material engineering database for design.

Priority & Equivalent Marine Steels

◆ Priority steels	◆ Equivalent steels
◆ HY 80	◆ A543
◆ A710 gr. A	◆ A736
◆ ABS EH36	◆ A737 gr. B
◆ A514E	◆ A517 E
◆ HY100	◆ A543 gr. C

Fatigue Data Needed for CPF Steels

- There is a need to generate fatigue data for critical design details manufactured from ASTM 715 gr.70, ASTM A570 and special alloy steels which are unique to CPF.
- Critical weldments has to identified for planning future maintenance.

Further Research on Ship Structural Details

- Develop a database of mechanical properties and characterize crack growth, propagation and arrest in critical details of the CPF.
- Conduct engineering analysis to determine stress levels acting on critical welded details using adequate modeling techniques.

Classes of Ship Details

- Type 1, non weldable details;
- Type 2, welded details on surface; and
- Type 3, welded details at end connections of joints.

Classification of Structural Details

- Details are classified in terms of the following variables:
  - Direction of applied stress relative to the structural detail;
  - Location (s) of possible crack initiation;
  - Geometrical configuration of the detail; and
  - Method of manufacture and inspection.

Cracked Fatigue Details and Availability of Data

- See Table 5.1 pg 39 in SSC 318, Fatigue Characterization of fabricated ship details
- Include structural details in fig. B.1 page 131-133.

Fatigue Cracking & Durability Design

- Fatigue Cracks occur at:
  - bracketed end connections of supporting structural details;
  - openings & cut-outs in primary structures;
  - intersection of welded detail with bulkheads;
  - discontinuities in highly stressed details, and
  - bad weld profiles .

Causes of Fatigue Failure of Welded Ship Details

- Low quality construction, poor welding, assembly & maintenance practices;
- Weld failure, incomplete fusion, undercut;
- Inappropriate design or poor materials;
- Inadequate NDT inspection; and
- Frequency and amplitude of random loading at low temperature.

Common Problems in Fatigue Design of Ship Details

- ◆ Service loads differ greatly from loads that are used in laboratory simulation.
- ◆ Fatigue design criteria are based on constant amplitude/Cycle fatigue data from smooth specimens in the laboratory.
- ◆ Fatigue resistance information is not available for all the structural details currently found in ship construction.

Issues That Impede Reliable Design

- ◆ There is a lot of variety of welded joints;
- ◆ Weldments of the same joint type are not usually alike;
- ◆ The behavior of simple weldments can be very complex; and
- ◆ Stresses in a weldment are not precisely known.

Factors Affecting Fatigue Behavior of Welded Details

- Geometry and Configuration of the detail;
- Stresses and Loading conditions including: amplitude, frequency, directionality of random loads and residual stresses;
- Steels from which the structure is fabricated (yield strength ranges from 30 to 100 ksi)
- Quality and integrity of the Weld .

Fatigue Design Process

- SSC 318- FATIGUE CHARACTERIZATION OF FABRICATED SHIP DETAILS FOR DESIGN (PHASE 1), 1983
- SSC 346- FATIGUE CHARACTERTIZATION OF FABRICATED SHIP DETAILS FOR DESIGN (PHASE 2), 1990
- D-03-002-008/SG-001- DESIGN PROCDURES FOR CF SURFACE SHIP STRUCTURES 1993/94
- D-03-002-008/SG-002- STRUCTURAL DESIGN OF CF SURFACE SHIPS. 1993/94

Design Parameters for Ship Structures

- Component Characteristics and Structural Details.
- Global Configuration
- Material Selection.
- Fabrication procedures and Specifications.

Design Parameters

Primarily Affect →	
GLOBAL CONFIGURATION	Applied Forces Structure Response Structure Redundancy
COMPONENT CHARACTERISTIC AND STRUCTURAL DETAILS	Stress Levels Stress Concentration Access, Workmanship and Details
MATERIAL SELECTION	Chemical Composition and Weldability Mechanical Properties and HAZ Corrosion Fatigue Behavior
FABRICATION PROCEDURE AND SPECIFICATIONS	Local Deformations and Residual Stress Pattern Defect Distribution and Initial Rate of Growth

Fabrication and Post-Fabrication Parameters

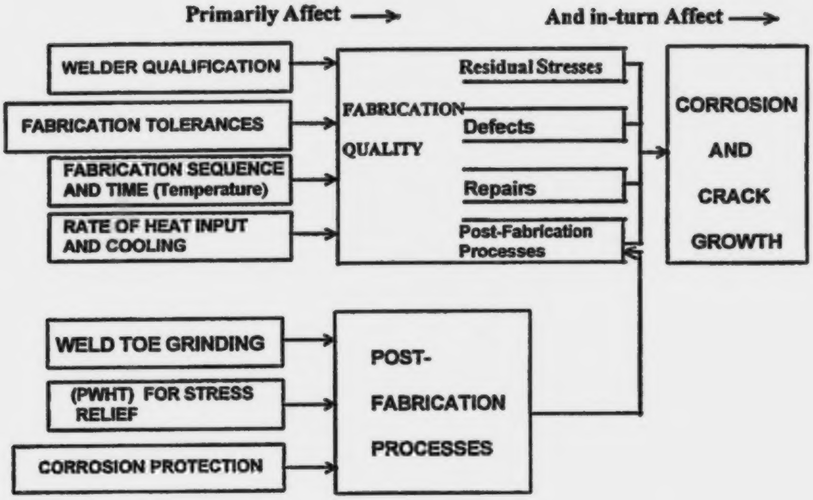

Primarily Affect →

And in-turn Affect →

WELDER QUALIFICATION

FABRICATION TOLERANCES

FABRICATION SEQUENCE AND TIME (Temperature)

RATE OF HEAT INPUT AND COOLING

FABRICATION QUALITY

Residual Stresses

Defects

Repairs

Post-Fabrication Processes

CORROSION AND CRACK GROWTH

WELD TOE GRINDING

(PWHT) FOR STRESS RELIEF

CORROSION PROTECTION

POST-FABRICATION PROCESSES

In-Service Parameters

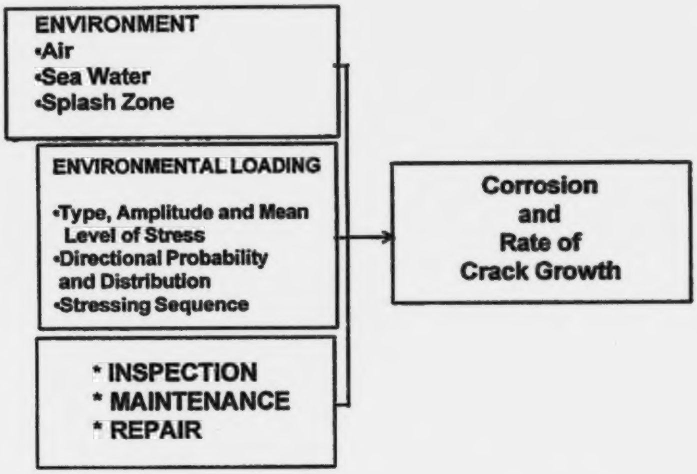

ENVIRONMENT
- Air
- Sea Water
- Splash Zone

ENVIRONMENTAL LOADING
- Type, Amplitude and Mean Level of Stress
- Directional Probability and Distribution
- Stressing Sequence

* INSPECTION
* MAINTENANCE
* REPAIR

Corrosion and Rate of Crack Growth

Fatigue Anlaysis Models & Parameters

- **SSC 346 1990**
- **SSC-367 May 93**
- **Naval Platform Fatigue Considerations by J.F. Porter, DREA, Halifax, December 1993**
- **Residual Strain Effects on Fatigue Crack Initiation and Growth in Marine Structures- Literature Review by L.Malik, Fleet Technology Inc., Ottawa 1993**

Global Parameters

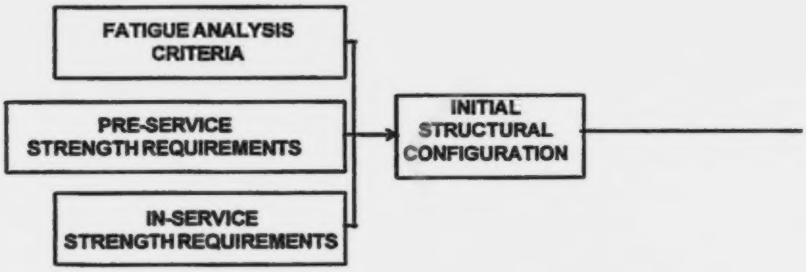

FATIGUE ANALYSIS CRITERIA

PRE-SERVICE STRENGTH REQUIREMENTS

IN-SERVICE STRENGTH REQUIREMENTS

INITIAL STRUCTURAL CONFIGURATION

Stress Model Parameters

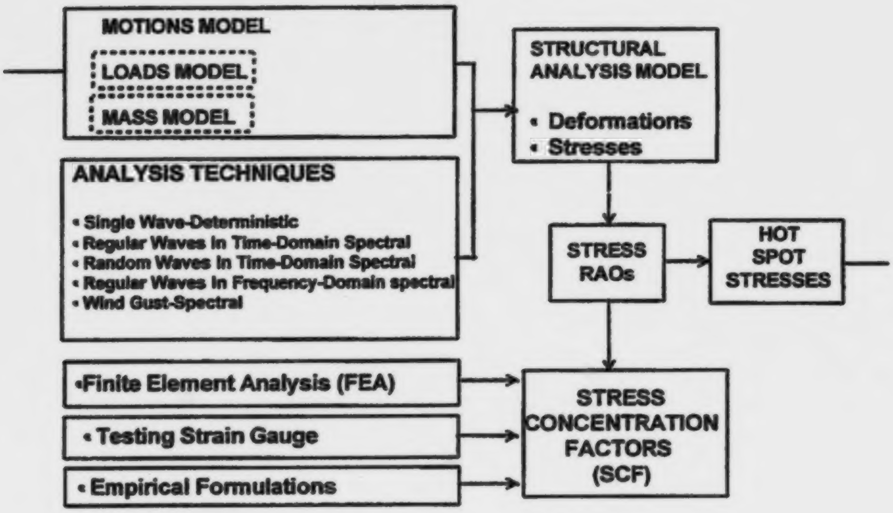

MOTIONS MODEL

LOADS MODEL

MASS MODEL

ANALYSIS TECHNIQUES

- Single Wave-Deterministic
- Regular Waves in Time-Domain Spectral
- Random Waves in Time-Domain Spectral
- Regular Waves in Frequency-Domain spectral
- Wind Gust-Spectral

STRUCTURAL ANALYSIS MODEL

- Deformations
- Stresses

STRESS RAOs

HOT SPOT STRESSES

- Finite Element Analysis (FEA)
- Testing Strain Gauge
- Empirical Formulations

STRESS CONCENTRATION FACTORS (SCF)

Stress History Model Parameters

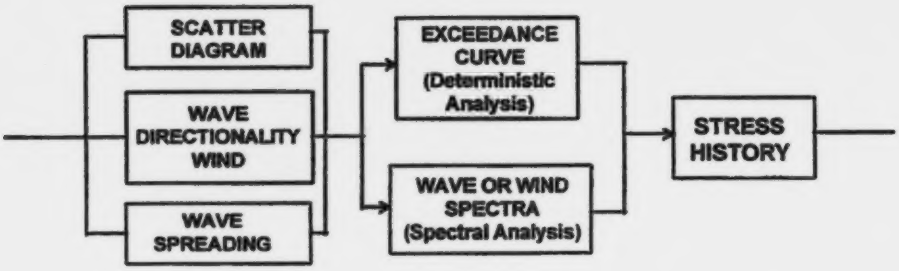

SCATTER DIAGRAM

WAVE DIRECTIONALITY WIND

WAVE SPREADING

EXCEEDANCE CURVE (Deterministic Analysis)

WAVE OR WIND SPECTRA (Spectral Analysis)

STRESS HISTORY

Fatigue Damage Computation Parameters

S-N CURVE

FATIGUE DAMAGE COMPUTATION

TYPICALLY UNACCOUNTED PARAMETERS

- Stress Sequence
- Maintenance/ Repairs
- Lapses in Corrosion Protection

Effect of Materials on the Integrity of Welded Details

◆ Ship steels exhibit adequate damage/ flaw tolerance under service conditions IF the structural details and welds are designed and fabricated properly.

◆ Fatigue crack initiation and propagation lives are insensitive to material properties of welded structural details.

◆ The quality and integrity of the welds are the main controlling factors.

Effect of Weld Profile and Attachment Thickness

- Improved weld profiles delay crack initiation and increase propagation lives.
- Concave weld profiles reduce stress concentrations at the toes, which in turn, extend fatigue life of the structure.
- Fatigue strength is reduced when the section thickness of the detail is increased.

Effect of Stress Cycles on Fatigue of Weldments

- (S-N) Fatigue data are generated under constant amplitude cyclic conditions;
- Fatigue resistance is a function of the alternating stress range and mean stress;
- The Stress range is the most important factor controlling the fatigue life of welded ship details.

Effect of Stress on Fatigue Behavior of Details

- Residual stresses caused by welding and/or assembly may significantly affect fatigue life of cetrtain types of structural details.
- Variable alternating random loads may degrade fatigue life.
- Repeated loadings and stress concentration factors tend to equalize the fatigue resistance of the structural detail regardless of the type of steel used.

Conclusions

- Fatigue strength of steel weldment does not increase in proportion to the increase in yield or ultimate strength. Increased strength is beneficial only in the initiation phase in smooth specimens.
- Fatigue life of weldments is dominated by crack propagation phase.
- The use of high strength steels in fabricated ship details facilitates fatigue cracking .

Fatigue Behavior of Welded Details

- Effects of Residual Stresses: may be negligible.
- Effect Of Material: may be negligible since fatigue life of the weldment is spent in propagating welding flaws and/or internal defects.

Ways to Control Fatigue and Fracture

- **Minimize weld defects during fabrication;**
- **Minimize Stress Concentrations and misalignments in structural weldments;**
- **Avoid welded joint eccentricity;**
- **Design the details for NDT inspection;**
- **Enforce adequate QA/QC procedures; and**
- **Minimize degradation of the assembled details.**

Improvement of Fatigue Behavior of Welded Details

- Reduction in stress concentrations by modifying the weld profile;
- Removal of Weld toe defects;
- Improvement of welding practices and control;
- Introduction of Local Compressive stresses by shot-peening of the weld;

MARINE STRUCTURAL Integrity PROGRAM (MSIP)

SSC-365/1991

Summary

Marine Structural Integrity Program (Msip)

- The objective is to develop procedures for the definition of advanced marine structural integrity program that would ensure more effective inspection, proper maintenance, and economical operation of naval vessels.

Msip- Design Objectives

- Create an efficient and durable Ship structural details which are devoid of unanticipated costly maintenance requirements.
- Ensure that the structure is able to withstand the expected maximum lifetime loading without significant deformation.

Components of MSIP

- Identification of critical components and potential failure modes
- Material selection
- Durability and damage tolerance analysis.
- Inspection strategy
- Tracking of individual structures.
- Full scale testing of critical structures.
- Management of aging structures
- Record keeping of structural maintenance.

Durability & Design Considerations

- Materials
- Connections, welding and fasteners systems;
- Structural configuration,
- Design stress levels,
- Manufacturing Processes & controls,
- Inspection level and quality,
- Interacting variables during design and fabrication.

Fatigue Analysis Tasks

- Characterization of short and long term cyclic loading conditions.
- Determination of the cyclic forces and strains in the critical details and components.
- Determination of potential degradation in strength and corrosion resistance of weldments.

MSIP- Fatigue Fracture Control Approaches

- Design and Fabrication of the Detail IAW to Specific Codes;
- Structural design based on redundancy and multiple load paths;
- Fail-safe design by including crack arrest provisions, such as using damage tolerant steels and geometric interruptions.

#510369

(26)

Novel Industrial Process and Equipment for Wear Resistant and Antifriction Coating of Large Diesel Engine Components

Abstract

V. Gorokhovsky*, S. Das Gupta*, A. Ginovker**†, V. Gelfandbein**

* The Electrofuel Manufacturing Co., 37 Hanna Ave., Toronto, Ont. M6K 1Y3

** Department of Physics, Dalhousie University, Halifax, N.S. B3H 3J5

1. A Large Area Filtered Arc Deposition System (LAFAD) including a rectangular two-channel macroparticle filter and two rectangular cathodic arc sources allows the production of vacuum coating deposition on articles of complex shape, with practically unlimited height. In this process a pure, strongly ionized gas-metal plasma flow containing multicharged ions without macroparticle impurities is created. The interaction of this plasma flow with the negatively charged substrate results in the deposition of coatings with an amorphous and ultra-microcrystalline structure. These coatings are characterized by a number of unique mechanical properties such as: high microhardness, high corrosion resistance and low friction. This allows the coatings to be used for improving wear resistance of marine diesel parts:

Application of LAFAD equipment allows several surface modifications and coating steps to be performed in one uninterrupted process.

The performance of several vital engine systems has been evaluated as a result of surface modification of parts using the LAFAD system.

1. Combustion subsystems - piston rings and cylinder liners
2. Power transmission subsystems - crankshafts and bearings
3. Fuel distribution - camshafts and valves

Obviously it is difficult to satisfy all demands with one coating material. Therefore, complex, multiphase, multilayer coating technology is being developed for engine part surface modification. The most suitable coating process for piston rings has been found to be a multistage process involving: ion nitriding (≤ 50mm), an intermediate layer of Cr-CrN (≤5 mm) and then an antifriction Mo_2N layer (~ 5 mm). Good results on cylinder liners have been provided by Cr-Si and Cr-Si-N coating systems. The best coatings for crankshafts were diamond-like coatings (DLC) with a thickness of less than 5mm using an Al_2O_3 intermediate layer. Ti -TiN coating systems were found to be most suitable for valve surface modification.

Diesel part surface modification can greatly increase the endurance and ease of maintainence of an engine.

---

† To whom correspondence should be addressed.

#510370 (27)

X-ray Diffraction Determination of Residential Strain for Marine Platforms

by

John F. Porter*, Micheal E. Brauss** and James A. Pineault**

* Defence Research Establishment Atlantic, Dockyard Lab,
FMO Halifax, Halifax, Nova Scotia, Canada, B3K 2X0

** Proto Manufacturing Ltd., 2175 Solar Crescent,
Oldcastle, Ontario, N0R 1L0

ABSTRACT

While x-ray diffraction techniques have long been applied for the determination of surface residential strain states, the bulky nature of the required apparatus has severely limited the usage of these techniques. Advances in solid state x-ray detection devices and computing systems have permitted the development of a fully portable miniature x-ray diffraction system (MXRD) for application on complex welded structures such as marine platforms. Residential strain is defined as the aggregate of those strains which are present in the structure in the absence of external loading. In marine platforms, these strains include the welding residual strain component, the restraint strain component as a result of joining structural sections and the dockside strain component present due to the weight of the structure. MXRD is capable of fully characterising the residential strain states in complex welded structures as well as the applied strain states due to external static loading conditions.

Recent advances in the current MXRD development activity will be described with an emphasis on the differences between this system and earlier diffractometers. The potential for the use of portable x-ray diffraction systems in non-destructive testing on marine platforms will be discussed, as well as several relevant case studies, involving the application of MXRD for the measurement of residential strain.

#510371 (

Diffraction Measurements on CPF Steel Fatigue Samples

by

Percy Clark*, Tom Holden*, John F. Porter** and Richard Yee***

* Atomic Energy of Canada Limited, Chalk River Laboratories,
Chalk River, Ontario, Canada, N0R 1L0

** Defence Research Establishment Atlantic, Dockyard Lab,
FMO Halifax, Halifax, Nova Scotia, Canada, B3K 2X0

*** Fleet Technology Limited, Kanata, Ontario, Canada, K2K 1Z8

ABSTRACT

In an effort to develop a non-destructive means of quantifying fatigue damage in cyclically loaded marine materials, prior to the formation of a detectable fatigue crack, a series of hourglass shaped specimens were fabricated from 350WT steel, cyclically loaded to various percentages of their fatigue crack initiation life, and examined via neutron diffraction methods. Diffraction line parameters were observed which varied strongly with distance from the waist of each speciman. These parameters correlated with the degree of induced fatigue damage. Comparisons were made between these experiments and earlier less successful similar experiments conducted on HY80 samples. The limitations and potential for the application of diffraction technologies to non-destructively define the remaining fatigue life in marine components and structures is reviewed.

1.0 INTRODUCTION

Diffraction techniques are possible non-destructive methods of evaluating plastic deformation or fatigue damage in marine components which have been subjected to cyclic loading. This makes them attractive for assessing remaining fatigue life in naval vessels.

Several workers have tried to assess the accumulation of fatigue damage by monitoring the changes in residual stress and line broadening with fatigue life using x-rays. Both Goto[1] who studied fatigued 17-4 PH steel and Pangborn *et al*[2] who studied aluminum alloys found that line broadening was more sensitive to 'fatigue damage' in the first and last 10% of fatigue life. Pangborn *et al* suggested that 'fatigue damage' was accumulated in the interior of the specimen and recommended the use of more penetrating Mo k_α x-rays to study this possibility. For steel specimens, sufficient penetration can only be achieved by employing neutron scattering techniques.

To study the behaviour of residual strains and line broadening in fatigued CPF steels and to test the feasibility of predicting remaining fatigue life using neutron diffraction, samples of CPF steel were fatigue tested by Fleet Technology Ltd. under varying stress ranges and these samples were then examined using neutron diffraction techniques at Chalk River Laboratories.

1.1 Line Broadening Measurements

A peak measured in a diffraction experiment using a perfectly collimated, zero wavelength spread instrumental set-up and a large, defect free diffracting crystal has the general form of a near delta-function due to the coherently scattered radiation superimposed on a slowly varying background. The width of the sharp coherent component has a predicted full width at half intensity (FWHM) of 7.61 arcseconds[3], called the Darwin width.

If the crystal is plastically deformed, the generation of dislocations broadens the diffraction peak through two mechanisms. The dislocations allow a non-uniform strain field to exist within the crystal which introduces a Gaussian component to the lineshape. With sufficient deformation, the dislocations can form tangled walls that break up the coherently scattering crystal into small sub-grains. This produces a particle size broadening effect, giving rise to a Lorentzian component to the lineshape. It is possible to separate the two effects by Fourier analysis using careful measurements of the lineshape for multiple peaks over a range of diffraction angles (Warren-Averbach analysis)[3]. For the purpose of the current work a simpler and more direct approach was preferred.

Kurita and Chiaki[4] used the FWHM (Δ_o) obtained from a Gaussian fit to a single diffraction peak in an attempt to assess plasticity in mild steels. They found that the linewidth varied linearly with the logarithm of the plastic strain (ε) according to the form

$$\epsilon = A \times 10^{C\Delta_o} \tag{1}$$

Where A and C are empirical constants. This approach is reasonable, in this case, since both the non-uniform strain and particle size effects are the result of dislocation based plastic deformation; the parameter of interest.

In any real diffraction experiment, the spread of radiation wavelength and the finite angular collimations of the incident and scattered beams contribute to an additional instrumental linewidth Δ_I. From a measurement of the linewidth of a well annealed reference nickel powder with negligible deformation broadening, Δ_I can be determined. The intrinsic deformation linewidth (Δ) can be found by subtracting the instrumental linewidth from the observed linewidth (Δ_o) in quadrature as follows

$$\Delta^2 = \Delta_o^2 - \Delta_I^2 \tag{2}$$

2.0 EXPERIMENTAL

2.1 Samples

Fleet Technology Ltd. fatigue tested 11 standard hourglass specimens of 350WT CPF steel at various stress ranges to determine an approximate S-N curve. Samples 1 and 3 were tested at low stresses and did not fail, while samples 2, 4-11 were tested to failure. The samples were tested at a stress ratio of 0.05. Samples 2-11 were shipped to Chalk River for neutron diffraction analysis. An additional set of 6 samples (A-F) were subjected to a varying number of cycles at various stress ranges. These unbroken samples were sent to Chalk River 'blind', that is, with unknown stress ranges and numbers of cycles to investigate the possibility of determining remaining fatigue life from diffraction measurements.

2.2 Neutron Diffraction

The experiments were carried out at the NRU reactor, Chalk River. The L3 spectrometer was used in a high resolution configuration, with the (331) planes of a Germanium monochromator selecting neutrons of wavelength 1.9895Å at a take-off angle, $2\theta_m=100°$. The angular collimations between the monochromator and sample, and the sample and the detector were 0.16° and 0.125° respectively. Accurate linewidth measurements require high statistical definition of the peak and typically the peak intensity was about 5000 counts. The wavelength of the neutron beam was calibrated with a standard Ni powder. The (111) powder peak of Ni is very close in scattering angle to the (110) iron reflection and the former gives a measure of the instrumental contribution to the linewidth of 0.256±.003°. The lattice parameter used in the calculation of lattice strain was determined from an untested fatigue specimen and was found to be 2.0270±0.0001Å.

The incident and diffracted neutron beams were spatially defined by slits placed in neutron absorbing cadmium. The intersection of the two beams defines the region from which the diffraction information is obtained, the gauge volume. In this case, the gauge volume was approximately cubical, 1.5mm on a side. By placing the samples on a computer controlled xyz stage the location of the gauge volume could be arbitrarily positioned in the sample. The diffraction peak was measured using a position sensitive detector and recorded in the form of intensity versus diffraction angle, 2θ. The peak position, $2\theta_{hkl}$, the integrated intensity, I_{hkl}, and the line width, Δ_o, were obtained by fitting a Gaussian distribution plus a sloping background to the data.

For each of the samples tested to failure (samples 2, 4-11), one remnant was measured at five axial positions: 2, 4, 6, 8 and 10mm from the break. The samples fatigued to a fixed number of cycles before failure (samples 3, A-F) were measured at the waist and 5mm above and below.

3.0 RESULTS

3.1 Fatigue Testing

The results of fatigue testing on samples 1-11 by Fleet Technology Ltd. is shown in Table I. It was determined that the fatigue life (N) could be represented by the following function of the stress range (S) in MPa

$$\log(N) = 118.3 - 42.18 \log(S) \tag{3}$$

The diameter of the samples was measured as a function of axial position after testing. Using the measured starting diameters of the specimens, the true macro-strain was calculated as a function of axial position and is shown in figure 1 for each of the broken samples.

Specimen Number	Stress Range (MPa)	Life Cycles
1	422	>3.8 million
3	446	>7 million
5,8	455	327 770, 289 320
4,11	485,484	208 490, 114 890
2,10	496, 498	46 410, 40190
9	506	2 870

Table I Specimens Tested to Establish the S-N Curve

3.2 Neutron Diffraction

Figure 2 shows the results of the diffraction measurements on the broken samples as a function of axial position. Both the line width (Δ), after correction for instrumental broadening, and the residual lattice strains were fit with a linear function of the axial position. From the linear fits the lattice strain and line broadening were calculated at the 0mm and 5mm positions and show a rough linear behaviour when plotted against the fatigue stress range as shown in figures 3 and 4.

The results of the broadening and lattice strain measurements at the waist position for the 6 'blind' samples are plotted in figures 5 and 6 as a function of the true macro-strain derived from diameter measurements before and after testing.

4.0 ANALYSIS

From the calculated macro-strain as a function of axial position and the linear fits of Δ versus sample position it was possible to infer the variation of Δ with true macro-strain for each sample as shown in figure 7. This was done to separate the role of fatigue damage from the effect of the considerable plastic deformation due to necking that can be seen in figure 1.

Inspection of figure 7 indicates that the data from all the broken samples lies on a single curve that is well described by a logarithmic relationship between macro-strain and the instrumental corrected broadening

$$\Delta = (0.071 \pm 0.001) \times \ln(\epsilon) + 0.322 \pm 0.002 \qquad (4)$$

This Kurita-Chiaki behaviour indicates that the broadening behaviour is dominated by the overall plastic deformation and that the number of cycles or remaining fatigue life may have little impact. That is, if the broadening were dominated by remaining fatigue life, samples tested at lower stress ranges and failing at lower macro-strains should deviate from the overall curve of the samples failing at high cycles. For example, if fatigue damage was a significant component of the observed broadening, the terminal broadening of samples 5 and 8 at ε=0.35 and e=0.73, respectively, should be much higher than the broadening of samples 2, 10 and 11 (which have much larger remaining fatigue life and a lower number of cycles at the corresponding strains and axial positions) . This is not a surprising result given the large degree of plastic deformation due to necking apparent in figure 1.

A similar approach was used to derive figure 8, which relates the measured residual lattice strain as a function of ε. Clearly, the data from the different samples do not follow a single master curve as closely as in figure 7. However, this is due to the relatively larger error of the lattice strain measurement. The data from all the samples actually do agree within the estimated error. Figure 9 shows the results of plotting the lattice strain along two constant ε slices through the data in figure 8. There is a large scatter and the slopes are on the order of the uncertainty. As well, following the argument in the previous paragraph, fatigue damage-induced broadening should yield a negative slope in figure 9. That the slope is actually positive is further evidence that the fatigue damage is completely swamped by the necking-induced plastic deformation.

Accepting it is the gross plastic deformation that dominates the broadening and lattice strain behaviour, the increasing Δ and increasing compressive lattice strain with increasing stress range seen in figures 3 and 4 is understandable. Since the samples tested at high stress ranges failed after fewer cycles and therefore in a more ductile failure mode, the macro-strains at the 0 and 5mm positions away from the break were higher.

In both figures 7 and 8 the data from the seven unbroken samples were also plotted and agree well with the overall behaviour of the broken samples.

5.0 CONCLUSIONS

Line broadening and lattice strain measured using neutron diffraction in CPF steels fatigue tested to failure are both sensitive indicators of the total plastic strain to which the material has been subjected. The line broadening was found to follow a logarithmic function of the plastic strain as reported by Churita and Chiaki[5]. However, it was found that neutron scattering measurements on samples cycled to failure did not provide indication of fatigue damage. Therefore, it was not possible to predict the remaining fatigue life in the 'blind', unbroken samples.

There are several possible reasons why the measurements reported here were insensitive to fatigue history. Since the samples were measured after failure, it was not possible to make measurements exactly at the waist. As well, it is possible that any effect of the fatigue damage was erased by plastic flow during the final ductile necking failure. The effect of the ductile necking was enhanced since the samples investigated had been tested in the low-cycle fatigue regime. Therefore, more experiments should be performed before and after failure on samples tested at lower nominal stress ranges where failure is expected at lower plastic strains.

6.0 REFERENCES

1. Goto, T., "Material Strength Evaluation and Damage Detection by X-ray Diffraction", in Advances in X-ray Analysis, v35, 1992, pp 489-501.1.

2. Pangborn, R.N., et. al, "Dislocation Distribution and Prediction of Fatigue Damage", Met. Trans A, V12A, Jan. 1981, pp 109-120.

3. B.E. Warren, X-Ray Diffraction, Addison Wesley : Reading Mass. (1969).

4. M. Kurita and K. Chiaki, Advances in X-ray Analysis, ed. by C.S. Barrett, Plenum Press: New York 34, 633 (1991)

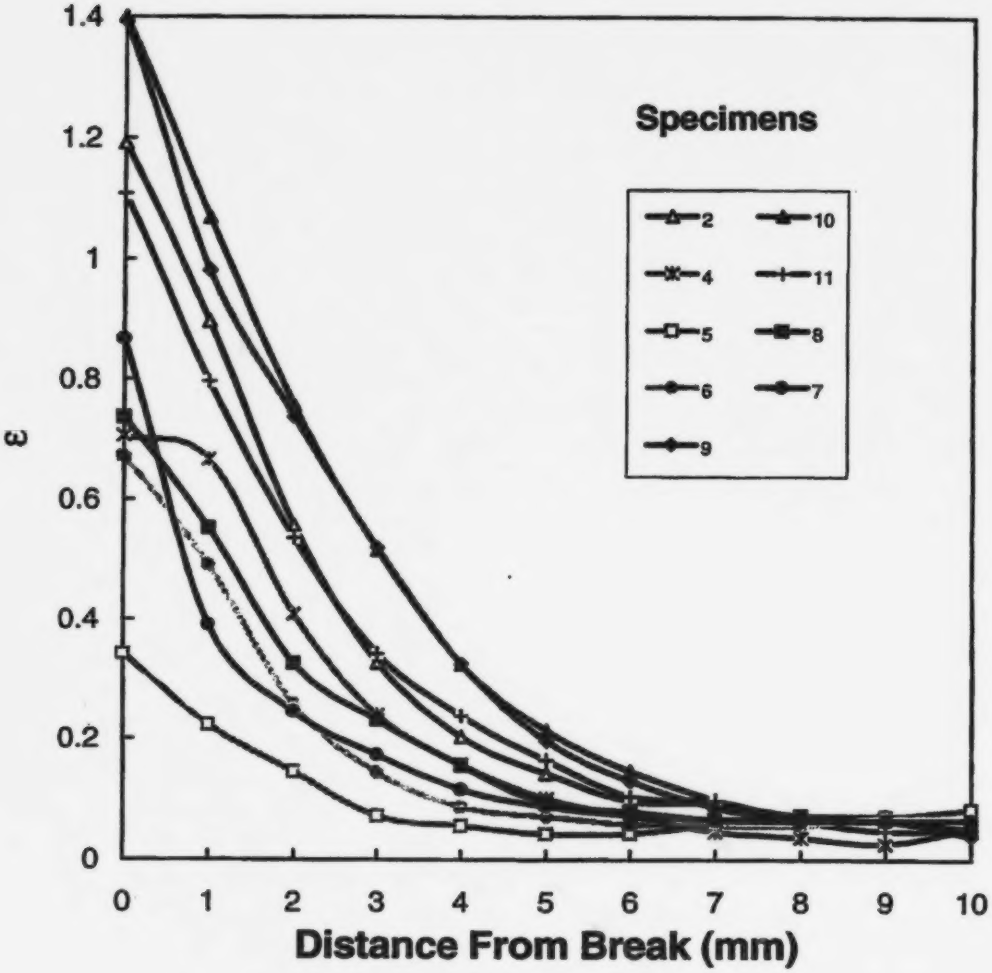

Figure 1 True plastic strain as a function of axial position away from the break for nine samples cycled to failure.

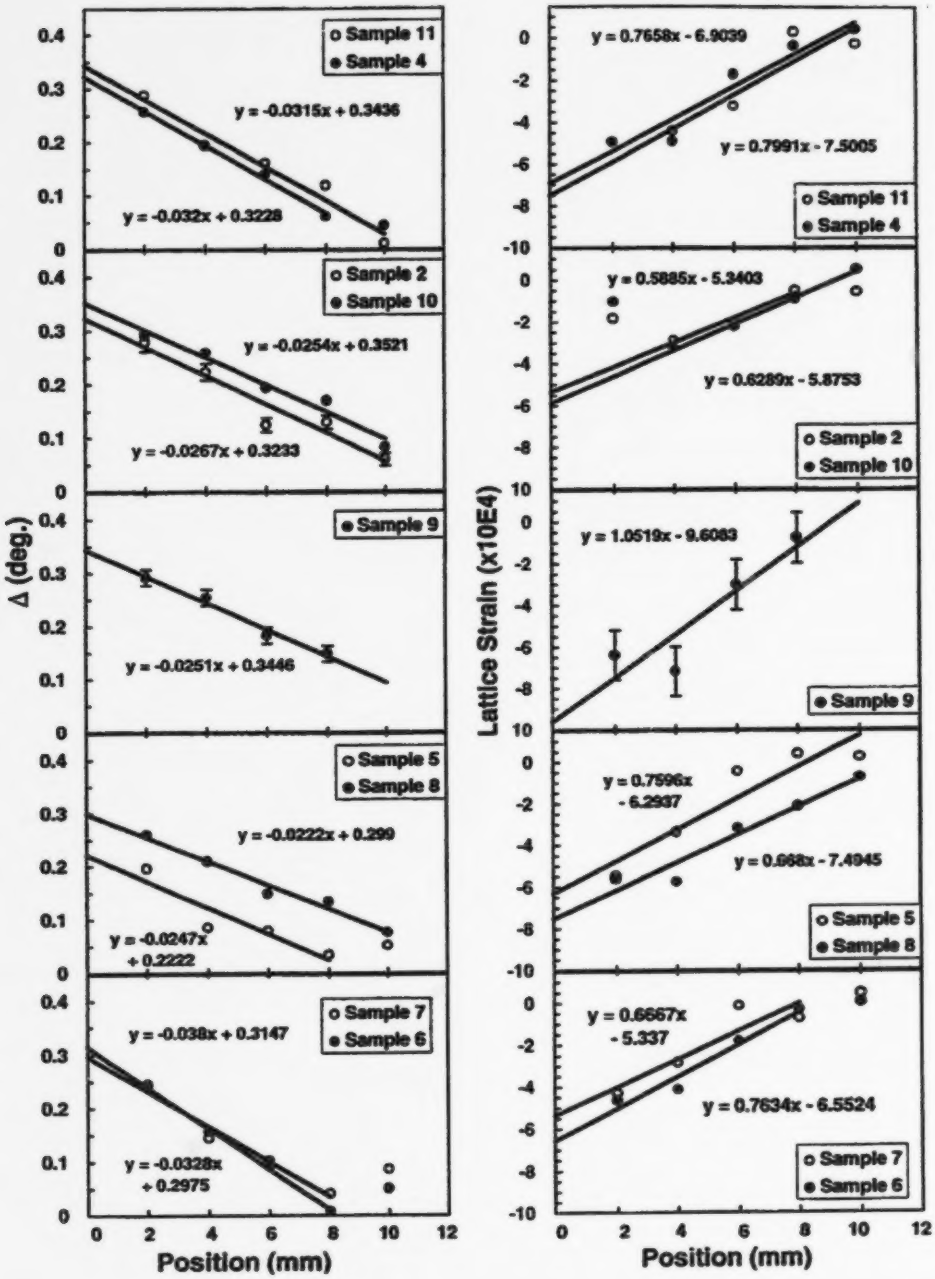

Figure 2 The (110) diffraction linewidth corrected for instrumental broadening and residual lattice strain for nine samples cycled to failure.

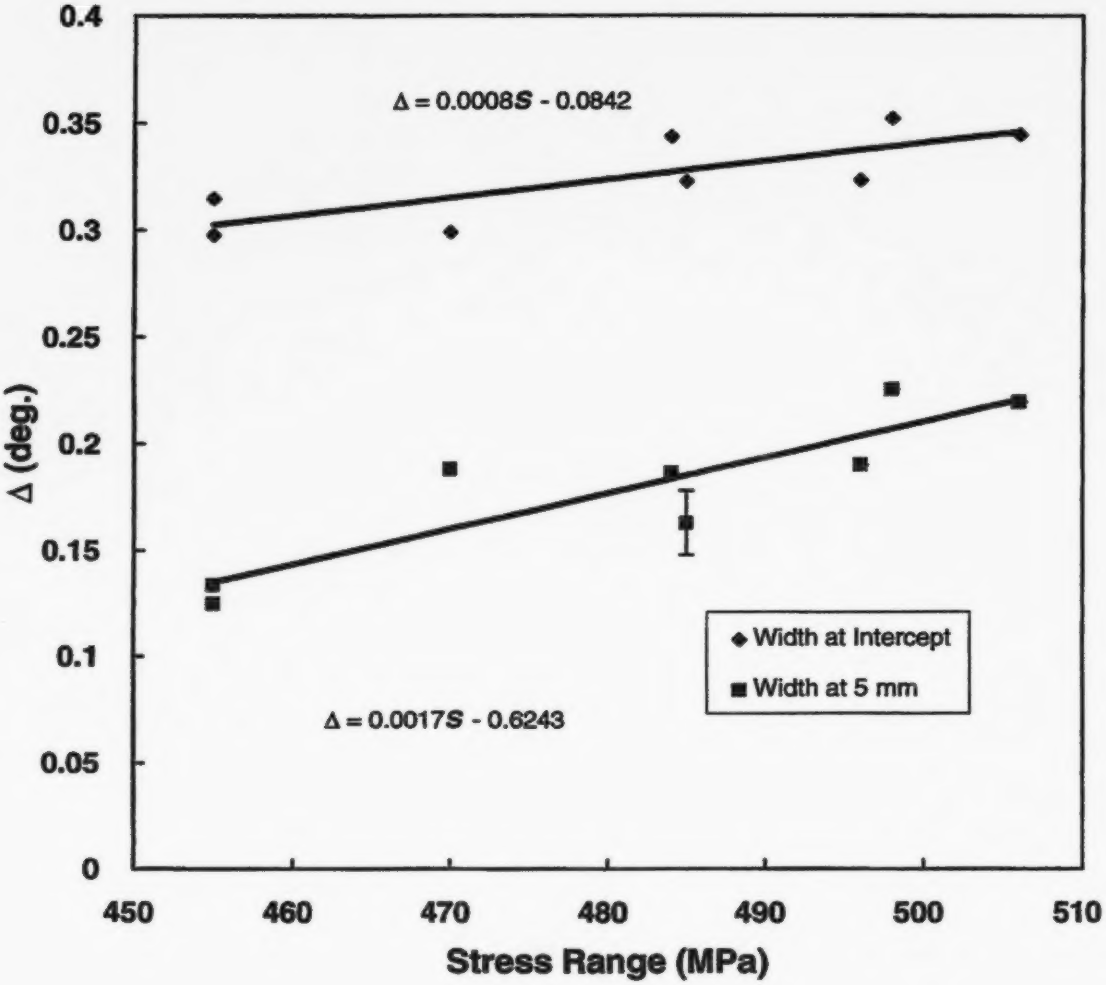

Figure 3 The diffraction linewidth at the break and 5mm away from the break as a function of fatigue stress range for nine samples cycled to failure.

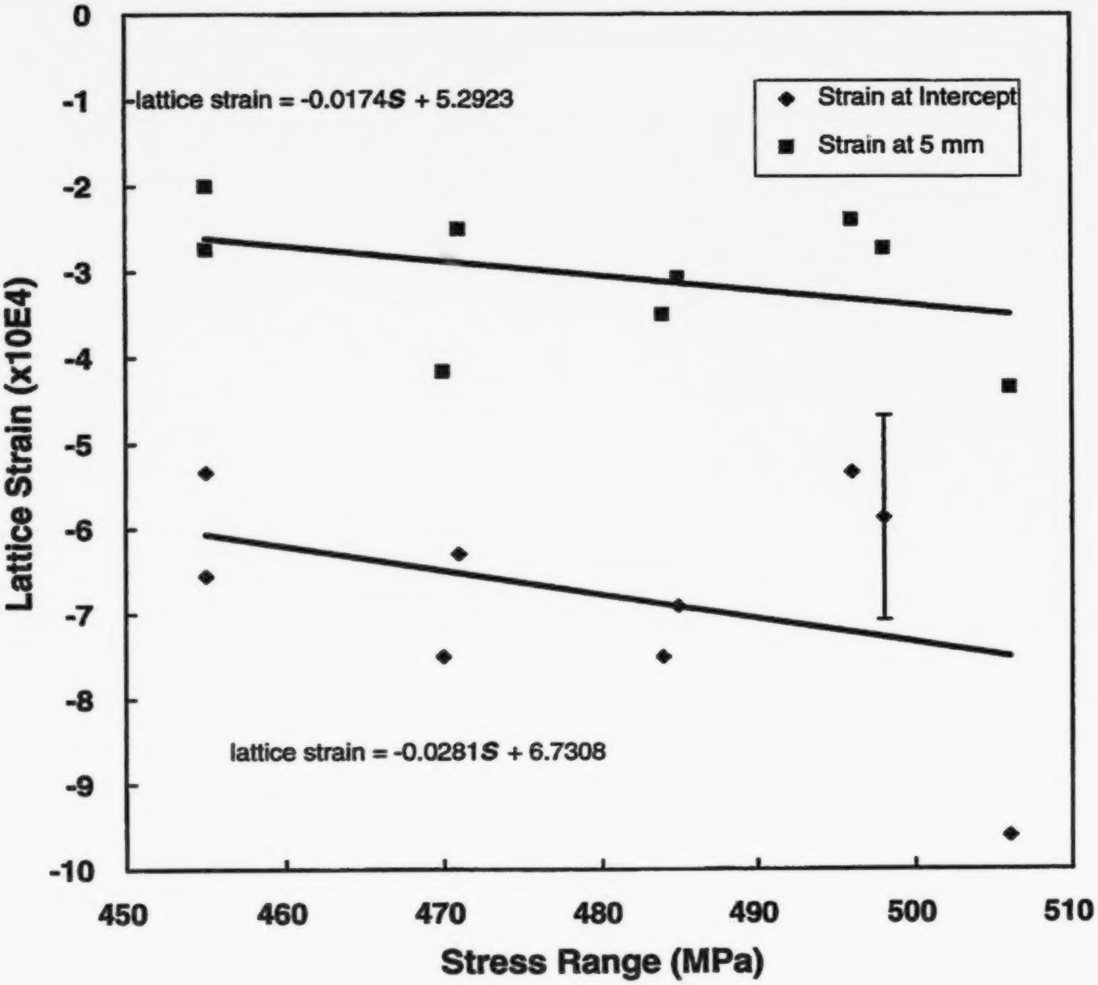

Figure 4 The residual lattice strain at the break and 5mm away from the break as a function of fatigue stress range for nine samples cycled to failure.

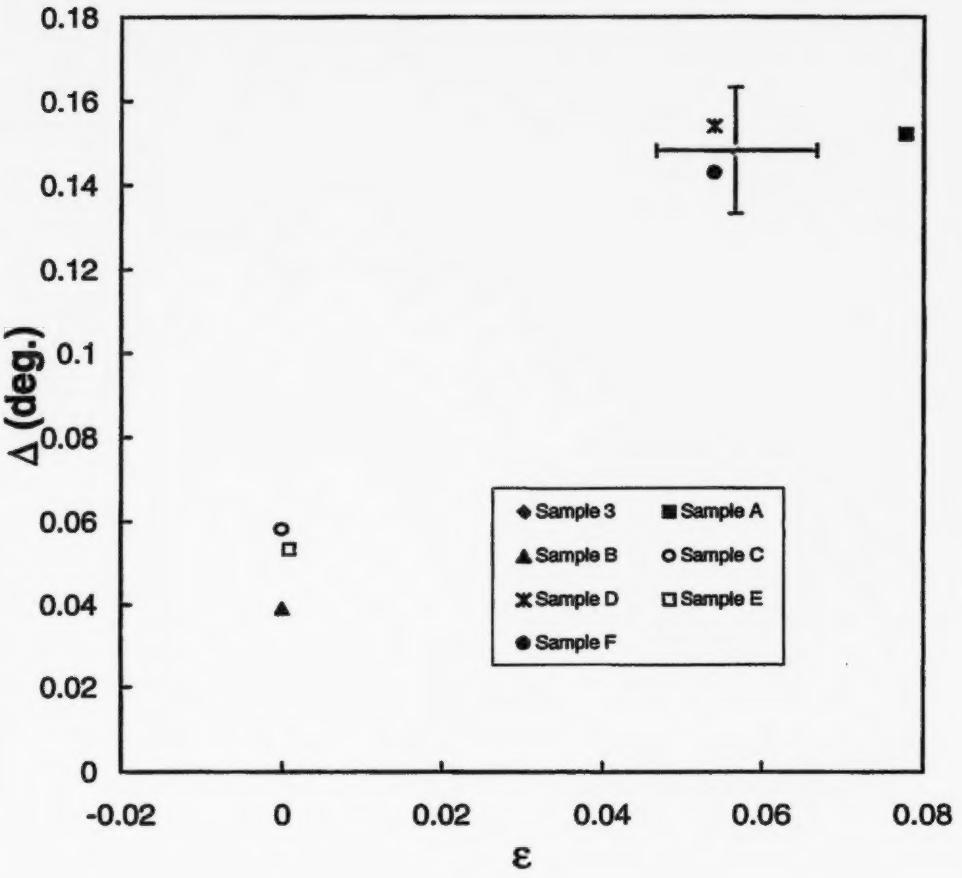

Figure 5 The diffraction linewidth at the waist as a function of true macrostrain for seven unbroken samples.

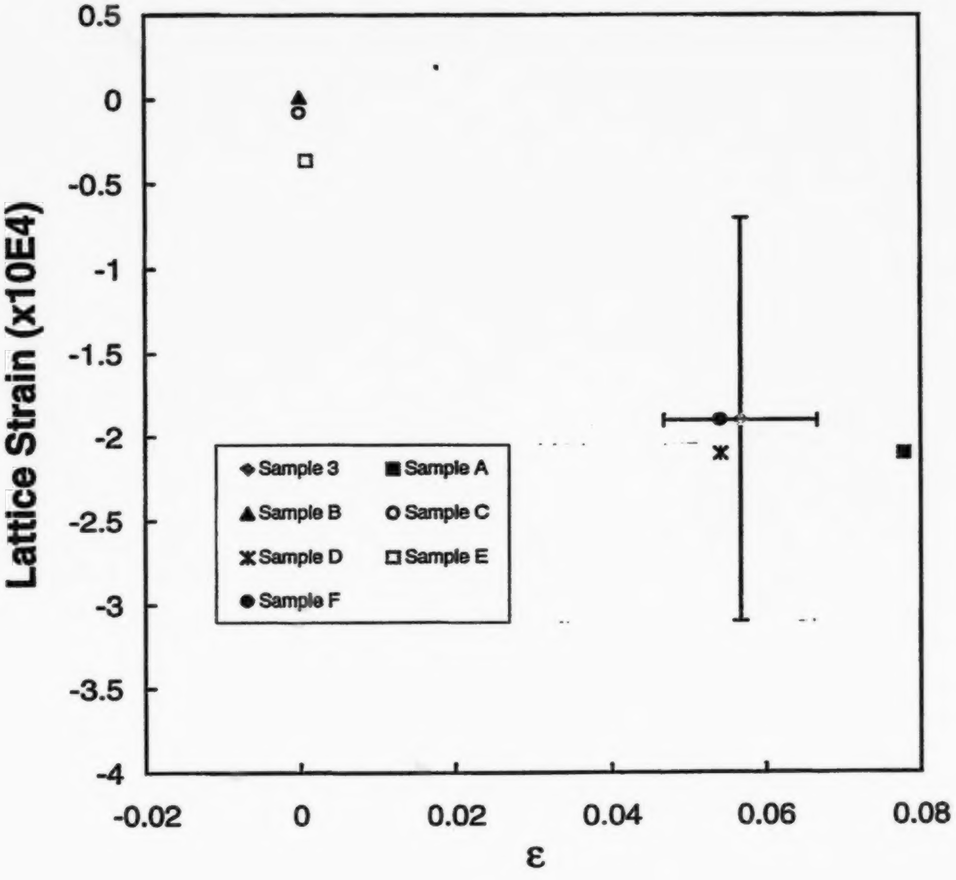

Figure 6 The residual lattice strain at the waist as a function of true macro-strain for seven unbroken samples.

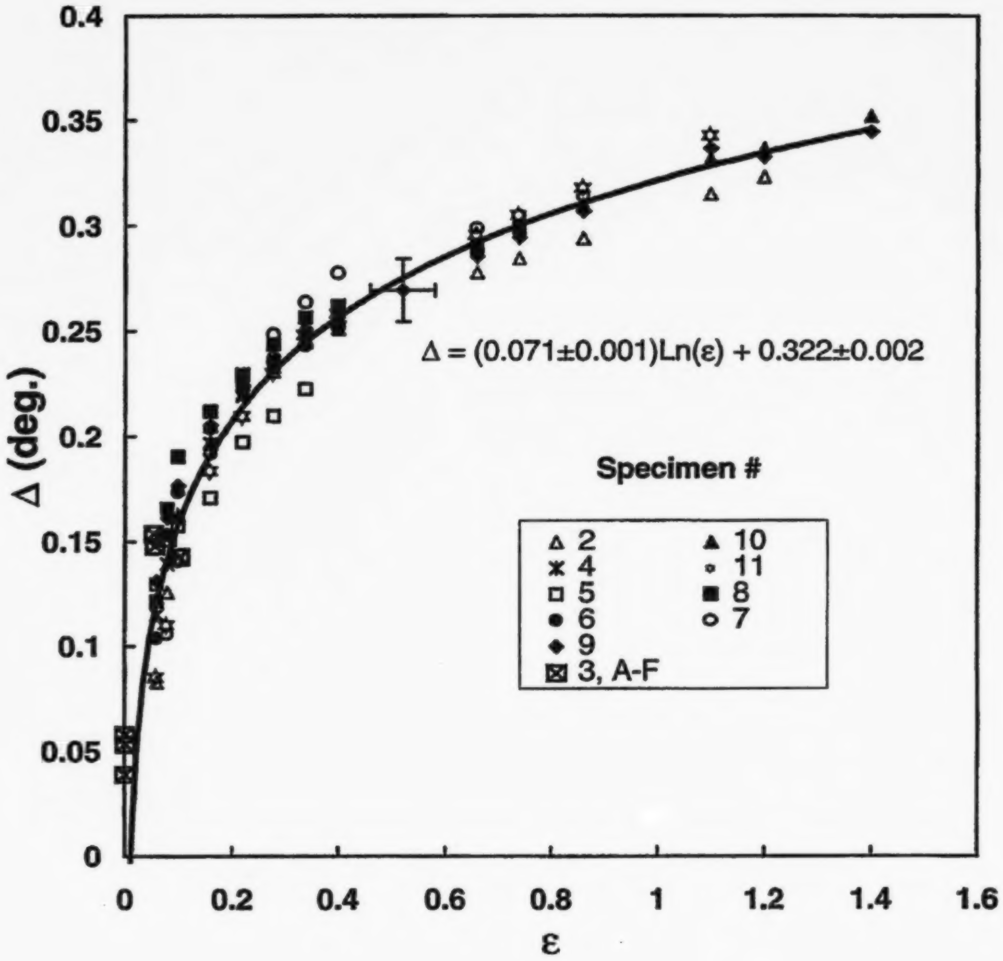

Figure 7 The (110) diffraction linewidth corrected for instrumental broadening as a function of true macro-strain for nine samples cycled to failure and seven unbroken samples.

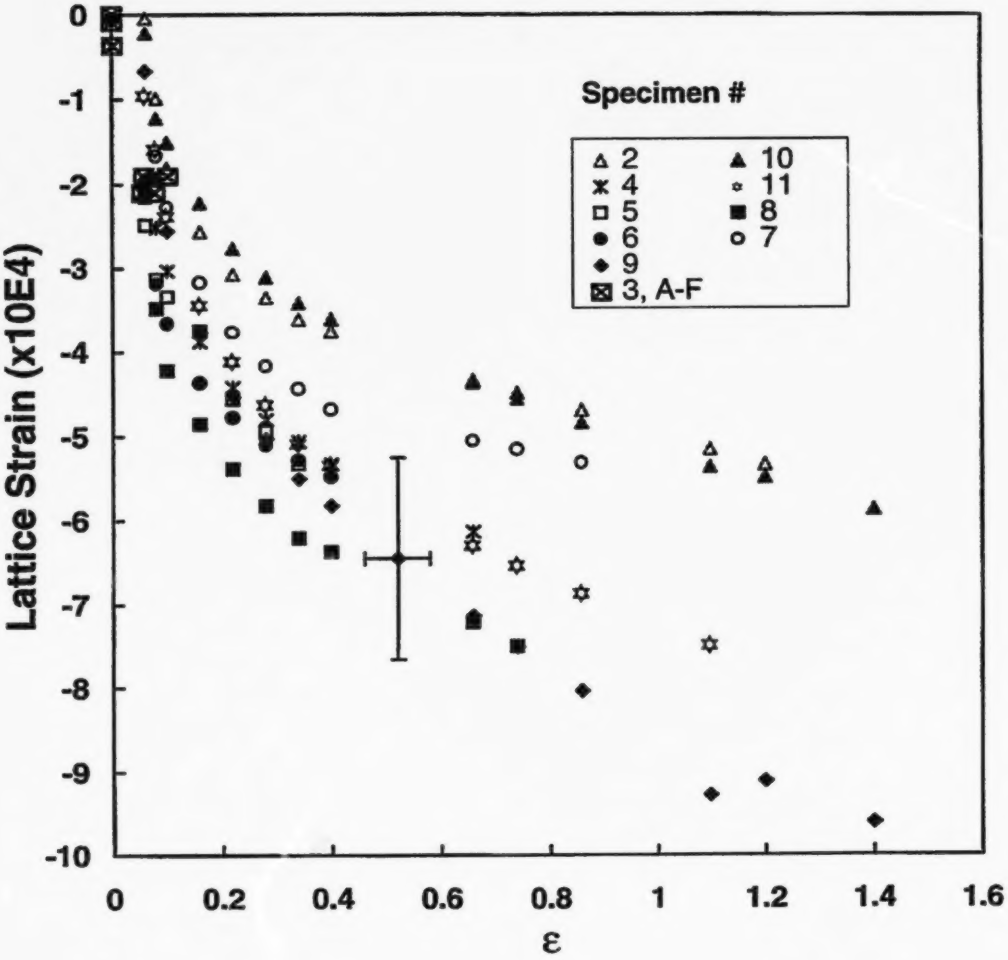

Figure 8 The residual lattice strain as a function of true macro-strain for nine samples cycled to failure and seven unbroken samples.

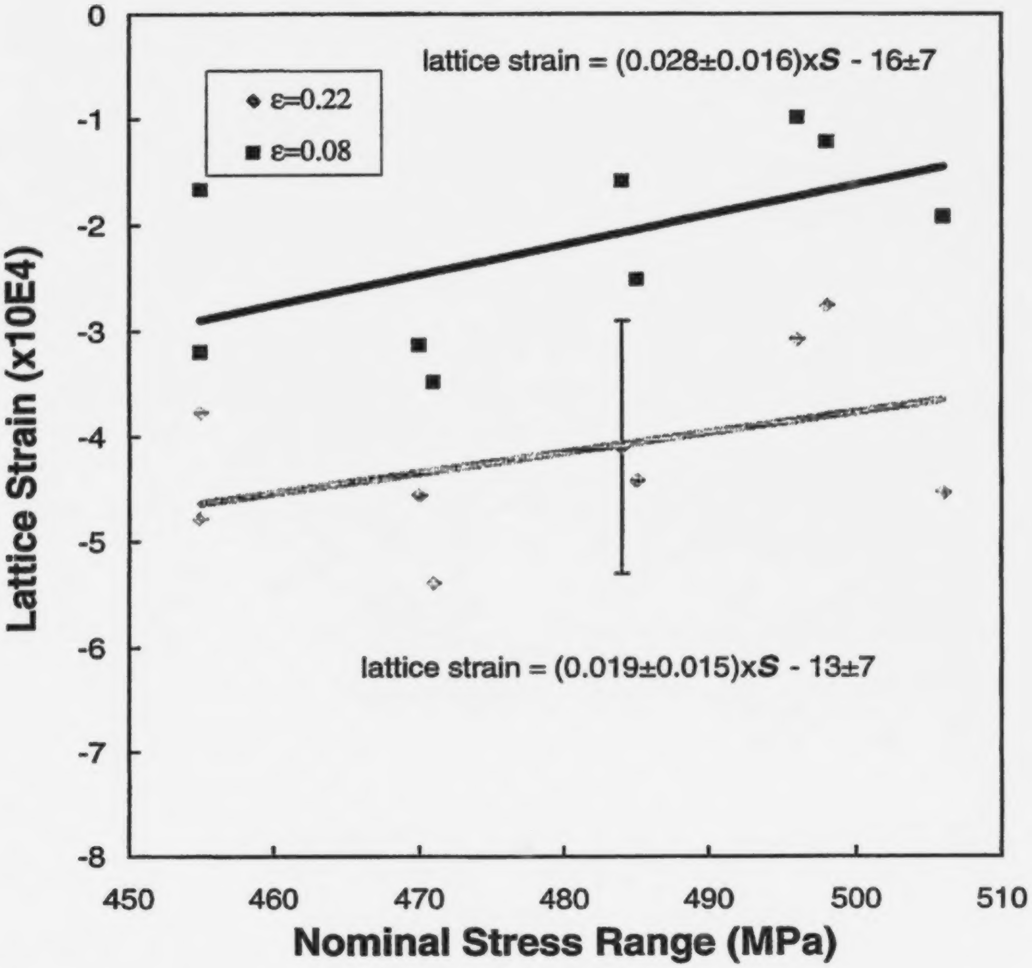

Figure 9 The residual lattice strain as a function of fatigue stress range at two constant strain values for nine samples cycled to failure.

#510372 (29)

Implementation of Accuracy Control on the Canadian Patrol Frigate Program

by

B.C. McGrath, P. Eng.

Saint John Shipbuilding Limited
Saint John, New Brunswick, Canada, E2J 4E5

ABSTRACT

Marine structural materials technology has gained much attention from researchers due to the condition of structural designs being limited by materials capabilities.

In addition to the materials and joining technologies, structural performance is affected by initial states of alignment, distortion and residual stress. Since each of these areas adds expense to shipyard construction efforts, they are as much concern to the builder as they are to the research community. The formation of an Accuracy Control Department in 1985 was the Saint John Shipbuilding Limited (SJSL) response to these causes of unwanted rework.

This presentation traces the growth and accomplishments of SJSL Accuracy Control in the quantification of dimensional performance as practiced on the Canadian Patrol Frigate Program. Special studies and in-process guidance and direction required for final product conformance is described. Impacts to structural integrity due to trends in construction methodologies is reviewed.

ACCURACY CONTROL

ACTIVITIES DIRECTED AT IMPROVING ELEMENTS OF COST/SCHEDULE PERFORMANCE THAT ARE IMPACTED BY DIMENSIONAL VARIABILITY OF INTERIM PRODUCTS

- Saint John Shipbuilding Limited -

SPECIFIC AREAS OF ACCURACY CONTROL ACTIVITY

RESIDUAL STRESSES

DISTORTION CONTROL

ALIGNMENT

- Saint John Shipbuilding Limited -

RESIDUAL STRESSES

REQUIREMENTS FOR OUTFITTING FOUNDATIONS

FLATNESS 0.1 - 0.5 MM

LEVEL 5 - 20 ARC MINUTES

MINIMIZE MACHINING ALLOWANCES

MINIMIZE MACHINING ON BOARD

PAGE__ OF__

CONDITION REPORT

HULL NO: 1222 | **UNIT NO:** 1250 | **ITEM:** 57mm GUN SEAT

STATUS: FLATNESS CHECK - SEAT RESTING FREE ON DECK | **DATE:** MARCH 30/88

36 BOLTS

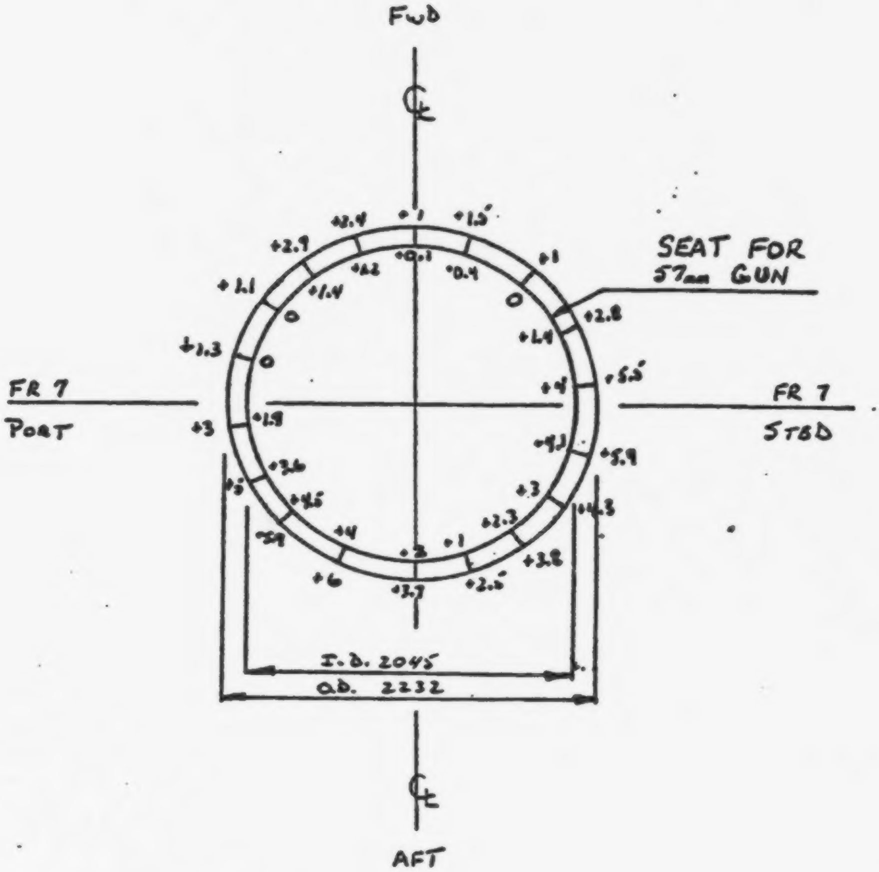
FWD
℄
+2.4
+1
+1.5
+2.9
+0.1
+0.4
+1
+2.2
+1.1
+1.4
0
0
+2.8
+1.4
+1.3
0
+5.5
+4
FR 7
PORT
+3
+1.9
FR 7
STBD
+4.1
+5.9
+3.6
+5
+4.5
+3
+4.3
+2.3
+5.9
+4
+3
+1
+3.8
+6
+3.7
+2.5
SEAT FOR 57mm GUN
I.D. 2045
O.D. 2232
℄
AFT

SURVEYOR: M. LANNIGAN, B. BROWN

REMARKS: 1) DEVIATIONS ARE FROM LOWEST POINT ON SEAT

CPF-04 Gun Seat Flatness

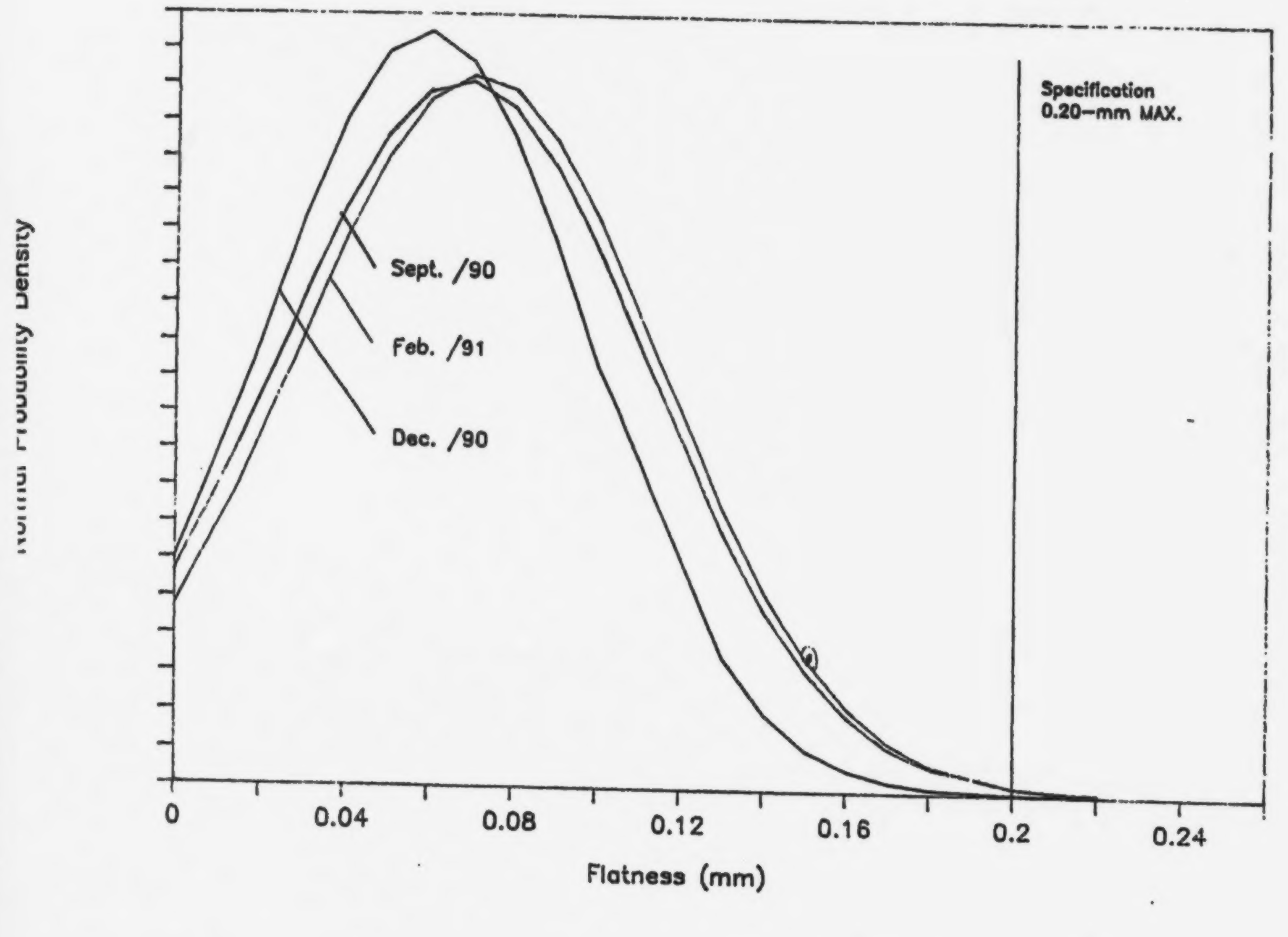

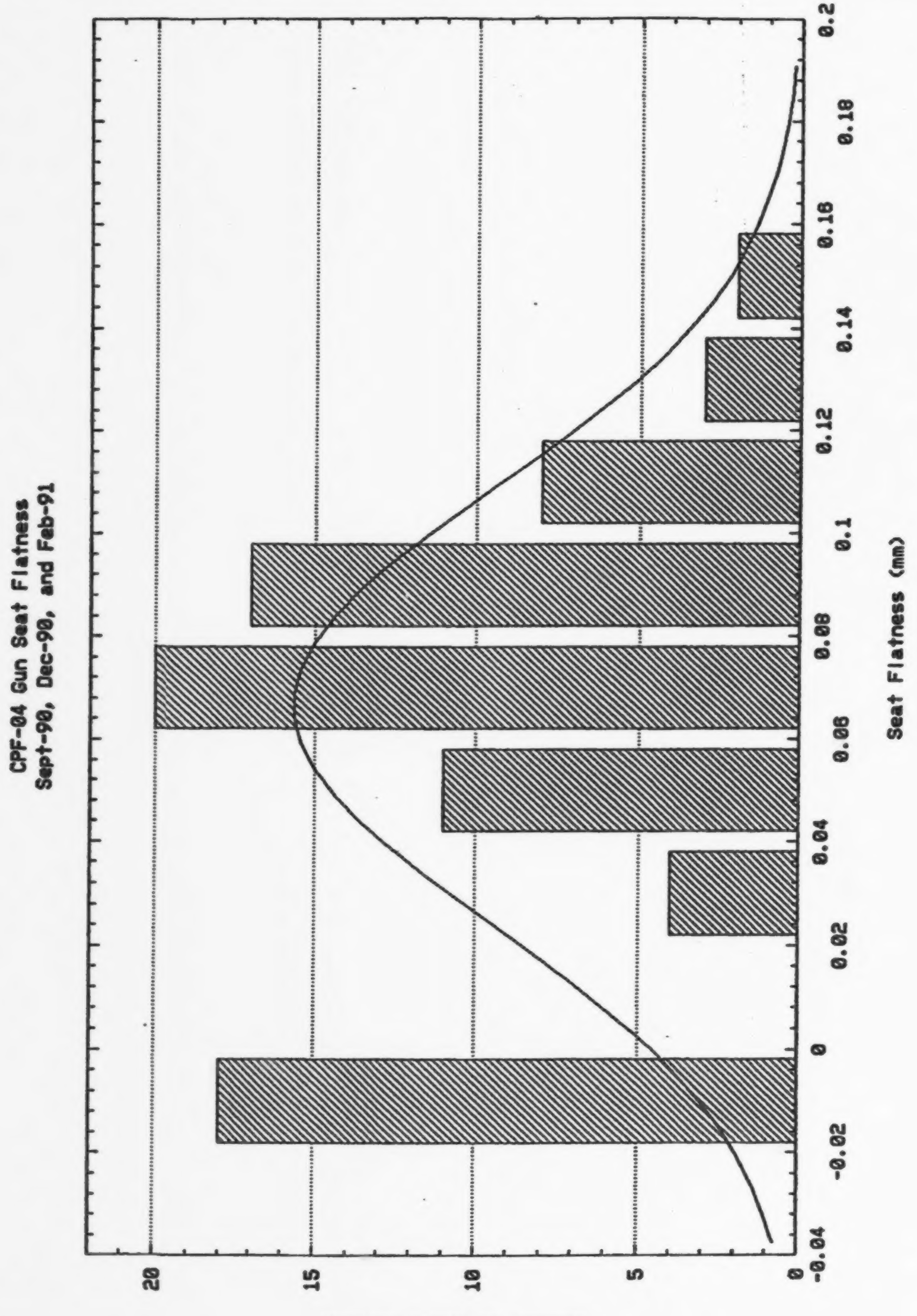
CPF-04 Gun Seat Flatness
Sept-90, Dec-90, and Feb-91

ACCURACY CONTROL AC36

PAGE __ OF __

CONDITION REPORT

HULL NO: 2252	UNIT NO: 1250	ITEM: 57mm Gun Seat
STATUS: After welding completed & hotwork		DATE: 13 May '94

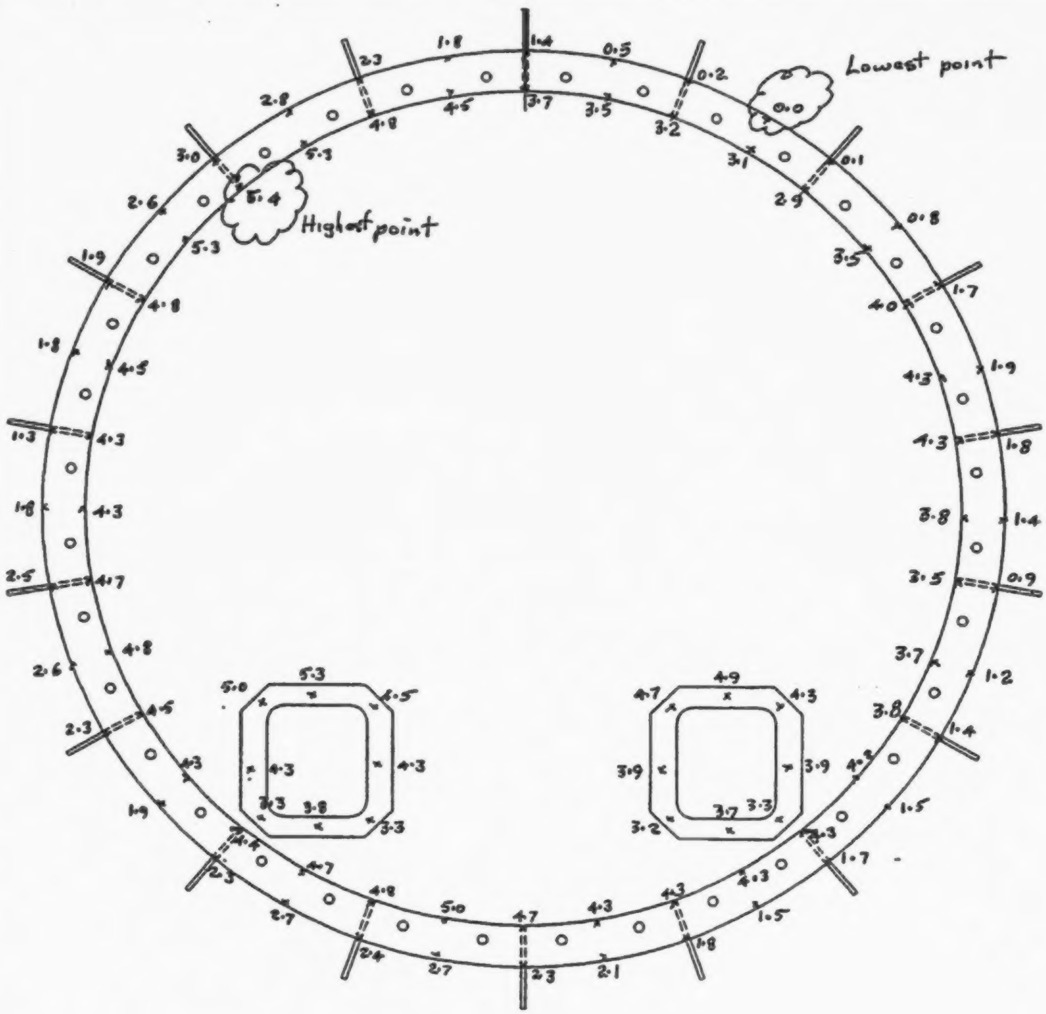
1.8
1.4
0.5
2.3
0.2
Lowest point
0.0
2.8
4.5
3.7
3.5
4.8
3.2
3.0
5.3
3.1
0.1
5.4
Highest point
2.6
2.9
0.8
5.3
3.5
1.9
4.8
1.7
4.0
1.8
4.5
4.3
1.9
1.3
4.3
4.3
1.8
1.8
4.3
3.8
1.4
2.5
4.7
3.5
0.9
4.8
3.7
2.6
1.2
5.0
5.3
5.5
4.7
4.9
4.3
2.3
4.5
3.8
1.4
4.3
4.3
4.3
3.9
3.9
4.2
1.9
3.3
3.8
3.3
3.7
3.3
3.2
1.5
2.4
3.3
4.7
1.7
2.3
4.8
5.0
4.7
4.3
4.3
4.3
2.7
1.5
2.4
2.7
2.3
2.1
1.8

SURVEYOR: R. Cassidy, H. Payne

REMARKS: 1) Lowest point shown as zero (0)
2) Deviations relate to lowest point

COPY: W. Mc Monigle

DISTORTION IN ASSEMBLIES

REQUIREMENTS FOR DISTORTION CONTROL

MAINTAIN DESIGN DIMENSIONS FOR ASSEMBLIES
WITH LOW STIFFNESS AND WELDING
UNBALANCED ABOUT THE NEUTRAL AXIS

- Saint John Shipbuilding Limited -

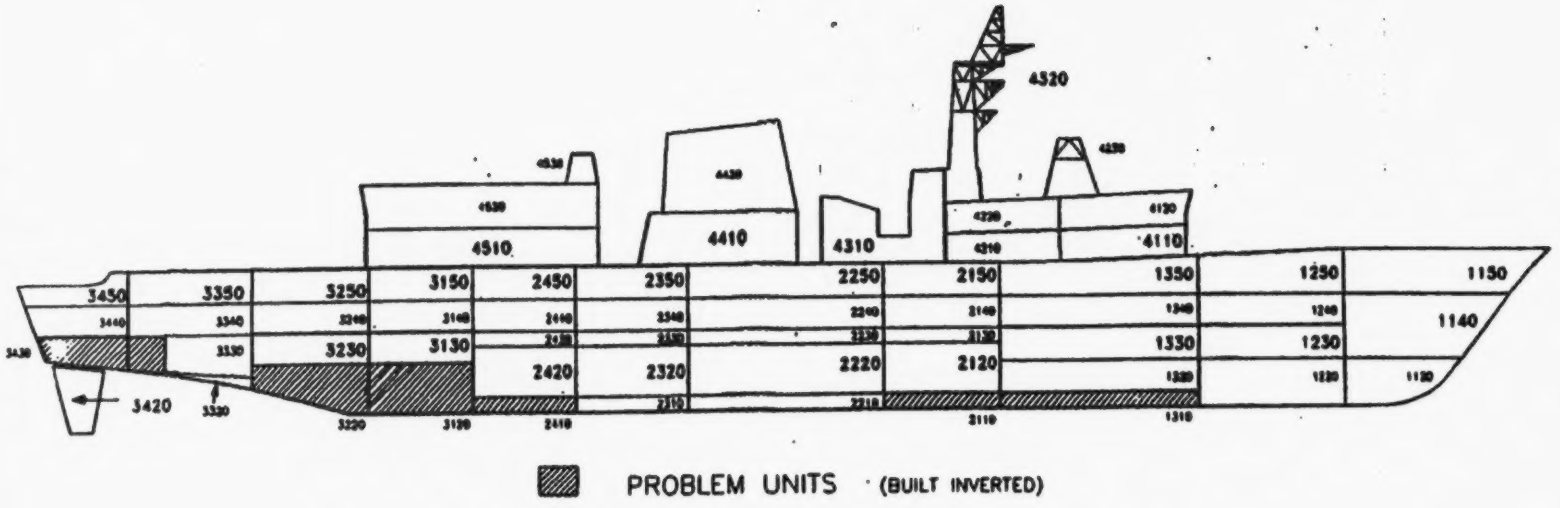
4520
4530
4510
4420
4410
4310
4320
4230
4220
4210
4120
4110
3430
3450
3440
3420
3350
3340
3330
3320
3250
3240
3230
3220
3150
3140
3130
3120
2450
2440
2430
2420
2410
2350
2340
2330
2320
2310
2250
2240
2230
2220
2210
2150
2140
2130
2120
2110
1350
1340
1330
1320
1310
1250
1240
1230
1220
1150
1140
1130
▨ PROBLEM UNITS (BUILT INVERTED)

CPF - 01
PROFILE

Exhibit 3: CPF - 01 UNIT DRAWING

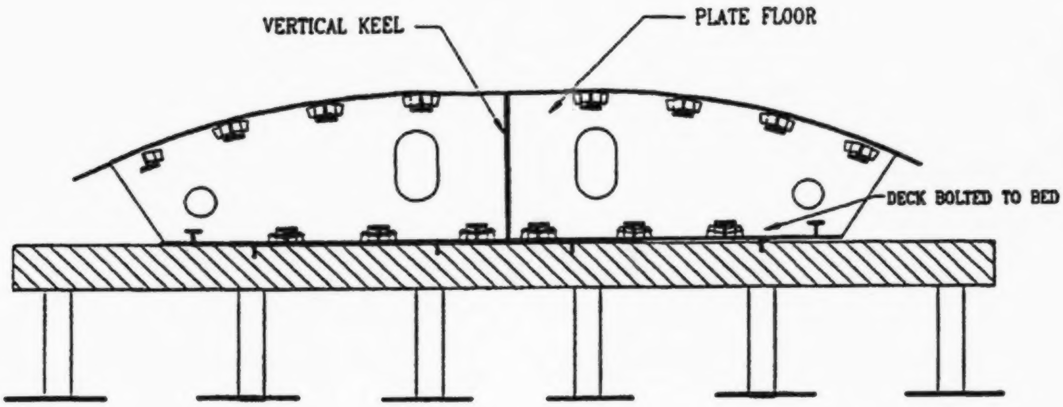
VERTICAL KEEL
PLATE FLOOR
DECK BOLTED TO BED

CONSTRUCTION BED
(INVERTED UNITS)

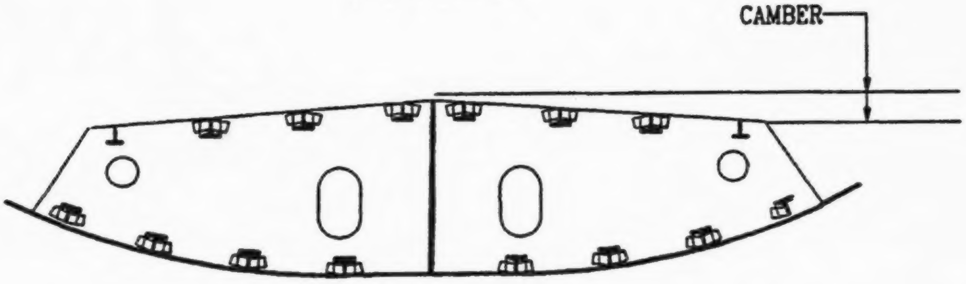

TRANSVERSE SECTION

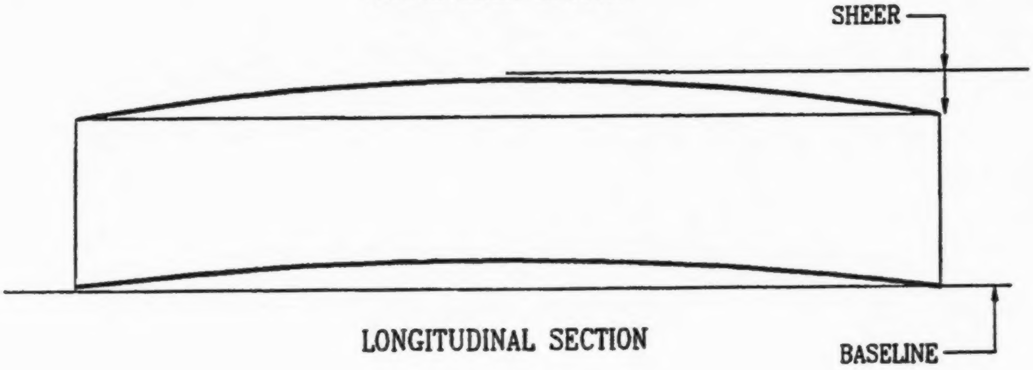
SHEER
BASELINE

LONGITUDINAL SECTION

(DISTORTION SCALE EXAGERATED)

Exhibit 2: INVERTED UNIT DISTORTION

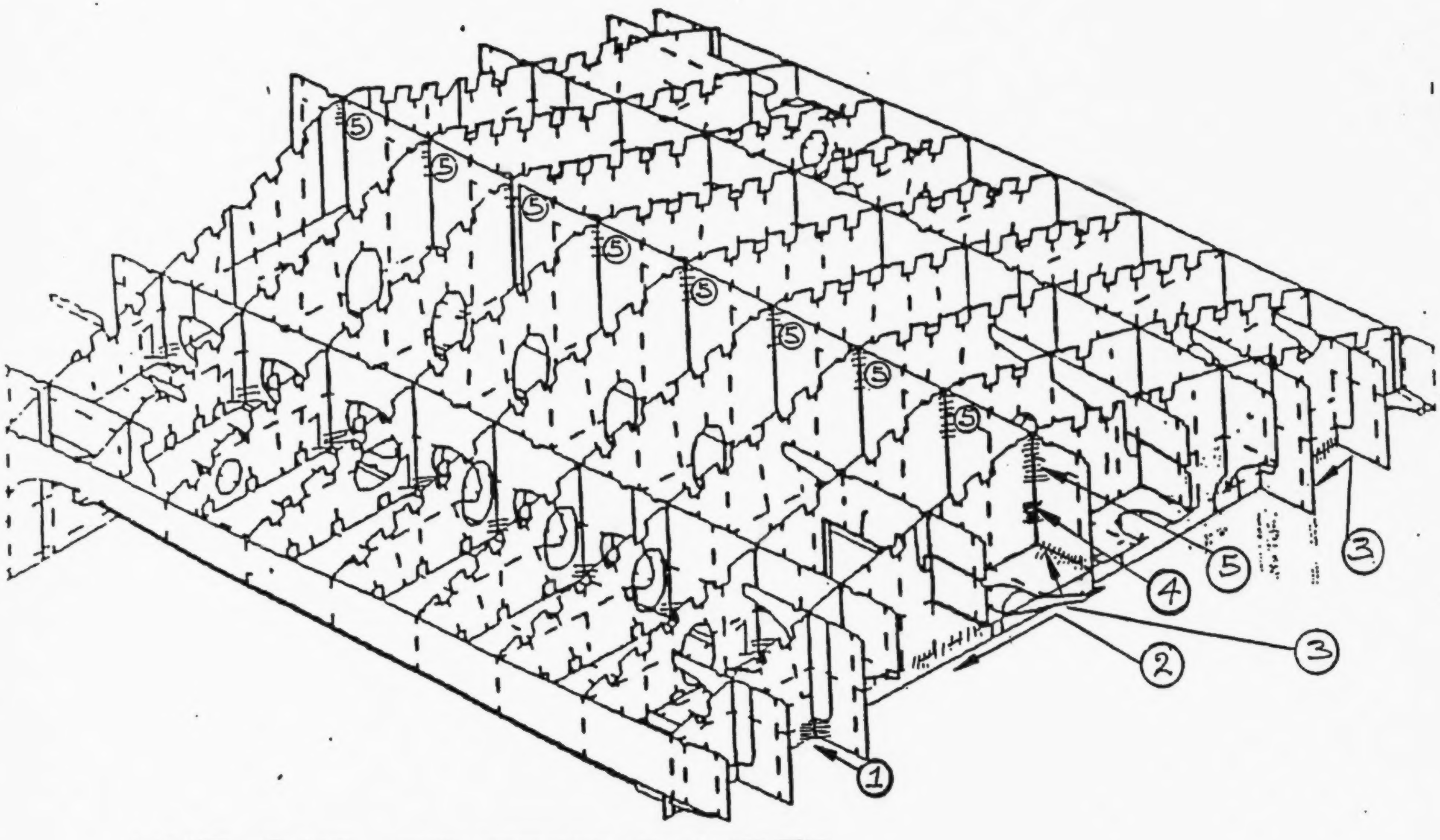
5
5
5
5
5
5
5
5
5
1
2
3
4
5
3

UNIT 2410 REVERSE CAMBER

ACCURACY CONTROL CHECK SHEET AC36

CONDITION REPORT

HULL NO.: 1222
UNIT NO.: 2110
ITEM: SHELL AS-BUILT
STATUS: COMPLETED - PRIOR JOINING TO 2120

DATE: MAR. 13/87
PAGE 1 OF

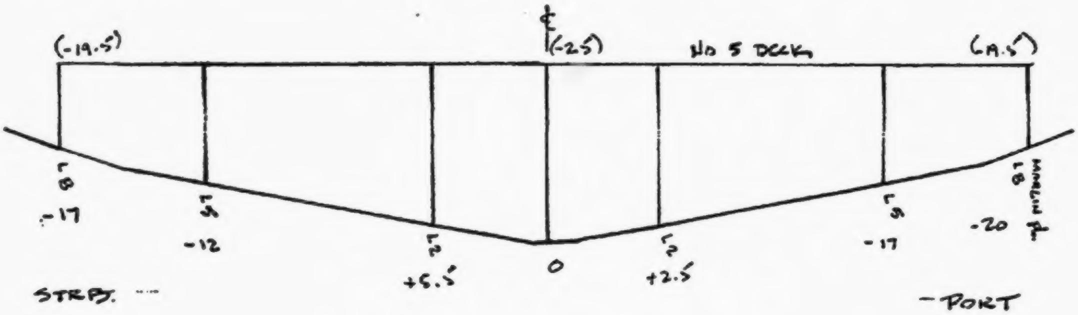
℄
(-19.5)
(-2.5)
NO 5 DECK
(-19.5)
L8
-17
L5
-12
L2
+5.5
0
L2
+2.5
L5
-17
L8
-20
MARGIN PL
STRBD.
PORT

DETAIL 6C
SECTION AT FR. 25
LOOKING AFT.

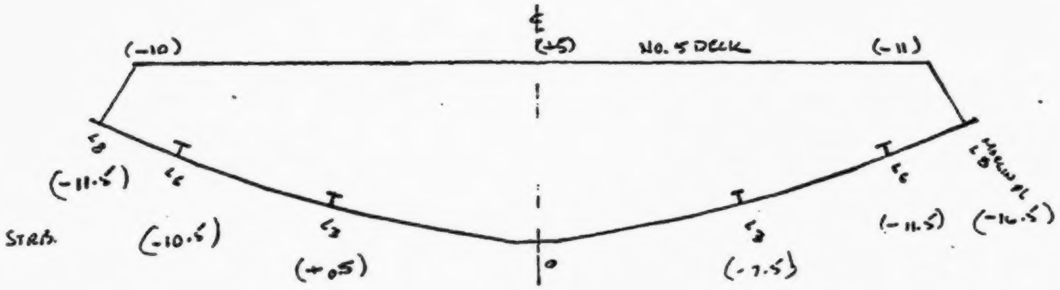
℄
(-10)
(+5)
NO. 5 DECK
(-11)
L8
(-11.5)
L6
(-10.5)
L3
(+0.5)
STRB.
0
L3
(-7.5)
L6
(-11.5)
L8
MARGIN PL
(-16.5)

DETAIL 7A
SECTION AT FR. 20.5
LOOKING AFT.

SURVEYOR: H. LONIGAN, H. PAYNE
TECHNICIAN:

REMARKS:
NUMBERS IN BRACKETS REPRESENT DEVIATION OF SHELL HEIGHTS FROM DESIGN HEIGHTS

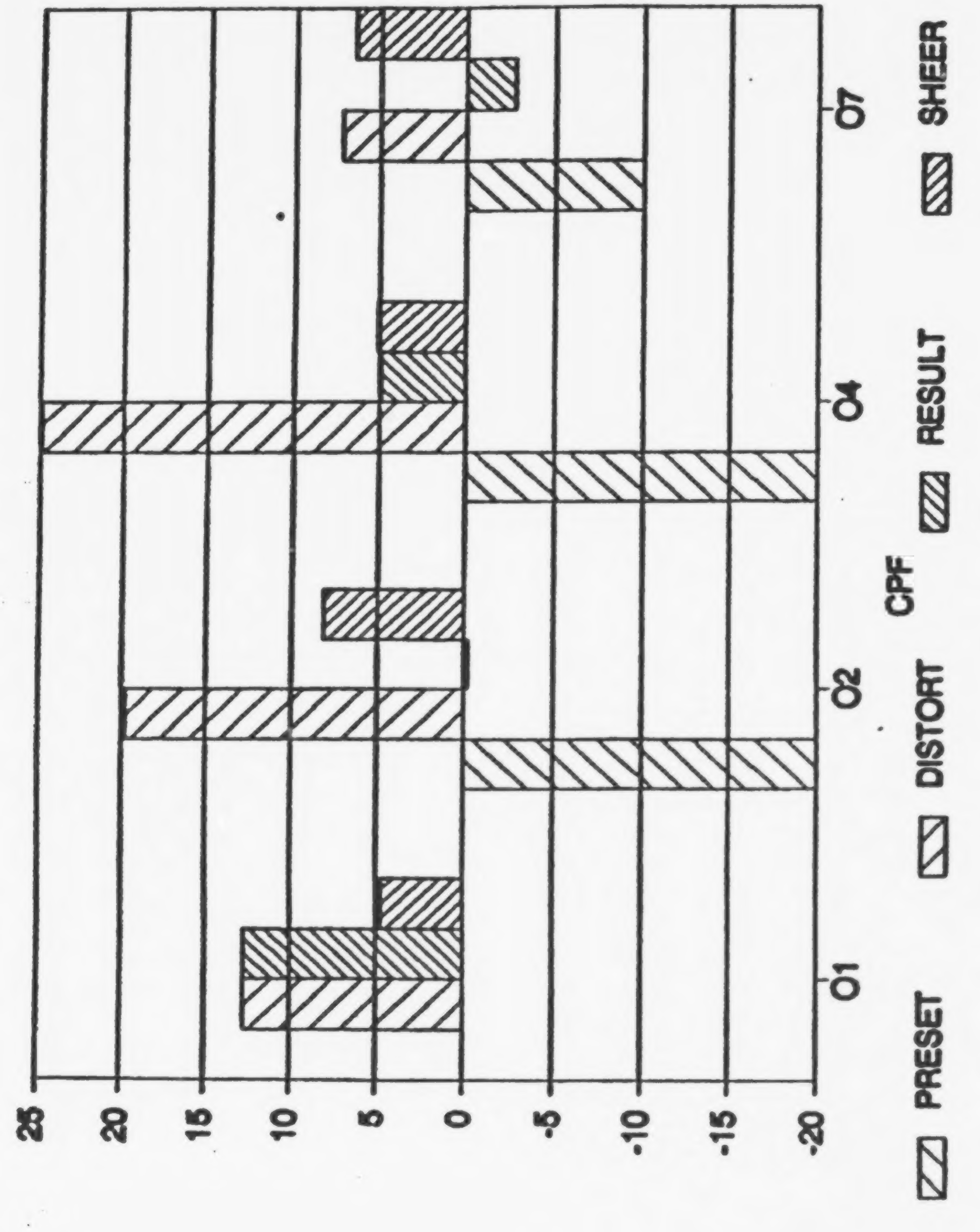
25
20
15
10
5
0
-5
-10
-15
-20
O1
O2
O4
O7
CPF
PRESET
DISTORT
RESULT
SHEER

Exhibit 17: CPF - 04 UNIT 2110 CAMBER

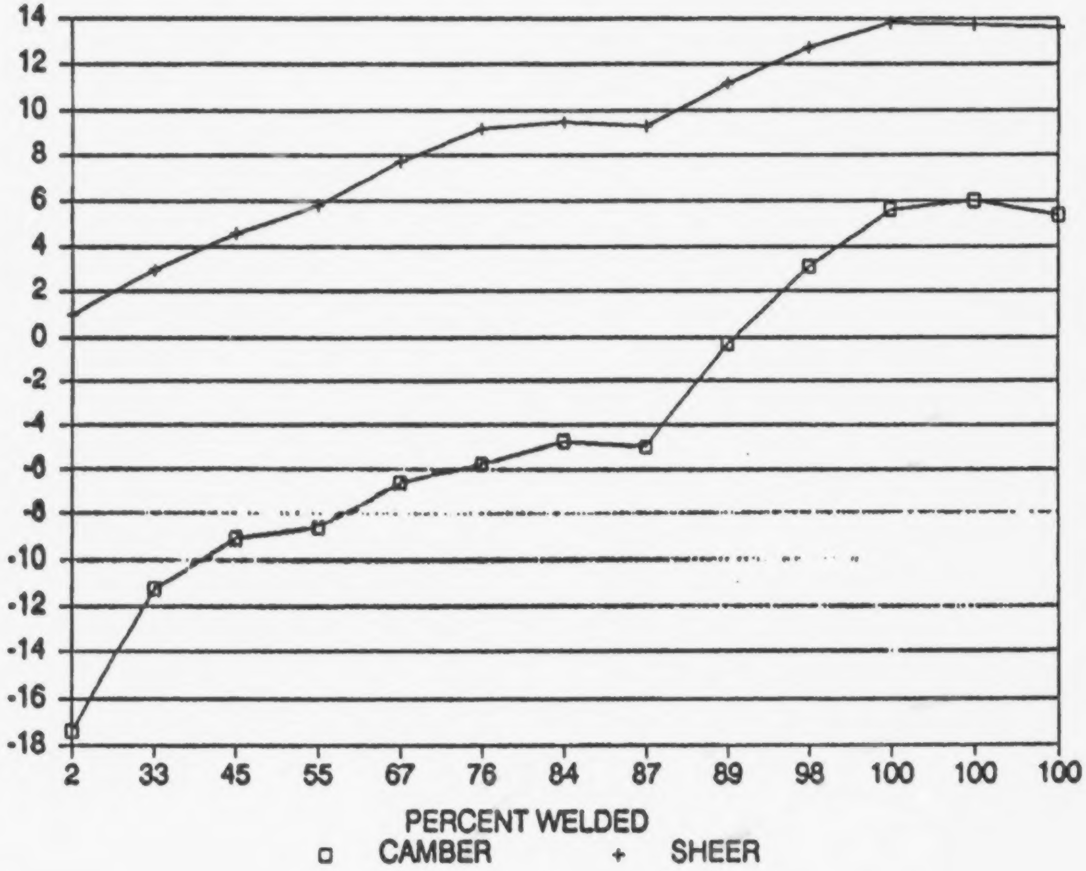

Exhibit 18: CPF - 04 UNIT 2110 -- Distortion

ALIGNMENT OF STRUCTURE

REQUIREMENTS FOR MAINTENANCE OF ALIGNMENT

MINIMIZE PLATE TUCKING

MINIMIZE FAIRING OR FRAMES/BARS AT UNIT JOINS

APPENDIX "A"

Test Panel #1
November 1990

Attachment to
AC Report
Nov. 23/90

Thin Plate Welding Distortion Test

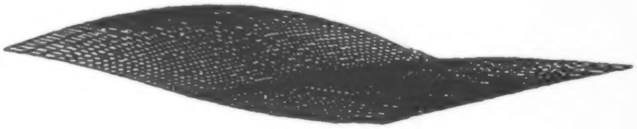

Butt Tacked

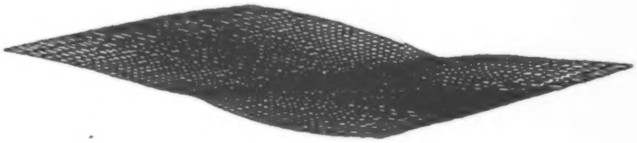

Butt Welded

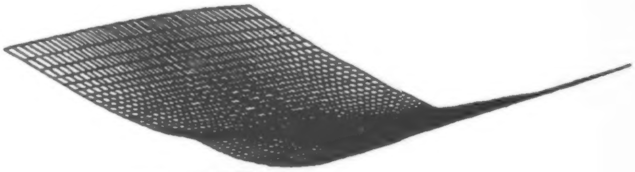

Bars Tacked

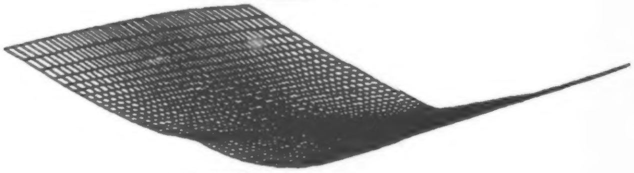

Bars Welded

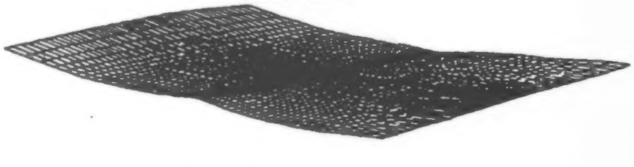

Tripping Brackets Tacked

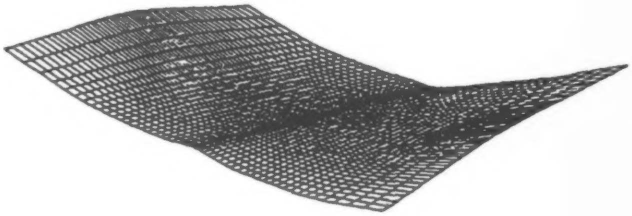

Tripping Brackets Weled

Note: Deflections perpendicular to plane magnified by 5X

Accuracy Control

APPENDIX "A"

Test Panel #2
November 1990

Attachment to
AC Report
Nov. 23/90

Thin Plate Welding Distortion Test

Butt Tacked

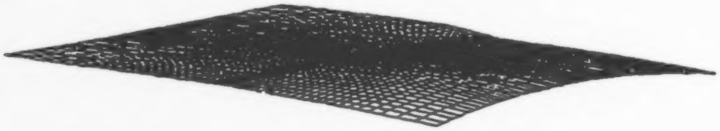

Butt Welded

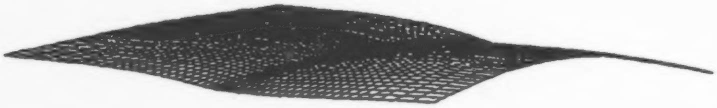

Bars Tacked

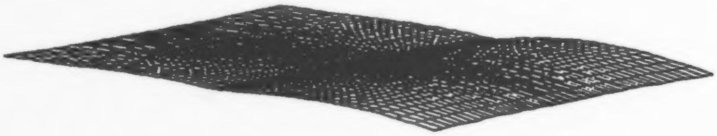

Bars Welded

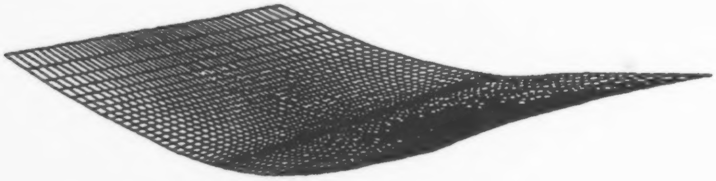

Tripping Brackets Tacked

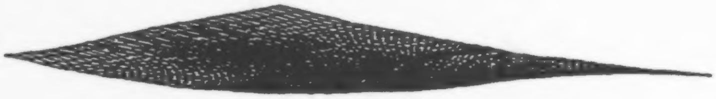

Tripping Brackets Weled

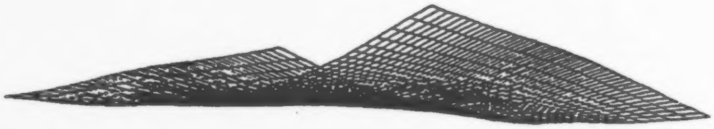

Note: Deflections perpendicular to plane magnified by 5X

Accuracy Control

APPENDIX "A"

Test Panel #3
November 1990

Attachment to
AC Report
Nov. 23/90

Thin Plate Welding Distortion Test

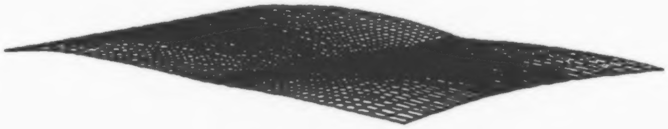

Butt Tacked

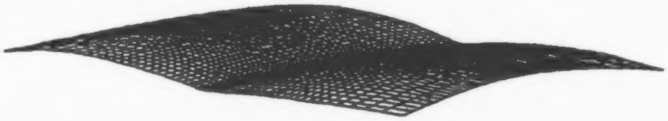

Butt Welded

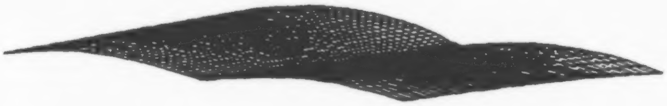

Bars Tacked

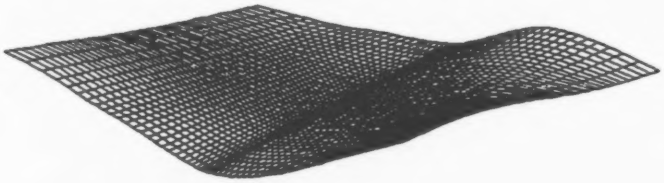

Bars Welded

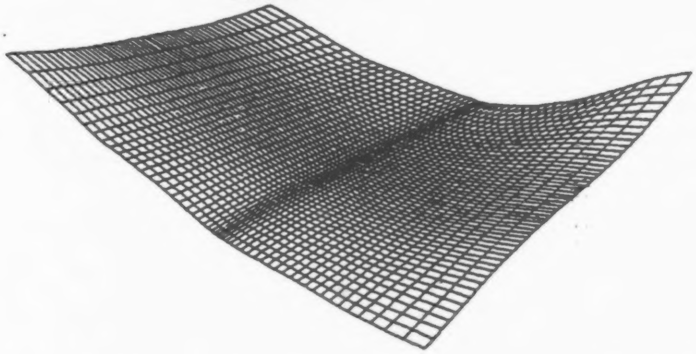

Tripping Brackets Weled

Note: Deflections perpendicular to plane magnified by 5X

Accuracy Control

APPENDIX "A"

Test Panel #4
November 1990

Attachment to
AC Report
Nov. 23/90

Thin Plate Welding Distortion Test

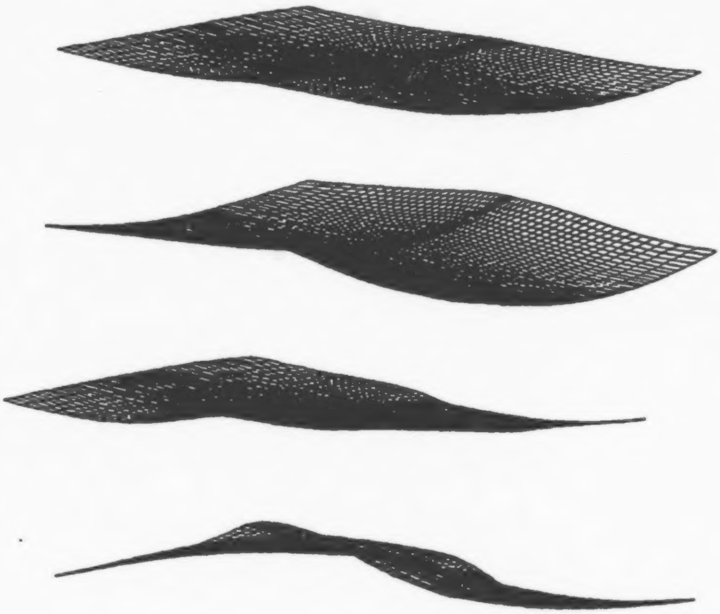
Butt Tacked
Butt Welded
Bars Tacked
Bars Welded

Note: Deflections perpendicular to plane magnified by 5X

Accuracy Control

WELDING PANEL TESTS - OCTOBER 1990

WELDING PARAMETERS

PANEL #1

	HEAT (J/mm)			SEQUENCE			RESTRAINT			FITUP		
CONDITION	SEAM	BARS	TRIPPING BRACKETS	SEAM	BARS	TRIPPING BRACKETS	SEAM	BARS	TRIPPING BRACKETS	SEAM	BARS	TRIPPING BRACKETS
FITTED	-	-	——	L-R	L-R	CL-OUT				1	0	0-2
WELDED	460	340		L-R	L-R	CL-OUT	NO	NO	——			

PANEL #2

	HEAT (J/mm)			SEQUENCE			RESTRAINT			FITUP		
CONDITION	SEAM	BARS	TRIPPING BRACKETS	SEAM	BARS	TRIPP	SEAM	BARS	TRIPPING BRACKETS	SEAM	BARS	TRIPPING BRACKETS
FITTED	-	-	——	L-R	L-R	CL-OUT				1	0	0-2
WELDED	400	340		L-R	L-R	CL-OUT	YES	YES	——			

PANEL #3

	HEAT (J/mm)			SEQUENCE			RESTRAINT			FITUP		
CONDITION	SEAM	BARS	TRIPPING BRACKETS	SEAM	BARS	TRIPPING BRACKETS	SEAM	BARS	TRIPPING BRACKETS	SEAM	BARS	TRIPPING BRACKETS
FITTED	-	-	——	L-R	L-R	CL-OUT				1	0	0-2
WELDED	320	620		L-R	L-R	CL-OUT	YES	YES	——			

PANEL #4

	HEAT (J/mm)			SEQUENCE			RESTRAINT			FITUP		
CONDITION	SEAM	BARS	TRIPPING BRACKETS	SEAM	BARS	TRIPPING BRACKETS	SEAM	BARS	TRIPPING BRACKETS	SEAM	BARS	TRIPPING BRACKETS
FITTED	-	-	——	CL-OUT	CL-OUT	CL-OUT				1	0	0-2
WELDED	687	711		CL-OUT	CL-OUT	CL-OUT	NO	NO	——			

WELDING PANEL TESTS - OCTOBER 1990
PANEL DEFLECTION (mm)

	AFTER SEAM WELDED			AFTER BARS WELDED			AFTER T/B WELDED	
	SEAM	BARS		SEAM	BARS		SEAM	BARS
PANEL #1	3.2	.73		2.1	0.4		1.05	0.8
	SEAM	BARS		SEAM	BARS		SEAM	BARS
PANEL #2	3.1	.81		1.5	0.6		1.5	1.1
	SEAM	BARS		SEAM	BARS		SEAM	BARS
PANEL #3	6.0	1.3		3.6	0.8		2.95	0.75
	SEAM	BARS		SEAM	BARS		SEAM	BARS
PANEL #4	3.8	.81		0.6	0.6		NA	NA

RATIO	CPF	TEST
PANEL BREADTH TO PLATE THICK	75	138
LENGTH TO BREADTH	1.7	4.5

ACCURACY CONTROL CHECK SHEET AC 38

PAGE 3 OF 9

CONDITION REPORT

HULL NO: 1222 | UNIT NO: 1150 | ITEM: Deck # 1 (HEIGHTS)

STATUS: Before erection

DATE: Feb 22 '88

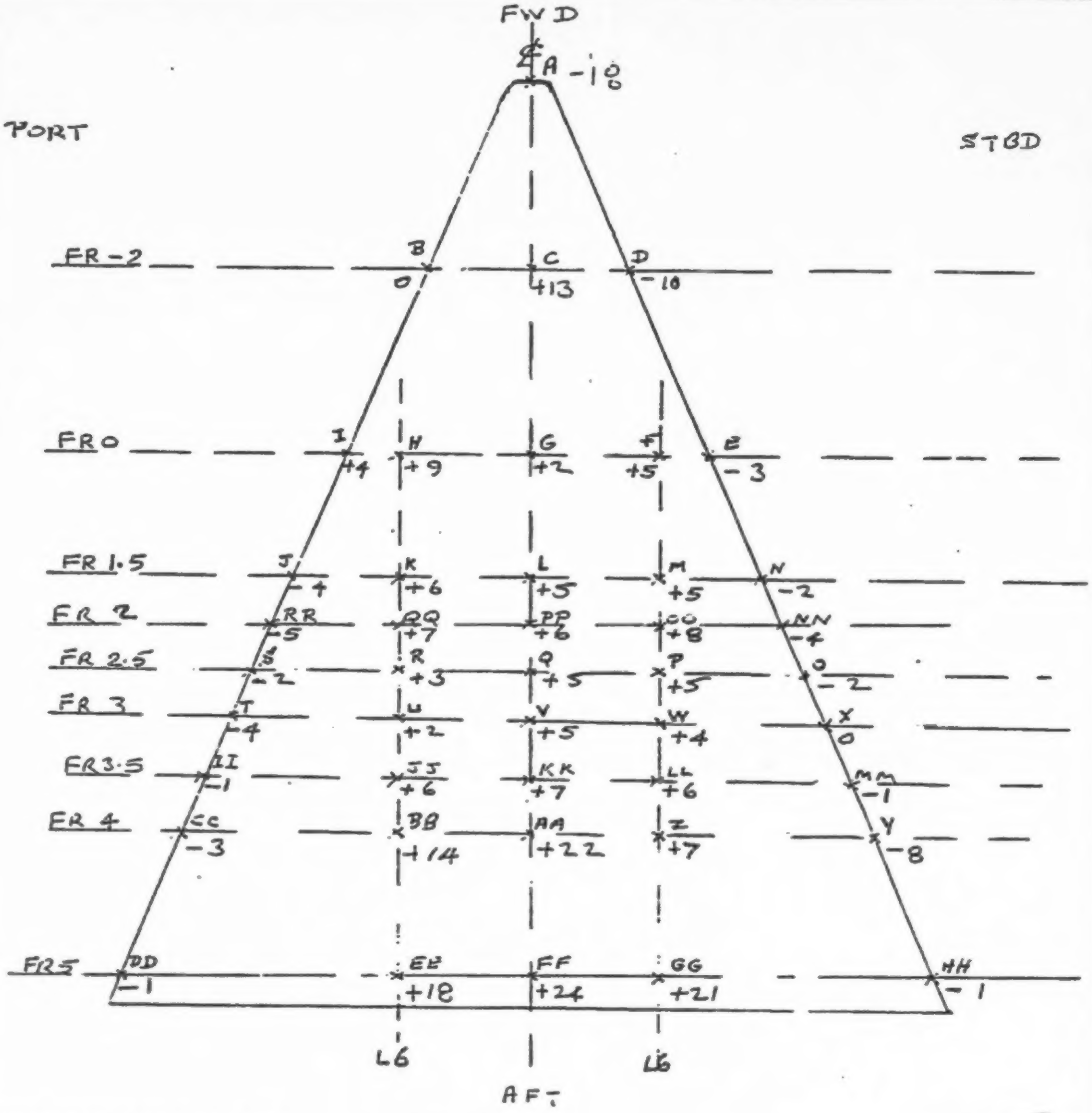
FWD
℄
A -10
PORT
STBD
FR -2
B 0
C +13
D -10
FR 0
I +4
H +9
G +2
F +5
E -3
FR 1.5
J -4
K +6
L +5
M +5
N -2
FR 2
RR -5
QQ +7
PP +6
OO +8
NN -4
FR 2.5
S -2
R +3
Q +5
P +5
O -2
FR 3
T -4
U +2
V +5
W +4
X 0
FR 3.5
II -1
JJ +6
KK +7
LL +6
MM -1
FR 4
CC -3
BB +14
AA +22
Z +7
Y -8
FR 5
DD -1
EE +18
FF +24
GG +21
HH -1
L6
L6
AFT

SURVEYOR: H. Payne R. Cassidy

REMARKS: 1) Deviations are from design

ACCURACY CONTROL AC36 PAGE __ OF __

CONDITION REPORT

HULL NO: *2262*	UNIT NO: *1150*	ITEM: *DECK #1*
STATUS: *As built prior to Blast & Paint*		DATE: *01 November 1994*

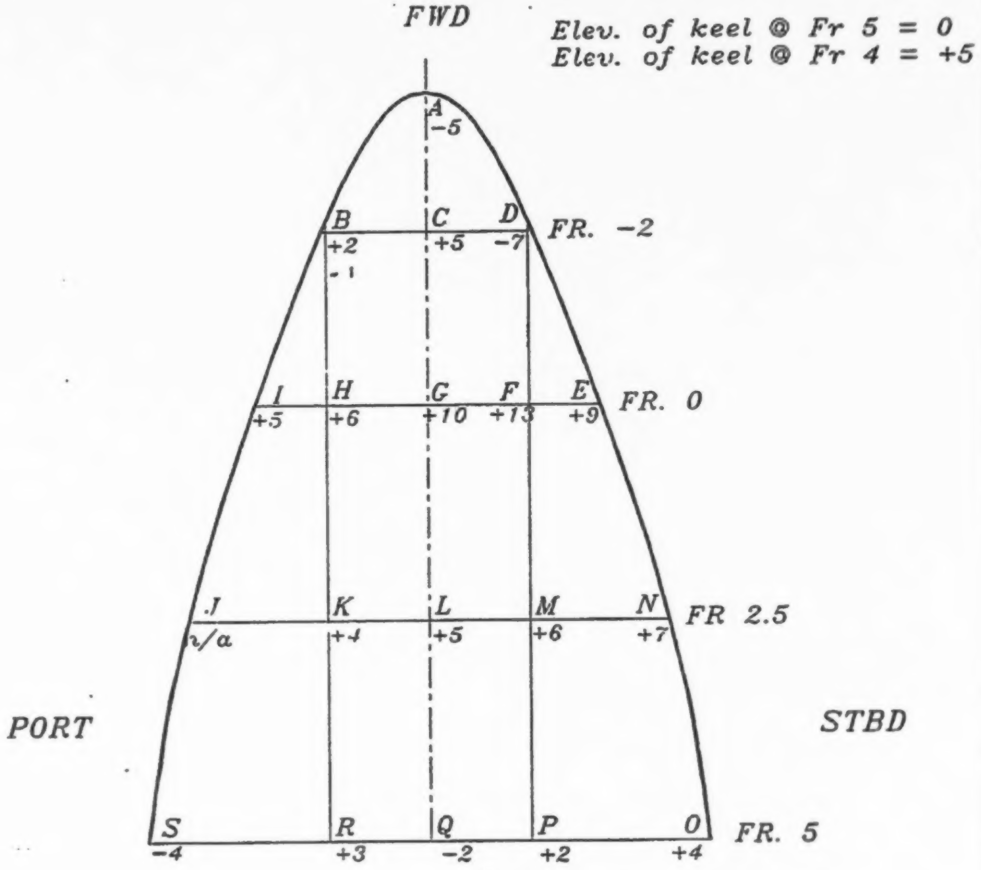
FWD
A
-5
B
+2
-1
C
+5
D
-7
FR. -2
I
+5
H
+6
G
+10
F
+13
E
+9
FR. 0
J
n/a
K
+4
L
+5
M
+6
N
+7
FR 2.5
PORT
STBD
S
-4
R
+3
Q
-2
P
+2
O
+4
FR. 5

Elev. of keel @ Fr 5 = 0
Elev. of keel @ Fr 4 = +5

PLAN VIEW DECK 1

SURVEYOR: *R. Cassidy, H. Payne*

REMARKS:
1. *DEVIATIONS ARE FROM DESIGN*
2. *U/S Keel @ Fr 5 held as design*
3. *TARGET ELEVATION = +9*

FILE NAME: MM1DECK1.DWG

SAINT JOHN SHIPBUILDING LTD. ACCURACY CONTROL

MEGA MODULE ERECTION PACKAGE

HULL: 2232

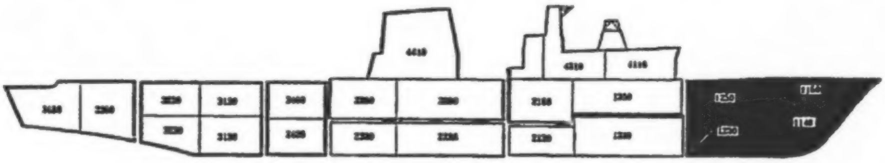

MEGA MODULE #1

3/16

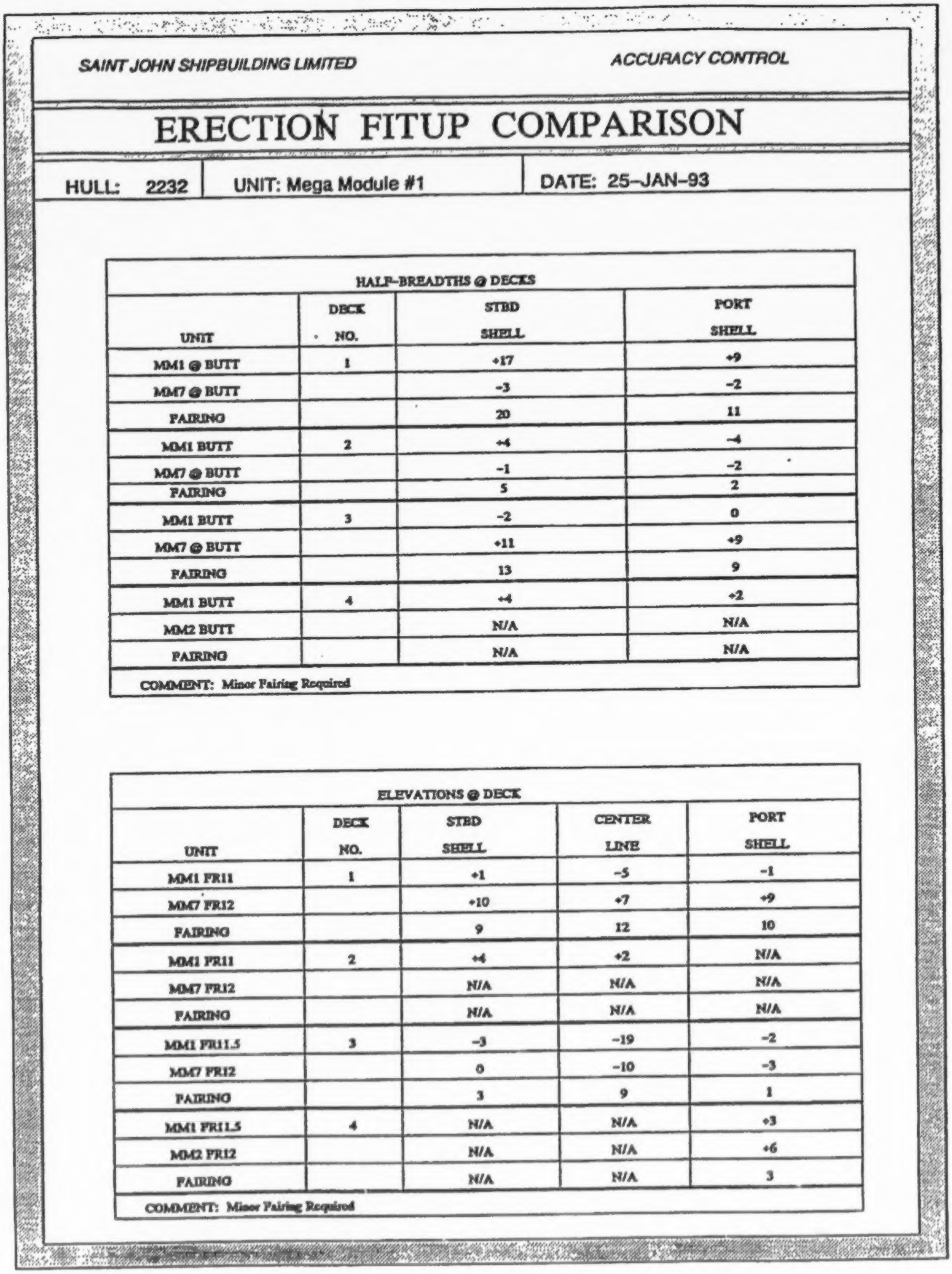

SAINT JOHN SHIPBUILDING LIMITED

ACCURACY CONTROL

ERECTION FITUP COMPARISON

HULL: 2232 | UNIT: Mega Module #1 | DATE: 25-JAN-93

HALF-BREADTHS @ DECKS

UNIT	DECK NO.	STBD SHELL	PORT SHELL
MM1 @ BUTT	1	+17	+9
MM7 @ BUTT		-3	-2
FAIRING		20	11
MM1 BUTT	2	+4	-4
MM7 @ BUTT		-1	-2
FAIRING		5	2
MM1 BUTT	3	-2	0
MM7 @ BUTT		+11	+9
FAIRING		13	9
MM1 BUTT	4	+4	+2
MM2 BUTT		N/A	N/A
FAIRING		N/A	N/A

COMMENT: Minor Fairing Required

ELEVATIONS @ DECK

UNIT	DECK NO.	STBD SHELL	CENTER LINE	PORT SHELL
MM1 FR11	1	+1	-5	-1
MM7 FR12		+10	+7	+9
FAIRING		9	12	10
MM1 FR11	2	+4	+2	N/A
MM7 FR12		N/A	N/A	N/A
FAIRING		N/A	N/A	N/A
MM1 FR11.5	3	-3	-19	-2
MM7 FR12		0	-10	-3
FAIRING		3	9	1
MM1 FR11.5	4	N/A	N/A	+3
MM2 FR12		N/A	N/A	+6
FAIRING		N/A	N/A	3

COMMENT: Minor Fairing Required

#510373

Fatigue Crack Initiation Prediction for Naval Platform Weldments

by

John F. Porter* and Richard Yee**

* Defence Research Establishment Atlantic, Dockyard Lab,
FMO Halifax, Halifax, Nova Scotia, Canada, B3K 2X0

** Fleet Technology Limited, Kanata, Ontario, Canada, K2K 1Z8

ABSTRACT

While fatigue in metals has been extensively studied for over 150 years, fatigue crack initiation and propagation in marine platforms remains one of the most common and serious challenges facing the maintainers and operators of these structures. An inability to satisfactorily quantify all of the factors which contribute to the formation of cracks has led to the creation of design methods for fatigue avoidance which are conservative in many situations and inaccurate in others. This paper reviews the current popular fatigue control methodologies and outlines recent experimental efforts to better understand the role of residential strain on the formation of fatigue cracks in complex welded joints. The fatigue control methodologies have been applied to the experimental weld joint configurations to predict initiation lives for comparison with the experimental results.

INTRODUCTION

Fatigue cracking of naval platforms remains one of the more common challenges facing the maintainers of these structures. While numerous tankers and bulk carriers have been lost or severely damaged due to the extension of fatigue cracking to the point where fracture has occurred, naval platforms are generally much more robust, use higher notch toughness materials and have considerably more redundant structural features. Consequently, catastrophic fracture originating from a fatigue crack is a very rare occurrence in naval platforms. Nevertheless, the repair of fatigue cracking represents a significant percentage of a naval platform's lifetime maintenance costs and with shrinking maintenance budgets, fatigue crack avoidance remains a priority. In addition, as modern navies reduce the number of their platforms, potential restrictions in the availability of these platforms due to cracking repair requirements becomes a serious consideration.

The degree to which fatigue poses problems in naval platforms varies significantly from one class of vessel to another and is dependent on many factors. A recent survey of defect identification in Royal Navy warships [1] indicated that, spanning a six year period, fatigue cracking accounted for 55% and 76% of the total defects requiring repairs in Leander class frigates and Type 42 class destroyers, respectively. In contrast, a study on Canadian Iroquois class destroyers entering TRUMP refits concluded that cracking accounted for only 10% of the total defects encountered.

Fatigue cracking in naval platforms can be divided into two categories. The first category is made up of those cracking incidents which are a direct result of poor fabrication practice. These cracks initiate from welds with very sharp root radii, unground flame cut edges, undetected weld defects or other situations where unusually high stress concentration factors exist. Usually these regions of the magnified stress are localised and these cracks often arrest when the crack tips enter the lower nominal stress state regions. Another characteristic of this category of cracking is that they do not constitute a class problem. That is they do not necessarily occur at similar locations on vessels of the same design. Their occurrence is random and can not be predicted during the design process. Repair of these cracks involves rewelding and recracking rarely occurs. Stringent application of weld inspection guidelines during fabrication have a direct beneficial influence on the total number of cracking incidents during a vessel's lifetime.

The second category of fatigue cracking can be defined as those which occur as a result of insufficient fatigue resistance through inadequate design. Empirical design practices, based on experience, often resulted in robust structures with high hidden factors of safety which compensated for the lack of understanding in design against fatigue. Pressure to reduce weight and cost through the use of higher strength steels and the use of numerical methods to optimise design have reduced or eliminated the hidden safety factors and thus increased the requirement to better understand the factors which influence crack initiation. Cracking resulting from a flawed design is a vessel class problem and often requires structural modification to prevent recracking.

These cracks are considered more serious as the potential to adversely effect structural integrity is higher.

One significant unknown in the prediction of fatigue crack initiation in naval platforms is the role played by residential strain states. The term residential strain is defined as the aggregate of those strains which are present in the structure in the absence of external loading. In a naval platform these strains include a residual strain component as a result of coldworking, machining or welding, a restraint strain component as a result of joining ship sections or flame straightening of deck plates, and a stillwater strain component present due to the weight of the platform. One obvious manner in which these strains modify fatigue damage accumulation is through mean strain effects during cyclic loading.

Welding residual strains are present in all welded joints as a result of nonuniform cooling of the weld metal and surrounding parent metal. Heat input, sequencing, constraint, number of weld passes, yield properties of the materials, cooling rates, and occurrence of phase transformations are only a few of the factors which play a strong role in defining a resultant welding residual strain field. There are no clear guidelines which permit the accurate prediction of these strain fields. As a consequence tensile yield level strains are often assumed to be present at the weld center. Restraint or assembly strains are due to the joining of plates or sections which do not fit precisely together. Geometric mismatches and eccentricities combine to generate far reaching restraint strains as plates or sections are forced into place. These strains are significant in that their influence extends over a much larger region than the more localised welding residual strains. Also these strains are uniform through the plate thickness. Due to difficulties in experimentally quantifying these strains, very little information is available on typical restraint strains in marine platforms. It was observed in a study, conducted in 1946 on a Destroyer Escort [2] that restraint strains varied from approximately a third of the yield strength of the steel in tension to a third of the yield strength of the steel in compression, depending on the sequence of the subassembly joining. In a more recent study on a modular constructed B.C. ferry [3], the long range assembly strains exceeded three quarters of the yield strength of the material in tension in some locations.

Difficulties in accurately determining structural residential strain states, conflicting experimental conclusions, and an inability to discern the effects of the various components of residential strain on the various stages of fatigue life have combined to produce a less than clear understanding of the manner in which these strains impact upon fatigue. While a great deal has been written on the effects of residential strain on fatigue, the vast majority of this literature has been devoted to small laboratory specimen responses. A current theoretical summation of residential strain influences on fatigue can be found in Reference 4.

Research efforts conducted by the Dockyard Laboratory of the Defence Research Establishment Atlantic (DREA) have concluded that a portable system based on x-ray diffraction techniques is the best manner to obtain in-service measurements of residential strains in naval platforms. As such, the development of a Miniature X-Ray Diffractometer (MXRD) has been pursued. It is envisioned that this device could be used to measure total strains (applied strains and residential strains) at critical locations in naval platforms and that the results of these surveys could serve as primary inputs for fatigue crack initiation assessments.

In an effort to determine the feasibility of applying diffraction data to enhance fatigue damage assessments in complex welded joints, a series of welded specimens were fabricated, instrumented, inspected via diffraction methods and cyclically loaded to failure. This paper briefly reviews key aspects of current fatigue control methodologies and outlines the results of these experimental efforts.

CURRENT FATIGUE CONTROL METHODOLOGIES

A number of different approaches have been developed to attempt to quantify the effects of cyclic loading on the fatigue response of marine structures. Total fatigue life (N_T) is defined as the sum of the initiation and early growth phase (N_I), and the macroscopic crack propagation phase (N_P) until final fracture. The stress-life (S-N) design curve approach, the hot spot strain approach and/or the local notch tip strain (strain-life) approach may be applied during design to ensure that the material, geometry and loading influences combined do not lead to fatigue crack initiation and significant propagation during the expected life of the structure. These methods are reviewed in Reference 4.

S-N Approach

The stress-life (S-N) or nominal stress approach to assessing joint configurations in marine platforms remains the most universally accepted methodology for fatigue crack initiation avoidance. Based on S-N (alternating stress versus cycles to failure or crack initiation) curves for specific welded joint geometries, this method has proved effective in predicting fatigue where cycles to failure are very high and the plastic component of the cyclic strain is very low. The generation of extensive sets of experimentally derived S-N curves for welded joints has led to the creation of sets of standard fatigue design curves such as provided in BS 5400 Part 10 [5], which have been adopted for use in naval structures. Potential crack initiation sites in basic welded details are classified into eight categories. The fatigue curves can be defined by

$$N_f = A\,(\Delta\sigma)^{-b}$$

where N_f is the number of cycles to failure,
$\Delta\sigma$ is the local nominal stress range,
and A and b are constants for each of the eight design detail classes.

The constants were derived assuming that the stress ranges in the welded joints are entirely tensile with a minimum stress of zero (R=0). The nominal axial stress range employed excludes stress concentration effects that are already built into the S-N design curves (i.e. due to misalignments, weld toes, weld reinforcements). Welded joints in naval platforms are usually embedded in global stress concentration regions of complex structural detail. These global stress concentrations must be explicitly included in the local nominal stress range. Therefore, the relevant local nominal stress range for a given crack initiation site is not equal to the stress range defined by simple ship bending theory. Unfortunately, there is no generally accepted method to separate stress concentration effects that are implicitly accounted for in the S-N curves from the complex structural detail's global stress concentration effects, when analyzing finite element or strain gauge data. Load spectrum of different stress ranges can be accounted for using a linear cumulative fatigue damage theory such as the Palmgren-Miner rule. If the summation of the various damage ratios associated with each segment of the lifetime load spectrum is less than 1, it is concluded that fatigue cracking will not initiate.

In recent years a number of sophisticated variations of the S-N theme have been proposed. The primary common features include (1) the use of actual observed or realistic wave data spectra, (2) the use of empirical, experimental or numerically (global finite element analysis) derived transfer functions to relate a unit amplitude wave to the cyclic stress range at the location of interest, (3) derivation of the cyclic stress spectrum, (4) calculation of fatigue damage ratios (using the BS5400 classification constants) for each response spectrum and (5) summation to calculate the total fatigue damage ratio [6-10]. Despite these advances, there remain several concerns with the application of the (S-N) design curve approach to complex welded structures such as naval platforms. The value of N or fatigue life associated with these curves corresponds to the number of cycles to failure at a particular cyclic load level. (failure is usually defined as the point at which a crack initiates, grows through the plate thickness and extends several centimeters along the surface). The method assumes that stress concentration effects and welding residual strains are incorporated within the relevant design curves, are similar for all joints of the same geometry and are reflected by the responses of the laboratory samples employed to generate the curves. Variations in the weldment residual strains and stress concentration factors due to the use of different materials and welding processes are not accounted for with this approach. Similarly, the effects of the other components of the residential strains (restraint strains, stillwater strains, etc.), built in during fabrication are not simulated or accounted for in subsequent analysis. The residential strain states and the other non-wave induced cyclic loading influence the stress ratio R ($\sigma_{min} / \sigma_{max}$), which in turn influence fatigue life prior to initiation. Also, inelastic behaviour at stress risers or notches is not adequately handled. High residential strains may interact with applied strains at locations with high stress concentration factors leading to localised plasticity and strain field modifications.

Several other concerns with the use of S-N design curves include the multi-axial nature of the strain fields in complex naval platform structural members, difficulties in the correct selection of the appropriate curve for complex weld joints, the effect of a corrosive sea water environment on fatigue life, the application of damage accumulation rules which do not account for load sequencing influences and are strain amplitude independent, the effects of material tensile strength on fatigue life, and size effects associated with the use of thin plates on naval platforms.

Hot Spot Stress Approach

The hot spot stress approach differs from the previous method in that crack initiation life is predicted using a stress range estimate at the point of initiation and one nominal S-N design curve. In this approach, the global geometric stress concentration factor effects are accounted for, however, the localised stress concentrations due to the weld itself (defined by the weld shape, toe angle, etc.) are ignored. This is because these effects are incorporated in the hot spot fatigue design curves. Different approaches have been developed for calculating hot spot stresses; by finite element analysis using shell elements or by extrapolating stresses obtained from strain gages, mounted outside the influence of the weld toe or reinforcement yet within the region affected by the global stress concentrations. The recommended distance from the weld toe to the closest strain gage location ranges from 0.4t to t, where t is the wall thickness. One of the difficulties associated with this method is the inconsistent definition of the position of the reference stress locations. In complex structural details, with very high stress gradients, the resultant hot spot stresses will be sensitive to the placement and length of the strain gages or to the mesh sizes employed in a finite element analysis. While this approach removes the complication of multiple S-N curves and the difficulties in assessing the correct joint classification, many of the afore mentioned concerns associated with the nominal S-N approach remain.

Local Notch Tip Strain

In recent years, there has been considerable interest in the use of fracture mechanics models to predict total fatigue life of welded joints, based on the assumption that crack-like defects are invariably present along weld toes. It is now recognized that crack initiation in sound welds can form a significant fraction of the total fatigue life. Because cyclic plasticity does occur along weld toes even in the high cycle regime (due to the presence of high tensile residential strains and high stress concentration factors), the classical Wohler S-N curve approach is not applicable for predicting crack initiation along weld toes. It is for this reason that attempts have been made to apply the local strain approach to welded joints. The major advantage of this method is that once the total strain range at the potential crack initiation site has been defined (numerically or experimentally), fatigue resistance assessments can be based on comparisons with joint geometry independent material strain versus N curves.

For the case of high cycle fatigue (low strain amplitudes and minimal plastic strain) the relationship between strain and number of cycles to initiation (N_I) is [4];

$$\Delta\varepsilon/2 = \sigma'_f (2N_I)^b \;/\, E$$

where σ'_f is the fatigue strength coefficient,
b is the fatigue strength exponent,
and E is Young's modulus.

The expression can be expanded to include plasticity effects in low cycle fatigue. It has been shown that residential strains do not significantly directly affect fatigue life in the low cycle regime. However for high cycle fatigue, the above equation can be modified to account for the shift in mean stress as a result of residential strains (stresses);

$$\Delta\varepsilon/2 = (\sigma_f - \sigma_m)(2N_I)^b \;/\, E$$

where σ_m is the mean or average stress modified by residential stresses. A more detailed explanation of the application of this approach to weldment details, while incorporating residential strain effects, is presented in Reference 4.

General acceptance of the local strain approach for welded joints has been hindered by several factors. Crack size corresponding to a predicted crack initiation life must be clearly defined so that the local strain approach can be properly interfaced with linear elastic fracture mechanics models for crack propagation. Since this crack size increases with increasing notch size and increasing severity of any crack-like defects along weld toes, it must be calibrated for different combinations of welding procedures, welding consumables, and base metals. Stable and transient mean stresses can significantly influence fatigue crack initiation at a notch root, and various corrections for mean stress effects in steels and aluminum alloys have been developed for the local strain approach [11,12]. It has been assumed in applications of the local strain approach to welded joints, that the local weld toe stresses cycle down from yield strength levels due to the presence of high tensile welding residual stresses. Fatigue testing results indicate that this assumption is reasonable for simple welded joints subjected to constant amplitude loading; however, there is little experimental data on the magnitude of short-term and long-term residential strains in naval platforms.

FATIGUE ASSESSMENT OF STIFFENED BEAMS

The experimental program employed to illustrate the application of the current fatigue design philosophies involved the fabrication, instrumentation and constant amplitude cyclic loading of six welded I-beams with a welded longitudinal attachment. Direct current potential drop techniques were employed to detect fatigue crack initiation in each specimen. X-ray diffraction techniques were employed to measure the initial residential strains at the anticipated crack initiation sites in each specimen and the total strains at the sites (with and without an applied load) following shake-down of the specimens. Strain gauges were also used to estimate the nominal stress ranges and hot spot stress ranges at the initiation sites in each test specimen. The combined experimental results were analyzed and used with the relevant S-N curves to predict the fatigue crack initiation lives. In addition, the local strain approach was used to predict the crack initiation life of each test specimen. The cyclic material data for the local strain analyses was gathered with small scale fatigue specimens.

Experimental Procedure

The test specimens (Figure 1) were fabricated from 2.54 cm thick CSA G40.21 350 WT steel plates. The fillet welds in these specimens were produced by a shielded metal arc welding process with E7018 electrodes. The most fatigue-prone areas in each specimen were the fillet welds at the ends of the longitudinal attachment (category F2 details according to BS 5400). The fillet weld at one end of the attachment was ground and hammer-peened so that fatigue cracks would only initiate at the opposing end.

Before the specimens were tested, x-ray diffraction measurements of initial residential strains were made at three locations along the weld toe at the unground end of each specimen's longitudinal attachment (at the longitudinal centre line and 5 mm to either side of the centre line). Additional measurements of the total (residential and applied) longitudinal strains at the unground end of each specimen's longitudinal attachment were taken after the first 10 loading cycles. These measurements were taken under mean, minimum, and maximum loads at three locations along the longitudinal centre line (at the unground weld toe, 1 mm from the weld toe, and 2 mm from the weld toe).

The top flange of each specimen was instrumented with five strain gauge rosettes, mounted along the longitudinal centre line at the locations shown in Figure 2. The first three rosettes were located in accordance with the IIW's recommended procedure for estimating hot spot stresses [3] and were used to estimate the hot spot stresses after the first 5 to 10 loading cycles. The other two rosettes were located outside the stress concentration region of the longitudinal attachment and were used to calibrate the applied loads against the nominal bending stresses in the outer fibre of the top flange.

The specimens were tested under constant amplitude cyclic loading in the servo-hydraulic test rig shown in Figure 3. All the specimens were tested under four-point bending at a nominal stress range of 100 MPa between the inner loading points. Three specimens (#1, #3, and #5) were tested at a mean stress of 0 MPa between the inner supports ($R = -1$), while the remaining specimens (#2, #4, and #6) were tested at a mean stress of 50 MPa between the inner supports ($R = 0$).

A local direct current drop potential system was used to detect fatigue crack initiation along the weld toe at the unground end of the longitudinal attachment in each specimen. Three active potential drop probes were spot-welded along the weld toe and a reference probe was spot-welded a few centimeters back from the weld toe as shown in Figure 4. Three readings were taken from each probe every 20,000 to 50,000 cycles. These readings were taken while the nominal bending stress in the outer fibre of the top flange was maintained at its maximum tensile test value. The average of the three readings from each active probe were normalized with respect to the average of the three readings from the reference probe to compensate for temperature and current fluctuations. The initiation and subsequent growth of a fatigue crack along the weld toe was indicated by monotonically increasing normalized potential drop readings from active probes straddling the crack plane. In order to assess the crack detection capability of the potential drop system, blue machinist ink was sprayed along the unground weld toe once the normalized potential drop readings from any active probe consistently exceeded its initial value by more than 1% to 2%.

Subsequent crack shape development was tracked by producing two to four beachmarks on crack surfaces before the end of each test. These beachmarks were produced by elevating the minimum nominal bending stress in the outer fibre of the top flange between the inner loading points to the mean bending stress in this region for 10,000 to 50,000 load cycles.

Experimental Results

The initial residential strains as measured with x-ray diffraction, along the unground weld toes of the welded beams before shake-down, are plotted in Figure 5. In most cases, the strains decreased along the weld toe at a rate of 55 to 185 microstrain/mm. Seventeen of the eighteen measurements were tensile. The most tensile measurement was 1350 microstrain, while the lone compressive measurement was -620 microstrain. The corresponding stresses derived with Hooke's Law for plane stress conditions were 280 MPa and -130 MPa, respectively.

Total strains (residential and applied) were measured with x-ray diffraction techniques along the longitudinal centreline of the welded beams after shake-down. Figure 6 shows the weld toe region total strain states as a function of the applied bending for specimen #3. Without any applied loading, the recorded strains were compressive in each sample. The weld toe region surface residential strains were probably modified by the light grinding and polishing conducted to mount the strain gauges (these surface preparations were conducted after the initial residential strain measurements). In all but one case, the weld toe strain ranges, measured at minimum and maximum applied loading, were 760 +/- 30 microstrain. The strain range at the weld toe in the remaining beam was 935 microstrain.

The fatigue testing of specimens #2 and #6 was terminated before any fatigue cracks were detected by the potential drop crack monitoring system. Specimen #6 was overloaded after 438,000 load cycles, while specimen #2 was recorded as a run-out after 4,390,850 load cycles. The four remaining specimens initiated and propagated similar fatigue cracking (Figure 7). In each case, microscopic fatigue cracks initiated along the instrumented weld toes and coalesced into a single macroscopic surface crack, which propagated through the thickness of the top flanges and into the webs before reaching the edges of the flange. Once the through-thickness cracking reached the edges of the flanges, it propagated rapidly through the webs. Each test was stopped before the crack tip reached the bottom flange due to excessive specimen deflection.

The stability of the normalized potential drop readings was such that fatigue crack initiation could be detected once the readings increased monotonically above 1.005. The crack depth at this detection level was less than 1.3 mm and possibly as small as 0.3 mm according to ink stains on the crack surfaces of the specimens. Table 1 summarizes the number of load cycles at which fatigue cracks were first detected. These crack detection lives (N_D) fall within a narrow range and are 11% to 20% of the corresponding total fatigue lives (N_T). Figure 8 is a plot of a/T versus N/N_T for the beams, where a is the maximum crack depth as indicated by the ink stains and beachmarks, T is the thickness of the top flange, N is the number of load cycles at the associated crack depth, and N_T is the number of load cycles to failure. This figure shows that 20% to 30% of the total fatigue life was spent in initiation and propagation of a crack to a depth of .1T (1.5 mm). Approximately 60% of the total fatigue lives of specimens #1, #3, and #5 was spent in initiation and propagation of a crack to a depth of .7T (9 mm). Similarly, approximately 70% of the fatigue life of specimen #4 was spent developing a crack to a depth of .6T (7.5 mm).

Table 1: Crack Detection Lives (N_D).

Specimen	$\Delta\sigma_o$ (MPa)	mean $\Delta\sigma_o$ (MPa)	N_D (cycles)	N_D/N_T
1	100	0	250,000	0.16
3	100	0	350,000	0.18
4	100	50	230,000	0.11
5	100	0	350,000	0.2

The total fatigue lives of the specimens are summarized in Table 2 and plotted in Figure 9 against the nominal bending stress range. Superimposed on this figure is the BS 5400 mean S-N curve for category F2 details and the corresponding 95% confidence limits. The fatigue lives of the specimens fall between the mean curve and the upper 95% confidence interval.

Table 2: Total Fatigue Lives (N_T).

Specimen	$\Delta\sigma_o$ (MPa)	mean $\Delta\sigma_o$ (MPa)	N_T (cycles)
1	100	0	1,570,950
3	100	0	1,914,900
4	100	50	2,132,340
5	100	0	1,755,870

The fatigue lives of these specimens are re-plotted in Figure 10 against the hot spot stress range. The hot spot stresses applied were estimated by quadratic extrapolation of the maximum principal stresses obtained from strain gauge rosette measurements. Superimposed on Figure 10 is the BS 5400 mean S-N curve for category E details and the 95% confidence limits. The ABS Guide for the Fatigue Strength Assessment of Tankers [10] has adopted the lower 95% confidence limit for category E details as the appropriate fatigue design curve for use with hot spot stress range.

LOCAL STRAIN ANALYSIS

Figure 11 is a micrograph of a longitudinal section through the crack initiation site in specimen #1 which shows that the fatigue cracking had initiated in the weld metal on a well defined weld toe radius (r). Specimen #3 had a similar crack initiation in the weld metal and a well defined toe radius. In contrast, there was no well-defined weld toe radius for specimens #4 and #5. For specimen #5, it was not clear whether the fatigue crack in this specimen initiated in the weld metal or heat affected zone. The elastic stress concentration factors (K_t) for the well-defined weld toe radii of specimens #1 and #3 were 2.49 and 2.27 respectively; as calculated from empirical relationships derived from finite element analysis.

The local stress ranges ($\Delta\sigma$) and local strain ranges ($\Delta\varepsilon$) at the crack initiation sites for specimens #1 and #3 were estimated by iteratively solving the cyclic form of Neuber's rule [14]

$$\Delta\sigma\Delta\varepsilon = (K_t\, \Delta S)^2 / E$$

where the elastic stress concentration factors were substituted for K_t, the hot spot stress ranges derived from strain gauge measurements were substituted for ΔS, and $\Delta\sigma$ was related to by the cyclic stress-strain curve. The estimated local strain ranges were then used in conjunction with the Smith-Topper-Watson equation [15]

$$\sigma_{max}\, \Delta\varepsilon/2 = \sigma_f^2 N^{2b}/E + \Delta\sigma_f \varepsilon_f N^{b+c}$$

to predict fatigue crack initiation lives for different maximum local stresses (σ_{max}), where σ_f, ε_f, b and c are material constants for the weld metal's strain-life curve [16].

Elastic stress concentration factors could not be calculated for specimens #4 or #5 as the local weld toe was sharp without a well-defined radius. The local strain and stress ranges at the crack initiation sites of these specimens was estimated by Lawrence's worst-case notch approach [17], whereby K_t in Neuber's rule was replaced by the highest possible value of Peterson's fatigue notch factor for steels [18];

$$K_f = 1 + (K_t - 1)/(1 + a/r)$$

$$a = .025\ (2068/UTS)^{1.8}$$

This worst-case value corresponded to a notch radius **r** equal to a. Table 3 summarizes the worst-case fatigue notch factors (K_f^{max}) and the corresponding critical weld toe radii (r_{crit}) that were calculated for specimens #4 and #5 from ultimate tensile strength (UTS) values estimated from hardness measurements at the crack initiation sites.

Table 3: Worst-Case Fatigue Notch Factors

Specimen	r_{crit} (mm)	K_f^{max}
4	0.17	3.13
5	0.18	3.1

The predicted values of local stress and strain ranges at the crack initiation sites of Specimens #1, #3, #4, and #5 are summarized in Table 4.

Table 4: Local Stress Range and Local Strain Range.

Specimen	Δε (μstrain)	Δσ (MPa)	R
1	2,234	522	-1
3	2,526	463	-1
4	3,042	615	0
5	2,654	547	-1

The corresponding crack initiation lives for various maximum local stresses are plotted in Figures 12 to 15. The calculated crack initiation lives decrease asymptotically with increasing magnitude of the assumed maximum local stress at the crack initiation site, and that these lives approached the experimental crack detection lives at maximum local stresses values of 368 MPa to 438 MPa (near the monotonic yield strength of the weld metal). This is consistent with the argument that the local stresses along a weld toe cycle down from yield strength levels following shake-down because of the initial presence of high tensile welding residual stresses.

DISCUSSION

The fatigue lives of the four successfully tested specimens fell between the BS 5400 F2 detail mean curve and the upper 95% confidence interval. This is consistent with the classification for fillet welds at the end of longitudinal attachments, assuming the presence of high tensile residual stresses along the weld toes (as assumed during the development of BS 5400's S-N design curves). It must be remembered that these laboratory experiments were similar to those conducted to generate the BS 5400 curves. Similarly, for the cyclic nominal stress ranges applied in these trials, the fatigue life limits corresponding to the lower and upper 95% confidence levels are approximately 400,000 and 2,500,000 cycles, respectively. With this broad a range and the scale of experiments conducted, it is not surprising that the fatigue lives of these samples fell within these bounds.

The total fatigue lives of the four specimens fall above the mean S-N curve for category E details, and the fatigue lives for three specimens fall above the upper 95% confidence limit. This indicates that the lower 95% confidence limit is an overly conservative design curve for the critical welded detail in these test specimens, when used in conjunction with hot spot stresses. This conservatism may be partially attributed to the fact that the hot spot stress range overestimates the driving force for crack growth through the thickness of the top flange and across the width of the top flange, particularly once the crack is longer than the thickness of the longitudinal attachment.

A portable x-ray diffraction system could be used to measure the residential strains at critical locations in a ship. The cyclic strain range at these notches could also be monitored. Unfortunately, this present study failed to conclusively demonstrate this capability. The compressive values of residential (zero applied load) strains that were derived from the post-shake-down x-ray diffraction measurements can be attributed to the surface preparation (light grinding and polishing) for the mounting of the strain gauges. The x-ray diffraction measured local cyclic strain ranges were similar for all samples, however they differed significantly from the predicted values of local strain range as shown in Table 5. The source of this discrepancy is as yet unclear and warrants further investigation.

Table 5: Predicted and Measured Local Strain Range.

Specimen	Δε (μstrain) Predicted	Δε (μstrain) X-ray
1	2,234	790
3	2,526	700
4	3,042	730
5	2,654	735

CONCLUSIONS

A brief review of the current state of fatigue crack initiation technology has been presented. The majority of cracks in naval platforms are the result of poor fabrication practice and are relatively insignificant from a structural reliability perspective. For those remaining cracking occurrences, determination of the total strain states at these locations enhances the ability to assess the problem.

Four welded I-beams with longitudinal stiffeners were successfully tested under constant amplitude cyclic loading. The weld toe at one end of each specimen's stiffener was ground and hammer peened so that fatigue cracks would only initiate along the weld toe at the opposing end. A direct current potential drop system was used to detect the initiation of these cracks. X-ray diffraction techniques were used to measure the initial residential strains at the anticipated crack initiation sites and the total cyclic strain ranges in each specimen. During cyclic loading, microscopic fatigue cracks initiated along the unground weld toe at the end of the longitudinal stiffener and coalesced into a single macroscopic surface crack. This crack propagated through the thickness of the top flange and into the web before reaching the edges of the flange.

Up to 30% of the total fatigue life of each failed specimen was spent in the initiation of a crack and the propagation of this crack to a maximum depth of 10% of the flange thickness (1.5 mm). Approximately 60% of the total fatigue lives of three of the four failed specimens was spent in the initiation of a fatigue crack and the propagation of this crack to a maximum depth of 70%

of the flange thickness (9 mm), and approximately 70% of the total fatigue life of the fourth failed specimen was spent in the initiation of a fatigue crack and the propagation of this crack to a maximum depth of 60% of the flange thickness (7.5 mm).

The total fatigue lives of all four specimens fell between BS 5400's mean S-N curve and its upper 95% confidence interval for category F2 details when plotted against the nominal bending stress ranges at the crack initiation sites. The total fatigue lives of all four specimens fell on the safe side of the mean S-N curve for category E details and the fatigue lives for three of the four failed specimens fell on the safe side of the upper 95% confidence limit, when they were plotted against the hot spot stress ranges at crack initiation sites. This indicates that the lower 95% confidence limit is an overly conservative design curve for the critical welded detail in the test specimens. This may be due to the fact that the hot spot stress range overestimates the driving force for crack growth through the thickness of the top flange and across the width of the top flange, particularly once the crack is longer than the thickness of the longitudinal attachment.

The crack initiation lives were calculated by the local strain approach and decreased asymptotically with increasing magnitude of the assumed maximum local stress at the crack initiation site, and approached the experimental crack detection lives at maximum local stresses near the monotonic yield strength of the weld metal. This is consistent with the presence of high initial tensile welding residual stresses along the weld toes.

A portable x-ray diffraction system could be used to measure the short-term and long-term residential stresses/strains at critical notches in a ship. Such a device could also be used to monitor the cyclic strain range at these notches. The feasibility of these applications could not be properly fully assessed in this study.

REFERENCES

1. Clark, J.D., "Fatigue Crack Initiation and Propagation in Warship Hulls", Proceedings of International Conference on Advances in Marine Structures - 2, ARE Dunferline, May 1991.

2. Ffield, P., "Control of Welding Stresses by Welding Sequence", American Welding Journal, November 1946.

3. "The Measurement of Long Range Reaction Stresses and Shakedown Effect", Materials Technology Centre, Fleet Technology Limited, Kanata, Ontario, August 1992.

4. Malik, L., "Residual Strain Effects on Fatigue Crack Initiation and Growth in Marine Structures - A Literature Review", Materials Technology Centre, Fleet Technology Limited, Kanata, Ontario.

5. BS 5400: Part 10: Code of Practice for Fatigue, 1980.

6. Hughes, O and Franklin, P., "Rationally-Based Fatigue Design of Tankers", proceedings of Ship Structures Symposium, Arlington, Virginia, November 1993.

7. Ma, Kai-tung, "Durability Considerations for New and Existing Ships", University of California, Berkley, SMP-5-1 report, September 1992.

8. Gurney, T.R., "Fatigue Design Rules for Welded Steel Joints", The Welding Institute Research Bulletin, Vol. 17, May 1976.

9. Sikora, J., Dinsenbacher, A., Beach, J., "A Method for Estimating Lifetime Loads and Fatigue Lives for Swath and Conventional Ships", Naval Engineers Journal, May 1983.

10. Guide for the Fatigue Strength Assessment of Tankers, American Bureau of Shipping, New York, NY, 1992.

11. Morrow, J., Fatigue Design Handbook, Society of Automotive Engineers, Warrendale, Pa., 1968.

12. Manson, S.S. and Halford, G.R., "Practical Implementation of the Double Linear Damage Rule and Damage Curve Approach for Treating Cumulative Fatigue Damage", Int. J. Fract., Vol. 17, No. 2, 1981, pp 169-172.

13. "Recommendations Concerning Stress Determination for Fatigue Analysis of Welded Components", prepared by ad hoc group of IIW Commissions XIII and XV, IIW Doc. XIII-1458-92, June, 1993.

14. Neuber, H, "Theory of Stress Concentration for Shear-Strained Prismatical Bodies with Arbitrary Non-Linear Stress-Strain Laws", Trans. ASME, J. Applied Mechanics, Vol. E28, 1961, p544.

15. Smith, K.N., Watson, P., and Topper, T.H., "A Stress-Strain Function for the Fatigue of Metals", J. Materials, Vol. 5, No. 4, 1970, pp 767-778.

16. Yee, R., "Cyclic Material Data for 350WT Welds and X-Ray Diffraction Measurements of Residential and Applied Strains Along Weld Toes", FTL Report 3762-17FR for DSE Fatigue and Fracture TIES Task 17, Jan. 24, 1995.

17. Lawrence, F.V., Mattos, R.J., Higashida, Y., and Burke, J.D., "Estimating the Fatigue Crack Initiation Life of Welds", Fatigue Testing of Weldments, ASTM STP 648, 1978, pp 134-158.

18. Peterson, R.E., Stress Concentration Factors, John Wiley & Sons, New York, 1974.

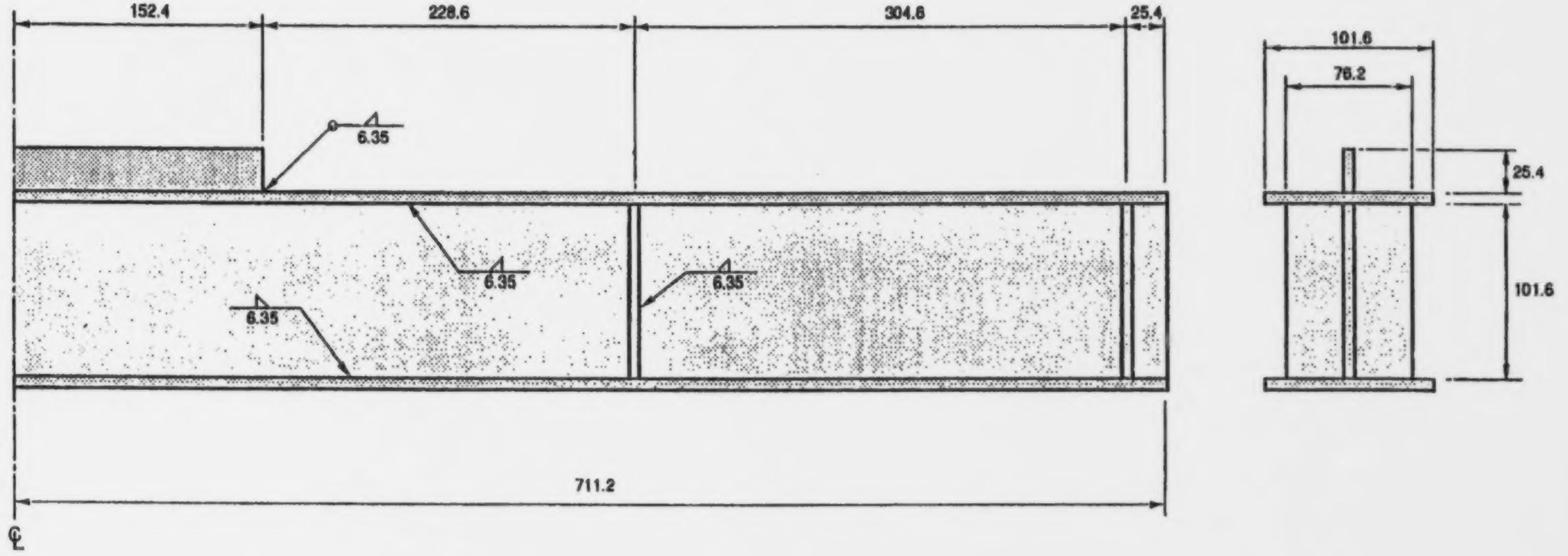
152.4
228.6
304.8
25.4
6.35
6.35
6.35
6.35
711.2
℄
101.6
76.2
25.4
101.6

12.7 mm thick 350 WT plates

All dimensions in mm.

Figure 1: Test specimen for fatigue testing and x-ray diffraction measurements of residential and applied strains.

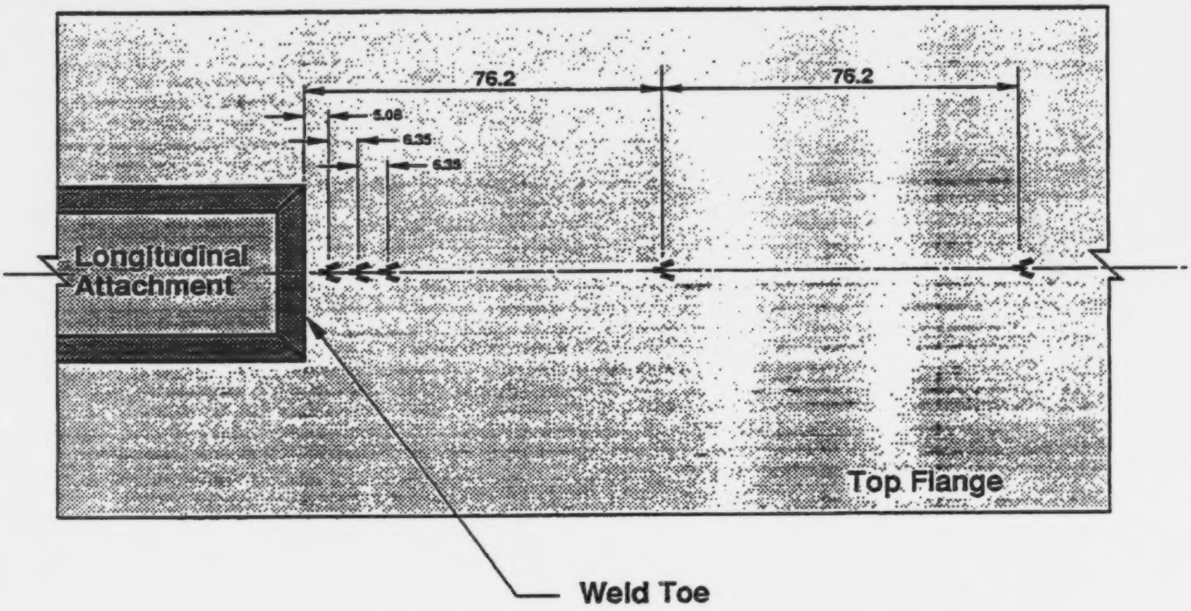
76.2
76.2
5.08
6.35
6.35
Longitudinal Attachment
Top Flange
Weld Toe

All dimensions in mm.

Figure 2: Locations of strain gauge rosettes along longitudinal centre line of top flange.

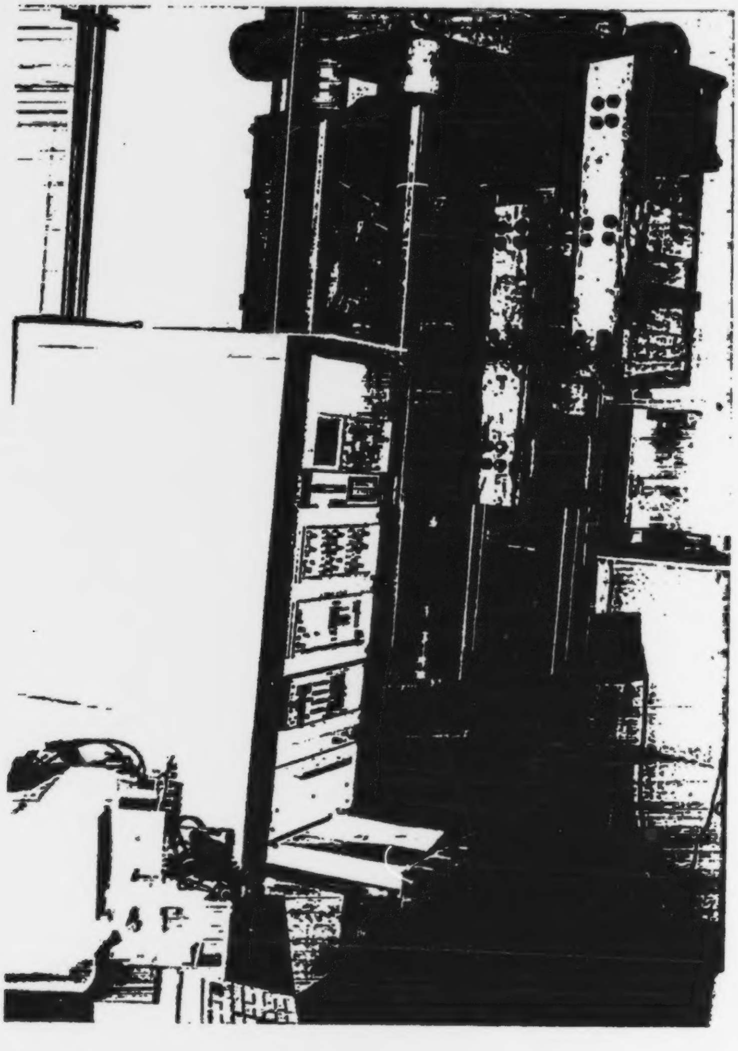

Figure 3: Servo-hydraulic test machine with four-point bending fixture.

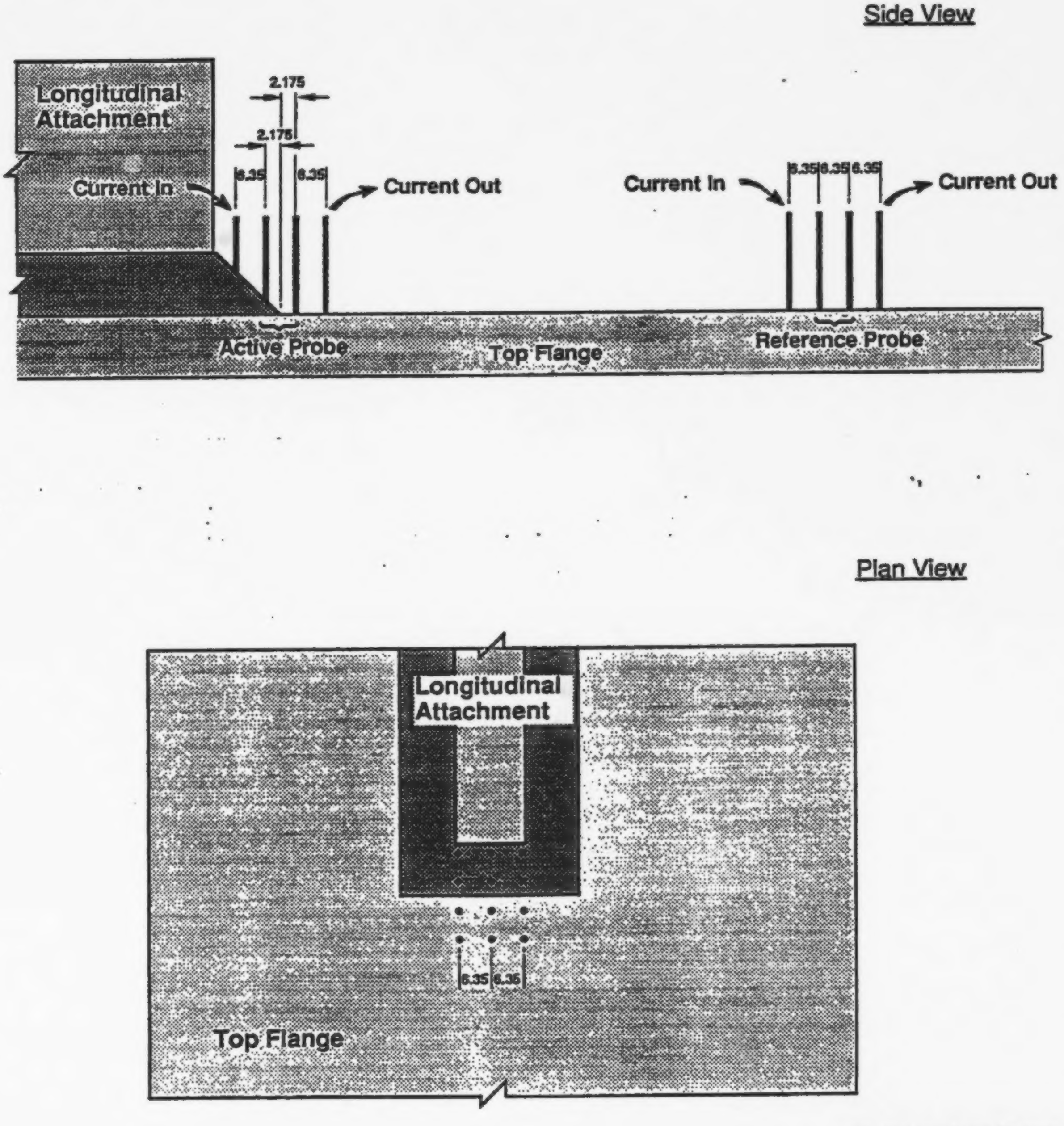
Side View
Longitudinal Attachment
2.175
2.175
6.35
6.35
Current In
Current Out
Active Probe
Top Flange
Current In
6.35
6.35
6.35
Current Out
Reference Probe
Plan View
Longitudinal Attachment
6.35
6.35
Top Flange

All dimensions in mm.

Figure 4: Layout of potential drop probes.

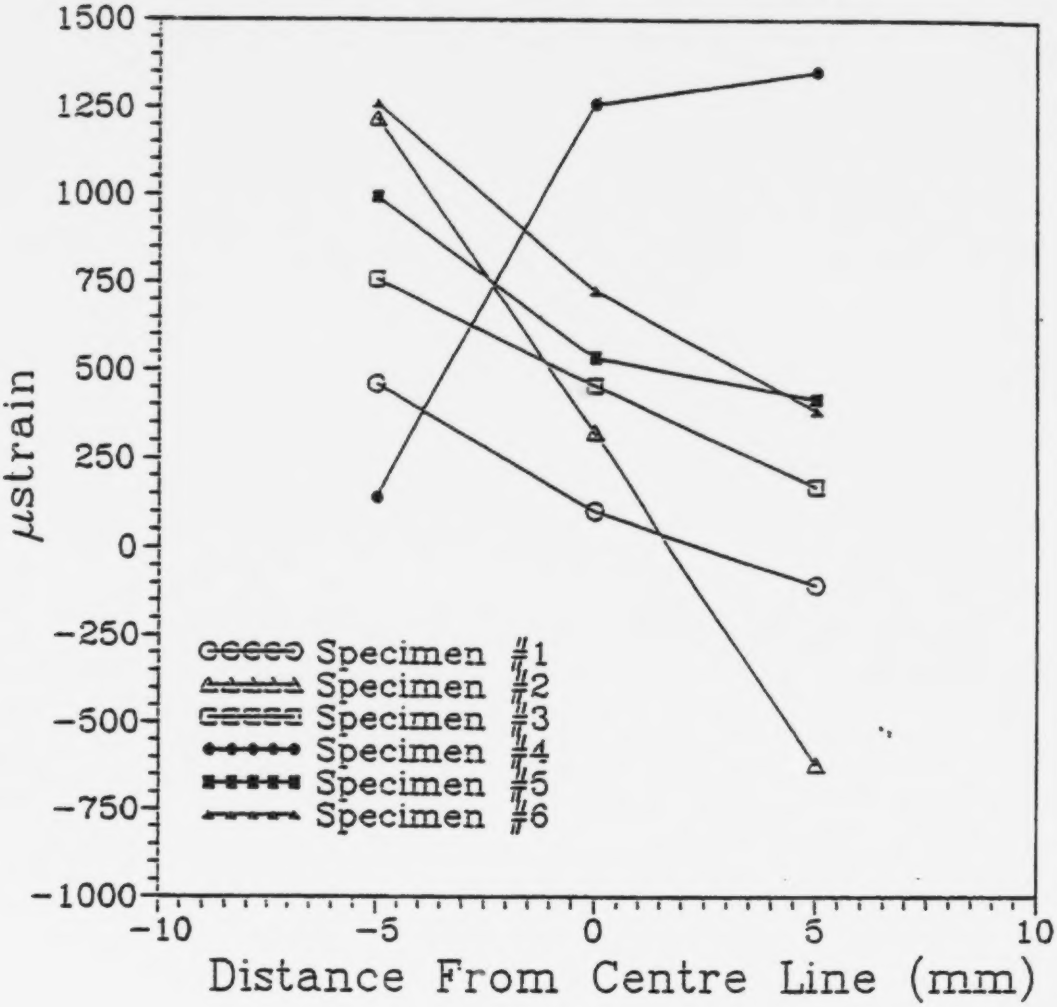

Figure 5: X-ray diffraction measurements of the residential strains along the weld toe at the unground end of the longitudinal attachment in specimens #1-#6.

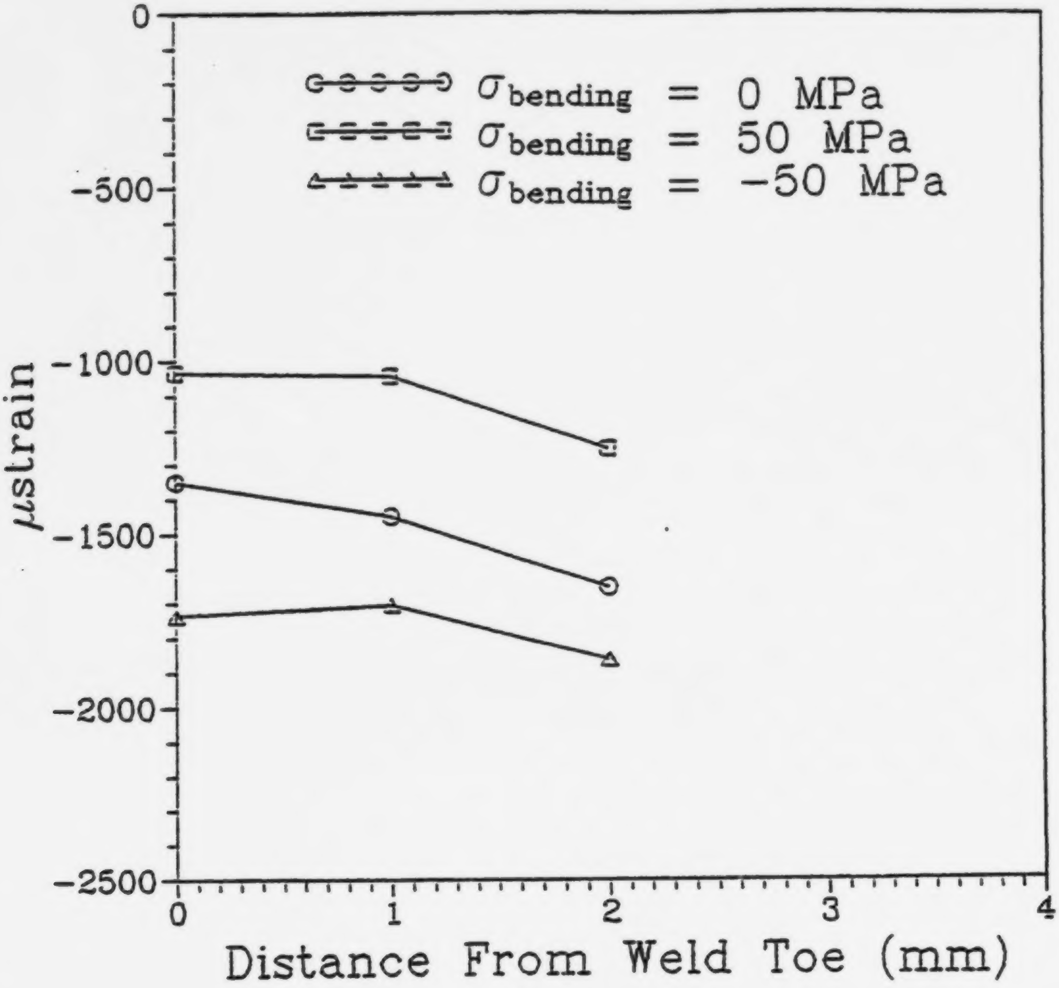

Figure 6: X-ray diffraction measurements of the total surface strains along the centre line of th top flange of specimen #3 vs distance from the weld toe at the unground end of the longitudin attachment.

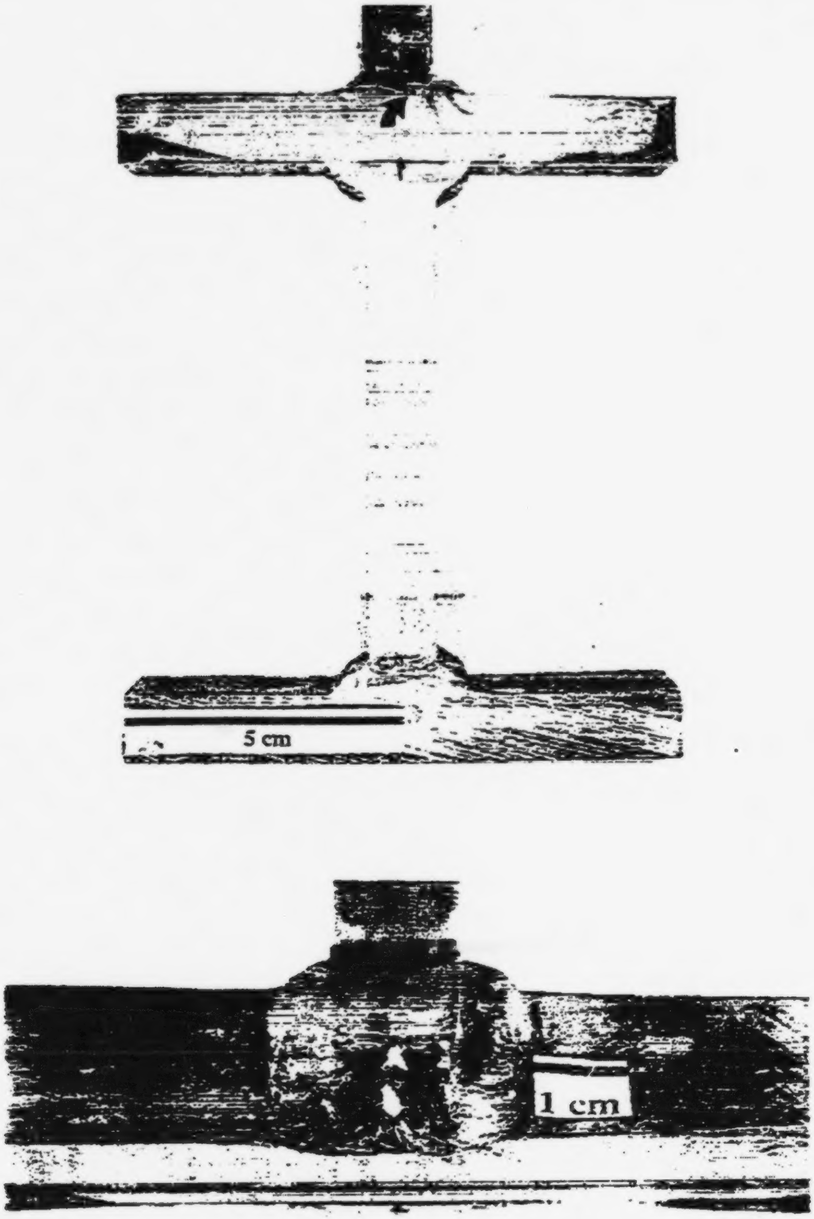

Figure 7: Fracture surface of specimen #3. Crack initiation site is indicated by ink stain.

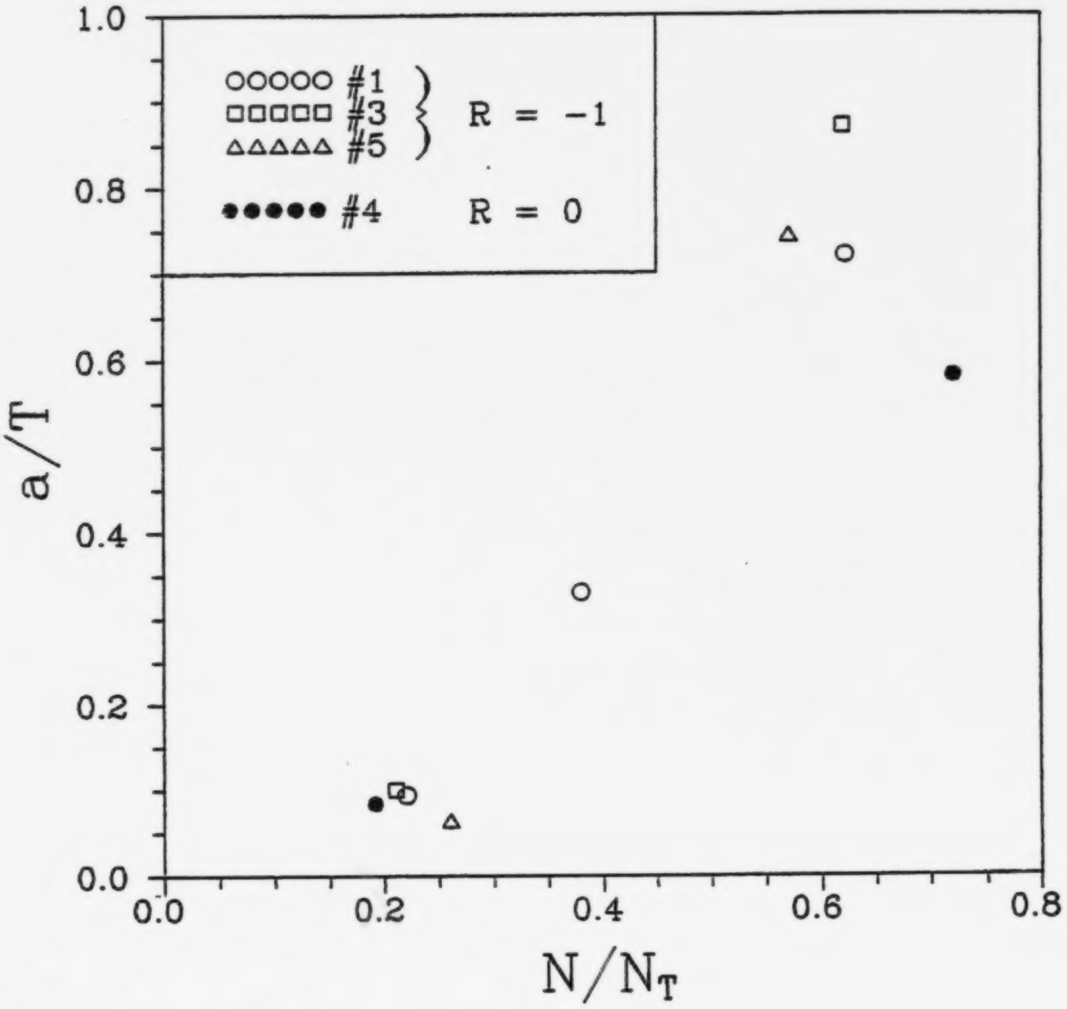

Figure 8: a/T versus N/N_T in specimens #1, #3, #4, and #5, where a is the maximum depth of ink stains and beachmarks, T is the thickness of the top flange, N is the number of load cycles at which a particular ink stain or beachmark was produced, and N_T is the total fatigue life or the number of load cycles to final failure.

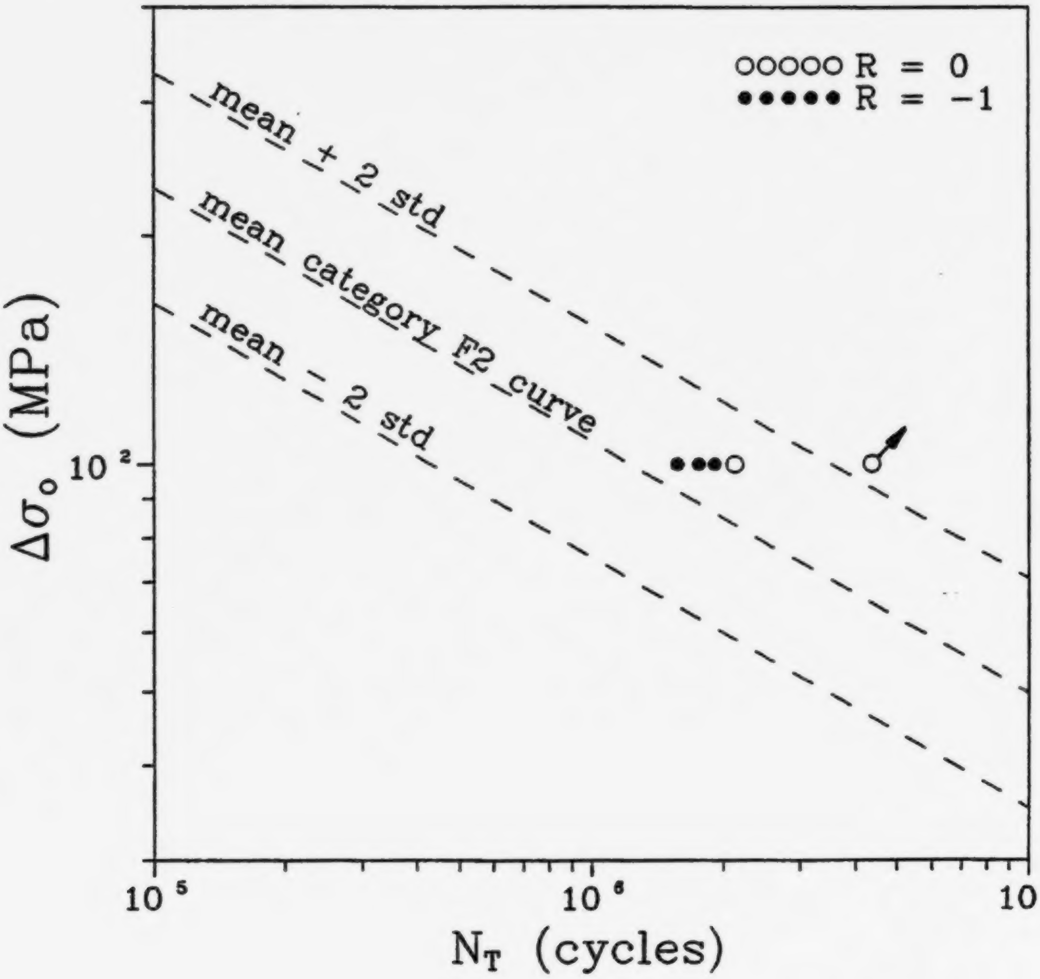

Figure 9: Total fatigue life (N_T) versus nominal bending stress range at crack initiation sit ($\Delta\sigma_o$).

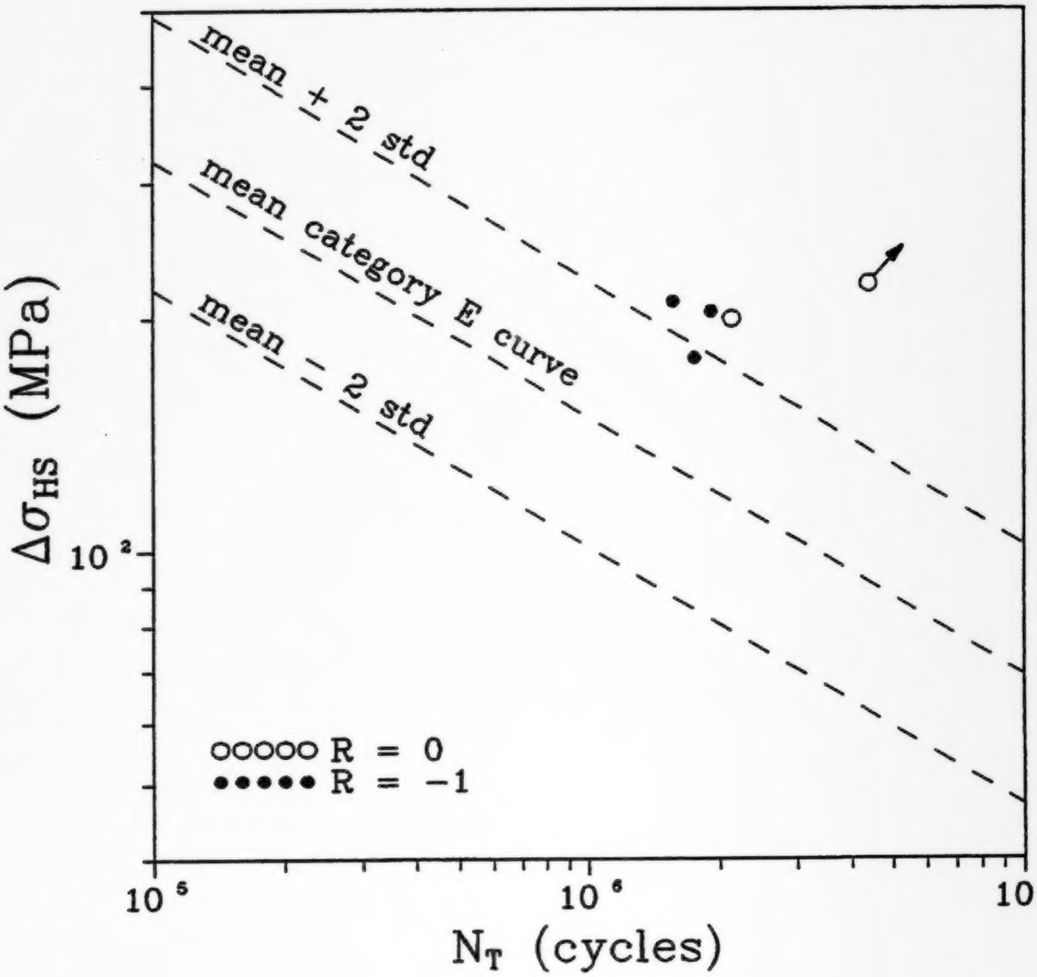

Figure 10: Total fatigue life (N_T) versus hot spot stress range at crack initiation site ($\Delta\sigma_{HS}$).

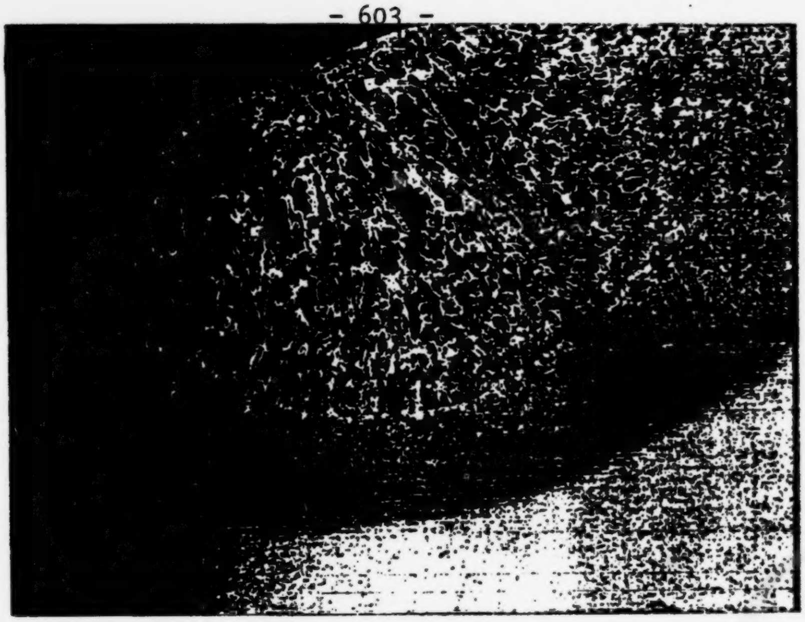

(a)

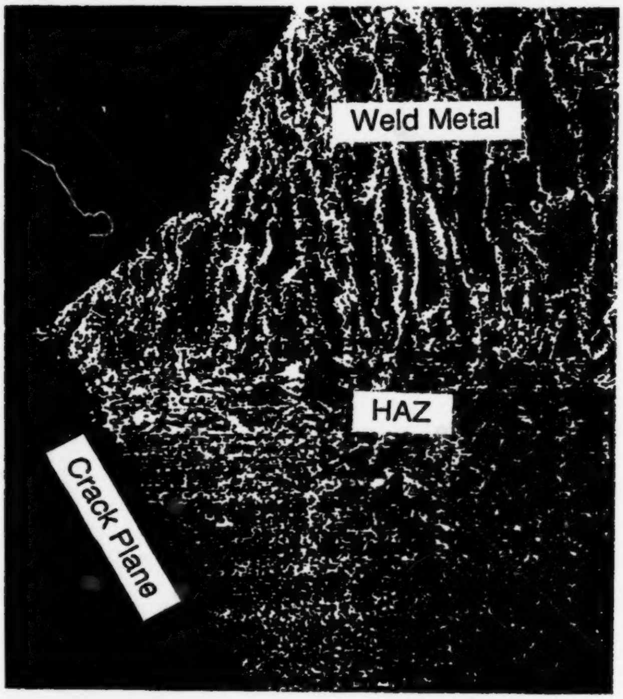

Weld Metal
HAZ
Crack Plane

(b)

Figure 11: Etched longitudinal section (2% nital) through crack initiation site in specimen #1 (a) 2X magnification (b) 50X magnification.

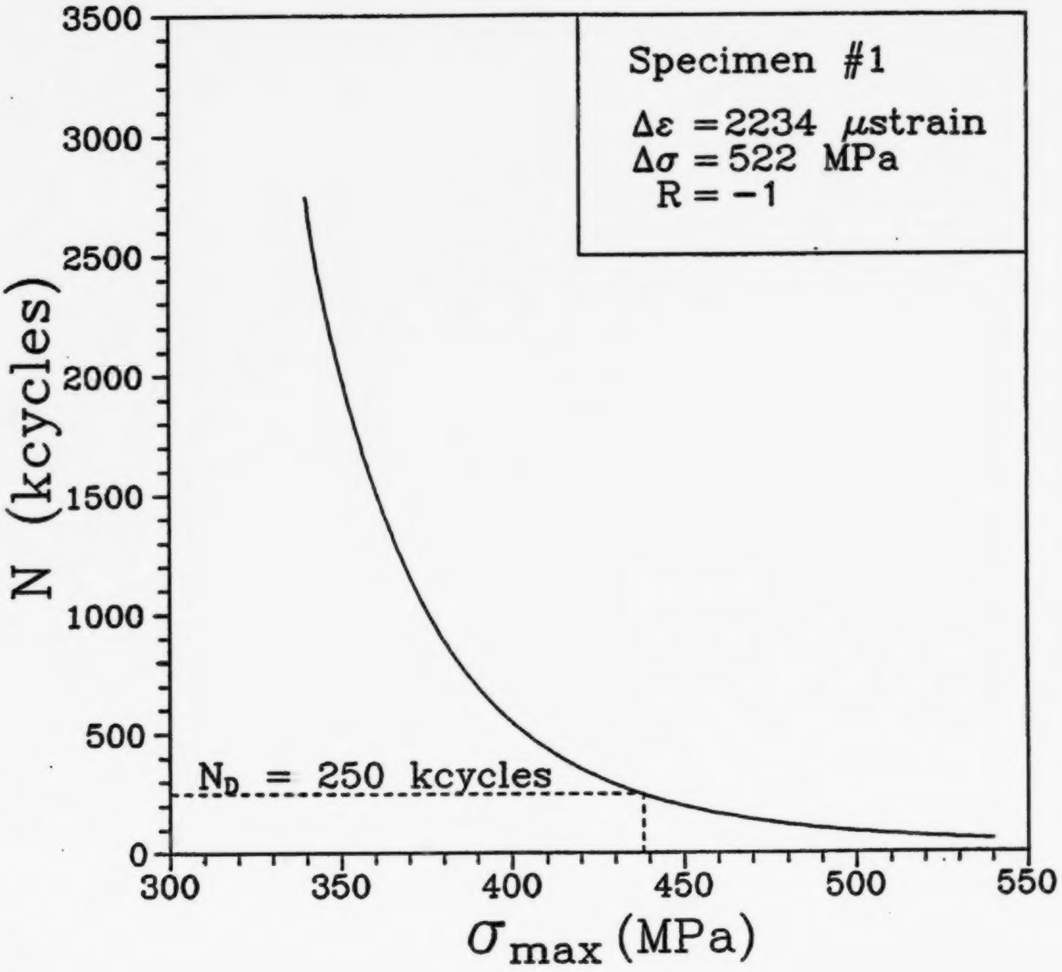

Figure 12: Predicted crack initiation life versus maximum stress at crack initiation site of Specimen #1. Actual crack initiation detected at 250 kcycles.

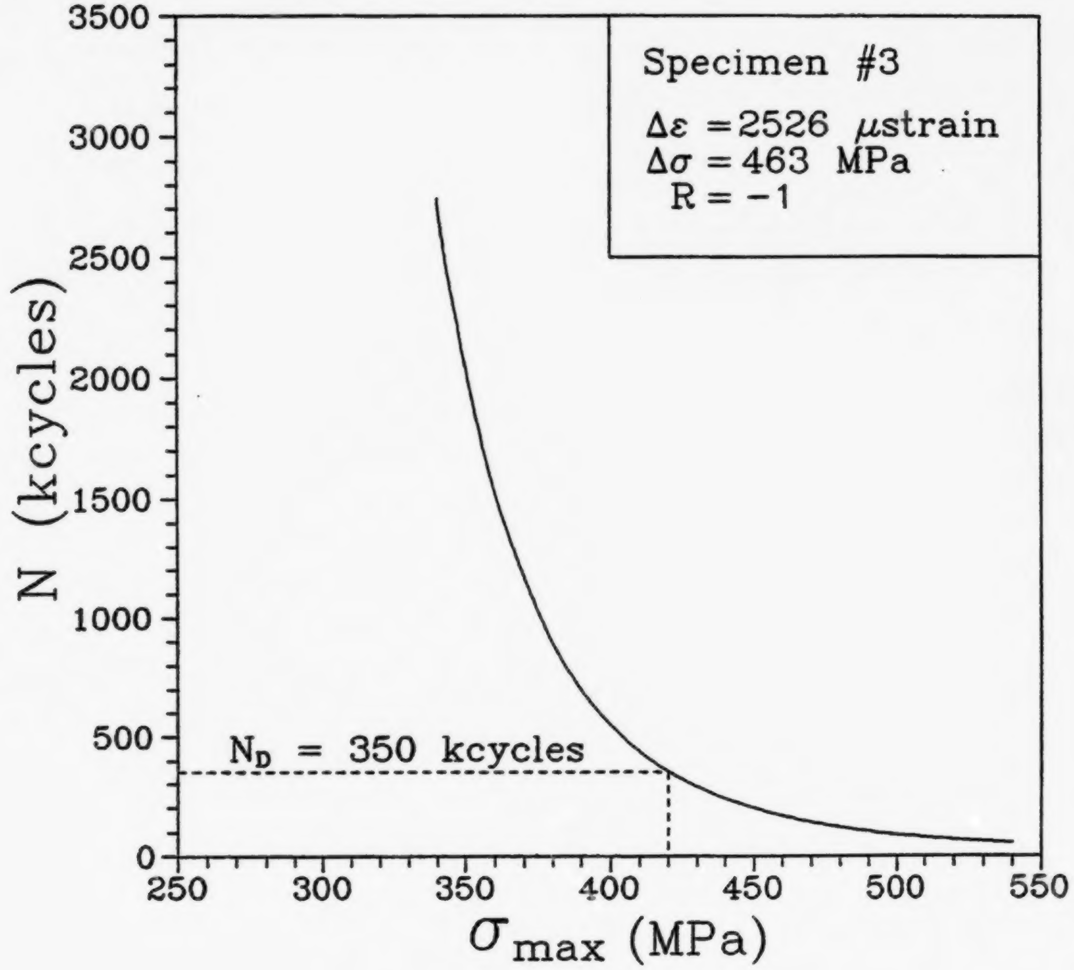

Figure 13: Predicted crack initiation life versus maximum stress at crack initiation site of Specimen #3. Actual crack initiation detected at 350 kcycles.

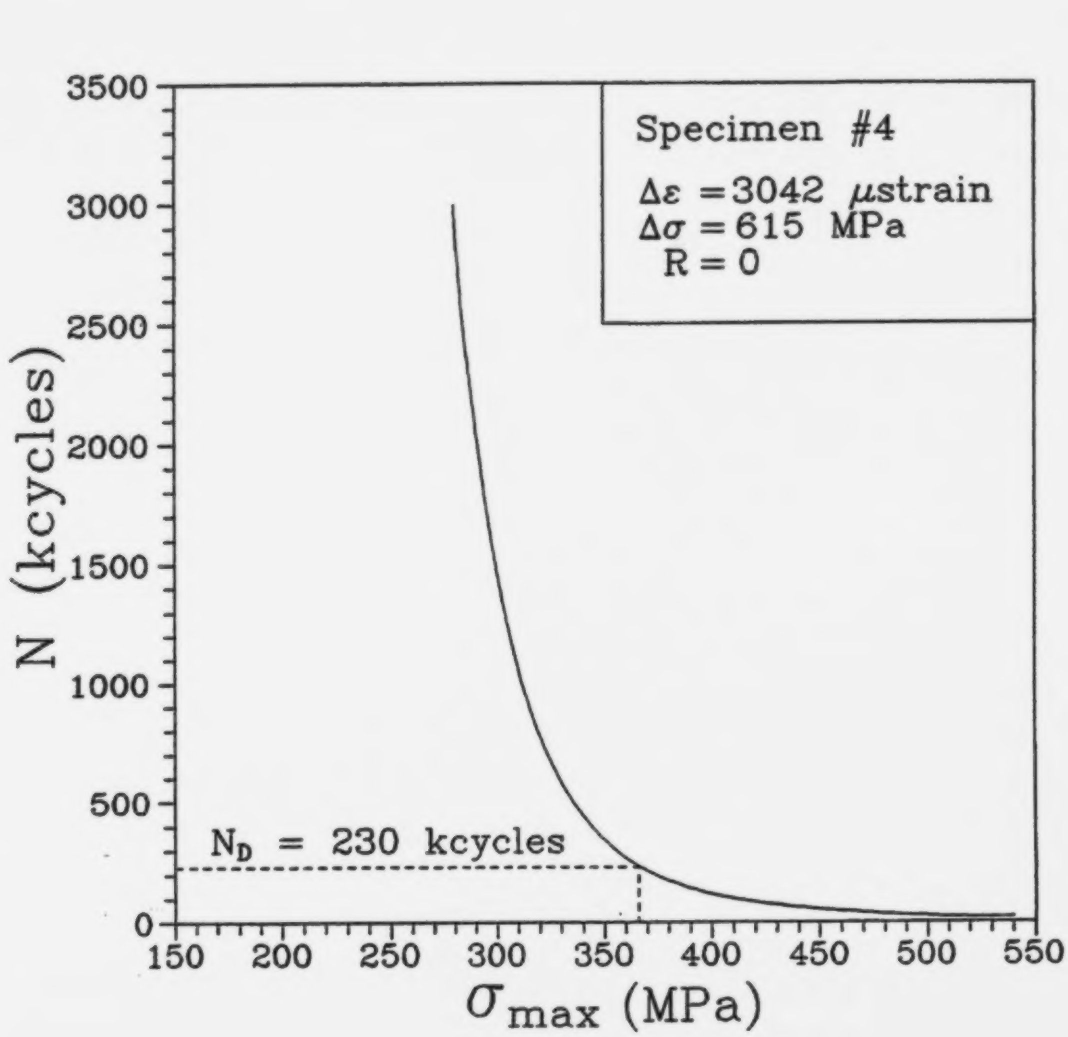

Figure 14: Predicted crack initiation life versus maximum stress at crack initiation site of Specimen #4. Actual crack initiation detected at 230 kcycles.

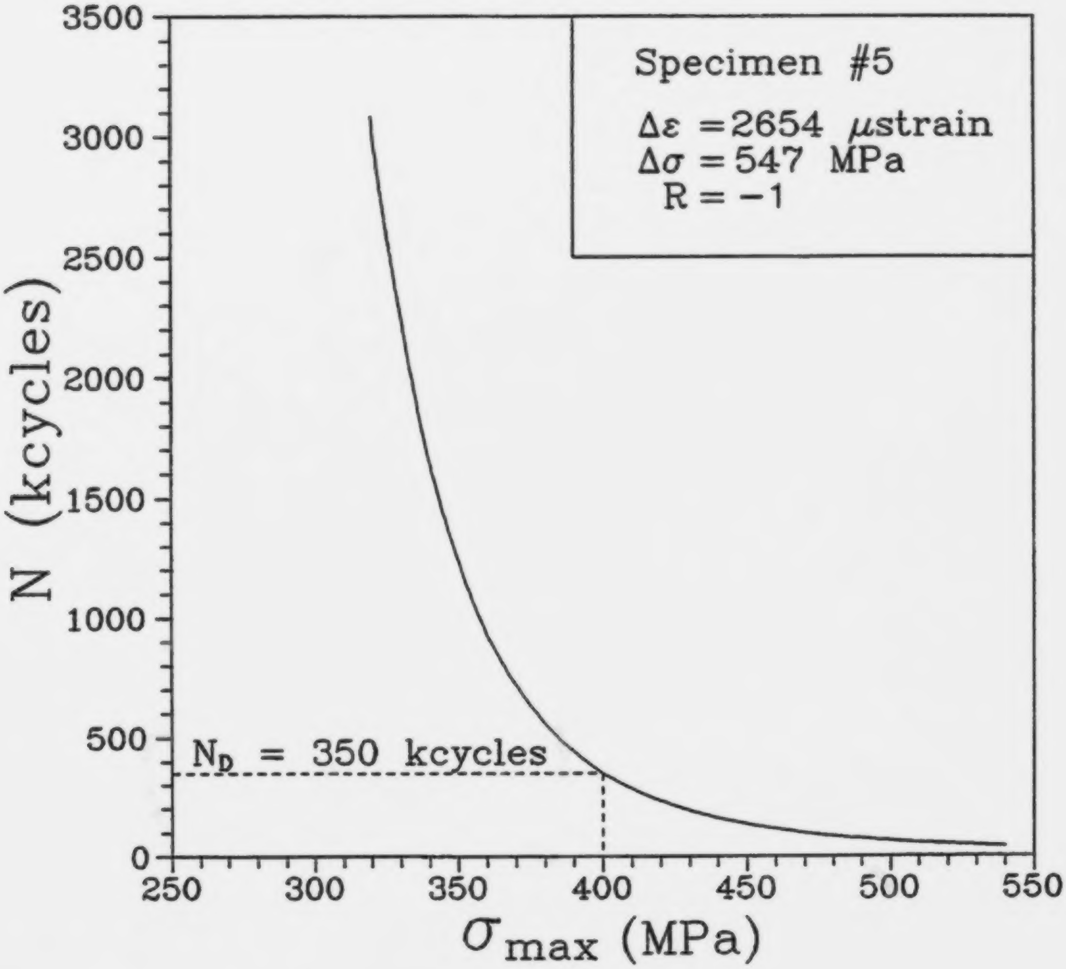

Figure 15: Predicted crack initiation life versus maximum stress at crack initiation site of Specimen #5. Actual crack initiation detected at 350 kcycles.

#510374 ㉛

Acoustic Emission Inspection of Compressed Gas Cylinders

D.R. Hay

Tektrend International Ltd.

ABSTRACT

Cylinders used to store compressed gases ranging from air and natural gas to hydrogen and inert compositions must be tested periodically usually by a hydrostatic test. In addition to insensitivity of the hydrotest to small service-induced defects, this test involves removal of the vessel from service and contamination of the vessel interior with water. Results of a program that compared acoustic emission testing with the hydrotest will be discussed showing much higher defect sensitivity for acoustic emission. These results combined with the ability to monitor in situ with acoustic emission recommend the latter in a number of applications.

TEKTREND

APPLICATIONS

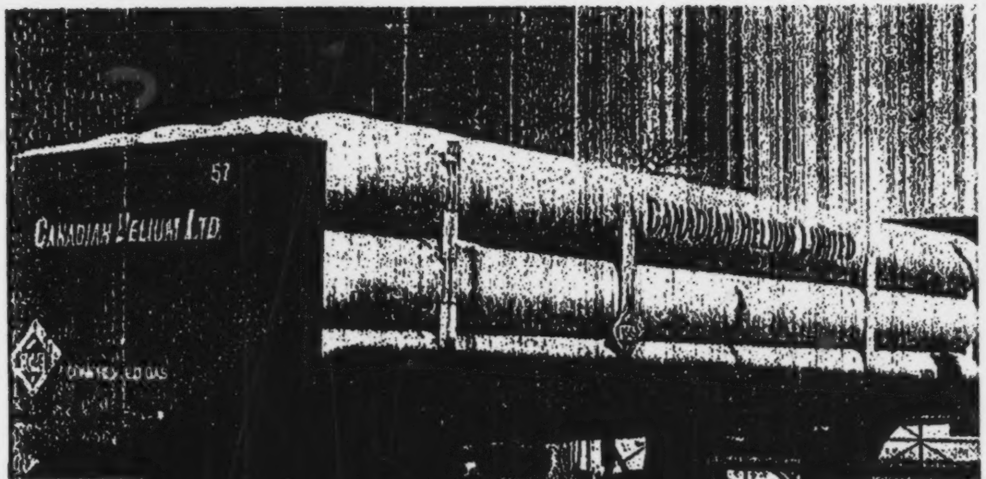
57
CANADIAN HELIUM LTD.
COMPRESSED GAS

JUMBO
12-TUBE TRAILER

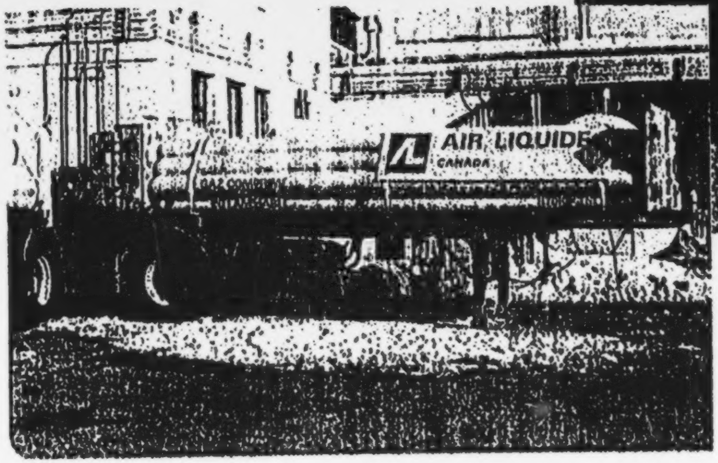
AIR LIQUIDE
CANADA

STANDARD
32-TUBE TRAILER

TEKTREND

PROJECT OBJECTIVES

ENHANCED SAFETY

OF

TUBE TRAILERS

THROUGH MORE SENSITIVE AND DETAILED INSPECTION

TEKTREND

COMPRESSED GAS TRANSPORT

COMMONLY TRANSPORTED GASES:

- OXYGEN
- HYDROGEN
- HELIUM
- NITROGEN
- ARGON
- AIR

OTHER GASES:

- NEON
- KRYPTON
- XENON

TEKTREND

TUBE SPECIFICATIONS

STAINLESS STEEL TUBES
DESIGN AND MATERIALS STANDARDS

CANADA: CTC REGULATIONS
UNITED STATES: DOT REGULATIONS

ASME BOILER AND PRESSURE VESSEL CODE SECTION VIII, DIVISION I, CODE CASE 1205, SPECIAL RULING, INTEGRALLY FORCED VESSELS, SA-372, SECTION VIII.

- MATERIAL PROPERTIES
- WALL THICKNESS
- MODES OF TRANSPORTATION AND PACKAGING
- SERVICE PRESSURE AND FILLING LIMITS
- RETESTING AND REINSPECTION INTERVALS AND REQUIREMENTS

MANDATORY REQUIREMENTS

At the time of manufacture a hydrostatic proof test must be performed. After this test, the cylindrical section of each seamless vessel must be examined using the ultrasonic angle beam technique in accordance with ASTM Standard A-388. DoT Specification 178.45-82 requires that the equipment must be calibrated to detect a notch equal to five percent of the design minimum wall thickness. The following ASTM Standards also are applicable.

E 114-82	Recommended Practice for Ultrasonic Pulse-Echo Straight-Beam Testing by the Contact Method
E 317-82	Practice for Evaluating Performance Characteristics of Ultrasonic Pulse-Echo Testing Systems Without the Use of Electronic Measurement Instruments
E 500-82	Definition of Terms Relating to Ultrasonic Testing

TEKTREND

FAILURE EXPERIENCE
IN
NORTH AMERICA AND EUROPE

GASES: HYDROGEN, NATURAL GAS, CARBON MONOXIDE AND ITS MIXTURES.

ENGLAND: Stress corrosion due to moisture and sulfur impurities and pressure-induced hydrogen environment cracking in a tube made from a chromium-molybdenum steel.

ITALY: Failure of low alloy chromium-molybdenum steel carrying carbon monoxide attributed to stress corrosion attack by hydrogen sulfide.

U. S. A.: Failure of a large seamless steel pressure tube attributed to environmentally assisted cracking due to high concentrations of hydrogen sulfide an sulfur compounds.

Natural Gas: Internal corrosion due to chemical reaction of the acid solution formed by the dissolution of carbon dioxide in water vapour contained in the gas.

TEKTREND

FAILURE MODES

CORROSION AND ENVIRONMENT-ASSISTED CRACKING

- GENERAL CORROSION INCLUDING PITTING
- SULFIDE STRESS CRACKING (SCC)
- HYDROGEN EMBRITTLEMENT

GENERAL CORROSION CAN BE INTERNAL OR EXTERNAL.

EXTERNAL CORROSION IS COMMON TO ALL TYPES OF STEEL CONTAINERS.

SURFACE ROUGHNESS OR SMALL DISCONTINUITIES ON THE INNER TUBE WALL CAN ACCELERATE THE INTERNAL CORROSION PROBLEM.

TEKTREND

FAILURE CHARACTERISTICS

- The fracture initiated on the inner surface in the position where the thin-walled parallel section meets the thicker knuckle region.
- In most of the failures, the fractures initiated at inner wall surface defects about 0.1 mm deep on the inner wall and had propagated in a brittle manner by a mixed intergranular/transgranular mode.
- The cracks tended to follow the distribution of the inclusions which are mainly manganese sulfide.
- The metallurgical structure in the vicinity of the cracks was tempered.
- The quality of the containers met required specifications.
- There was no evidence of any manufacturing defects or defective material
- NDT tests showed that the material quality in the region of the failure was equal to material quality in the parallel wall section. Toughness was at the expected level for quenched and tempered steels at that strength level.
- The absence of gross defects, the good quality of the steel, and the indications on the fracture surface establish that the fractures grew in service and were not manufacturing faults.

TEKTREND

CONVENTIONAL INSPECTION REQUIREMENTS

VISUAL INSPECTION: EVERY TWO (2) OR THREE (3) YEARS

HYDROSTATIC: EVERY FIVE (5) YEARS

HYDROSTATIC TEST IS CARRIED OUT IN A WATER JACKET OR ALTERNATE APPARATUS TO DETERMINE THE EXPANSION OF THE TUBE.

TEKTREND

TEST METHOD OVERVIEW

CANDIDATE METHODS

	ADVANTAGES	DISADVANTAGES
CONVENTIONAL NDT	DETECTION CHARACTERIZATION	100% VOLUME COVERAGE REQUIRED
HYDROTEST ACOUSTIC EMISSION	"REMOTE"	DETECTION ONLY

LABORATORY TESTING PROGRAM

OBJECTIVES:

- Effect a direct comparison of acoustic emission testing with the water jacket test for sensitivity to plastic instability.
- To evaluate the acoustic emission behavior of cylinders.
- To measure crack growth rates.
- To measure crack retardation due to overstressing at the hydrostatic proof load.

TEKTREND

PROOF TEST

PROOF TEST +

FRACTURE MECHANICS

↓

LARGEST FLAW IN THE STRUCTURE

ADDITIONAL DESIRABLE INFORMATION

LOCATE SUBCRITICAL DEFECTS
ASSESS SIZE AND SHAPE
MEASURE GROWTH BETWEEN TESTS

TEKTREND

ADVANTAGES
OF
ACOUSTIC EMISSION TESTING

HIGH SENSITIVITY

FAST
(IN-SITU TUBE TESTING)

TEKTREND

EXPERIMENTAL PROGRAM
LABORATORY TESTS

HYDRO AND AE

PURPOSE: COMPARE RELATIVE SENSITIVITY
VERIFY COMPUTATIONS

ARTIFICIAL AND NATURAL FLAWS

ARTIFICIAL:	FATIGUED	5
	WELD ARC	3
NATURAL:	GROUND FLAT	5
	SAW CUT (LONG.)	5
VS a/t	SAW CUT (TRANS.)	5
TOTAL SPECIMENS		23

CYLINDER TESTING

LABORATORY SETUP

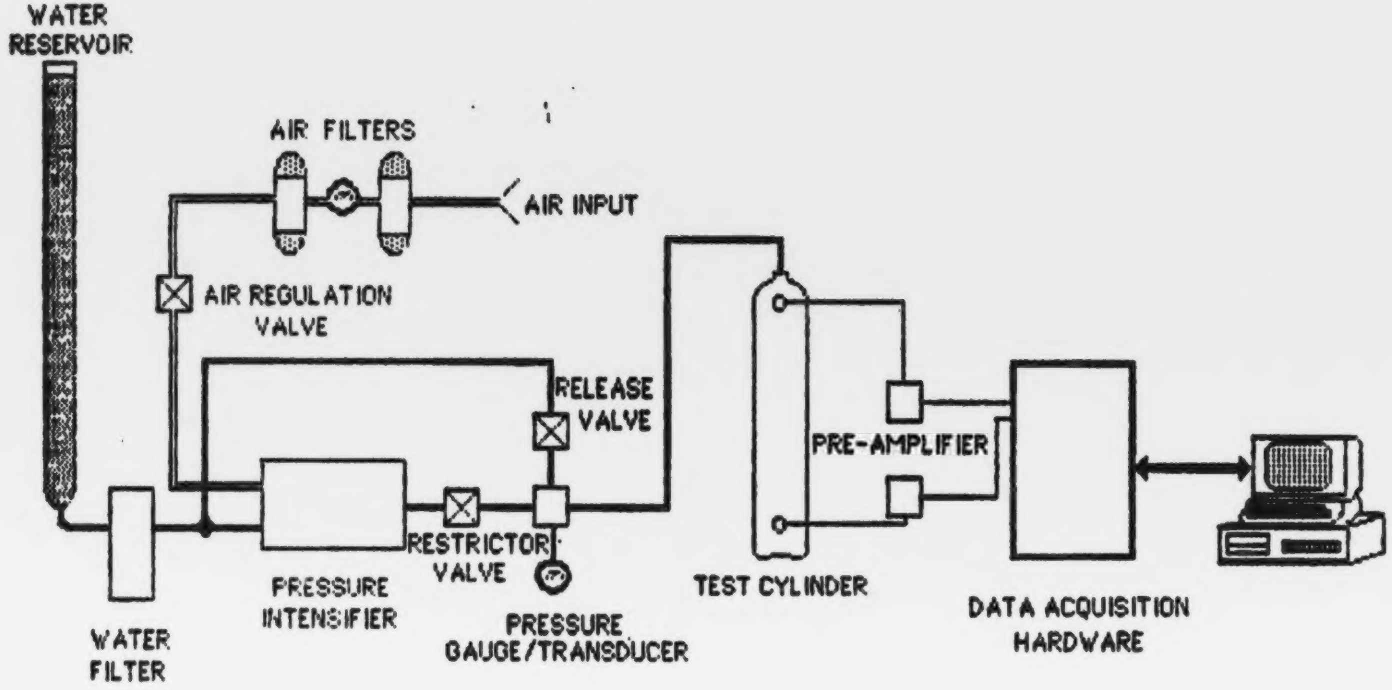
WATER
RESERVOIR
AIR FILTERS
AIR INPUT
AIR REGULATION
VALVE
RELEASE
VALVE
PRE-AMPLIFIER
WATER
FILTER
PRESSURE
INTENSIFIER
RESTRICTOR
VALVE
PRESSURE
GAUGE/TRANSDUCER
TEST CYLINDER
DATA ACQUISITION
HARDWARE

TEKTREND

TEST CYLINDERS

No.		Flaw Type	Dimensions	No.		Flaw Type	Dimensions
1.	Artificial	Longitudinal Cut	5.08cm x 0.16cm	2.	Artificial	Longitudinal Cut	5.08 x .3175
3.	Artificial	Longitudinal Cut	5.08cm x .477cm	4.	Artificial	Longitudinal Cut	10.16 x .157
5.	Artificial	Longitudinal Cut	10.16 x .3175	6.	Artificial	Longitudinal Cut	10.16 x .477
7.	Artificial	Longitudinal Cut	15.24 x .157	8.	Artificial	Longitudinal Cut	15.24 x .3175
9.	Artificial	Longitudinal Cut	15.24 x .477	10.	Artificial	Longitudinal Cut	.3175
11.	Artificial	Longitudinal Cut	.477	12.	Natural	Arc Strike	
13.	Natural	Arc Strike		14.	Natural	Crack (5400 cycles)	
15.	Natural	Crack (9400 cycles)		16.	Natural	Corroded Crack	
17.	No flaw						

PRESSURIZATION SCHEDULE

The pressure was increased incrementally by cycling between zero and the following values until failure:

0-10.3 MPa 0-13.8 MPa 0-14.5 MPa 0-15.2 MPa

0-5.9 MPa 0-17.25 MPa 0-20.7 MPa 0-24.8 MPa

0-24.1 MPa, then in 3.5 MPa increments until failure.

This cycling back to zero permitted measurement of the expansion by the direct method for each incremental pressure level.

TEKTREND

PRESSURIZATION
TEST RESULTS

OF THE FOURTEEN (14) CYLINDERS TESTED:

- FIVE (5) WOULD HAVE BEEN DETECTED BY THE HYDROTEST BY BURSTING AND WOULD HAVE BEEN UNDETECTED BY THE WATER JACKET.
- FIVE (5) OF THE CYLINDERS WOULD HAVE BEEN REJECTED BY ACOUSTIC EMISSION AT AN OVERPRESSURE OF 115%.
- NINE (9) OF THE CYLINDERS WOULD HAVE BEEN REJECTED BY ACOUSTIC EMISSION AT AN OVERPRESSURE OF 5/3.
- AMONG THE LATTER NINE (9), THREE (3) WOULD NOT HAVE BEEN DETECTED BY HYDROTEST, BUT AE REVEALED CRACK EXTENSION DURING THE TEST ITSELF.
- VOLUMETRIC EXPANSION DID NOT REVEAL ANY OF THE CRACK-LIKE DEFECTS.

ACOUSTIC EMISSION BEHAVIOR
OF
CYLINDERS

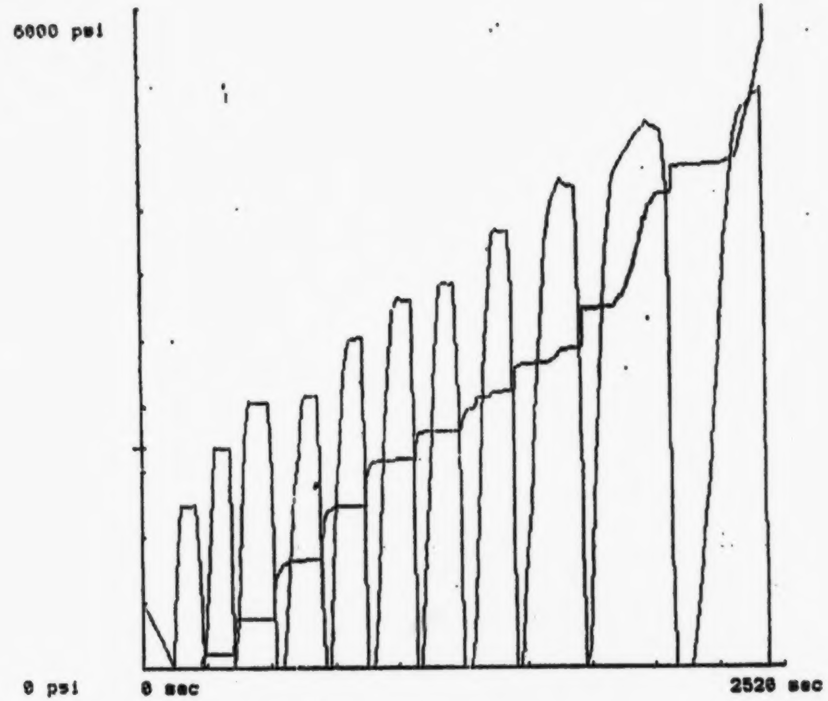

Starting Pressure : 628
Minimum Pressure : 0
Maximum Pressure : 5270
Total Events recorded : 641

ACOUSTIC EMISSION BEHAVIOR OF CYLINDERS

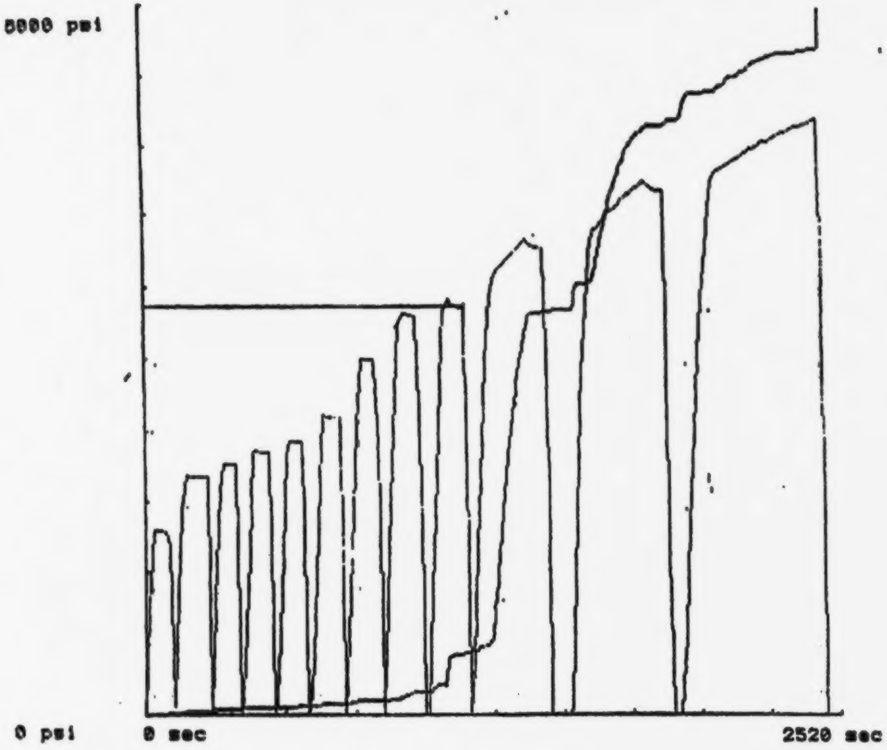

Starting Pressure : 0
Minimum Pressure : 0
Maximum Pressure : 5004
Total Events recorded : 1070

TEKTREND

HYDROTEST AND AE

In this option, the hydrostatic test is retained and acoustic emission testing is used in lieu of the water jacket. This is an extremely conservative approach which retains the high retest pressure of the current testing procedure and simply replaces the water jacket with the more sensitive acoustic emission monitoring. Testing at 5/3 service pressure would excite activity in smaller flaws than the lower pressures in the second option outlined below and this level of test pressure, combined with considerations of crack propagation rates and crack retardation effects induced at this level of pressure provides a margin of safety consistent with a 10-year retesting interval.

This option thus retains the advantages of the currently mandated retest methods, namely, the "proof test" character of the hydrotest and supplements it with the additional sensitivity of acoustic emission monitoring. In the case of vessels that would be rejected by the water jacket due to in-service induced deterioration, such wall thinning is produced by corrosion where cracking of the corrosion products are readily detected by acoustic emission.

TEKTREND

IN-SITU ACOUSTIC EMISSION

In this option, compressed gas tubes and cylinders would be pressurized using the product gas normally transported by the vessels as the pressurization fluid and monitored using acoustic emission. For reasons of safety and availability of pressurization pumping equipment at the filling station and the presence of overpressurization safety devices in the system, the test pressure is generally limited to 110% of normal service pressure. Pressurization would be carried out to the highest value deemed reasonable from test practicalities, namely, pressurization capabilities at the filling station and the presence of overpressurization safety devices in the system. This is of the order of 110% to 115% of the service pressure. If there have been accidental overloads or pressure excessions due to temperature cycling to pressures of 110% or over, testing under this option risks being ineffective due to the Kaiser Effect.

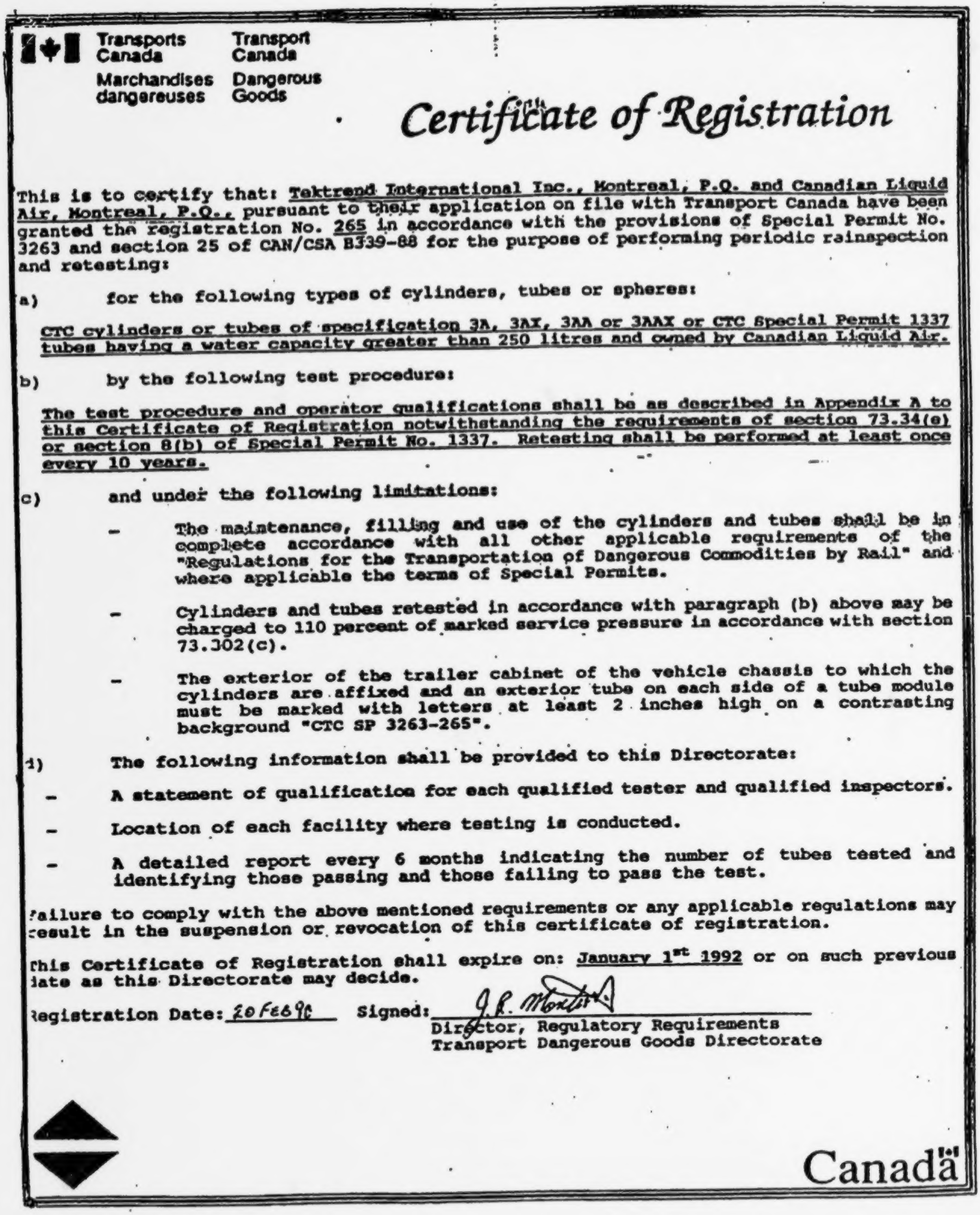

Transports Canada Transport Canada
Marchandises dangereuses Dangerous Goods

Certificate of Registration

This is to certify that: Tektrend International Inc., Montreal, P.Q. and Canadian Liquid Air, Montreal, P.Q., pursuant to their application on file with Transport Canada have been granted the registration No. 265 in accordance with the provisions of Special Permit No. 3263 and section 25 of CAN/CSA B339-88 for the purpose of performing periodic reinspection and retesting:

a) for the following types of cylinders, tubes or spheres:

CTC cylinders or tubes of specification 3A, 3AX, 3AA or 3AAX or CTC Special Permit 1337 tubes having a water capacity greater than 250 litres and owned by Canadian Liquid Air.

b) by the following test procedure:

The test procedure and operator qualifications shall be as described in Appendix A to this Certificate of Registration notwithstanding the requirements of section 73.34(e) or section 8(b) of Special Permit No. 1337. Retesting shall be performed at least once every 10 years.

c) and under the following limitations:

- The maintenance, filling and use of the cylinders and tubes shall be in complete accordance with all other applicable requirements of the "Regulations for the Transportation of Dangerous Commodities by Rail" and where applicable the terms of Special Permits.
- Cylinders and tubes retested in accordance with paragraph (b) above may be charged to 110 percent of marked service pressure in accordance with section 73.302(c).
- The exterior of the trailer cabinet of the vehicle chassis to which the cylinders are affixed and an exterior tube on each side of a tube module must be marked with letters at least 2 inches high on a contrasting background "CTC SP 3263-265".

d) The following information shall be provided to this Directorate:

- A statement of qualification for each qualified tester and qualified inspectors.
- Location of each facility where testing is conducted.
- A detailed report every 6 months indicating the number of tubes tested and identifying those passing and those failing to pass the test.

Failure to comply with the above mentioned requirements or any applicable regulations may result in the suspension or revocation of this certificate of registration.

This Certificate of Registration shall expire on: January 1st 1992 or on such previous date as this Directorate may decide.

Registration Date: 20 Feb 90 Signed: J.R. Montier
Director, Regulatory Requirements
Transport Dangerous Goods Directorate

Canada

#510375 ㉜

Prediction of Hydrogen Cracking in Multipass Welds in Low Carbon Steels

by

B.A. Graville*, L.N. Pussegoda**, and L. Malik**

*Graville Associates Inc, Georgetown, Ontario

**Fleet Technology Limited, Kanata, Ontario

ABSTRACT

Enormous advances have been made in recent years to improve the hydrogen cracking resistance of steels during welding by using low carbon levels coupled with thermo-mechanical controlled processing, precipitation hardening, or other strengthening methods. As the resistance to heat affected zone cracking has improved, however, the region of greatest risk of cracking has shifted from the HAZ to the weld metal, or as experienced in pipelines, the reheated HAZ of multipass welds.

Whereas the critical problem with older steels was the determination of a suitable preheat to allow the root pass to be deposited without HAZ cracking, with modern steels the challenge is to determine welding procedures that prevent critical hydrogen levels being reached at any critical location throughout a multipass weld. The initial preheat may be less important than, say, the number and size of passes, the geometry of the weld, or the time/temperature experience between passes. Time between passes is rarely specified in a welding procedure but may have a decisive effect on local hydrogen concentrations and the risk or weld metal cracking.

In the present work, hydrogen distribution is modelled using a simple finite difference approach that accounts for the major factors influencing hydrogen levels. Hydrogen diffusivity is expressed in terms of a trap model allowing calibration of two parameters from simple experiments. Experiments have been performed using bend specimens with various hydrogen removal aging treatments between passes. The deflection to failure of the bend tests was used as an index of sensitivity to hydrogen cracking. The results showed good agreement with the model for room temperature aging but effects of temperature were not accurately predicted. The results suggest, however, that for the purposes of welding procedure development, a simple hydrogen distribution model coupled with a local critical hydrogen concentration cracking criterion is a practical approach.

A. BACKGROUND

1. Modern day weldable steels have low carbon and low carbon equivalent. The HAZ thus has high resistance to weld hydrogen induced cold cracking.

2. However, there is still a risk of cold cracking in weld metal, and in the case of pipelines, in the relatively soft reheated HAZ.

3. Most of the weldability assessment methodologies (CTS test, Tekken test, restraint test etc.) are based on single pass welds and are suitable for preheat or welding procedure determination for root pass or fillet weld without HAZ cracking.

4. The weld metal and reheated HAZ cracking in comparison are problems of multipass welds.

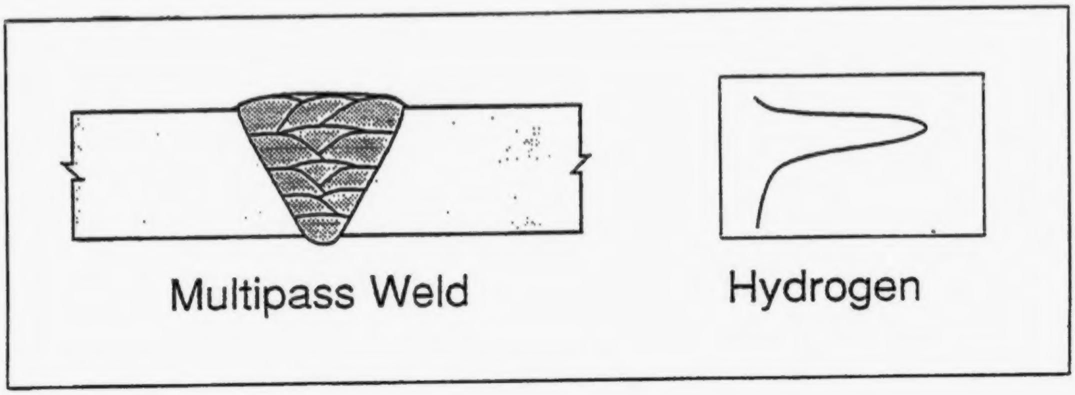
Multipass Weld
Hydrogen

Hydrogen in Multipass Welds

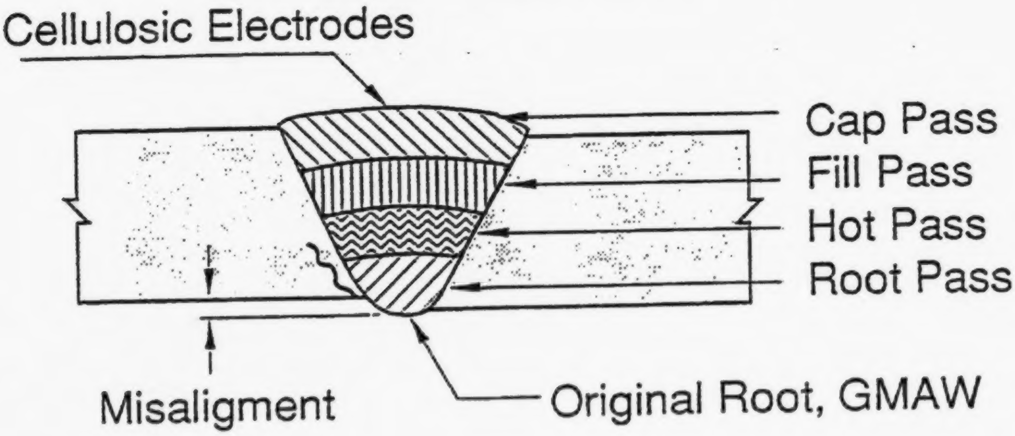
Cellulosic Electrodes
Cap Pass
Fill Pass
Hot Pass
Root Pass
Misaligment
Original Root, GMAW

Cracking in Reheated HAZ during Repair Welding

5. Instead of the initial preheat, the important variables are number and size of the weld passes, the geometry of the weld, and interpass time and temperature. Interpass time is rarely specified in welding procedure but may have a decisive influence on the incidence or absence of cracking in the welds.

6. The challenge in the case of weld metal and reheated HAZ cracking is therefore to optimize some of the above mentioned variables so as to prevent critical hydrogen levels being reached at any critical location throughout a multipass weld.

B. OBJECTIVE

To develop a hydrogen distribution model for pipeline girth welds that would account for the effect of major factors influencing hydrogen levels and susceptibility to hydrogen cracking in the reheated HAZ.

C. APPROACH

- Use a simple finite difference modelling approach;
- Employ simple experiments to estimate diffusivity of hydrogen;
- Experiments involve simple 'slow' bend tests on welds with various intra-pass or post weld aging treatments to create different hydrogen distributions (see **Figures 1 and 2**).

In these tests, the deflection to failure in the bend tests serves as an index of sensitivity to hydrogen cracking, dependent upon the **local hydrogen concentration in the HAZ** of the root pass near the stress concentration.

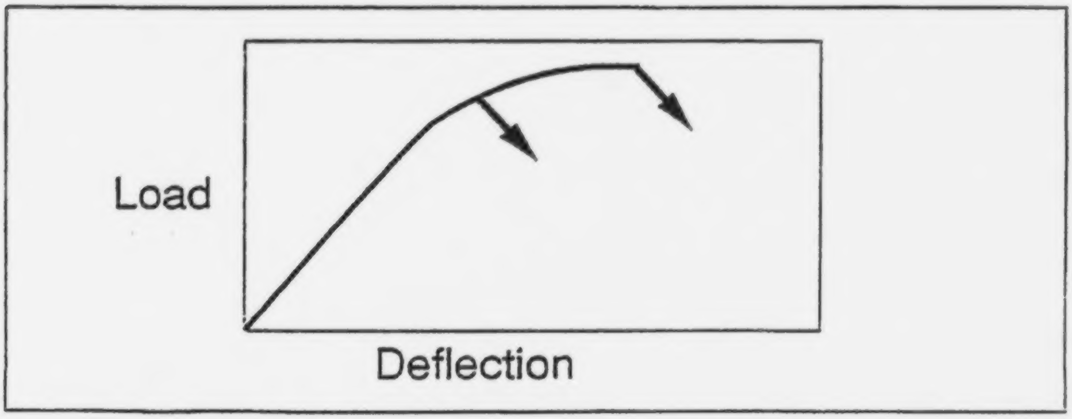

Slow Bend Test

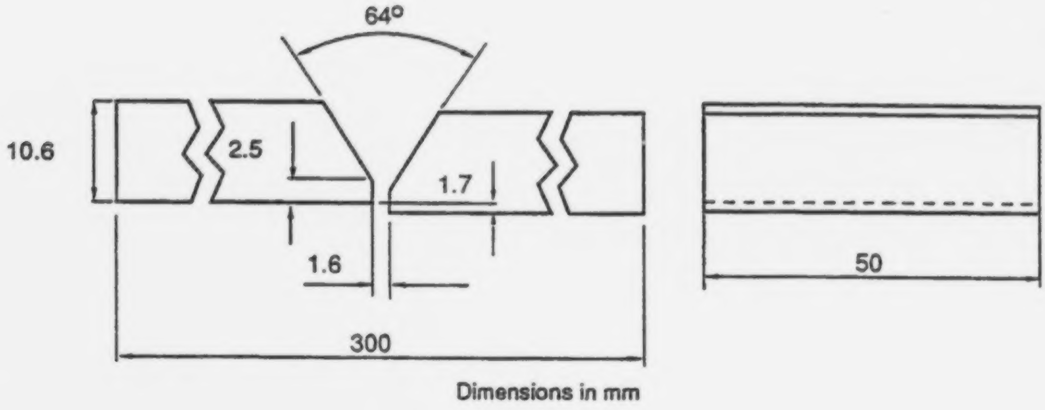
64°
10.6
2.5
1.7
1.6
300
50
Dimensions in mm

Joint preparation for the bend test

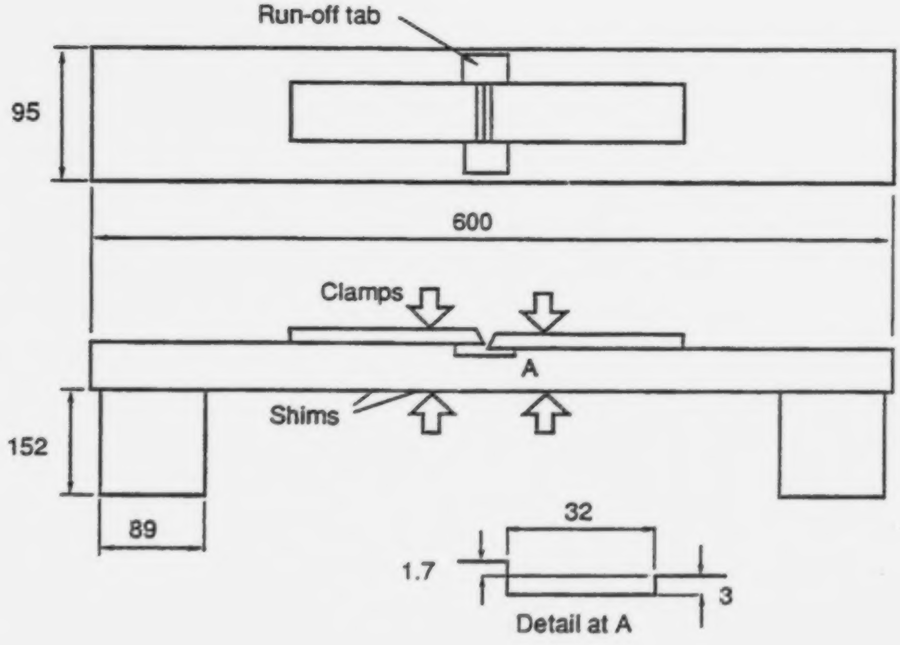
Run-off tab
95
600
Clamps
A
Shims
152
89
32
1.7
3
Detail at A

Welding jig for the bend test.

Figure 1. Details of the bend test preparation.

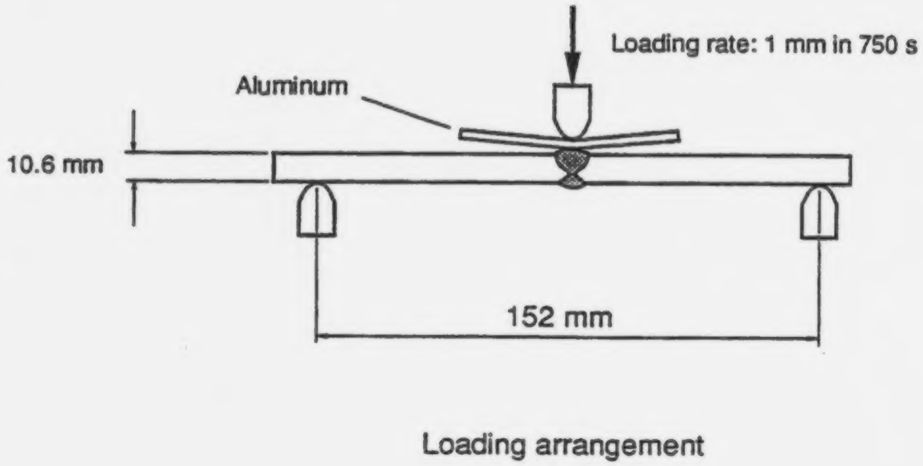
Loading rate: 1 mm in 750 s
Aluminum
10.6 mm
152 mm
Loading arrangement

Figure 2. Loading arrangement for the bend test.

D. EXPERIMENTS & RESULTS

D.1 TASK 1

Slow bend specimens welded according to normal procedure. Then aged at 20° or 70°C for various times (0 to 64 hours) prior to slow bend tests. Measure total diffusible hydrogen content on tested samples after tests. From the results so obtained (**Figures 3 and 4**),

$$D(70) = 9.14\,D(20)$$

where D(70) and D(20) are hydrogen diffusion coefficients in the weld zone at 70° and 20°C, respectively. Also, the activation energy for hydrogen diffusion can be calculated to be 37 kJ/mole which is higher than expected.

Figures of deflection versus hydrogen (**Figure 5**) and deflection difference (with respect to zero aging time) vs adjusted time (**Figure 6**) indicate that

$$D(70) = 5\,D(20)$$

and Activation Energy = 27 kJ/mm (expected value)

Prediction of the Model for Total Remaining Hydrogen in the Specimens after Ageing

Figure 7 shows the calculated vs measured global hydrogen.

- Good correlation between the calculated and measured values;
- Discrepancy could be due to the assumed initial hydrogen level (20 ml/100g) or the effect of plastic deformation during the test.
- Ideally, should have measured hydrogen on untested duplicate specimens.

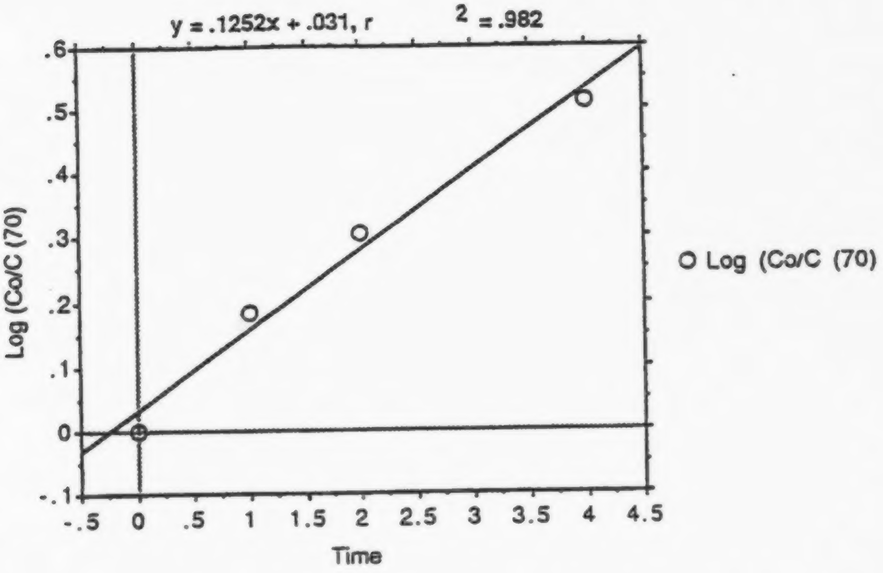

Figure 3. Regression plot for measured hydrogen contents for 70°C ageing.

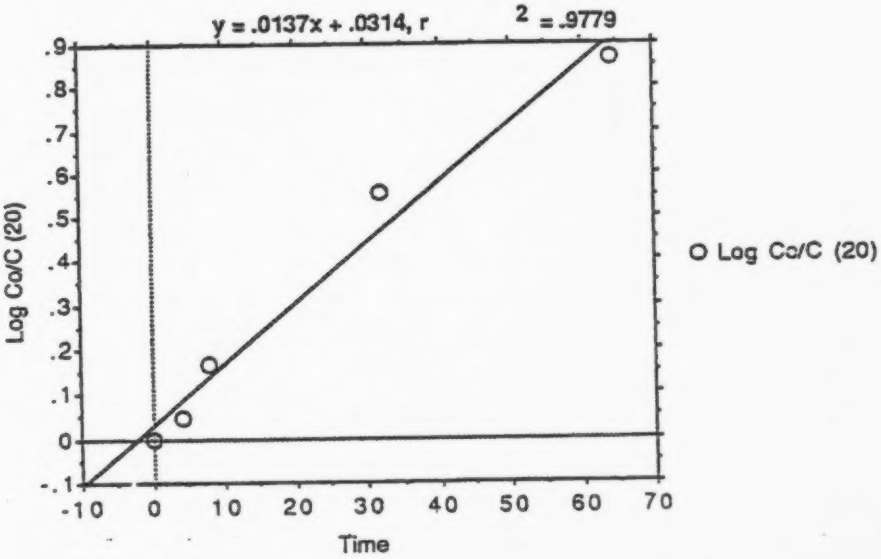

Figure 4. Regression plot measured hydrogen for 20°C ageing. Time in hours.

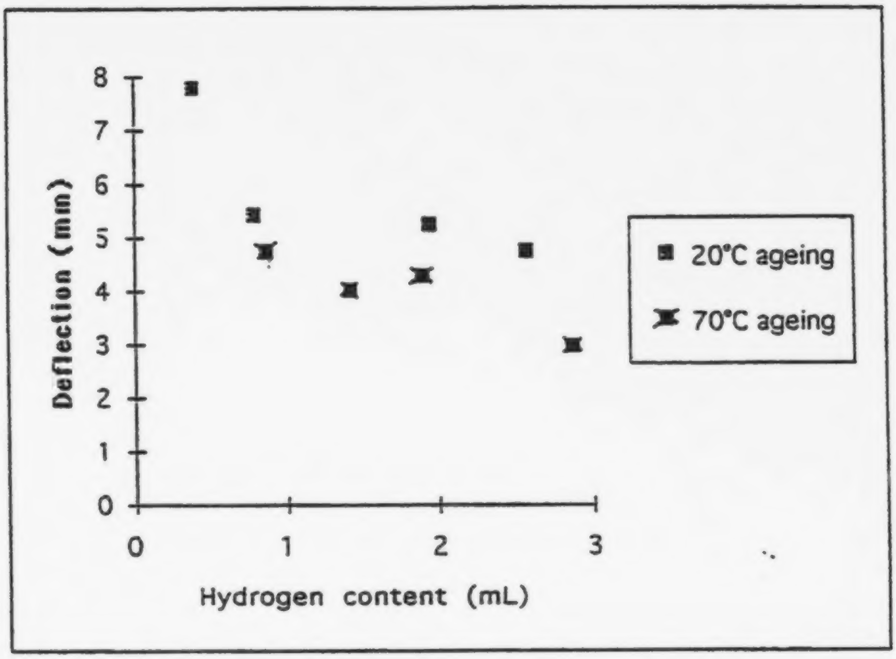

Figure 5. Deflection against measured hydrogen content for two aging temperatures. Measurements from Task 1 fractured bend specimens.

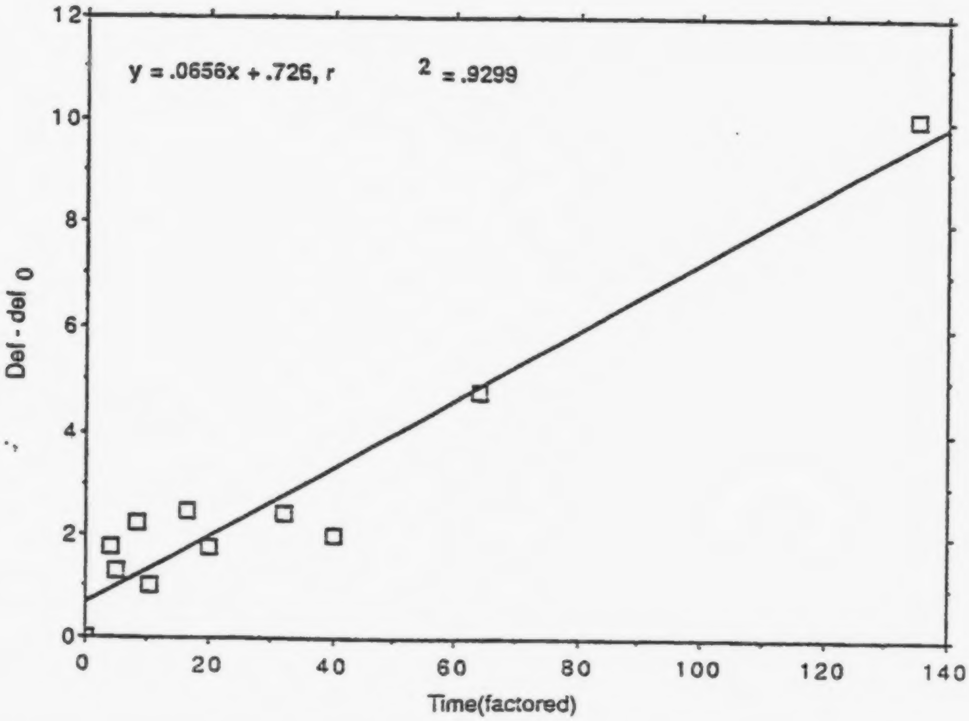

Figure 6. Results of fitting deflection data. Deflection is def - def at zero time. Time for 70°C data is multiplied by factor 5. This factor was found by trial and regression analysis to give best fit of data.

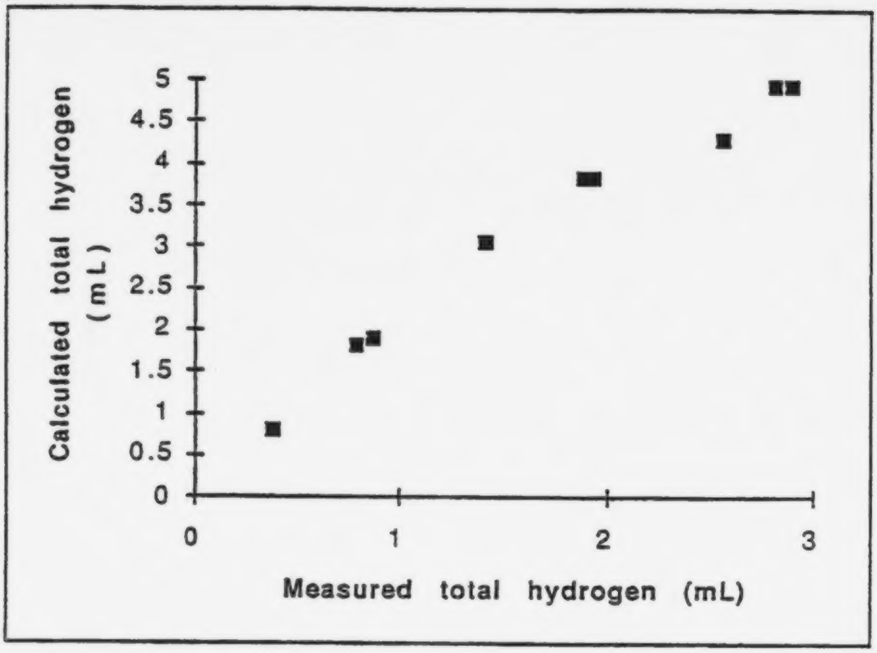

Figure 7. Total hydrogen content calculated from the model versus the measured values from fractured bend specimens. Data from Task 1 tests. The calculated values assumed a weld metal hydrogen content of 20 mL /100g of fused metal.

D.2 TASK 2

- Explore the effect of hydrogen diffusion distance.
- Welding procedure incorporated an ageing treatment (**up to 8 days at 20°C**) after the root pass (Series 1, smaller diffusion distance) or after the root and hot pass (series 2, larger diffusion distance). Then age after weld completion.
- The slow bend test results are shown in table below.

Table 7. Results of Task 2 bend tests.

Sample ID	Age temp (°C)	Age time (hours)	Deflection (mm)	Max load (kN)	Test duration (min)
Series 1					
2-1	19	0	2.90	27.7	44
2-2	19	4	2.80	26.1	42
2-3	19	24	5.24	31.0	78
2-4	19	96.5	7.78	34.1	115
Series 2					
3-3	19	0	4.92	31.6	70
3-1	19	16	4.29	30.7	64
3-4	19	96	8.41	35.7	125*
3-2	19	193	9.05	35.4	134**

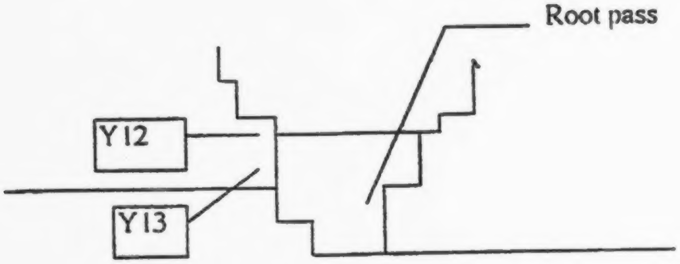

Model Predictions

Figures 8 and 9 show changes in hydrogen concentration with time in the HAZ at location Y12 adjacent to hot pass boundary. In Figure 8, the local hydrogen concentration decreases steadily with time as expected. When aging is done after the hot pass, the hydrogen concentration is initially zero at Y12 but rises as hydrogen diffuses from fill and cap passes. After reaching a peak at about 8 hours, the level starts to decline and follow a path similar to that in Figure 8. Thus in the second set of experiments, there is a period of a few hours after welding where the specimen hydrogen is decreasing but the local hydrogen in the root region is increasing.

This can also be in seen in the 2-D hydrogen distributions seen in **Figures 10 and 11.** Figure 10 shows the distribution immediately after depositing the cap pass when the total hydrogen content is at its maximum. Figure 11 shows the distribution after the weld has cooled to 50°C prior to aging. Total hydrogen content has increased but hydrogen has spread through to the root pass. **These are the conditions symptomatic of delayed cracking.**

In **Figure 12**, the measured deflection to first load drop in the bend tests is plotted against the local HAZ concentration at Y12 for all tests involving aging at 20°C. An acceptably good correlation is observed. This result should be compared with that shown in **Figure 13** where the deflection is plotted against the total (or average) hydrogen concentration and the resulting correlation is poorer.

E. CONCLUSIONS

- A simple model can provide a reasonable prediction of the local hydrogen concentration which can predict the cracking behavior in bend tests welded with different procedures.
- With suitable experimental/joint simulation calibration, the model can be used to predict cracking behavior in other multipass welds.

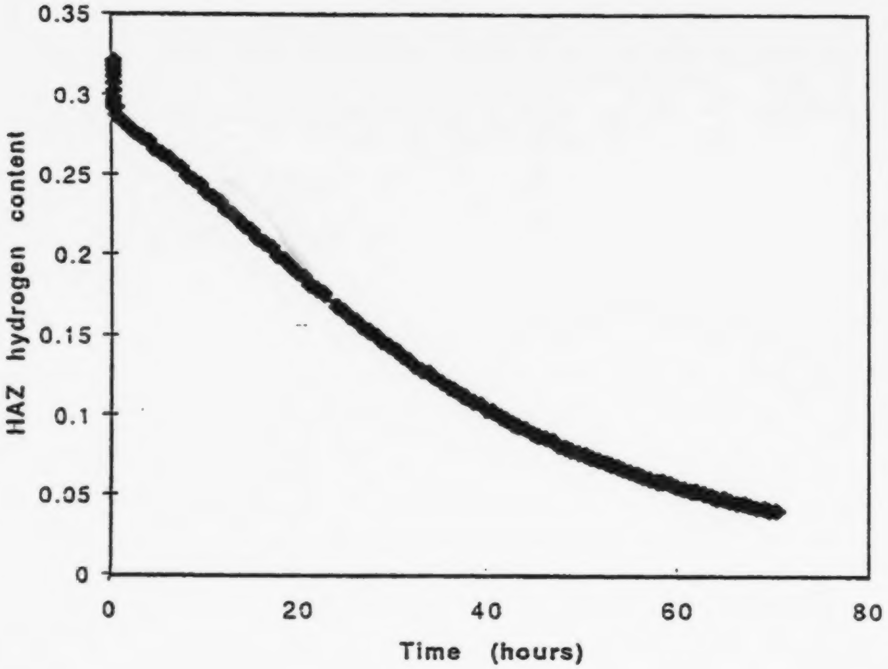

Figure 8

Ageing after Root Pass
H_2 decline starts
immediately.

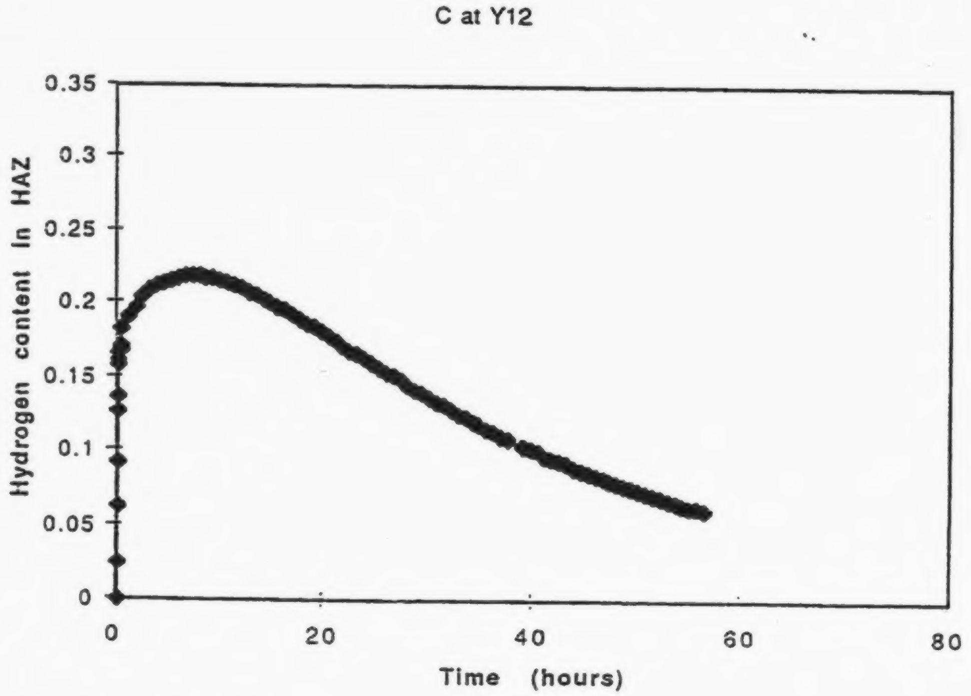

Figure 9
Ageing after Hot Pass
H_2 builds up first,
then declines.

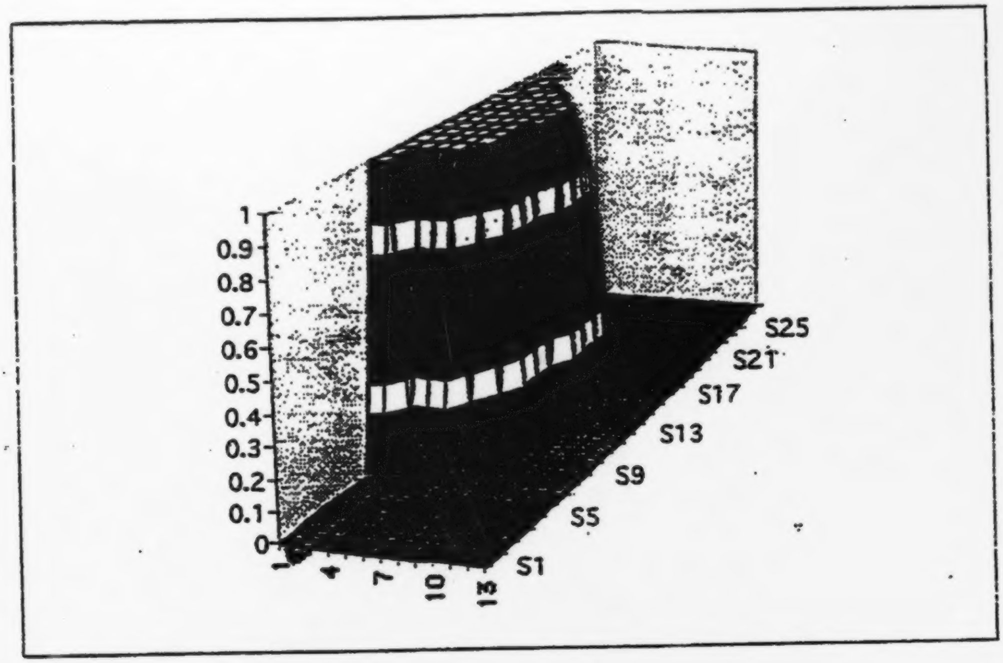

Figure 10. Task 2 series 2. Hydrogen distribution immediately after depositing the cap pass.

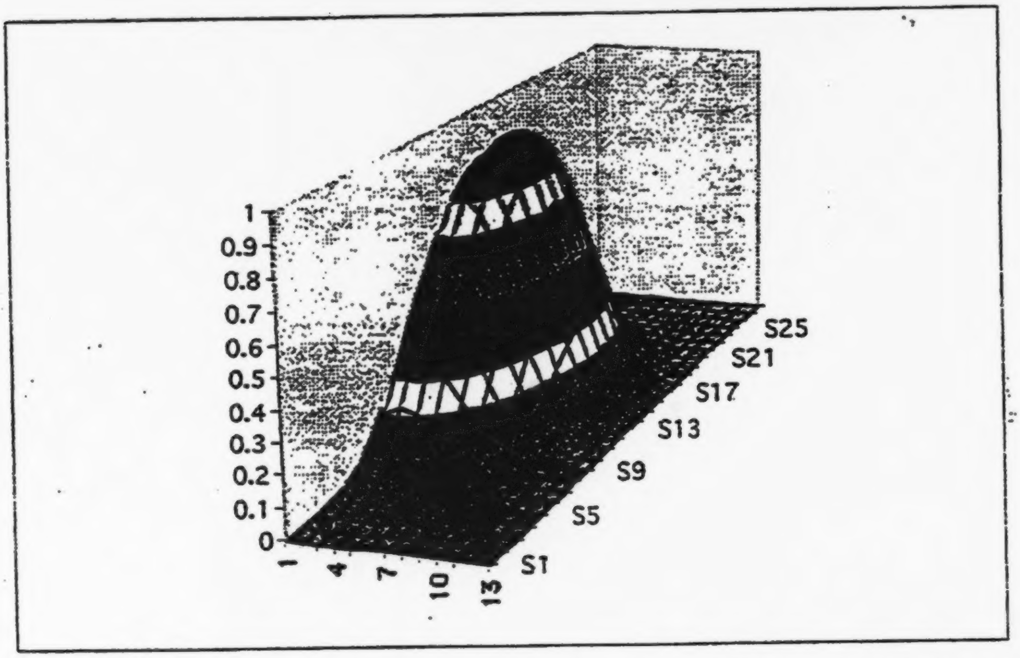

Figure 11. Task 2 series 2. Hydrogen distribution after weld has cooled to 50°C at beginning of ageing time.

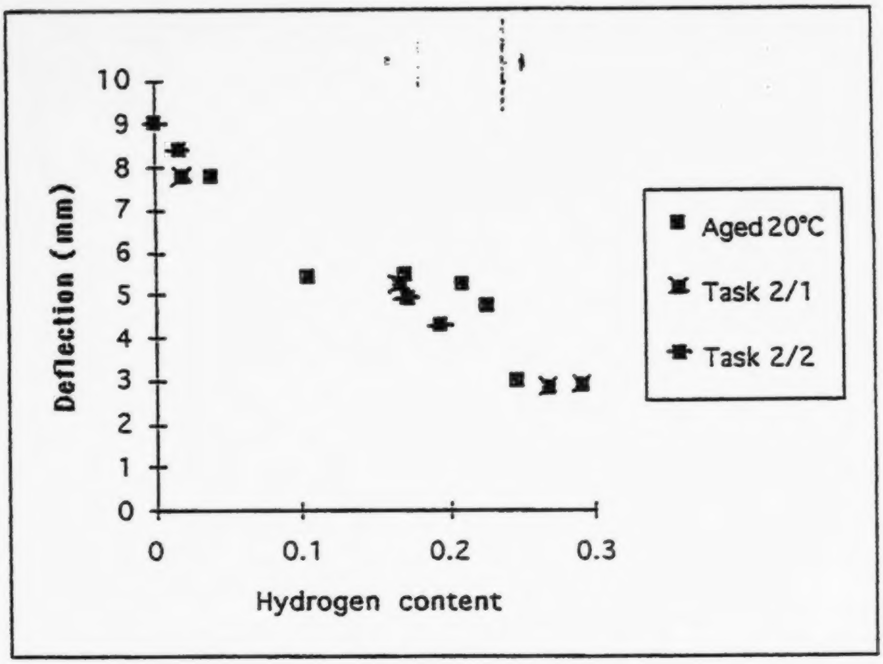

Figure 12. All data for tests aged at 19 or 20°C. Shows good relation between deflection and local HAZ hydrogen content for Tasks 1 and 2.

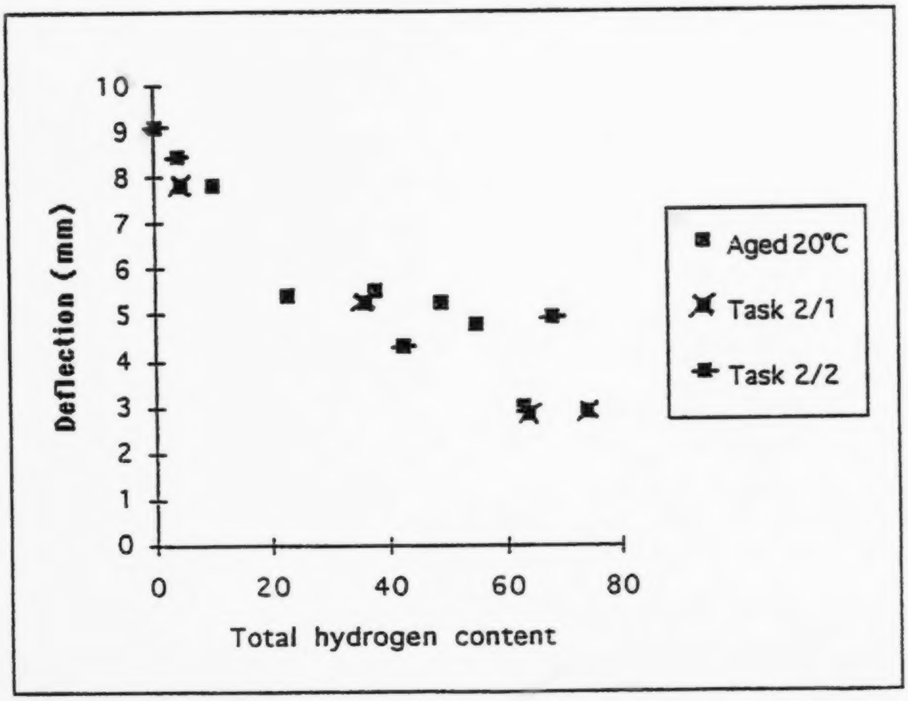

Figure 13. All data for 19 or 20°C ageing plotted against total hydrogen content. Agreement is less good especially for the Tasks 2/2 data.

#510376 ㉝

ACOUSTIC PROPERTIES OF SONAR DOME MATERIALS

by

Dr. Jacques Yves Guigné[1], Dr. Jeff P. Szabo[2] and Mr. Quanshun Liu[1]

1. Guigné International Ltd., 82 St. Thomas Line, Paradise, Newfoundland, Canada A1L 1C1
2. Defense Research Establishment Atlantic (DREA), Dockyard Laboratory, HMC Dockyard, Bldg D-17, FMO Halifax, Halifax, Nova Scotia, Canada B3K 2X0

ABSTRACT

As part of a development project sponsored by DRDM and DMCS on Spectra Fiber composite sonar domes, DREA has been tasked to provide data on the acoustic properties of glass and Spectra Fiber based composite panels in a 2 - 10 kHz range. The low frequency and high level of accuracy desired presented a number of challenges for carrying out insertion loss measurements. This paper introduces the use of parametric arrays to generate broad frequency responses off sonar dome materials. Particular attention is placed on the generation of low kHz signals in a laboratory limited tank setting and the resultant measurements produced.

INTRODUCTION

The two main functions of a sonar dome are to protect hull-mounted sonar equipment from physical damage as a ship moves through the water, and to displace the turbulent boundary layer away from the ship hull to reduce flow noise. Ideally, the dome should have a minimal effect on the propagation of sound from the target to the ship and from the ship to the target. This may be achieved by using materials for dome construction that have a low insertion loss, *IL*, defined as the reduction in sound pressure resulting from insertion of a test panel between a source and a receiver. Unfortunately, materials which have low insertion losses, such as elastomers, are usually not stiff enough to be self-supporting and do not have the required strength for sonar domes. One solution is to use fibre-reinforced plastic (FRP) composite materials with high strength-to-weight ratios, which enable thin panels with relatively low insertion loss to be used. In addition to low insertion loss, FRPs may offer better noise characteristics than metallic structures due to higher internal damping, since the dome itself may contribute to the noise level via flow excitation at resonnances within the structure.

This paper focuses on the acoustic characterization of several candidate materials being considered as sonar dome construction materials. In addition to metallic-based panels and glass-reinforced materials, composites reinforced with Spectra Fiber were examined. Spectra Fiber, from Allied Signal Corporation, is polyethylene prepared in such a manner that it is highly crystalline, with the crystals aligned along the fiber axis. Examination of the acoustic properties of Spectra Fiber panels is part of a larger effort to develop Spectra Fiber sonar domes, sponsored by Chief Research and Development and Director Maritime Combat Systems.

COMPOSITE PANELS

Spectra Fiber composite panels were prepared by Advanced Composite Technology (ACT), Sparks, Nevada using two different resin systems and two different weaves, Table 1. The resin systems used for the prepregs were based either on a cyanate ester (BTCY-3) or an epoxy, Shell EPON 828 (BT250F). The plasma treated Spectra Fiber reinforcing fibres were configured in either a 985-8H satin weave or a 988-4H satin weave, as shown in Table 1. In each case, the panels contained 50% ± 2% by weight resin, and were 1 m x 1 m x 10 mm in size.

Glass reinforced composite panels were fabricated by ACT using the same resin systems (cyanate and epoxy) as the Spectra Fiber panels, using an 8H satin weave.

TABLE 1

SAMPLE IDENTIFICATION			**DIMENSION (MM)**
Spectra Fiber Composite Panels		**Weave**	
985PT/BT250E	(Epoxy-based)	8H	1005 x 1005 x 10
988PT/BT250E	(Epoxy-based)	4H	1005 x 1005 x 10
985PT/BTCY-3	(Cyanate-based)	8H	1005 x 1005 x 10
988PT/BTCY-3	(Cyanate-based)	4H	1005 x 1005 x 10
GRP Panels			
7H5100LN016/001	(Epoxy-based)	8H	1020 x 1080 x 10
7H5100LN016/002	(Cyanate-based)	8H	1010 x 1255 x 10
Standard Calibration Panel			
Stainless Steel Plate			1219 x 1168 x 0.92

EXPERIMENTAL FACILITY

This investigation required acoustic measurements of sound, propagated at normal incidence to a panel immersed in water. The use of a parametric source was strategic to the study. With conventional sources, measurements on panels of limited size are affected by diffraction from the edges of the test panels. At low frequency ranges, approaching 1 kHz, diffraction is most pronounced, making it difficult to resolve the diffracted signal from the main transmitted signal. To minimize such effects, the energy at the edge must be reduced. With conventional acoustic transmission, it is very difficult to generate small spot insonification at low frequencies; directionality is a function dictated by frequency.

In view of this, a parametric source was designed and developed with a small beam cross-section. The basic principles of a parametric source can be found in Westervelt (1963), Clay and Medwin (1977), Berktay *et al.* (1979) and Humphrey (1985). Briefly, when two intense sound waves of slightly different frequencies are generated coaxially in water, they interact to produce secondary signals that contain a band of frequencies. These include both the sum and difference frequencies. Of particular importance are the low difference frequency signals generated. These signals possess many attractive attributes suited for material testing which include narrow beamwidth, no sidelobes, and broadband capabilities even at the lower kHz range. Therefore, material testing in a small tank is possible with parametric arrays since diffraction and sidelobe interference problems are made negligible. In addition, the broad bandwidth inherent in the parametric source allows material testing over a wide range of frequencies to be executed with a single small transducer.

In the experiments, a process called "self-demodulation" was used to create the secondary signals of the parametric array. In this method, a pulse-modulated carrier wave is radiated from the acoustic transducer with nonlinear interactions occurring in the water between all the frequencies radiated to yield a band of secondary frequencies.

The source for the study involved a wideband transducer resonant at 500 kHz, driven by a modulated carrier waveform obtained from the transmitting electronics. A short carrier pulse with a smooth envelope was transmitted. A "raised cosine bell" was generated as the modulating function. For our application, the parametric source was deliberately truncated within the Rayleigh distance by placing a "low-pass acoustic filter" across the primary beam at one metre from the transducer. This approach attenuated the higher frequency primary waves while transmitting the low-frequency secondary waves without significant loss. The truncator design was not a trivial task, but involved careful matching of characteristics of the primary beam to minimize spreading of the secondary wave after termination. Distances between hydrophones and panels had to be considered in the design of the truncator panel. A plate made of 20 gauge stainless steel was used as truncator.

Newfoundland's Marine Institute's flume laboratory was the site for the tests. Its dimensions consisted of a large, rectangular concrete windowed tank; 21.5 metres long, 8 metres wide and 4 metres deep, ideal for low frequency material evaluation.

The general geometry used in the study is shown in Figure 1A with a time history example of a signal received after the test panel exhibited in Figure 1B.

MEASUREMENTS

The setup for making the loss measurements is shown in Figure 2. A reference signal was first acquired; the transmitted signal was then recorded with the test panel placed between the truncator and hydrophone. The echo reduction measurements utilized a similar experimental setting (see Figure 3). Once a reference signal was recorded without the panel being present, then reflected signals could be captured with the same hydrophone placed in front of the test panel.

The insertion loss of a panel was defined in terms of the complex incident sound pressure and complex transmitted sound pressure:

$$IL = 20\log_{10}\left|\frac{\textit{incident sound pressure } p_i}{\textit{transmittted sound pressure } p_t}\right| = 20\log_{10}\left|\frac{1}{T}\right| \tag{1}$$

T is the complex transmission coefficient.

The echo reduction (*ER*) of a panel was also defined in terms of its complex incident sound pressure and complex reflected sound pressure:

$$ER = 20\log_{10}\left|\frac{\textit{incident sound pressure } p_i}{\textit{reflected sound pressure } p_r}\right| = 20\log_{10}\left|\frac{1}{R}\right| \tag{2}$$

R is the complex reflection coefficient and the function | • | represents the magnitude.

Computations of the complex reflection and transmission coefficient were performed in the frequency domain via the Fast Fourier Transform (FFT). In each case, the complex Fourier coefficients for each pulse were used in the division. In addition, the Hilbert Transform was employed to better display and calculate changes in the waveform. Such a response analysis involves taking the imaginary part of the signal along with the real part. The resulting analytic signal is displayed as time or frequency envelopes. Such transformed data allows for precise time representation of both the peak values and instantaneous phases of the signal. The Hilbert-transformed series were detrended and the energy envelopes were log transformed (see Figure 1B). (Guigné *et al.* (1991) and Guigné and Chin (1989) provide details on the application of the Hilbert Transform to underwater acoustics).

RESULTS

Ideally, the properties of a sonar dome would be such as to allow the propagation of acoustic radiation through with minimal reflection, absorption, or distortion. Examination of the Hilbert Transforms is one way of determining the amount of distortion due to the panel. The shape of the transmitted waveforms for the cyanate-based Spectra Fiber panels (Figures 4A, 5A and 6A) are very close to those of the Reference waveforms, while the epoxy-based Spectra Fiber and GRP panel waveshapes are slightly more distorted (Figures 7A, 8A and 9A). The Hilbert Transform of a thin (0.92 mm) stainless steel panel is shown for comparison in Figure 10A. Note how the waveshape is altered considerably more than for the composite panels.

The amount of reflection and absorption may be quantified by their echo reduction and insertion loss spectra, shown in Figures 11 and 12 for the panels listed in Table 1. The Spectra Fiber panels had relatively flat insertion loss spectra of less than 1dB up to 35 kHz (Figure 12), whereas the GRP panels had losses that increased more sharply with frequency, with values of 2.5 - 3.5 dB at the higher end of the freuency range examined (40kHz). The cyanate-based panels had slightly better (lower insertion losses) performance than the epoxy-based panels for Spectra Fiber panels, but the opposite was true for the GRPs (i.e. the epoxy resins were superior). The 8H weave was found to have slightly lower insertion losses than the 4H weave for the Spectra Fiber/cyanate resin system. The Spectra Fiber panels also had low reflectivity, or high echo reduction, in the 1 - 40 kHz frequency range (Figure 11). The least reflective panel was the 8H cyanate resin Spectra Fiber panels, which had echo reductions of 15 - 22 dB.

SUMMARY

From the data collected, it is clear that the Spectra Fiber Composite Panels have very low insertion losses compared to the glass fiber composites of the same thickness. In particular, the 988 PT/BT250E epoxy-based panel and 985PT/BTCY3 cyanate-based panel have remarkable responses producing very little waveshape distortion and losses (see Figure 12). The Spectra Fiber echo reduction characteristics also concurred with the goal for the sonar dome material to remain low in reflectivity.

Overall, it would appear that significant gains would be made using Spectra Fiber Composite materials over glass fiber and metallic composite sonar domes. In addition to being non-corroding and having high strength to weight ratio, their acoustic properties appear well-matched in impedance to water, and also appear well suited to low frequency propagation.

REFERENCES:

Berktay, H.O., B.V. Smith, H.B. Braithwaite and M. Whitehouse, 1979, Subbottom profilers with parametric sources, *Underwater Applications of Nonlinear Acoustics*, Institute of Acoustics, University of Bath, England, Session 1.2, pp. 1-10.

Clay, C.S., and H. Medwin, 1977. Acoustical Oceanography: Principles and Applications, *Wiley-Interscience*, New York, pp. 185-187.

Guigné, J.Y., N. Rukavina, P.H. Hunt and J.S. Ford, 1991, An acoustic parametric array for measuring the thickness and stratigraphy of contaminated sediments. *J. Great Lake Res.* **17**: 120-131.

Guigné, J.Y. and V.H. Chin, 1989, Acoustic imaging of an inhomogeneous sediment matrix, *Marine Geophysical Research,* **11**:301-317.

Humphrey, V.F., 1985, The measurement of acoustic properties of specimens of limited size by use of a parametric source, *Journal of Sound and Vibration,* **98**(1) pp 67-81

Westervelt, P.J. 1963, Parametric acoustic array, *J. Acous. Soc. Am.* **35**:535-537.

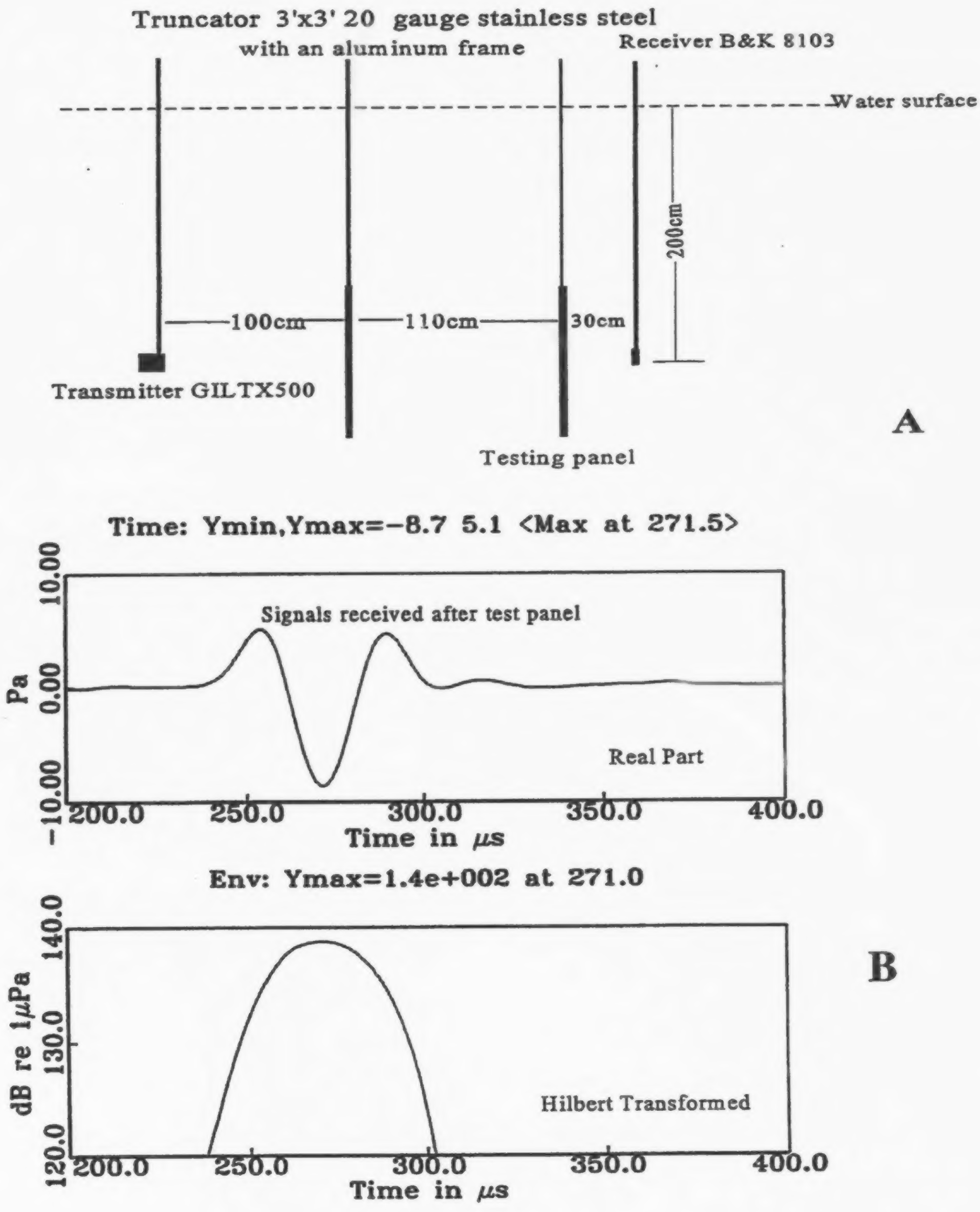
Truncator 3'x3' 20 gauge stainless steel
with an aluminum frame
Receiver B&K 8103
Water surface
200cm
100cm
110cm
30cm
Transmitter GILTX500
Testing panel
A
Time: Ymin,Ymax=-8.7 5.1 <Max at 271.5>
Signals received after test panel
Real Part
Pa
10.00
0.00
-10.00
200.0
250.0
300.0
350.0
400.0
Time in μs
Env: Ymax=1.4e+002 at 271.0
Hilbert Transformed
dB re 1μPa
140.0
130.0
120.0
200.0
250.0
300.0
350.0
400.0
Time in μs
B

Figure 1

Setup for Insertion Loss Measurements

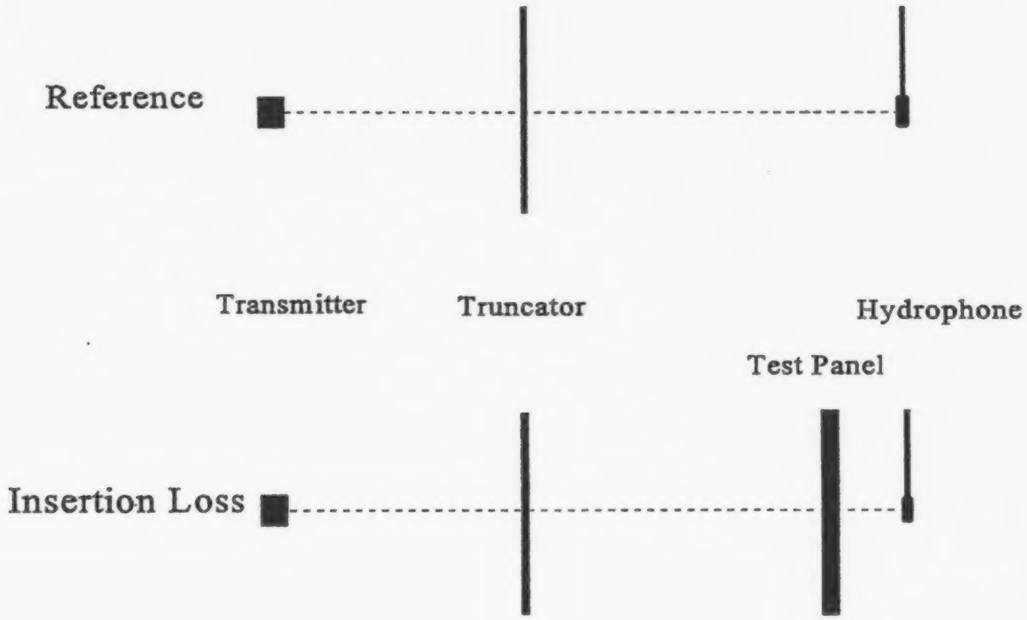
Reference
Transmitter
Truncator
Hydrophone
Test Panel
Insertion Loss

Figure 2

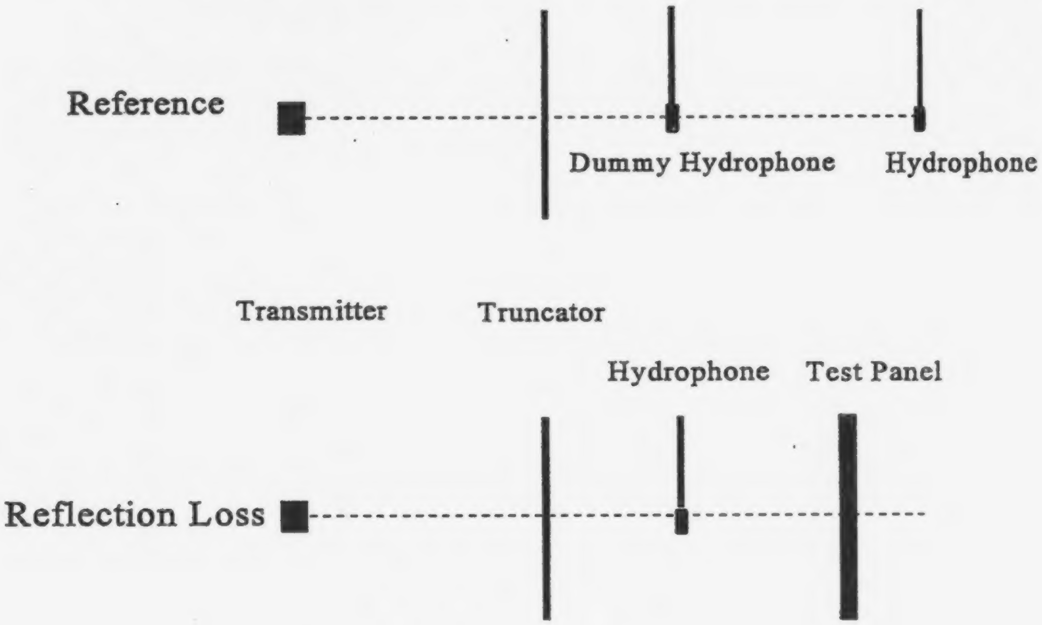

Setup for Reflection Loss Measurements

Reference
Dummy Hydrophone
Hydrophone
Transmitter
Truncator
Hydrophone
Test Panel
Reflection Loss

Figure 3

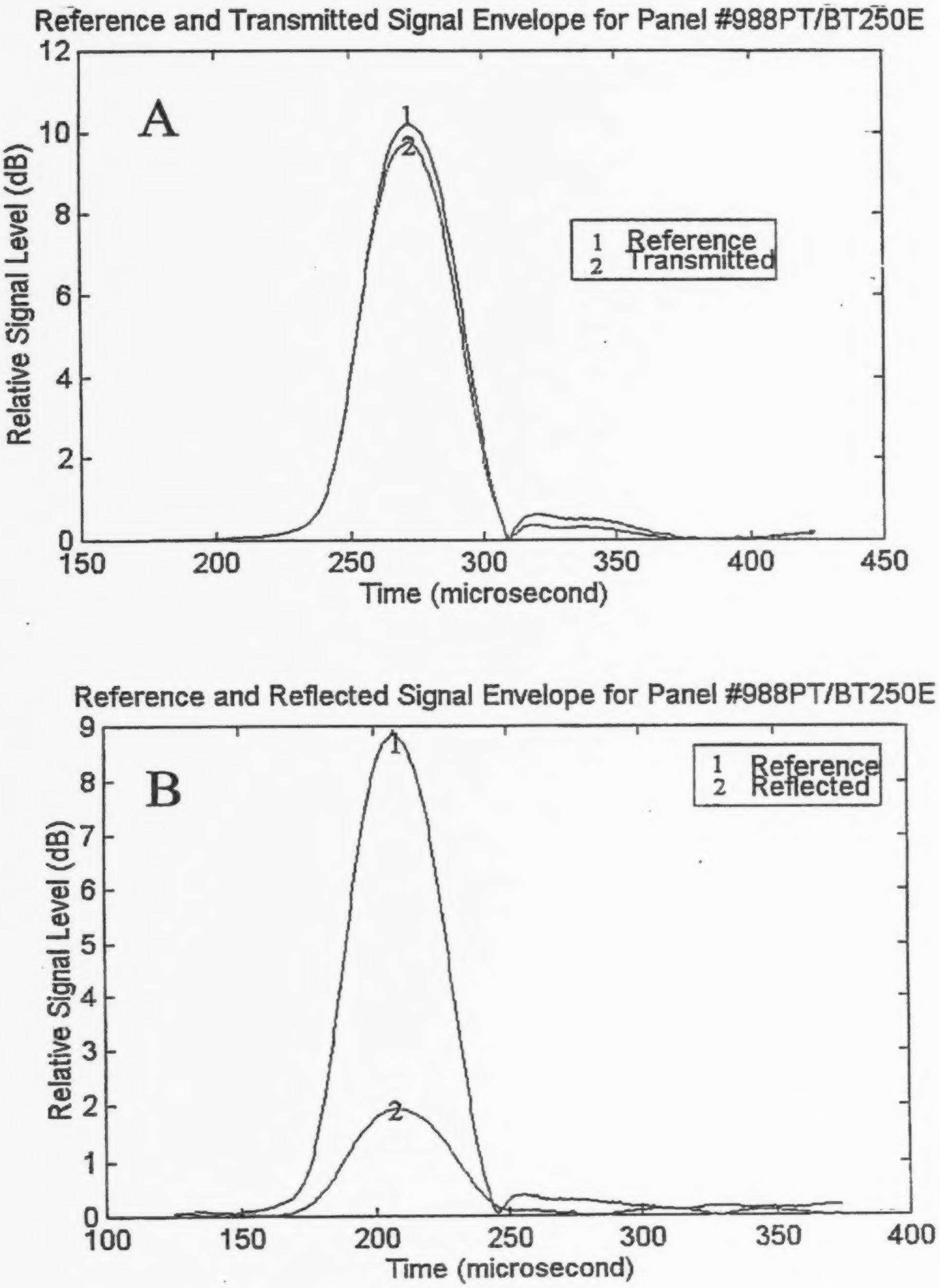
Reference and Transmitted Signal Envelope for Panel #988PT/BT250E
A
Relative Signal Level (dB)
0
2
4
6
8
10
12
150
200
250
300
350
400
450
Time (microsecond)
1 Reference
2 Transmitted
1
2
Reference and Reflected Signal Envelope for Panel #988PT/BT250E
B
Relative Signal Level (dB)
0
1
2
3
4
5
6
7
8
9
100
150
200
250
300
350
400
Time (microsecond)
1 Reference
2 Reflected
1
2

Figure 4

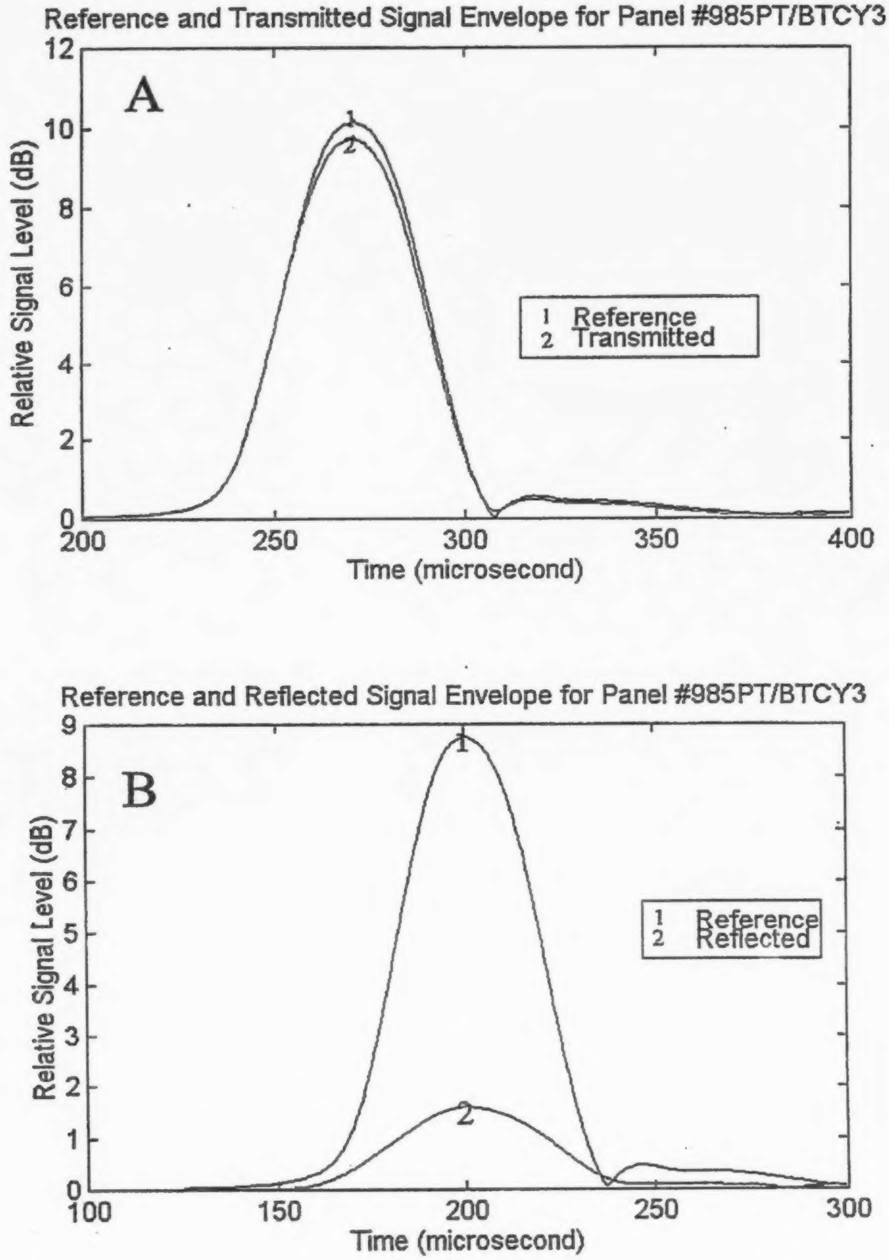
Reference and Transmitted Signal Envelope for Panel #985PT/BTCY3
A
Relative Signal Level (dB)
12
10
8
6
4
2
0
200
250
300
350
400
Time (microsecond)
1
2
1 Reference
2 Transmitted
Reference and Reflected Signal Envelope for Panel #985PT/BTCY3
B
Relative Signal Level (dB)
9
8
7
6
5
4
3
2
1
0
100
150
200
250
300
Time (microsecond)
1
2
1 Reference
2 Reflected

Figure 5

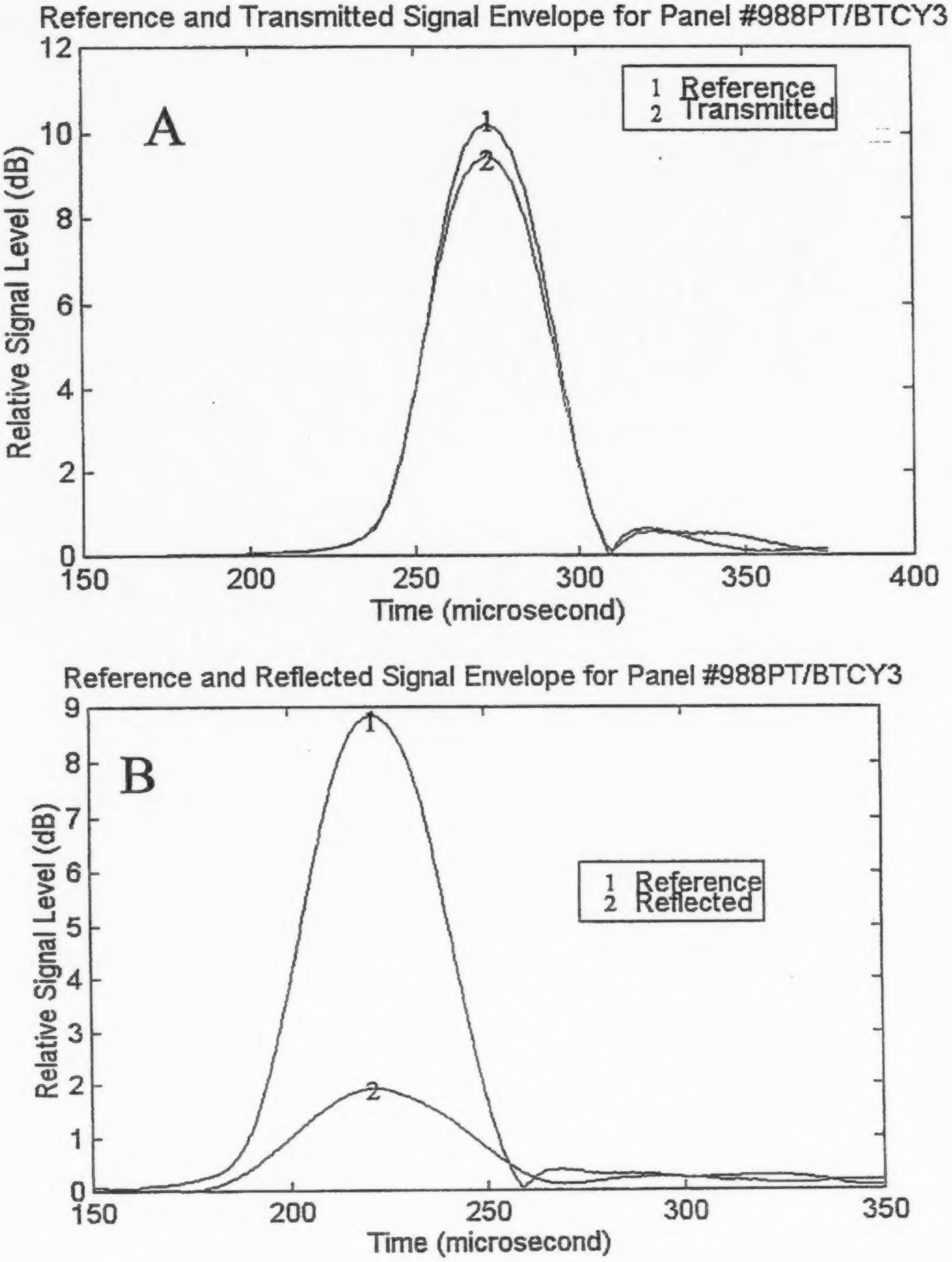
Reference and Transmitted Signal Envelope for Panel #988PT/BTCY3
A
1 Reference
2 Transmitted
Relative Signal Level (dB)
0
2
4
6
8
10
12
150
200
250
300
350
400
Time (microsecond)
1
2
Reference and Reflected Signal Envelope for Panel #988PT/BTCY3
B
1 Reference
2 Reflected
Relative Signal Level (dB)
0
1
2
3
4
5
6
7
8
9
150
200
250
300
350
Time (microsecond)
1
2

Figure 6

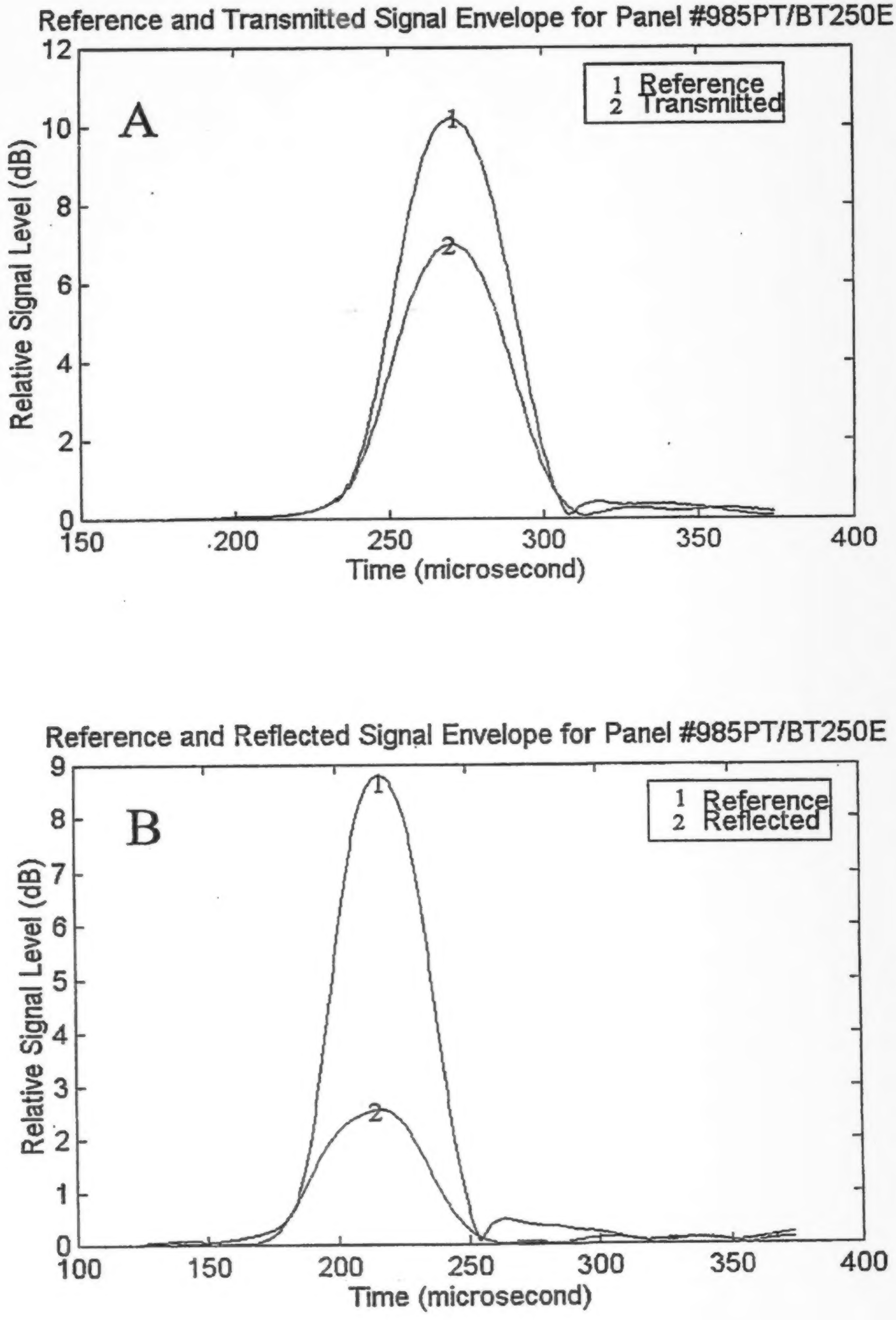

Reference and Transmitted Signal Envelope for Panel #985PT/BT250E

Reference and Reflected Signal Envelope for Panel #985PT/BT250E

Figure 7

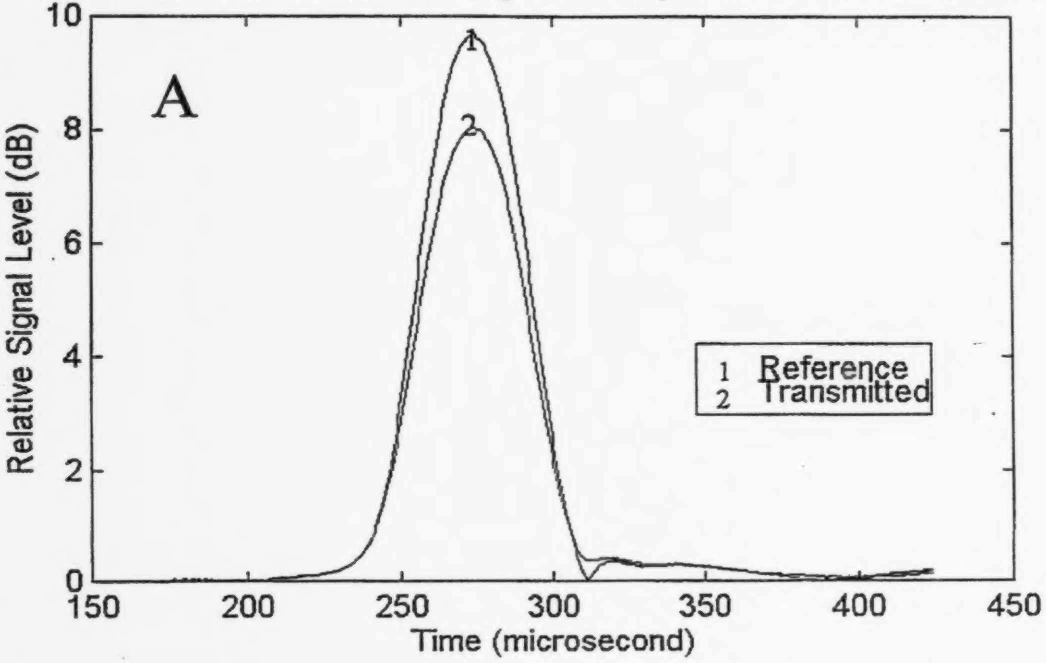
Reference and Transmitted Signal Envelope for GRP Panel #1 Blue

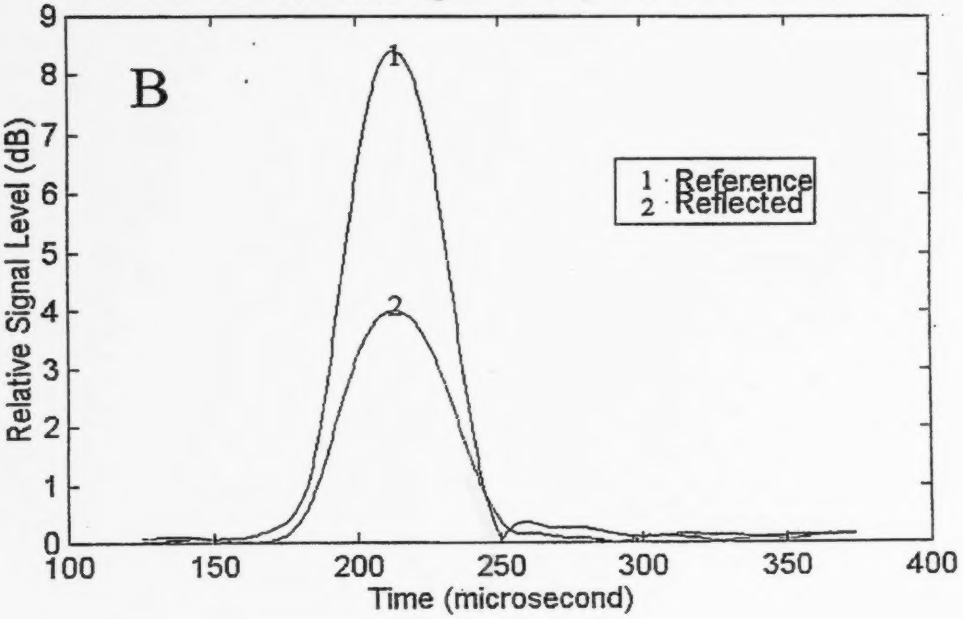
Reference and Reflected Signal Envelope for GRP Panel #1 Blue

Blue - Epoxy

Figure 8

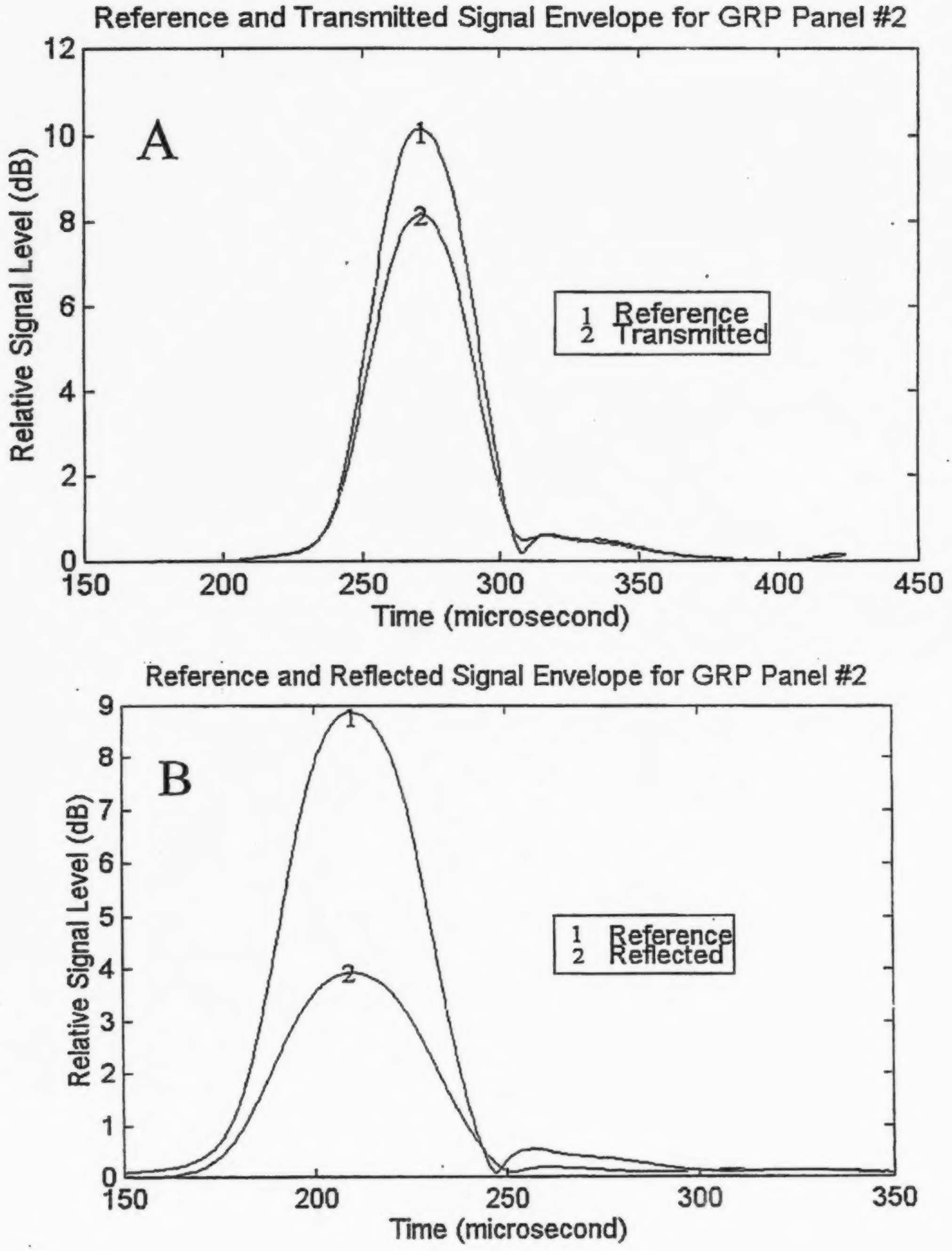

Brown - Cyanate

Figure 9

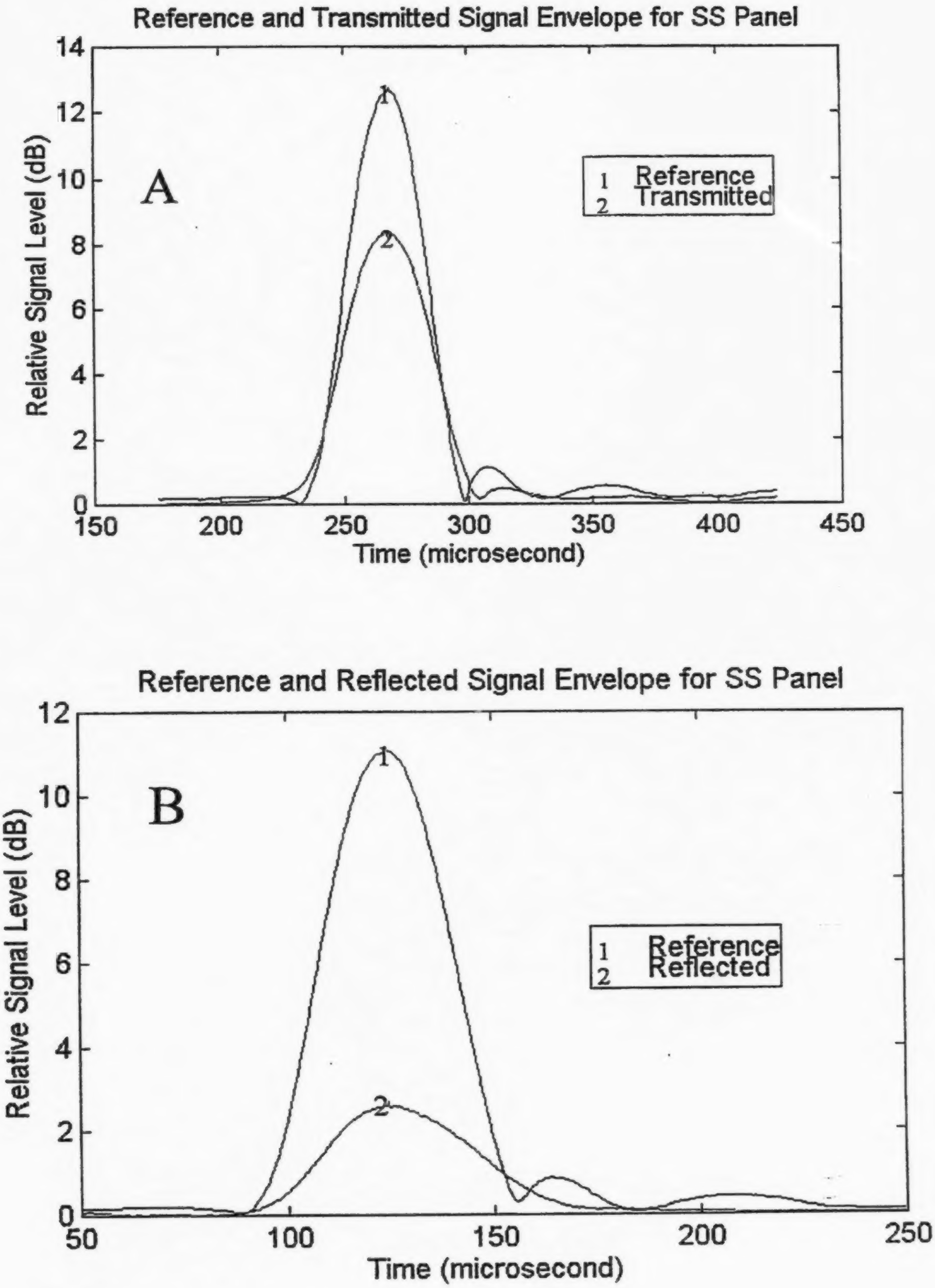

SS - Stainless Steel

Figure 10

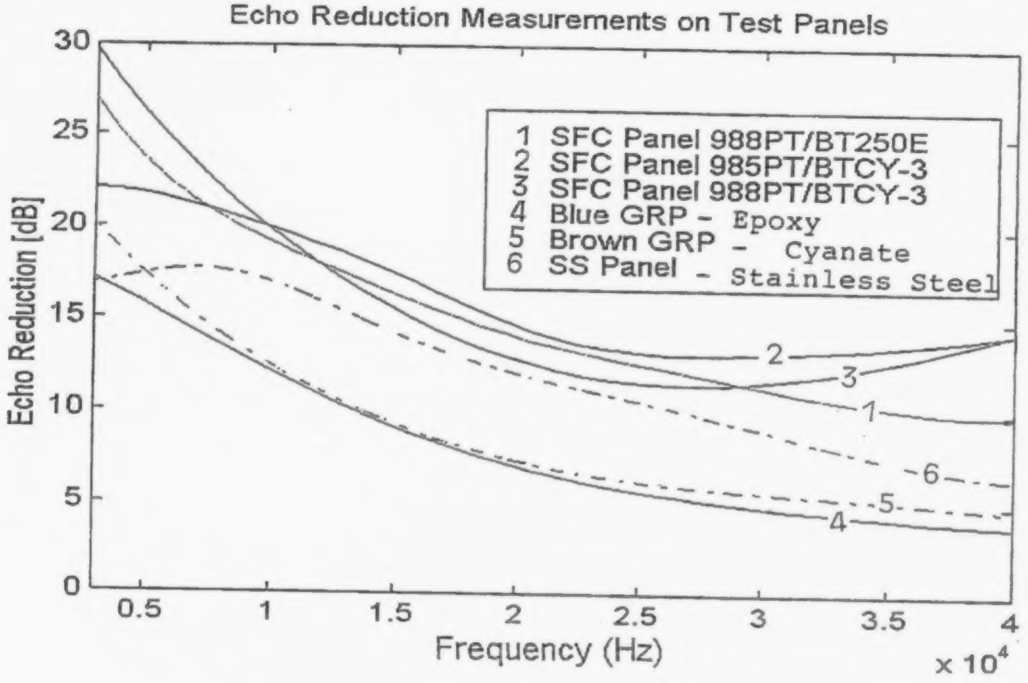
Echo Reduction Measurements on Test Panels
Echo Reduction [dB]
30
25
20
15
10
5
0
0.5
1
1.5
2
2.5
3
3.5
4
Frequency (Hz)
x 10^4
1 SFC Panel 988PT/BT250E
2 SFC Panel 985PT/BTCY-3
3 SFC Panel 988PT/BTCY-3
4 Blue GRP - Epoxy
5 Brown GRP - Cyanate
6 SS Panel - Stainless Steel
2
3
1
6
5
4

Figure 11

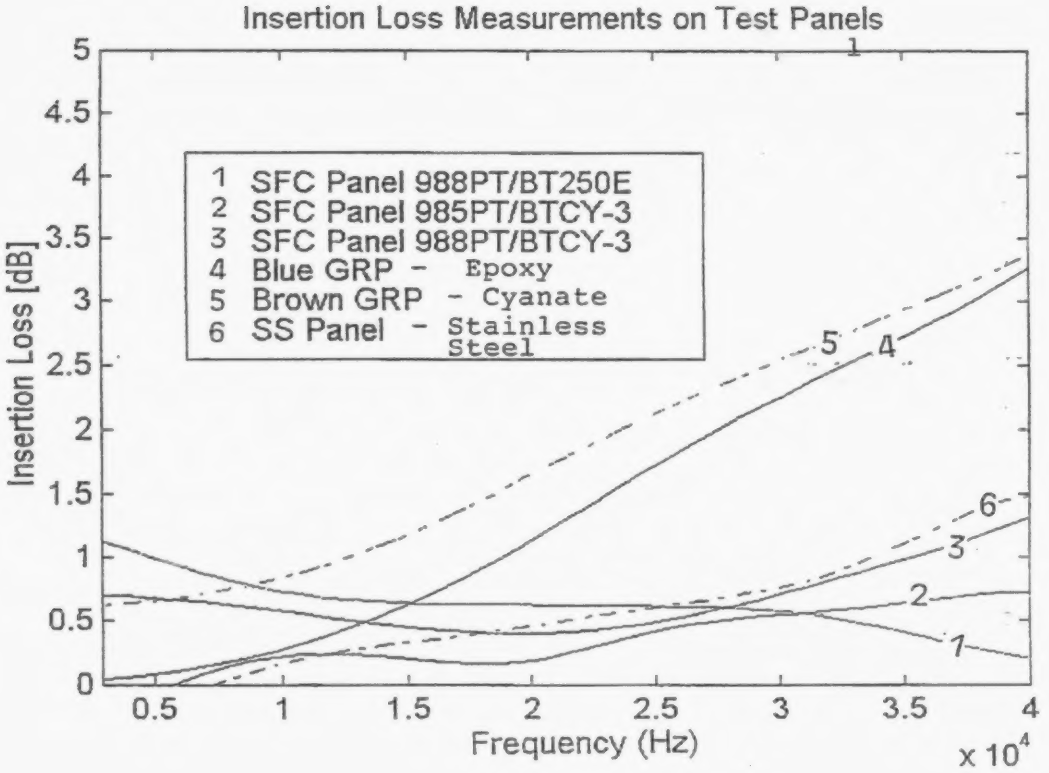
Insertion Loss Measurements on Test Panels
Insertion Loss [dB]
Frequency (Hz)
x 10^4
0
0.5
1
1.5
2
2.5
3
3.5
4
4.5
5
0.5
1
1.5
2
2.5
3
3.5
4
1 SFC Panel 988PT/BT250E
2 SFC Panel 985PT/BTCY-3
3 SFC Panel 988PT/BTCY-3
4 Blue GRP - Epoxy
5 Brown GRP - Cyanate
6 SS Panel - Stainless Steel
1
2
3
4
5
6

Figure 12

Dr. A.M. Abdel-Latif
Quality Engineering Test Establishment
Materials Engineering and Applied Physics
Ottawa, Ontario
K1A 0K2

David Allison
(Non-Metallic Materials, Paints, etc)
Head, Section 114
Director of Naval Architecture
Ministry of Defence
Block F. Foxhill
Bath
UK BA1 5AB

Dr. M.N. Bassim
Dept. of Mechanical Engineering
University of Manitoba
Winnipeg, Manitoba R3T 5V6

Ray Beazley Bldg D200
Welding Supervisor
Fleet Engineering Maintenance Unit
FMO Halifax
Halifax, Nova Scotia B3K 2X0

Mr. Jorgen Bernt and Mr. Dat Nguyen
J.O.Bernt and Associates Limited,
3375 Laird Road, Unit 3
Mississauga,Ontario,Canada
L5L 5R7

Ms Teresia Betancourt
Nova Scotia Research Foundation
100 Fenwick St. Box 790
Dartmouth, Nova Scotia B2Y 3Z7

Charles Billard
MetaSoudage
c/o Centre R & D Metallurgie
MIL Davie Inc.
Case Postale 130
22 Geo D. Davie
Levis, Quebec, G6V 6N7

Mr. Mike Brauss
Proto Manufacturing Ltd.
2175 Solar Cr.
Oldcastle, Ontario N0R 1L0

Dave Brennan
Martec Ltd. Suite 400
1888 Brunswick St.
Halifax, Nova Scotia B3F 3F8

Larry Brown
Annapolis Detachment
Caederock Division
Naval Surface Warefare Center
Code 2815
Annapolis Maryland 21402-5067

Mr. Bob Caswell
Canadian Patrol Frigate Detachment
Brunswick House Suite 500
44 Chipman Hill
St John New Brunswick E2L 2A9

Dr. M.K. Chernuka
Martec Ltd. Suite 400
1888 Brunswick St.
Halifax, Nova Scotia B3F 3F8

Capt(N) G.D. Humby
Commanding Officer
Ship Repair Unit Atlantic
FMO Halifax
Halifax Nova Scotia B3K 2X0

Mr. Perry Clarke
Atomic Energy of Canada Ltd.
Chalk River Nuclear Laboratories
Chalk River, Ontario N0R 1L0

Terry Culliton
Saint John Shipbuilding Ltd.
Bayside Drive
P.O.Box 300
St John, New Brunswick E2L 4E5

Dr Virginia DeGiorgi
Code 6382
Naval Research Laboratory
Washington, D.C.
USA 20375-5000

Johnnie DeLoach
Annapolis Detachment
Caederock Division
Naval Surface Warefare Center
Annapolis Maryland 21402-5067

R. DeNale
Annapolis Detachment
Caederock Division
Naval Surface Warefare Center
Annapolis Maryland 21402-5067

Mr Duane Tuttle/
Mr Duane Giffin/
Mr Ralph Wallis/
Mr Sean Bartlett
Mr Fred Grainger
NDT D200
FMO Halifax
Halifax, Nova Scotia B3K 2X0

Mr Stephane Garneau DSE
National Defence Headquarters
101 Colonel By Drive
Ottawa, Ontario K1A 0K2

Mr Jim Gianetto
Metals Technology Labs
Energy Mines and Resources Canada
555 Booth St.
Ottawa, Ontario K1A 0G1

Dr. Andrey Ginovker
Dalhousie University
Department of Physics
Halifax N.S.
B3H 3J5

Mr. Sherman Goucher
Canadian Patrol Frigate Program
Brunswick House Suite 501
44 Chipman Hill
St John New Brunswick E2L 2A9

Dr. Jacques Guigné
Guigné International Limited
82 St. Thomas Line
RR#1, P.O. Box 13, Site 21
Paradise, Newfoundland A1C 1C1

Mr Randy Haggett
Defence Research Establishment Atlantic
FMO Halifax
Halifax, Nova Scotia B3K 2X0

Craig Hamm
Guigné International Limited
82 St. Thomas Line
RR#1, P.O. Box 13, Site 21
Paradise, Newfoundland A1C 1C1

Dr. Bob Hay
President
Tektrend International Ltd.
2755 Pitfield
Ville St. Laurent, Quebec H4S 1G3

John Hewitt
The Laser Institute
9924-45 Ave
Edmonton Alta T6E 5J1

Dr John Hiltz
Defence Research Establishment Atlantic
FMO Halifax
Halifax, Nova Scotia B3K 2X0

Dr. Roger S. Hollingshead
Defence Research Establishment Atlantic
FMO Halifax
Halifax, Nova Scotia B3K 2X0

Mr. Paul Holsberg
Annapolis Detachment
Caederock Division
Naval Surface Warefare Center
Code 2810
DTNSRDC
Annapolis, Maryland 21402

Mr Don Hussey
Donelad Ltd.
Suite 720 Sun Tower
1550 Bedford Highway
Bedford N.S. B4A 1E6

Dr Calvin Hyatt
Defence Research Establishment Atlantic
FMO Halifax
Halifax N.S. B3K 2X0

Head/Hydronautics Section
Defence Research Establishment Atlantic
P.O.Box 1012
Dartmouth, Nova Scotia B2Y 3Z7

Dr. S. Das Gupta and Mr. S. Johar
Electrofuel Manufacturing Company Ltd.
21 Hanna Avenue
Toronto, Ont., Canada
M6K 1W8

Dr. R.L. Jones
Materials Engineering Division
Admiralty Research Establishment
Holton Heath
Poole
Dorset, U.K. BH16 6JU

Mr Ken KarisAllen
Facts Engineering
P.O.Box 20039
Halifax, Nova Scotia B3R 2K9

Lt(N) Kirk Kirkoff DSE 5-3-3
National Defence Headquarters
101 Colonel By Drive
Ottawa, Ontario K1A 0K2

Ms Carol Lebowitz
Annapolis Detachment
Caederock Division
Naval Surface Warefare Center
Code 2815
Annapolis Maryland 21402-5067

Kelly-Anne Lively
10 Jersey Drive
Dartmouth N.S. B2W 1V6

Quan Shun Liu
Guigné International Limited
82 St. Thomas Line
RR#1, P.O. Box 13, Site 21
Paradise, Newfoundland A1C 1C1

Gord MacDonald D22
Welding Officer
Fleet Engineering Maintenance Unit
FMO Halifax
Halifax, Nova Scotia B3K 2X0

Dr. L. Malik
Materials Technology Centre
311 Legget Drive
Kanata, Ontario K2K 1Z8

Terri Ann Marsico
Applied Research Laboratory
The Pennsylvania State University
P.O. Box 30
165 Applied Science Building
State College
University Park PA 16804

Dr. James R. Matthews
Defence Research Establishment Atlantic
FMO Halifax
Halifax, Nova Scotia B3K 2X0

Lt(N) L.M. Maxwell
Canadian Patrol Frigate Detachment
Brunswick House Suite 500
44 Chipman Hill
St John New Brunswick E2L 2A9

Dr. K.M. Valter McConville
Aastra Aerospace Inc.,
1685 Flint Rd.
Downsview, Ont
M3J 2W8

Brian McGrath
St.John Ship Building Ltd.
300 Union St.
P.O. Box 5111
St. John N.B.
E2L 4L4

Ken McRae
Esquimalt Defence Research Detachment
FMO Esquimalt
Victoria, B.C. V0S 1B0

Dr. Richard Morchat DRDM 8
National Defence Headquarters
101 Colonel By Dr
Ottawa Ontario

Dr. M.K.Murthy
MKM Consultants International
10 Avoca Avenue,Unit 1906
Toronto,Ont.
M4T 2B7

LCdr D. Peer D200
Industrial Engineering
FMO Halifax
Halifax, Nova Scotia B3K 2X0

Bob Pemberton Bldg D166
Fleet Engineering Maintenance Unit
FMO Halifax
Halifax, Nova Scotia B3K 2X0

Mr. John Porter
Defence Research Establishment Atlantic
FMO Halifax
Halifax, Nova Scotia B3K 2X0

Rajean Rene
Centre R & D Metallurgie
MIL Davie Inc.
Case Postale 130
22 Geo D. Davie
Levis, Quebec, G6V 6N7

Mr. Richard Robicheau
216-55 Highfield Park Drive
Dartmouth, Nova Scotia
B3A 4S3

Dr. Alan Russell
Head/Materials Engineering Section
Esquimalt Defence Research Detachment
FMO Esquimalt
Esquimalt, British Columbia V0S 1B0

Dr. Mahi Sahoo
Metals Technology Labs
Energy Mines and Resources Canada
555 Booth St.
Ottawa, Ontario K1A 0G1

Frank Smith
German Marine
71 Ilsley Avenue
Dartmouth N.S.
B3B 1L5

Dr Jeff Szabo
Defence Research Establishment Atlantic
FMO Halifax
Halifax, Nova Scotia B3K 2X0

Mr. Dwight Veinot
Defence Research Establishment Atlantic
FMO Halifax
Halifax, Nova Scotia B3K 2X0

Mr. Tom West
FEMU
FMO Halifax
Halifax, Nova Scotia B3K 2X0

Richard Yee
Materials Technology Centre
311 Legget Drive
Kanata, Ontario K2K 1Z8